ROLE OF DELAMINATION AND INTERLAMINAR FATIGUE IN THE FAILURE OF LAMINATES WITH PLY DROPOFFS

by

Dong Jin Shim

B. S., Aerospace Engineering
Seoul National University (1994)

S. M., Aerospace Engineering
Seoul National University (1997)

Submitted to the Department of Aeronautics and Astronautics
in Partial Fulfillment of the Requirements for the Degree of

Doctor of Philosophy
in Aeronautics and Astronautics
at the
Massachusetts Institute of Technology

June 2002

Signature of Author.....
Department of Aeronautics and Astronautics
May 13, 2002

Certified by.....
Paul A. Lagace
Professor of Aeronautics and Astronautics and Engineering Systems
Chair, Thesis Committee

Certified by.....
John W. Hutchinson
Gordon McKay Professor of Applied Mechanics, Harvard University
Thesis Committee

Certified by.....
S. Mark Spearing
Associate Professor of Aeronautics and Astronautics
Thesis Committee

Accepted by.....
Wallace E. Vander Velde
Professor of Aeronautics and Astronautics
Chair, Committee on Graduate Students

Role of Delamination and Interlaminar Fatigue in the Failure of Laminates with Ply Dropoffs

by
DONG JIN SHIM

Submitted to the Department of Aeronautics and Astronautics on May 13, 2002 in partial fulfillment of the requirements for the Degree of Doctor of Philosophy

Abstract

Analytical and experimental investigations were conducted on laminates with ply dropoffs to better understand the interlaminar stress field and delamination/damage characteristics in such laminates, as well as the relationship between the two based on the strength of materials approach. To gain key insights into the mechanisms and structural parameters that cause interlaminar stresses, analytical models for laminates with simple ply dropoff configurations were developed based on a systematic and hierarchical approach. Mathematically, these individual models are formulated using the stress function method in which the form of the admissible stress field is assumed *a priori* based on the stress field from the classical laminated plate theory and other functional constraints of the problem. The results are validated via comparisons with numerical solutions from previous investigations and as performed in the current work. Various structural parameters such as the taper angle and the location of the terminated plies are found to affect the interlaminar stress distribution. Careful consideration of the characteristics and trends of the interlaminar stresses in such laminates reveals that two fundamental mechanisms give rise to interlaminar stresses: the *termination effect*, that is caused by the load transfer from the terminated ply group to the continuous plies; and the *offset effect*, that is caused by the redistribution of the load from the undropped region to the dropped region in the outer continuous plies through an offset in the through-thickness direction. These mechanisms, the factors that affect them, and their utility are described and discussed in detail. Factors of particular importance are the magnitudes of the far-field loads in the terminated and the outer continuous ply groups, the offset distance, and the taper angle. Experiments are conducted on unidirectional laminate configurations under static and cyclic loads to establish delamination/damage trends when the number and location of the terminated plies are varied. Under both loading conditions, delamination is found to be the dominant damage mode, although other modes, *e.g.*, ply splits, occur. In certain types of specimens under cyclic loading, delaminations in different regions have different growth characteristics causing delaminations in one region to be a greater concern than in another region because the length of the delaminations increases indefinitely. In general, the experimental observations regarding delamination/damage are consistent with expectations based on the stress analysis. Delaminations are generally observed along interfaces where the interlaminar stresses are greatest, and static delamination loads are higher in laminates with lower interlaminar stresses. Quantitative predictions of the delamination loads using the Quadratic Delamination Criterion with the average stress method do not agree as well with the experimental data because a single value for the averaging length could not be

obtained. The possible causes for the apparent non-uniqueness of the averaging length and its implications are further discussed. Based on this investigation, further recommendations for work on laminates with ply dropoffs are proposed.

Thesis Supervisor: Paul A. Lagace

Title: Professor of Aeronautics and Astronautics and Engineering Systems

ACKNOWLEDGEMENTS

This work would not have been possible had it not been for the contributions from numerous people, and they deserve acknowledgement. First and foremost, I would like to thank Prof. Lagace for the support and guidance he provided throughout this work, and for being a great advisor, mentor, and friend. It has been a pleasure working with him. Prof. Spearing and Prof. Hutchinson have provided valuable suggestions throughout this research, and I would like to thank them as well. I am grateful to Prof. Cesnik and Prof. Dugundji whose questions have helped me to frame this work better. I would like to thank John Kane for all his help manufacturing and testing those specimens, Ping for making sure that I always got paid and her kind words of support, and Cathy. My four years in TELAC have been very enjoyable because of all the great officemates I have had. Some have long gone, Brian W., Mike T., Jose M., Ariela G., and Stacy J., some have graduated not so long ago, Barb H. (soon to be Mrs. Wong), Randel G., Dennis B., and Seth K. (always circle the dog), and others are still here at the time of this writing, Chris D., Mark "Chewy" K., Chris "Sopps" G., Torrey R. (get rid of those damn red bars), Kevin T., Jeremy G., and Linda M. I should also note my UROPs for helping me out with the manufacturing and testing.

Finally, I would like to thank my wife, Eunseon, for her love, patience and understanding, my parents, Mr. and Mrs. Shim, for their love and support, my brother, Dong Uk, and sister, Jeong Yun, for always caring and looking out for their younger brother, and my son, Brian, for always providing laughter and joy.

I thank the Lord who is my rock, my strength and my salvation.

"I can do everything through him who gives me strength." - Philippians 4:16

And... Go Sox! This *is* the year.

FORWARD

This work was performed in the Technology Laboratory for Advanced Composites (TELAC) of the Department of Aeronautics and Astronautics at the Massachusetts Institute of Technology. This work was sponsored by Sikorsky Aircraft under Purchase Order #N5609206.

TABLE OF CONTENTS

LIST OF FIGURES

LIST OF TABLES

NOMENCLATURE

α	taper angle
n	number of plies in one half of a symmetric laminate in the undropped region
m	number of plies in one half of a symmetric laminate in the dropped region
x_1, x	lengthwise direction
x_2	widthwise direction
z	global thickness direction
z_i	local thickness direction defined in each ply
S_{ijkl}	compliance matrix
F_i, G_i	stress functions defined at the interfaces between two plies for region A
H_i, K_i	stress functions defined at the interfaces between two plies for region B
t_i (or t)	thickness of the *i*th ply (when constant)
a_j, b_j	constants for stress functions
λ_j, μ_j	eigenvalues for regions A and B, respectively
Φ_j, Ψ_j	eigenvectors for region A
Θ_j , Γ_j	eigenvectors for region B
$\tilde{\psi}_i$, $\tilde{\phi}_i$, κ	Lagrange multipliers
a	delamination length in laminate with existing delamination
l_d	length of dropoff region
t_d	offset distance
σ_0	applied far-field stress at undropped end due to in-plane load
σ_s	applied far-field stress at undropped end due to bending load
N	applied in-plane load

M	applied bending load
n_c	number of continuous plies in a geometrically unsymmetric laminate
l_{ave}	averaging length

Subscripts and supercripts

A	region A
B	region B
D	terminated plies

CHAPTER 1

INTRODUCTION

The use of composite materials in structural components has been steadily rising due to the advantages of composite materials in comparison to conventional materials. These advantages include high specific strength and stiffness and better resistance to fatigue [1]. Although composite materials are used in many applications such as automobiles, ships, and bridges, they are particularly useful in the aerospace industry where the benefits of saving weight are especially important and sometimes critical. As such, composites have been used extensively in military applications such as airplanes, helicopters, and satellites for many years. In the commercial sector, use of composite materials in structural components has been increasing at a slower rate due to the higher cost of composite materials in comparison to conventional materials. The rules and regulations for safety and reliability are more stringent for commercial aircraft compared to military aircraft and the consequences in the event of failure are much greater such that there is also more risk involved in introducing composite materials (or any other new material) in the commercial sector. This has also hindered use of composite materials in commercial aircraft.

Composite materials have been in use in commercial airplanes as secondary structures such as spoilers in the Boeing 737 since the 1970s [2]. The first all-composite commercial aircraft was the Beechcraft Starship, which is a small eight-passenger airplane, built in the mid-1980s. The first primary structure made of composites in a large passenger airplane was the fin of the Airbus A300/310 series in the late-1980s. The A300/310 series fin, which is made of carbon fiber reinforced plastic, weighs approximately 20% less and requires approximately 95% fewer parts compared to an aluminum alloy design [3]. More recently, the empennage of the Boeing 777 was built

using composite materials.

With the increasing use of composite materials in structural applications in general, there is a need to understand in greater detail how to design and analyze structures with such materials both statically as well as for fatigue considerations in order to ensure safe operation. However, designing with composite materials, especially continuous fibrous composites, is very different from designing with most conventional materials. In addition to being anisotropic, continuous fibrous composite materials are commonly used in laminated form. These characteristics make structures that are relatively simple to design using conventional materials more complex using composite materials. An example of such a structure is the tapered laminated plate. Since each layer, or ply, of the composite laminate is constant in thickness, the taper can only be achieved by terminating the appropriate number of plies at the necessary locations. These ply "dropoffs" are commonly used in composite laminates when laminate properties, such as stiffness, along the length need to be varied. They are used, for example, in aircraft wing skins, leaf springs, and composite flexbeams.

Of particular interest in this work is the case of the composite flexbeam. This is a structure used in bearingless and hingeless rotorhub assemblies for helicopters. A diagram of such a rotorhub assembly is shown in Figure 1.1. Traditional rotorhub assemblies consist of a complex arrangement of bearings and hinges to support the lead-lag, flapping, and feathering motions of the rotor blades. These mechanical components increase the overall weight of the rotorhub and require a significant amount of time for maintenance, in addition to the cost of the components themselves. The flexbeam eliminates the need for any mechanical hinges, which results in significantly fewer parts and a decrease in weight. In the case of the bearingless main rotor of the MD 900 Explorer, the composite bearingless rotor design has 76% fewer parts and weighs 14.5% less compared to a metal rotor design [4]. Moreover, the flexbeam can be designed to minimize vibration. Therefore, there are significant advantages to be gained by using

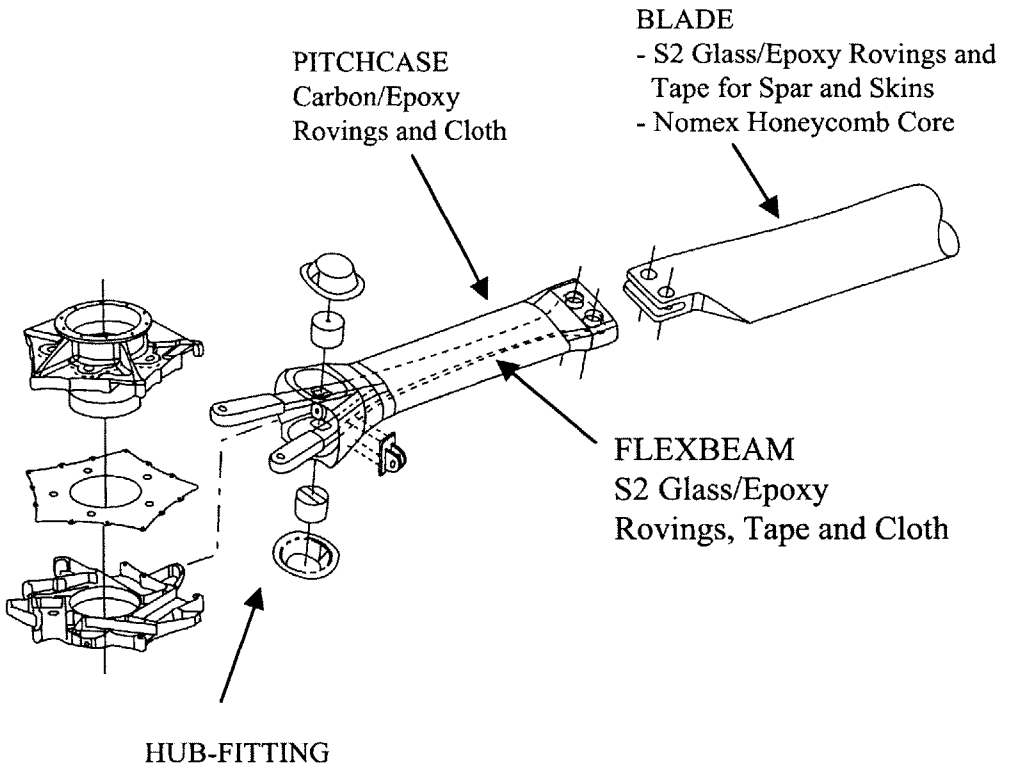

Figure 1.1 Diagram of bearingless and hingeless rotorhub assembly of MD900 Explorer [4].

composite flexbeams.

However, these advantages are not gained without cost. It is well known that ply dropoffs act as stress raisers in composite laminates. Ply dropoffs represent discontinuities in the load path that complicate the stress state under applied load, giving rise to high in-plane and interlaminar stresses in the vicinity of the ply dropoffs [5]. These interlaminar stresses are a key concern in composite flexbeams as well as other laminates with ply dropoffs since they can cause delaminations [6]. Such delaminations not only decrease the load-carrying capability of the structure, but can also lead to other types of damage to induce premature failure.

The problem is especially critical in the case of flexbeams because they are primary load-bearing structures undergoing coupled tensile, bending and twisting cyclic loads. As such, it is important to be able to assess the integrity of the flexbeams under circumstances where delaminations have originated. Therefore, the damage tolerance aspect of the structure under cyclic load needs to be known in order to use it with confidence. Due to the lack of understanding and reliable prediction methodologies, such structures continue to be assessed mainly using costly experiments. Such experimentally based assessment of flexbeams is not only undesirable due to the cost, but also of little use when there is a need to design new flexbeams with improved or different performance requirements. Thus, a fundamental understanding of the effects of ply dropoffs on the damage/failure of composite laminates would be very useful. This understanding is also crucial in developing reliable prediction methodologies that may help to reduce the number of experiments necessary to show damage tolerance.

Many researchers have therefore investigated laminates with ply dropoffs both experimentally and analytically. As expected, experiments have shown that, in most cases, delamination at the interfaces between the terminated and continuous plies is the initial type of damage, although other types of damages such as matrix cracking and fiber breakage have been observed, *e.g.*, [7,8]. The majority of the previous work on stress

analyses of laminates with ply dropoffs has been accomplished through the use of the finite element (FE) method, *e.g.*, [5,8]. These analyses have shown that stress concentrations occur in the region where the plies are dropped off. The interlaminar stresses in this region are very high, and possibly singular at certain points, and decay rapidly to zero away from this region, much like interlaminar stresses at straight free edges.

A review of previous work shows that although much information on the damage/failure and stress field characteristics has been gathered, a clear understanding of the mechanisms giving rise to interlaminar stresses and subsequent delaminations in laminates with ply dropoffs is inadequate. An understanding of such mechanisms and effects would be particularly important in the preliminary design stages when the overall laminate configuration needs to be chosen. One of the main reasons for the lack of general understanding is that many investigations have conducted case-specific studies. This not only limits the applicability of the results but can also cause some ambiguity. Specific configurations have been considered in most of the previous experimental work as well as in much of the previous analytical work. The results have shown that some experimental observations, such as the nature and location of damage initiation, do not seem to have any definitive trends and at times seem to contradict one another. In order to establish meaningful trends and to clarify these issues, the parameters that affect laminates with ply dropoffs need to be systematically investigated. Similarly, despite the number of investigations on stress analysis of laminates with ply dropoffs, there is yet no accepted baseline for the stress field characteristics. The specific laminate configurations considered in previous investigations generally preclude the comparison of stress fields obtained from different investigations using different stress analysis methods. Therefore, a need exists to establish the baseline stress field characteristics in laminates with ply dropoffs through reliable and accurate stress analysis.

The objective of this work is to obtain a *fundamental understanding* of the

mechanisms and related structural parameters that give rise to interlaminar stresses in laminates with ply dropoffs and how the interlaminar stress field characteristics are related to the damage characteristics, particularly delamination initiation characteristics, under static and fatigue loads. An understanding of the mechanisms and parameters that give rise to interlaminar stresses can be obtained through careful exploration of the nature of the stress field. This is particularly important in preliminary design. Therefore, a sub-objective is to develop accurate and reliable tools for stress analysis. Another sub-objective is to obtain general trends that show how different structural parameters affect laminates with ply dropoffs through a systematic experimental program. Such trends will be used to gain insights into the relationship between the interlaminar stress field characteristics and damage characteristics. The current work will focus on the overall effects of ply dropoffs on composite laminates. Ply dropoffs have implications to the laminate as a whole and affect the interlaminar stress field not only in the immediate vicinity of the dropoffs but also away from this region. The former issue has been the subject of most previous investigations and is better understood, and thus, the current work can build on this.

The work in this thesis is organized as follows. A brief summary of the previous work accomplished on this topic is presented in Chapter 2. In this chapter, the current status and understanding of laminates with ply dropoffs are assessed, and areas of research that require further investigation are identified. This is followed by an approach in Chapter 3 to accomplish the stated objectives where the problem definition and the analytical and experimental work performed as part of the research are described in detail. The formulation and solutions to the analytical models used to obtain interlaminar stresses are presented in Chapter 4. In Chapter 5, the manufacturing process and the testing procedures are described. The results from the analytical work are presented in Chapter 6. Here, the validity of the analytical models is shown by comparing results with those from previous investigations and additional FE analyses. Subsequently, a

parametric study is performed to explore the characteristics of the interlaminar stress field when structural parameters are varied, and the insights gained are discussed. In Chapter 7, the experimental results are presented and their implications and significance are discussed. The characteristics and trends of the analytical and experimental results are examined in Chapter 8 to correlate the two results both qualitatively and quantitatively based on the strength of materials approach. Finally, in Chapter 9, the conclusions and recommendations for future work based on the results of the current work are listed.

CHAPTER 2

PREVIOUS WORK

A review of the literature on laminates with ply dropoffs is presented in this chapter. Due to the complex configuration of laminates with ply dropoffs, it is important to establish first the terminology that will be used throughout the thesis. This is followed by a discussion of basic properties of laminates with ply dropoffs such as strength, damage/failure modes, and fatigue characteristics that have been observed through experiments. The next section deals with stress analysis, which is the first step toward the prediction of failure in these structures. In the final section, the methods that have been used to predict failure under static and cyclic loads are discussed. The bases of these methods are the strength of materials approach and the strain energy release rate approach.

2.1 Laminate Configuration and Terminology

A laminate that has one or more terminated plies, or ply dropoffs, is called a laminate with ply dropoffs. The dropoffs can occur either internally or externally, and they can be symmetric or unsymmetric about the mid-plane of the laminate. A diagram of a typical laminate with symmetric internal ply dropoffs is shown in Figure 2.1. The configuration is divided into three regions based on the thickness. The uniform thickness regions before and after the terminated plies are called the *undropped* region and the *dropped* region, respectively, and the region in which the plies are terminated is called the *dropoff* region. The matrix region at the tip of the terminated plies in laminates with internal ply dropoffs, which is usually triangular in shape when viewed from the edge, is called the *resin pocket.* Voids can form inside these resin pockets due to lack of resin

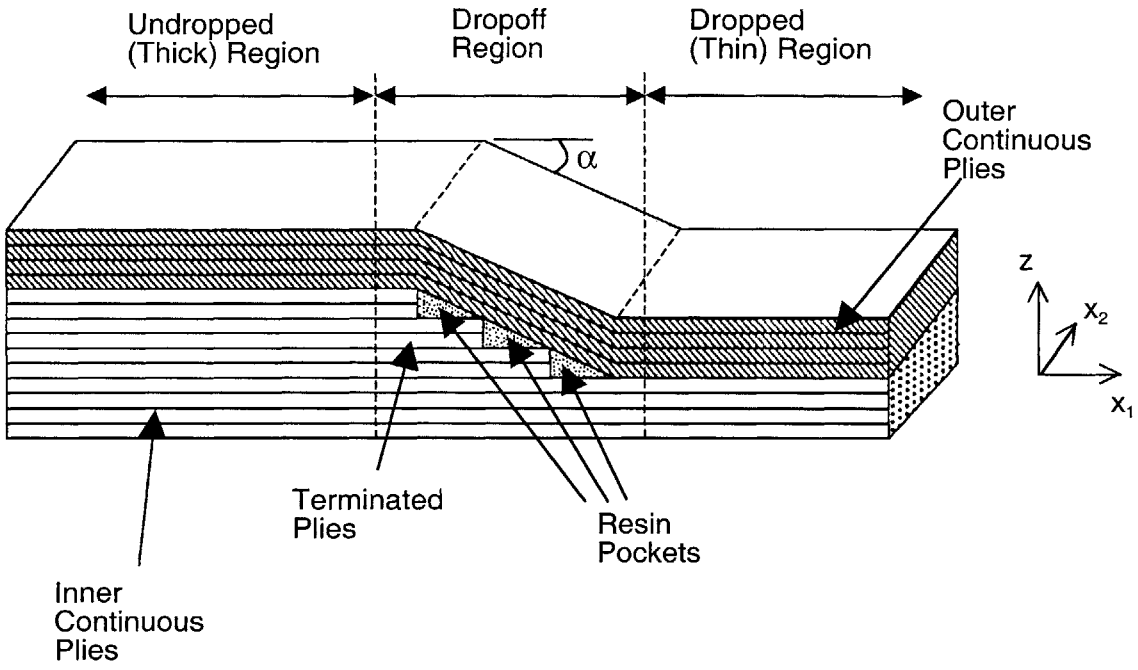

Figure 2.1 Diagram of a typical laminate with ply dropoffs.

flow during the manufacturing process. In order to reduce the volume of the resin pockets, and thus, reduce the probability of void formation, plies are sometimes terminated in several distinct steps. The laminate shown in Figure 2.1 has plies terminated in three distinct steps.

The coordinate system used to define the axes is also shown in Figure 2.1. Standard definitions for the ply orientation angle in the x_1-x_2 plane, θ, are used, *i.e.*, 0° coincides with the x_1-axis and θ is measured positive in the counterclockwise direction. The angle that the dropped region makes in the x_1-z plane with respect to the x_1-axis is defined as the taper angle, α. The layup of a laminate with ply dropoffs is denoted by the layup of the undropped region of the laminate with the terminated ply groups followed by a subscript 'D' (for dropped). For example, a laminate whose layup is $[0/90/\pm\theta]_s$ in the undropped region and $[0/90]_s$ in the dropped region with $[\pm\theta]_s$ as the terminated ply group is expressed as $[0/90/(\pm\theta)_D]_s$.

2.2 Experimental Characterization of Laminate Properties

One of the most important properties of structural components is the failure load. Several researchers have conducted extensive experimental programs in order to identify the factors that affect this property in laminates with ply dropoffs. The need to do so stems from the fact that ply dropoffs create a discontinuity in the load path. This may cause stress concentrations in the dropoff region such that the failure loads of laminates with ply dropoffs cannot be deduced simply from those of flat laminates whose layups are equivalent to either the undropped or dropped regions. Cannon [9] performed tensile tests on several different layups of graphite/epoxy laminates with ply dropoffs consisting of ±45° and 0° plies, and for each layup, two flat laminates whose layups were equivalent to the undropped and dropped regions of the laminate with ply dropoffs. The results showed that the failure loads were not bounded by those of the corresponding two flat laminates, but were higher than those of the corresponding flat laminate whose layup was

equivalent to the dropped region for some laminates and lower for other laminates, although the differences were within experimental scatter. Therefore, the failure load may depend on the layup of the laminate and/or the terminated ply group.

More specifically, experiments have shown that many factors may affect the failure load of a laminate with ply dropoffs under in-plane loads. These factors include the number of terminated plies, *e.g.*, [10], the layups of the terminated ply group (or groups), *e.g.*, [11] and the geometry of the dropoff region, *e.g.*, [12]. However, it is not clear how these factors each affect the failure load and this is complicated by interaction of these factors. For example, tests were performed on graphite/epoxy laminates with ply dropoffs using the number of terminated plies as one of the test variables [10]. The test matrix consisted of laminates whose layup in the undropped region varied with the number of terminated plies and remained constant in the dropped region. The results showed that the tensile and compressive strengths generally decrease as the number of terminated plies increases. It was also observed that the reduction in strength of the laminates with ply dropoffs tested when compared with the strength of the flat laminates with layups equivalent to the dropped regions is directly related to the increase in axial stiffness of the undropped region, implying a correlation between the stiffness and strength. However, in other types of laminates with ply dropoffs no such correlation between the two properties was observed. In other experiments [7], tests were conducted on two glass/epoxy laminates with ply dropoffs with different layups that both had the same axial stiffnesses in the undropped and dropped regions, and one of the laminates exhibited an increase in strength, while the other exhibited a decrease compared to the flat laminates with layups equivalent to the respective dropped regions.

Although the strength of laminates with ply dropoffs generally decreases with an increase in the number of terminated plies [13], this is not always the case, as shown in experiments by Grimes and Dusablon [11]. Static tension and compression tests were conducted on three types of laminates, a flat laminate that consisted of thirty plies with

0°, 90°, and ±45° orientations, and two laminates with ply dropoffs. The first laminate with ply dropoffs had two 0° plies terminated and the second laminate had two pairs of ±45° plies terminated from the layup of the flat laminate. The results showed that the mean tensile strength of the laminate with four ply dropoffs is 19% higher than the laminate with two ply dropoffs at dry conditions in room temperature, while the tensile strength of both laminates with ply dropoffs is slightly higher than that of the flat laminate. The results indicate that the layup of the terminated plies can have a greater effect on the strength of the laminate than the number of terminated plies.

Due to the catastrophic nature of static failure modes, documentation of such have not been very useful in clarifying the issue of the effects of ply dropoffs. According to the experimental results reported by Cannon [9], the static tensile failure modes of laminates with ply dropoffs generally resemble those of flat laminates whose layups are equivalent to the dropped region. The static compressive failure modes have been observed to be characterized by local crushing in the vicinity of the dropoff region in the absence of buckling [10]. Buckling and post-buckling behavior of laminates with ply dropoffs has also been investigated [14]. These investigations have shown that unlike flat laminates, laminates with ply dropoffs exhibit complex buckling modes and that the buckling load was bounded by the buckling loads of the flat laminates with layups equivalent to the undropped and dropped regions.

In order to obtain a better understanding of the effects of ply dropoffs on the static strength of composite laminates, it may be more important to characterize the initiation of damage. The reason is that although the initial damage may not cause final failure of the laminate, it can lead to other types of damage that will cause the laminate to fail [6]. Composite laminates often fail as a result of a combination of several local damage types occurring progressively [15], and thus, knowledge of the initial of damage is critical.

In general, the onset of damage in laminates with ply dropoffs under static in-plane loads is characterized by delaminations in the vicinity of the dropoff region,

although the exact nature and location of the damage may depend on several factors such as those affecting the failure load. According to some investigations, transverse matrix cracks in the resin pockets occur prior to the onset of delamination [13]. This implies that load transfer between the terminated plies and the resin pockets at the tip of the terminated ply groups does not occur, *i.e.*, the tip of the terminated plies is stress-free. Delamination onset in laminates with ply dropoffs in a single step has been observed to occur in the undropped region adjacent to the dropoff region between the terminated ply groups and the continuous plies for both laminates under tension [16] and compression [10]. For laminates with ply dropoffs in multiple steps, delamination onset has been observed to occur in the dropped and dropoff regions at the terminated ply group closest to the dropped region in some cases [7], as shown in Figure 2.2. In other cases, no delaminations were observed until catastrophic failure [17].

One set of experiments on laminates with symmetric external ply dropoffs in multiple steps under a bending load has shown that delamination is the main mode of damage [18]. In this case, delaminations occurred on both the tensile and compressive sides of the laminate. However, another set of experiments on laminates with external ply dropoffs under combined in-plane and bending loads has shown that the mode of damage initiation is dependent on the layups of the continuous and terminated plies [8]. It was observed that delamination would occur initially only in the case where the interface of the continuous and terminated plies was located between two 0° plies. In other cases, such as when the interface was located between two angle plies or an angle ply and a 0° ply, matrix cracking would occur initially. For laminates with internal dropoffs, experiments have shown that tensile fracture of the outer continuous plies can occur before delamination [19].

A factor that may further complicate delamination initiation in laminates with ply dropoffs is the presence of straight free edges. It is well known that laminates with straight free edges are prone to delamination [20] for certain layups and configurations.

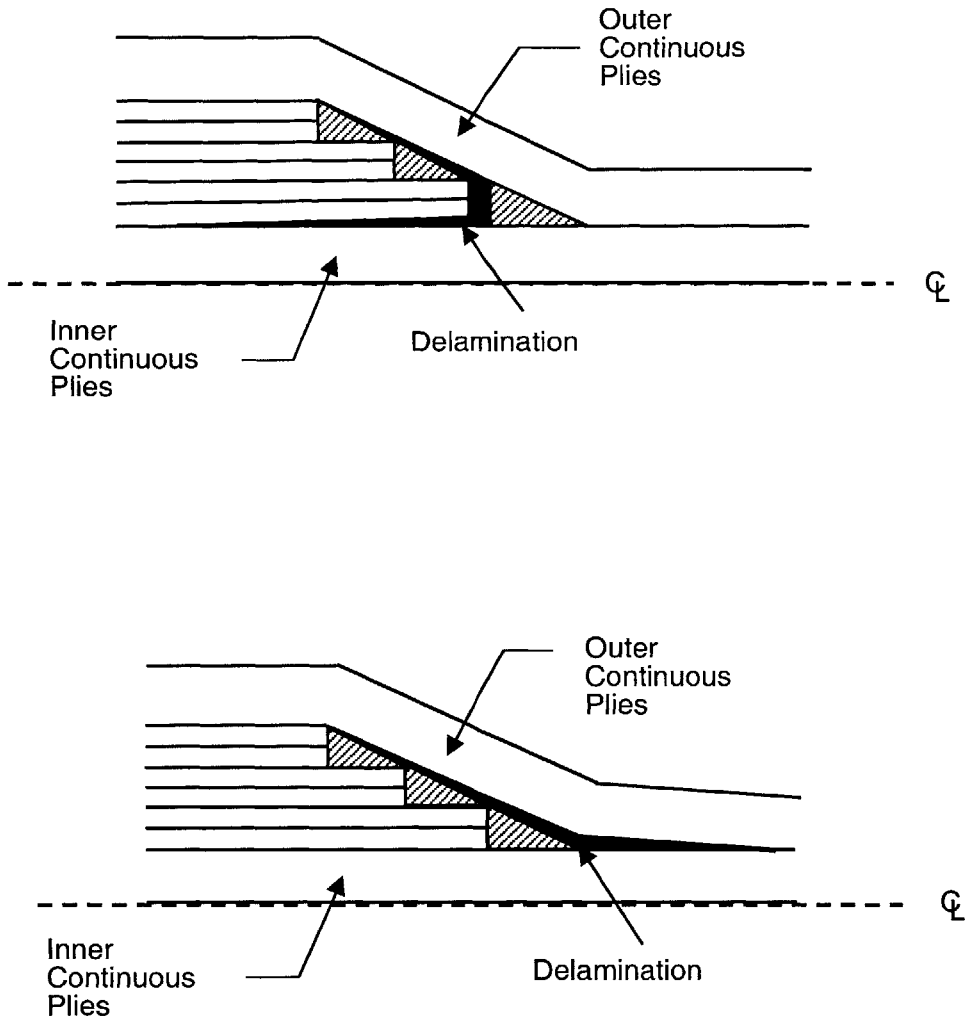

Figure 2.2 Schematics of delamination initiation and subsequent growth at two different locations in the dropoff region: *(upper)* delamination at last terminated ply group and *(lower)* delamination at tip of resin pocket.

In laminates with ply dropoffs, the situation is compounded because of the possibility of interaction between the free edge and the ply dropoffs. Therefore, it is necessary to isolate the effects of the ply dropoffs from the effects of the free edges by considering layups with little or no free edge effects. Many investigations of laminates with ply dropoffs under static tensile loads have therefore appropriately considered unidirectional laminates with ply dropoffs, *e.g.*, [21], or layups known to have small free edge effects, *e.g.*, [7].

The effects of ply dropoffs in composite laminates may be better understood if the factors that affect delamination can be isolated and characterized separately. It has been suggested that one of these factors may be the effect of the discontinuous plies [21,22], and experiments have been performed in order to show that flat laminates with cut internal plies could be used to simulate delamination behavior of laminates with ply dropoffs. However, flat laminates with cut internal plies can be used to characterize delamination only if such delaminations occur in the undropped region of the laminate. As mentioned previously, delaminations have been observed to occur in the dropoff and dropped regions in some laminates with ply dropoffs [7]. Therefore, a better method to isolate and characterize the factors that affect delamination needs to be devised.

The occurrence of delaminations causes a change in the load-carrying path of the laminate and this is accompanied by an instantaneous drop in load carried by the laminate. Such load drops may be observed when testing under displacement control in a hydraulic testing machine and, in some cases, audible cracking noises can be heard [7]. However, in general, it is difficult to observe precisely when and where the damage initiation events occur because they may not be manifested clearly. Furthermore, in certain laminates where internal flaws exist, initiation may occur in the interior regions of the laminate, making it extremely difficult to observe such. Thus, it is important to design experimental procedures such that initiation events may be observed.

Since the initiation of delamination does not necessarily mean failure, it may also

be important to characterize the growth of delamination subsequent to initiation. In some experiments, the occurrence of the initial delaminations was seen to be sudden and unstable, which implies that a growth stage cannot be separated from an initiation stage [16]. In cases where the initial delaminations were stable, delaminations were observed to grow in a stable manner into the dropped region for some laminate configurations [7], and into the undropped region for other laminate configurations [17].

Significantly less work on laminates with ply dropoffs under cyclic loads exists in the literature. Subsequently, much less is understood on the fatigue behavior of these types of laminates such as their initiation and growth characteristics. Based on the limited number of experimental results, the fatigue characteristics are also highly dependent on many factors such as the material properties and layup of the laminate.

In glass/epoxy laminates with ply dropoffs under tension-tension loading, delaminations have been observed to be the main cause of failure in some investigations, *e.g.*, [23,24], while fiber breakage was the cause of failure with no delaminations in the dropped region near the dropoffs in another investigation [17]. The main difference in the two investigations was the number of continuous plies in the layups of the laminates with ply dropoffs. In the former investigation, laminates with 26 continuous and 12 terminated plies were considered, whereas in the latter investigation, laminates with 8 continuous and 12 terminated plies were considered. This indicates that the ratio of continuous plies to terminated plies may affect the type of failure mode in laminates with ply dropoffs.

In graphite/epoxy laminates under tension-tension loading, delaminations were initially seen in the dropped region growing in a stable manner into the undropped region before other delaminations initiated at the tip of the resin pocket and grew unstably along the entire length of the laminate (see Figure 2.2) [23]. In another investigation [17], delaminations were observed to initiate in the terminated plies closest to the top and bottom surfaces of the laminates near the undropped region and grow into the undropped

region with no delaminations in the dropped region. Again, one of the main differences in the two experiments was in the layup of the laminates with ply dropoffs. In the former investigation, 0° laminates with plies terminated in groups of two in three distinct steps were considered, whereas in the latter investigation, more complex laminates with 0° and ±45° plies with the terminated ply groups separated intermittently by continuous plies in several steps were considered. Another difference was the existence of an interleaf (toughened thermoset adhesive layer) on one side of the plies in the composite material used in the former investigation.

Based on experiments with 0° laminates with ply dropoffs and flat laminates with cut internal plies, delamination growth rates for different specimen configurations exhibit different growth rates [13]. Delamination growth rate may be influenced by several factors, such as material properties, ratio of continuous and discontinuous plies and the layup of the terminated ply group. Flat laminates with cut internal plies were observed to delaminate faster than the laminates with ply dropoffs.

As in the case of other types of composite laminates, matrix cracks tend to occur along with delaminations in adjacent plies for laminates with angle plies [24]. This further complicates the damage modes and makes it more difficult to identify the role of delamination in laminates with ply dropoffs. In addition, the existence of straight free edges in such laminates would be another source of concern. Subsequently, it would not be appropriate to attribute all of the experimental fatigue characterizations of laminates with ply dropoffs as the effect of the terminated plies. The effects of the interaction between free edges and ply dropoffs is discussed further in the next section.

As discussed in this section, some of the experimental observations show definitive trends with respect to a certain characteristic of the laminate. For example, most experimental results indicate that the larger the ratio of the number of terminated plies to continuous plies, the lower the failure load. However, other experimental observations, such as the nature and location of ply dropoffs, do not seem to have any

trends and at times seem to contradict one another. Thus, although many experimental investigations have been performed on laminates with ply dropoffs, there is no general understanding as to what the overall effects of ply dropoffs are on the damage and failure of these laminates. The main reason for the lack of general understanding lies in the fact that specific laminate configurations have been considered in previous experiments. Such experiments, as described in this section, yield results that are only relevant to the characteristics of the particular laminates considered and cannot be generalized to apply for other laminate configurations. Thus, in order to obtain a more general understanding of the effects of ply dropoffs on the damage and failure of laminates with ply dropoffs, systematic experimental programs are needed.

2.3 Stress Analysis

The experimental investigations presented in the previous section show that the main mode of damage in laminates with ply dropoffs under both static and cyclic loads is delamination. From investigation of other types of laminates prone to delamination, such as laminates with straight free edges and cutouts, it is well known that high interlaminar stresses are the main cause of delamination [6]. In laminates with ply dropoffs, regions of high interlaminar stresses are caused by a change in the load path due to the terminated plies. Thus, a careful analysis of the stress field in these laminates is the first step toward a methodology to predict when and where delaminations will occur.

The majority of the stress analyses of laminates with ply dropoffs in the literature has been accomplished through the use of finite element (FE) methods. Many different types of FE methods have been developed and/or employed such as two-dimensional (2D) displacement-based formulations, *e.g.*, [16,23,25], quasi-three-dimensional (3D) displacement-based formulations, *e.g.*, [26,27], 3D displacement-based formulations, *e.g.*, [28,29], hybrid formulations, *e.g.*, [5,7], and nonlinear formulations, *e.g.*, [30]. In general, these analyses have shown that concentrations of in-plane stress components

occur and interlaminar stresses arise in the dropoff region where the plies are terminated. The interlaminar stresses in this region are very high, and possibly singular at certain points, and decay rapidly to zero away from this region, much like interlaminar stresses at straight free edges.

These FE analyses have considered different types of laminates with ply dropoffs that show different stress field characteristics. Therefore, it is difficult to establish the validity and compare the accuracy of each method to choose the simplest method that can be used with confidence. However, as is the case with any FE analysis, it is important to understand the scope and limitations of the method before applying it. For example, the stress field in unidirectional laminates with ply dropoffs loaded along the fiber direction can be expected to be well-predicted by a 2D FE model because the stress components in the width-wise direction (y-direction) is zero. For laminates with angle plies, a quasi-3D or 3D model would be required in order to predict the non-zero y-direction stress components. Likewise, in order to account for interaction between the effects of free edges and ply dropoffs in laminates with angle plies, a 3D model would be required. Such FE analyses have shown that the stress field characteristics in the vicinity of the ply dropoffs near the free edges may be very different compared to the interior part of the laminate [5].

Since delamination is the failure of the interface between two plies, some investigators have focused on calculating stress concentrations in this region. Previous work on composite laminates has shown that a very thin layer of matrix forms at the interface between plies [6]. This matrix (resin) layer, which is approximately on the order of one fiber diameter in size in graphite/epoxy laminates [31], has been modeled with the appropriate matrix material properties separate from the plies, which are modeled with the ply material properties, *e.g.*, [32,33]. Such analyses have shown that there could be significant differences in the stress state obtained by modeling the matrix layer compared to analyses without the matrix layer, and that the stress field also depends

on the thickness of the matrix layer. However, from a practical point of view, such a precise analysis may not be very useful because realistic laminates with ply dropoffs would contain other irregularities of similar length-scales, such as variable matrix layer thickness and misaligned ply dropoffs [34].

Although the FE method can be a very accurate and powerful tool for stress analysis, it does not provide a clear picture of how stresses are transferred across the dropoff region. This insight can lead to a better understanding of the basic mechanisms that give rise to interlaminar stresses. Another drawback of the FE analysis is the large amount of time (and resources) required in performing the analysis. This is particularly true in preliminary design phases where a number of configurations and variations in parameters need to be considered. In the case of laminates with ply dropoffs, very fine elements are required to obtain converged values of interlaminar stresses in the vicinity of the dropoffs. This can lead to FE models with a very large number of degrees-of-freedom. Reducing the number of elements through the use of ply dropoff elements has been proposed [35], but the formulation only provides for accurate displacements and requires an additional local FE analysis in order to obtain stress distributions. Another problem with very fine elements is the danger of using elements whose size are on the order of or smaller than the characteristic dimensions of the fiber/matrix structure. In such cases, it would be inappropriate to use the macroscopic ply properties since the assumptions of material homogeneity would no longer be valid.

Some analytical methods that have focused on the local interlaminar stresses in the region where the plies are dropped off have been proposed, *e.g.*, [36-40]. These methods have provided more insight into the nature of interlaminar stresses for specific laminates with ply dropoffs compared to numerical methods. For example, it has been shown that interlaminar shear stresses in the region where plies are dropped off can be approximated by using a shear-lag analysis [37]. This suggests that the load transfer between terminated plies and neighboring continuous plies occurs mainly through shear

stresses in the resin layers. It has also been shown that in addition to the distributed shear stresses in the resin layers, load transfer can occur through concentrated forces at the tip of the terminated plies in certain dropoff configurations [36]. However, in general, analytical methods are limited in utility because they are either applicable only to certain types of problems or are difficult to implement. Some efficient analytical methods that are relatively easy to implement have been proposed for laminates with external ply dropoffs [38,41]. These can be used to obtain stress fields at the skin-stiffener interfaces of stiffened panels.

Despite the number of investigations on stress analysis of laminates with ply dropoffs, there is yet no accepted baseline for the stress field characteristics. This is due to the fact that there can be an unlimited number of possible configurations in the dropoff region, and as such, specific laminate configurations have been considered in previous investigations. This generally precludes the comparison of stress fields obtained from different investigations using different stress analysis methods. Based on the results for specific laminate configurations, very high interlaminar shear and normal stresses exist in the immediate vicinity of local discontinuities in the dropoff region, such as at the ply termination sites or the tip of the resin pocket. Away from the immediate vicinity of local discontinuities, the interlaminar stresses decay rapidly toward zero. Thus, plots of the interlaminar stresses evaluated along the length of the laminate at a particular interface of the terminated and continuous ply groups appear to be a series of "spikes" located at the local discontinuities in the dropoff region. However, it is not clear whether the interlaminar stresses are tensile or compressive in nature at these locations and this is very important in the prediction of delamination onset. For example, in one investigation, the stress analysis of a unidirectional laminate with ply dropoffs showed that the interlaminar normal stress at the tip of the resin pocket is tensile [23]; whereas in another investigation of a laminate with similar layup and geometry the interlaminar normal stress was found to be compressive [5].

Although the highest stress concentration in laminates with ply dropoffs occurs in the region where plies are dropped off and, as such, many previous investigations have focused on the determination of interlaminar stresses in this region, it is also important to have a good understanding of the effects of ply dropoffs on the interlaminar stresses from an overall viewpoint. Such an understanding would be extremely useful in preliminary design phases where the laminate layup and dropoff sequence need to be decided. Moreover, one of the difficulties in modeling and analysis of laminates with ply dropoffs lies in the fact that there can be substantial differences between the idealized structure and the real structure. It has been shown the interlaminar stresses calculated using realistic ply dropoffs differ significantly from those calculated using idealized ply dropoffs [34]. Actual laminates with ply dropoffs may contain defects such as voids, sloped plies, and misaligned terminations of plies due to manufacturing irregularities. Such defects are not homogeneous and may differ from laminate to laminate. Although laminates with specific defects can be modeled and analyzed, the results from such, for the most part, cannot be generalized. Therefore a global analysis that allows one to obtain an overall view of the stress field is not only useful, but in certain cases, may be sufficient.

2.4 Prediction of Damage and Failure

The ultimate goal of much research in laminates with ply dropoffs, as in other composite structures, is to predict accurately when and where damage will occur and how it will progress until failure under a certain type of loading. There are two approaches to predict damage and failure in laminates with ply dropoffs: that based on strength of materials and that based on fracture mechanics. The former approach has been used to predict delamination initiation loads in laminates with ply dropoffs. The latter approach has been used to predict loads at which delamination will start to grow, and the rate of growth. Previous work using the two approaches are summarized and discussed in the

following sub-sections.

2.4.1 Strength of Materials Based Approach

The strength of materials approach is based on the assumption that damage will occur in the composite laminate when the magnitude of the stress field at a particular point or region is equal to or larger than its strength. Therefore, in order to predict the damage loads in laminates with ply dropoffs, a reliable criterion is needed along with an accurate method of obtaining the stress field.

Since many different types of failure (damage) criteria exist in the literature [1], it is necessary to use the appropriate criterion(a) that corresponds to the type of damage observed through experimental studies. As presented previously, the main mode of damage initiation in laminates with ply dropoffs is delamination. Thus, it would be most appropriate to use a damage criterion that predicts delamination such as the Quadratic Delamination Criterion (QDC) [42]. Some of the criteria that have been used are the maximum stress criterion for matrix cracking in the matrix layer between plies, *e.g.*, [7,26], the von Mises criterion for the matrix layer between plies, *e.g.*, [12], a modified version of the Tsai-Wu criterion to account for delamination, *e.g.*, [7], and a modified version of the Hashin criterion to account for delamination, *e.g.*, [10].

The results for the predicted delamination loads have been mixed compared to the observed experimental results. In all cases, delaminations were predicted to initiate at the tip of the terminated ply group, *i.e.*, at the interface of the resin pocket and terminated ply group, between the ply either above or below it [7,10,12,26]. These predictions generally agree well with the observed results, although, as previously mentioned, the exact location of delamination is uncertain. However, the predicted initiation loads did not match well with the experimental results. In some cases, the delamination loads were predicted to be overly conservative [10], while in other cases, they were predicted to be greater than those obtained experimentally [7]. It is noted, however, that the exact load at which delamination occurs is difficult to obtain experimentally, as mentioned in the

Section 2.2.

Previous work on delaminations have shown that when applying a delamination criterion, it may be more appropriate to use average stress values rather than point-wise values [42]. The concept of average stress stems from the fact that the possibility of failure of a larger volume of material subjected to some stress state is greater than that of a smaller volume of material because the probability of the existence of a critical flaw in the larger material is greater [43]. Therefore, the average stress values should be more meaningful than point-wise values. In the case of laminates with ply dropoffs where singularities in the stress field may exist, the use of the average stress concept is even more attractive since these singularities may be weak and integrable as in the case of interlaminar stresses at free edges [31].

An important parameter in using the average stress concept is the characteristic distance over which the stresses are averaged. This value can be determined through correlations with experimental results and should be a material system constant [42]. The average stress values along with damage criteria have been used to predict delamination initiation loads in glass/epoxy laminates with ply dropoffs, *e.g.*, [7,12]. These studies have shown that an averaging distance of one ply thickness gives the best fit to experimental results when maximum shear stress failure criterion is used for the matrix layer [7]. This averaging distance is on the same order of magnitude as those suggested by others for laminates with straight free edges [42,44].

2.4.2 Strain Energy Release Rate Based Approach

According to linear elastic fracture mechanics, a crack will start to advance under static, monotonic loading when the strain energy release rate or the stress intensity factor becomes greater than its critical value. There are three components of the strain energy release rate (or stress intensity factor), modes I, II and III, depending on the loading condition and/or the local stress distribution near the crack-tip. These components correspond to different modes of crack propagation, and each component has a different

critical value. The total strain energy release rate is the sum of the strain energy release rates for each mode and represents the overall change in the strain energy of a structure with respect to crack advance. The strain energy release rate is generally easier to obtain than the stress intensity factor because it only requires calculation of the change in strain energy of the structure with respect to crack growth. In contrast, accurate crack tip stress fields are required to obtain accurate stress intensity factors.

Fracture mechanics can be useful in the analysis of delaminations in composite structures because delaminations can be modeled as cracks between two plies. Unlike other types of damage modes in composites such as fiber breakage, delamination can grow in a self-similar manner, which makes it possible to use fracture mechanics [1]. In order to use fracture mechanics concepts, either the strain energy release rate or the stress intensity factor needs to be calculated for a given delamination. Due to the complexities involved in problems with composite materials such as anisotropy and the length-scales associated with the crack tip where the homogenized properties of the fiber/matrix material may no longer be valid, an accurate stress field at the crack tip is difficult to obtain. The stress field at the crack tip is generally singular and oscillatory in nature, which adds to the complexity [45]. On the other hand, the total strain energy release rate is easier to obtain as was described for the isotropic case. In general, simple two-dimensional FE models can be used to obtain the change in strain energy due to crack growth via the virtual crack closure (or extension) technique [46]. This being the case, the strain energy release rate is often used in delamination problems involving composite laminates. In some special cases, simple analytical expressions may exist for the total strain energy release rate. However, the fact that the critical strain energy release rate is often used does not necessarily mean that it is a valid criterion to predict delamination growth. It has been shown that the total critical strain energy release rate is laminate dependent [42,47], and, it is still unclear how much each of the individual components of the strain energy release rate affect delamination [48].

The critical strain energy release rate is generally obtained via experiments on test specimens with intentional pre-cracks. This allows one to observe the advance of such cracks relatively easily. For isotropic materials, pre-cracks are commonly used in standardized tests, *e.g.*, [49]. The expression for the strain energy release rate (or the stress intensity factor) can generally be obtained as a function of the test specimen geometry and load applied [50]. The critical strain energy release rate (or the stress intensity factor) can then be obtained using this equation and the applied load at which crack advance is observed from experiments.

For composite materials, pre-cracks are used in some cases such as the double cantilever beam (DCB) test [51], while in other cases they are not, *e.g.*, free edge delamination test [52]. For the latter type of tests, delamination "onset" load (or strain) at which delamination is first detected through the inspection method used is obtained from the tests. However, the concept of the strain energy release rate is generally related to the *growth* of a pre-existing delamination, not its onset. Delamination onset cannot be determined using the critical strain energy release rate. Thus, in such tests, the term delamination onset is used to circumvent the problem of having to detect the growth of microscopic flaws in the material (in the absence of a pre-crack), which is impractical. The critical strain energy release rate is obtained using a similar procedure outlined for isotropic materials.

For delaminations growing symmetrically into the undropped region in laminates with symmetric ply dropoffs, approximate analytical expressions for the total strain energy release rate as a function of the delamination length, applied load and material properties have been derived [53]. In the special case where the ply dropoffs are located at the mid-plane of the laminate with a delamination growing symmetrically into the undropped region under in-plane load, as shown in Figure 2.3, the total strain energy release rate can be expressed as;

$$G = \frac{P^2(E_0 - E^*)}{4E_0E^*} \tag{2.2}$$

where P is the applied load per unit width, E_0 is the in-plane stiffness of the undelaminated laminate in the undroppped region, and E^* is the in-plane stiffness of the delaminated laminate in the undropped region [17]. Equation (2.2) implies that the total strain energy release rate is independent of the delamination length, *a*, shown in Figure 2.3. This expression is similar to the total strain energy release rate for delamination at straight free edges. This can be expressed as;

$$G = \frac{h\varepsilon^2}{2}(E_{lam} - E^*) \tag{2.3}$$

where h is the laminate thickness, ε is the strain, E_{lam} is the longitudinal modulus of the undelaminated laminate, and E^* is the weighted average longitudinal modulus of the sublaminates after delamination [52]. In both cases, FE calculations using virtual crack extension (or closure) techniques can be performed to show that the total strain energy release rate is independent of the delamination length, once the delamination has initially grown a short length [16,52].

For the case of delamination at the free edges, there has been some success in predicting static delamination onset through equation (2.3) and the critical strain energy release rate, *e.g.*, [42,52]. However, the critical value of the total strain energy release rate does not seem to be a material system parameter, since different values are obtained even for laminates with the same layup, but different thickness plies [42]. It has been suggested that instead of the critical value of the total strain energy release rate, only the mode I contribution, *i.e.*, G_{Ic}, may govern delamination onset [47].

For laminates with ply dropoffs, similar observations have been made. There has been some success in predicting when delamination will occur by using equation (2.2) and comparing such with the critical total strain energy release rate obtained via experiments of other laminates with ply dropoffs [21]. However, the critical total strain

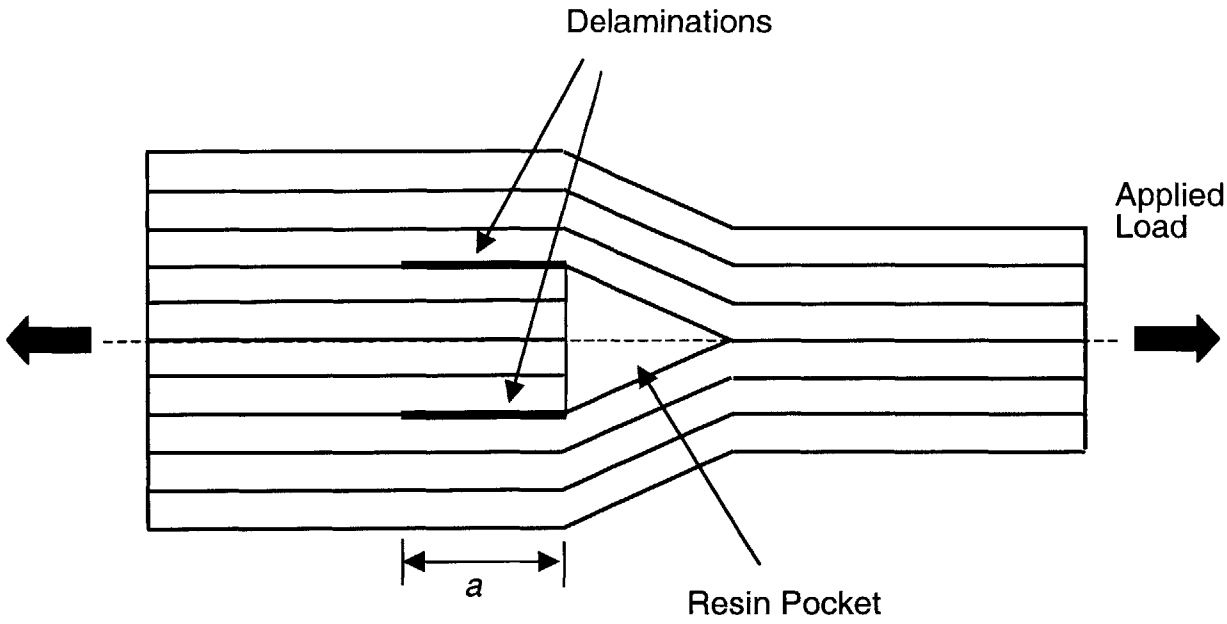

Figure 2.3 Edge view of a laminate with ply dropoffs located at the mid-plane of the laminate under in-plane load with delaminations of length *a* growing into the undropped region.

energy release rates for various ply dropoff configurations with the same material system obtained through numerous experiments were shown to be very different even for unidirectional laminates [16]. Subsequently, a method to calculate or, more appropriately, "curve-fit" the critical total strain energy release rate has been proposed [16,54]. The critical total strain energy release rate is assumed to be a linear function of the average interlaminar normal stress ahead of the delamination and an exponential function of the specimen thickness. The expression for the critical total strain energy release rate is then obtained through a least squares method to fit the experimental data from previous investigations, *e.g.*, [17,22]. However, there are at least two issues that need to be addressed before such a method can be used with confidence. One, no theoretical basis for the particular assumed functional dependence of critical total strain energy release rate on the average interlaminar normal stress and the specimen thickness is given. Two, numerous experiments need to be performed on many different types of laminate configurations to generate the experimental data required to curve fit for the critical total strain energy release rate.

Under cyclic loads, the growth of inherent microscopic flaws can occur even before the critical value of the strain energy release rate is reached. The relationship between the cyclic stress intensity factor, ΔK, and the rate of crack growth, da/dN, can be generally characterized by an empirical power law suggested by Paris and Erdogan [55],

$$\frac{da}{dN} \propto (\Delta K)^m \tag{2.4}$$

where m is a constant that depends on factors such as the material properties, frequency, load ratio and loading mode [56]. For composite materials, a similar relationship has been used with the cyclic or maximum strain energy release rate in place of the cyclic stress intensity factor, *e.g.*, [52].

As with other composite laminates under cyclic load, the power law has been used to characterize the delamination growth behavior due to ply dropoffs, *e.g.*, [13,17].

Specifically, delamination growth rates have been characterized for laminates with simple ply dropoffs [13], and used to predict growth in laminates with more complex dropoff configurations based on empirical power laws [17]. Although the correlation between the predicted and observed delamination lengths was not very good, this methodology is widely used for other types of materials and configurations, and seems to be promising. However, since delaminations in different laminate configurations may exhibit different growth characteristics, and thus may require different power laws, it is important to establish the configuration of laminates with ply dropoffs to which empirical laws obtained from a specific laminate can be applied.

Some investigators have suggested that since the crack grows much faster in composite materials over a small range of loads as compared to metallic structures, the power law may not be as useful in characterizing such materials [57]. The reason is that small uncertainties in applied load may large cause uncertainties in delamination growth. They therefore proposed an empirical technique that uses the concept of a strain energy release rate threshold for no delamination growth [57] and applied this to laminates with ply dropoffs [23,24,58]. In this methodology, the fatigue life of a laminate with ply dropoffs is defined as the number of cycles to unstable delamination onset, and is predicted using the empirical number of cycles to delamination initiation obtained in double cantilevered beam (DCB) tests of the same composite material. It is postulated that the number of cycles to delamination onset in laminates with ply dropoffs is equal to that of DCB specimens if the total strain energy release rate in laminates with ply dropoffs equals the total cyclic strain energy release rate at which delamination initiated in DCB specimens. The total strain energy release rates were normalized by the square of the applied loads and the laminate thickness. Although the predicted and observed numbers of cycles to delamination for the laminates with ply dropoffs considered showed good correlation, *e.g.*, [24], the methodology lacks a theoretical basis for a correlation in the strain energy release rate from the DCB tests, which is for a mode I crack, and the

laminate with ply dropoffs, which is for a mixed-mode crack.

In addition, a major obstacle to applying this technique to laminates with ply dropoffs is that the location of the critical delamination onset is unknown. To use this technique, the location of the critical delamination onset must be known in order to calculate the strain energy release rate and correlated with data from the DCB tests. However, the location of delamination initiation and subsequent growth in laminates with ply dropoffs is still unclear. Some, *e.g.*, [23], believe that the delamination originates at the sharp tip of the resin pocket based on the fact that interlaminar shear stresses are highest at this location (see Figure 2.2). Others, *e.g.*, [5], have maintained that both interlaminar shear and normal stresses are higher at the ply drop-off location compared to the sharp tip of the resin pocket, and thus, this should be the critical location (see Figure 2.2). Experimental observations, as previously mentioned, indicate dependence of the initiation location on the configuration of the laminate.

In summary, the predictive capabilities for laminates with ply dropoffs have been investigated through the use of both the strength of materials based approach and the strain energy release rate based approach. Although the results of these investigations show that the two methods may be used to predict loads at which delamination initiates and grows unstably until failure with reasonable accuracy, the procedures for prediction of damage and failure for laminates with ply dropoffs have not yet matured, and thus need further investigation.

CHAPTER 3

APPROACH

The objective of this work is to provide an overall understanding of the mechanisms that cause interlaminar stresses in laminates with ply dropoffs and how such stresses can be related to the delamination characteristics under static and cyclic loads. To accomplish this objective, both analytical and experimental work was performed. As discussed in Chapter 2, most of the previous work on stress analysis of laminates with ply dropoffs has focused on the local interlaminar stresses of specific laminate configurations. This limits the general applicability of the results. The current analytical work focuses on capturing the overall effects of the ply dropoffs on the interlaminar stress field to establish baseline stress field characteristics in such laminates. The experiments were designed to establish definitive trends that help to supplement and extend the understanding obtained from the analytical work.

In this chapter, the overall approach to accomplish the objective is discussed in detail. An overview of the approach is given in the first section, followed by a discussion of the analytical models that are developed to help identify the mechanisms causing interlaminar stresses in the second section. In the final section, the experimental work used to characterize delamination initiation and growth is described.

3.1 General Overview

Laminates with ply dropoffs may contain many material and geometric details that make it difficult to model and analyze in a general manner. A diagram of a generic laminate with ply dropoffs was shown in Figure 2.1. Depending on the particular application of interest, the laminate may contain terminated plies in several distinct steps

with many different possibilities for the sequence of the steps. The laminate may also consist of several different composite materials or may be unsymmetric, and the taper in the dropoff region may be non-linear. Therefore, in order to investigate the overall effects of ply dropoffs on composite laminates, there is a need to define a simplified structure that includes the key features of laminates with ply dropoffs while excluding the material and geometric specifics. For this purpose, the framework of the building block approach (BBA) philosophy [59], which provides a systematic method to reduce complex problems into less complex sub-components, was used. A diagram of the BBA applied to design and analysis of general structures is shown in Figure 3.1.

The BBA requires one to identify and isolate the key features and components that comprise the problem and consider the structure with the lowest level of structural complexity as the baseline. As shown in Figure 3.1, in the design and analysis of generic structures, this lowest level component is the coupon test specimen. Subsequently, more levels of complexity are added to the baseline component as a better understanding is acquired.

A simplified configuration of laminates with ply dropoffs can be defined in a similar manner. Although many factors may affect the interlaminar stress field in generic laminates with ply dropoffs, the key factors are the presence of the terminated plies and the resulting taper in the dropoff region. The specifics such as the termination sequence and taper geometry are of secondary importance in the overall laminate configuration.

Thus, in the analytical and experimental work, the following configuration of laminates with ply dropoffs is considered. In the dropoff region, all ply dropoffs are considered to occur in a single step. This configuration greatly simplifies the geometry of the dropoff region while allowing the effects of the ply dropoffs to be present. The configuration may also be thought of as representing a more detrimental ply dropoff case since several steps would generally be used in the case where many plies are terminated as a group to "mitigate" the dropoff effect, *e.g.*, [35]. The taper angle in the dropoff

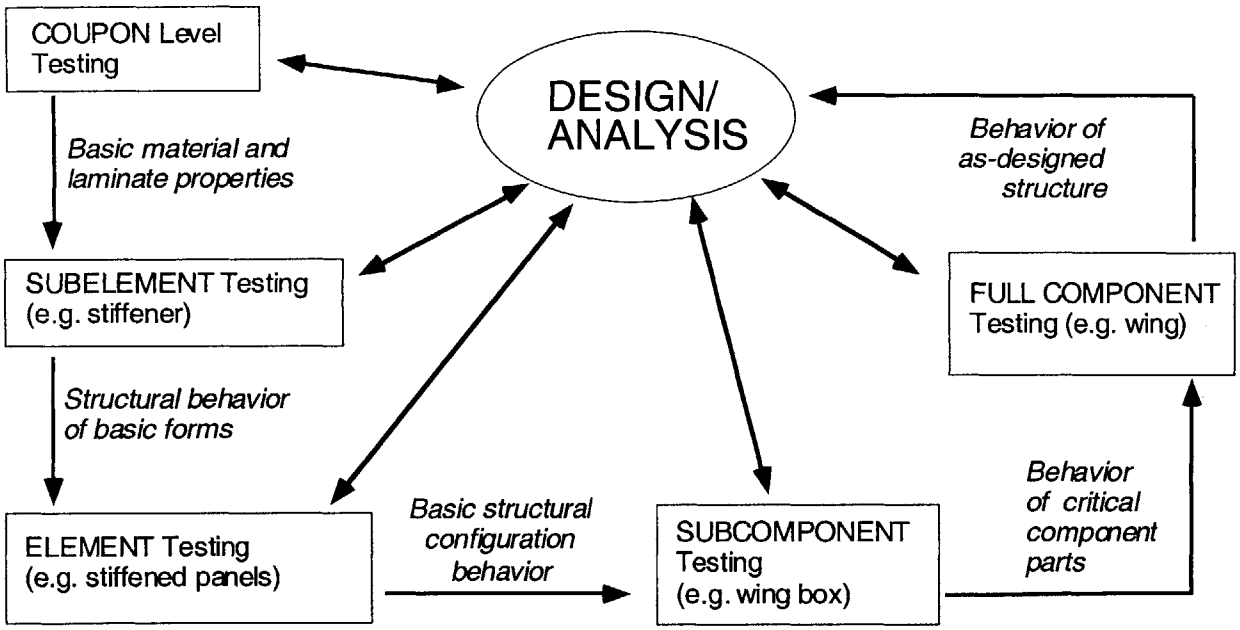

Figure 3.1 Flowchart of the building-block approach for the design and analysis of generic structures [59].

region is assumed to be constant over the region. In addition, laminates with symmetric layups and ply dropoffs that occur symmetrically with respect to the mid-plane of the laminate are considered. This geometrical symmetry allows the in-plane and bending responses to be de-coupled and considered separately. The in-plane and bending responses can later be combined to consider general cases. A diagram of the baseline laminate configuration is shown in Figure 3.2 along with the terminology used in the current work. The direction of the in-plane load is perpendicular to the terminated plies such that there is a difference of in-plane stresses in the undropped and dropped regions. The bending load generates a moment about the y-direction (or width-direction).

In the current work, models to determine the stress field through analytical means are developed. Analytical methods can provide better insights into the physical nature of the stress field in laminates with ply dropoffs through appropriate conceptual models, as compared to numerical methods, in addition to providing accurate and reliable stress fields. Such insights are needed to better understand the mechanisms and structural parameters that give rise to interlaminar stresses. To acquire such understanding, the analytical models are used to investigate the effects of various structural parameters on the interlaminar stress field. Most previous work has focused on the local effects of ply dropoffs such as the effects of different termination sequences [12] and the shape of the dropoff region and resin pocket [28]. However, the overall effects of ply dropoffs in composite laminates have not been investigated and thus are not clearly understood. The parameters to be considered are the layups in the undropped and dropped regions, the number and location of the terminated plies along the thickness of the laminate, and the taper angle in the dropoff region. General trends obtained from this investigation, along with the importance of these parameters on different laminate configurations and load types are presented in this work.

The experimental work is performed in order to observe and characterize delamination initiation and growth under static and cyclic loads in laminates with simple

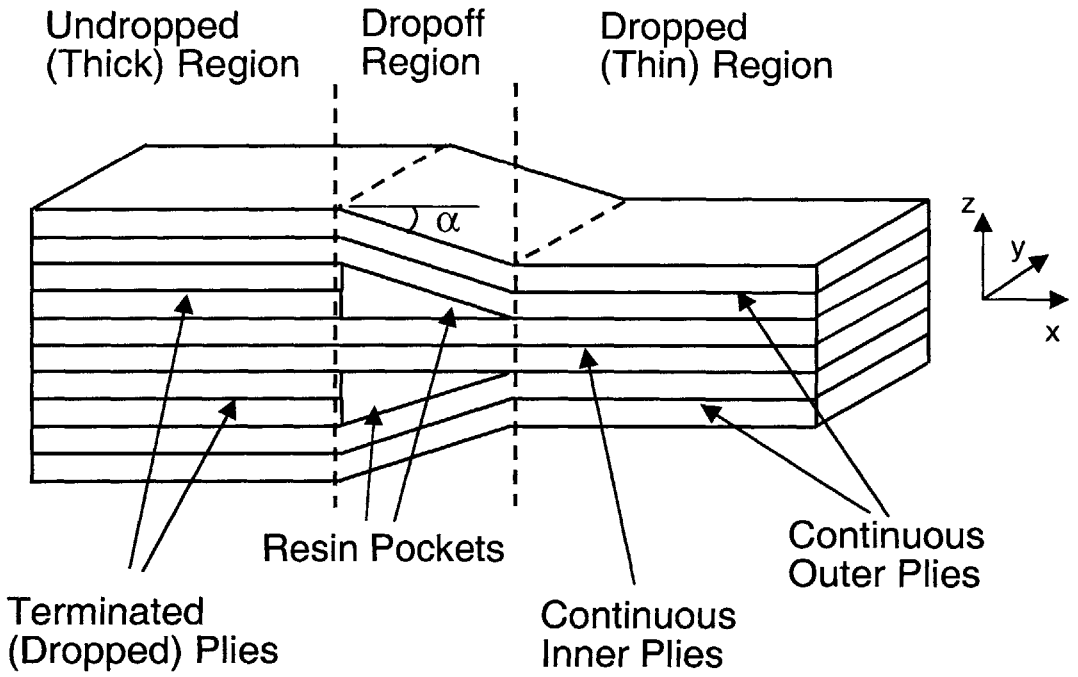

Figure 3.2 Configuration of the baseline laminate with ply dropoffs showing terminology.

ply dropoff configurations consistent with those that are modeled analytically. The similarities and differences between static and cyclic damage initiation characteristics for each specimen, as well as the overall initiation and growth trends are examined. Previous work has shown that delamination is the dominant mode of damage, although other damage modes, such as matrix ply cracks and fiber breakage, have been observed. Of particular interest are the effects that different factors, such as the number and location of terminated plies, have on the delamination characteristics of the laminate. Such experimental data are not available in the literature.

Using the results from the analysis and experiments, qualitative and quantitative examinations of the stress field and the delamination characteristics are performed to find the relationship between them. Since delamination initiation characteristics are of particular interest, the current work focuses on stress-based methodologies for quantitative predictions, such as the Quadratic Delamination Criterion for static cases, as these are more suitable for such purposes. Previous investigations have shown that the Quadratic Delamination Criterion is very effective in predicting the occurrence of delamination in composite laminates, *e.g.*, [42]. Once a firm understanding of the relationship between the stress field and the delamination characteristics is established, extensions to more complex laminates, such as unsymmetric laminates under in-plane loads and/or bending loads, are considered through analysis in order to further extend the understanding.

3.2 Analytical Models

The framework of the BBA is particularly suited for use in the development of analytical models. Since this approach requires one to break down the factors that cause interlaminar stresses and consider these factors in a hierarchical manner for models with increasing complexity, it helps to understand better the mechanisms causing such stresses. To obtain accurate and reliable interlaminar stress fields in each such analytical

model, the stress function method is used. This method, in which an assumption for the form of the stress field is made in terms of unknown stress functions that are determined using the principle of minimum complementary energy, has been used in previous work on laminates with straight free edges [20], circular free edges [60] and material discontinuities [61] with great success. The validity of each analytical model is established by comparing results with those from the open literature or through finite element (FE) analysis at each step of the building block. The ABAQUS® finite element (FE) package is used for the latter purpose [62].

Three analytical models are developed to calculate the stress field in the baseline laminate. Using the methodology of the BBA, the factors that cause such stresses are first identified and subsequently incorporated in general analytical models. In the baseline laminates with ply dropoffs, the factors that cause interlaminar stresses are the sources of discontinuities in the load path. These can be divided into two categories based on length-scales. From a *global* viewpoint, discontinuities arise due to the differences in laminate properties from the undropped region to the dropped region, and due to the termination of the plies. These global discontinuities, that depend only on the layups of the laminate in the undropped and dropped regions and are independent of the specifics of the ply dropoffs in the dropoff region, give rise to interlaminar stresses. The other lengthscale deals with a *local* viewpoint where discontinuities arise due to the differences in the material properties of the plies and the resin pockets at the tip of the terminated plies, and due to the geometric specifics of the dropoff region such as the ply path and taper angle. These local discontinuities depend only on the specifics of the ply dropoffs and also cause interlaminar stresses. In addition to these two considerations, the boundary conditions of the edges of laminates with ply dropoffs are stress-free. They therefore provide yet another source of interlaminar stresses. The focus of the current work is on the effects of terminated plies, therefore, these free-edge effects are not considered. Thus, it can be seen that interlaminar stresses in laminates with ply dropoffs

arise due to a combination of global and local factors, and therefore, it is important to consider the interlaminar stresses from each source separately because they may possess very different characteristics including different associated length-scales.

Following the basic methodology of the BBA, the first step is to identify the structure with the lowest level of complexity. In the case of the analytical method, the structure with the lowest level of complexity is one where only the global discontinuities are considered. Herein, this model is called the "global" model. The next step of the building block is to add more factors to the model with the lowest level of complexity. This is done by adding the effects of local discontinuities to the global model. Herein, this model is called the "mixed" model. The global and mixed models are developed as part of the analytical work. Subsequent models with increasing complexity can be developed, as illustrated in Figure 3.3 where a diagram of the analytical models with hierarchical levels of complexity based on the concept of the BBA is shown. Note that models with greater complexity than that of the mixed model require specific details of the terminated plies in the dropoff region. This is beyond the scope of the current analytical work. Such laminates are most suited for analysis using numerical methods.

In the global model, the interlaminar stresses in symmetric laminates with ply dropoffs due to the global discontinuities are considered by modeling the laminate as two laminates of uniform thicknesses whose layups are equivalent to that of the undropped and dropped regions. This is achieved by "cutting off" the dropoff region and replacing it with appropriate boundary conditions at the two interfaces, or *cutoffs*, where the dropoff region meets the undropped region and the dropped region. Consideration of the global effects in isolation may aid in better understanding the key parameters in the laminate and provide the basis to determine the overall stress field in laminates with ply dropoffs. Moreover, this model is also directly applicable for consideration away from the specifics of the ply dropoffs and to certain types of laminates for which the interlaminar stresses due to the local discontinuities vanish or are small. Examples of such laminates are

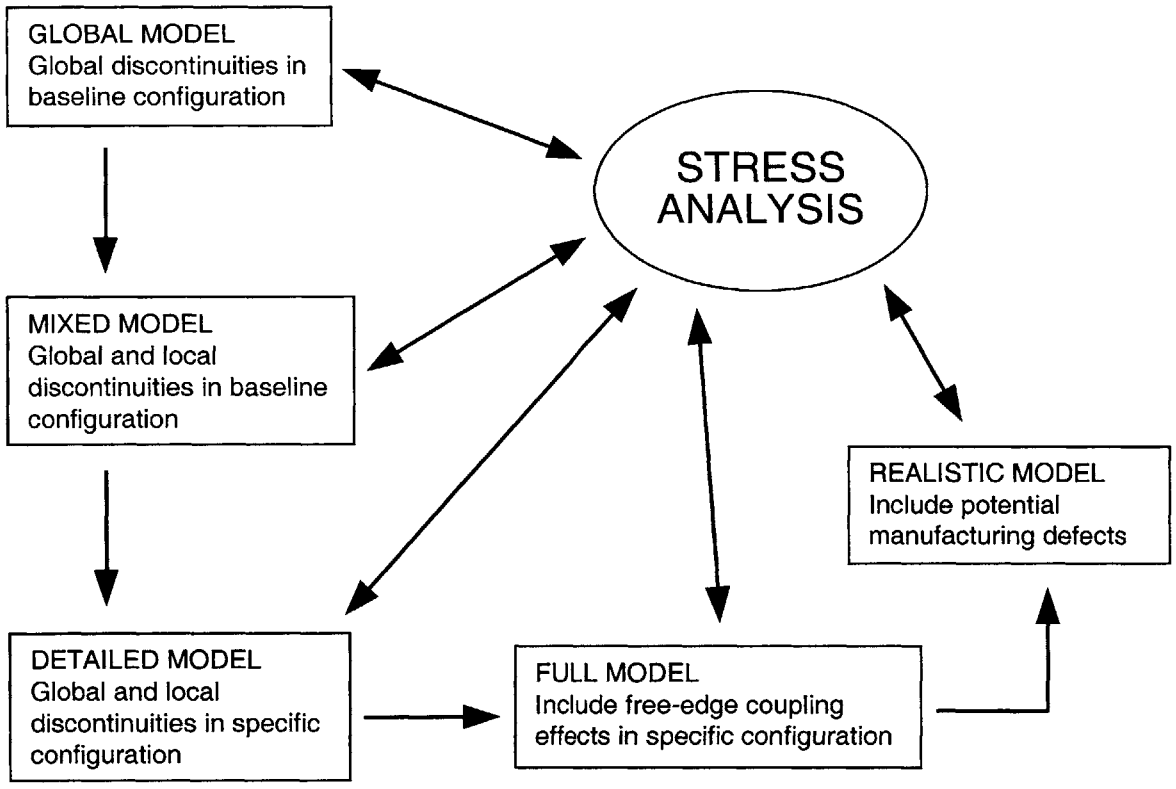

Figure 3.3 Flowchart of the building-block approach adapted for analysis of laminates with ply dropoffs.

laminates with external ply dropoffs or with ply dropoffs whose taper angle is small.

In the mixed model, the local effects of the ply dropoffs are considered along with the global effects. In the baseline laminate configuration, the only local effect is the constant taper angle in the dropoff region. This is a key parameter not only in the dropoff region, but also in the overall geometry of the laminate because it specifies the length of the dropoff region. The effect of the taper angle is included in the analytical model by considering the equilibrium of the dropoff region as a unit.

The two analytical models are developed based on the baseline laminate with symmetric ply dropoffs under in-plane and bending loads. These are used to obtain the stress field characteristics of laminates with ply dropoffs in general and, through parametric studies, to help understand the mechanisms that give rise to interlaminar stresses. In addition, the two models can be combined to obtain interlaminar stresses in more complex configurations such as laminates with geometrically unsymmetric ply dropoffs. Since the analyses are linear, the stress field obtained from the analytical model for each loading condition can be superposed in an appropriate manner to consider such laminate configurations. This feature of the analytical method is exploited to explore the nature of the interlaminar stress field in laminates with symmetric ply dropoffs under bending loads and laminates with unsymmetric ply dropoffs under in-plane loads.

As a further extension of the analytical model, a third model is developed for laminates with ply dropoffs that have existing delaminations. In the baseline laminate configuration, delamination can occur along several interfaces as illustrated in Figure 3.4. Considering each delaminated segment of the laminate as a unit, the stress field using similar methods for the first and second analytical models can be obtained approximately. This model may be useful in understanding and characterizing growth of delamination after initiation, especially under fatigue loads. Since the current work focuses on delamination initiation under static and fatigue loads, this analytical model is developed only for in-plane loading conditions to show feasibility, but could straightforwardly be

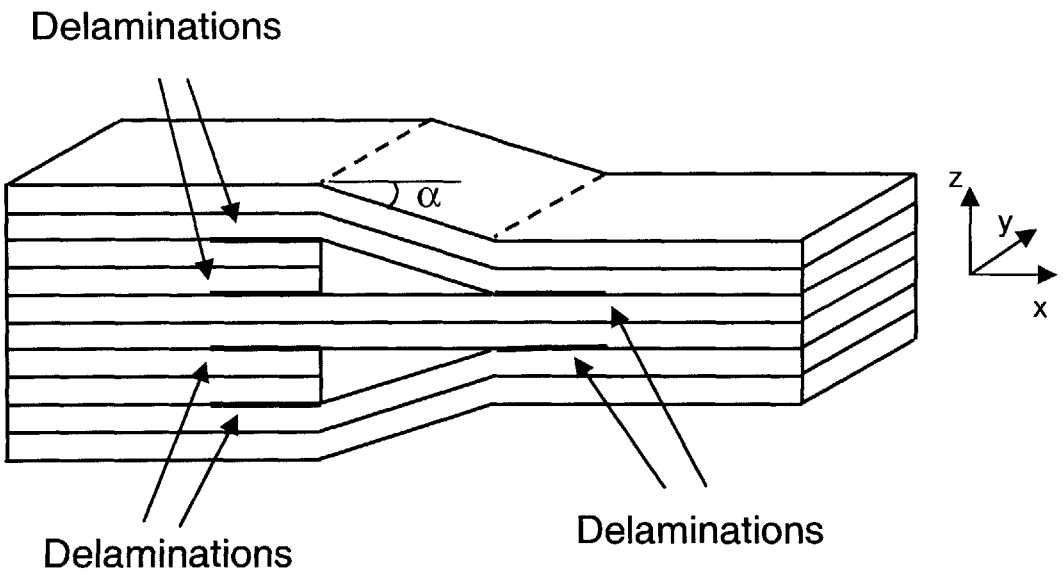

Figure 3.4 Possible delamination sites in the baseline laminate with ply dropoffs.

extended to other considerations and configurations.

3.3 Experiments

The experimental work consists of static and cyclic tensile tests on several types of laminates with ply dropoffs and the observation of damage initiation and growth characteristics. The types of laminates and the geometry of the specimens considered in the experiments were selected based on the BBA and the baseline laminate configuration. This allows one to compare damage characteristics from different types of laminates and identify any general trends that may exist. A key concern is the possibility of irregularities in the actual specimens that may cause a significant change in the damage characteristics. As mentioned in Chapter 2, irregularities from manufacturing defects may exist in actual specimens, and they have been found to affect the local stress field significantly [34]. As such, it is important to manufacture the specimens with a high degree of consistency and reliability. The manufacturing procedures used in this work to ensure the quality of the specimens are discussed further in Chapter 5.

Following the baseline laminate configuration, the terminated plies in the coupon specimens are geometrically symmetric about the mid-plane of the laminate such that the in-plane and bending coupling effects are eliminated. The ply dropoffs are located at the mid-section of the coupon specimen along the length such that the tabs (and, therefore, the grips when testing) are sufficiently far away from the dropoff region. The taper angle in the dropoff region is fixed at 7° based on actual composite flexbeam geometries. A factor that may further complicate delamination initiation in laminates with ply dropoffs is the presence of straight free edges. It is well known that laminates with straight free edges are prone to delamination, *e.g.*, [20], for certain layups and configurations. In laminates with ply dropoffs, the situation is compounded because of the possibility of interaction between the free edge and the ply dropoffs. Therefore, it is necessary to isolate the effects of the ply dropoffs from the effects of the free edges by considering

layups with little or no free edge effects. In the current work, laminates with 0° plies are used, and thus, there is no elastic mismatch from ply to ply thereby eliminating free-edge effects.

Six types of specimens are considered in the experiments. Among the many factors that may affect the interlaminar stress field, and therefore, the damage characteristics, two factors were selected. They are the number of terminated plies and the location of the terminated ply group. Laminates with four and eight terminated plies, and three different dropoff locations through the thickness are considered. Specifically, from a total of 16 plies in the undropped region, one set of laminates has two symmetric ply dropoffs, and another set has four symmetric ply dropoffs. Three locations for the ply dropoffs are considered for each set of laminates with ply dropoffs. For the laminates with two symmetric ply dropoffs, the dropoffs occur in a single step as in the baseline configuration. However, for the laminates with four symmetric ply dropoffs, the dropoffs occur in two distinct steps. The reason for using two distinct steps is to avoid the possibility of irregular, large void formation in the resin pockets.

The specific characteristics of interest from the static and cyclic tension tests are the damage modes and the damage initiation location and load. Based on test results from previous investigators, delamination is expected to be the dominant mode of damage. To determine the load at which delamination initiates under static load, the load drop method in conjunction with edge replication techniques are used. In the load drop method, an instantaneous drop in the load, which may indicate a delamination, is constantly monitored. This method has been used successfully in previous work to detect free edge delamination initiation events [42]. The fatigue tests are performed in order to observe the damage modes, determine the location at which damage initiates, and obtain the number of cycles to damage initiation and observe delamination growth characteristics. In this case, the specimens were examined for detectable damage through visual inspection of the top and bottom surfaces, edge replication, and X-ray radiographs

at pre-determined intervals. Port-mortem fracture surface analyses were also performed to identify possible causes of delamination.

CHAPTER 4

ANALYTICAL MODELS

The analytical models developed in the current work to obtain the interlaminar stress field in laminates with ply dropoffs are described in this chapter. Three analytical models are developed in hierarchical levels of complexity based on the building block philosophy. The three analytical models developed herein are based on the same theoretical and mathematical formulations. These formulations are described in the first section. Following the formulation, the general solution methodology to obtain the stress field is discussed in the second section. In the third section, the global model, which is the model with the lowest level of complexity, is presented. In this model, the effects of the global factors such as the layup of the laminate and number and location of the terminated plies are considered. In the mixed model, the effect of the taper angle is also considered in addition to the global factors. This model is presented in the fourth section. As a further extension of the analytical models, a model for laminates with existing delaminations is considered in the fifth section. In order to obtain the interlaminar stress field using such models efficiently, the analytical procedures were implemented using a computer program. The computer implementation of the analytical models is discussed in the final section.

4.1 General Formulation

It is well-known that ply dropoffs in composite laminates give rise to regions of high in-plane and interlaminar stresses. These stresses arise due to discontinuities in the material and geometric properties of the undropped, dropoff, and dropped regions of the laminate that complicate the load transfer from the undropped region to the dropped

region. Hence, the regions of in-plane stress concentrations and high interlaminar stresses in the baseline laminate configuration will occur in the vicinity of the region where the load transfer takes place. In order to facilitate the development of the analytical methods that model this load transfer accurately in an overall sense, three simplifying assumptions are made.

The first assumption is that the undropped and dropped regions are sufficiently long such that the effects of the terminated plies taper to zero away from the dropoff region within the undropped and dropped regions. Based on this assumption, the laminate with ply dropoffs can be divided into regions where two different states of stress exist. One, a state of complex three-dimensional stress is expected to exist in the vicinity of the dropoffs since the load transfer takes place near the dropoff region. Two, a state of plane stress is expected far away from the dropoff region since the load transfer in the dropoff region does not affect regions sufficiently distant from the dropoff region. Since this plane stress state is relatively easy to obtain, this assumption simplifies the problem and is very useful for solving the stress field using analytical methods.

The second assumption is that the triangular region at the tip of the terminated plies in the dropoff region, *i.e.*, the resin pocket, does not transfer stress. This assumption is based on physical observations by previous investigators from experiments where the resin pocket was found to crack at very low loads, *e.g.*, [13]. This is an exaggeration of the resin crack and represents a more severe case of termination because no load can be transferred across the terminated plies, *i.e.*, the terminated plies carry no load at the termination location in the dropoff region. In addition, other traction-free surfaces exist in the dropoff region if it is assumed that no load is transferred in this triangular region, simplifying the problem further. In reality, in laminates with undamaged resin pockets, the presence of the resin pocket would allow some load to be transferred at the termination locations.

The third assumption is that the stress field does not vary in the widthwise

direction parallel to the ply dropoffs. This assumption is based on the fact that ply dropoffs will not give rise to in-plane or interlaminar stresses that vary parallel to the ply dropoffs. In reality, other factors such as free edges may be present such that the stress field does vary with respect to the widthwise direction. Such factors are not considered in the current work.

The focus of the current work is to provide a clear view of how the load transfer from the undropped region to the dropped region occurs. This knowledge will contribute toward a more complete understanding of the overall effects of the ply dropoffs. Therefore, the stress distributions in the undropped and dropped regions, particularly in the vicinity of the dropoff region, are sought from the analysis. The dropoff region that connects the undropped region to the dropped region provides the path through which the load transfer occurs. Therefore, modeling the dropoff region is a key step in the analytical work. Three models are developed in this work to model the dropoff region in increasing levels of complexity. These models are described in detail in sections 4.3 through 4.5.

The stress field in the dropoff region itself is not, however, expected to be of significance. Since the ply dropoffs occur in a single step in the baseline laminate configuration (see Figure 3.4) and no type of discontinuity exists in the dropoff region to cause stress redistribution, the stress state in this region is not expected to yield any valuable insights to the overall load transfer mechanism. Thus, the stress distribution in the dropoff region itself is not considered.

To obtain the stress field in the undropped and dropped regions, the baseline laminate is modeled as two separate uniform thickness laminates with the appropriate boundary conditions at the interfaces of the undropped and dropoff regions, and the dropped and dropoff regions. These interfaces are referred to as the "cutoffs". A diagram of the baseline laminate configuration modeled as two uniform thickness regions is shown in Figure 4.1. To identify the two regions conveniently, the uniform thickness

region whose layup is equivalent to that of the undropped region is referred to as "region A". The uniform thickness region whose layup is equivalent to that of the dropped region is referred to as "region B". Since symmetric laminates with ply dropoffs are considered in the current work, only half of the laminates in regions A and B need to be analyzed. Based on the first simplifying assumption discussed previously, the regions in the vicinity of the cutoffs are in a state of three-dimensional stress, and the regions sufficiently far away from the cutoffs are in a state of plane stress. It is therefore convenient to divide the problem into two parts based on the superposition principle: the classical laminated plate theory (CLPT) problem and the companion problem. The companion problem is an auxiliary problem that is formulated based on the boundary conditions the CLPT solution does not fully satisfy in the original problem. Under in-plane load, the CLPT problem yields a constant in-plane stress field that describes the regions near the ends of each region but that does not satisfy the boundary conditions at the cutoffs of the original problem. Under bending load, the CLPT problem yields a piecewise linear in-plane stress field that describes the region near the ends of each regions but that, again, does not satisfy the boundary conditions at the cutoffs of the original problem. Therefore, the companion problem is formulated such that it yields a three-dimensional stress field that varies along the length of the laminate and can satisfy the appropriate boundary conditions when superposed with the CLPT solution. The stress field from the companion problem should vanish sufficiently far away from the cutoffs such that the CLPT stress field is recovered. The desired solution is obtained by superposing the two stress fields from the CLPT and companion problems. A graphical representation of superposition of the CLPT stress field and the companion stress field is shown in Figure 4.2. Similar superposition methods have previously been applied successfully for interlaminar stress analysis at free edges [60,63] and at other discontinuities [61,64].

The CLPT problem consists of solving for the in-plane stresses in regions A and B when in-plane or bending loads are applied. The formulation and solution for the

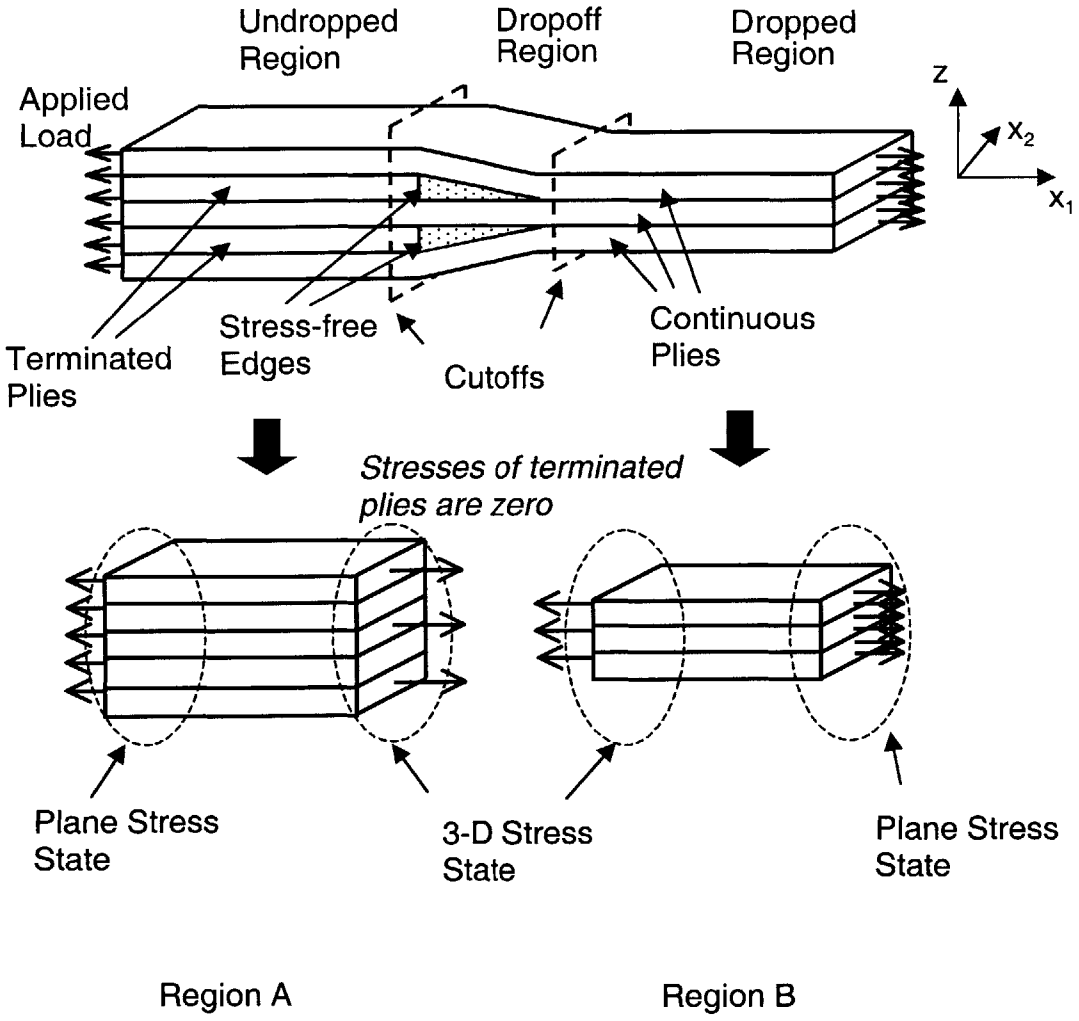

Figure 4.1 Diagram of *(top)* baseline laminate with ply dropoffs, and *(bottom)* model of a laminate with ply dropoffs.

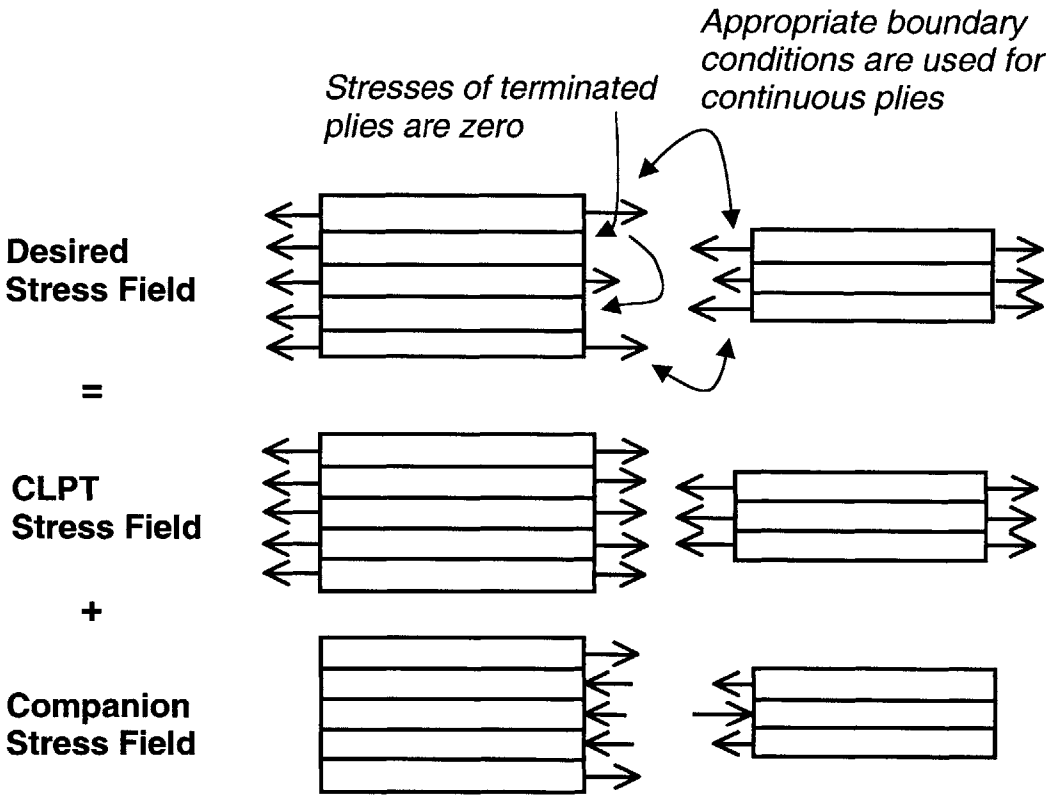

Figure 4.2 Graphical representation of the superposition of the CLPT stress field and the companion stress field to yield the desired stress field.

CLPT problem are readily available in the literature from standard textbooks, *e.g.*, [1], and are not presented here. The solution to this problem yields the CLPT stress field that exists in the regions away from the cutoffs. The companion problem consists of solving for the ply-by-ply three-dimensional stress field in regions A and B such that the stress boundary conditions are satisfied at the cutoffs and the stresses decay to zero away from the cutoffs. Thus, the companion problem needs to be formulated based on the ply-by-ply equilibrium equations. These two problems are superposed to yield the solution to the actual case.

The baseline laminate is described as having $2n$ plies in region A and $2m$ plies in region B with n greater than m. Thus, the number of continuous plies in the laminate is $2m$ and the number of terminated plies is $2(n-m)$. A diagram of regions A and B and the associated axis system is shown in Figure 4.3. Since the stress fields are considered only in the undropped and dropped regions, *i.e.*, the dropoff region is not explicitly considered, an axis system in which region A lies in the negative region of the lengthwise direction coordinate, x_1, and region B in the positive region of x_1 is used. The thickness direction coordinate, z_i, is defined locally in each ply with the origin at the mid-point of the ply thickness, as shown in Figure 4.3. A global thickness direction coordinate, z, whose origin is at the mid-plane of the laminate, is also defined.

Stress equilibrium on a ply-by-ply basis for each ply requires for both regions A and B, that:

$$\sigma_{ij,j} = 0 \tag{4.1}$$

where σ_{ij} are the components of the companion stress. As is the case with standard tensor notation, Latin subscripts denote three-dimensional problems and take on values from 1 to 3. A comma denotes a derivative. Since the applied load does not vary with respect to the x_2-direction of the laminate, the stresses in the undropped and dropped regions may be assumed to be functions of only two spatial coordinates, x_1 and z, with no variation in

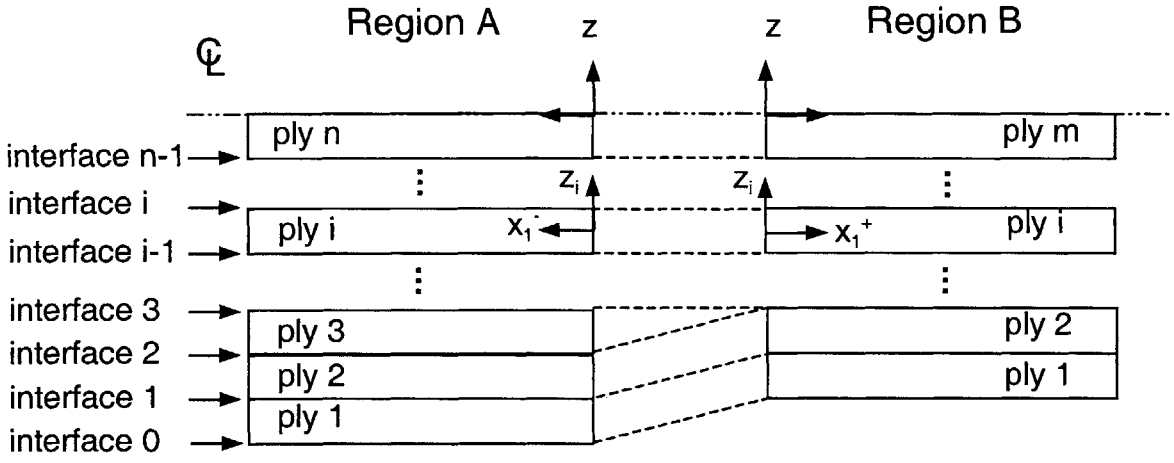

Figure 4.3 Diagram of the global model for the bottom half of a symmetric laminate with ply dropoffs showing the ply numbering scheme and the associated axis systems.

the x_2-direction. This condition is known as the state of generalized plane deformation [65]. Under this condition, the equilibrium equations in (4.1), expressed in expanded form, become:

$$\frac{\partial \sigma_{11}}{\partial x_1} + \frac{\partial \sigma_{1z}}{\partial z} = 0 \tag{4.2}$$

$$\frac{\partial \sigma_{12}}{\partial x_1} + \frac{\partial \sigma_{2z}}{\partial z} = 0 \tag{4.3}$$

$$\frac{\partial \sigma_{1z}}{\partial x_1} + \frac{\partial \sigma_{zz}}{\partial z} = 0 \tag{4.4}$$

Using the stress-strain relation,

$$\varepsilon_{ij} = S_{ijkl}\sigma_{kl} \tag{4.5}$$

where S_{ijkl} is the compliance matrix and ε_{ij} are the components of strain. The expression for the in-plane stress σ_{22}, which is not explicitly related to the other stress components in the equilibrium equations, can be obtained as a function of the in-plane strains and stresses. This is accomplished by taking the stress-strain relation in equation (4.5), for the case of i and j equal to 2, and solving for σ_{22}, *i.e.*:

$$\sigma_{22} = -\left(\frac{\varepsilon_{22}}{S_{2222}} + \frac{S_{1122}}{S_{2222}}\sigma_{11} + \frac{S_{2233}}{S_{2222}}\sigma_{33} + \frac{S_{2212}}{S_{2222}}\sigma_{12} \right) \tag{4.6}$$

Based on the second simplifying assumption, the terminated plies are assumed to carry no loads at the cutoffs in the undropped region. This implies that at the cutoffs, *i.e.*, $x_1 = 0$, the terminated plies are traction-free. Therefore, the stress boundary condition at the cutoff in region A for the terminated plies can be expressed as:

$$\sigma_{1j}^{A}(0,z)=0 \tag{4.7}$$

where the superscript "A" refers to region A. Equation (4.7) is comprised of both the CLPT and the companion stresses because the traction-free condition requires the sum of these stresses to be zero.

The CLPT and companion problems as formulated yield the solution for the stresses in the two uniform thickness laminates in regions A and B under in-plane or bending loads. The stresses satisfy equilibrium in equations (4.2) through (4.4) and the traction boundary condition in equation (4.7). The details of the solution procedure using the stress function method for the companion problem are described in the next section.

4.2 Stress Function Method

The solution to the companion problem formulated in the previous section is obtained by using the stress function method. In this method, a set of admissible stress fields that satisfy equilibrium in equations (4.2) through (4.4) is first assumed. The admissible stress field is based on the assumptions that each component of stress is separable and can be expressed in terms of a set of unknown stress functions of x_1, and known functions of z. The stress functions are subsequently determined by using the principle of minimum complementary energy. In using this method, the initial assumption for the stress field is important because the accuracy of the interlaminar stresses and the applicability of the methodology depend on the initial assumption. For the case of in-plane loading conditions, the assumption for the stress field used in previous work is utilized [61]. For the case of bending loads, a new set of stress functions based on the functional constraints of the problem such as the global force and moment equilibrium is developed.

4.2.1 In-plane Load

For laminates under in-plane load, the in-plane stresses are assumed to first order to be constant through the thickness within each ply. This assumption follows directly

from the constant in-plane stress in each ply based on the CLPT. Use of the stress equilibrium equations then yields that the shear stress components, σ_{1z} and σ_{2z}, are linear in z, and that the normal stress component, σ_{zz}, is parabolic in z. The general expression for the companion stress field can be simplified by introducing stress functions, $F_i(x_1)$ and $G_i(x_1)$, that are defined at the interfaces between plies (see Figure 4.3). This allows the interlaminar shear stress continuity conditions at ply interfaces to be automatically satisfied. Using this definition, the in-plane stresses for the *i*th ply in region A are expressed as the weighted (by the thickness of the *i*th ply, t_i) difference of the stress functions at the top and bottom interfaces of the ply:

$$\sigma_{11}^{(i)} = \frac{1}{t_i}\left(F_{i-1}(x_1) - F_i(x_1)\right) \tag{4.8a}$$

$$\sigma_{12}^{(i)} = \frac{1}{t_i}\left(G_{i-1}(x_1) - G_i(x_1)\right) \tag{4.8b}$$

The dimension of these stress functions is force per length.

The out-of-plane stresses are obtained by substituting these expressions into the equilibrium equations (4.2) through (4.4) on a ply-by-ply basis. Using a prime to represent the derivative with respect to x_1, the out-of-plane stresses for the *i*th ply in region A are expressed as:

$$\sigma_{1z}^{(i)} = F_i'(x_1)\left(\frac{z_i}{t_i} + \frac{1}{2}\right) - F_{i-1}'(x_1)\left(\frac{z_i}{t_i} - \frac{1}{2}\right) \tag{4.8c}$$

$$\sigma_{2z}^{(i)} = G_i'(x_1)\left(\frac{z_i}{t_i} + \frac{1}{2}\right) - G_{i-1}'(x_1)\left(\frac{z_i}{t_i} - \frac{1}{2}\right) \tag{4.8d}$$

$$\sigma_{zz}^{(i)} = \frac{t_i F_{i-1}''(x_1)}{2}\left(\frac{z_i}{t_i} - \frac{1}{2}\right)^2 - \frac{t_i F_i''(x_1)}{2}\left(\frac{z_i}{t_i} + \frac{1}{2}\right)^2 - \sum_{j=1}^{i-1} t_i F_j''(x_1) \tag{4.8e}$$

This form of the companion stress field has been used previously for stress analysis of composite laminates with material discontinuities [61]. Note that the interlaminar stresses in equations (4.8c) through (4.8e) have been expressed in terms of the local z-direction coordinate.

The general form of the companion stresses in region B is identical to that for region A as shown in equation (4.8). However, the stress functions in region B differ from those in region A. Since the solution procedure for region B is almost identical to that for region A, the procedure for region B is not discussed separately and can be inferred from that for region A unless otherwise noted. The companion stress field in region B is expressed using the stress functions $H_i(x_1)$ and $K_i(x_1)$ in place of $F_i(x_1)$ and $G_i(x_1)$ in equation (4.8).

Due to anti-symmetry, the interlaminar shear stresses must vanish at the mid-plane of the laminate under in-plane loads. According to equations (4.8c) through (4.8e), the interlaminar shear stresses at the mid-plane are equal to the first derivatives of the stress functions, $F_n'(x_1)$ and $G_n'(x_1)$. In addition, the outer surface of the half-laminate must be traction-free, *i.e.*, interlaminar shear and normal stresses must be equal to zero. The interlaminar shear stresses at the outer surface are equal to the first derivatives of the stress functions, $F_0'(x_1)$ and $G_0'(x_1)$, and the interlaminar normal stress at the outer surface is equal to the second derivative of the stress function, $F_0''(x_1)$. Thus, the two constraints at the mid-plane and outer surface can be expressed as:

$$F_0' = F_0'' = F_n' = G_0' = G_n' = 0 \tag{4.9}$$

As mentioned previously, the companion stresses in both regions A and B must vanish sufficiently far away from the cutoffs such that the CLPT stresses are recovered. Therefore, additional constraints are placed on the stress functions that can be obtained from the stress functions and their derivatives that appear in the expressions for the stresses in equations (4.8a) through (4.8e). For region A, these constraints can be

expressed as:

$$\lim_{x_1 \to -\infty} F_i, F_i', F_i'' = 0 \qquad \text{for i = 0 to n} \tag{4.10a}$$

$$\lim_{x_1 \to -\infty} G_i, G_i' = 0 \qquad \text{for i = 0 to n} \tag{4.10b}$$

Equations (4.9) and (4.10) imply that at the outer surface and mid-plane of region A, $F_i(x_1)$ and $G_i(x_1)$ are zero. This can be seen by integrating equation (4.9) with respect to x_1, which results in constants, and setting these constants to zero according to equation (4.10).

In addition to the differential form of the equilibrium equations, the general expression for the companion stress field in equation (4.8) must also satisfy the integral form of the equilibrium equations, *i.e.*, the x_1 and x_2-direction force equilibrium equations. Since the desired stress field is obtained by the superposition of the CLPT stress field and the companion stress field, the sum of the integrals of the CLPT stresses and the companion stresses through the thickness must equal the applied in-plane forces. However, the CLPT problem is formulated based on in-plane force equilibrium, and thus, the integrals of the CLPT stresses are exactly equal to the applied in-plane forces. This implies that the integrals of the companion stresses must always equal zero. Therefore, at any location along the length of region A, x_1-direction and x_2-direction force equilibrium of the half-laminate requires,

$$\int_{-\frac{h}{2}}^{0} \sigma_{1\alpha}\, dz = \sum_{i=1}^{n} \sigma_{1\alpha}^{(i)} t_i = 0 \tag{4.11}$$

where h is the thickness of region A. Substituting equations (4.8a) and (4.8b) into equation (4.11), it can be immediately seen that the current assumption for the companion stress field satisfies the force equilibrium equations. This is not a coincidence; it is the result of the particular choice for the companion stress field that satisfies equilibrium in

equations (4.2) through (4.4) and the constraints in equations (4.9) and (4.10).

The next step is to determine the unknown stress functions in the companion stress field expression in equation (4.8) through the use of the principle of minimum total complementary energy. This principle states that the solution to the problem is the stress field that minimizes the total complementary energy. The total complementary energy, π^*, for the global model can be expressed as,

$$\pi^* = \frac{1}{2}\int_{V^A+V^B} \sigma_{ij} S_{ijkl} \sigma_{kl} dV + \int_{S^A+S^B} \sigma_{ij} n_j \tilde{u}_i dS \tag{4.12}$$

where V^A and V^B represent volume integrals in regions A and B, respectively, S^A and S^B represent surface integrals in regions A and B, respectively, where the displacements are prescribed, and $\tilde{u}_i$ are the prescribed displacements. The stresses, σ_{ij}, in equation (4.12) are composed of the CLPT part and the companion part. The CLPT stresses for regions A and B are obtained by solving for the in-plane ply-by-ply stresses in each region when in-plane loads are applied, and are known values. Thus, they do not contribute to the variation of the total complementary energy. Therefore, only the companion stresses need to be considered when the total complementary energy is minimized. Since there are no prescribed displacements in the current problem, taking the first variation of the total complementary energy in equation (4.11) and setting it to zero results in the following equation:

$$\delta\pi^* = \frac{1}{2}\delta\int_{V^A} \sigma_{ij}^A S_{ijkl} \sigma_{kl}^A dV^A + \frac{1}{2}\delta\int_{V^B} \sigma_{ij}^B S_{ijkl} \sigma_{kl}^B dV^B = 0 \tag{4.13}$$

This equation can be simplified by eliminating the in-plane companion stress σ_{22} via equation (4.6) whose expression is not explicitly related to the other companion stress components through ply-by-ply equilibrium in equations (4.2) through (4.4). Since the in-plane strains are constant values according to the CLPT solution, the in-plane strain ε_{22} in equation (4.6) is also assumed to be constant. Hence, it does not contribute to the

variation of the complementary energy in equation (4.13). Therefore, a modified expression for the stress-strain relation can be obtained by ignoring ε_{22} and substituting equation (4.6) for σ_{22} in the stress-strain relation in equation (4.5). The modified expression for the stress-strain relation can be expressed as,

$$\varepsilon_{ij}^{*} = S_{ijkl}^{*}\sigma_{kl}^{*} \tag{4.14}$$

where

$$\tilde{\varepsilon}^{*} = [\varepsilon_{11} \quad \varepsilon_{33} \quad \varepsilon_{23} \quad \varepsilon_{13} \quad \varepsilon_{12}]^{T} \tag{4.15}$$

$$\tilde{\sigma}^{*} = [\sigma_{11} \quad \sigma_{33} \quad \sigma_{23} \quad \sigma_{13} \quad \sigma_{12}]^{T} \tag{4.16}$$

and

$$S_{ijkl}^{*} = S_{ijkl} - \frac{S_{22kl}S_{22ij}}{S_{2222}} \tag{4.17}$$

Using equation (4.14) and matrix notation, the expression for the minimization of the total complementary energy in equation (4.13) can be simplified as:

$$\delta\pi^{*} = \frac{1}{2}\delta\int_{V^{A}} \tilde{\sigma}^{*A}\mathbf{S}^{*}\tilde{\sigma}^{*A}dV^{A} + \frac{1}{2}\delta\int_{V^{B}} \tilde{\sigma}^{*B}\mathbf{S}^{*}\tilde{\sigma}^{*B}dV^{B} = 0 \tag{4.18}$$

Substituting the general expression for the companion stress field in equation (4.8) into equation (4.18) and performing the minimization results in two distinct systems of ordinary differential equations, one for region A and another for region B. The general form of the system of ordinary differential equations for region A is,

$$\begin{bmatrix}\mathbf{A}_{11} & \mathbf{0}\\ \mathbf{0} & \mathbf{0}\end{bmatrix}\begin{Bmatrix}\mathbf{F}\\ \mathbf{G}\end{Bmatrix}^{IV} + \begin{bmatrix}\mathbf{B}_{11} & \mathbf{B}_{12}\\ \mathbf{B}_{12} & \mathbf{B}_{22}\end{bmatrix}\begin{Bmatrix}\mathbf{F}\\ \mathbf{G}\end{Bmatrix}'' + \begin{bmatrix}\mathbf{C}_{11} & \mathbf{C}_{12}\\ \mathbf{C}_{12} & \mathbf{C}_{22}\end{bmatrix}\begin{Bmatrix}\mathbf{F}\\ \mathbf{G}\end{Bmatrix} = \mathbf{0} \tag{4.19}$$

where

$$\mathbf{F} = [F_1 \quad F_2 \quad \ldots \quad F_{n-1}]^T \tag{4.20a}$$

and

$$\mathbf{G} = [G_1 \quad G_2 \quad \ldots \quad G_{n-1}]^T \tag{4.20b}$$

The elements of the matrices, **A**, **B** and **C**, in equation (4.19) are *(n–1)* by *(n–1)* sub-matrices whose components can be expressed as follows.

$$[\mathbf{A}_{11}]_{ij} = \begin{cases} e_i\left(e_j g_j - 2L_3^{j+1} t_j\right) + L_1^j + L_1^{j+1} & \text{for} \quad \mathrm{j} = \mathrm{i} \\ e_i\left(e_j g_j + L_3^j t_j - L_3^{j+1} t_{j+1}\right) - L_2^j & \text{for} \quad \mathrm{j} = \mathrm{i}+1 \\ e_i\left(e_j g_j + L_3^j t_j - L_3^{j+1} t_{j+1}\right) & \text{for} \quad n-1 \geq j > \mathrm{i}+1 \end{cases} \tag{4.21}$$

$$[\mathbf{B}_{11}]_{ij} = \begin{cases} 2e_i\left(-2L_8^{j+1} t_{j+1}\right) + L_4^j + L_4^{j+1} & \text{for} \quad \mathrm{j} = \mathrm{i} \\ e_i\left(L_8^j t_j - L_8^{j+1} t_{j+1}\right) + L_5^j & \text{for} \quad \mathrm{j} = \mathrm{i}+1 \\ e_i\left(L_8^j t_j - L_{12}^{j+1} t_{j+1}\right) & \text{for} \quad n-1 \geq j > \mathrm{i}+1 \end{cases} \tag{4.22}$$

$$[\mathbf{B}_{12}]_{ij} = \begin{cases} L_7^{j+1} & \text{for} \quad \mathrm{j} = \mathrm{i}-1 \\ \left(-e_i L_{12}^j t_j + L_6^j + L_6^{j+1}\right) & \text{for} \quad \mathrm{j} = \mathrm{i} \\ \left(e_i\left(L_{12}^j t_j - L_{12}^{j+1} t_{j+1}\right) + L_7^j\right) & \text{for} \quad \mathrm{j} = \mathrm{i}+1 \\ e_i\left(L_{12}^j t_j - L_{12}^{j+1} t_{j+1}\right) & \text{for} \quad n-1 \geq j > \mathrm{i}+1 \end{cases} \tag{4.23}$$

$$[\mathbf{B}_{22}]_{ij} = \begin{cases} -2\left(L_{11}^j + L_{11}^{j+1}\right) & \text{for} \quad \mathrm{j} = \mathrm{i} \\ -L_{11}^j & \text{for} \quad \mathrm{j} = \mathrm{i}+1 \\ 0 & \text{for} \quad n-1 \geq j > \mathrm{i}+1 \end{cases} \tag{4.24}$$

$$[\mathbf{C}_{11}]_{ij} = \begin{cases} \left(L_9^j + L_9^{j+1}\right) & \text{for} \quad \mathrm{j} = \mathrm{i} \\ -L_9^j & \text{for} \quad \mathrm{j} = \mathrm{i}+1 \\ 0 & \text{for} \quad n-1 \geq j > \mathrm{i}+1 \end{cases} \tag{4.25}$$

$$[\mathbf{C}_{12}]_{ij} = \begin{cases} -L_{10}^{i} & \text{for} \quad j = i - 1 \\ \left(L_{10}^{j} - L_{10}^{j+1}\right) & \text{for} \quad j = i \\ -L_{10}^{i} & \text{for} \quad j = i + 1 \end{cases} \tag{4.26}$$

$$[\mathbf{C}_{12}]_{ij} = \begin{cases} \left(L_{13}^{j} + L_{13}^{j+1}\right) & \text{for} \quad j = i \\ -L_{13}^{j} & \text{for} \quad j = i + 1 \\ 0 & \text{for} \quad n - 1 \geq j > i + 1 \end{cases} \tag{4.27}$$

The constants, e_i, g_i and L_i are:

$$e_i = \frac{1}{2}\left(t_i + t_{i+1}\right) \qquad g_i = \sum_{j=i+1}^{n} L_{14}^{j} t_j^2$$

$$L_1^i = S_{3333}^{*(i)} \frac{h_i^3}{10} \qquad L_2^i = S_{3333}^{*(i)} \frac{h_i^3}{60}$$

$$L_3^i = S_{3333}^{*(i)} \frac{h_i}{3} \qquad L_4^i = \frac{2}{3} S_{2233}^{*(i)} h_i - \frac{8}{3} S_{2323}^{*(i)} h_i$$

$$L_5^i = -\frac{2}{3} S_{2233}^{*(i)} h_i - \frac{4}{3} S_{2323}^{*(i)} h_i \qquad L_6^i = \frac{2}{3} S_{3312}^{*(i)} h_i - \frac{8}{3} S_{1323}^{*(i)} h_i$$

$$L_7^i = -\frac{2}{3} S_{3312}^{*(i)} h_i - \frac{4}{3} S_{1323}^{*(i)} h_i \qquad L_8^i = \frac{2 S_{2233}^{*(i)}}{h_i}$$

$$L_9^i = \frac{2 S_{2222}^{*(i)}}{h_i} \qquad L_{10}^i = \frac{4 S_{2212}^{*(i)}}{h_i}$$

$$L_{11}^i = \frac{4}{3} \frac{S_{1313}^{*(i)}}{h_i} \qquad L_{12}^i = 4 \frac{S_{3312}^{*(i)}}{h_i}$$

$$L_{13}^{i} = 8\frac{S_{1212}^{*(i)}}{h_i} \qquad L_{14}^{i} = 2\frac{S_{3333}^{*(i)}}{h_i}$$

The solution to the system of ordinary differential equations (4.19) yields the stress functions, which can be expressed as a summation of exponential functions, *i.e.*,

$$\mathbf{F}(x_1) = \sum_{j=1}^{3(n-1)} a_j \Phi_j e^{\lambda_j x_1} \tag{4.28a}$$

$$\mathbf{G}(x_1) = \sum_{j=1}^{3(n-1)} a_j \Psi_j e^{\lambda_j x_1} \tag{4.28b}$$

where λ_j are the eigenvalues, and Φ_j and Ψ_j are the eigenvectors of equation (4.19). For region B, the general form of stress functions can be obtained similarly as,

$$\mathbf{H}(x_1) = \sum_{j=1}^{3(m-1)} b_j \Theta_j e^{\mu_j x_1} \tag{4.29a}$$

$$\mathbf{K}(x_1) = \sum_{j=1}^{3(m-1)} b_j \Gamma_j e^{\mu_j x_1} \tag{4.29b}$$

where μ_j are the eigenvalues, and Θ_j and Γ_j are the eigenvectors of the equation corresponding to equation (4.19) for region B. The values for a_j and b_j depend on which model is used for the dropoff region. The solution procedure for obtaining these values is described in sections 4.3 through 4.5.

4.2.2 Bending Load

For laminates under bending loads, the in-plane stresses are assumed to vary linearly through the thickness of each ply. This assumption follows directly from the CLPT under bending load where the in-plane stresses are linear in each ply and discontinuous through the entire thickness of the laminate in general. Use of equilibrium represented in equations (4.2) through (4.4) yields quadratic functions in z for the

interlaminar shear stresses and cubic functions in z for the interlaminar normal stresses.

The general expression for the companion stress field under bending load is more complicated than that for the in-plane load. The reason is that the in-plane stresses under bending load have two values at the interfaces in general because they are assumed to be piecewise linear and discontinuous. In order to allow the in-plane stress field to be dual-valued at the interfaces, three stress functions are defined in each ply, *e.g.*, in the *i*th ply $F_{2i-2}(x_1)$, $F_{2i-1}(x_1)$ and $F_{2i}(x_1)$ for σ_{11}, and $G_{2i-2}(x_1)$, $G_{2i-1}(x_1)$ and $G_{2i}(x_1)$ for σ_{12}. The in-plane stresses at the two interfaces of each ply are then expressed as a difference of two stress functions multiplied by a constant, which is a function of the ply thickness. This multiplier is required in order to satisfy moment equilibrium. For example, the in-plane stress σ_{11} in the *i*th ply is proportional to $\left[F_{2i-2}(x_1) - F_{2i-1}(x_1)\right]$ at the *(i–1)*th interface and to $\left[F_{2i-1}(x_1) - F_{2i}(x_1)\right]$ at the *i*th interface (see Figure 4.3 for ply and interface number definitions). The in-plane stress in the *i*th ply is then expressed as a linear function in z connecting the stresses at the two interfaces. Note that exceptions occur at the outer surface and the mid-plane of the laminate where the in-plane stresses are single-valued. Thus, the in-plane stresses for the *i*th ply in region A are expressed as the difference of the combinations of stress functions at the *(i–1)*th and *i*th interfaces multiplied by a linear function in z:

$$\sigma_{11}^{(i)} = \frac{1}{t_i\left(3\sum_{j=i}^{n} t_j - 2t_i\right)}\left[F_{2i-1}(x_1) - F_{2i}(x_1)\right]\left(\frac{z_i}{t_i} + \frac{1}{2}\right) - \frac{1}{t_i\left(3\sum_{j=i}^{n} t_j - t_i\right)}\left[F_{2i-2}(x_1) - F_{2i-1}(x_1)\right]\left(\frac{z_i}{t_i} - \frac{1}{2}\right) \tag{4.30a}$$

$$\sigma_{12}^{(i)} = \frac{1}{t_i\left(3\sum_{j=i}^{n} t_j - 2t_i\right)}[G_{2i-1}(x_1) - G_{2i}(x_1)]\left(\frac{z_i}{t_i} + \frac{1}{2}\right) - \frac{1}{t_i\left(3\sum_{j=i}^{n} t_j - t_i\right)}[G_{2i-2}(x_1) - G_{2i-1}(x_1)]\left(\frac{z_i}{t_i} - \frac{1}{2}\right) \tag{4.30b}$$

At the bottom surface, which corresponds to the *0*th interface, equations (4.30a) and (4.30b) yield in-plane stresses that are proportional to the sum of stress functions, $F_{-1}(x_1) - F_0(x_1)$ and $G_{-1}(x_1) - G_0(x_1)$. Similarly, at the mid-plane, which corresponds to the *n*th interface, the in-plane stresses are proportional to the sum of stress functions, $F_{2n-1}(x_1) - F_{2n}(x_1)$ and $G_{2n-1}(x_1) - G_{2n}(x_1)$. Since the in-plane stresses are single-valued at the bottom surface and the mid-plane, only one independent arbitrary function of x is needed. Therefore, the stress functions $F_{-1}(x_1)$, $G_{-1}(x_1)$, $F_{2n}(x_1)$ and $G_{2n}(x_1)$ are set equal to zero, *i.e.*,

$$F_{-1} = G_{-1} = F_{2n} = G_{2n} = 0 \tag{4.31}$$

Equation (4.31) implies that derivatives of the stress functions of $F_{-1}(x_1)$, $G_{-1}(x_1)$, $F_{2n}(x_1)$ and $G_{2n}(x_1)$ are also equal to zero.

It is noted that the current definition of the stress functions allows the moment equilibrium to be satisfied automatically, as discussed later in this sub-section. If the stress functions had been defined at the interfaces as in the in-plane load case, an additional equation for the moment equilibrium would be required because the condition is not automatically satisfied. This leads to the approach of defining three separate stress functions, using their combinations to express values of the stresses at the interfaces and then using weighted values of these combinations to determine the stresses through the ply depending on the defined through-thickness variation.

The interlaminar shear stresses can be obtained by substituting equation (4.30) into equations (4.2) and (4.3), and performing the required integration on a ply-by-ply

basis. The constants of integration were obtained by imposing interlaminar shear stress continuity at all ply interfaces and the boundary condition of a zero interlaminar shear stress at the outer surface. The resulting expressions for interlaminar shear stresses, σ_{1z} and σ_{2z}, are:

$$\sigma_{1z}^{(i)} = -\frac{1}{2\left(3\sum_{j=i}^{n} t_j - 2t_i\right)}[F'_{2i-1}(x_1) - F'_{2i}(x_1)]\left(\frac{z_i}{t_i} + \frac{1}{2}\right)^2$$

$$+\frac{1}{2\left(3\sum_{j=i}^{n} t_j - t_i\right)}[F'_{2i-2}(x_1) - F'_{2i-1}(x_1)]\left(\frac{z_i}{t_i} - \frac{1}{2}\right)^2$$

$$-\frac{1}{2}\sum_{j}^{i}\left(\frac{1}{\left(3\sum_{k=j}^{n} t_k - t_j\right)}[F'_{2j-2}(x_1) - F'_{2j-1}(x_1)]\right. \tag{4.30c}$$

$$\left. +\frac{1}{\left(3\sum_{k=j-1}^{n} t_k - 2t_j\right)}[F'_{2j-3}(x_1) - F'_{2j-2}(x_1)]\right)$$

$$\sigma_{2z}^{(i)} = -\frac{1}{2\left(3\sum_{j=i}^{n} t_j - 2t_i\right)}[G'_{2i-1}(x_1) - G'_{2i}(x_1)]\left(\frac{z_i}{t_i} + \frac{1}{2}\right)^2$$

$$+\frac{1}{2\left(3\sum_{j=i}^{n} t_j - t_i\right)}[G'_{2i-2}(x_1) - G'_{2i-1}(x_1)]\left(\frac{z_i}{t_i} - \frac{1}{2}\right)^2$$

$$-\frac{1}{2}\sum_{j}^{i}\left(\frac{1}{\left(3\sum_{k=i}^{n} t_k - t_j\right)}[G'_{2j-2}(x_1) - G'_{2j-1}(x_1)]\right.$$

$$\left.+\frac{1}{\left(3\sum_{k=j-1}^{n} t_k - 2t_j\right)}[G'_{2j-3}(x_1) - G'_{2j-2}(x_1)]\right) \tag{4.30d}$$

Similarly, the interlaminar normal stress, σ_{zz}, was obtained by substituting equation (4.30c) into the z-direction equilibrium equation (4.4) and performing the required integration on a ply-by-ply basis. Again, the constants of integration were obtained by imposing interlaminar normal stress continuity at all ply interfaces and the boundary condition of a zero interlaminar normal stress at the outer surface. The resulting expression for the interlaminar normal stress can be expressed as:

$$\sigma_{zz}^{(i)} = \frac{t_i}{6\left(3\sum_{j=i}^{n} t_j - 2t_i\right)}[F''_{2i-1}(x_1) - F''_{2i}(x_1)]\left(\frac{z_i}{t_i} + \frac{1}{2}\right)^3$$

$$- \frac{t}{6\left(3\sum_{j=i}^{n} t_j - t_i\right)}[F''_{2i-2}(x_1) - F''_{2i-1}(x_1)]\left(\frac{z_i}{t} - \frac{1}{2}\right)^3$$

$$- \frac{1}{2}t_i \sum_{j}^{i}\left(\frac{1}{\left(3\sum_{k=j}^{n} t_k - t_j\right)}[F''_{2j-2}(x_1) - F''_{2j-1}(x_1)]\right.$$

$$\left. + \frac{1}{\left(3\sum_{k=j-1}^{n} t_k - 2t_j\right)}[F''_{2j-3}(x_1) - F''_{2j-2}(x_1)]\right)\left(\frac{z_i}{t} - \frac{1}{2}\right) \qquad (4.30e)$$

$$+ t_i \sum_{j}^{i}\left(\left(\frac{1}{3} + \frac{i-j}{2}\right)\frac{1}{\left(3\sum_{k=j}^{n} t_k - t_j\right)}[F''_{2j-2}(x_1) - F''_{2j-1}(x_1)]\right.$$

$$\left. + \left(\frac{2}{3} + \frac{i-j}{2}\right)\frac{1}{\left(3\sum_{k=j-1}^{n} t_k - 2t_j\right)}[F''_{2j-3}(x_1) - F''_{2j-2}(x_1)]\right)$$

As in the case of the assumed stress field under in-plane load, the expression for the stress field in region B is identical to that expressed in equation (4.30) but with different arbitrary functions. Thus, these are not discussed separately and can be inferred from that of region A unless otherwise noted. In such cases, the functions $H_i(x_1)$ and $K_i(x_1)$ are used in place of $F_i(x_1)$ and $G_i(x_1)$ in equation (4.30) for region B.

The boundary conditions at the mid-plane and outer surface of the half-laminate require some of the arbitrary stress functions in x_1 to be equal to zero. According to equations (4.30c) and (4.30d), the interlaminar shear stresses at the bottom surface are

proportional to derivatives of the stress functions, $F_0'(x_1)$ and $G_0'(x_1)$, and the interlaminar normal stress at the outer surface is proportional to the second derivatives of the stress functions, $F_0''(x_1)$. These functions must be equal to zero since the outer surface is traction-free. In addition, since the interlaminar normal stress is anti-symmetric about the thickness of the laminate under bending load, it must vanish at the mid-plane. From equation (4.30e), the interlaminar normal stress at the mid-plane is proportional to $F_{2n}''(x_1)$, which is already equal to zero according to equation (4.31). Thus, the boundary conditions require the following constraints:

$$F_0' = G_0' = F_0'' = 0 \tag{4.32}$$

As in the in-plane load case, all arbitrary functions of x must vanish far away from the cutoffs such that the companion stresses are zero and the CLPT stress field is recovered. This implies that in region A the arbitrary functions converge to zero in the limit of negative x at infinity:

$$\lim_{x_1 \to -\infty} F_i, F_i', F_i'' = 0 \qquad \text{for i = 0 to 2n} \tag{4.33a}$$

$$\lim_{x_1 \to -\infty} G_i, G_i' = 0 \qquad \text{for i = 0 to 2n} \tag{4.33b}$$

Combining equations (4.32) and (4.33), it can be seen that at the mid-plane and outer surface of the half-laminate the derivatives of the stress functions, $F_0'(x_1)$ and $G_0'(x_1)$, are zero. This can be obtained by integrating the equations in (4.32), which results in constants, and setting these constants to zero according to equations (4.33a) and (4.33b).

It is noted that, in general, the assumed stress field for the *i*th ply in equation (4.30) is not only a function of the ply thickness, t_i, but also a function of the thickness of other plies. This complicates the expression for the assumed stress field. This is the result of the requirement that the integral form of the equilibrium equations be satisfied along with the differential form of the equilibrium equations. For a symmetric laminate

under bending, force equilibrium is automatically satisfied because the in-plane stresses are assumed to be anti-symmetric about the mid-plane through the thickness. The moment equilibrium requires that the sum of the integrals of the in-plane stresses from the CLPT and the companion problem multiplied by the moment arm equal the applied moment. However, the CLPT problem for bending is formulated based on moment equilibrium, and thus, the integral of the CLPT in-plane stresses multiplied by the moment arm is equal to the applied moment. This implies that the integral of the companion stresses multiplied by the moment arm at any location along the length of region A is always equal to zero, *i.e.*,

$$\int_{-\frac{h}{2}}^{0} \sigma_{1\alpha} z \, dz = 0 \tag{4.34}$$

where z denotes the global thickness direction coordinate. Since the companion stresses are defined in the local z-coordinate, a relationship between z and z_i is needed to perform the integration:

$$z = z_i - (\sum_{j=i}^{n} t_j - \frac{1}{2} t_i) \tag{4.35}$$

Upon substituting equation (4.35) into equation (4.34), and performing the integrations, the following equation is obtained:

$$\sum_{i=1}^{n} \int_{-\frac{t_i}{2}}^{\frac{t_i}{2}} \sigma_{1\alpha}^{(i)} \left[z_i - (\sum_{j=i}^{n} t_j - \frac{1}{2} t_i) \right] dz = 0 \tag{4.36}$$

This equation shows that in order for the in-plane stresses to satisfy the moment equilibrium equation, they must be, in general, functions of the ply thickness. Substituting equations (4.30a) and (4.30b) into equation (4.36), it can be immediately verified that the current choice of the assumed stress field satisfies moment equilibrium.

The solution methodology to determine the unknown stress functions in the

companion stress field is similar to that used for the in-plane load case as described in section 4.2.1. The principle of minimum total complementary energy is again used to obtain the solutions for the stress functions. Since the applied moment acts only about the x_2-direction, the in-plane strain ε_{22} is assumed to be negligible. Hence, equations (4.30a) through (4.30e) are substituted into the total complementary energy equation in equation (4.18), and the required minimization performed. This leads to two distinct systems of ordinary differential equations, one for region A, and another for region B. The general form of the system of ordinary differential equations is identical to those obtained for the in-plane load case, *i.e.*:

$$\begin{bmatrix} \mathbf{A}_{11} & \mathbf{0} \\ \mathbf{0} & \mathbf{0} \end{bmatrix} \begin{Bmatrix} \mathbf{F} \\ \mathbf{G} \end{Bmatrix}^{IV} + \begin{bmatrix} \mathbf{B}_{11} & \mathbf{B}_{12} \\ \mathbf{B}_{12} & \mathbf{B}_{22} \end{bmatrix} \begin{Bmatrix} \mathbf{F} \\ \mathbf{G} \end{Bmatrix}'' + \begin{bmatrix} \mathbf{C}_{11} & \mathbf{C}_{12} \\ \mathbf{C}_{12} & \mathbf{C}_{22} \end{bmatrix} \begin{Bmatrix} \mathbf{F} \\ \mathbf{G} \end{Bmatrix} = \mathbf{0} \tag{4.37}$$

where

$$\mathbf{F} = [F_1 \quad F_2 \quad \ldots \quad F_{2n-1}]^T \tag{4.38a}$$

$$\mathbf{G} = [G_1 \quad G_2 \quad \ldots \quad G_{2n-1}]^T \tag{4.38b}$$

However, it is emphasized that the values and dimensions of the matrices **A**, **B** and **C** in equation (4.38) are different from those in equation (4.19).

The elements of the matrices, **A**, **B**, and **C** in equation (4.38) are *(2n–1)* by *(2n–1)* sub-matrices. The expressions for the components of these matrices are significantly more complicated and lengthier than those for the in-plane load case, and thus, were evaluated numerically. In order to facilitate the numerical evaluation, each element of the matrices is expressed using the matrix form of the assumed stress functions. For example, the in-plane stress, $\sigma_{11}^{(i)}$, in equation (4.30a) can be expressed in matrix form as,

$$\sigma_{11}^{(i)} = \begin{bmatrix} g_1^{(i)}(z) & g_2^{(i)}(z) & \cdots & g_{2n-1}^{(i)}(z) \end{bmatrix} \begin{Bmatrix} F_1(x) \\ F_2(x) \\ \vdots \\ F_{2n-1}(x) \end{Bmatrix} \equiv \mathbf{g}_{11}^{(i)}\mathbf{F} \tag{4.39a}$$

where $\mathbf{g}_{11}^{(i)}$ is a function of z only. Comparing equations (4.39a) and (4.30a), it can be seen that $\mathbf{g}_{11}^{(i)}$ is equal to:

$$\mathbf{g}_{11}^{(i)} = \begin{Bmatrix} g_1^{(i)}(z_i) \\ \vdots \\ g_{2i-2}^{(i)}(z_i) \\ g_{2i-1}^{(i)}(z_i) \\ g_{2i}^{(i)}(z_i) \\ \vdots \\ g_{2n-1}^{(i)}(z_i) \end{Bmatrix} = \begin{Bmatrix} 0 \\ \vdots \\ -\dfrac{1}{t_i\left(3\sum_{j=i}^{n} t_j - t_i\right)}\left(\dfrac{z_i}{t_i} - \dfrac{1}{2}\right) \\ \dfrac{1}{t_i\left(3\sum_{j=i}^{n} t_j - 2t_i\right)}\left(\dfrac{z_i}{t_i} + \dfrac{1}{2}\right) + \dfrac{1}{t_i\left(3\sum_{j=i}^{n} t_j - t_i\right)}\left(\dfrac{z_i}{t_i} - \dfrac{1}{2}\right) \\ -\dfrac{1}{t_i\left(3\sum_{j=i}^{n} t_j - 2t_i\right)}\left(\dfrac{z_i}{t_i} + \dfrac{1}{2}\right) \\ \vdots \\ 0 \end{Bmatrix} \tag{4.40}$$

Since σ_{11} is a scalar value, and the transpose of a scalar value is itself, σ_{11} can also be expressed as:

$$\sigma_{11}^{(i)} = \sigma_{11}^{(i)T} = \mathbf{F}^T\mathbf{g}_{11}^{(i)T} \tag{4.41}$$

The other components of the assumed stress field in equation (4.30) can be similarly expressed in matrix form for both the undropped and dropped regions:

$$\sigma_{12}^{(i)} = \mathbf{g}_{12}^{(i)}\mathbf{G}' = \mathbf{G}'^T\mathbf{g}_{12}^{(i)T} \tag{4.39b}$$

$$\sigma_{1z}^{(i)} = \mathbf{g}_{1z}^{(i)}\mathbf{F}' = \mathbf{F}'^T\mathbf{g}_{1z}^{(i)T} \tag{4.39c}$$

$$\sigma_{2z}^{(i)} = \mathbf{g}_{2z}^{(i)}\mathbf{G}' = \mathbf{G}'^{T}\mathbf{g}_{2z}^{(i)^T} \tag{4.39d}$$

$$\sigma_{zz}^{(i)} = \mathbf{g}_{zz}^{(i)}\mathbf{F}'' = \mathbf{F}''^{T}\mathbf{g}_{zz}^{(i)^T} \tag{4.39e}$$

Substituting the matrix form of the assumed stress field in equations (4.39a) through (4.39e) into the expression for the total complementary strain energy in equation (4.18) and performing the required minimization yields the expressions for the matrices **A**, **B** and **C**.

For simplicity, consider the contribution from region A to the total complementary strain energy in equation (4.18). The procedure for region B is identical. The first term in equation (4.18) can be expanded as:

$$\begin{aligned}
&\frac{1}{2}\delta\int_{V^A}\tilde{\sigma}^{*A}\mathbf{S}^{*}\tilde{\sigma}^{*A}dV^A \\
&\quad=\frac{1}{2}\delta\int_{V^A}\Big(S_{1111}^{*}{\sigma_{11}}^2+S_{1313}^{*}{\sigma_{13}}^2+S_{3333}^{*}{\sigma_{33}}^2+S_{1212}^{*}{\sigma_{12}}^2+S_{2323}^{*}{\sigma_{23}}^2 \\
&\qquad\qquad+2S_{1133}^{*}\sigma_{11}\sigma_{33}+2S_{1112}^{*}\sigma_{11}\sigma_{12}+2S_{1323}^{*}\sigma_{13}\sigma_{23}+2S_{1233}^{*}\sigma_{12}\sigma_{33}\Big)dV
\end{aligned} \tag{4.42}$$

Substituting equations (4.39a) through (4.39e) into equation (4.42) yields the following equation:

$$\begin{aligned}
&\frac{1}{2}\delta\int_{V^A}\tilde{\sigma}^{*A}\mathbf{S}^{*}\tilde{\sigma}^{*A}dV^A \\
&=\frac{1}{2}\delta\int_{V^A}\Big[S_{1111}^{*}\mathbf{F}^{T}{\mathbf{g}_{11}}^{T}\mathbf{g}_{11}\mathbf{F}+S_{1313}^{*}\mathbf{F}'^{T}{\mathbf{g}_{13}}^{T}\mathbf{g}_{13}\mathbf{F}'+S_{3333}^{*}\mathbf{F}''^{T}{\mathbf{g}_{33}}^{T}\mathbf{g}_{33}\mathbf{F}'' \\
&\quad+S_{1212}^{*}\mathbf{G}^{T}{\mathbf{g}_{12}}^{T}\mathbf{g}_{12}\mathbf{G}+S_{2323}^{*}\mathbf{G}'^{T}{\mathbf{g}_{23}}^{T}\mathbf{g}_{23}\mathbf{G}'+S_{1133}^{*}\Big(\mathbf{F}^{T}{\mathbf{g}_{11}}^{T}\mathbf{g}_{33}\mathbf{F}''+\mathbf{F}''^{T}{\mathbf{g}_{33}}^{T}\mathbf{g}_{11}\mathbf{F}\Big) \\
&\quad+S_{1112}^{*}\Big(\mathbf{F}^{T}{\mathbf{g}_{11}}^{T}\mathbf{g}_{12}\mathbf{G}+\mathbf{G}^{T}{\mathbf{g}_{12}}^{T}\mathbf{g}_{11}\mathbf{F}\Big)+S_{1323}^{*}\Big(\mathbf{F}'^{T}{\mathbf{g}_{13}}^{T}\mathbf{g}_{23}\mathbf{G}'+\mathbf{G}'^{T}{\mathbf{g}_{13}}^{T}\mathbf{g}_{23}\mathbf{F}'\Big) \\
&\quad+S_{1233}^{*}\Big(\mathbf{G}^{T}{\mathbf{g}_{12}}^{T}\mathbf{g}_{33}\mathbf{F}''+\mathbf{F}''^{T}{\mathbf{g}_{12}}^{T}\mathbf{g}_{33}\mathbf{G}\Big)\Big]dV
\end{aligned} \tag{4.43}$$

Note that the volume integral in equation (4.43) reduces to an area integral in the x_1 and z directions for generalized plane deformation cases. Since only the $\mathbf{g}_{ij}$'s are a function of

z, the integration over the z-coordinate can be evaluated before the minimization is performed. This leaves the minimization in equation (4.43) to be performed for the arbitrary stress functions **F** and **G**, which are functions of x_1. Performing the minimization results in the system of ordinary differential equations in the form of equation (4.37), with the components of the matrices **A**, **B** and **C** as:

$$\mathbf{A}_{11} = S^*_{3333}\int_{-\frac{h}{2}}^{0} \mathbf{g}_{33}{}^T \mathbf{g}_{33} dz \tag{4.44}$$

$$\mathbf{B}_{11} = -S^*_{1313}\int_{-\frac{h}{2}}^{0} \mathbf{g}_{13}{}^T \mathbf{g}_{13} dz + S^*_{1133}\left(\int_{-\frac{h}{2}}^{0} \mathbf{g}_{11}{}^T \mathbf{g}_{33} dz + \int_{-\frac{h}{2}}^{0} \mathbf{g}_{33}{}^T \mathbf{g}_{11} dz\right) \tag{4.45}$$

$$\mathbf{B}_{12} = -S^*_{1323}\left(\int_{-\frac{h}{2}}^{0} \mathbf{g}_{13}{}^T \mathbf{g}_{23} dz + \int_{-\frac{h}{2}}^{0} \mathbf{g}_{23}{}^T \mathbf{g}_{13} dz\right) + S^*_{1233}\left(\int_{-\frac{h}{2}}^{0} \mathbf{g}_{12}{}^T \mathbf{g}_{33} dz + \int_{-\frac{h}{2}}^{0} \mathbf{g}_{33}{}^T \mathbf{g}_{12} dz\right) \tag{4.46}$$

$$\mathbf{B}_{22} = -S^*_{2323}\int_{-\frac{h}{2}}^{0} \mathbf{g}_{23}{}^T \mathbf{g}_{23} dz \tag{4.47}$$

$$\mathbf{C}_{11} = S^*_{1111}\int_{-\frac{h}{2}}^{0} \mathbf{g}_{11}{}^T \mathbf{g}_{11} dz \tag{4.48}$$

$$\mathbf{C}_{12} = S^*_{1112}\left(\int_{-\frac{h}{2}}^{0} \mathbf{g}_{11}{}^T \mathbf{g}_{12} dz + \int_{-\frac{h}{2}}^{0} \mathbf{g}_{12}{}^T \mathbf{g}_{11} dz\right) \tag{4.49}$$

$$\mathbf{C}_{22} = S^*_{1212}\int_{-\frac{h}{2}}^{0} \mathbf{g}_{12}{}^T \mathbf{g}_{12} dz \tag{4.50}$$

Since the functions $\mathbf{g}_{ij}$ are polynomials in z, the exact values of the components of each integral can be obtained if the appropriate order of Gauss integration is used [66]. For example, the integrand in equation (4.44) is a polynomial in which the highest power of z

is six. This number can be obtained by noting that the $\mathbf{g}_{33}$ is a polynomial whose highest power of z is three and multiplying by two. Since a polynomial of *(2n–1)* is integrated exactly with *n*th order Gauss integration, a fourth-order Gauss integration needs to be used.

As in the case of the in-plane load, the solution to the system of ordinary differential equations (4.37) yields the stress functions, which can be expressed as a summation of exponential functions, *i.e.*,

$$\mathbf{F}(x_1) = \sum_{j=1}^{3(2n-1)} a_j \Phi_j e^{\lambda_j x_1} \tag{4.51a}$$

$$\mathbf{G}(x_1) = \sum_{j=1}^{3(2n-1)} a_j \Psi_j e^{\lambda_j x_1} \tag{4.51b}$$

where λ_j are the eigenvalues, Φ_j and Ψ_j are the eigenvectors of equation (4.37), and a_j are unknown constants. Note that there are more terms in the expression for the stress function in the bending load case *(3(2n–1)* terms) than the in-plane load case *(3(n–1)* terms). There are more terms in the bending load case since more stress functions are needed to describe the stress state under bending load due to the dual-valued nature of the in-plane stresses at the interfaces. This results in larger **A**, **B** and **C** matrices in equation (4.37). For region B, the general form of stress functions can be obtained in a similar manner as,

$$\mathbf{H}(x_1) = \sum_{j=1}^{3(2m-1)} b_j \Theta_j e^{\mu_j x_1} \tag{4.52a}$$

$$\mathbf{K}(x_1) = \sum_{j=1}^{3(2m-1)} b_j \Gamma_j e^{\mu_j x_1} \tag{4.52b}$$

where μ_j are the eigenvalues, and Θ_j and Γ_j are the eigenvectors of the equation

corresponding to equation (4.37) for region B. The procedures for obtaining the values for a_j and b_j are discussed in the following sections.

4.3 Global Model

In the global model, the load transfer from the undropped region to the dropped region is modeled by considering only the global discontinuities. The global discontinuities are those that arise due to the differences in laminate properties from the undropped region to the dropped region, and due to the termination of the plies. The most effective method to consider the global discontinuities is to assume that the length of the dropoff region is effectively zero. This assumption completely eliminates the need to include the specifics of the discontinuities due to the geometric specifics of the dropoff region. The load transfer from the undropped region to the dropped region across the dropoff region is then assumed to occur directly through the continuous plies only. The triangular region at the tip of the terminated plies is assumed to carry no loads implying that the terminated plies are stress-free at the cutoffs. An illustration of the global model is shown in Figure 4.4.

Mathematically, the two conditions at the cutoffs can be expressed as follows. For each continuous ply, all components of stresses at the cutoffs ($x_1 = 0$) in regions A and B are equal. This condition can be expressed as,

$$\sigma_{1j}^{A}(0,z) - \sigma_{1j}^{B}(0,z) = 0 \tag{4.53}$$

where the superscripts denote the stresses in regions A and B, respectively. It is emphasized that the stresses in equation (4.53) are comprised of the CLPT part and the companion part. The stress-free boundary conditions at the cutoffs were shown in equation (4.7).

The two conditions in equations (4.7) and (4.53) are used to compute the two

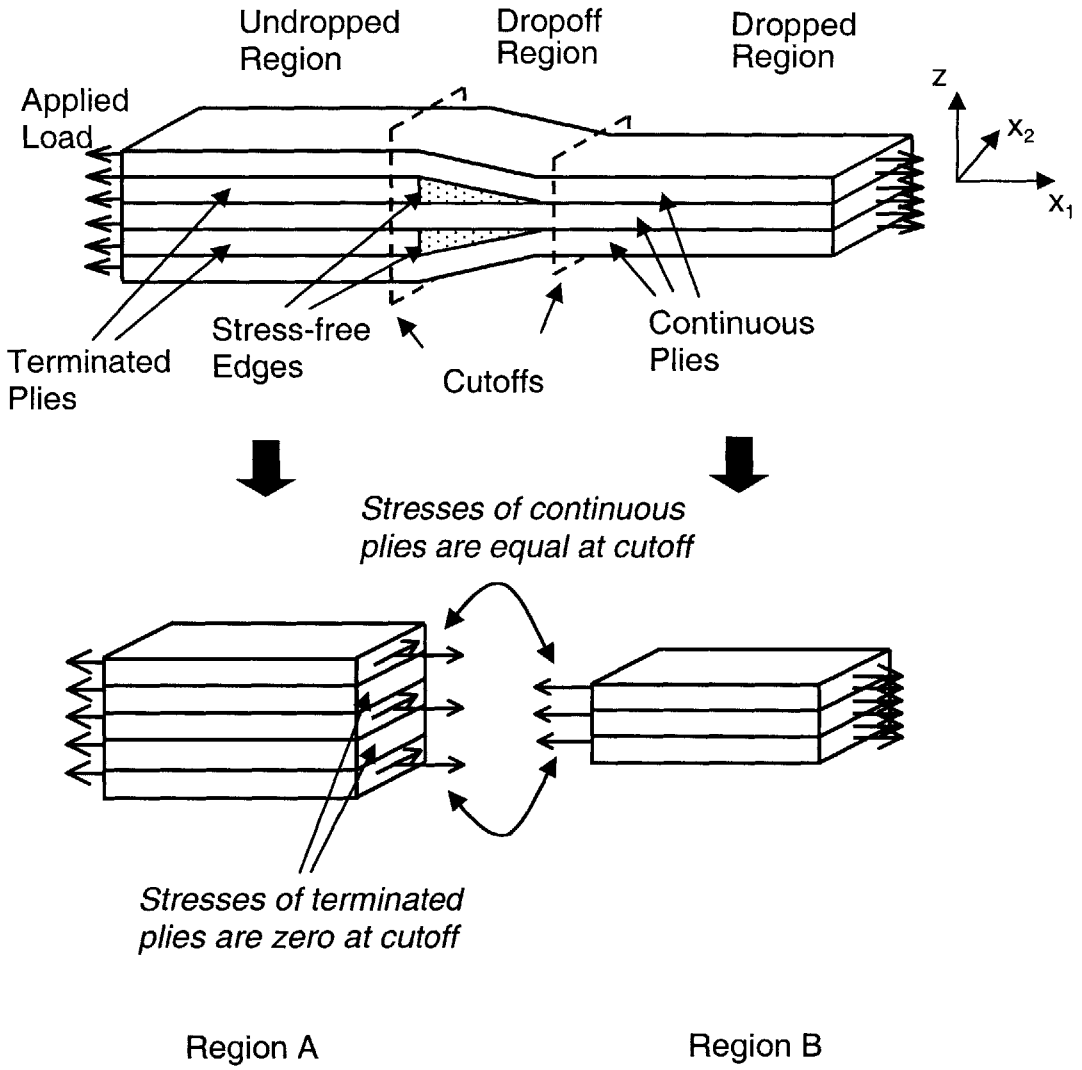

Figure 4.4 Illustration of global model where the stresses of terminated plies are equal to zero at the cutoff, and the stresses of continuous plies are matched at the cutoff.

unknown constants, a_j and b_j, in equations (4.28) and (4.29) for the in-plane load case, and equations (4.51) and (4.52) for the bending load case. The additional boundary conditions that result from performing the minimization in equation (4.18) are also needed to find the unknown constants. However, in general, these additional boundary conditions are very lengthy and complex, and thus, are difficult to implement into an efficient computational procedure. Therefore, an approximate method that is computationally easier to implement is used in the current work. This method is essentially a Ritz method with the unknown constants a_j and b_j as the coefficients and the exponential form of the stress functions obtained in equations (4.28) and (4.29) used as the assumed coordinate functions for the in-plane load case, and equations (4.51) and (4.52) multiplied by their respective eigenvectors used as the assumed coordinate functions for the bending load case. The stress boundary conditions in equations (4.7) and (4.53) are imposed using Lagrange constraints. The total complementary energy is then minimized with respect the Ritz coefficients.

The total complementary energy can be expressed as,

$$\begin{aligned}\pi^* = &\frac{1}{2}\int_{V^A} \tilde{\sigma}^{*A}\mathbf{S}^*\tilde{\sigma}^{*A}dV^A + \frac{1}{2}\int_{V^B} \tilde{\sigma}^{*B}\mathbf{S}^*\tilde{\sigma}^{*B}dV^B \\ &+ \tilde{\psi}_1\left[\tilde{\sigma}^A_{11}(0,z) - \tilde{\sigma}^B_{11}(0,z)\right] + \tilde{\psi}_2\left[\tilde{\sigma}^A_{12}(0,z) - \tilde{\sigma}^B_{12}(0,z)\right] \\ &+ \tilde{\psi}_3\left[\tilde{\sigma}^A_{1z}(0,z) - \tilde{\sigma}^B_{1z}(0,z)\right] + \tilde{\phi}_1\left[\tilde{\sigma}^A_{11}(0,z)\right] + \tilde{\phi}_2\left[\tilde{\sigma}^A_{12}(0,z)\right] + \tilde{\phi}_3\left[\tilde{\sigma}^A_{1z}(0,z)\right]\end{aligned} \tag{4.54}$$

where $\tilde{\psi}_i$ and $\tilde{\phi}_i$ are vectors of Lagrange multipliers for the continuous and terminated plies, respectively. The Lagrange constraints in equation (4.54) are identical to equations (4.7) and (4.53) but expressed in vector form. Since there are *(n–m)* terminated plies, the Lagrange constraints for the terminated plies can be expressed as:

$$\tilde{\sigma}^A_{1j}(0,z) = \left[\sigma^1_{1j}(0,z) \quad \sigma^2_{1j}(0,z) \quad \ldots \quad \sigma^{n-m}_{1j}(0,z)\right]^T \tag{4.55a}$$

For the *m* continuous plies the Lagrange constraints can be expressed as,

$$\tilde{\sigma}_{1j}^{A}(0,z)-\tilde{\sigma}_{1j}^{B}(0,z)=\left[\sigma_{1j}^{1}(0,z)\quad\sigma_{1j}^{2}(0,z)\quad\ldots\quad\sigma_{1j}^{k}(0,z)\right]_{A}^{T}-\left[\sigma_{1j}^{1}(0,z)\quad\sigma_{1j}^{2}(0,z)\quad\ldots\quad\sigma_{1j}^{k}(0,z)\right]_{B}^{T} \tag{4.55b}$$

where the subscripts "A" and "B" in the left-hand side indicate regions A and B, respectively. In the in-plane load case, the stresses in only *(m–1)* plies are matched in equation (4.55b) because the companion stresses in each region already satisfy the force equilibrium equation (4.11). This reduces the number of independent equations by one. In the bending load case, the stresses in all m plies are matched. Thus, the unknown constants, a_j and b_j, in equations (4.28) and (4.29) and equations (4.51) and (4.52) can be completely determined through this procedure.

4.4 Mixed Model

In the global model, the geometry of the dropoff region is not considered. This allows only the global effects of the ply dropoffs to be included in the stress field. Following the building-block approach, the next step is to add more complexity to the global model by considering the geometrical effects in the dropoff region. In the baseline laminate configuration, the geometry in the dropoff region can be defined by the taper angle. Note that a finite taper angle implies a finite length of the dropoff region, unlike the global model where the length of the dropoff region is assumed to be zero. In the mixed model, the load transfer from the undropped region to the dropped region via the tapered geometry in the dropoff region is of key interest. Since the stress field in the dropoff region itself is not sought from the analysis, a rigid model of the tapered geometry that allows the load to be transferred directly from the undropped region to the dropped region is used. An illustration of the baseline laminate configuration modeled as two laminates of uniform thickness with a rigid dropoff region is shown in Figure 4.5.

In general, the dropoff region can be further divided into two regions; the sloped region and the non-sloped region. The two regions are shown in Figure 4.5. There are

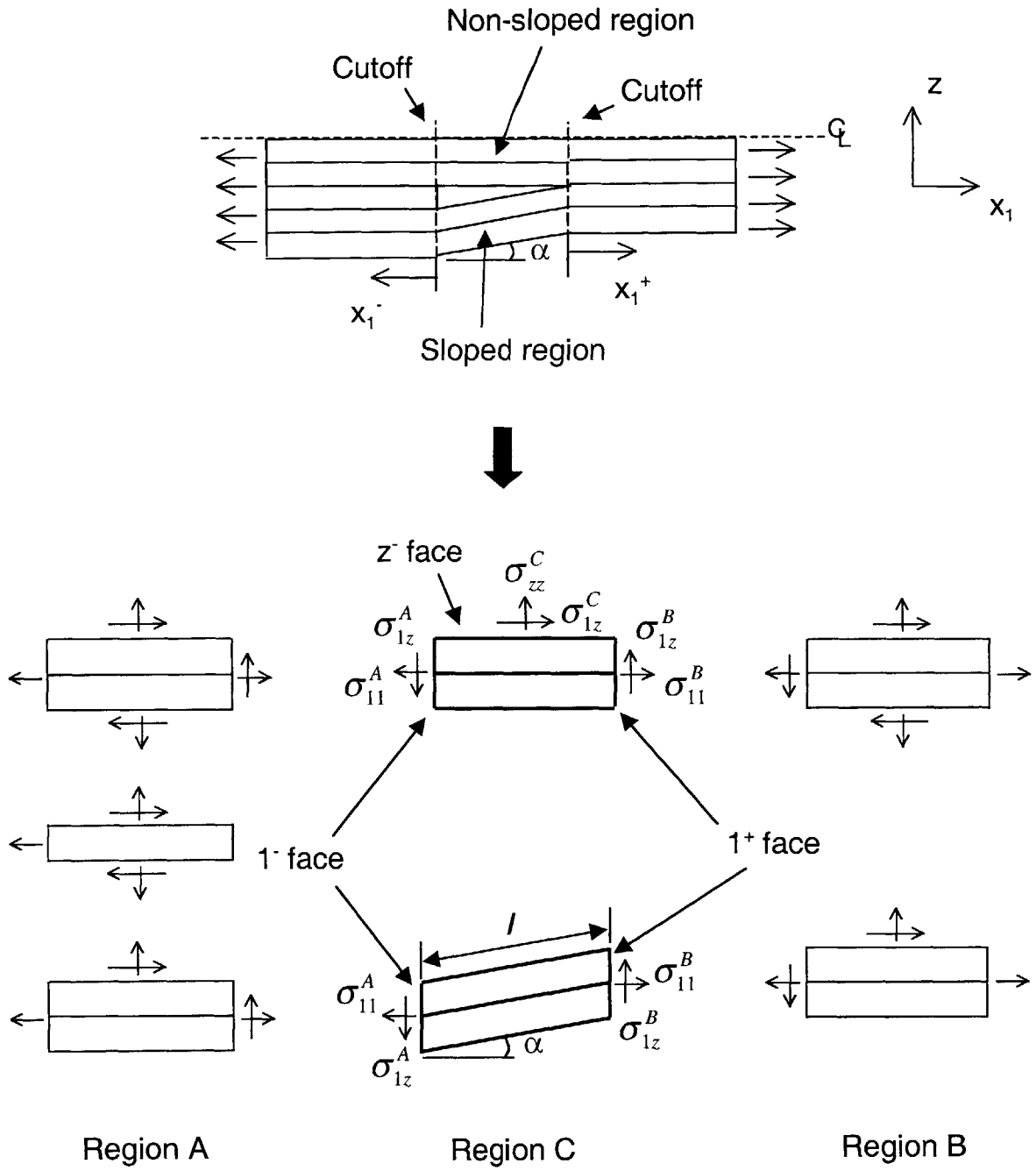

Figure 4.5 Diagram of the mixed model, where *(top)*, the laminate configuration and coordinate system is defined, and *(bottom)* free body diagrams of the undropped, dropoff and dropped regions are shown.

two special cases where only one of these regions would exist. In the case of laminates with external ply dropoffs, only the non-sloped region exists, and in the case of laminates with ply dropoffs located at the mid-plane, only the sloped region exists. At the two cutoff locations, *i.e.*, at $x_1 = 0^+$ and $x_1 = 0^-$, the stresses must be continuous. Thus, the stresses at the interfaces of the cutoffs in the dropoff region can be expressed as stresses in the undropped and dropped regions. The relations between the stresses at the two cutoff locations are found by using the force and moment equilibrium of the sloped and non-sloped regions on a global basis, *i.e.*, the integral form of the equilibrium equations. Since the problem is formulated based on generalized plane deformation assumptions, there are three force equilibrium equations and one moment equation to be considered. Note that due to the assumption that the resin pocket at the tip of the terminated plies carries no load, the upper surface in the sloped region and the lower surface in the non-sloped region in Figure 4.5 are traction-free.

The global equilibrium equations of both the non-sloped and sloped regions are not needed because the equilibrium equations are not independent. In Figure 4.5, the laminate with ply dropoffs is divided into four main regions, the undropped region, the dropped region, the non-sloped region and the sloped region. In each region, the force and moment equilibrium equations must be satisfied. Equilibrium in the undropped and dropped regions are already imposed and satisfied through the judicious selection of the assumed stress field. In addition, equilibrium of the entire laminate is also assumed. This implies that the equilibrium equations of either the non-sloped region or the sloped region are redundant. Since it is more convenient to consider the sloped region due to the traction-free top and bottom surfaces, the equilibrium equations in this region are used in the current work.

From the free body diagram of the sloped region in Figure 4.5, the integral form of the force equilibrium in all three directions requires that:

$$\int_{1^-} \sigma_{1j}^{A}(0,z)dz - \int_{1^+} \sigma_{1j}^{B}(0,z)dz = 0 \tag{4.56}$$

It is noted that the x_2-direction and the corresponding stresses, σ_{12}'s, are not shown in Figure 4.5 to keep the diagram from being too cluttered. Since the stresses are defined on a ply-by-ply basis, equation (4.56) can also be expressed as a sum of the integrals over each ply, *i.e.*:

$$\sum_i \int_{-\frac{t}{2}}^{\frac{t}{2}} \sigma_{1j}^{A(i)} dz - \sum_i \int_{-\frac{t}{2}}^{\frac{t}{2}} \sigma_{1j}^{B(i)} dz = 0 \tag{4.57}$$

The moment equilibrium equation about the x_2-direction of the sloped region can be expressed as,

$$\int_{1^-} \sigma_{11}^{A}(0,z) z\, dz + \int_{1^+} \sigma_{1z}^{B}(0,z) l\cos\alpha\, dz - \int_{1^+} \sigma_{11}^{B}(0,z)(z + l\sin\alpha)\, dz = 0 \tag{4.58}$$

where α is the taper angle and l is the length of the sloped region. As in the case of the force equilibrium equations, the moment equilibrium equations can also be expressed in terms of a summation of the integrals over each ply, *i.e.*:

$$\sum_i \int_{-\frac{t}{2}}^{\frac{t}{2}} \sigma_{11}^{A(i)} z dz + \sum_i \int_{-\frac{t}{2}}^{\frac{t}{2}} \sigma_{1z}^{B(i)} l\cos\alpha\, dz - \sum_i \int_{-\frac{t}{2}}^{\frac{t}{2}} \sigma_{11}^{B(i)} (z + l\sin\alpha) dz = 0 \tag{4.59}$$

Again, it is emphasized that the stresses in equations (4.57) and (4.59) are comprised of both the CLPT part and the companion part.

The force and moment equilibrium equations in the sloped region, as expressed in equations (4.57) and (4.59), relate the stresses at the cutoffs of the undropped and dropped regions. These conditions, along with the conditions that terminated plies carry no load at the cutoffs in equation (4.7) are used to determine the unknown constants, a_j and b_j. The procedure to obtain these constants is similar to that described in section 4.3 for the global model, *i.e.*, they are obtained through the minimization of the total

complementary energy. For the mixed model, the total complementary energy can then be expressed as,

$$\begin{aligned}\pi^* = &\frac{1}{2}\int_{V^A}\tilde{\sigma}^{*A}\mathbf{S}^*\tilde{\sigma}^{*A}dV^A + \frac{1}{2}\int_{V^B}\tilde{\sigma}^{*B}\mathbf{S}^*\tilde{\sigma}^{*B}dV^B \\ &+\psi_j\left[\sum_i\int_{-\frac{t}{2}}^{\frac{t}{2}}\sigma_{1j}^{A(i)}dz - \sum_i\int_{-\frac{t}{2}}^{\frac{t}{2}}\sigma_{1j}^{B(i)}dz\right] + \kappa\left[\sum_i\int_{-\frac{t}{2}}^{\frac{t}{2}}\sigma_{11}^{A(i)}zdz\right. \\ &\left.+\sum_i\int_{-\frac{t}{2}}^{\frac{t}{2}}\sigma_{1z}^{B(i)}l\cos\alpha dz - \sum_i\int_{-\frac{t}{2}}^{\frac{t}{2}}\sigma_{11}^{B(i)}(z+l\sin\alpha)dz\right] \\ &+\tilde{\phi}_1\left[\tilde{\sigma}_{11}^A(0,z)\right] + \tilde{\phi}_2\left[\tilde{\sigma}_{12}^A(0,z)\right] + \tilde{\phi}_3\left[\tilde{\sigma}_{1z}^A(0,z)\right]\end{aligned} \tag{4.60}$$

where ψ_j, κ and $\tilde{\phi}_i$ are Lagrange multipliers for the force and the moment equilibrium in the sloped region, and terminated plies in the undropped region, respectively. The Lagrange multiplier for the terminated plies, $\tilde{\phi}_i$, is a vector, and the Lagrange constraints are identical to equation (4.55a). As in the global model, the stress field in laminates with ply dropoffs under both in-plane and bending loads can be obtained using the mixed model.

4.5 Model for Laminates with Existing Delaminations

Experiments have shown that some types of laminates with ply dropoffs have a tendency to delaminate in the undropped region [17]. Such a delaminated configuration is shown in Figure 2.3. In order to obtain the stress field in such configurations, a model for laminates with existing delaminations in the undropped region was developed as an extension of the analytical models.

In the analytical model for laminates with existing delaminations, the baseline laminate with delaminations in the undropped region is considered. The analysis is restricted to delaminations that occur symmetrically about the mid-plane and equal in length. A diagram of such a laminate is shown in Figure 4.6. In addition, to simplify the

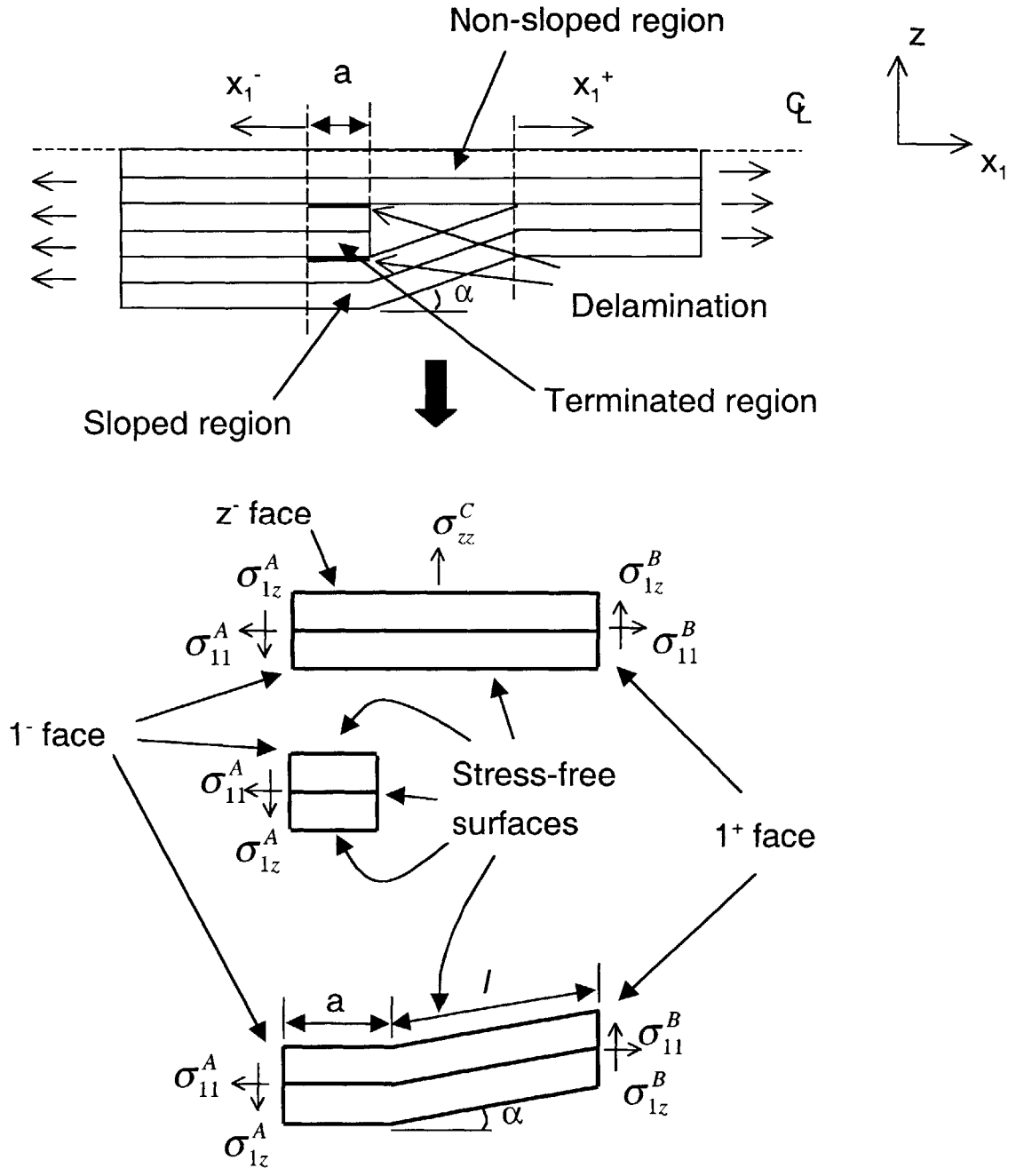

Figure 4.6 Diagram of the model with existing delamination, where *(top)*, the laminate configuration and coordinate system is defined, and *(bottom)* free body diagrams of the undelaminated part of the undropped region, the delaminated region, and dropped regions are shown.

analysis, the length of the delamination is assumed to be at least as long as the decay length for the stresses in the delaminated region. The decay length in a laminate with a semi-infinite delamination is defined as the distance from the delamination tip ($x_1^- = 0$) to the point where the magnitude of the interlaminar shear stress, σ_{1z}, has decayed to 1% of its maximum value. Under such a condition, the stress field away from the delaminated region will not be affected by the length of the delamination.

The general formulation discussed in section 4.2 is applicable for this model as well. However, unlike the previous two models, the laminate is divided into three regions corresponding to the undropped region that has not delaminated, the delaminated region including the dropoff region, and the dropped region. An illustration of the model is shown in Figure 4.6. The load transfer from the undelaminated part of the undropped region to the dropped region is modeled by assuming that the delaminated region including the dropoff region is rigid. Therefore, as in the mixed model, the load transfer occurs through forces and moments near the cutoffs of the delaminated region. It is noted that this model is developed only for the in-plane loading condition. This development does show, however, that further extensions to the current analytical framework based on the building-block approach can be made.

The delaminated region is further divided into three regions; the sloped region, the non-sloped region and the terminated region. Since it is assumed that the delaminated region is rigid, no deformation will occur in this region. Therefore, it is further assumed that the delamination interfaces of the sloped region and the terminated region, and the non-sloped region and the terminated region are stress-free. This assumption is also consistent with the fact that the load across the delaminated region is only transmitted through the cutoffs. However, these assumptions may be an over-simplification of the problem because laminates under in-plane load would tend to deform in a manner such that the terminated region and the sloped and non-sloped regions are in contact. Such contact would give rise to interlaminar normal stresses. In addition, the interlaminar

shear stresses at the delamination interfaces may exist due to friction. Thus, the current analysis is expected to yield a first order approximation of the general stress field in the undelaminated part of the undropped region and the dropped region. Modeling the contact and friction behavior at the delamination interfaces is beyond the scope of this work. Such models require the geometry of the laminate to be specified. This should be considered at a higher level of complexity in terms of the building-block approach.

The force and moment equilibrium equations of the three regions in the delaminated region can be obtained by considering the free body diagram in Figure 4.6. As in the mixed model, the global equilibrium equations in each of the three delaminated regions are not independent. Since the equilibrium of the entire laminate and the undropped and dropped regions are already satisfied, the equilibrium equations of only two of the three regions are independent. Equilibrium of the sloped region and the terminated region are considered in this work.

From the free body diagram of the sloped region in Figure 4.6, the force equilibrium equations in the x_1, x_2 and z-directions can be obtained and expressed as:

$$\int_{1^-} \sigma_{1j}^{A}(0,z)dz - \int_{1^+} \sigma_{1j}^{B}(0,z)dz = 0 \tag{4.61}$$

Note that this expression is identical to the force equilibrium equations for the sloped region in the mixed model (see equation (4.56)). This expression can be simplified as a summation of the integrals of the stresses on a ply-by-ply basis, *i.e.*:

$$\sum_i \int_{-\frac{t}{2}}^{\frac{t}{2}} \sigma_{1j}^{A(i)} dz - \sum_i \int_{-\frac{t}{2}}^{\frac{t}{2}} \sigma_{1j}^{B(i)} dz = 0 \tag{4.62}$$

The moment equilibrium equation about the x_2-direction can be expressed as:

$$\int_{1^-} \sigma_{11}^{A}(0,z) z\,dz + \int_{1^+} \sigma_{1z}^{B}(0,z)(a + l\cos\alpha)dz - \int_{1^+} \sigma_{11}^{B}(0,z)(z + l\sin\alpha)dz = 0 \tag{4.63}$$

Again, this expression can be simplified as:

$$\sum_i \int_{-\frac{t}{2}}^{\frac{t}{2}} \sigma_{11}^{A(i)} z dz + \sum_i \int_{-\frac{t}{2}}^{\frac{t}{2}} \sigma_{1z}^{B(i)} (a + l\cos\alpha) dz - \sum_i \int_{-\frac{t}{2}}^{\frac{t}{2}} \sigma_{11}^{B(i)} (z + l\sin\alpha) dz = 0 \quad (4.64)$$

For the terminated region, the force equilibrium equations in the x_1, x_2 and z-directions can be expressed as:

$$\int_{1^-} \sigma_{1j}^{A}(0,z) dz = 0 \quad (4.65)$$

This expression can be simplified by substituting the ply-by-ply stress field into equation (4.65). This yields:

$$\sum_i \int_{-\frac{t}{2}}^{\frac{t}{2}} \sigma_{1j}^{A(i)} dz = 0 \quad (4.66)$$

This equation differs from equation (4.7) in that the integral of the stresses at the cutoffs in the terminated ply group are required to be zero instead of the stresses in each ply being zero. Thus, in general, the stresses in each ply at the cutoffs are not equal to zero. Note that the stress field in the terminated region is self-equilibrating and any non-zero stresses at the 1^- face must decay to zero at the stress-free end. The moment equilibrium equation about the x_2-direction is found to be:

$$\int_{1^-} \sigma_{11}^{A}(0,z) z\, dz = 0 \quad (4.67)$$

Similarly, this equation can be simplified as:

$$\sum_i \int_{-\frac{t}{2}}^{\frac{t}{2}} \sigma_{11}^{A(i)} z dz = 0 \quad (4.68)$$

Note that equations (4.66) and (4.68) describe the equilibrium conditions at the cutoffs for the terminated plies. These equations are used in place of the stress-free conditions at

the cutoffs that were used for the global and mixed models in equation (4.7).

The equilibrium equations in the sloped and terminated regions are used to obtain the total complementary energy. Using Lagrange multipliers, the total complementary energy can be expressed as,

$$\begin{aligned}\pi^* = &\frac{1}{2}\int_{V^A}\tilde{\sigma}^{*A}\mathbf{S}^*\tilde{\sigma}^{*A}dV^A + \frac{1}{2}\int_{V^B}\tilde{\sigma}^{*B}\mathbf{S}^*\tilde{\sigma}^{*B}dV^B \\ &+\psi_j\left[\sum_i\int_{-\frac{t}{2}}^{\frac{t}{2}}\sigma_{1j}^{A(i)}dz - \sum_i\int_{-\frac{t}{2}}^{\frac{t}{2}}\sigma_{1j}^{B(i)}dz\right] + \kappa\left[\sum_i\int_{-\frac{t}{2}}^{\frac{t}{2}}\sigma_{11}^{A(i)}zdz\right. \\ &\left.+\sum_i\int_{-\frac{t}{2}}^{\frac{t}{2}}\sigma_{1z}^{B(i)}(a+l\cos\alpha)dz - \sum_i\int_{-\frac{t}{2}}^{\frac{t}{2}}\sigma_{11}^{B(i)}(z+l\sin\alpha)dz\right] \\ &+\phi_1\left[\sum_i\int_{-\frac{t}{2}}^{\frac{t}{2}}\sigma_{11}^{A(i)}dz\right] + \phi_2\left[\sum_i\int_{-\frac{t}{2}}^{\frac{t}{2}}\sigma_{11}^{A(i)}\bar{z}dz\right]\end{aligned} \tag{4.69}$$

The procedure for obtaining the unknown constants, a_j and b_j, is similar to those for the global and mixed models. Note that for this model, only the in-plane loading case is considered. Therefore, the assumed stress field in equations (4.8) expressed in terms of the exponential functions in equations (4.28) and (4.29) multiplied by the eigenvectors and the unknown constants, a_j and b_j, are substituted for the stress field in equation (4.69). The total complementary energy is then minimized to obtain the unknown constants.

Extension to laminates under bending load can be made using the same solution procedure described herein for laminates under the in-plane load. However, in this case, the assumed stress field equations for the bending load case in equation (4.30) expressed in terms of the appropriate exponential functions need to be substituted into equation (4.69).

4.6 Computer Implementation

In order to solve for the stress field in laminates with ply dropoffs using the three

analytical models described in the previous sections, a computer code was written using the program Matlab®. The code for the analytical models, called "Matlab script", is listed in Appendix A for the in-plane load case and in Appendix B for the bending load case.

The structure of the Matlab codes follows the general solution procedure described in the previous sections and can be divided into two parts. The first part of the scripts is identical for all three analytical models. In this part, the user is prompted to input the laminate configuration and material properties. The three dimensional ply-by-ply material constants are found and the CLPT solutions obtained. Subsequently, the components of the **A**, **B** and **C** matrices shown in equation (4.19) for the in-plane load case, and in equation (4.37) for the bending load case are determined. For the in-plane load case, equations (4.21) through (4.27) are implemented in the script, whereas in the bending load case, equations (4.44) through (4.50) are evaluated using Gauss integration points and weights. The matrices **A**, **B** and **C** are used to obtain the eigenvalues and eigenvectors for equations (4.28) and (4.29), and (4.51) and (4.52). In the second part, the unknown constants a_j and b_j are obtained using one of the three equations (4.54), (4.60) and (4.69), depending on which model is being used.

The stress distribution in the undropped and dropped regions, that are obtained as results of the analysis, can be viewed in the form of plots at any point along either the x_1-direction or the z-direction. All the components of stresses can be viewed using the scripts.

CHAPTER 5

EXPERIMENTS

The experimental procedures designed and used to observe and characterize static and fatigue behavior of laminates with simple dropoff configurations under in-plane load are described in this chapter. The objective of the experimental work is to obtain definitive trends of damage/delamination occurrences to help better understand the overall effects of ply dropoffs. Such trends can be obtained through a set of systematic experiments on laminates with ply dropoffs. To this end, two parameters were selected and varied to investigate their effects on damage/delamination of composite laminates. The complete test matrix, including the two parameters and associated levels, is described in the first section. In order to be able to compare the results from the experimental work with those from the analytical work, it is important for the geometry of the specimens to closely match that of the baseline laminate configuration. The specimen geometry chosen for the experimental work is described in the second section. In the third section, the procedures used to manufacture the coupon specimens are described. Particular attention was taken to manufacture high quality specimens consistently and to minimize random irregularities. Finally, the testing procedures including the methods used to detect damage/delamination during the static and fatigue tests are described in the fourth section.

5.1 Test Matrix

As discussed in Chapter 2, previous experimental investigations of laminates with ply dropoffs have shown that many factors affect the failure load and/or the onset of damage. These factors include the number of terminated plies, the layup of the

terminated ply group, and the geometry of the dropoff region. However, the individual and combined effects of such factors are not yet clearly understood. The main reason for this lack of understanding, despite numerous experimental investigations, is the specific laminate configurations considered in the previous experiments. Results from such case-specific experiments are limited in their applicability, and have hindered the acquisition of a general understanding of the effects of ply dropoffs.

In the current work, a systematic experimental program with a test matrix in which two parameters are varied at different levels is considered to help better understand their effects. The two key factors are the number of terminated plies in the dropoff region and the location of terminated plies through the thickness of the laminate. These factors were chosen because they are fundamental parameters that define the laminate, and also because it is relatively easy to manufacture such laminates. In addition, the effect of these factors on the interlaminar stress field can be analyzed using the analytical models and thereby compared with experimental results. The number of terminated plies is varied between four and eight, and three locations for the terminated plies are considered. To eliminate the in-plane and bending coupling effect due to the geometry, the terminated plies are placed symmetrically about the mid-plane of the laminate across the thickness. In addition, laminates with 0° plies are used to eliminate elastic mismatch from ply to ply. This eliminates the possibility of delamination due to free edge effects that may interact with the effects of ply dropoffs and further complicate the damage/delamination process in the laminate.

The number of plies in the undropped region for all specimens was chosen to be sixteen. Thus, for the set of laminates with four terminated plies, the number of plies in the dropped region is twelve; and for the set of laminates with eight terminated plies, the number of plies in the dropped region is eight. Note that for the former case, two plies are terminated on each side of the laminates about the mid-plane for symmetry, while for the latter case, four plies are terminated on each side about the mid-plane. All terminated

plies are dropped in a group of two plies in order to avoid the possibility of random, large void formation in the resin pockets. Thus, for the set of laminates with eight terminated plies, there are two distinct steps in the dropoff region due to the termination.

Three locations are considered for the terminated plies through the thickness of the laminate. For one set of laminates, the terminated plies are located at the top and bottom surfaces. This configuration is called the *external dropoffs*. For the other two sets of laminates, the terminated plies are in the interior regions of the laminate. These configurations are called the *internal dropoffs*. Two different internal ply dropoff configurations are considered with the terminated plies of one set of laminates located closer to the top and bottom surfaces and those of another set of laminates located further away from these surfaces. The complete test matrix is shown in Table 5.1.

Static and cyclic tensile tests were performed on the specimens. For each type of specimen, four static tests and three cyclic tests were conducted. Static tests were conducted to obtain damage/delamination initiation loads and modes, and the location at which it initiates. Cyclic tests were conducted to obtain the number of cycles to damage/delamination initiation and growth characteristics.

5.2 Specimen Geometry and Material

The overall geometry of the specimens with ply dropoffs is similar to that of standard composite tensile test coupons found in the ASTM standard [67]. The coupon specimens are 350 mm in length and 31 mm in width. The ply dropoffs are located at the mid-section of the coupon along its length. Glass/polyester tabs, with lengths of 50 mm and widths of 31 mm, are bonded at the two ends of the coupon specimens to prevent stress concentrations and resulting premature failure at the grips of the mechanical testing machine. Since only symmetric specimens are considered, no bending is induced by the thickness difference in the undropped and dropped regions. The tabs are beveled at an angle of 30° on one side to ensure that the load transfer from the grips to the coupon

Table 5.1 Test Matrix

Specimen Type		Layup	Number of Static Tests	Number of Cyclic Tests
Number of Terminated Plies	Dropoff Location			
4	External	$[0_{2D}/0_6]_s$	4	3
	Internal	$[0_2/0_{2D}/0_4]_s$	4	3
	Internal	$[0_4/0_{2D}/0_2]_s$	4	3
8	External	$[0_{4D}/0_4]_s$	4	3
	Internal	$[0_2/0_{4D}/0_2]_s$	4	3
	Internal	$[0_3/0_{4D}/0]_s$	4	3

specimen occurs smoothly. Due to the use of the tabs, the length of the test section is 250 mm. For laminates with internal dropoffs, a taper angle of 7° in the dropoff region was used based on actual geometries of composite flexbeams. For laminates with external dropoffs, a sudden dropoff exists between the undropped region and the dropped region with no taper. A diagram of the specimen geometry is shown in Figure 5.1.

This geometry allows the undropped and dropped regions to be significantly longer than the dropoff region. The dropoff region must be as far away from the tabs as possible for two reasons. One is that in the baseline laminate configuration, the undropped and dropped regions were assumed to be sufficiently long such that the effects of the load transfer in the dropoff region do not affect regions far away from the dropoff region. Another reason is that the load is introduced to the coupon specimen through the grips, and therefore, is not the desired uniform in-plane load that should be applied at the test section. There is a complex three-dimensional state of stress near the grips that gradually transforms, within approximately a tab length, to uniform in-plane load according to St. Venant's principle.

All specimens were made of AS4/3501-6 graphite/epoxy composite from Hexcel®. The raw composite material is supplied in the form of 375 mm wide pre-impregnated unidirectional tape (or pre-preg) in a roll and stored at temperatures below −18°C to prevent curing. This fiber/resin system has been used extensively at TELAC, and the manufacturing procedures and material properties are well-known. The material properties are shown in Table 5.2.

5.3 Manufacturing Procedures

As discussed in Chapter 2, there may be significant differences between the idealized and the actual geometries of laminates with ply dropoffs. Due to manufacturing irregularities, actual laminates may contain defects such as voids, kinked plies, irregular

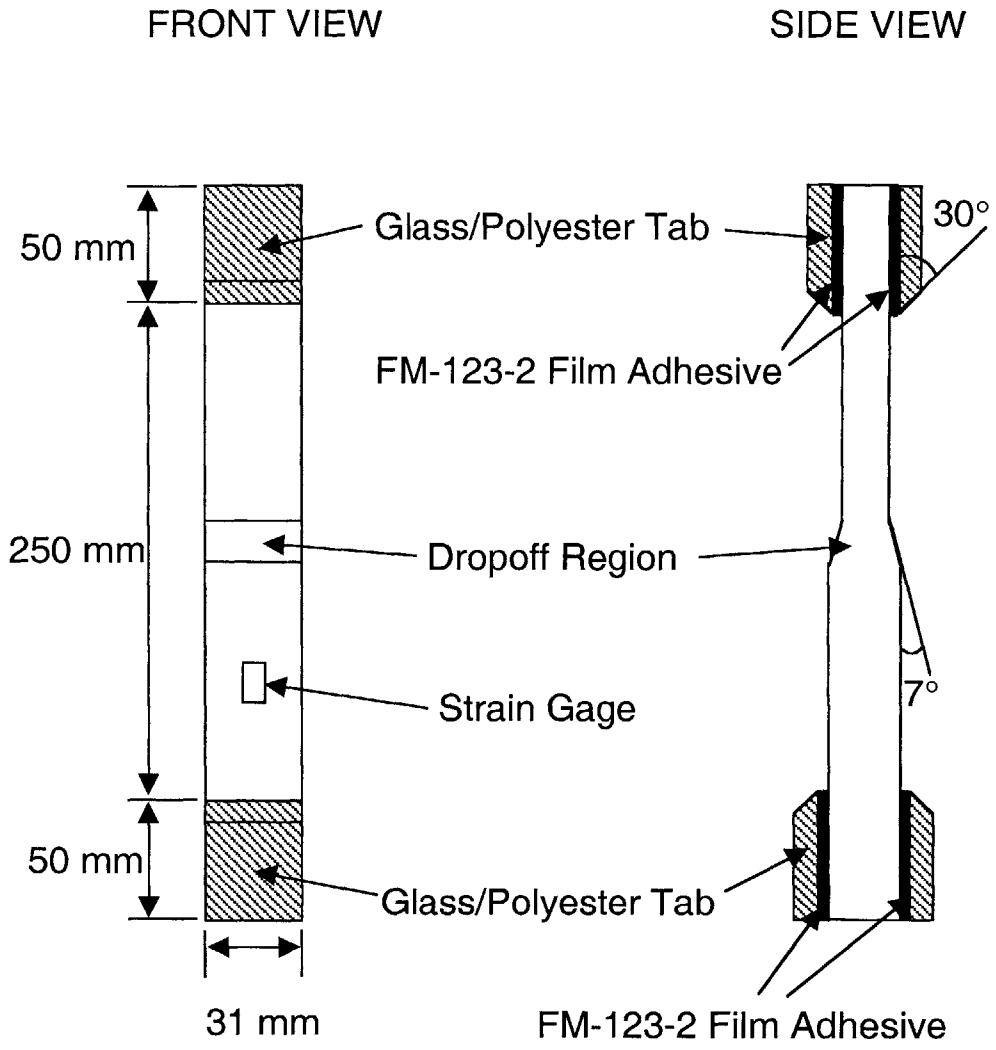

Figure 5.1 Geometry of coupon specimens.

Table 5.2 Material Properties of AS4/3501-6 Composite System[1]

Property	AS4/3501-6
E_L	142 GPa
E_T	9.81 GPa
E_Z	9.81 GPa
G_{LT}	6.0 GPa
G_{LZ}	6.0 GPa
G_{TZ}	4.8 GPa
ν_{LT}	0.30
ν_{LZ}	0.30
ν_{TZ}	0.34
t	0.132 mm

[1] From Hexcel®.

tapers and misaligned termination of plies that are not represented in the idealization. Since stress fields in such laminates may differ significantly from those obtained for the idealized geometry [34], the damage/delamination characteristics may also be very different. In addition, since these defects are not homogeneous and may differ from specimen to specimen, they would further hinder efforts to identify the precise effects of ply dropoffs. Therefore, it is essential that specimens with the least amount of defects be produced consistently. Although some of the previous investigations have cited the occurrence of such defects, few have documented methods to suppress the formation of such.

Many of the defects found in laminates with ply dropoffs occur in the dropoff region. Some defects such as misaligned termination of plies may occur due to human errors during the layup process, while others such as the formation of voids and irregular tapers may occur due to material properties and ambient conditions during the curing process. The former type of defects can be controlled within finite tolerances through careful layup procedures. Although the latter type of defects cannot be controlled as easily, they can be suppressed by ensuring good consolidation in the dropoff region. This can be implemented by the use of composite spacers. Pre-cured composite spacers with one edge of the spacers beveled to the desired taper angle are used as molds that fit into the dropoff and dropped regions of the specimen. The spacers allow the top and bottom surfaces of the cure assembly to be flat such that uniform pressure can be applied to achieve good consolidation in the composite part. Note that for specimens with external ply dropoffs there is no taper, and thus, the composite spacers do not need to be beveled in these cases. A diagram of the composite part/spacer assembly is shown in Figure 5.2.

The main advantage of using composite spacers as molds instead of conventional metallic molds is that the thickness of the composite spacers can be designed to match the desired thickness of the terminated ply group with great ease. For the current experimental work, composite spacers with thicknesses equal to two plies and four plies

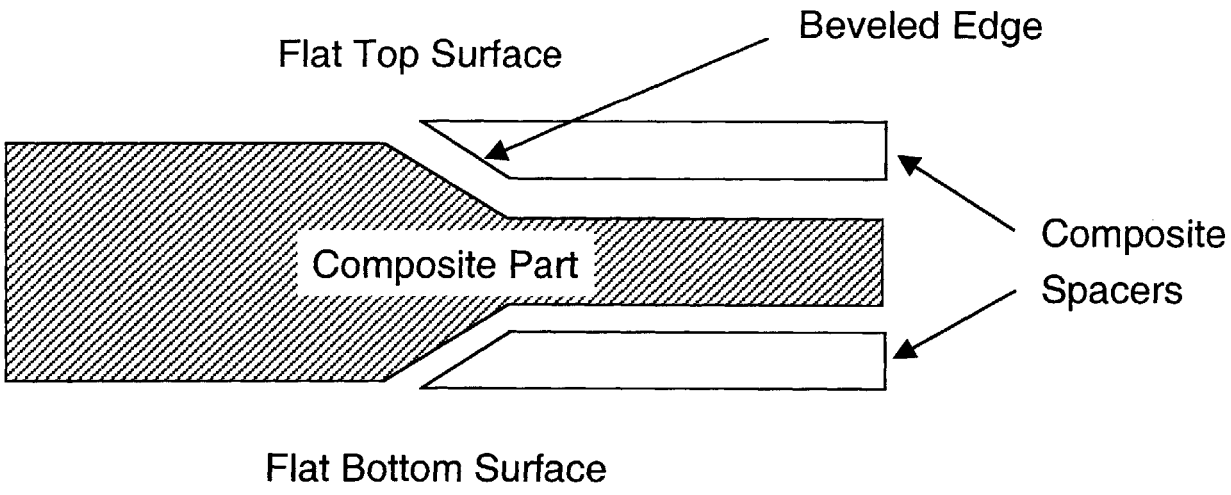

Figure 5.2 Illustration of composite part/spacer assembly used to manufacture laminates with ply dropoffs.

are needed to manufacture specimens with four and eight ply dropoffs, respectively. Using metals, it would be more difficult to manufacture molds to such specifications.

The manufacturing procedure is a two-step process. The first step is to manufacture the composite laminates to be used as spacers and to bevel the spacers at a constant angle across one edge. The second step is to manufacture the specimens with ply dropoffs using the spacers. To simplify the manufacturing process, composite laminates with dimensions of 350 mm in length by 300 mm in width are manufactured and cut into coupon specimens with dimensions of 350 mm by 31 mm. A 350 mm by 300 mm laminate yields up to eight coupon specimens of the desired dimensions after trimming the edges. Therefore, one laminate for each type of specimen needs to be manufactured to obtain all of the specimens for the static and cyclic tests. Based on the dimensions of the composite laminate, the dimensions of the composite spacers need to be 175 mm in length and 300 mm in width. The manufacturing procedure for the composite spacer is described in the following sub-section. This is followed by the manufacturing procedure for the specimens.

5.3.1 Composite Spacers

As previously described, composite spacers with two different thickness are needed to manufacture the specimens in the test matrix. The spacers with two plies must have a unidirectional layup to prevent warping, and thus, a layup of $[0_2]$ was chosen. The layup of the spacers with four plies was chosen to be $[0/90]_s$ for convenience in manufacturing. Composite laminates with dimensions of 350 mm by 300 mm were manufactured and then cut to the required dimensions of the spacer using a milling machine. For alignment purposes, the dimensions of the spacers were 10 mm wider than the dimensions of the dropped region. This is discussed further when the cure setup is described. All laminates with 8-ply dropoffs can be manufactured using a pair of 4-ply spacers, and all laminates with 4-ply dropoffs can be manufactured using a pair of 2-ply spacers. Since the spacers are reusable, only two pairs of spacers are required to

manufacture all the laminates. However, in order to manufacture multiple composite laminates in one cure cycle, four spacers of each type were manufactured. The $[0_2]$ spacer is very brittle in the direction perpendicular to the fibers and may break easily. Thus, an extra set of $[0_2]$ spacers was manufactured.

Since the spacers are flat composite laminates, standard manufacturing procedures can be used [68]. The pre-preg is cut using a 350 mm by 300 mm aluminum template covered with non-porous teflon and razor knifes, and laid up on a layup jig in the appropriate lamination sequence. Once the laminate has been laid up, it is put on an aluminum cure plate and the cure assembly is prepared by setting the cure materials. The entire cure assembly is covered with vacuum bagging. A 0.9 m diameter by 1.5 m long autoclave is used to apply the appropriate combination and sequence of heat, pressure and vacuum required to cure the composite laminates. The manufacturer's recommended cure cycle for the AS4/3501-6 composite material is shown in Figure 5.3.

Initially, the spacers were beveled using a 15 cm-wide belt sander. However, this method yielded uneven angles along the edge of the spacer due to the vibration of the belt sander table. For the $[0_2]$ spacers with a thickness of approximately 0.27 mm, small vibrations can lead to large variations in the beveled angles. The uneven surface of the metal backing plate behind the sanding belt also contributed to make it practically impossible to bevel the long edge of the spacers at a constant angle. Therefore, a beveling table was built such that the spacers can be beveled to a smooth and constant angle. The beveling table consists of a 500 mm long by 500 mm wide by 50 mm thick block of aluminum with a groove across the length, and a small fiber-glass tool-piece with sandpaper attached to a beveled face. The fiber-glass tool-piece is 63 mm long by 13 mm wide by 3 mm thick in size and attached via a bolt to a sliding bar of dimensions 500 mm long by 20 mm wide by 15 mm thick that fits snug in the groove. One face of the tool-piece is beveled to the desired angle of 7° using the belt sander. Due to its thickness and width, the fiber-glass tool-piece is less susceptible to the vibration and

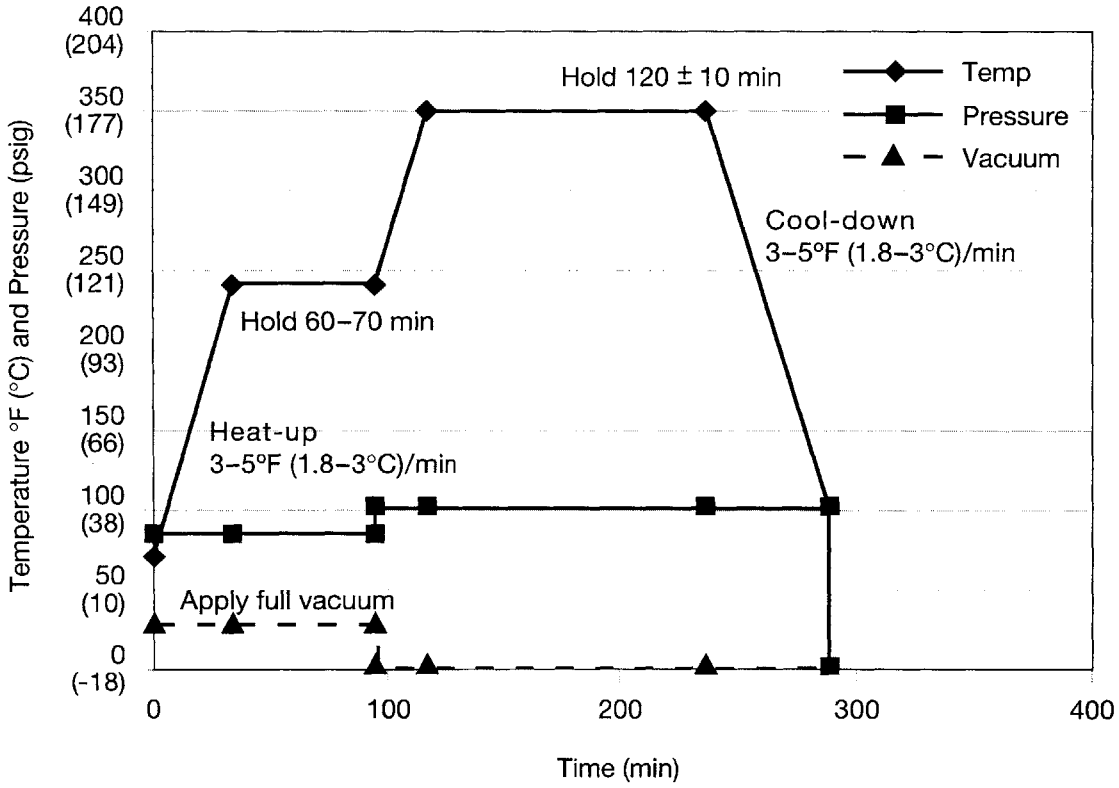

Figure 5.3 Manufacturer's recommended cure cycle for the 3501-6 epoxy matrix (from Hexcel® product data sheet).

uneven metal plate, and an accurate constant angle can be obtained. A diagram of the beveling table is shown in Figure 5.4.

The procedure for beveling the spacer using the beveling table is as follows. The spacer is set and fixed on the level, rectangular beveling table with the groove that runs across the length of the table parallel to the edge. Double-sticky tape is used to fix the spacer flat on the beveling table. At this point, the spacer is perfectly aligned with the edge of the groove. The sliding bar is placed into the groove such that the sand paper attached to the fiber/glass tool-piece touches the edge of the spacer. A 1800-grit sandpaper is used in performing wet-sanding to ensure that a smooth beveled surface is obtained. The edge of the spacer is beveled by sliding the tool-piece attached to the bar back and forth along the groove. Once the spacer is beveled, it is cut to the appropriate dimensions using the milling machine. The angles at different cross-sections of the spacers were measured and found to vary by approximately $\pm 0.2°$. This is a significant improvement over the belt sander where the angles were observed to vary by more than $\pm 1°$.

5.3.2 Laminate Layup and Curing Procedures

The manufacturing procedure for the composite laminates with ply dropoffs begins with cutting and laying up the pre-preg for the curing procedure. The pre-preg is cut to the desired dimensions using razor knifes around templates of three different dimensions. These templates are also covered with non-porous teflon to prevent sticking to the pre-preg. Two templates are used to cut the pre-preg to the size of the terminated plies, while the third template is used to cut the pre-preg to the size of the continuous plies. The dimensions of the templates for the terminated plies are 350 mm by 175 mm and 350 mm by 177 mm. The latter template is used for the slightly longer terminated plies in the specimens with 4-ply dropoffs where dropoffs occur in two distinct steps. The dimension of the third template is 350 mm by 300 mm.

After cutting, the pre-preg is laid up according to the appropriate lamination

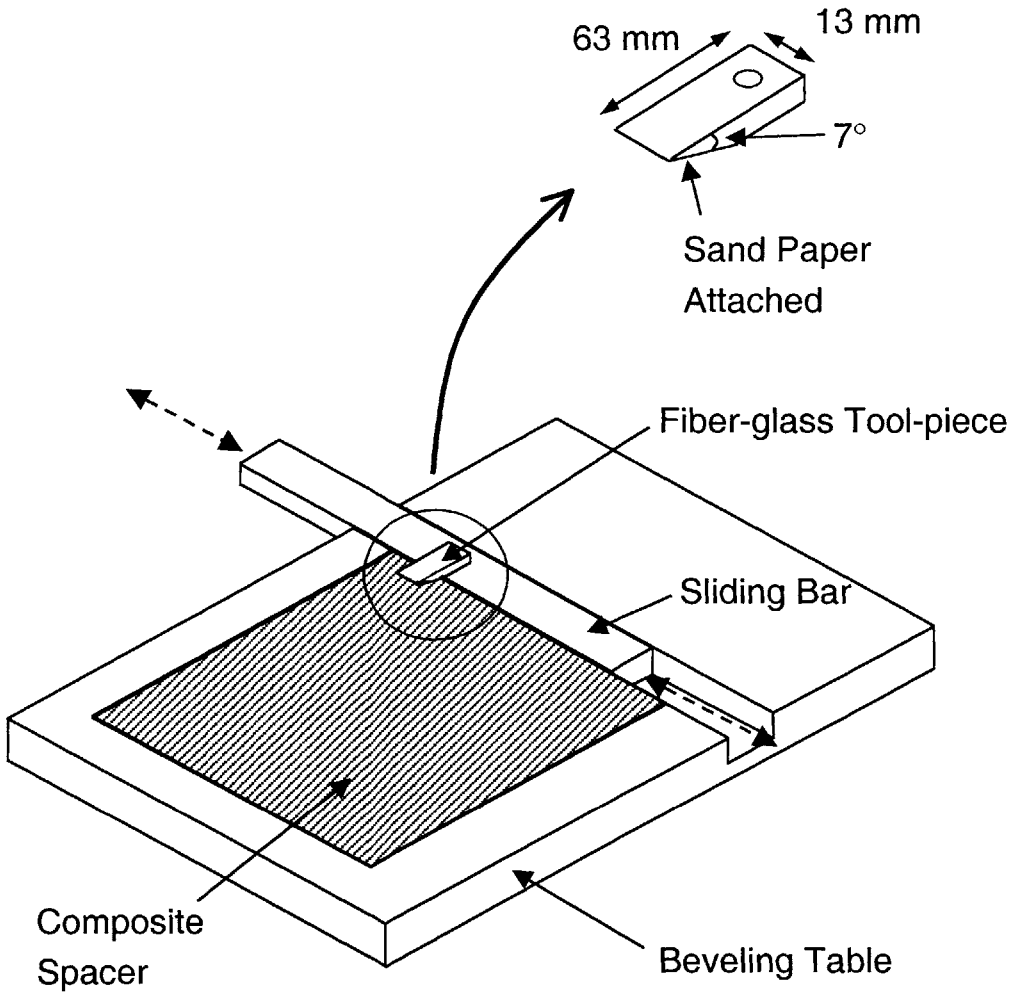

Figure 5.4 Diagram of the beveling table used in beveling the edge of composite spacers.

sequence in a layup jig. The bottom spacer is placed on the layup jig before any of the pre-preg is laid up. This not only ensures that the laminate conforms to the desired shape of the taper in the dropoff region but also ensures that the bottom spacer is aligned with the terminated plies. The layers of pre-preg cut using the templates are carefully laid up on the jig by aligning the pre-preg against the right-angled fence of the jig. A roller is used to apply pressure after each layer such that wrinkles or voids can be pressed down and suppressed. For laminates with external ply dropoffs the beveled edge of the spacers were aligned with the end of the laminate such that the dropoff occurs in a sudden step instead of a taper.

There are two important steps in manufacturing good quality laminates with symmetric ply dropoffs. One is the alignment of the beveled edge of the top spacer and the bottom spacer. This alignment process is important because it determines how well the dropoff region of the cured composite laminate is aligned and defined. The beveled edge of the top spacer is aligned by viewing the edges of the composite part with a magnifying glass and matching the top and bottom spacers with the terminated plies. This procedure is easier to perform by laying the composite part/spacer assembly flat on a table and aligning the region of the top spacer that extends over the composite part across the width with the corresponding region of the bottom spacer. Therefore, it is useful to have composite spacers that are slightly larger than the width of the composite part.

The other important step is the cure assembly (or setup) as this can significantly influence the formation of the dropoff region. A cure assembly that is similar to that for regular flat composite laminates, as in the case of spacers, can be used by considering the composite part/spacer assembly to be a flat laminate assembly. The entire cure assembly is shown in Figure 5.5. The composite part/spacer assembly is placed on a large flat aluminum cure plate that can be rolled into the autoclave. The cure plate is sprayed with a layer of release agent, Frekote 700, and covered with guaranteed non-porous teflon (GNPT) to avoid excess resin from bonding to it. Several layers of cure material such as

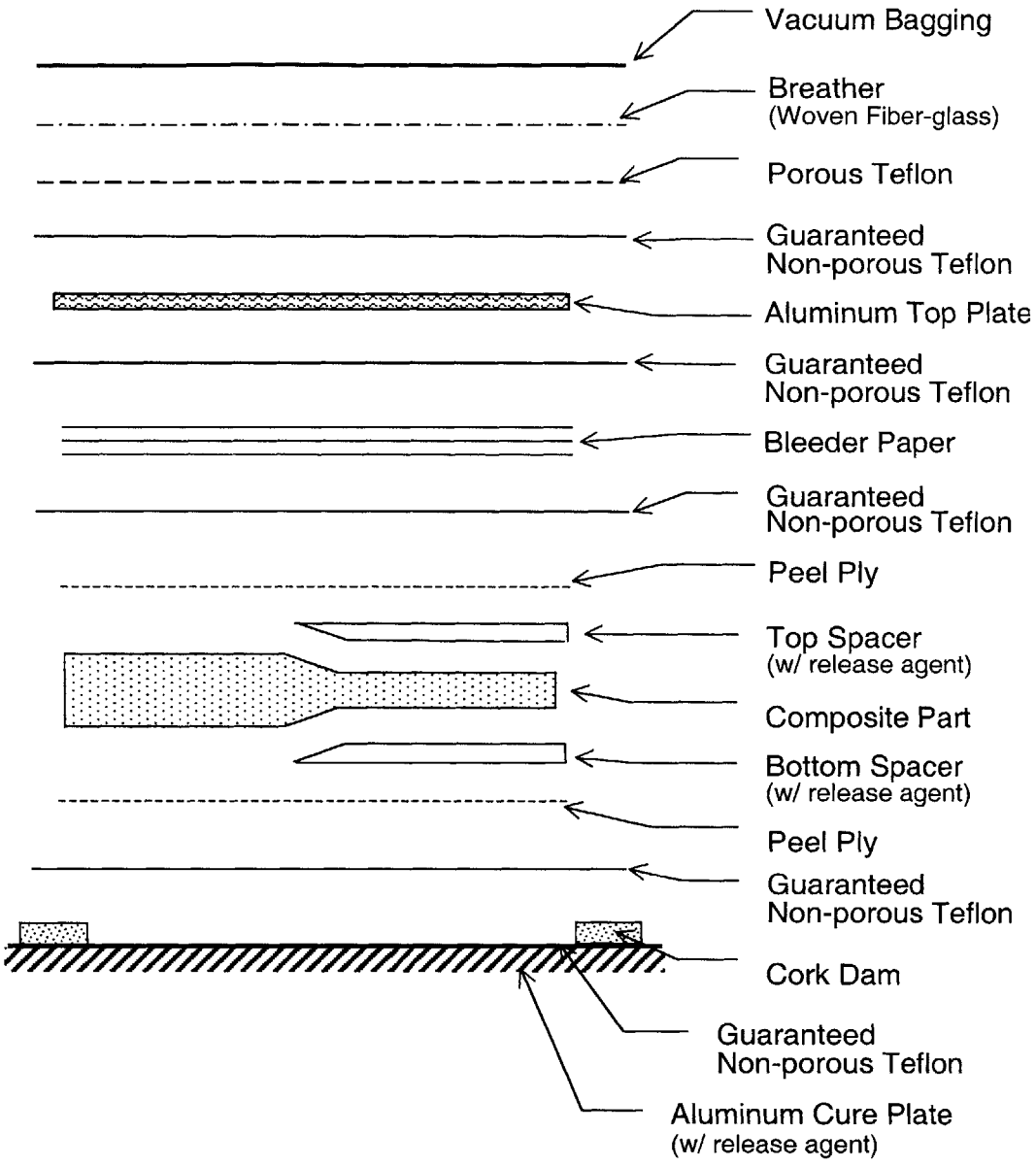

Figure 5.5 Diagram of the cure assembly for the composite laminates with ply dropoffs.

bleed paper used to soak up excess resin during the flow stage of the curing process are placed on top of the composite part/spacer assembly. An aluminum cover plate (or top plate) is placed above the cure material to ensure that pressure is applied uniformly to the composite part/spacer assembly for good consolidation and well-defined taper angle. No cure material is placed between the composite part and spacers. The top plate is also sprayed with layers of release agent and covered with GNPT. To ensure that the composite spacers do not attached to the composite part, they were coated with generous layers of release agent. To prevent the laminate from moving during the cure, dams made of aluminum or cork were used along the perimeters of the laminate. The entire cure assembly is covered by a vacuum bag sealed at the edges with vacuum tape to allow a vacuum to be drawn during the curing process. It is essential that vacuum is maintained at least through the flow stage to ensure that the formation of voids is minimized and good consolidation is achieved. Up to six laminates with dimensions of 350 mm by 300 mm can be setup on the cure plate and, as noted previously, several laminates were cured simultaneously to reduce the number of total autoclave runs.

The cure assembly is rolled into the autoclave and cured using the manufacturer's recommended cure cycle. Care must be taken during the cool-down stage to keep the laminates from thermal shock by gradually lowering to room temperature. Once the autoclave is cooled down, the cure setup is taken apart using particular care when detaching the composite spacers from the composite parts such that they do not break. The laminates are then placed in an unpressurized post-cure oven at 177°C for eight hours to complete the cross-linking of the epoxy matrix.

5.3.3 Tabbing and Final Preparation

The 350 mm by 300 mm laminates with ply dropoffs manufactured using the aforementioned procedures were trimmed at the edges and cut into 350 mm by 31 mm coupons using a water-cooled milling machine with a silicon-carbide blade. Glass/polyester tabs were cut, using a bandsaw, into 50 mm by 31 mm pieces and bonded

to the coupon specimens using FM-123-2 film adhesive via a secondary bond cure. The nominal thickness of the tabs is 3 mm. The bond cure is performed in the autoclave by applying 0.07 MPa of pressure and 107°C for two hours under full vacuum.

Final preparations for the coupon specimens were made by polishing the edges of the laminates using a felt tip bobbin and fine colloidal abrasive. The average particle size of the abrasive is 0.7 μm. The felt tip bobbin is attached to a drill press, and the bobbin is dipped in the colloidal abrasive solution (two parts water for one part of abrasive). The edge of the coupon specimen is then polished by pressing it against the rotating felt tip bobbin while moving the specimen back and forth. This smoothing of the edges serves two purposes: one, it allows a clear view of the edges when inspecting for damage/delamination; and two, it allows a good imprint of the edges to be obtained using replicating tapes. The use of the replicating tapes is discussed further in section 5.5.

A strain gage was attached on each static test specimen at the mid-point along the length of the undropped region to record strain data in the lengthwise direction. This was used to obtain the longitudinal modulus. The location is deemed sufficiently far away from the dropoff region such that the effects of load transfer in that region do not affect the strain gage readings. The strain gages used were a general purpose, type EA-06-125AD-120 gages from the Measurements Group, Inc.

5.4 Quality Assessment

The quality of the coupon specimens was assessed by checking for the occurrence of voids and other irregularities in the dropoff region at the specimen edges through an optical microscope with magnification up to 100X, and by measuring the thickness at various locations in the undropped and dropped regions. The observations and measurements revealed that the quality of the specimens were fairly uniform, although there were misaligned termination of plies in some specimens. Overall, the dropoff

region at the top and bottom surfaces of the specimens was well-defined and the taper angles were within ±0.3° of the nominal value of 7°.

Photographs of the dropoff regions of two typical specimens are shown in Figure 5.6. The two photographs show close-ups of the dropoff region of a laminate with eight internal ply dropoffs and a laminate with four internal ply dropoffs. It is clear from the figure that both laminates have well-defined dropoff regions and resin pockets. Voids in the resin pockets that were visible from the edges were found in less than 10% of coupon specimens. Specimens with voids in multiple resin pockets were excluded from the tests. Although it is not very clear from the photographs, the terminated ply groups in the upper and lower halves of the laminates are not perfectly aligned. The misalignment is more pronounced in the specimen with 8-ply dropoffs, and is on the order of 0.5 mm. A misalignment on the order of 0.5 mm was observed in other specimens with 8-ply dropoffs as well.

The thickness measurements were taken both in the undropped and dropped regions. A total of 18 points were measured on each specimen using micrometers. The location of the measurement points is shown in Figure 5.7. The width is also measured at six locations, as indicated in Figure 5.7, using calipers. The average values for the thickness and width of each specimen are shown in Table 5.3. It can be seen from the table that the coefficient of variation for the thickness is within 6% and for the width is within 0.5%. The average per ply thickness can be obtained by dividing the average thickness by the number of plies. The average per ply thickness in laminates with 4-ply dropoffs is 0.124 mm in both the undropped and dropped regions, and in laminate with 8-ply dropoffs is 0.122 mm in the undropped region and 0.126 mm in the dropped region. This represents a 3% difference in the average per ply thickness of specimens with 8-ply dropoffs, which is within reasonable scatter. The average per ply thicknesses of the current specimens show a maximum of 7.5% difference as compared to the manufacturer's nominal thickness of 0.132 mm. Note that, in general, the width in the

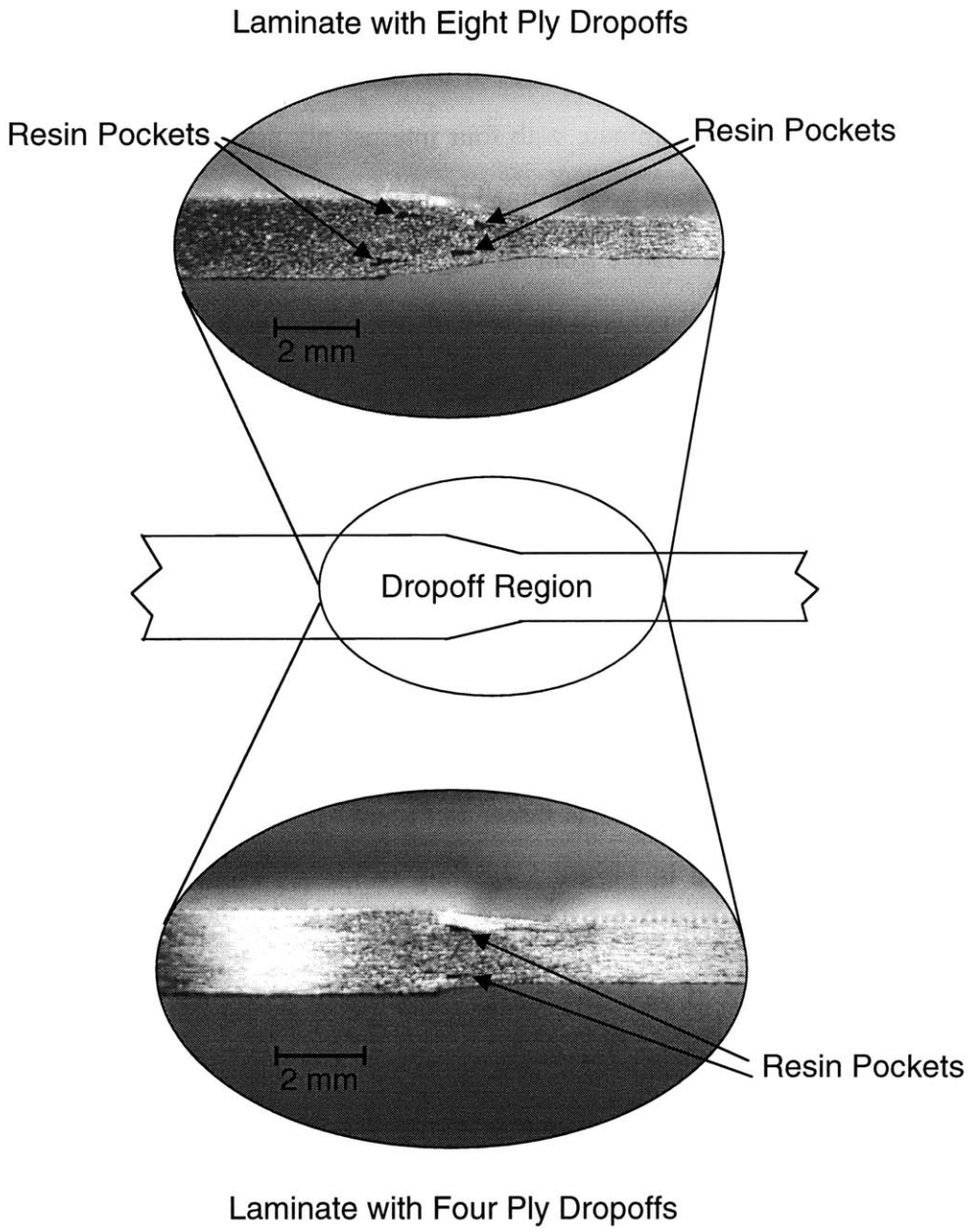

Figure 5.6 Photographs of *(top)*, a specimen with eight internal ply dropoffs, and *(bottom)*, a specimen with four internal ply dropoffs.

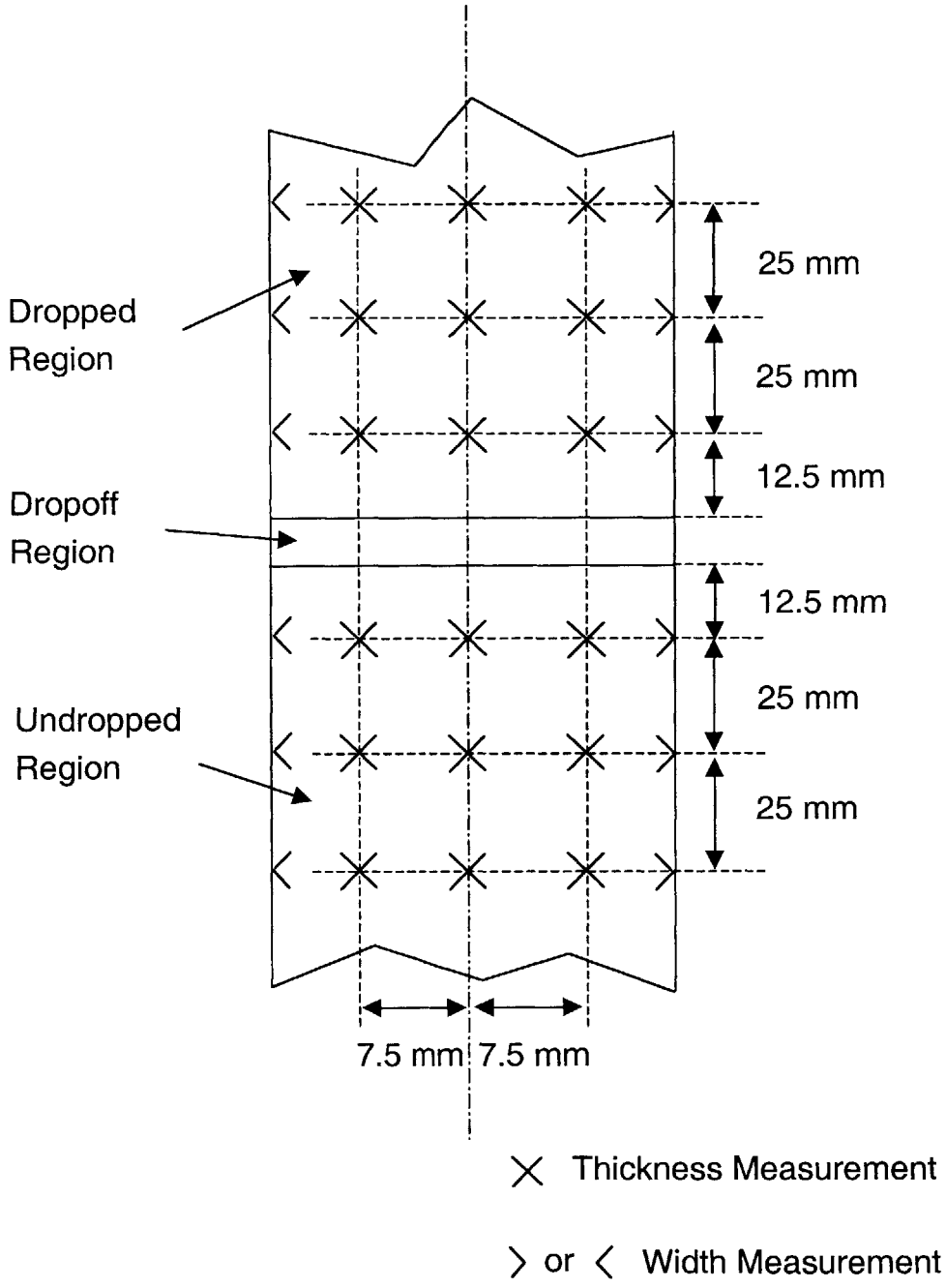

Figure 5.7 Location of thickness and width measurements taken on specimens as indicated by crosses and half-crosses, respectively.

Table 5.3 Average dimensions of coupon specimens

Layup	Average Thickness [mm]		Average Width [mm]	
	Undropped Region	Dropped Region	Undropped Region	Dropped Region
$[0_{2D}/0_2/0_4]_s$	1.99 (3.78%)*	1.50 (4.23%)	31.63 (0.41%)	31.61 (0.29%)
$[0_2/0_{2D}/0_4]_s$	1.99 (4.75%)	1.49 (5.53%)	31.68 (0.11%)	31.63 (0.09%)
$[0_4/0_{2D}/0_2]_s$	1.95 (2.58%)	1.46 (2.97%)	31.66 (0.23%)	31.59 (0.12%)
$[0_{4D}/0_4]_s$	1.97 (3.00%)	1.00 (3.91%)	31.65 (0.05%)	31.56 (0.12%)
$[0_2/0_{4D}/0_2]_s$	1.94 (2.84%)	1.02 (2.07%)	31.67 (0.17%)	31.58 (0.15%)
$[0_3/0_{4D}/0]_s$	1.93 (2.87%)	1.00 (1.87%)	31.69 (0.07%)	31.62 (0.06%)

* Coefficient of variation in parentheses.

undropped region is consistently larger than the width in the dropped region by a small amount on the order of 0.3%.

5.5 Testing Procedures

All static and cyclic tests were conducted on an MTS® hydraulic load frame fitted with an Instron® controller. The static tensile tests serve two purposes. One is to provide data as to when and how damage/delamination in laminates with ply dropoffs occurs. The other is to determine the limit loads for the fatigue tests. For the cyclic tests, specimens were loaded under cyclic tensile load with a stress ratio (or R-ratio) greater than zero up to 100,000 cycles or complete failure defined as the specimen being unable to carry any load. Specimens that did not show any damage up to 100,000 cycles were considered to have run-out. The details of the testing procedures for the static and cyclic tests are described in subsequent paragraphs, starting with the static tests.

The static tests were performed with the hydraulic load frame under displacement (or stroke) control. Since the objective of the static tests is to observe the damage/delamination initiation loads and modes, a low stroke-rate is needed to monitor the occurrence of such events and stop the testing machine. Two stroke rates were used during testing to reduce test time. For each specimen type, a stroke rate of 0.125 mm/min was used throughout the test for the first specimen. This corresponds to an average strain rate of approximately 500 μstrain/min in the specimen. Subsequent tests of the same specimen were conducted using a stroke-rate of 0.25 mm/min (or approximately 1000 μstrain/min) for loads smaller than approximately half the damage/delamination initiation load as determined for the first specimen. The stroke-rate was lowered to 0.125 mm/min for the remainder of the test.

The strain, displacement and applied load were recorded during the static tests. Data were recorded on a computer using Labview® through a connection to an analog-to-digital (A/D) board. The displacement readings were taken directly from the Instron®

controller and the load readings were taken from the load cell attached to the upper grips of the hydraulic load frame. The strain gage readings were taken via a Vishay® strain gage conditioner. All readings were recorded in a computer file using a sampling rate of 1 Hz.

Based on observations in previous investigations of laminates with ply dropoffs, delamination is expected to be the dominant mode of initial damage. To determine the load at which delamination initiates, the load drop method was used in conjunction with edge replication. During static testing under displacement-control, the load applied to the specimen being tested should always increase by a certain amount. If a damage event occurs in the specimen, a drop in the load may occur. The load drop method refers to the detection of drop in the load. This method is further described in a following sub-section. The load drop method and edge replication have been used successfully in previous work to detect free edge delamination initiation events [42], and can also detect other types of damage at the free edges.

A typical static test is performed as follows. Before placing the coupon specimen in the hydraulic load frame, the upper and lower grips are aligned using a thick, straight steel bar. The bar is placed in the testing machine and the upper and lower grips are closed to ensure that they are aligned. The specimen is placed in the testing machine and the upper grips are closed first making sure that it is perpendicular to the grips, and hence aligned vertically, using a machinist's square. This is the zero load position, and the strain gages are zeroed in this position. The lower grips are then closed. The data acquisition system is turned on and the testing machine is started at the desired stroke rate. The displacement and load are increased until one of two events occurred. One event is audible cracking noises and the other is a drop in load greater than a pre-determined value. This value is described further in a following sub-section on the load drop method. If cracking noises were heard, the testing machine was immediately stopped. A stop switch was programmed into the Labview program such that in such an

event, a button on the computer can be clicked to stop simultaneously the test and the data being recorded on the computer file. The drop in load was monitored using a computer program and the data acquired from the load cell in real-time. The testing machine was connected to the computer such that a load drop event triggered an automatic stoppage of the test. This is discussed further in a following sub-section. The data recorded on the computer file is reduced using Microsoft Excel®.

Once the test is stopped, the load is reduced to half the current load and the specimen is inspected for damage/delamination. The specimen is kept under load to keep the damage/delamination open and thus make such easier to detect via edge replication. The load is reduced to prevent an inadvertent increase in load while inspecting the specimen, which may cause catastrophic failure. The load at which the test is stopped is recorded in a lab notebook. The specimen is inspected visually and through replicating the edges. The edges are replicated via cellulose tape soaked in acetone, commonly referred to as replication tapes. The replication tapes are 25 mm wide and used to take an imprint of the edge. The details of the replication procedure are described in a following sub-section. The tape is then inspected under a microscope to check for damage/delamination using magnification up to 100X. Once a damage/delamination is detected, the specimen is not tested further. If the damage/delamination is not detected, the load is increased to approximately 95% of the load at which the test was stopped and testing is resumed.

The cyclic tensile tests are performed in order to observe the damage modes, to determine the location at which damage initiates, to obtain the number of cycles to damage initiation, and to observe delamination growth characteristics. This requires only the number of fatigue cycles the testing machine has conducted to be directly recorded. No strain gages were used in the cyclic tests. The cyclic tests were stopped every 1,000 to 5,000 cycles to inspect for damage/delamination initiation and growth, or when audible cracking noises were heard. Once the test is stopped, the specimen is inspected for

damage/delamination both visually and through edge replication, similar to the case of static tests. The number of cycles at which the test is stopped is recorded in a lab notebook.

For the cyclic tests, the testing machine is run under load control between a specified maximum and minimum load. Although it is desirable to use as high a frequency as possible during cyclic tests to reduce test time, the highest frequency at which any cyclic test can be conducted is limited by the capability of the testing machine to apply the specified load levels. For specimens whose maximum load is large, a lower frequency needs to be used in order to allow the testing machine to be able to apply the load levels within acceptable limits. For specimens whose maximum load is small, a higher frequency can be used. For the current tests, a maximum of 5 Hz and a minimum of 3 Hz was used. At these frequencies, heating due to the cyclic loading is not a concern. In general, such effects become important above 10 Hz in composite materials. The maximum and minimum loads were periodically monitored to check that load levels being applied were within acceptable limits.

The maximum load levels at which the specimens were tested under cyclic load were chosen as percentages of the static delamination initiation loads. The three specimens from each specimen type were tested under three different maximum load levels. Clearly, in order to avoid static failure, the maximum load for each specimen type must be smaller than the static delamination initiation load. In the current tests, maximum load levels between 60% and 86% of the static delamination initiation load minus one standard deviation was used to ensure that premature static failure did not occur. A fixed stress ratio of R equal to 1/8 was used throughout the tests. This stress ratio was chosen based on damage tolerance demonstration requirements for composite flexbeams. The actual load levels used in the fatigue tests are presented in Chapter 6.

After the static and cyclic tests were completed, all specimens were inspected for damage/delamination using x-ray. X-ray photomicrograph allows one to view the extent

of internal damage/delamination across the width of the specimens. To make the internal damage/delamination visible 1,4-diiodobutane was used. The chemical solution is dabbed on the edges and surfaces of the laminate using a swab to seep into the damaged and/or delaminated areas and allowed to dry. Any excess chemical solution left on the edges or surfaces was wiped off with paper towel soaked with water to prevent any erroneous damage/delamination markings from appearing on the photomicrographs. To further characterize the damage/delamination in the static and cyclic test specimens, a scanning electron microscope (SEM) was used to inspect the fracture surfaces at several locations. Since the epoxy matrix is non-conductive, an environmental SEM was used to view the fracture surfaces.

5.5.1 Edge Replication

Delamination can be very difficult to detect through visual inspection using a microscope especially when it is short and the interfaces are closed. Moreover, the unidirectional fibers reflect light from the light source, which makes it difficult to distinguish the dark matrix regions from delaminations. A more involved but accurate method of detecting such delaminations is edge replication. This allows an imprint of the edges to be taken by physically applying and pressing against the edges a strip of cellulose acetate tape softened with acetone. Since the softened tape can penetrate delaminated interfaces, delaminations and other types of cracks can be seen and identified clearly.

The replication procedure involves several steps. A 25 mm wide strip of cellulose acetate tape is cut and placed on the edge of the specimen centered at the dropoff region. The dropoff region is used as a reference to identify the location of the replication. Acetone is then squirted on the tape to dissolve the surface in contact with the edge. A small, flat roller is used to firmly press the tape on the edge. Any air pockets must be flattened out using the roller to ensure that a good imprint is taken. Once the acetone evaporates and the tape is dry, it is peeled carefully from the edges. A picture of the

replicating process is shown in Figure 5.8. The picture shows acetone being squirted on to the replication tape being held at the edges of the laminate under load.

Once a replication is taken, it is taped onto a microscope glass to prevent curling as the acetone dries completely. The microscope glass is then viewed under a microscope with magnification up to 100X to inspect for any damage/delamination in the dropoff region. Typical replications of the dropoff regions in two specimens before testing are shown in Figure 5.9. One is a replication of a specimen with four external ply dropoffs and the other is a replication of a specimen with four internal ply dropoffs. It can be seen that the replication technique yields a detailed view of the edge surface and provides an excellent means to inspect and detect delamination.

From the replication of the specimen with external ply dropoffs, it can be seen that a resin pocket exists at the tip of the terminated plies. Such resin pockets occur because the composite spacer does not fully abut the terminated plies during the manufacturing process. A small, circular-shaped void can be seen in the resin pocket. From the replication of the specimen with internal ply dropoffs, it can be seen that the geometry of the resin pocket is not a simple triangle, but consists of a main, triangular region and a secondary, trapezoidal region. The trapezoidal region occurs due to the difference in location of the terminated plies on the order of 200 μm.

5.5.2 Load Drop Phenomenon

Delamination events occurring across the width (or parts thereof) of the specimens during static testing are expected to cause a sudden drop in load because the load path through the specimen must change instantaneously. The cause of the load drop phenomenon for the current test is different from that for the straight free edge delamination case [42]. In straight laminates, delamination occurs at the free edges across the entire length of the specimen. A drop in load occurs due to a decrease in the overall modulus of the specimen that is caused by the delamination. The modulus of the delaminated specimen can be estimated by averaging the moduli of the remaining

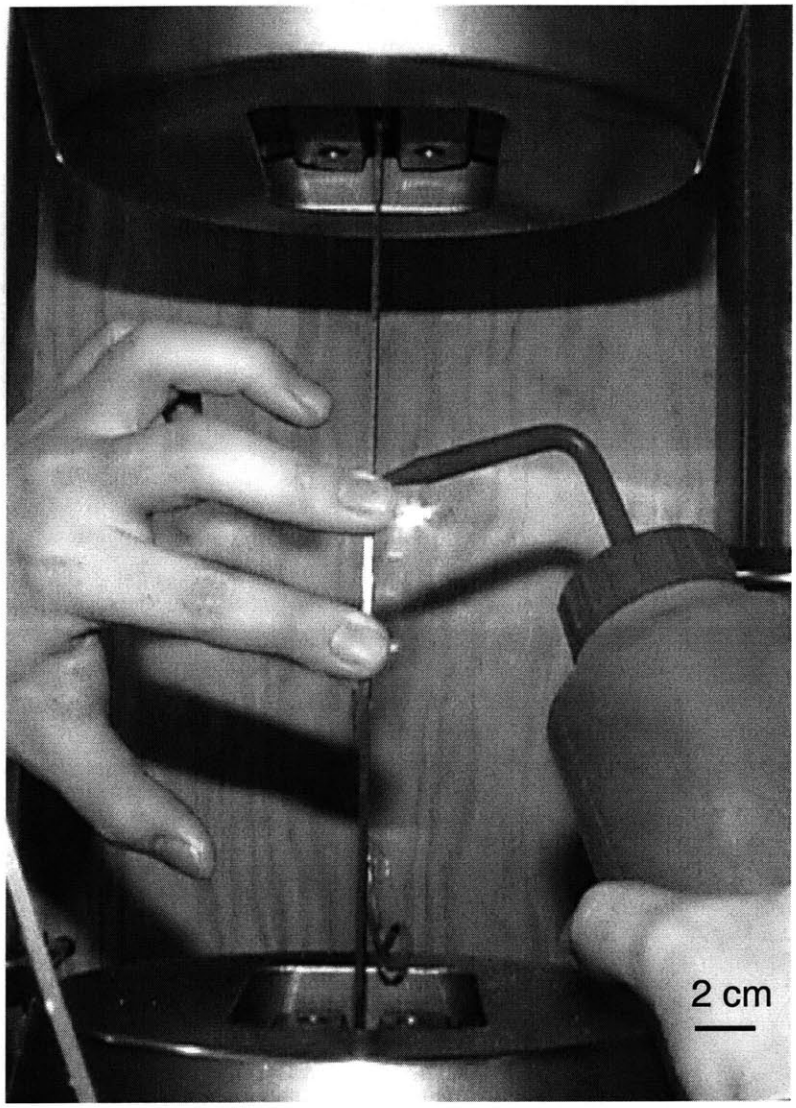

Figure 5.8 Photograph of edge replication being performed with coupon specimen under load.

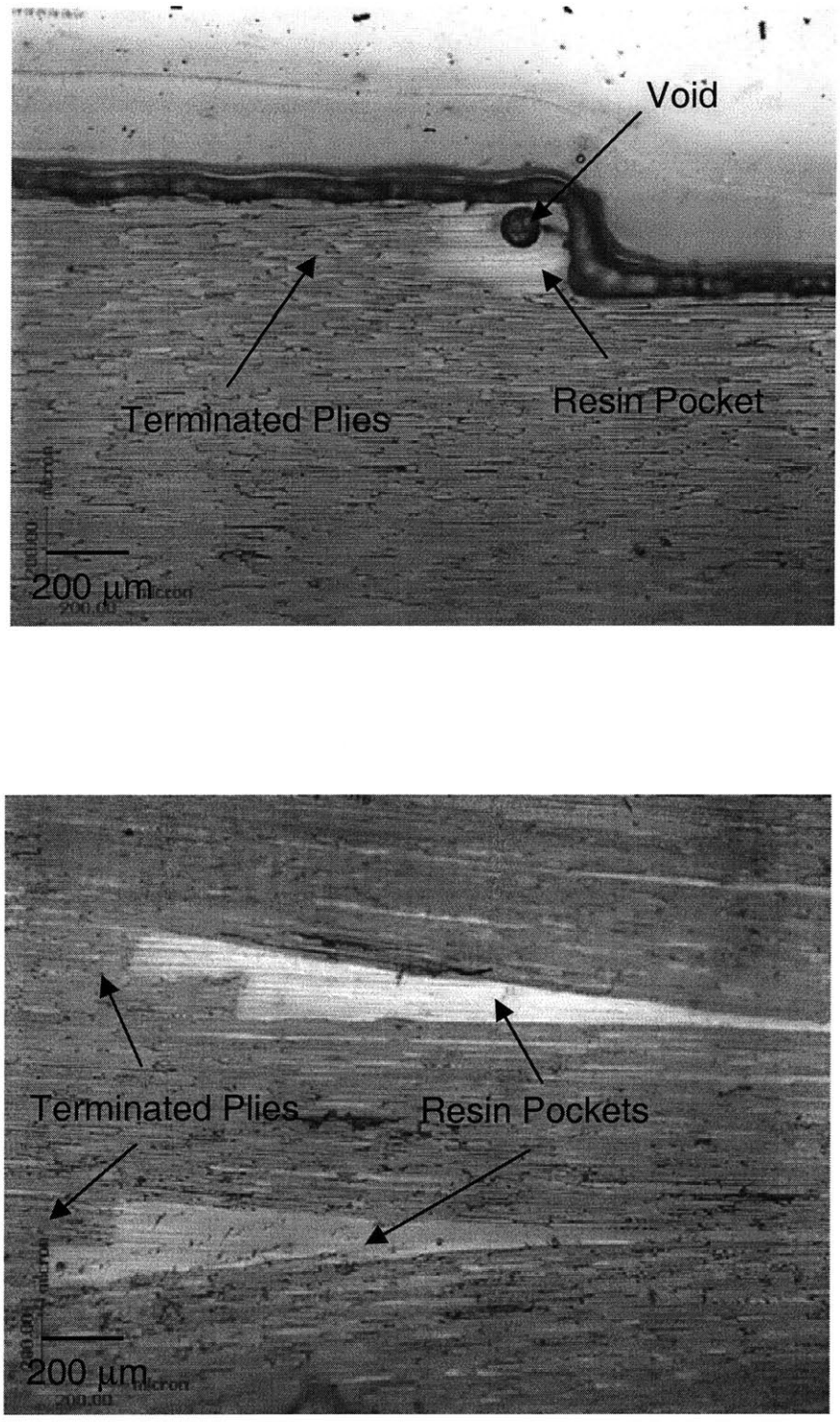

Figure 5.9 Photomicrographs of edge replications of the dropoff regions, *(top)* in a specimen with four external ply dropoffs, and *(bottom)*, in a specimen with four internal ply dropoffs.

sublaminates weighted by the thickness of the sublaminates. The magnitude of the drop in load can then be estimated as a function of the moduli of the undelaminated and delaminated specimen and the area of delamination.

Unlike the straight free edge case, it is difficult to predict the magnitude of the drop in load in the current specimens because the drop does not occur due to a change in the overall modulus but rather due to a change in the load path along the delaminated regions in the length of the specimen. Thus, the criterion for stopping the static test was established for each specimen type based entirely on trial and error during the test of the first specimen in that group. For each specimen, the average increase in force per sample interval was noted during initial static testing stages at loads below 2000 N, which was well before any damage events occurred. Ideally, since the hydraulic grips displace at a constant rate, the increase in force should also be constant. Thus, under ideal conditions, the increase in load while testing can be monitored and the testing stopped when the load does not increase by the constant amount. However, due to the noise in the data acquisition system combined with other tolerances in the overall testing system, the load did not always increase by a constant amount. Therefore, a "load drop margin" was chosen as a criterion to stop the test. If the difference in the current sampled load and the previous sampled load is smaller than the load drop margin, the testing is stopped. The load drop margin was chosen by considering the average increase in force per sample interval and the typical magnitude of the noise in the data that could obscure the load drop. The typical magnitude of the noise was determined from the load readings taken when no load was applied. It is important to choose the load drop margin such that it is conservative enough to ensure that delamination events are detected, yet not so conservative as to produce too many "false" stoppages.

Typical values for the load drop margin were between 22 N and 0 N depending on the stroke rate used and the magnitude of the load. Note that the load drop margin was not always fixed for each specimen and varied depending on the stage of testing. Once

the first specimen from a specimen group is tested and the delamination load obtained, subsequent specimens of the same type were tested using a higher value for load drop margin at lower loads and a lower margin as the load become closer to the previously observed delamination load. A computer program was written in Labview® such that the testing was automatically stopped when such an event occurred.

CHAPTER 6

STRESS FIELD CHARACTERIZATION

The characteristics of the interlaminar stress fields in laminates with ply dropoffs are presented and discussed in this chapter. Since new analytical models were developed and implemented in a computer code, the validity and applicability of the analytical work need to be assessed first. For this purpose, the stress fields in various composite laminates obtained using the current analytical methods and those obtained via finite element analyses including those from the open literature in the two such cases applicable were compared. This work is presented in the first section. In the second section, a parametric study is presented where several structural parameters that affect the interlaminar stress field are considered using laminates with different layups to help identify general trends and gain insight to key mechanisms. In the third section, the characteristics of the interlaminar stresses in laminates with combined in-plane and bending loads are presented. In this section, symmetric laminates with ply dropoffs are considered. Unsymmetric laminates with ply dropoffs are considered in the fourth section. Finally, in the fifth section, the fundamental mechanisms that cause interlaminar stresses and the limitations of the current analytical models are discussed based on results from the previous sections.

6.1 Validation of Analytical Methods

The validity and applicability of the current analytical methods described in Chapter 4 are established by comparing the stress fields obtained using the current methods with those obtained using numerical methods either from the open literature or via finite element analysis. This procedure is accomplished by considering two types of

laminates. One type of laminate considered is the flat multi-directional laminate with straight free edges, and the other is the unidirectional laminate with ply dropoffs. The two types of laminates are considered in order to take full advantage of the stress analysis results available in the open literature and from two-dimensional finite element (FE) analyses. Since all of the current analytical methods are linear analyses, validation of the stress fields for unidirectional laminates with ply dropoffs *and* of the stress field for multi-directional laminates with straight free edges is sufficient to establish validity of the current methods for multi-directional laminates with ply dropoffs.

Although it is convenient to use stress analysis results from previous investigations in the literature for validation purposes, there are only two such previous stress analyses available. One is for the case of a laminate with external ply dropoffs [27], and the other of a laminate with internal ply dropoffs [16]. As discussed in Chapter 2, most of the previous investigations on laminates with ply dropoffs have focused on local details of the dropoff region such as the precise geometry of the terminated plies. Although numerical stress analyses have been performed as part of such investigations in general, the overall stress fields in the undropped and dropped regions were not presented in most investigations. Therefore, in order to validate the current analytical methods for various layups and load types, finite element (FE) analyses were performed on laminates with ply dropoffs as a means to provide additional stress analysis results. Two-dimensional elements were used in the FE analyses for time effectiveness.

Since the two-dimensional FE analysis can only be used for laminates with unidirectional layups, laminates with straight free edges were also considered to supplement the validation for cases of laminates with arbitrary ply angles. Straight free edges in a flat composite laminate give rise to interlaminar stresses due to the stress-free condition at the edges and mismatch in elastic constants from ply to ply. Two-dimensional FE analysis does not account for the contribution to the stress field in the widthwise direction, and thus, cannot be used to obtain accurate stress fields in such

laminates. However, the stress distributions for such laminates under in-plane and bending loads are readily available in the open literature. The current analytical methods for laminates with ply dropoffs can be easily modified to handle such laminates. Therefore, the effects obtained from such analyses can be directly compared with those available in the open literature.

The details of the finite element analyses performed for the validation procedure are described in the first sub-section. In the next sub-section, comparisons of the stress fields in laminates with straight free edges are presented to validate the current methods for laminates with arbitrary ply angles. Three laminates under in-plane and bending loads are considered, and the stress fields obtained from the current work are compared with those from previous investigations in the literature. This is followed by comparisons of the stress fields for unidirectional laminates with ply dropoffs obtained using the global model and FE analysis and/or from previous investigations. Laminates with external and internal ply dropoffs are considered in this sub-section. The validity of the mixed model for laminates with internal ply dropoffs is established in the fourth sub-section. Two laminates with internal ply dropoffs are considered under both in-plane and bending loads. Finally, in the fourth sub-section, the model for laminates with existing delaminations is considered. Two laminates, one with external ply dropoffs and the other with internal ply dropoffs, under in-plane load are considered.

All laminates with ply dropoffs considered in the following examples are of unit width unless stated otherwise.

6.1.1 Finite Element Modeling

The FE analysis in the current work was performed using ABAQUS®. The CPS8 element, which is a two-dimensional 8-node rectangular plane stress element with full integration, is used. Only one half of the laminate was modeled for all laminates. For laminates under in-plane load, a symmetric boundary condition was specified at the mid-plane, and for laminates under bending load, an anti-symmetric boundary condition was

specified. A typical FE model is shown in Figure 6.1. For in-plane load cases, the left end of the undropped region is constrained in the x-direction, and uniform displacement is specified at the right end of the dropped region. For the bending load cases, a couple-force is applied at both ends creating moment through four-point bending. As shown in Figure 6.1, elements of different sizes are used in order to obtain better approximations of the stress field while reducing the total number of degrees-of-freedom in the FE model. The size of the smallest element in the length direction is 0.1t (where t is nominal ply thickness). In addition, the resin pockets are assumed to carry no load. This is consistent with the analytical models.

It is noted that the elements used in the current FE analysis are displacement-based elements that require the stresses to be calculated by numerical differentiation of nodal displacements. Thus, the stress field may not satisfy equilibrium in an integral sense and is not expected to be completely accurate in regions where stress gradients are high, such as in the immediate vicinity of the ply dropoffs. However, a converged FE solution should yield good approximations for the stress field away from the immediate vicinity of the ply dropoffs.

A mesh convergence study was performed on a $[0_4/0_D]_s$ laminate in order to choose the size of the elements in the thickness direction. The laminate has a taper angle of 5.7° and is under an in-plane stress of 1000 MPa applied at the dropped end. Material properties of a generic glass/epoxy, shown in Table 6.1, are used. The first model has a total of 2640 elements, which corresponds to elements with a thickness of 0.5t; the second model a total of 3960 elements, which corresponds to elements with a thickness of 0.25t; and the third model a total of 6600 elements, which corresponds to elements with a thickness of 0.1t. The interlaminar stress components σ_{xz} and σ_{zz} along the interface of the terminated and continuous plies ($z = t$) in the undropped region along the length of the laminate obtained using the three models are shown in Figures 6.2 and 6.3. It can be seen that there is no significant difference in the stress field characteristics

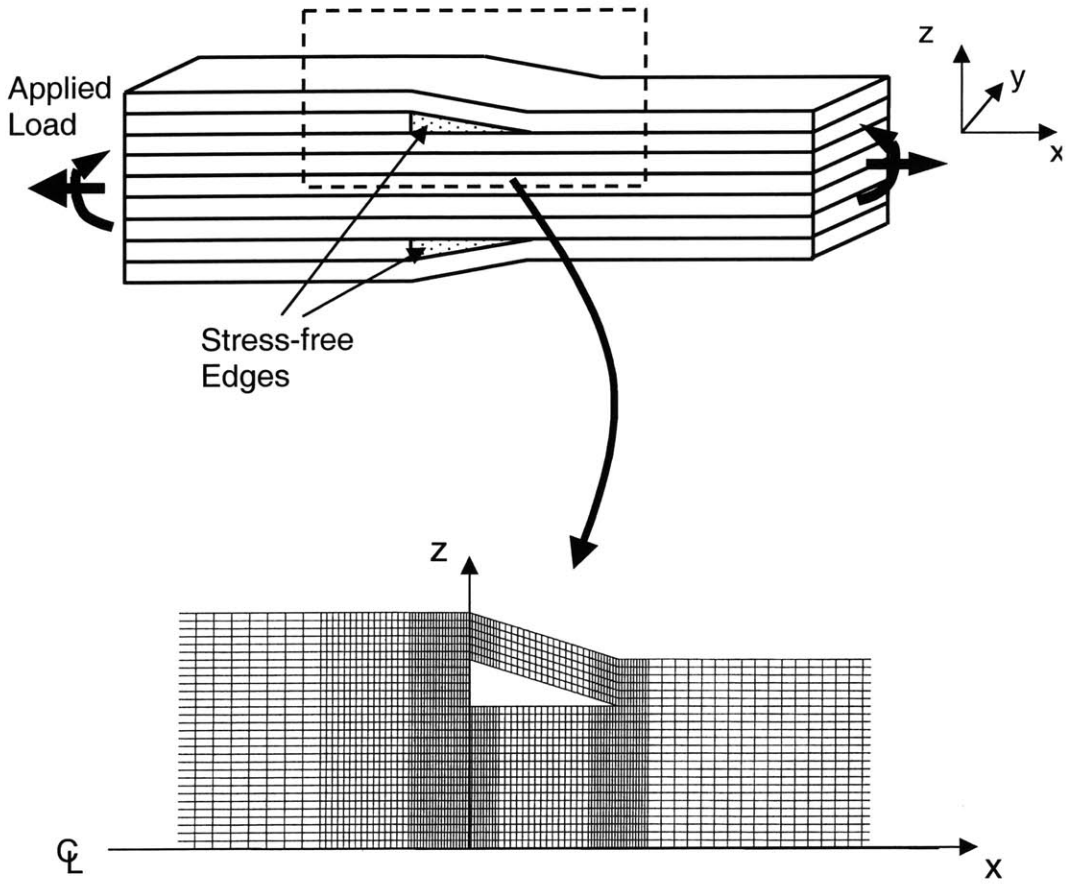

Figure 6.1 Typical finite element mesh used for validation of analytical results.

Table 6.1 Generic material properties of composite materials used in current work[1]

Property	Graphite/Epoxy[2]	Graphite/Epoxy[3]	Glass/Epoxy
E_L	20 Msi	130 GPa	43.9 GPa
E_T	2.1 Msi	9.0 GPa	15.4 GPa
E_Z	2.1 Msi	9.0 GPa	15.4 GPa
G_{LT}	0.85 Msi	4.8 GPa	4.34 GPa
G_{LZ}	0.85 Msi	4.8 GPa	4.34 GPa
G_{TZ}	0.85 Msi	4.8 GPa	4.34 GPa
ν_{LT}	0.21	0.28	0.30
ν_{LZ}	0.21	0.28	0.30
ν_{TZ}	0.21	0.28	0.30
t	-	0.125 mm	0.127 mm

[1] All material properties, including G_{TZ} and ν_{TZ} values, set to same values as used in previous work [16,27,69,70] to allow for direct comparison.

[2] Graphite/epoxy material properties in English units used for analyses of laminates with straight free edges under in-plane load and bending load.

[3] Graphite/epoxy material properties in SI units used for analysis of laminate with external ply dropoffs under in-plane load.

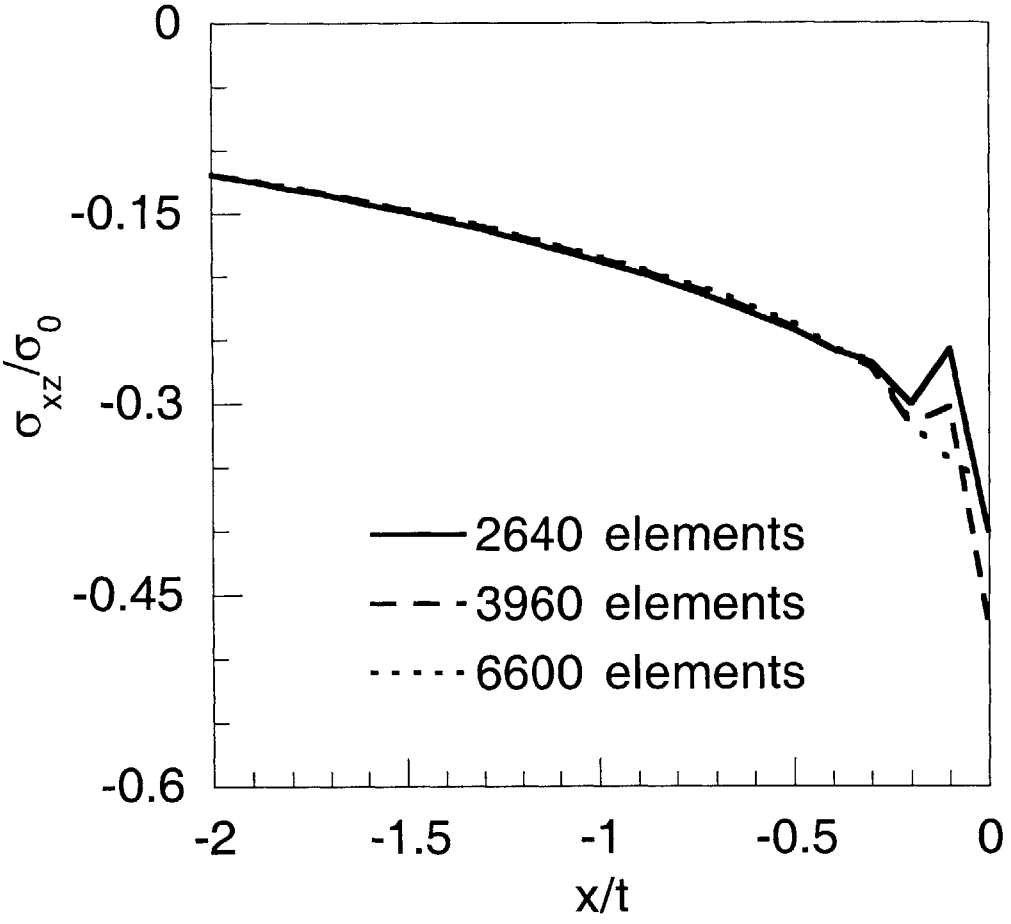

Figure 6.2 Interlaminar shear stresses along the interface of the continuous and terminated plies (z = t) in the undropped region in a $[0_4/0_D]_s$ laminate obtained using three different finite element meshes for convergence study.

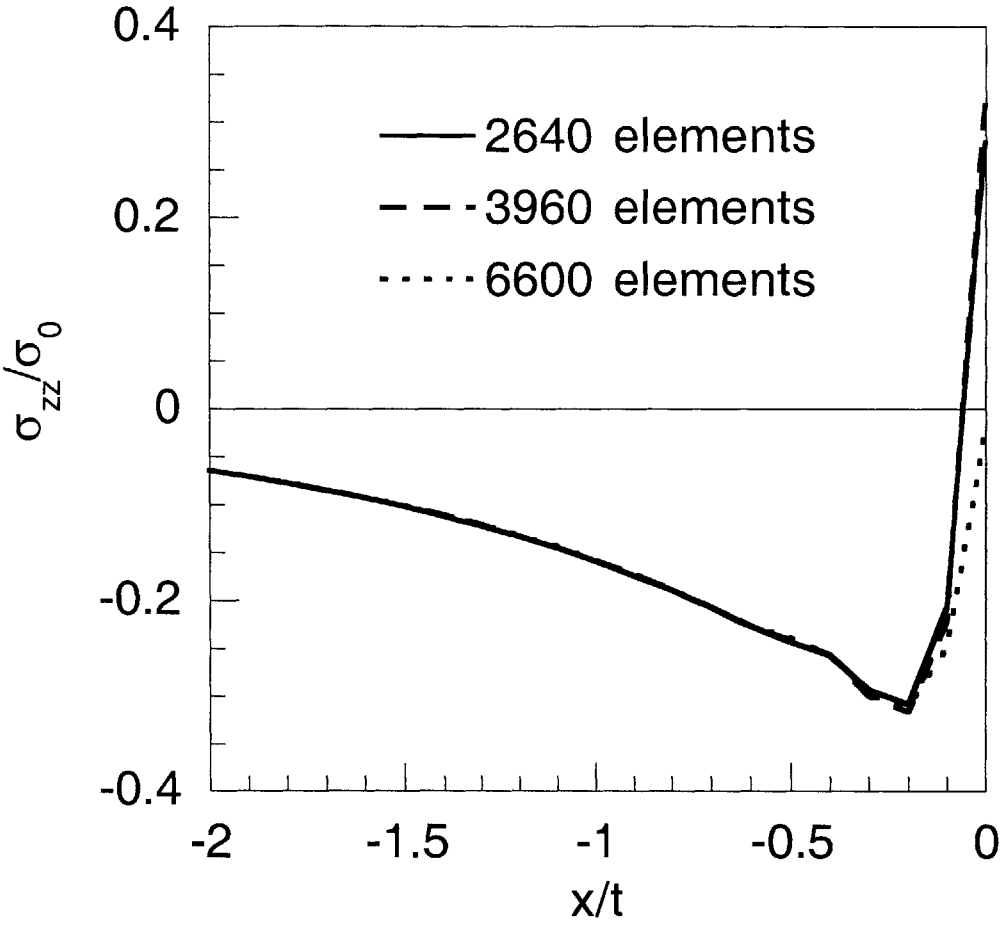

Figure 6.3 Interlaminar normal stresses along the interfaces of the continuous and terminated plies (z = t) in the undropped region in a $[0_4/0_D]_s$ laminate obtained using three different finite element meshes for convergence study.

except in the regions very close to where the ply dropoffs occur (x/t = 0). For distances larger than 0.25t from the termination location, the stress fields obtained using the three models match very well. This shows that the model with elements of thicknesses equal to 0.5t yields a sufficiently converged solution. In all FE analyses, the models used to calculate the stress fields are of one higher level of refinement having elements with thicknesses of 0.25t.

6.1.2 Laminates with Straight Free Edges

The current analytical method was slightly modified to analyze laminates with straight free edges. Using this modified analytical method, as subsequently described, three laminates that were previously considered in the literature are analyzed and the results compared with those presented in literature. For the in-plane load case, a laminate with a quasi-isotropic layup of $[\pm 45/0/90]_s$ is considered, while for the bending load case, two laminates with layups of $[90/0]_s$ and $[\pm 45]_s$ are considered.

A diagram of a generic laminate with straight free edges is shown in Figure 6.4. Comparing this figure with the model for a laminate with ply dropoffs in Figure 4.1, it can be seen that a laminate with straight free edges can be thought of as one of the uniform thickness regions with the load acting in the widthwise direction and different boundary conditions at the ends. To accommodate the differences in the loading direction and boundary conditions, two modifications to the analytical model for laminates with ply dropoffs need to be made. The first modification is to apply the loads in the direction parallel to the ply dropoffs. The cutoff, which is one end of the uniform thickness region, corresponds to the free edge, and the other end corresponds to the mid-section of the laminate with straight free edges. Thus, only half of the laminate with straight free edges is modeled. The second modification is to apply the stress-free condition at the cutoff to every ply as opposed to only at the terminated plies in the case of laminates with ply dropoffs.

The quasi-isotropic laminate with a layup of $[\pm 45/0/90]_s$ under in-plane load is

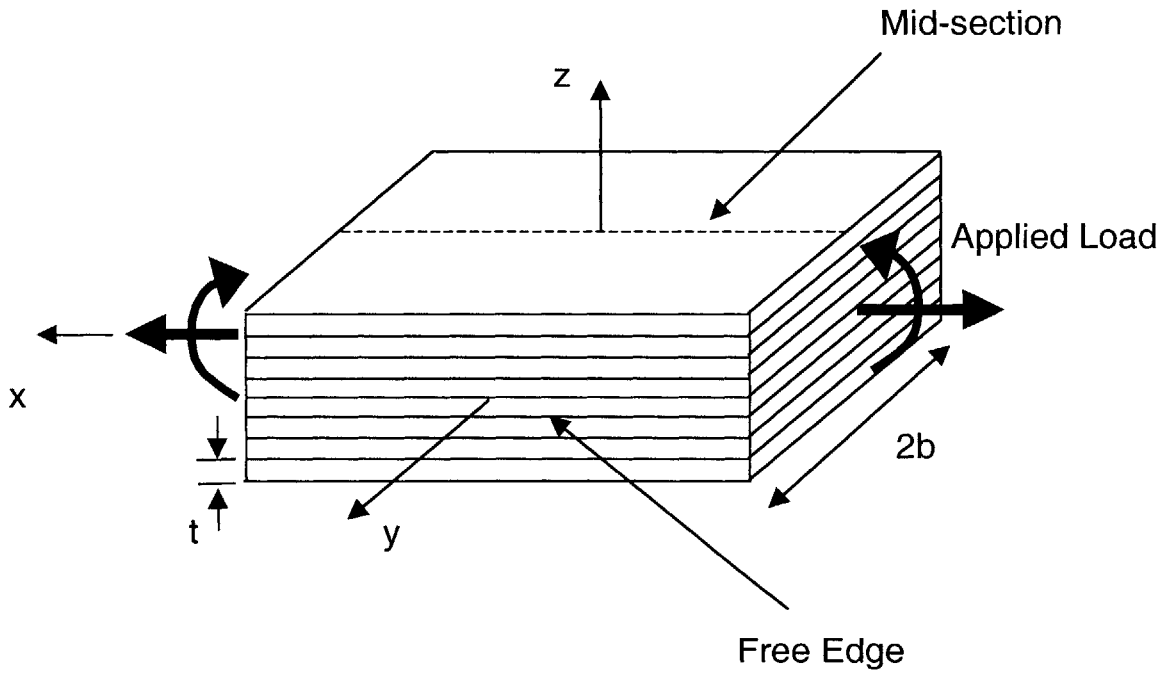

Figure 6.4 Diagram of a laminate with straight free edges showing the coordinate system and the direction of the applied load.

considered first. The material properties of a generic graphite/epoxy composite in English units are used. These are shown in Table 6.1. The laminate is under uniform axial strain, ε_0, equal to 1 μstrain. The geometry and coordinate system of a laminate with straight free edges is shown in Figure 6.4. The width of the laminate is 2b where b is equal to 16t and the thickness of a ply is t. The same laminate was previously considered by Wang and Crossman [69] using a finite difference method, and the results from their investigation are used for comparison.

The stress distributions along the y-direction for the interlaminar stresses at three locations through the thickness obtained using the current method and the finite difference method are shown in Figure 6.5. The y-direction coordinate is normalized by the half-width of the laminate, b. As shown in Figure 6.5, the interlaminar shear stress, σ_{yz}, obtained using the current analysis satisfies the stress-free boundary condition at the free edge (y/b = 1), while the interlaminar shear stress, σ_{xz} and interlaminar normal stress, σ_{zz} are very large near the edge, and possibly singular [71]. It can be seen from Figure 6.5 that the results obtained using the two methods show very good agreement, thereby validating the current method for in-plane load cases.

For the bending load case, two laminates with layups of $[90/0]_s$ and $[\pm 45]_s$ are considered. The same material properties of a generic graphite/epoxy composite that were used in the previous example, which are shown in Table 6.1, are used. The laminates are loaded in bending to produce a maximum bending strain of –0.001 (in/in) at the top surface in both cases. The geometry and coordinate system of the laminate considered are identical to that shown in Figure 6.4 with the exception of the number of plies. In this example, the laminates have four plies, and the width of the laminate is 2b where b is equal to 6t. The two laminates were considered in a previous investigation by Salamon [70] with the use of a finite difference method. The interlaminar stresses in the two laminates obtained using the current method and from the previous investigation are shown in Figures 6.6 and 6.7. In the previous work [70], all stresses were normalized by

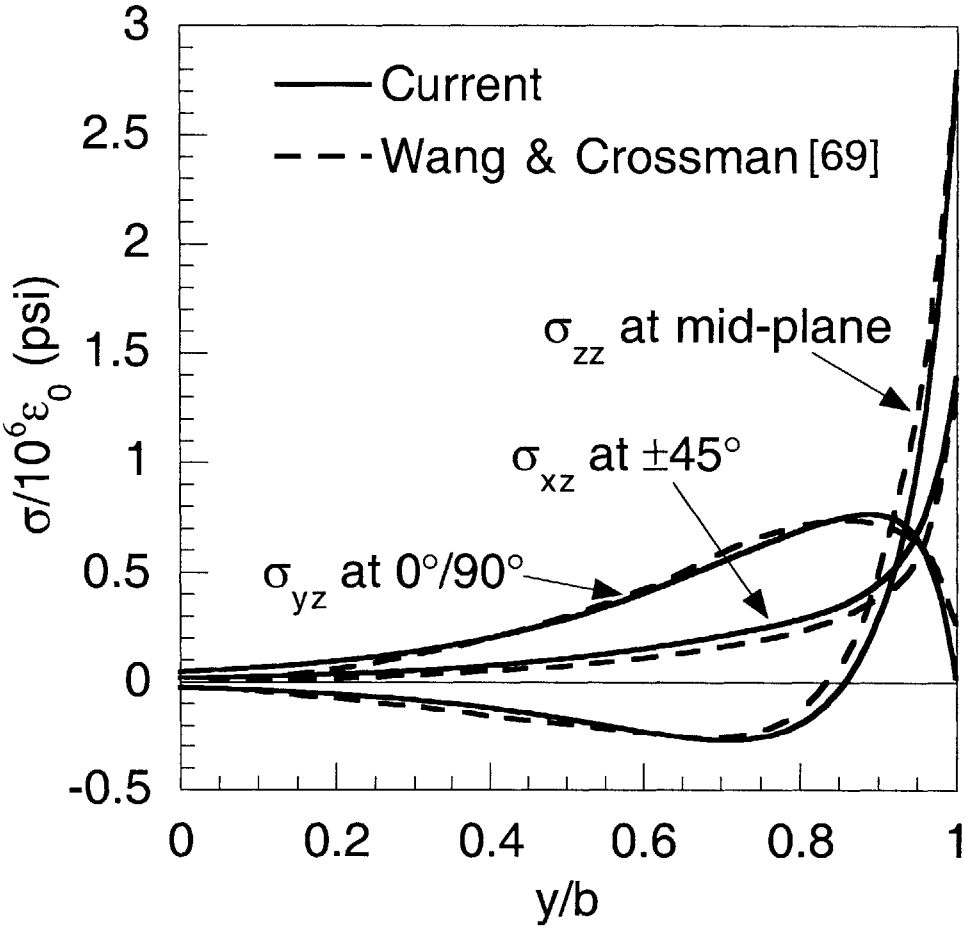

Figure 6.5 Interlaminar stresses obtained along various interfaces in a $[\pm 45/0/90]_s$ laminate with straight free edges under in-plane load using the global model and a finite difference method [69].

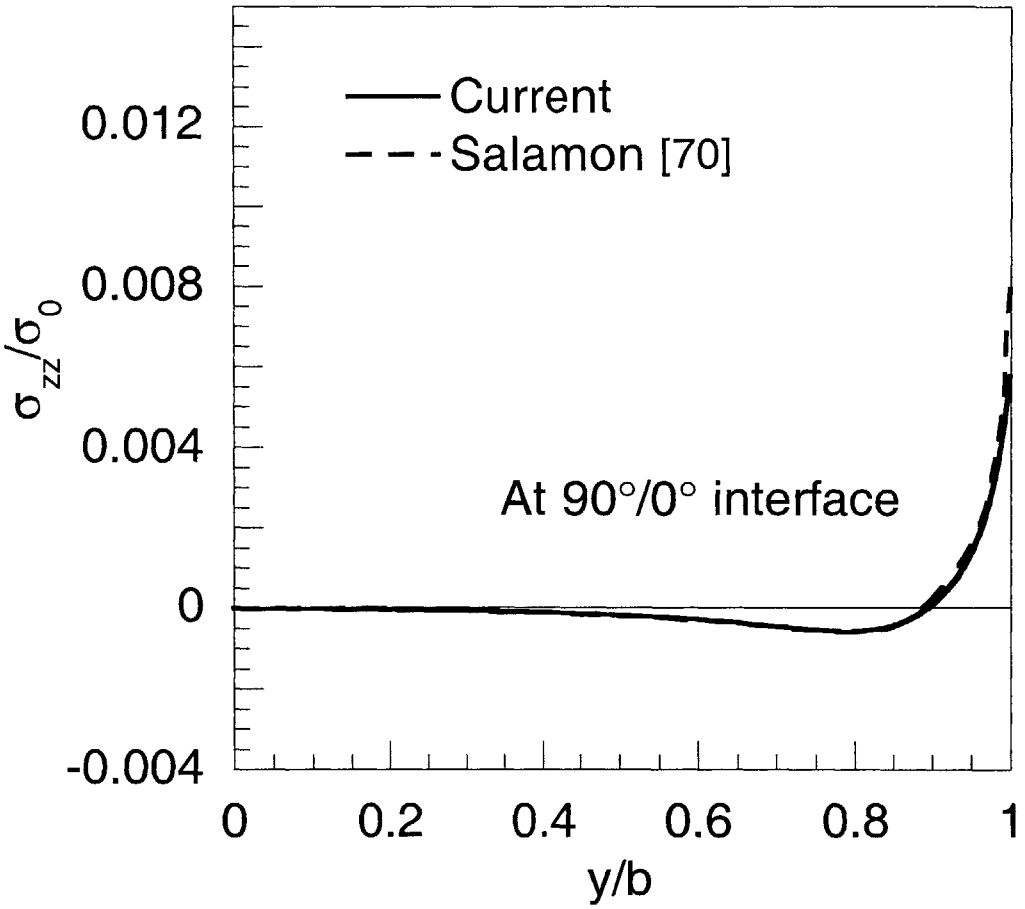

Figure 6.6 Interlaminar normal stresses along 90°/0° interface in a $[90/0]_s$ laminate with straight free edges under bending load obtained using the global model and a finite difference method [70].

a value of σ_0 equal to 10,000 psi, which is the in-plane stress in a $[0_2]_s$ laminate at z equal to –t for the bending strain as specified. The same normalization is used herein as well to allow for direct comparison. The interlaminar normal stresses along the y-direction of the $[90/0]_s$ laminate at the 90°/0° interface (z = –t) are shown in Figure 6.6. It can be seen that the stress distributions obtained using the current method and from the previous analysis match very well. Both stress distributions show that the interlaminar normal stress is very high at the free edge (y/b = 1) but decays rapidly to zero approximately one laminate thickness away from the free edge. The *crossover* point, which is defined as the point at which stress reversal from tensile to compressive, or vice versa, occurs in the stress distribution, as obtained using the current method nearly coincides with that from the previous analysis at approximately y/b equal to 0.9. The general trend of the interlaminar normal stress is very similar to that observed in laminates with straight free edges under in-plane loads (see Figure 6.5). The interlaminar shear and normal stresses in the $[\pm 45]_s$ laminate at the ±45° interface (z = –t) are shown in Figure 6.7. It can be seen that interlaminar stresses obtained using the current analytical method and the finite difference method are, again, in good agreement, thereby validating the current method for cases of bending load.

6.1.3 Global Model

Three laminates with external and internal ply dropoffs are considered for validation of the global model. A laminate with a layup of $[0_{2D}/0_2]_s$ is considered for the external ply dropoff case. This laminate has been considered in a previous investigation repeated in the literature [27], and the stress analysis results from that work are used for comparison. For the bending load case, a $[0_D/0_2]_s$ laminate is considered and the results compared with those obtained using the FE method. The laminate with internal ply dropoffs considered has a layup of $[0_4/0_D]_s$. For this laminate, three different taper angles of 0°, 1° and 5.7° in the dropoff region are considered via the FE method to assess applicability of the global model to these types of laminates. The results obtained using

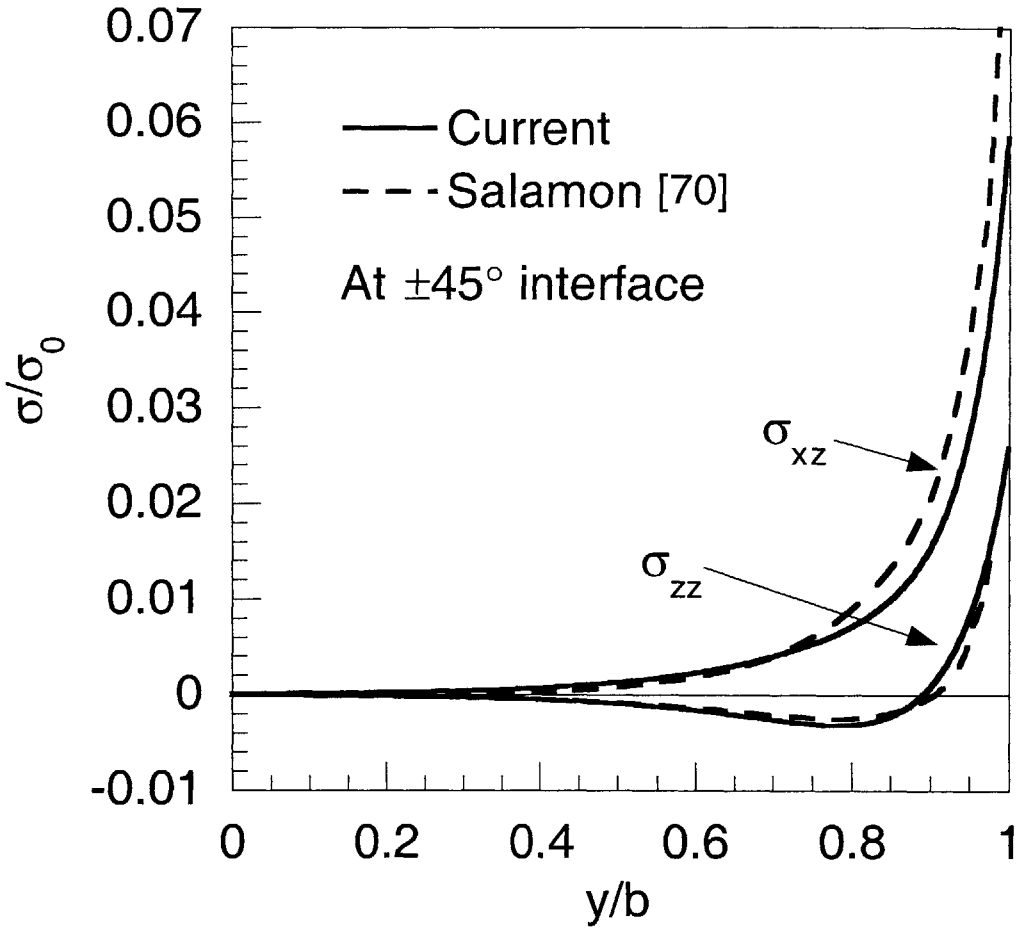

Figure 6.7 Interlaminar shear and normal stresses along the ±45° interface in a $[\pm 45]_s$ laminate with straight free edges under bending load obtained using the global model and a finite difference method [70].

the global model are compared with those obtained via FE analyses. In addition, the stress analysis result from a previous investigation is available for this laminate with a taper angle of 7°. This is also used to validate both the global and the FE models.

A diagram of the $[0_{2D}/0_2]_s$ laminate considered is shown in Figure 6.8 along with the dimensions and coordinate system. The length of the laminate is 2ℓ, where ℓ is equal to 8t and the thickness of each ply is t. Material properties of a generic graphite/epoxy composite in SI units shown in Table 6.1 are used. A uniform tensile stress, σ_0, is applied at the undropped end. The same laminate configuration was considered by Wu and Webber [27] using a quasi-three-dimensional displacement-based FE model. Their results are used for validation of the global model.

The in-plane and interlaminar stress distributions obtained using the global model and from the previous FE analysis are shown in Figures 6.9 and 6.10, respectively. All stresses are normalized by the applied stress, σ_0, and the x-direction coordinate is normalized by the length ℓ. The in-plane stresses within the continuous plies along the interface of the continuous and terminated plies (z = 2t) are shown in Figure 6.9. It can be seen that the stress distributions obtained using the global model and from the previous analysis generally follow the same trend, although the magnitudes differ over the entire undropped region and parts of the dropped region. At its peak, the in-plane stress from the global model is equal to $2.2\sigma_0$, while that from the FE model is equal to $5.2\sigma_0$. The difference in the overall magnitude is not unexpected because, in the current method, in-plane stress is assumed to be constant through-the-thickness and equal to the average in-plane stress in each ply. Thus, the average in-plane stress obtained using the global model along the interface of the continuous and terminated plies where the highest stress concentration occurs should be smaller than the in-plane stress obtained using an FE model where it is assumed to vary through-the-thickness of each ply.

In Figure 6.10, the interlaminar shear and normal stresses along the same interface (z = 2t) are shown. For the interlaminar stresses, it can be seen that the results from the

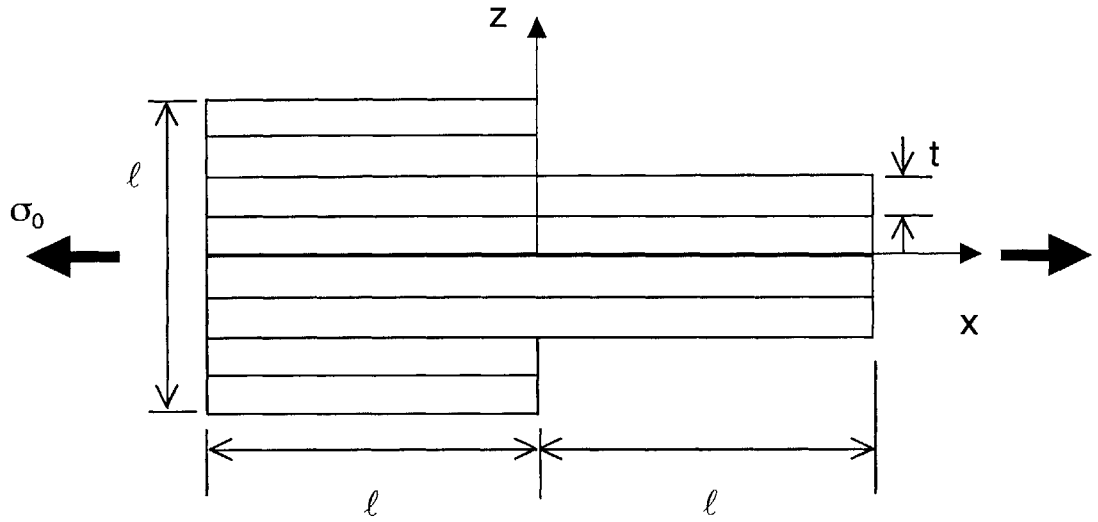

$\ell = 8t$

Figure 6.8 Diagram of a $[0_{2D}/0_2]_s$ laminate under uniform in-plane stress σ_0 applied at the undropped end.

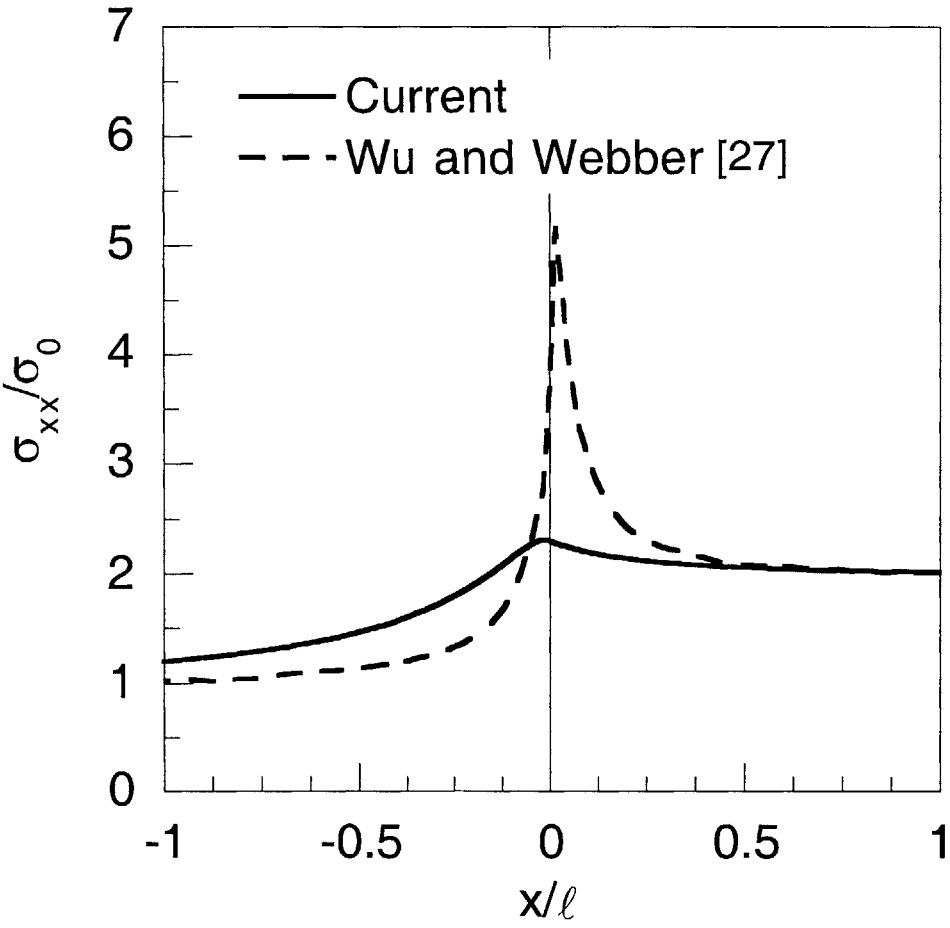

Figure 6.9 In-plane stresses within the continuous ply along the interface of z equal to t in the continuous ply in a $[0_{2D}/0_2]_s$ laminate under in-plane load obtained using the global model and a finite element method [27].

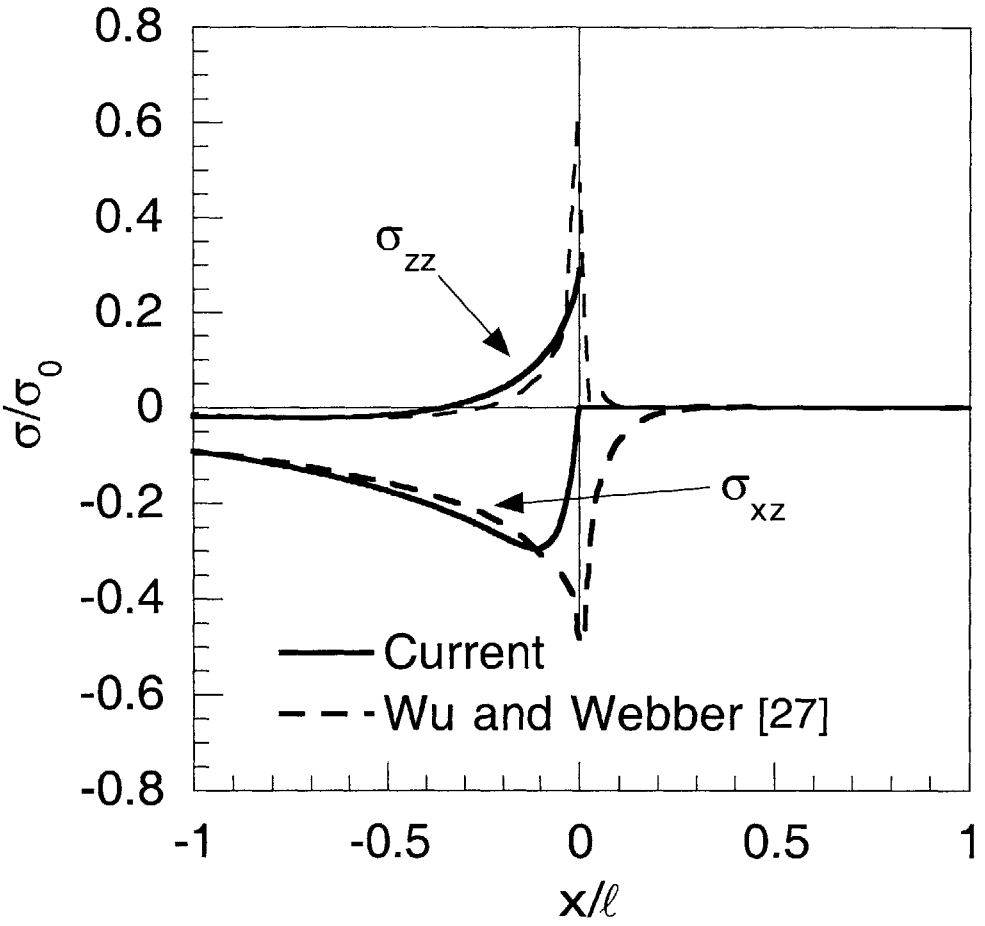

Figure 6.10 Interlaminar normal and shear stresses along the interface at z equal to t in a $[0_{2D}/0_2]_s$ laminate under in-plane load obtained using the global model and a finite element method [27].

current method not only follow the general trend of the previous analysis but are also comparable in magnitude except in the immediate vicinity of the cutoffs ($x/\ell = 0$). Since the case of z equal to 2t in the dropped region coincides with the outer surface of the laminate, both interlaminar shear and normal stresses should be zero. This is predicted by the current analytical method in contrast to the FE results where this traction-free condition at the outer surface of the dropped region is not satisfied at all points by the FE results.

The global model can be used to perform refined analyses by dividing each ply into thinner sub-plies. Note that the current analytical method is formulated by considering stress equilibrium on a ply-by-ply basis. This leads to the assumption for the stress field in each ply (see equations (4.8) for in-plane load and equation (4.30) for bending load). In the refined analysis, the same formulation is used on a sub-ply by sub-ply basis. This leads to the assumption for the stress field in each sub-ply. Since the stress field is assumed in each sub-ply, the refined analysis requires a greater number of stress functions. In this context, refining the global model is analogous to refining the FE analysis by using smaller elements.

Plots of the in-plane and interlaminar normal stresses obtained by refining each ply up to eight sub-plies in multiplies of two are shown in Figures 6.11 and 6.12. The interlaminar shear stresses are not shown because their characteristics are similar to those of the interlaminar normal stresses. It can be seen in Figure 6.11 that increasing the number of ply sub-divisions affects the in-plane stress distribution over a large portion of the length of the laminate including the peak stress value. The overall in-plane stress distribution obtained via dividing each ply into eight sub-plies is in good agreement with that obtained using the FE analysis. The peak stress value from this refined analysis is $4.2\sigma_0$, which is comparable to $5.2\sigma_0$ from the FE analysis. Note that the peak in-plane stress in the FE analysis occurs approximately one ply thickness away from the cutoff. This may be due to the fact that in a FE analysis, the stresses are obtained at discrete

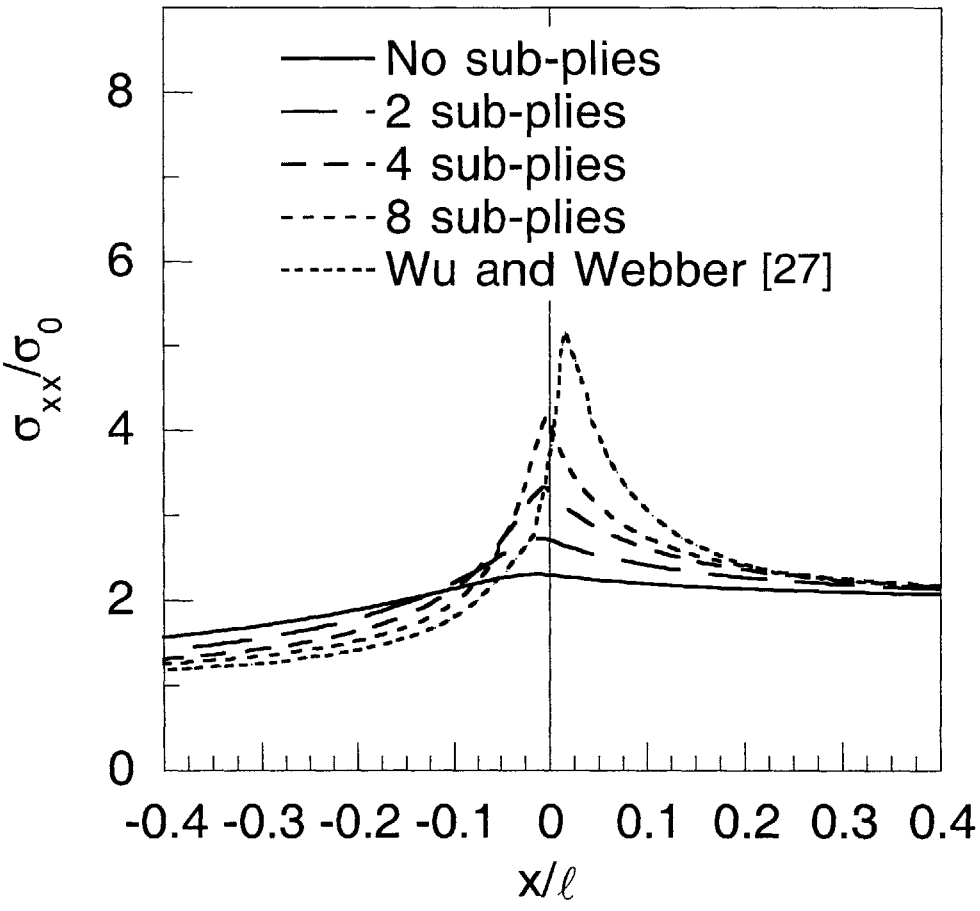

Figure 6.11 In-plane stresses obtained using refined analyses via ply sub-division within the continuous ply along the interface of z equal to t in a $[0_{2D}/0_2]_s$ laminate under in-plane load.

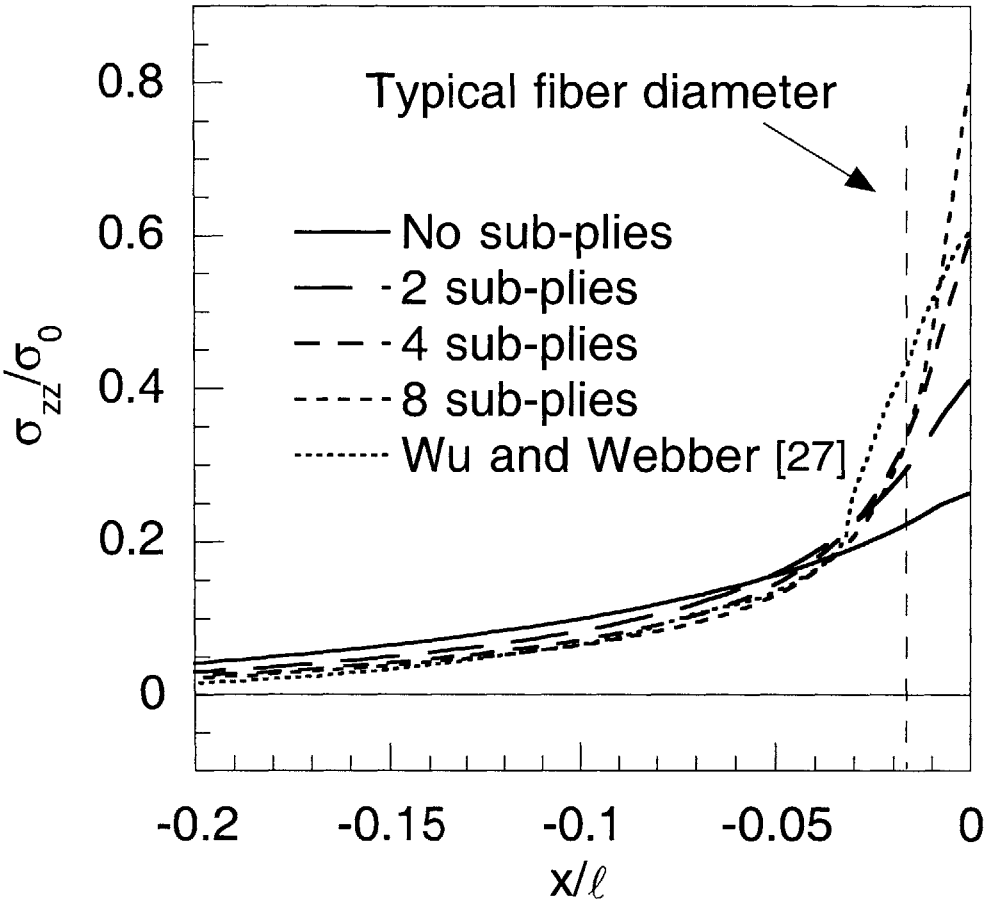

Figure 6.12 Interlaminar normal stresses obtained using refined analyses via ply subdivision along the interface of z equal to 2t in a $[0_{2D}/0_2]_s$ laminate under in-plane load.

points, and the stress at the cutoff was not calculated in the FE analysis. The peak interlaminar normal stress in Figure 6.12 is also seen to increase with increasing number of sub-plies and actually exceeds the peak value from the FE analysis for the most refined case. However, only a small region near the dropoff (a fraction of the ply thickness) is affected for this stress component. Note that only the undropped region is shown in Figure 6.12 since the interlaminar normal stress is zero in the dropped region.

The values of the peak interlaminar normal stress and the distance from the dropoff location for the interlaminar normal stress to reach 1% of the applied stress, σ_0, are shown in Table 6.2. The peak stress value obtained using the refined analysis with four sub-plies matches that obtained by Wu and Webber. It can be seen from Table 6.2 that the rate of increase of the peak interlaminar normal stress continues to grow as the analysis is refined. This suggests the possibility of the existence of a singularity at the dropoff location for the continuum as modeled. However, it is noted that although such a refined analysis may give more precise stress values at x equal to zero, the utility is questionable since the length-scales over which the stresses are refined are on the order of a fiber diameter where the assumptions of material homogeneity within a ply are no longer valid. The typical dimension of a fiber diameter is indicated in Figure 6.12.

For the bending load case, a laminate with a layup of $[0_D/0_2]_s$ is considered. The material properties of a generic glass/epoxy composite shown in Table 6.1 are used, and a bending moment, M, equal to 1 kNm is applied at the ends such that the lower half of the laminate is under compression. The coordinate system for this laminate is defined in the same manner as that shown in Figure 6.8. The length, ℓ, of the undropped and dropped regions is equal to 40t, where t is the thickness of a ply. Since no results for laminates with ply dropoffs under bending load are available in the literature, a FE analysis was performed using the general procedure described in Section 6.1.1.

The in-plane and interlaminar stress distributions obtained using the global model and the FE model described previously are shown in Figures 6.13 through 6.19. In

Table 6.2 Peak interlaminar normal stress and characteristic length[1] comparisons for refined analysis using ply sub-division of $[0_{2D}/0_2]_s$ laminate under in-plane load

	Number of Ply Sub-divisions				Wu and Webber [27]
	None	2	4	8	
Peak Interlaminar Normal Stress ($/\sigma_0$)	0.26	0.41	0.60	0.80	0.60
Characteristic Length (/b)	0.34	0.32	0.30	0.30	0.26

[1] Distance required for interlaminar normal stress to equal 1% of applied stress, σ_0.

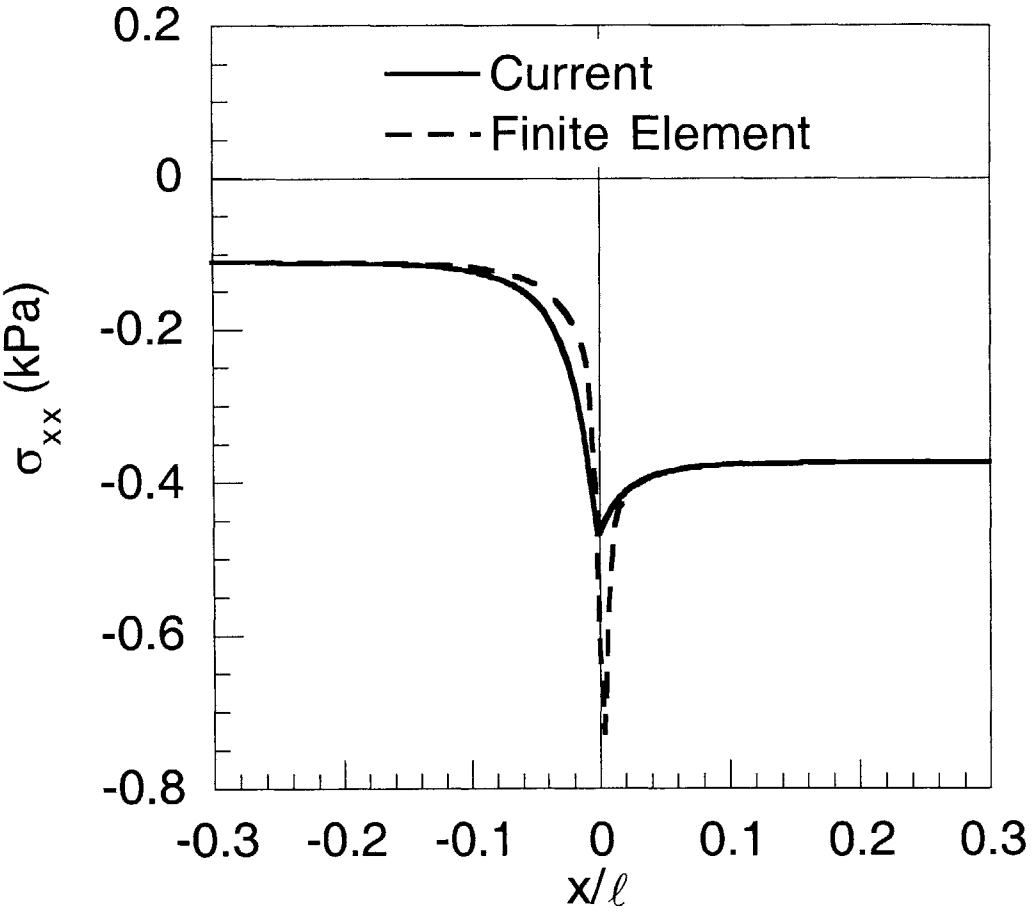

Figure 6.13 In-plane stresses along the interface of the continuous and terminated plies in the undropped region and outer surface in the dropped region ($z = -2t$) in a $[0_D/0_2]_s$ laminate under a bending load of 1 kNm obtained using the global model and FE method.

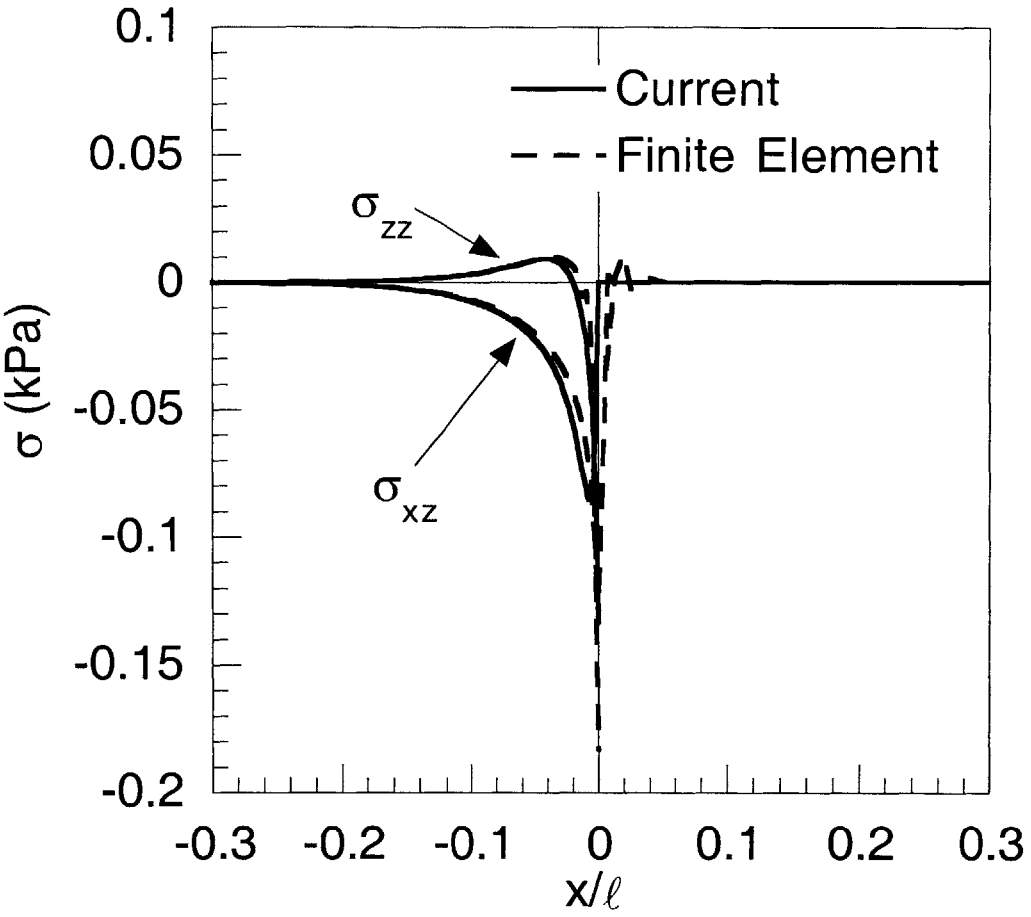

Figure 6.14 Interlaminar shear and normal stresses along the interface of the continuous and terminated plies in the undropped region and outer surface in the dropped region ($z = -2t$) in a $[0_D/0_2]_s$ laminate under a bending load of 1 kNm obtained using the global model and FE method.

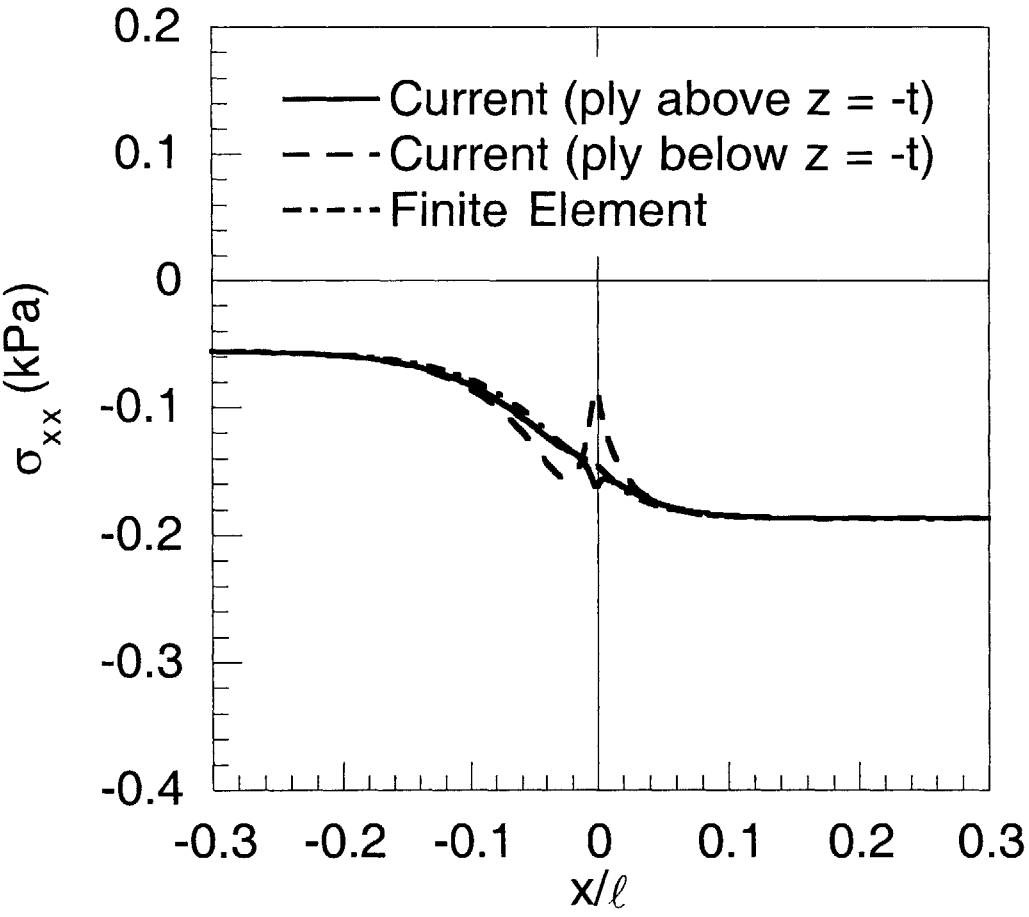

Figure 6.15 In-plane stresses along the interface of two continuous plies at z equal to –t in a $[0_D/0_2]_s$ laminate under a bending load of 1 kNm obtained using the global model and FE method.

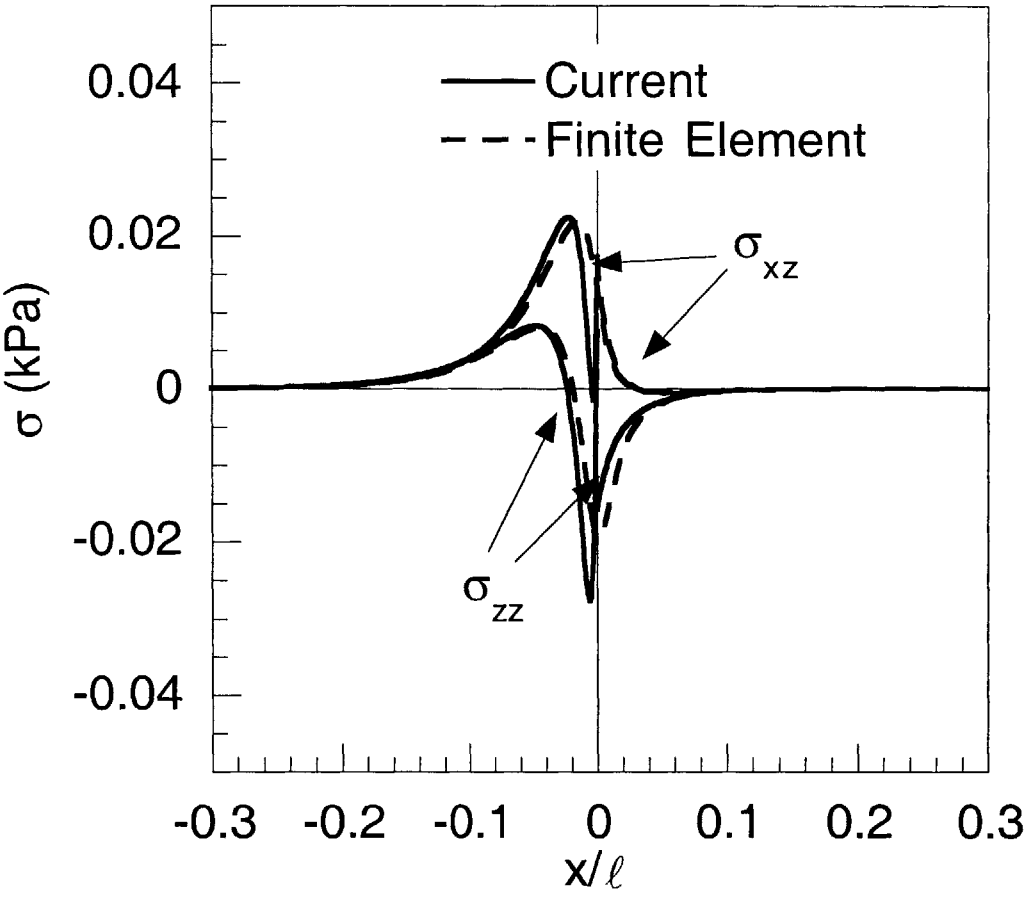

Figure 6.16 Interlaminar shear and normal stresses along the interface of two continuous plies at z equal to $-t$ in a $[0_D/0_2]_s$ laminate under a bending load of 1 kNm obtained using the global model and FE method.

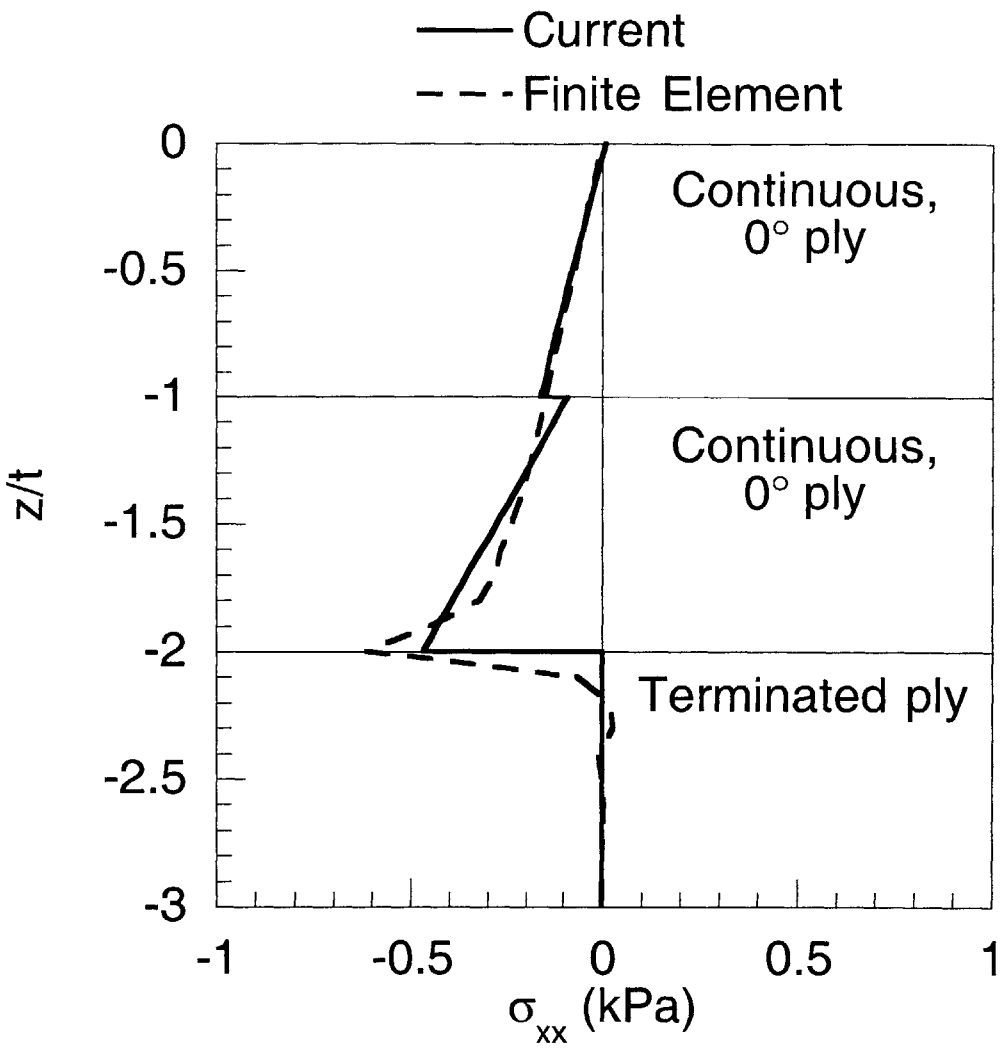

Figure 6.17 In-plane stresses through the thickness at the dropoff at the edge of the undropped region (x = 0) in a $[0_D/0_2]_s$ laminate under a bending load of 1 kNm obtained using the global model and FE method.

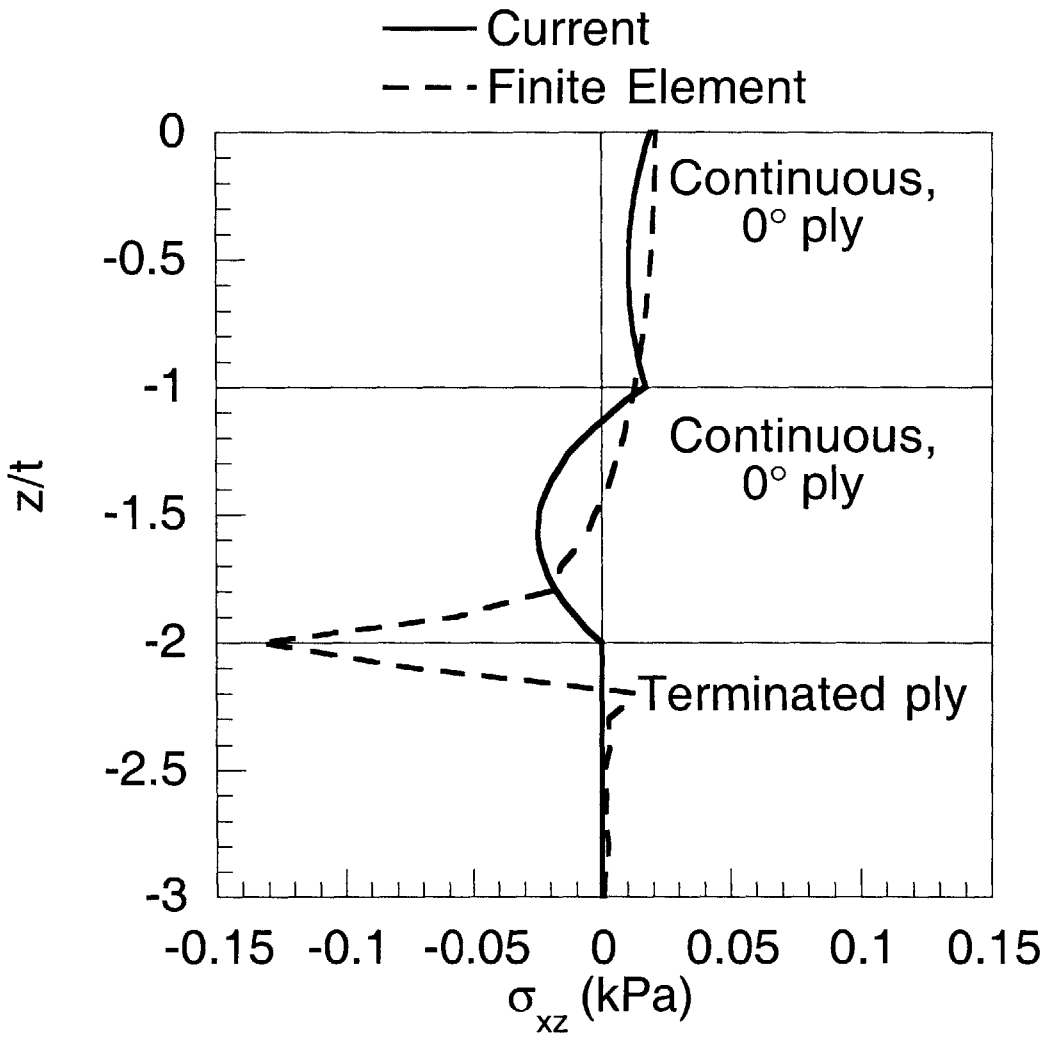

Figure 6.18 Interlaminar shear stresses through the thickness at the dropoff at the edge of the undropped region (x = 0) in a $[0_D/0_2]_s$ laminate under a bending load of 1 kNm obtained using the global model and FE method.

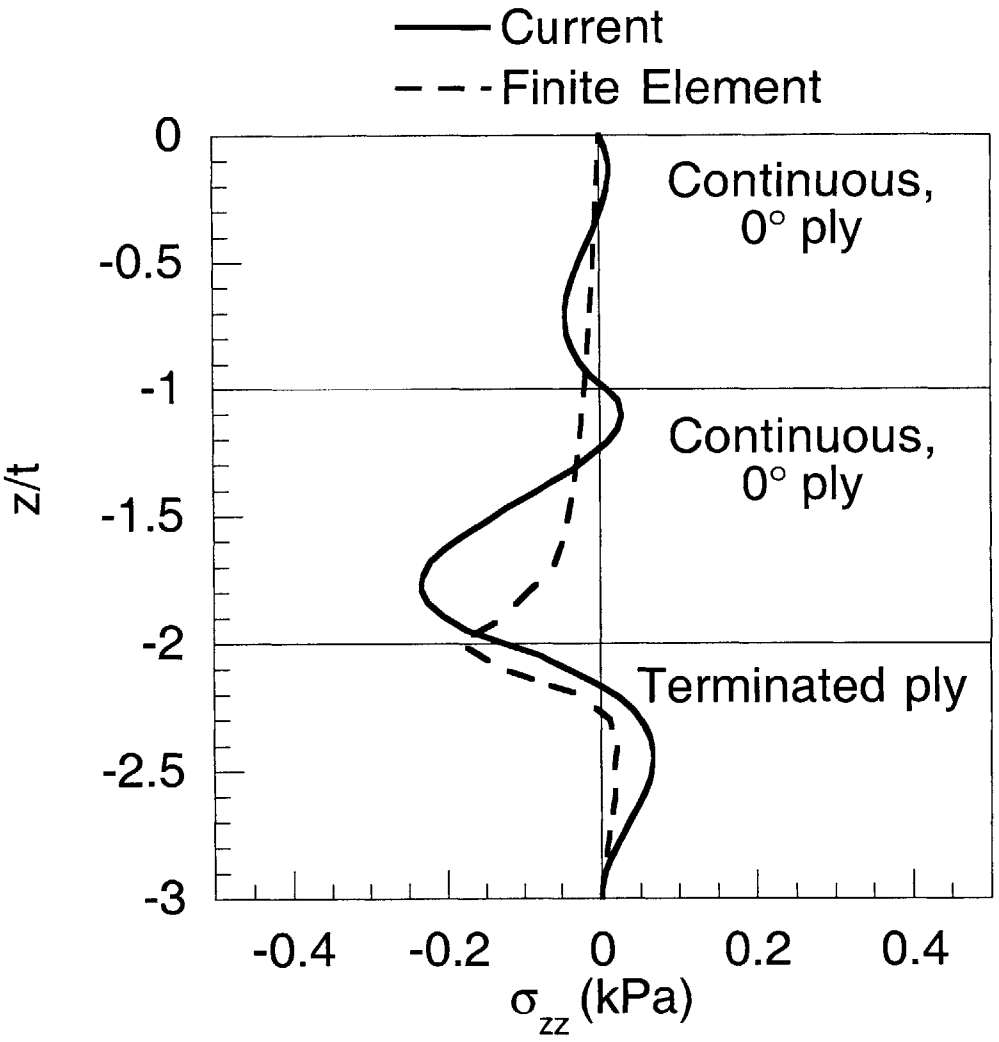

Figure 6.19 Interlaminar normal stresses through the thickness at the dropoff at the edge of the undropped region (x = 0) in a $[0_D/0_2]_s$ laminate under a bending load of 1 kNm obtained using the global model and FE method.

Figures 6.13 and 6.14, the stresses along the interface of the continuous and terminated plies in the undropped region and the outer surface in the dropped region ($z = -2t$) are shown. In Figures 6.15 and 6.16, the stresses along the interface of two continuous plies ($z = -t$) are shown. The stresses through the thickness in the lower half of the laminate at the dropoff ($x = 0$) at the edge of the undropped region are shown in Figures 6.17 through 6.19.

It can be seen from Figures 6.13 and 6.14 that the in-plane and interlaminar stresses along z equal to $-2t$ obtained using the global and the FE models match extremely well except in the immediate vicinity of the cutoff corresponding to values of x/ℓ less than 0.07. The in-plane stress along this interface is a minimum at the cutoff (maximum in magnitude) and decreases rapidly in magnitude to converge to the far-field applied stress values approximately one laminate thickness away from the cutoff in both the undropped and dropped regions. Similarly, the interlaminar stresses along this interface decay to zero within approximately one laminate thickness away from the cutoff. As was seen for the in-plane loading case, the interlaminar shear stress obtained using the analytical method satisfies the traction-free condition at x equal to 0 while that obtained using the finite element does not at all points. Since the current FE method is a displacement-based method, it is not capable of completely satisfying this traction-free condition. However, a better approximation to that condition would be obtained by refining the mesh.

As shown in Figures 6.15 and 6.16, the stresses along the interface of the two continuous plies ($z = -t$) obtained using the two methods also show very good agreement except in the vicinity of the dropoff location within x/ℓ less than 0.05. Note that two in-plane stress distributions along this interface can be obtained via the global model. One corresponds to the in-plane stress in the ply immediately below the interface, and the other corresponds to that in the ply immediately above the interface. Although both in-plane stress distributions show similar trends away from the cutoff, the one in the ply

immediately below the interface exhibits a deviation from the smooth transition across undropped and dropped regions in the vicinity of the dropoff location seen in the stress distribution from the FE analysis. The in-plane stress in the ply above the interface is seen to match that obtained using the FE analysis very well. The dual-valued nature of the in-plane stress obtained using the global model in this example is discussed further in the following paragraph. The interlaminar shear and normal stresses along z equal to –t is non-zero in the vicinity of the dropoff due to the terminated plies, although the magnitudes are smaller by approximately an order of magnitude than those along the interface of the continuous and terminated plies in Figure 6.14. It is noted that, as shown for the in-plane loading case in the previous example, refined analyses may be performed using the global model through sub-division of plies to obtain more refined stress distributions.

Based on the good agreement between the stresses obtained using the current analytical and FE methods, the through-the-thickness stress distributions are also expected to match well. In Figure 6.17, the in-plane stresses, σ_{xx}, obtained using the two methods meet such expectations. However, it can be seen that the results obtained using the global model satisfy the traction-free condition exactly in the terminated ply at x equal to 0 while the finite element method yields finite stresses in the vicinity of z equal to –2t in the terminated ply. Note that the in-plane stress obtained using the current analytical method is discontinuous at the ply interfaces at z equal to –t and –2t. Since each ply in the laminate has the same modulus, the discontinuity implies that the in-plane strain is also discontinuous, which is physically incorrect. This is a result of the fact that the current analytical method for bending load is a stress-based method in which the stress continuity conditions are explicitly enforced and satisfied but the strain continuity conditions are not. The reverse problem that strain continuity conditions are satisfied but stress continuity conditions are not, can be found in displacement-based analytical methods such as classical laminated plate theory and higher order plate theories for

bending loads [72]. It is noted that in the current analytical method, the discontinuity can be alleviated, although not eliminated, via ply sub-division. A similar discontinuity exists for the in-plane load cases, which is described in a later section. The interlaminar shear and normal stress states through the thickness at the dropoff obtained using the two methods as shown in Figures 6.18 and 6.19 do not match as well as the in-plane stresses, although the general trend is in agreement. In the case of the interlaminar shear stress in Figure 6.18, the traction-free condition in the terminated ply at z equal to 0 should also be satisfied as in the case of the in-plane stress. However, it can be seen that the interlaminar shear stress obtained using the finite element method fails to satisfy this condition completely, while the global model does.

The laminate with a layup of $[0_4/0_D]_s$ under in-plane load is considered next. A diagram of the laminate is shown in Figure 6.20 along with the coordinate system used. Note that the coordinate system is defined such that the negative lengthwise direction, x^-, corresponds to the undropped region and the positive lengthwise direction, x^+, corresponds to the dropped region. This coordinate system facilitates the comparison of interlaminar stresses obtained using the FE method and the analytical method because the stress field in the dropoff region is not considered using the analytical method. The lengths of the undropped and dropped regions are chosen to be 50t and 40t, respectively, where t is the thickness of each ply. These values for the length of the undropped and dropped regions were chosen such that the ratios of the length to the thickness of the laminate in each region are the same and equal to five. This is sufficiently long for the interlaminar stresses to decay to zero such that they are consistent with the assumption made in the analytical methods. The material properties of a generic glass/epoxy composite material are used as shown in Table 6.1, and a uniform tensile stress, σ_0, of 1000 MPa is applied at the dropped end for all laminates.

The $[0_4/0_D]_s$ laminate with three taper angles of 0°, 1° and 5.7° in the dropoff region are considered in the FE analysis. The three taper angles are considered in order

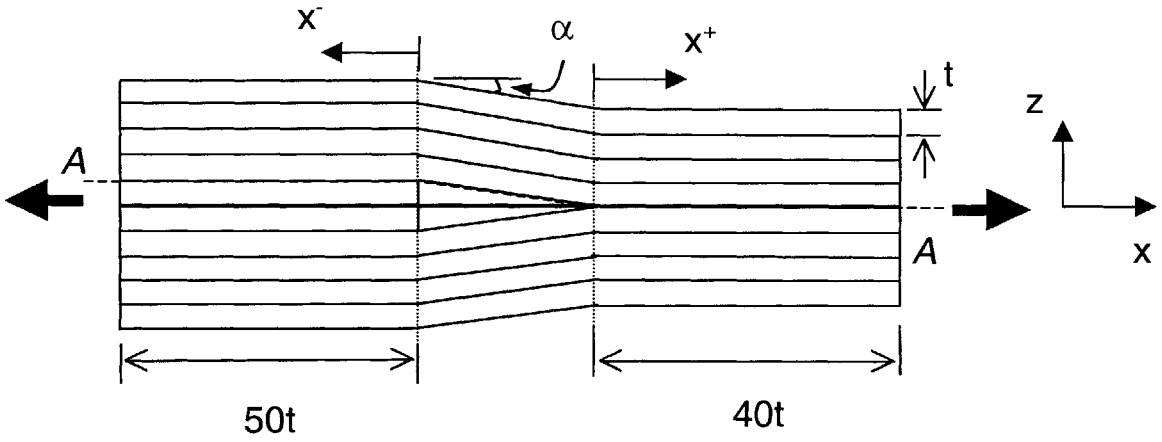

Figure 6.20 Diagram of a $[0_4/0_D]_s$ laminate under in-plane load.

to assess the applicability of the global model for internal dropoff cases. Note that the global model does not take the geometry of the dropoff region into account. Therefore, it is clear that the global model will not yield stress distributions that will match those in all three laminates with the three taper angles. Note that the configuration of the laminate with a taper angle of 0° is slightly different from the other two laminates. In such a laminate, the dropoff region is infinitely long, and thus, the laminate consists of only the undropped and dropoff regions; the dropped region does not exist.

The interlaminar stresses in the undropped region of the same laminate configuration is also available from a previous investigation by Cui, Wisnom and Jones [16]. They analyzed a laminate with the same layup and a taper angle of 5.7° but a shorter length of approximately 25t in the undropped region using a similar FE method. This is used to validate both the global model and the current FE analysis. The interlaminar shear and normal stresses, σ_{xz} and σ_{zz}, in the $[0_4/0_D]_s$ laminate with a taper angle of 5.7° obtained using the analytical method and the two FE methods are shown in Figures 6.21 and 6.22, respectively. The stresses are evaluated along the interface of the continuous and terminated plies in the undropped region (z = t), and the mid-plane in the dropped region (z = 0). This interface corresponds to the dashed line *AA* in Figure 6.20. The results shown in Figures 6.21 and 6.22 indicate that both the interlaminar shear and normal stresses calculated using the two FE analyses agree very well with each other in the undropped regions. The interlaminar shear stresses calculated using the global model and the two FE methods also match very well. At the mid-plane of the laminate in the dropped region, corresponding to z equal to 0, the interlaminar shear stress must equal zero under in-plane load due to anti-symmetry. The results shown in Figure 6.21 satisfy this condition. In Figure 6.22, it can be seen that the interlaminar normal stress calculated using the analytical method is an order of magnitude smaller than that obtained using the FE methods in the vicinity of the cutoff in the undropped region for x/t less than –5. In the dropped region, the interlaminar normal stresses obtained by the two different

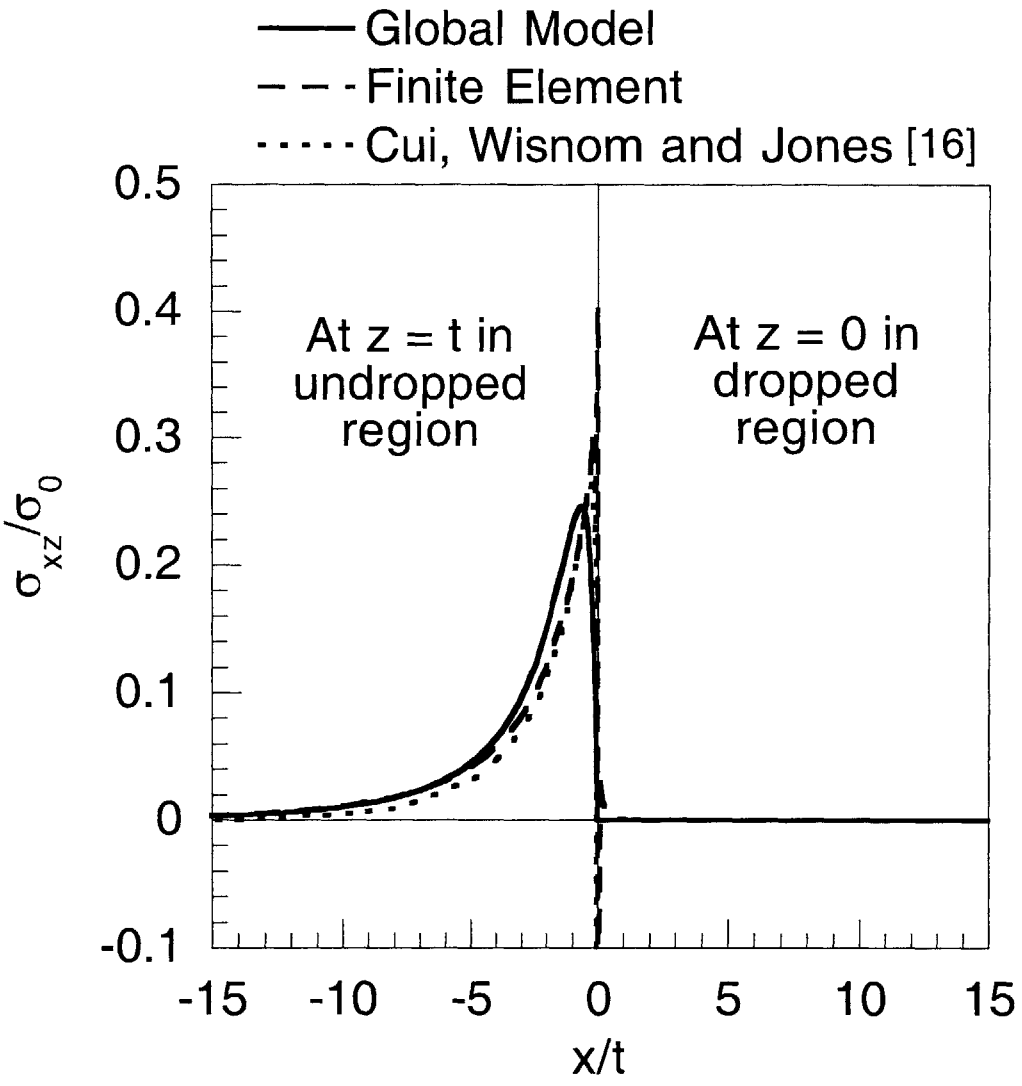

Figure 6.21 Interlaminar shear stresses along the interface at z equal to t in the undropped region and z equal to 0 in the dropped region in a $[0_4/0_D]_s$ laminate with a taper angle of 5.7° under in-plane load obtained using the global model, current FE model, and FE model from a previous investigation [16].

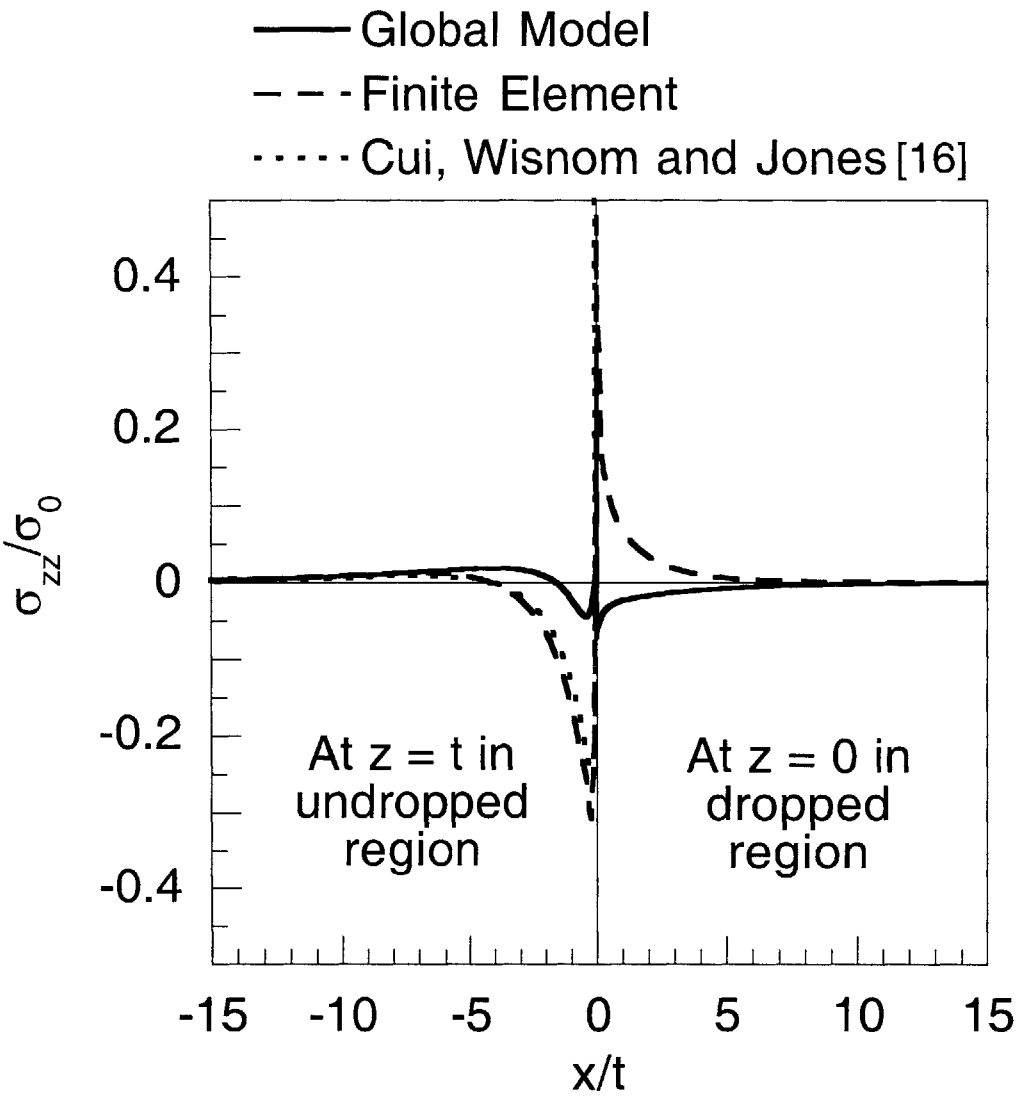

Figure 6.22 Interlaminar normal stresses along the interface at z equal to t in the undropped region and z equal to 0 in the dropped region in a $[0_4/0_D]_s$ laminate with a taper angle of 5.7° under in-plane load obtained using the global model, current FE model, and FE model from a previous investigation [16].

methods differ both in magnitude and sense.

The effects of the taper angle on the stress field obtained using the FE analysis can be seen in Figures 6.23 and 6.24. The results shown in Figure 6.23 indicate that there is no significant difference in the interlaminar shear stresses except in the vicinity of the cutoff within one ply thickness in the laminates with three different taper angles. The stress values at the cutoff can be ignored since the current displacement-based FE method is not expected to yield accurate values in this region. In the case of interlaminar normal stresses shown in Figure 6.24, significant differences in magnitude can be seen in the three laminates. In the undropped region, the magnitude of the peak interlaminar normal stress is smallest for the laminate with a taper angle of 0° and increases with the increasing angle of taper. In addition, the crossover distance, which is the distance measured from the cutoff that is required for the interlaminar normal stress to change from compressive to tensile, is shortest for the laminate with 0° taper and increases with increasing angles of taper. In the dropped region, the interlaminar normal stress is also affected by the change in taper angle. The trend clearly indicates that smaller angles of taper will reduce the tensile nature of the interlaminar normal stress significantly with regard to the magnitude and decay length. Such trends are investigated in greater detail in the Section 6.2. Note that since the dropped region does not exist in the laminate with 0° taper angle, the interlaminar stress in this region using the FE method cannot be obtained, and is not shown.

Since the global model does not take the dropoff region into account, the laminate with the taper angle of 0° is more representative of the global model. Thus, the results for this laminate should be the best match for the results of the global model. This can be verified through comparison of the interlaminar stresses in the laminate with a taper angle of 0° obtained using the two methods shown in Figures 6.21 through 6.24. For the interlaminar shear stresses, the results obtained using the global model show very good agreement with those obtained using the FE models for all three laminates with different taper angles including the 0° taper angle case. This can be seen immediately by

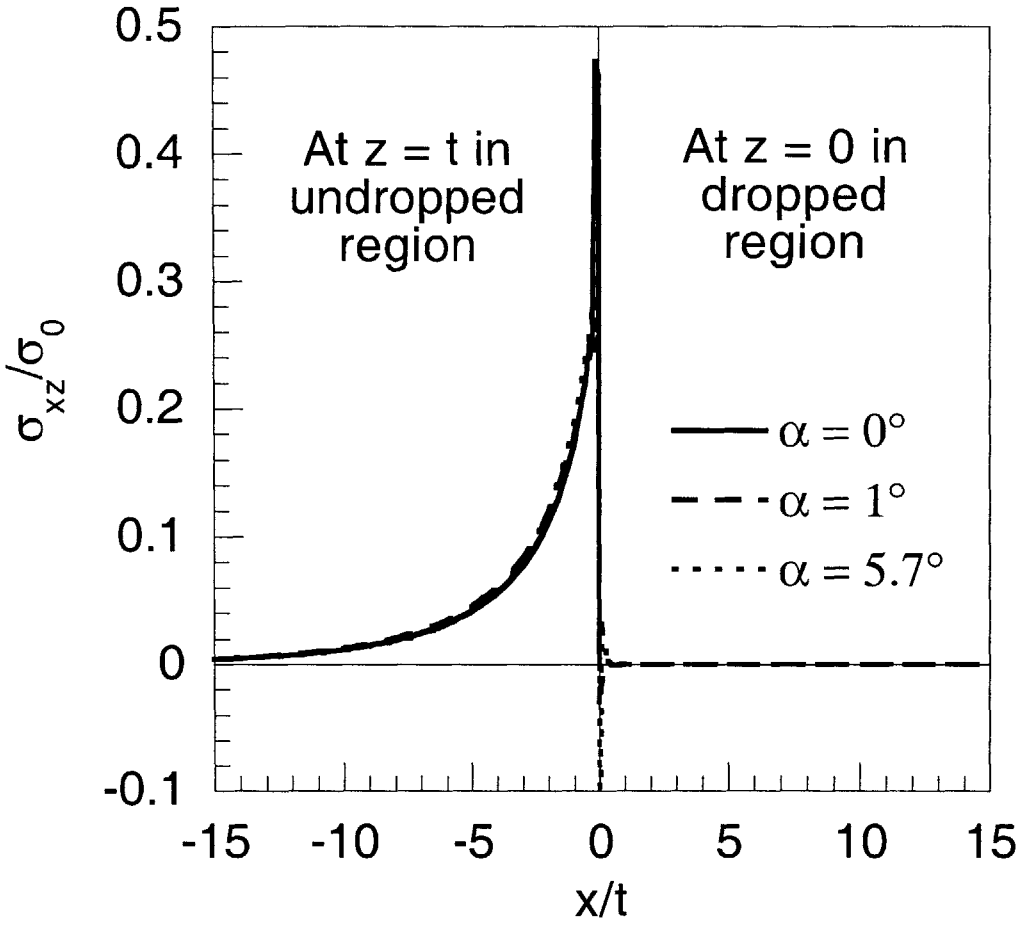

Figure 6.23 Interlaminar shear stresses along the interface at z equal to t in the undropped region and z equal to 0 in the dropped region in a $[0_4/0_D]_s$ laminate with three different taper angles under in-plane load obtained using the current FE method.

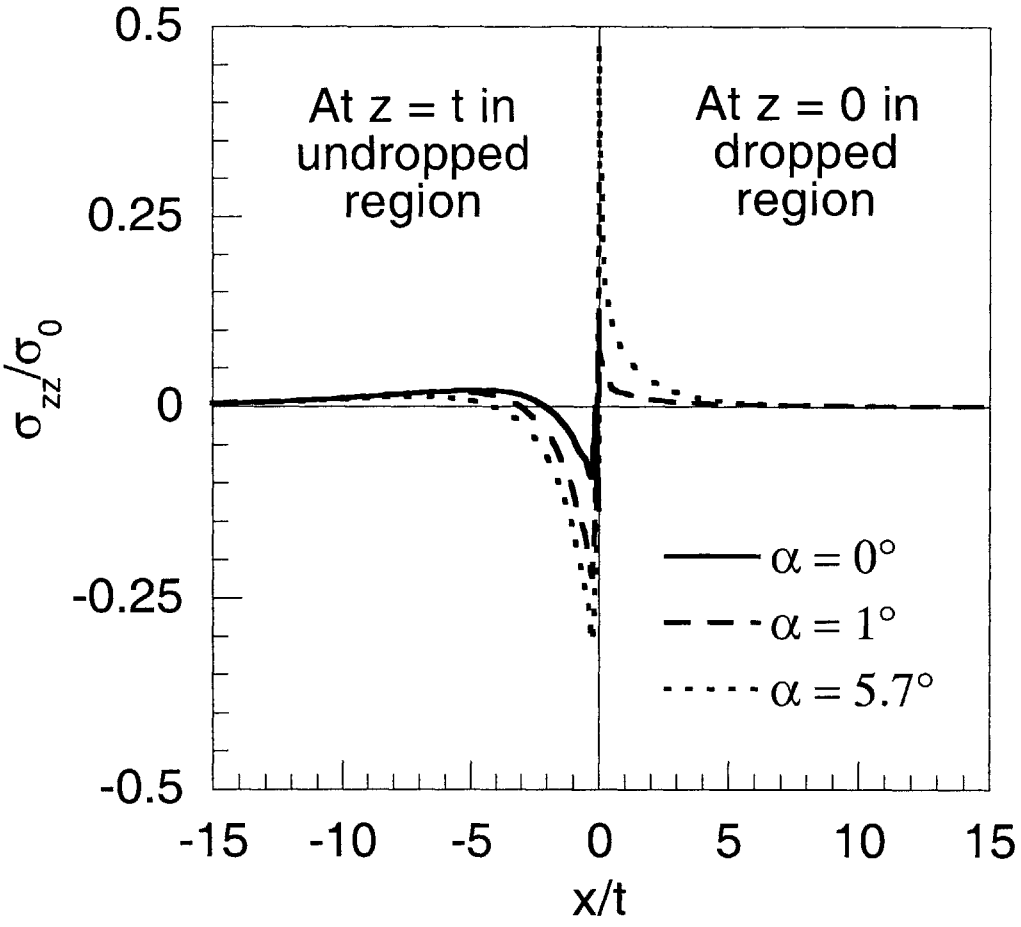

Figure 6.24 Interlaminar normal stresses along the interface at z equal to t in the undropped region and z equal to 0 in the dropped region in a $[0_4/0_D]_s$ laminate with three different taper angles under in-plane load obtained using the current FE method.

comparing the interlaminar shear stresses in Figures 6.21 and 6.23. For the interlaminar normal stress, the results for the laminates with a taper angle of 0° obtained using the global and FE models from Figures 6.22 and 6.24 are shown again in Figure 6.25. As expected, the interlaminar normal stresses in the undropped region are seen to match very well except in the vicinity of the cutoff for x/t less than –2.5t. At the cutoff, the interlaminar normal stress obtained using the global model is tensile while that obtained using the FE model is compressive. Otherwise, the magnitude and crossover points of the interlaminar normal stresses obtained using the two methods are seen to be in good agreement.

The results presented in this sub-section show that the stress fields calculated using the global model provide good first order approximations of the complete stress fields in laminates with external and internal ply dropoffs. The interlaminar stresses in the laminate with external dropoffs arise solely due to the global discontinuities, which are considered in the global model. Therefore, the global model where the laminate is modeled as two separate uniform thickness regions with the stresses being transferred only through the continuous plies is an exact representation of such a laminate. As a result, it is expected to yield the accurate stress field. Comparison with the solution obtained using the FE method not only shows that the global model yields valid interlaminar stress distributions, but one that satisfies the traction-free boundary conditions.

Interlaminar stresses in laminates with internal dropoffs arise due to both global and local discontinuities, the latter of which are not considered in the global model. Since this model does not take into account the geometry of the dropoff region, the effect of the taper angle is not captured. However, it was seen from the FE analysis that the effect of the taper angle is not significant for interlaminar shear stresses, and that the solution obtained using the analytical method is very close to those obtained using the FE method. For the interlaminar normal stresses, the results from the FE analysis indicate

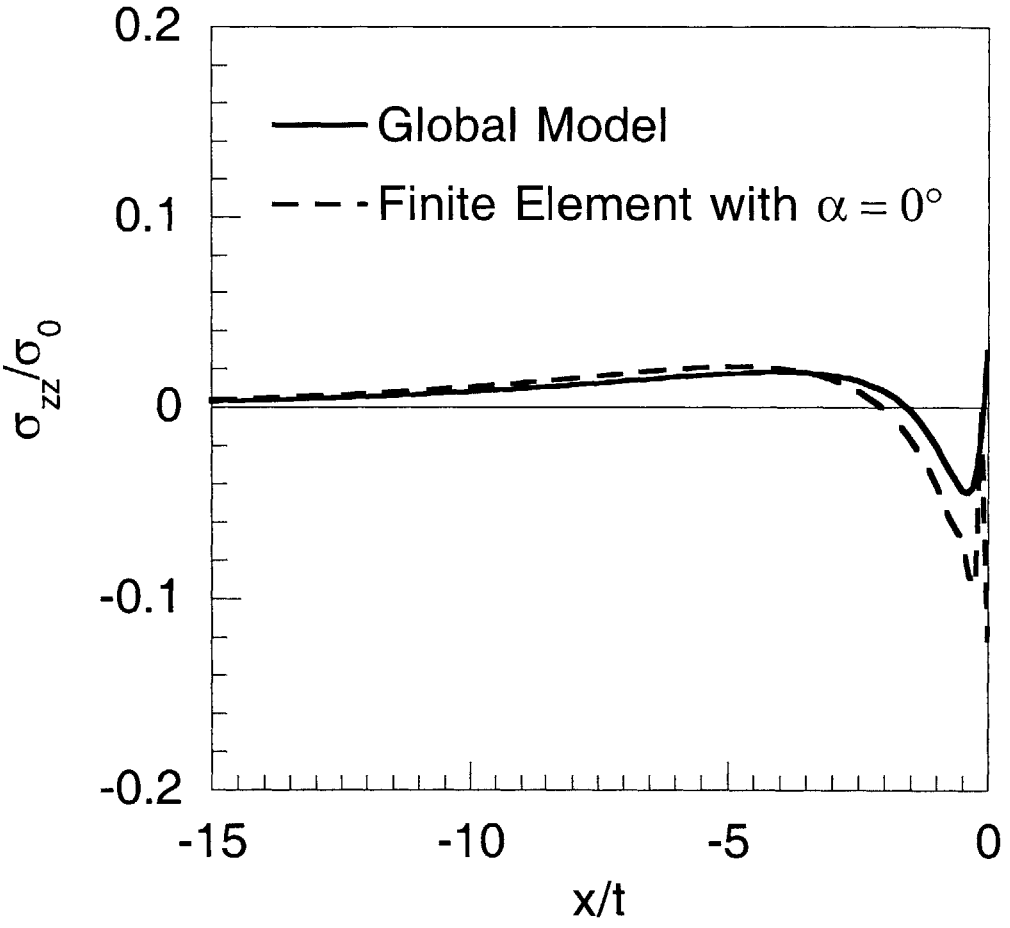

Figure 6.25 Interlaminar normal stresses along the interface at z equal to t in the undropped region in a $[0_4/0_D]_s$ laminate with a taper angle of 0° under in-plane load obtained using the global model and the current FE method.

that the effect of the taper angle is significant. It was seen that increasing the taper angle had the effect of increasing the magnitude and decay length (or crossover points) of the interlaminar normal stresses. The interlaminar normal stress distribution obtained using the analytical method was shown to match well with those obtained using the FE method for the laminate with a taper angle of 0°, but not for the laminate with a taper angle of 5.7°. This indicates that the global model correctly captures the effect of the global discontinuities in laminates with internal dropoffs, but not the effect of the local discontinuities, specifically the taper angle. The mixed model, which includes the effect of the taper angle, is considered in the next sub-section.

6.1.4 Mixed Model

Two laminates are considered for validation of the mixed model. One is a $[0_4/0_D]_s$ laminate, which was considered in the previous sub-section for the global model. The other is a laminate with the same number of continuous and terminated plies as the $[0_4/0_D]_s$ laminate but with the terminated plies located at a different thickness location. The layup of the second laminate is $[0_2/0_D/0_2]_s$, and it is evaluated for the in-plane load case only. The $[0_4/0_D]_s$ laminate under in-plane load is considered first, followed by the same laminate under bending load. The $[0_2/0_D/0_2]_s$ laminate is considered next to show validity and applicability of the mixed model to laminates with ply dropoffs located at arbitrary locations.

The geometry of the $[0_4/0_D]_s$ laminate is shown in Figure 6.20. The same lengths in the undropped and dropped regions, material properties, and in-plane load conditions described in the previous sub-section are used. The interlaminar shear and normal stresses, σ_{xz} and σ_{zz}, for the laminate with two taper angles, 1° and 5.7°, are shown in Figures 6.26 and 6.27, respectively. All stresses are evaluated along the interface of the continuous and terminated plies ($z = t$) in the undropped region and along the mid-plane ($z = 0$) in the dropped region corresponding to the dashed line *AA* in Figure 6.20. These values are normalized by the applied stress, σ_0, in the undropped region.

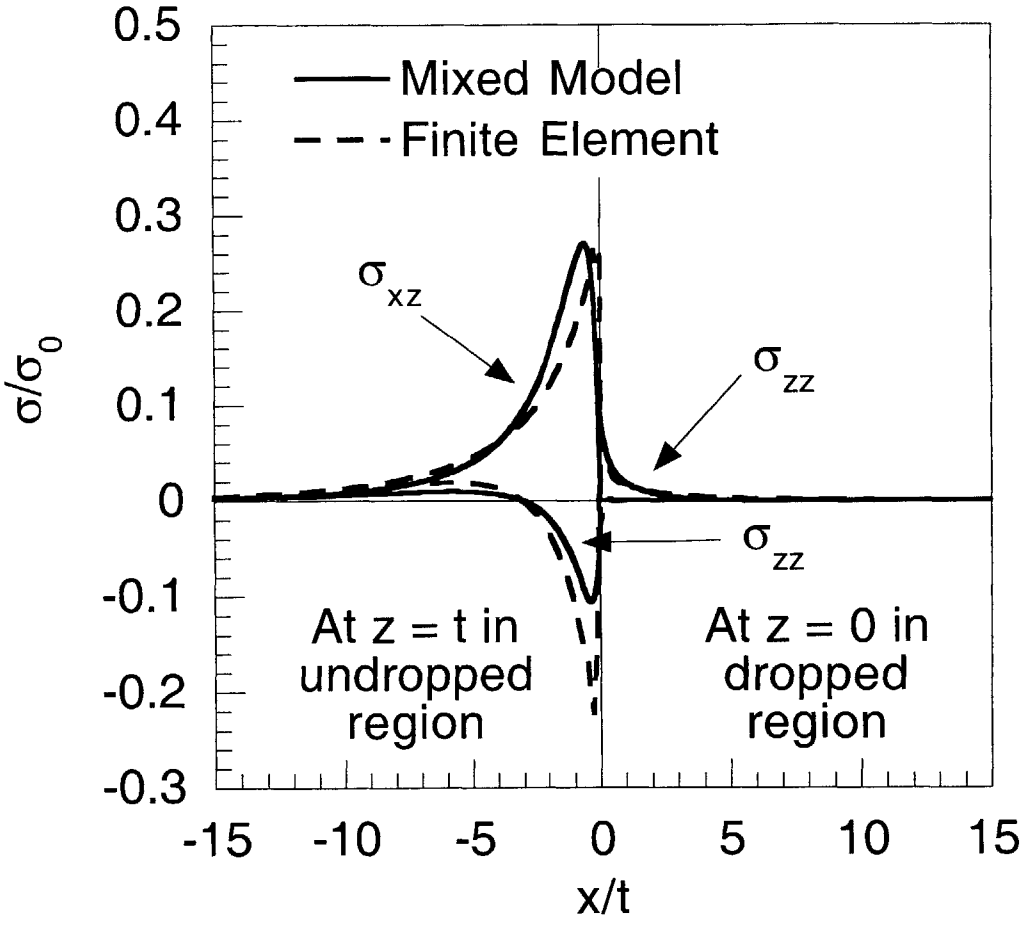

Figure 6.26 Interlaminar shear and normal stresses along the interface at z equal to t in the undropped region and z equal to 0 in the dropped region in a $[0_4/0_D]_s$ laminate with a taper angle of 1° under in-plane load obtained using the mixed model and the FE method.

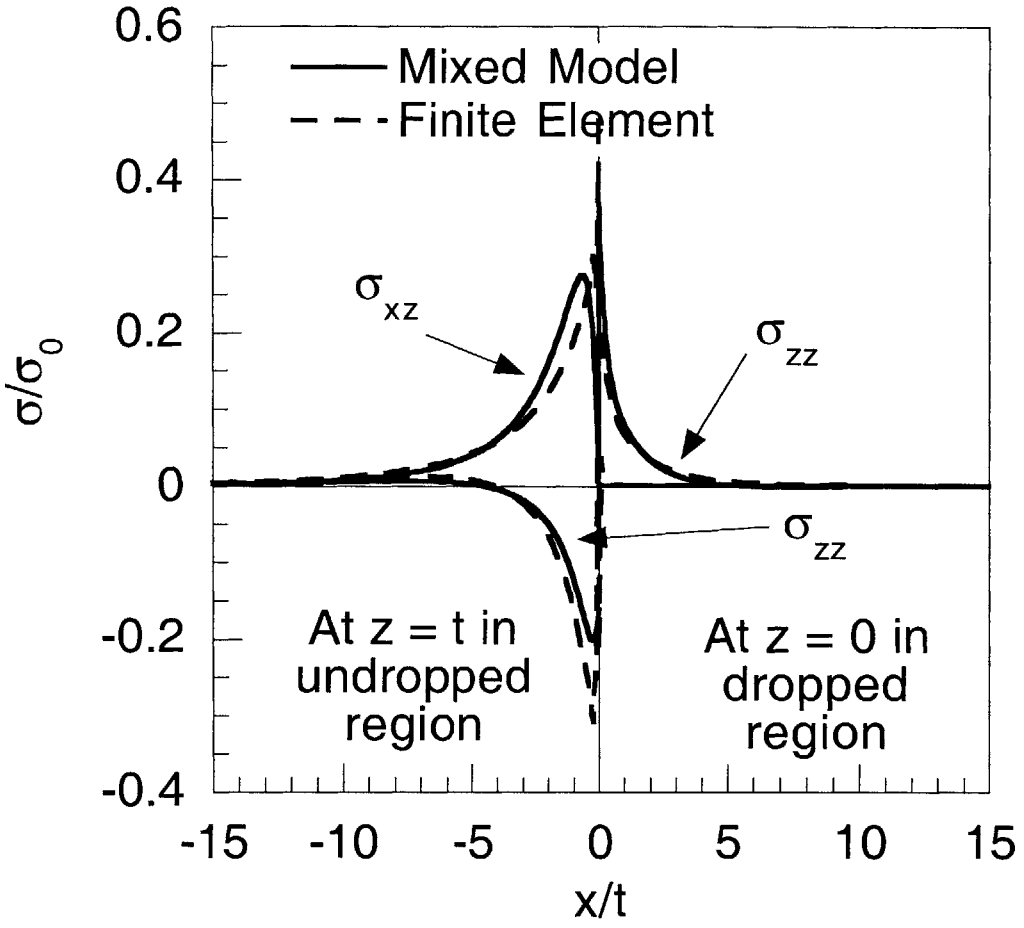

Figure 6.27 Interlaminar shear and normal stresses along the interface at z equal to t in the undropped region and z equal to 0 in the dropped region in a $[0_4/0_D]_s$ laminate with a taper angle of 5.7° under in-plane load obtained using the mixed model and the FE method.

It can be seen in Figures 6.26 and 6.27 that the interlaminar shear stresses obtained using the mixed model and the FE model match very well for both laminates with taper angles of 1° and 5.7°. This is consistent with the good agreement seen in the previous sub-section for stresses obtained using the global model and the FE method, and validates the current analytical models for interlaminar shear stress calculations. Again, due to anti-symmetry, the interlaminar shear stress in the dropped region at the mid-plane is equal to zero. The interlaminar normal stresses obtained using the mixed model also match very well with those obtained using the FE method for both laminates. As discussed in the previous sub-section, an increase in the taper angle tends to increase the magnitude and crossover distance of the compressive interlaminar normal stress in the undropped region according to the FE analysis. The interlaminar normal stress obtained using the mixed model predicts the same trend and shows very good agreement with that obtained using the FE analysis. In the dropped region, the interlaminar normal stress is tensile and its magnitude increases with increasing taper angle. The mixed model is able to capture this trend as well. In the vicinity of the dropoff location (x/t less than 1), the interlaminar normal stress increases rapidly for both taper angle cases, which suggests singular behavior. The mixed model can also be used in a refined analysis through sub-division of plies to investigate the existence of such as shown for the global model in the example of the laminate with external ply dropoffs.

The interlaminar shear and normal stresses along the interface between two continuous plies at z equal to 2t in the undropped region and z equal to t in the dropped region in the same laminate with a taper angle of 5.7° are shown in Figures 6.28 and 6.29, respectively, to further validate the mixed model. As for the stresses at the interfaces of the continuous and terminated plies, the results obtained using the two models show very good agreement, particularly for the interlaminar normal stress component. Note that along the interface of the two continuous plies, significantly less shear transfer occurs over the length of the undropped region as seen in Figure 6.28 compared to the interface

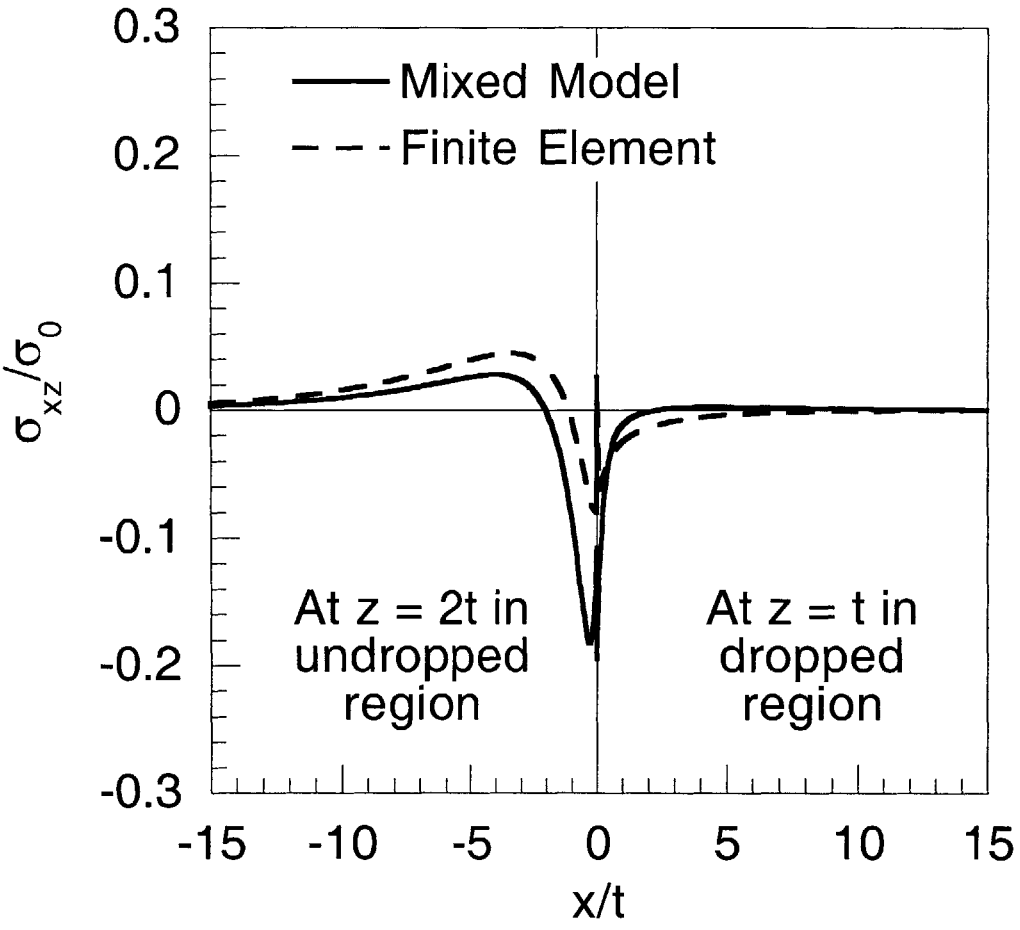

Figure 6.28 Interlaminar shear stresses along the interface at z equal to 2t in the undropped region and z equal to t in the dropped region in a $[0_4/0_D]_s$ laminate with a taper angle of 5.7° under in-plane load obtained using the mixed model and the FE method.

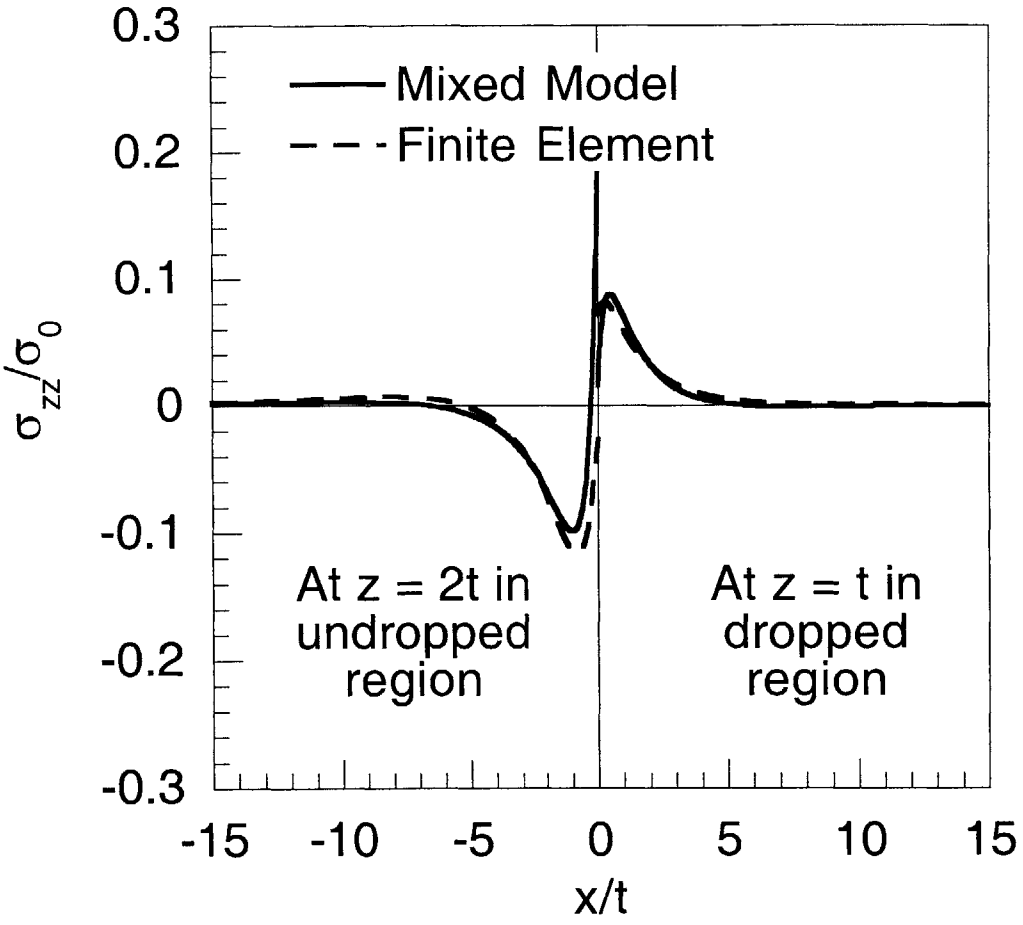

Figure 6.29 Interlaminar normal stresses along the interface at z equal to 2t in the undropped region and z equal to t in the dropped region in a $[0_4/0_D]_s$ laminate with a taper angle of 5.7° under in-plane load obtained using the mixed model and the FE method.

of the continuous and terminated plies in Figure 6.27. The magnitude of the interlaminar shear stress obtained via the mixed model differs by a factor of approximately two compared to the FE results in the vicinity of the cutoff. It can also be seen in Figure 6.29 that the magnitudes of the interlaminar normal stresses are smaller along the interfaces of the two continuous plies in the undropped and dropped regions compared to the interfaces considered in Figure 6.27.

The same laminate under bending load is considered, again with taper angles of 1° and 5.7°. The material properties of a generic glass/epoxy composite as found in Table 6.1 are again used. A moment, M, of $100t^2$ MNm is applied at both ends such that a positive moment creates tension in the plies in the upper-half of the laminate. The moment gives rise to a linear distribution of in-plane stress, σ_{xx}, through the thickness of the laminate in the undropped region far away from the ply dropoffs. The magnitude of the stress at the outer surfaces of the laminate is equal to 6 MPa. The interlaminar shear and normal stresses obtained using the mixed model and the FE model for the two cases with taper angles of 1° and 5.7° are shown in Figures 6.30 and 6.31, respectively. The interlaminar shear and normal stresses are evaluated along the interface of the continuous and terminated plies in the undropped region ($z = t$) and the mid-plane in the dropped region ($z = 0$). This corresponds to the dashed line *AA* in Figure 6.20.

The interlaminar stress distributions obtained using the two methods, shown in Figures 6.30 and 6.31, are generally in good agreement, although there are some differences in the magnitude of the interlaminar shear stress in the vicinity of the cutoff in the dropped region for values of x/t less than 3. As shown for the case of laminates with external ply dropoffs, a better approximation for the interlaminar shear stress can be obtained by performing a refined analysis, although the utility of such would be questionable. The interlaminar normal stresses show excellent agreement in the undropped region where the stress is compressive in the vicinity of the cutoff. Note that under bending load, the interlaminar normal stress at the mid-plane is zero due to anti-

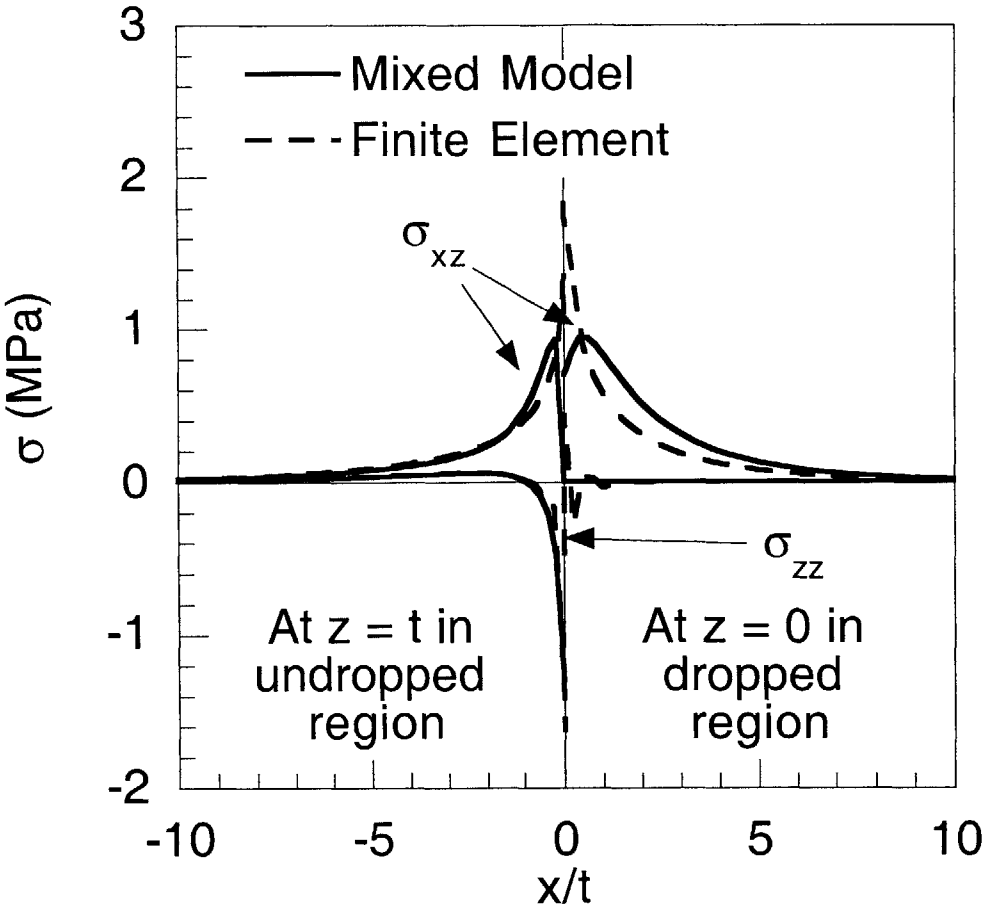

Figure 6.30 Interlaminar shear and normal stresses along the interface at z equal to t in the undropped region and z equal to 0 in the dropped region in a $[0_4/0_D]_s$ laminate with a taper angle of 1° under a bending load of $100t^2$ MNm obtained using the mixed model and the FE method.

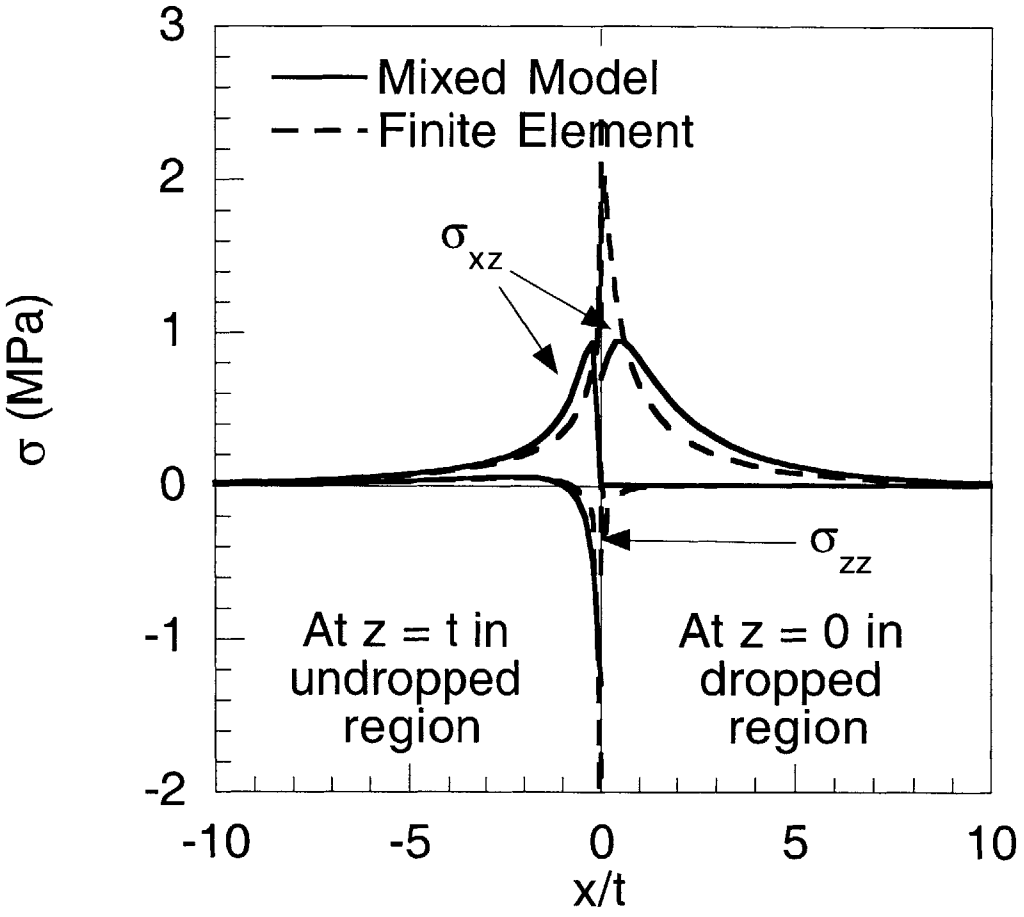

Figure 6.31 Interlaminar shear and normal stresses along the interface at z equal to t in the undropped region and z equal to 0 in the dropped region in a $[0_4/0_D]_s$ laminate with a taper angle of 5.7° under a bending load of $100t^2$ MNm obtained using the mixed model and the FE method.

symmetry. In the dropped region, it can be seen that the interlaminar normal stress obtained by the mixed model is identically zero, while the FE analysis yields some spurious stresses near the dropoff point (x/t = 0). Such spurious stresses also occur in the mixed model for in-plane components. This is discussed later in this sub-section.

An interesting observation can be made by comparing the interlaminar stress distributions obtained using the mixed model for the two cases. In Figures 6.30 and 6.31, it can be seen that the interlaminar stress distributions for laminates with taper angles of 1° and 5.7° appear to be very similar. In fact, it can be shown using the boundary conditions for the mixed model that the stress distributions for the two laminates are identical, and that, in general, the taper angle does not affect the stress field for laminates with ply dropoffs located at the mid-plane under bending load. Consider the z-direction force equilibrium in the dropped region (corresponding to region B in Figure 4.5). The applied moment is equivalent to applying a linear distribution of in-plane stress in the x_1-direction. Since there is no interlaminar normal stress at the mid-plane and the surface of the laminate is stress-free, the shear force in the z-direction at the cutoff must be zero for such laminates. The shear force in the z-direction is equal to the integral of the interlaminar shear stress along the 1^+ face and can be expressed as:

$$\int_{1^+} \sigma_{1z}^{B}(0,z)\,dz = 0 \tag{6.1}$$

Since the shear force in the z-direction at the cutoff in the dropped region is equal to zero, the shear force in the z-direction at the cutoff in the undropped region must also be equal to zero based on z-direction force equilibrium in the sloped region as expressed in equation (4.56), *i.e.*:

$$\int_{1^-} \sigma_{1z}^{A}(0,z)\,dz = 0 \tag{6.2}$$

Thus, the moment equilibrium about the x_2-direction of the sloped region must be

satisfied by the in-plane stresses in the x_1-direction acting at the cutoffs in the undropped and dropped regions, since the two other surfaces of the sloped region are stress-free. The equation for this condition can be obtained by substituting equation (6.1) into the equation for the moment equilibrium about the x_2-direction in equation (4.58). The resulting equation can be expressed as:

$$\int_{1^-} \sigma_{11}^{A}(0,z) z\, dz - \int_{1^+} \sigma_{11}^{B}(0,z)(z + l\sin\alpha)\, dz = 0 \tag{6.3}$$

The first integration term of equation (6.3) is equal to the moment about the x_2-direction due to the in-plane stress, σ_{11}, at the dropoff location in the undropped region. This term is always equal to zero because the assumed form of the stress field was chosen to satisfy the moment equilibrium equation (see equation (4.34)). Similarly, the second intergration term of equation (6.3) is the moment about the x_2-direction due to the in-plane stress, σ_{11}, at the dropoff location in the dropped region. This term is also equal to zero. Therefore, in laminates with ply dropoffs located at the mid-plane, the moment equilibrium equation is automatically satisfied, and there is no dependence on the taper angle.

Comparing the interlaminar stresses obtained using the FE method in Figures 6.30 and 6.31, it can be seen that the difference between the stresses in laminates with 1° and 5.7° taper angle is very small. This is consistent with the observation made for the stress distribution obtained using the mixed model. The small differences in the stresses for the laminates with the two taper angles can be attributed to the different meshes used in the two FE analyses and the effect of the compliant dropoff region. In the mixed model, the dropoff region is assumed to be rigid. It is noted that the stress field in laminates under bending load is independent with respect to the taper angle in the dropoff region only when the terminated plies are located at the mid-plane. For other types of laminates in general, the stress field is dependent on the taper angle.

A limitation of the analytical model for laminates under bending load is that it is

unable to predict zero in-plane stress at the mid-plane. The in-plane stress in a symmetric laminate due to bending load must be anti-symmetric about the mid-plane and continuous at the mid-plane. These two conditions imply that the in-plane stress at the mid-plane should be zero. The in-plane stress, σ_{xx}, along this location ($z = 0$) in the undropped and dropped regions in the $[0_4/0_D]_s$ laminate is shown in Figure 6.32. It can be seen that the mixed model yields non-zero in-plane stress in the undropped region in the undropped region. The result obtained using the FE method yields the correct zero in-plane stress along this location in the undropped region but does not yield zero in-plane stress at the mid-plane in the dropped region.

The non-zero in-plane stress at the mid-plane obtained using the analytical method arises due to the assumed form of the stress field in the companion problem. The assumed form of the in-plane stresses at the mid-plane are not explicitly required to equal zero (see equation (4.30)). However, the magnitude of the in-plane stress obtained using the mixed model is not significant. It is an order of magnitude lower than the in-plane stress at the outer surfaces, which is equal to 6 MPa. The magnitude of the spurious in-plane stress may be reduced if a more refined analysis is performed, either by subdividing plies or by using a higher-order assumed stress field. Furthermore, the presence of the non-zero in-plane stresses is not a serious limitation because the critical interfaces of interest in laminates with ply dropoffs based on previous investigations are generally those away from the mid-plane where delaminations tend to occur.

A laminate with ply dropoffs located away from the mid-plane is next considered to show the validity of the mixed model for laminates with ply dropoffs at arbitrary locations. A laminate with a layup of $[0_2/0_D/0_2]_s$ is considered for this purpose. The lengths in the undropped and dropped regions are 50t and 40t respectively, and the material properties of a generic glass/epoxy composite material, shown in Table 6.1, were used. A diagram of the laminate is shown in Figure 6.33. As in the previous example, an in-plane stress, σ_0, of 1000 MPa is applied at the undropped end. The interlaminar stress

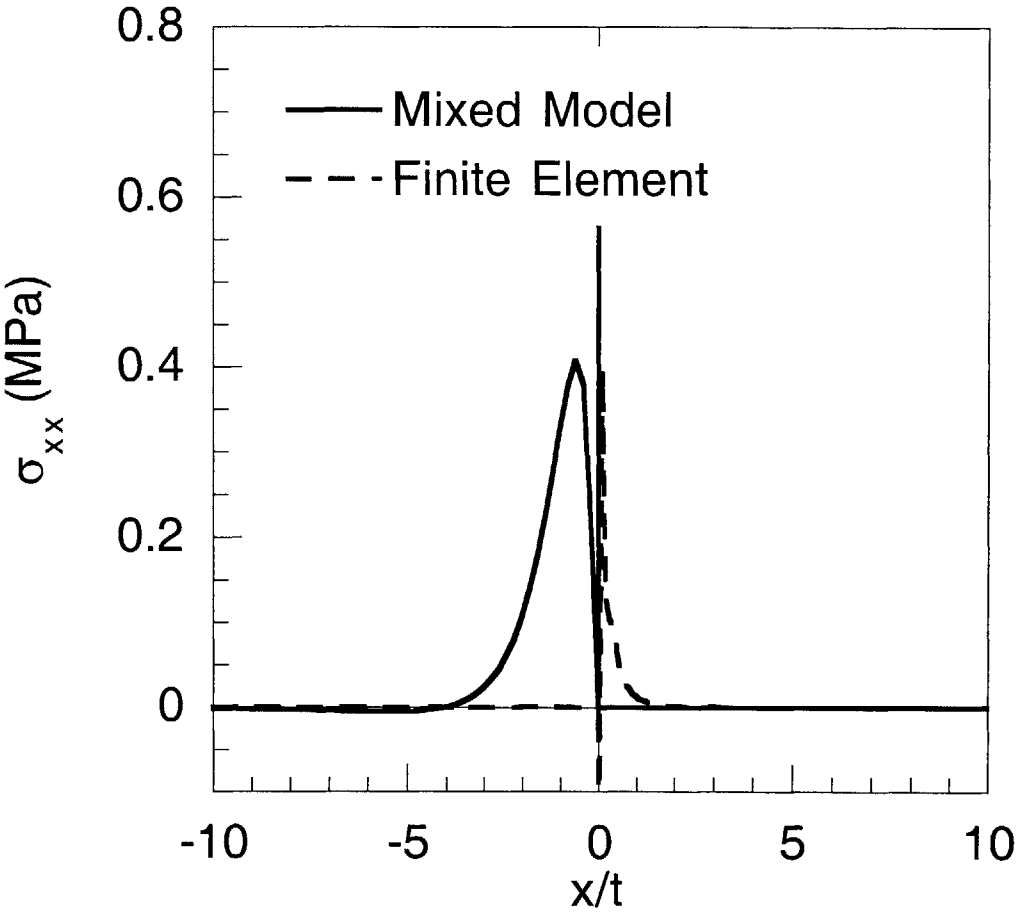

Figure 6.32 In-plane stress along the mid-plane in a $[0_4/0_D]_s$ laminate with a taper angle of 5.7° under a bending load of $100t^2$ MNm obtained using the mixed model and the FE method.

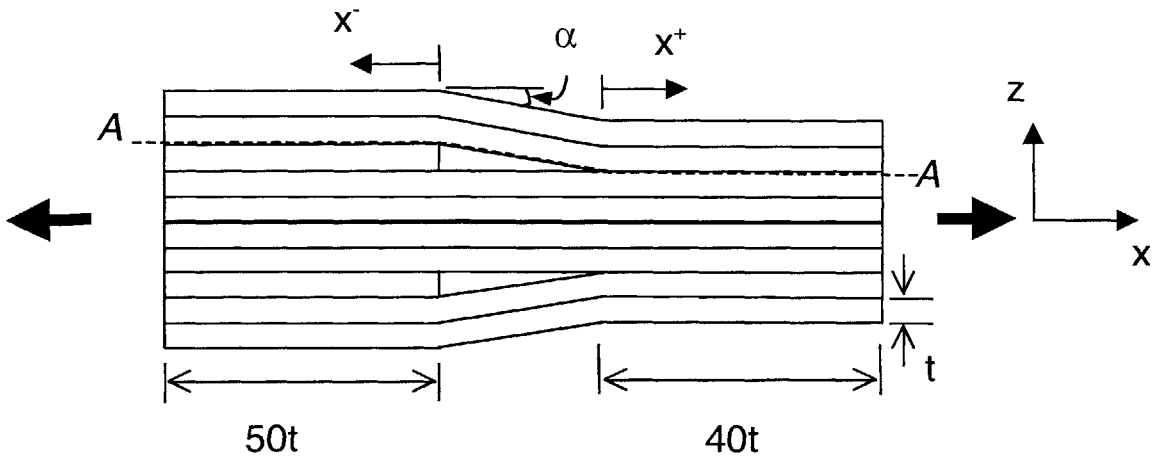

Figure 6.33 Diagram of laminate with a layup of $[0_2/0_D/0_2]_s$.

distribution in two laminates with taper angles of 1° and 5.7° are considered.

The interlaminar stresses obtained using the mixed model and the FE analysis are shown in Figures 6.34 and 6.35 for taper angles of 1° and 5.7°, respectively. All stresses are normalized by the applied stress in the undropped region, σ_0. The interlaminar stresses along the interface of the terminated and continuous plies (z = 3t) in the undropped region and the interface of the inner and outer continuous plies (z = 2t) in the dropped region are shown. These interfaces correspond to the dashed line *AA* in Figure 6.33. It can be seen from these figures that both the interlaminar shear and normal stresses obtained using the two methods match very well except in the immediate vicinity of the cutoffs (within two ply thicknesses). As in previous cases, the interlaminar shear stresses obtained using the mixed model are equal to zero at the cutoff due to the traction-free condition, while those obtained using the finite element method are not. The magnitude and crossover points of the interlaminar normal stresses in the undropped region are seen to increase with increasing taper angle, as observed for the $[0_4/0_D]_s$ case.

It is important to note that the mixed model was developed with the assumption that the dropoff region is rigid and transfers load without any deformation. In reality, the dropoff region is compliant and will deform under in-plane (or bending) load. In the FE analysis, the dropoff region was modeled as being compliant with the material properties of composite materials. Thus, to further validate the mixed model, the interlaminar normal stresses at the mid-plane of the laminate obtained using the two methods, including the dropoff region in the FE method, were compared. This is shown in Figures 6.36 and 6.37 for taper angles of 1° and 5.7°, respectively. In these figures, the interlaminar normal stresses along the entire length of the laminate are shown, and the x-direction coordinate is defined such that the origin coincides with the point x^- equal to 0 in Figure 6.33. Thus, for Figure 6.36, the negative x-direction corresponds to the undropped region, the region between x/t equal to 0 and 50 is the dropoff region, and the region for x/t greater than 50 is the dropped region. Similarly for Figure 6.37, the

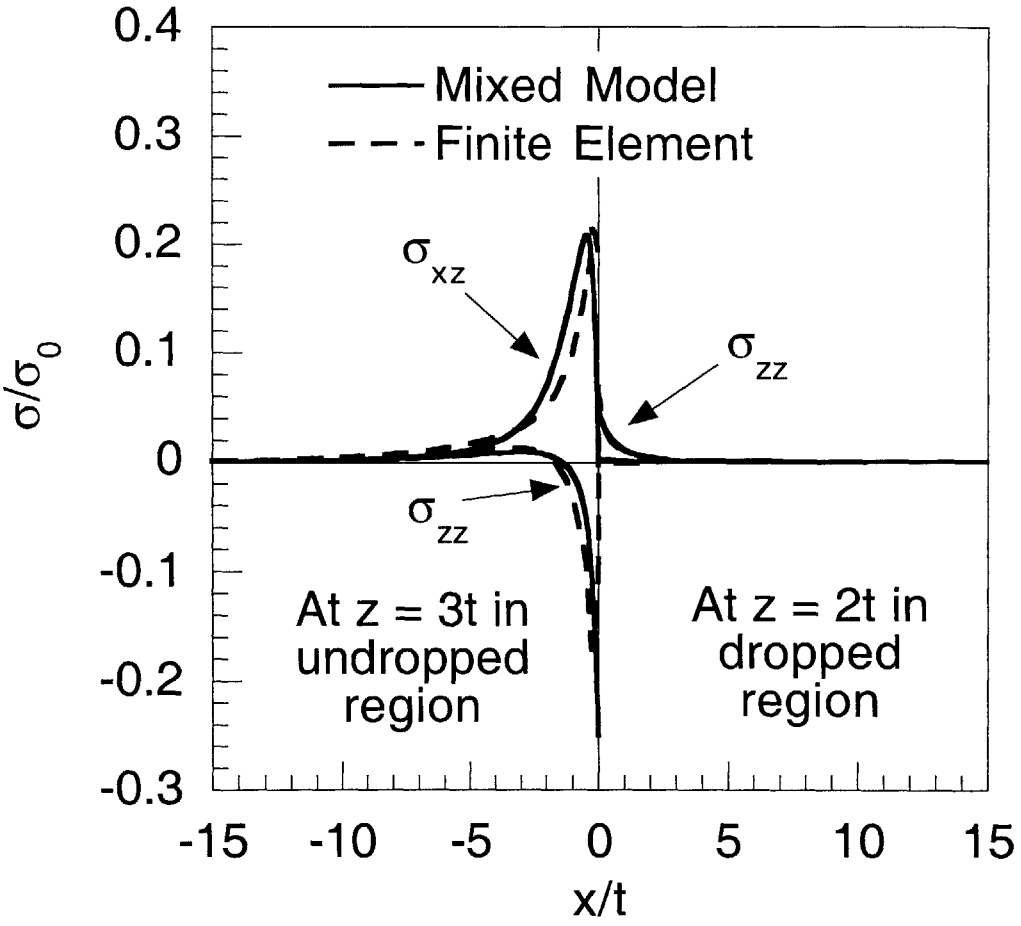

Figure 6.34 Interlaminar shear and normal stresses along the interface at z equal to 3t in the undropped region and z equal to 2t in the dropped region in a $[0_2/0_D/0_2]_s$ laminate with a taper angle of 1° under in-plane load obtained using the mixed model and the FE method.

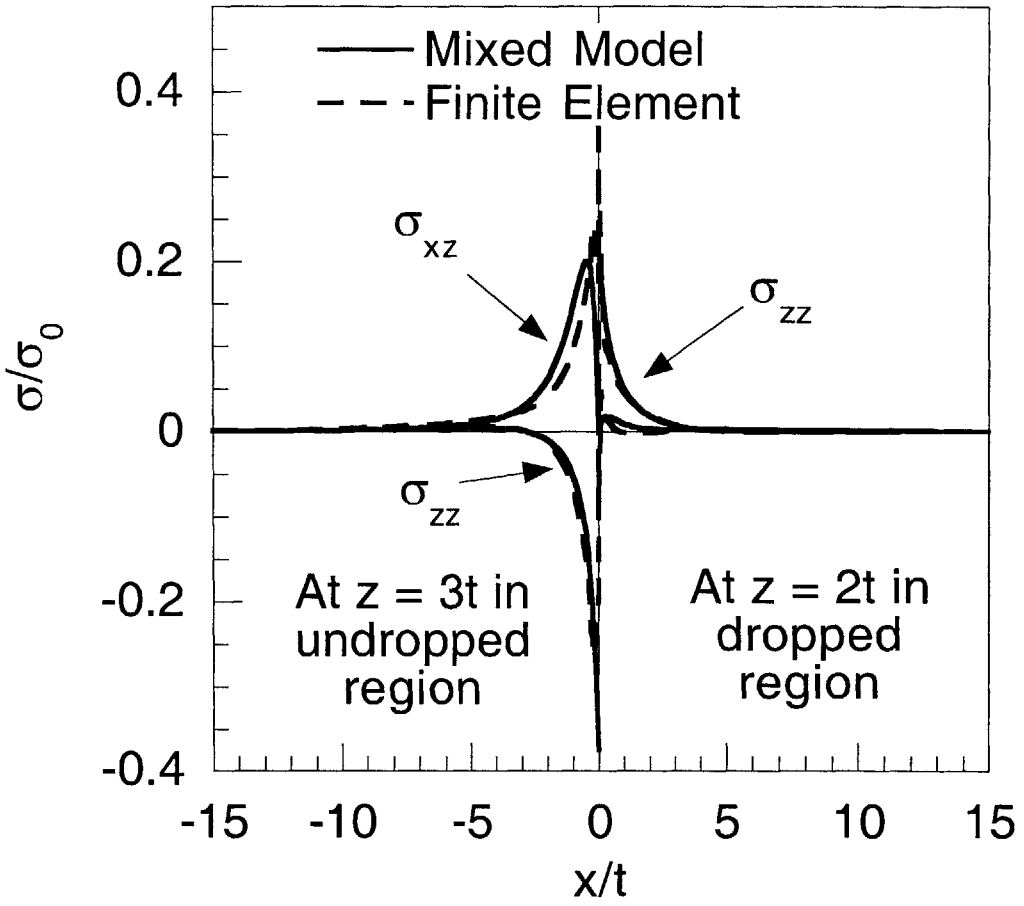

Figure 6.35 Interlaminar shear and normal stresses along the interface at z equal to 3t in the undropped region and z equal to 2t in the dropped region in a $[0_2/0_D/0_2]_s$ laminate with a taper angle of 5.7° under in-plane load obtained using the mixed model and the FE method.

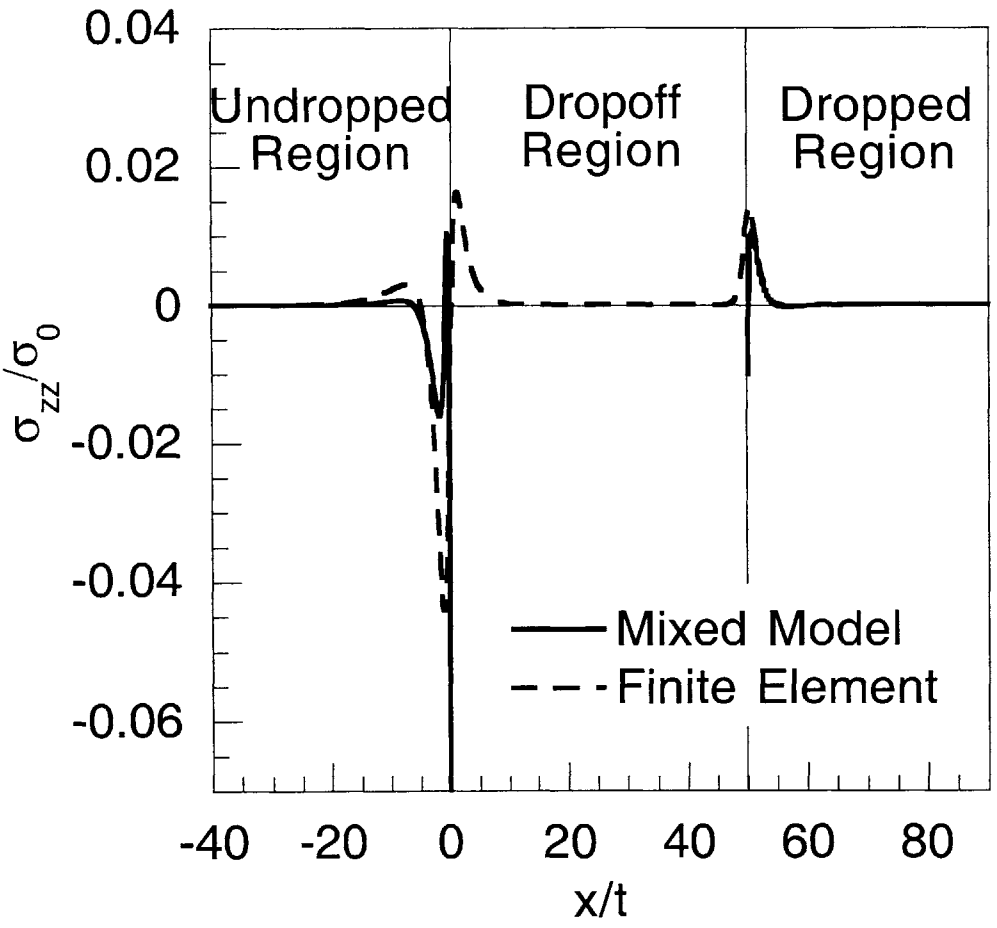

Figure 6.36 Interlaminar normal stresses along the mid-plane in a $[0_2/0_D/0_2]_s$ laminate with a taper angle of 1° under in-plane load obtained using the mixed model and the FE method.

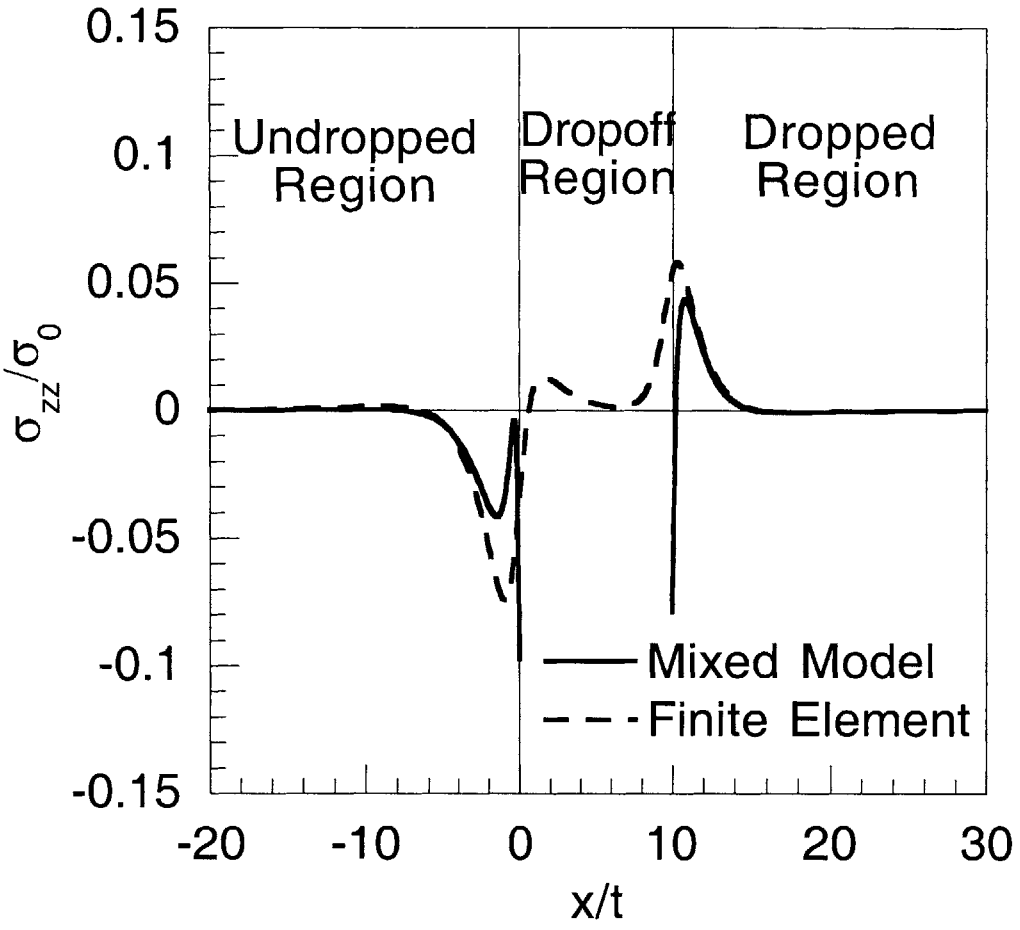

Figure 6.37 Interlaminar normal stresses along the mid-plane in a $[0_2/0_D/0_2]_s$ laminate with a taper angle of 5.7° under in-plane load obtained using the mixed model and the FE method.

negative x-direction corresponds to the undropped region, the region between x/t equal to 0 and 10 is the dropoff region, and the region for x/t greater than 10 is the dropped region. Stress distribution in the dropoff region can be obtained using only the FE analysis, which is shown in both figures.

The results shown in Figure 6.36 indicate that the interlaminar normal stress distribution along the length of the laminate in the undropped and dropped regions obtained using the two methods generally follow similar trends in the undropped and dropped regions. The interlaminar normal stresses in the dropped region obtained using the two methods overlap and indicates very good agreement away from the cutoff (x/t = 50) for x/t greater than 52. The magnitudes in the undropped region near the cutoff differ by a factor of more than two. In the immediate vicinity of the cutoffs at x/t equal to 2, the solution obtained using the analytical model shows a reversal of the interlaminar normal stress with the stress changing sign abruptly from tensile to compressive. A similar trend is also seen in Figure 6.37, with the difference in magnitude being somewhat smaller than in the case of a 1° taper angle. The two figures show that the rigid dropoff region assumption is a reasonable one, and does yield stress distributions that are comparable to the FE model including a compliant dropoff region away from the immediate vicinity of the cutoffs. The interlaminar shear stresses at the mid-plane are identically zero due to symmetry, and are not shown.

6.1.5 Laminates with Existing Delaminations

Two laminates are considered to validate the analytical model for laminates with existing delaminations at the dropoff in a symmetric configuration about the mid-plane. One is a laminate with external ply dropoffs with a layup of $[0_{2D}/0_3]_s$, and the other is a laminate with internal ply dropoffs with a layup of $[0_2/0_{2D}/0_2]_s$. For both laminates, the stress fields obtained using the analytical model are compared with those obtained using the FE model.

For the $[0_{2D}/0_3]_s$ laminate, the material properties of a generic glass/epoxy

composite material, shown in Table 6.1, are used. The lengths of the undropped and dropped regions are chosen to be 50t, which is sufficiently long such that the interlaminar stresses decay to zero far away from the dropoff and delaminated regions. The length of the delamination, a, is also chosen to be 50t. This is sufficiently long such that the stress fields in the undropped and dropped regions are unaffected by the length of the delamination, which is consistent with assumptions of the analytical model. A diagram of the laminate considered is shown in Figure 6.38.

The interlaminar shear and normal stresses in the undropped regions obtained using the analytical and FE methods are shown in Figure 6.39. These interlaminar stresses are evaluated along the interface of the continuous and terminated plies in the undropped region ($z = 3t$). Since the interface at z equal to 3t in the dropped region corresponds to the outer surface of the laminate, the interlaminar stresses in the dropped region are nonexistent, and thus, not shown. It can be seen that the stress distribution obtained using the current analytical model with existing delaminations shows very good agreement with that obtained using the FE analysis. Note that the interlaminar shear stress distribution obtained using the analytical model exhibits a reversal in trend near the cutoff approximately one ply thickness away from the cutoff. This reversal trend disappears as the analytical model is refined using ply sub-division. The overall stress distributions along this interface resemble those in a similar laminate without existing delaminations considered in Section 6.1.2 that are shown in Figure 6.7. The interlaminar normal stress is tensile at the cutoff and decreases in magnitude to zero far away from the cutoff, while the interlaminar shear stress is negative at the cutoff and monotonically decays in magnitude to zero. The negative interlaminar shear stress indicates that in-plane stresses in the terminated plies above this interface are transferred to the continuous plies below the interface.

The in-plane stresses through the thickness of the laminate at the cutoff ($x/t = 0$) in the upper-half of the laminate obtained using the analytical and FE methods are shown

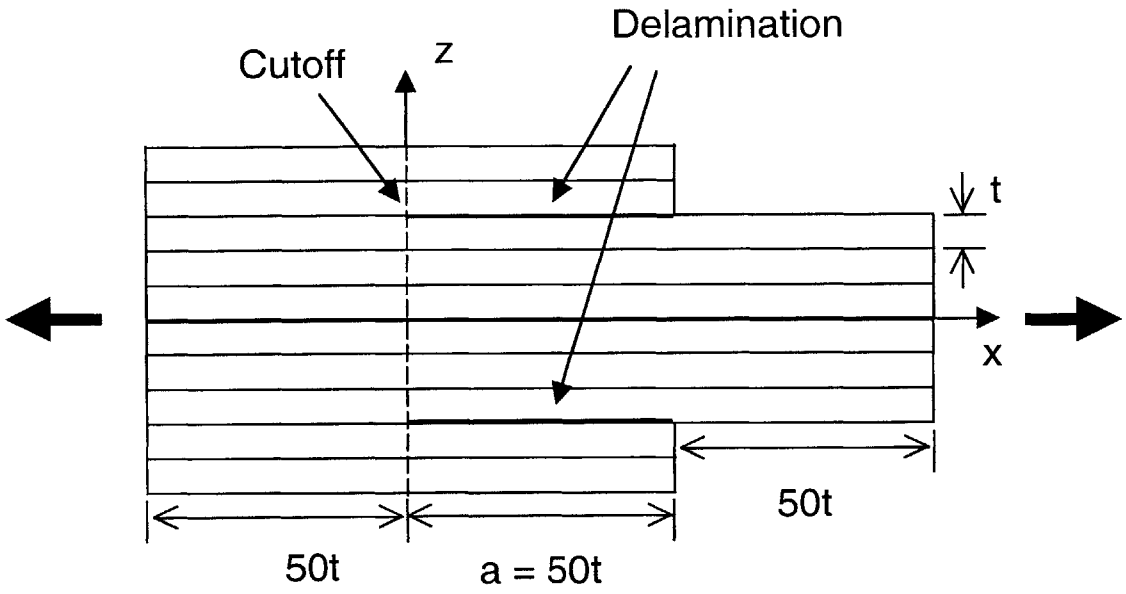

Figure 6.38 Diagram of a laminate with external ply dropoffs with existing delaminations of length a in the undropped region.

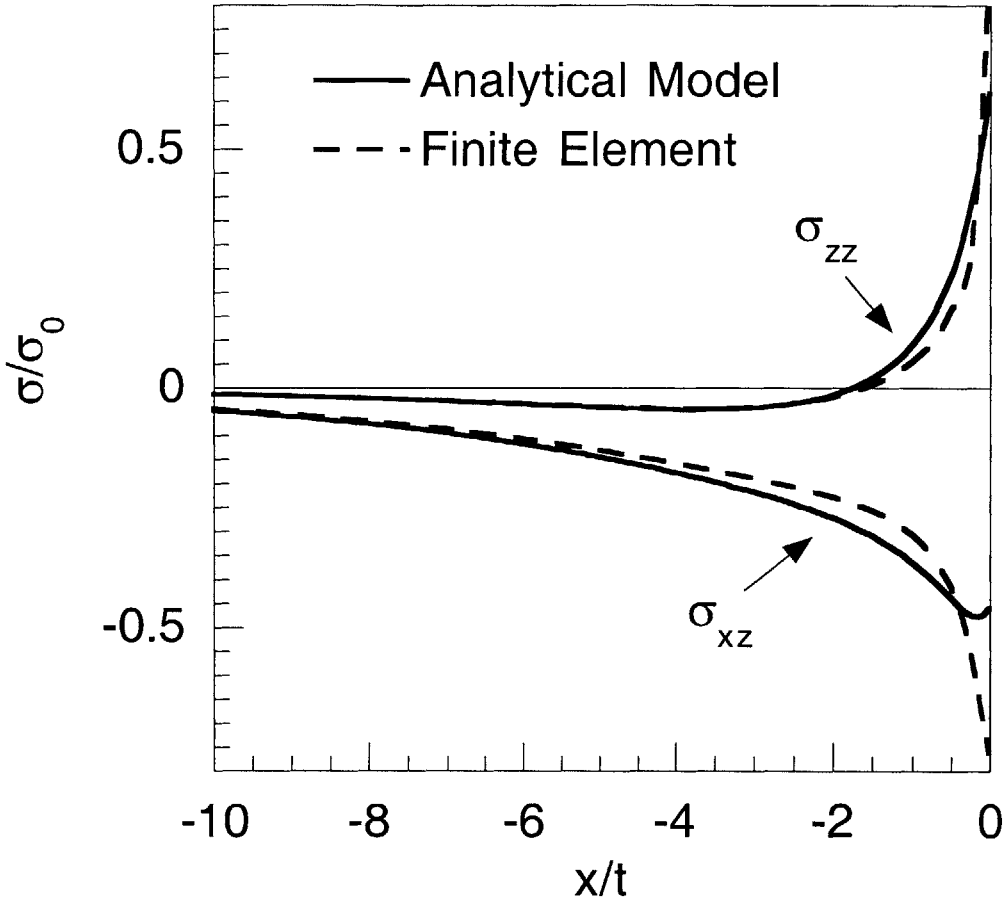

Figure 6.39 Interlaminar shear and normal stresses along the interface with existing delamination in the undropped region (z = 3t) in a $[0_{2D}/0_3]_s$ laminate obtained using the analytical model and the FE method.

in Figure 6.40. The in-plane stress field obtained using the analytical model is piecewise constant in each ply and discontinuous from ply to ply. The cause of this discontinuity is similar to that discussed previously for the bending load case in Section 6.1.2 in that the in-plane strain continuity condition across unidirectional plies is not satisfied by the current analytical model. Note that the in-plane stress field in the terminated ply group obtained using the analytical model is identically zero, while that obtained using the FE method is not. The analytical model yields in-plane stress equal to zero in the terminated plies because each ply was modeled as one layer. In the analytical model, the x-direction force and moment equilibrium must be satisfied at the cutoffs for laminates with existing delaminations (see equations (4.66) and (4.68)). If each ply is modeled as a single layer, these equations imply that the in-plane stresses must be identically zero. If the analysis were refined by subdividing each ply into multiple layers, the in-plane stresses would be non-zero with the integral in the terminated ply group being zero. A refined analysis with each ply subdivided into two layers was performed to illustrate this point. The in-plane stress distributions obtained using the analytical model with each ply divided into two sub-plies and the FE method are shown in Figure 6.41. It can be seen that, as expected, the in-plane stresses in the terminated plies are non-zero. In addition, it can be seen that a better approximation for the in-plane stress field is obtained.

The $[0_2/0_{2D}/0_2]_s$ laminate with internal ply dropoffs with existing delaminations is considered next. The lengths of the undropped and dropped regions are equal to 50t as in the previous example. The taper angle in the dropoff region is chosen to be 11°. The laminate configuration is shown in Figure 6.42. Note that the interfaces between the delaminated section of the laminate and the continuous plies are assumed to be stress-free in the analytical model. This follows from the assumption that the dropoff and delaminated regions are rigid and only transfer loads at the cutoffs. However, these assumptions may be an over-simplification of the problem because under in-plane load the actual laminate would intuitively deform in a manner such that the interfaces between

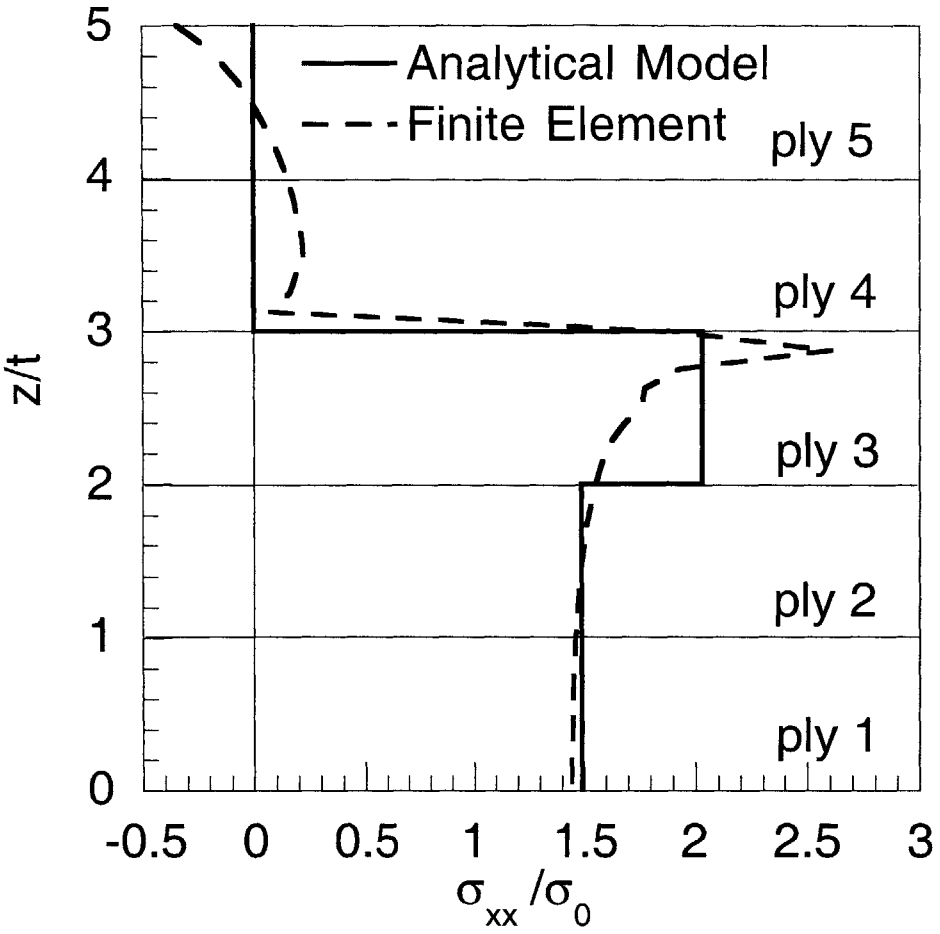

Figure 6.40 In-plane stresses through the thickness in the upper-half of the laminate at the cutoff in a $[0_{2D}/0_3]_s$ laminate with existing delaminations obtained using the analytical model and FE method.

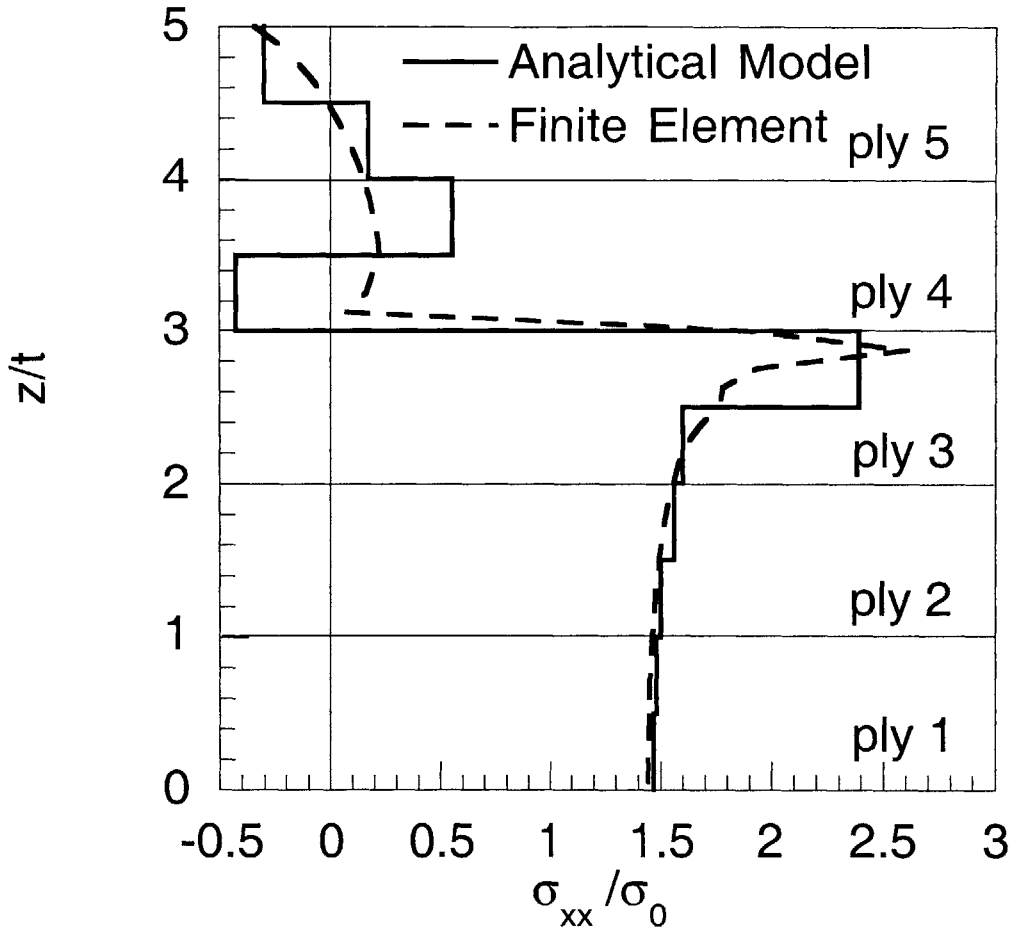

Figure 6.41 In-plane stresses through the thickness in the upper-half of the laminate at the cutoff in a $[0_{2D}/0_3]_s$ laminate with existing delaminations obtained using a refined analysis via ply subdivision and FE method.

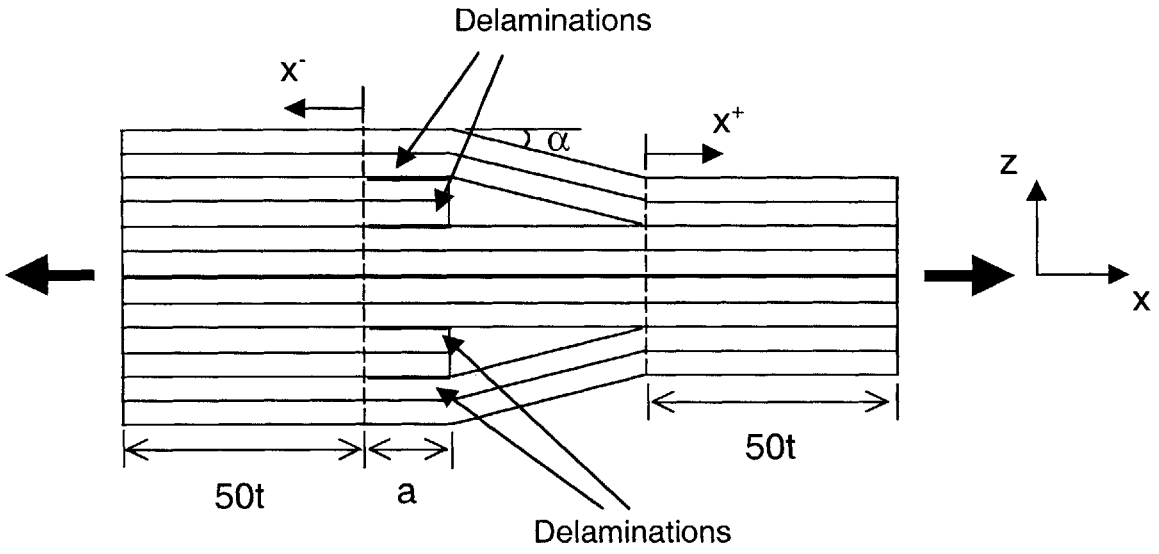

Figure 6.42 Diagram of laminate with internal ply dropoffs of length a and existing delaminations in the undropped region.

the delaminated section of the laminate and the continuous plies would be in contact. The deformed configuration of the laminate obtained via a FE analysis immediately confirms this intuition. The deformed configuration of the laminate as obtained is shown in Figure 6.43. The length of the delaminated region in this FE model is 5t. It can be seen that continuous plies in the dropoff and delaminated regions overlap the delaminated plies. This configuration is physically unrealistic, and therefore, the interfaces at which overlap occurs should be in contact. This would produce finite compressive interlaminar normal stresses at the interfaces and possibly induce finite interlaminar shear stresses via friction.

In order to assess applicability of the analytical model that does not take contact into account, the stresses in the $[0_2/0_{2D}/0_2]_s$ laminate with existing delamination obtained using a FE analysis with contact restrictions and those obtained using the analytical model are compared. Note that due to the iterative technique used to solve problems with contact restrictions via the FE method [62], larger contact regions can significantly increase the time required for the analysis to yield converged solutions. Thus, in the current example, the length of the delamination was chosen to be 10t.

The interlaminar shear and normal stresses along an interface with existing delamination ($z = 4t$ in the undropped region and $z = 2t$ in the dropped region) are shown in Figures 6.44 and 6.45, while the in-plane stress distributions through the thickness are shown in Figures 6.46 and 6.47. It can be seen in Figure 6.44 that despite the simplifying assumptions in the analytical method, the interlaminar shear stresses show good agreement, although the analytical method underestimates the peak stress near the cutoff for values of x/t less than one. The difference in magnitudes of the interlaminar normal stress shown in Figure 6.45 obtained using the two methods is more evident, although the trends are very similar. In the undropped region, the analytical method yields a stress distribution that is highly compressive in the vicinity of the cutoffs with the crossover distance being equal to approximately 2.5t, while the FE method yields one with a

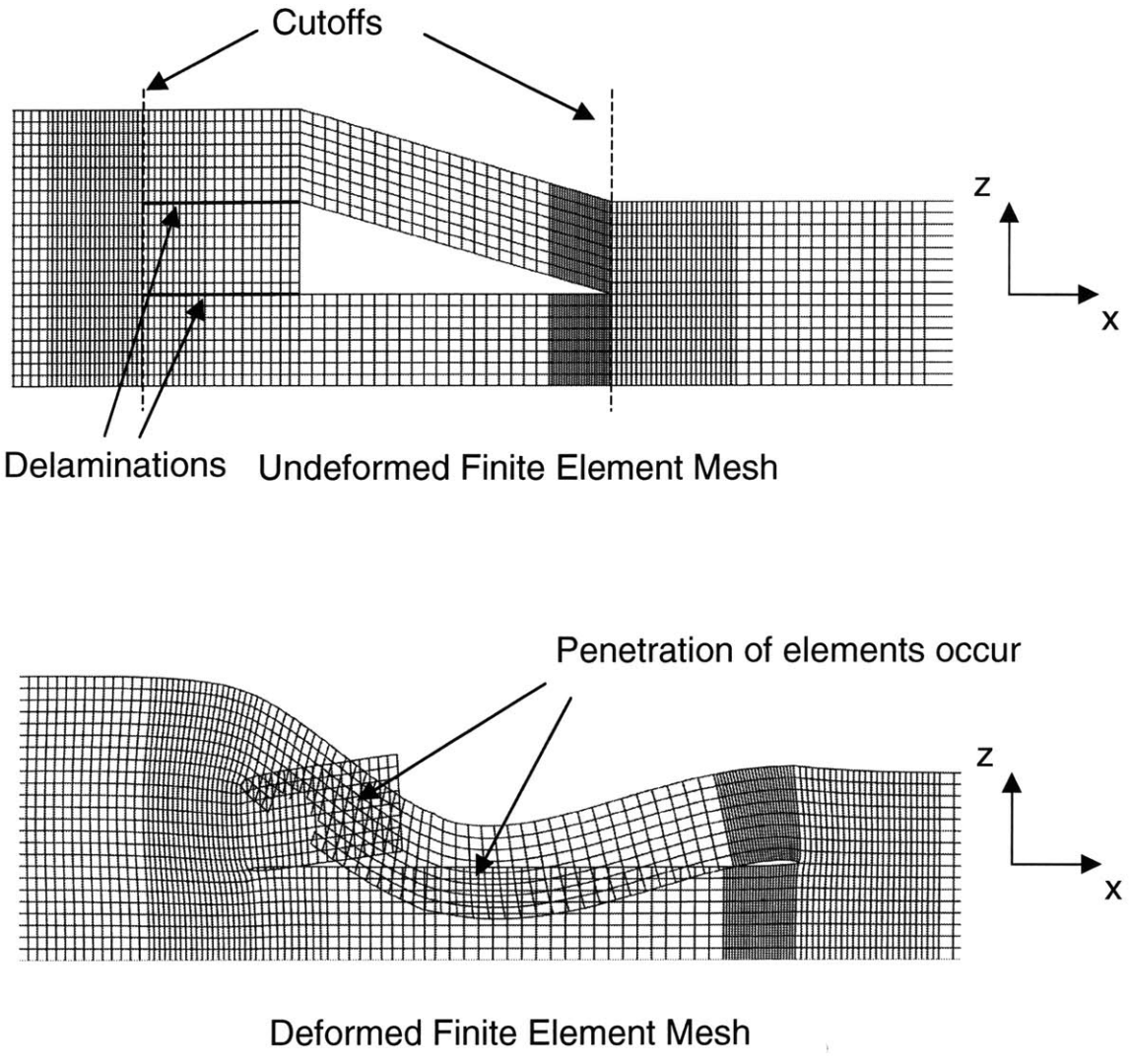

Figure 6.43 Finite element meshes of *(top)* undeformed configuration, and *(bottom)*, deformed configuration obtained using a model without contact elements at the delamination surfaces for the $[0_2/0_{2D}/0_2]_s$ laminate (deformations are magnified by 10,000,000X).

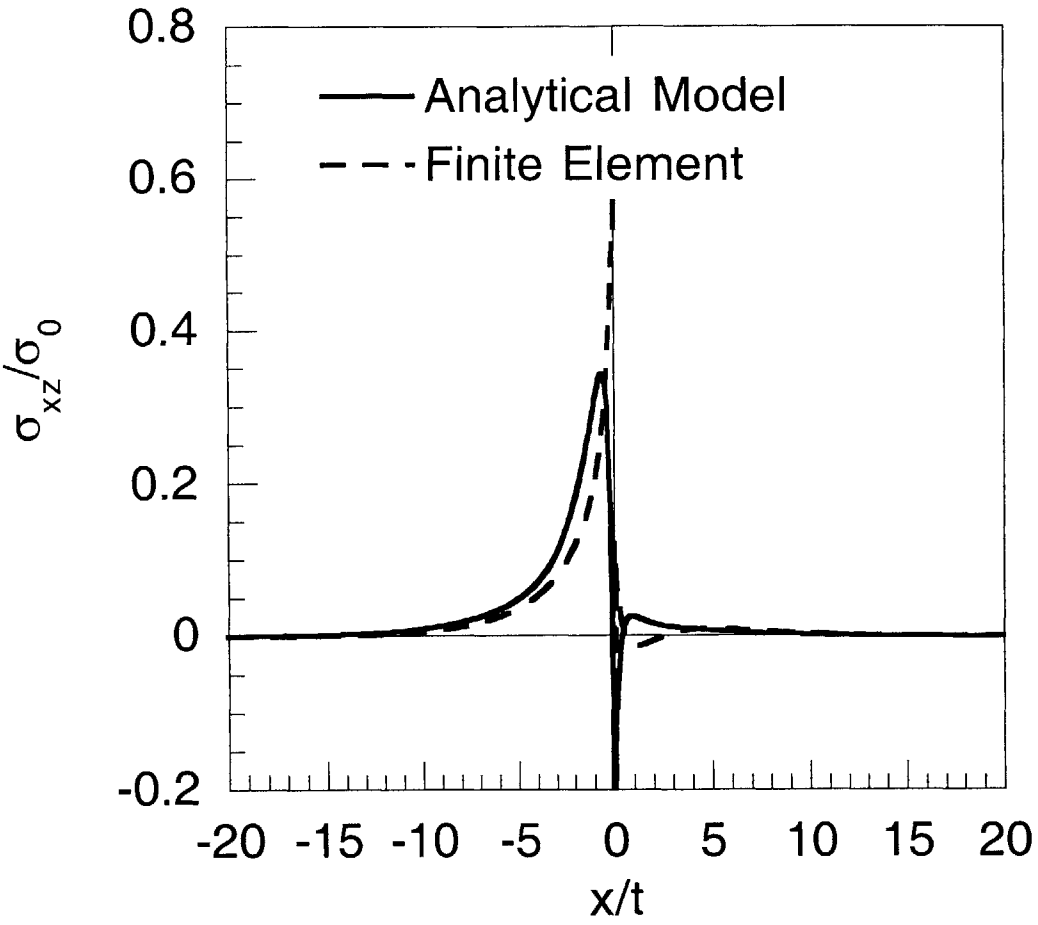

Figure 6.44 Interlaminar shear stresses along the interface with existing delamination (z = 2t) in a $[0_2/0_{2D}/0_2]_s$ laminate obtained using the analytical model and the FE method with contact restrictions.

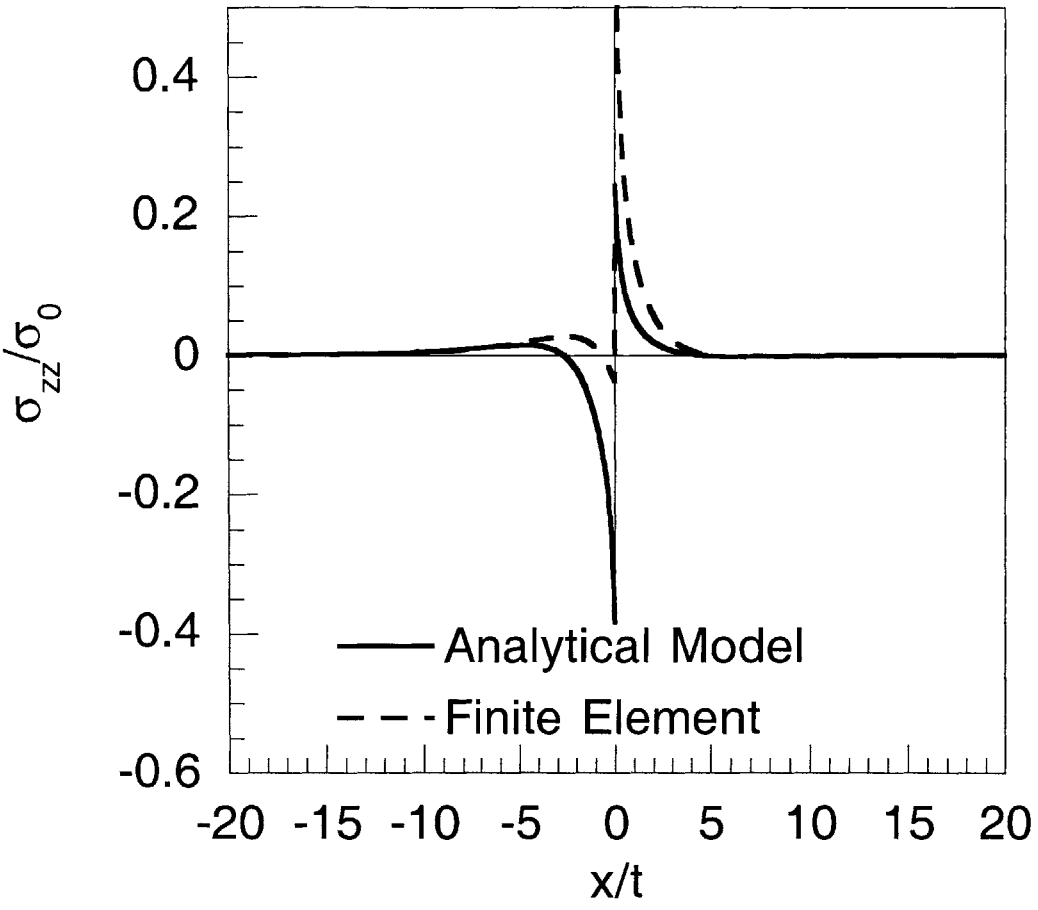

Figure 6.45 Interlaminar normal stresses along the interface with existing delamination ($z = 2t$) in a $[0_2/0_{2D}/0_2]_s$ laminate obtained using the analytical model and the FE method with contact restrictions.

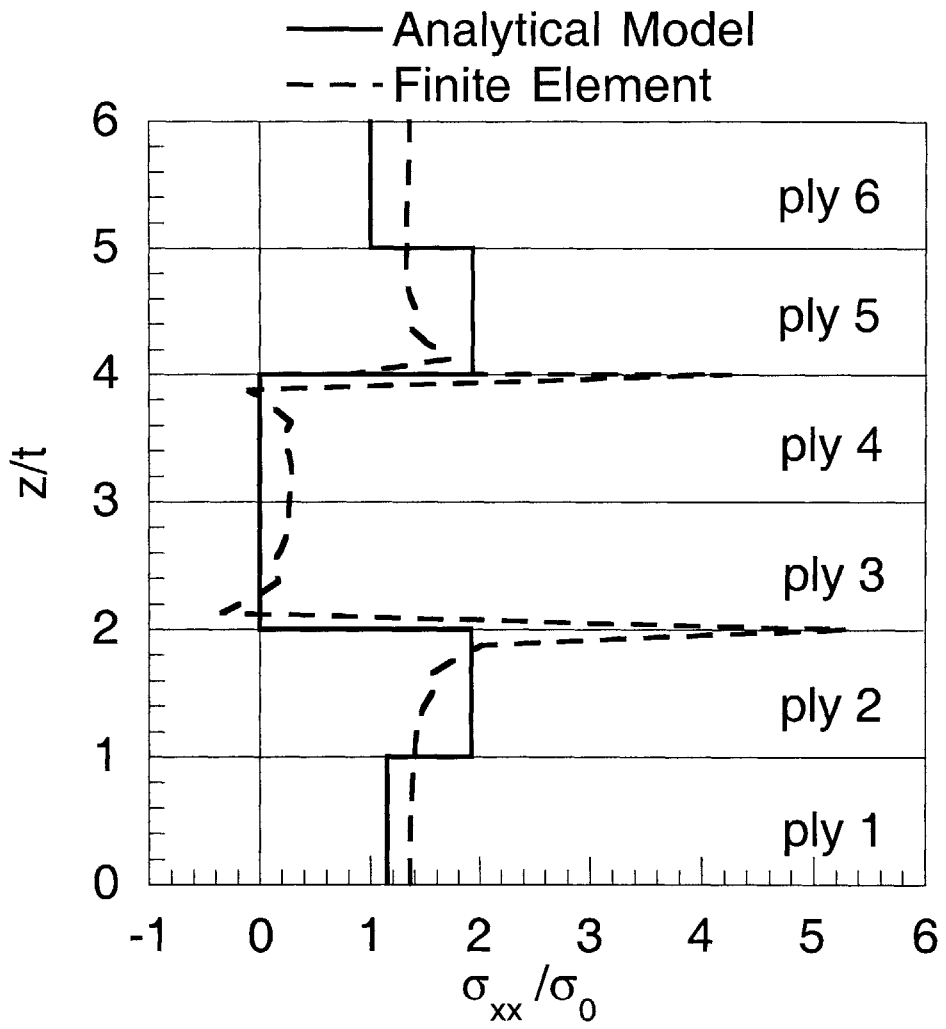

Figure 6.46 In-plane stresses through the thickness in the upper-half of the laminate at the cutoff in a $[0_2/0_{2D}/0_2]_s$ laminate with existing delaminations obtained using the analytical model and FE method.

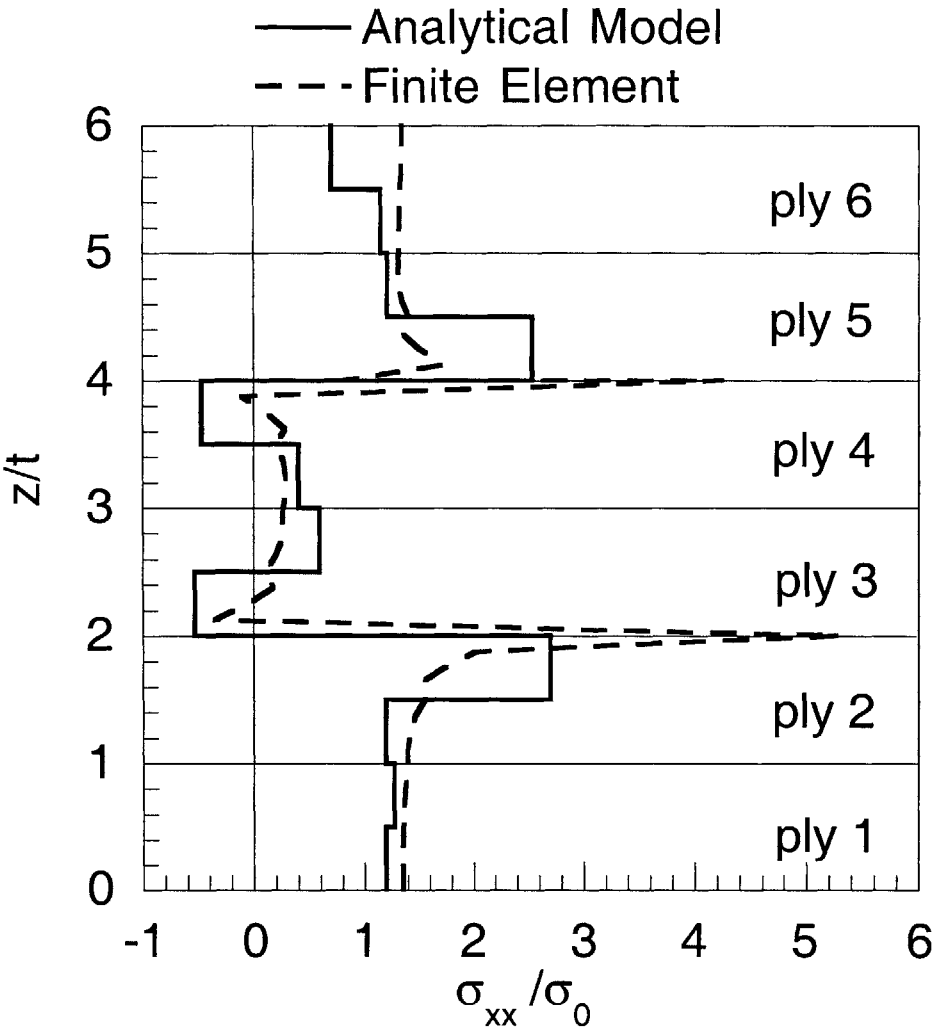

Figure 6.47 In-plane stresses through the thickness in the upper-half of the laminate at the cutoff in a $[0_2/0_{2D}/0_2]_s$ laminate with existing delaminations obtained using a refined analysis via ply subdivision and FE method.

significantly smaller compressive stress and a crossover distance of approximately one ply thickness. In the dropped region, the magnitudes of the stresses obtained using the two methods differ significantly. The fact that the interlaminar normal stresses do not match as well as the interlaminar shear stresses is not surprising, since the contact phenomenon of the delaminated interfaces is not modeled in the analytical method, which may transfer interlaminar normal stresses.

Similar trends in the through-thickness in-plane stress distributions at x equal to 0 in the undropped region can be seen in Figures 6.46 and 6.47. A plot of the in-plane stress distribution obtained using the analytical method without ply sub-division is shown in Figure 6.46, while one obtained using the analytical method with ply sub-division is shown in Figure 6.47. Each ply was divided into two sub-plies in the refined analysis. As in the case for the external ply dropoffs in the previous example, the refined analysis yields a better approximation to the overall in-plane stress distribution compared to that obtained using the FE method.

The two examples in this sub-section show that the current analytical method can be used to obtain accurate interlaminar stress fields for laminates with delaminations at external ply dropoffs. In the external case, the delaminated region does not come into contact with other parts of the laminate as it deforms. This allows the interlaminar stress field in the analytical model to closely match that of the FE model. For laminates with internal ply dropoffs, the delaminated region becomes a contact surface. This is not modeled in the analytical method, and the analytical method therefore does not yield accurate results. Nevertheless, comparison of the interlaminar stress field in a laminate with internal ply dropoffs shows that the current method yields similar trends as that of the FE analysis for the interlaminar shear stress. This indicates that the current method provides a good framework to further extend the model for laminates with internal ply dropoffs with existing delamination by considering the contact forces between the delaminated interfaces. For such an analysis, the deformation in the delaminated and

dropoff regions would need to be taken into account.

6.2 Parametric Study

In the previous section, it was seen that the distribution of the interlaminar stress fields in laminates with ply dropoffs varies depending on the laminate configuration. For example, it was seen in Section 6.1.3 that the magnitude of the interlaminar normal stress decreases with decreasing taper angle while the interlaminar shear stress distribution is not significantly affected. In this section, the structural parameters that affect interlaminar stresses in laminates with ply dropoffs under in-plane and bending loads are investigated in greater detail, including the effects of the taper angle. Specifically, five structural parameters are considered; the taper angle, the through-thickness location of the terminated ply group, the overall stiffness of the terminated ply group, the layup sequence of the terminated ply group, and the number of terminated plies. For each parameter, three or four laminates with different "levels" (*e.g.*, magnitude, location) of the parameter are considered in order to gain key insights. The material properties of the AS4/3501-6 composite material system shown in Table 5.2 are used in all of the examples in this section.

6.2.1 Taper Angle

Three $[0_2/0_{2D}/0_4]_s$ laminates with taper angles of 3.81°, 5.71° and 11.31° are considered in order to investigate the effects of the taper angle on the interlaminar stress field. The three taper angles correspond to lengths of the dropoff region of 30t, 20t, and 10t, respectively. A diagram of the $[0_2/0_{2D}/0_4]_s$ laminate considered is shown in Figure 6.48 along with the indications of the positive directions of the applied in-plane and bending loads. Interlaminar stresses along the two interfaces of the continuous and terminated plies in the undropped region and along the interface of the inner and outer continuous plies in the upper-half of the laminates are considered. Plots of the

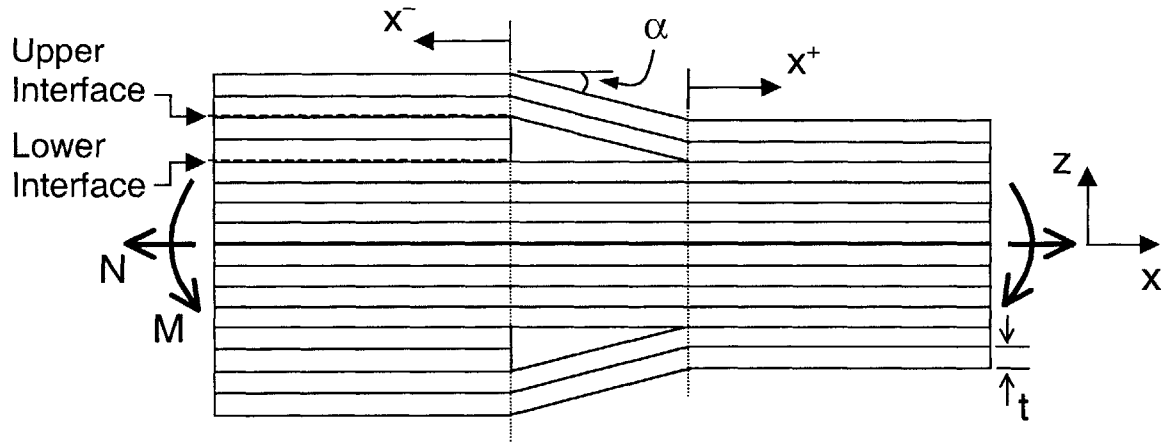

Figure 6.48 Diagram of a $[0_2/0_{2D}/0_4]_s$ laminate showing the positive directions of the applied loads with indications of "upper" and "lower" interfaces as referenced in Figures 6.49 through 6.52 and 6.58 through 6.62.

interlaminar stresses in the laminates under in-plane load are shown in Figures 6.49 and 6.50, and those in laminates under bending load are shown in Figures 6.51 and 6.52. Two plots are shown in each figure: one along the upper interface of the terminated ply group in the undropped region (z = 6t) and the inner and outer continuous plies in the dropped region (z = 4t), and the other along the lower interface of the terminated ply group in the undropped region (z = 4t) and along the inner and outer continuous plies in the dropped region (z = 4t). For the cases of in-plane load, the stresses are normalized by the applied in-plane stress at the undropped end, σ_0, and for the cases of bending load, by the in-plane stress at the outer surface at the undropped end, σ_s, due to the applied moment. All laminates are assumed to have unit width.

It can be seen in Figure 6.49 that the taper angle affects the interlaminar shear stress distribution in both the undropped and dropped regions. However, the change in the distribution is more evident in the dropped region where the magnitude of the stress increases in addition to changing signs with increasing taper angle. Although the rate of change of the magnitude of the interlaminar shear stress in the dropped region with respect to the taper angle is relatively high, the magnitude of the interlaminar shear stress there is significantly smaller than that in the undropped region. Even in the laminate with a taper angle of 11.31° where the magnitude of the interlaminar shear stress in the dropped region is the greatest among the three laminates considered, the magnitude in the dropped region is smaller by a factor of approximately three. Therefore, these stresses are not a key concern in the delamination of laminates as long as the taper angle is relatively small and within the range of those considered.

In the undropped region shown in the top plot of Figure 6.49, the interlaminar shear stress along the upper interface of the terminated ply group decreases with increasing taper angle. In contrast, the interlaminar shear stress along the lower interface of the terminated ply group increases as shown in the bottom plot of Figure 6.49. The reason for this opposing trend is that the interlaminar shear stresses along the two

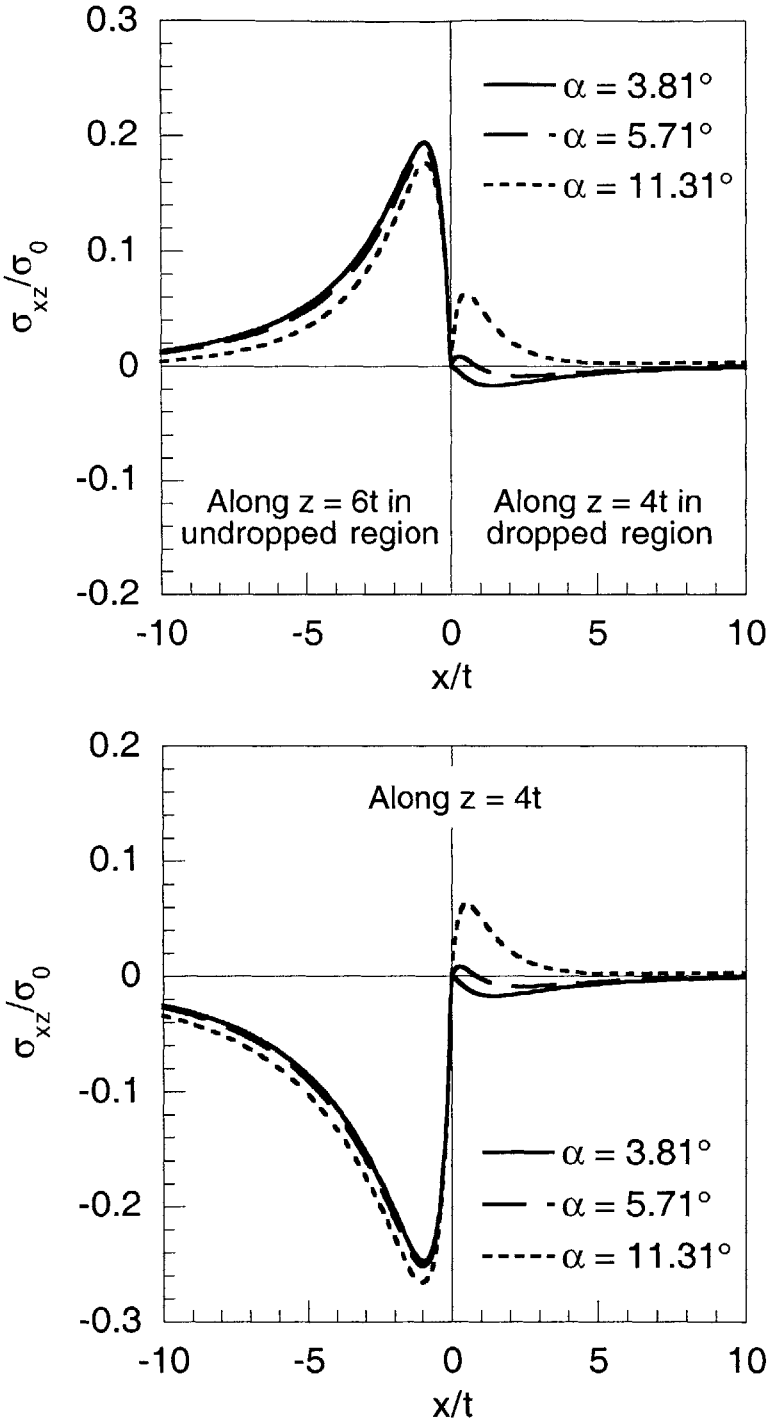

Figure 6.49 Interlaminar shear stresses along *(top)* the upper interface in the undropped region (z = 6t) and the interface of the inner and outer continuous plies in the dropped region (z = 4t), and *(bottom)*, the lower interface in the undropped and dropped regions (z = 4t) in $[0_2/0_{2D}/0_4]_s$ laminates with taper angles of 3.81°, 5.71° and 11.31° under in-plane load.

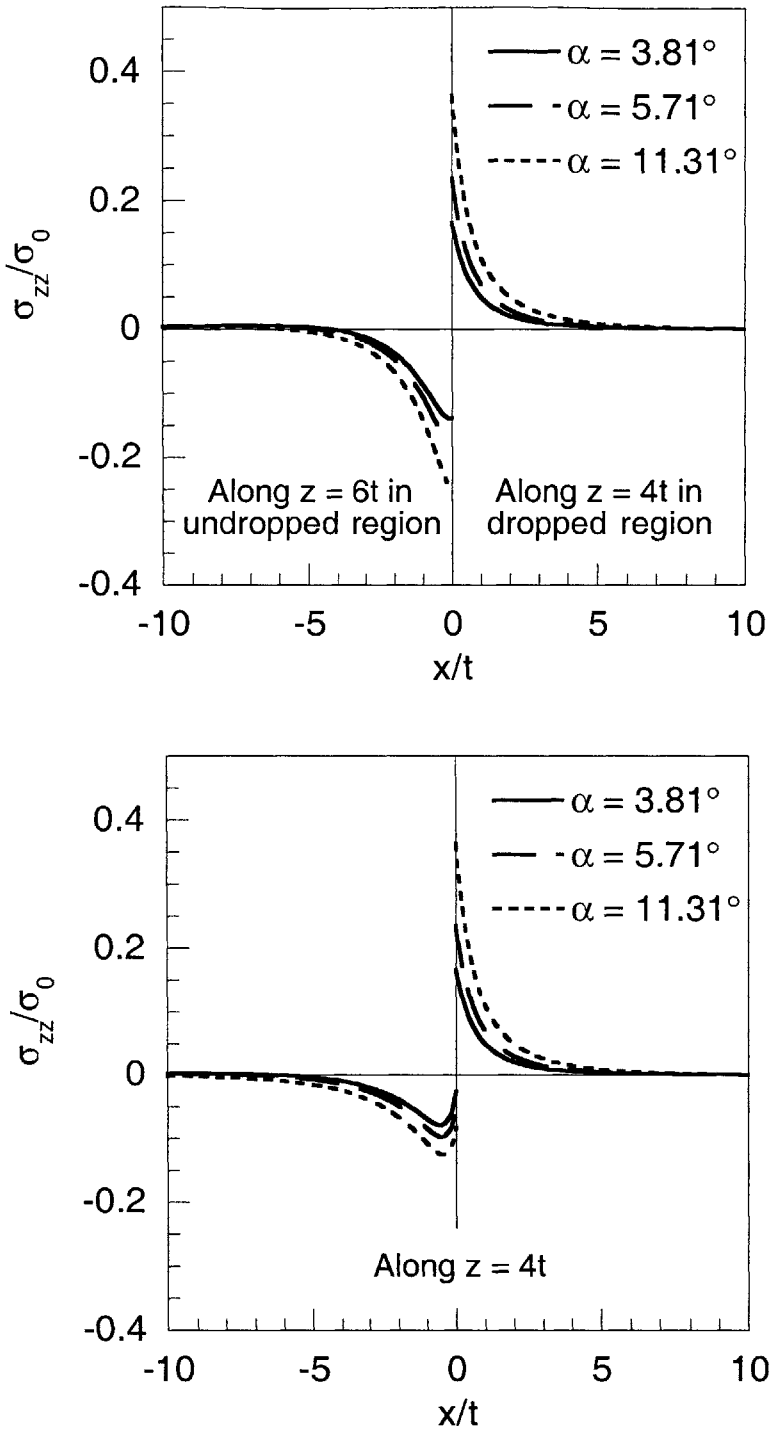

Figure 6.50 Interlaminar normal stresses along *(top)* the upper interface in the undropped region (z = 6t) and the interface of the inner and outer continuous plies in the dropped region (z = 4t), and *(bottom)*, the lower interface in the undropped and dropped regions (z = 4t) in $[0_2/0_{2D}/0_4]_s$ laminates with taper angles of 3.81°, 5.71° and 11.31° under in-plane load.

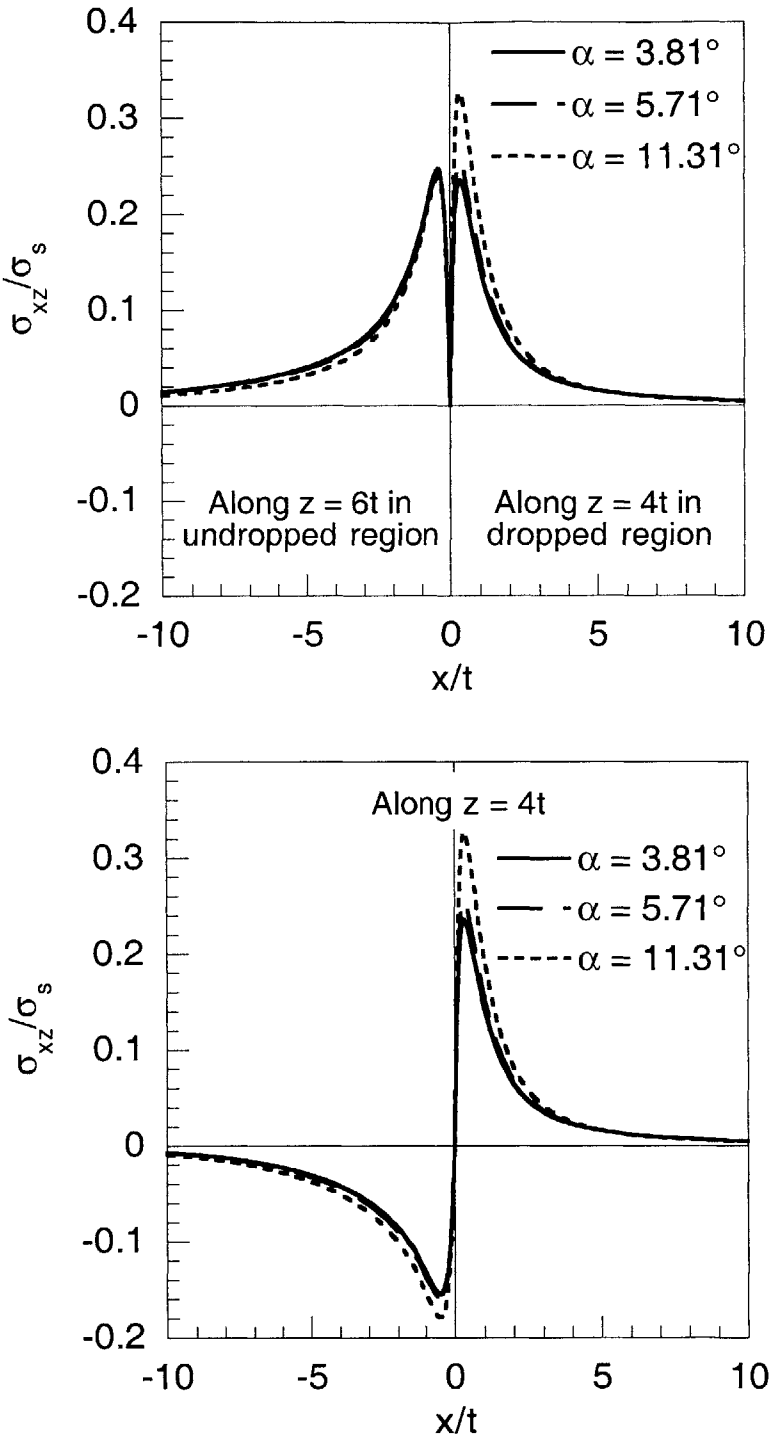

Figure 6.51 Interlaminar shear stresses along *(top)* the upper interface in the undropped region (z = 6t) and the interface of the inner and outer continuous plies in the dropped region (z = 4t), and *(bottom)*, the lower interface in the undropped and dropped regions (z = 4t) in $[0_2/0_{2D}/0_4]_s$ laminates with taper angles of 3.81°, 5.71° and 11.31° under bending load.

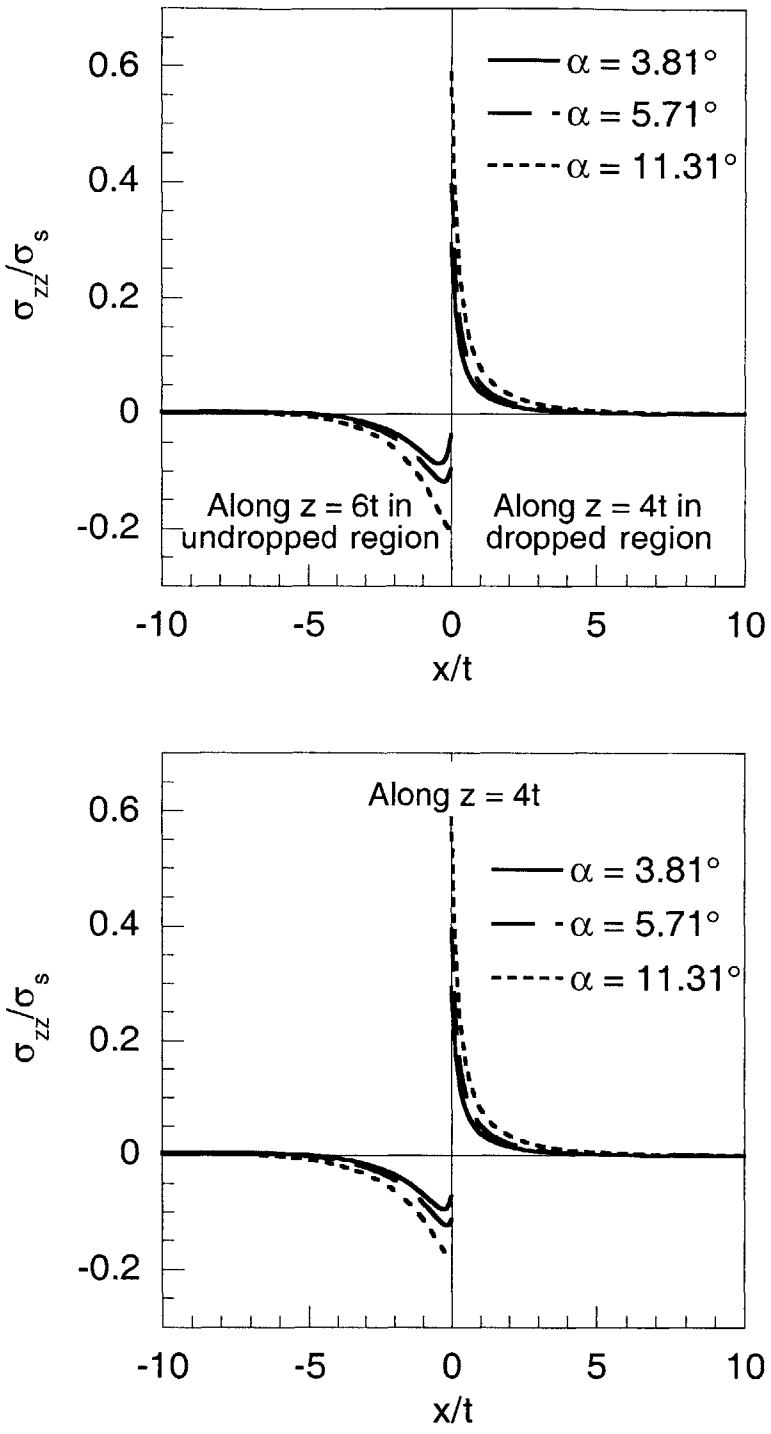

Figure 6.52 Interlaminar normal stresses along *(top)* the upper interface in the undropped region (z = 6t) and the interface of the inner and outer continuous plies in the dropped region (z = 4t), and *(bottom)*, the lower interface in the undropped and dropped regions (z = 4t) in $[0_2/0_{2D}/0_4]_s$ laminates with taper angles of 3.81°, 5.71° and 11.31° under bending load.

interfaces are not independent. The interlaminar shear stresses along these two interfaces represent the load transferred from the terminated ply group to the continuous plies above and below the terminated ply group. Therefore, the sum of the integral of the interlaminar shear stress, *i.e.*, total load transferred along these two interfaces, must remain constant and equal to the far-field load carried by the terminated ply group. Since there are two terminated plies, the far-field load in the terminated ply group is equal to $2\sigma_0 t$. The load transferred across each interface is shown in Table 6.3. As expected, based on the interlaminar stress distributions, the load transferred along the upper interface of the terminated ply group decreases while the load transferred along the lower interface of the terminated ply group increases with increasing taper angle. The sum of the load transferred is constant with respect to the taper angle and equal to $2\sigma_0 t$.

Two interesting trends in the total load transferred via interlaminar shear stresses along the two interfaces in the undropped region can be observed in Table 6.3. One, it can be seen that the load transferred along the lower interface of the terminated ply group to the four inner continuous plies is always greater than that transferred along the upper interface to the two outer continuous plies. Two, it can be seen that the ratio of the load transferred along the lower interface to that transferred along the upper interface increases with increasing taper angle. The ratio is 1.7 in the laminate with a taper angle of 3.81°, 1.9 in the laminate with a taper angle of 5.71°, and 2.9 in the laminate with a taper angle of 11.31°. These trends clearly show that the load transfer from the terminated ply group to the inner and outer continuous plies in laminate with internal ply dropoffs is closely related to the taper angle in the dropoff region.

The effects of the taper angle on the interlaminar normal stress distribution in both the undropped and dropped regions can be clearly seen in Figure 6.50. In the dropped region, the peak stress, which always occurs at the cutoff ($x = 0$), increases from $0.17\sigma_0$ in the laminate with a taper angle of 3.81° to $0.23\sigma_0$ in the laminate with a taper angle of 5.71° to $0.37\sigma_0$ in the laminate with a taper angle of 11.31°. In addition, the

Table 6.3 Load (per unit width) transferred along the two interfaces of the terminated ply group in the undropped region in $[0_2/0_{2D}/0_4]_s$ laminates with various taper angles under in-plane load

Interface	Taper Angle		
	3.81°	5.71°	11.31°
Upper Interface (z = 6t)	0.75*	0.69	0.51
Lower Interface (z = 4t)	1.25	1.31	1.49
Total	2.00	2.00	2.00

* All values normalized by $\sigma_0 t$.

magnitude of the interlaminar normal stress is smallest over the entire dropped region in the laminate with a taper angle of 3.81° followed by the laminate with a taper angle of 5.71°. The magnitude of the interlaminar normal stress is the greatest in the laminate with a taper angle of 11.31°. Since the interlaminar normal stresses in this region are tensile, this increasing trend of the interlaminar normal stress is a key concern in the delamination of the laminate. On the other hand, the peak stresses along the upper and lower interfaces in the undropped region are compressive and increase in magnitude with increasing taper angle. Since the interlaminar normal stress along these interfaces in the undropped region are compressive, they are not expected to contribute significantly to delamination. The trend of increasing magnitude of the tensile and compressive interlaminar normal stresses in the undropped region and the dropped region is consistent with the trend observed in Section 6.1.3. It is noted that although the interlaminar normal stress distributions along the upper and lower interfaces approximately one ply thickness away from the cutoff exhibit slightly different trends, the integrals of the interlaminar normal stresses, *i.e.*, the net compressive force along the two interfaces are equal. This is described in greater detail in Section 6.4.

The trends of the interlaminar shear stress distributions in laminates under bending load are similar to those in laminates under in-plane load as seen in Figure 6.51. As in the in-plane load case, the change in the distribution is more evident in the dropped region compared to that in the undropped region. However, in laminates under bending load, the magnitude of the interlaminar shear stress in the dropped region is comparable to and in some cases larger than that in the undropped region, causing delamination in the dropped region to be a key concern. For example, it can be seen that the peak interlaminar shear stress of $0.33\sigma_s$ in the dropped region of the laminate with a taper angle of 11.31° is greater than that of $0.24\sigma_s$ along the upper interface of the terminated ply group in the undropped region. Therefore, the change in the interlaminar shear stress distribution in the dropped region may affect the delamination behavior of the laminate.

In the undropped region shown in the top plot of Figure 6.51, the interlaminar shear stress distribution along the upper interface exhibits a decreasing trend in magnitude with increasing taper angle, while along the lower interface shown in the bottom plot of Figure 6.51, the opposite trend is seen. This trend is identical to that of the in-plane load case. The load transferred along the each interface in the undropped region is shown in Table 6.4. It can be seen that the sum of the load transferred along the two interfaces is constant with respect to the taper angle and equal to $1.25\sigma_s t$, which is the far-field load in the terminated ply group. It can also be seen that the load per unit width transferred along the upper interface is always greater than that transferred along the lower interface, which is in contrast to the trend observed in the laminates under in-plane load. In laminates under bending load, the far-field in-plane stress carried by the terminated ply group varies linearly through the thickness, and thus, the stress at the upper interface of the terminated ply group is greater than that at the lower interface. Therefore, it is not surprising that the load transferred along the upper interface is greater than that transferred along the lower interface. However, the ratio of the load transferred along the lower interface of the terminated ply group to the load transferred along the upper interface is seen to increase with increasing taper angle in laminates under bending load consistent with the case of the laminates under in-plane load. The ratio is 0.6 in the laminate with a taper angle of 3.81°, 0.7 in the laminate with a taper angle of 5.71°, and 0.9 in the laminate with a taper angle of 11.31°. This, again, shows that the load transfer from the terminated ply group to the inner and outer continuous plies is closely related to the taper angle in the dropoff region.

The characteristics and trends of the interlaminar normal stresses in the upper-half of laminates under bending load shown in Figure 6.52 are, again, similar to those in laminates under in-plane load. The peak tensile interlaminar normal stress occurs in the dropped region at the cutoff and monotonically decreases away from the cutoff while the interlaminar normal stresses in the undropped region are compressive and smaller in

Table 6.4 Load (per unit width) transferred along the two interfaces of the terminated ply group in the undropped region in $[0_2/0_{2D}/0_4]_s$ laminates with various taper angles under bending load

Interface	Taper Angle		
	3.81°	5.71°	11.31°
Upper Interface (z = 6t)	0.75*	0.73	0.65
Lower Interface (z = 4t)	0.49	0.51	0.60
Total	1.25	1.25	1.25

* All values normalized by $\sigma_s t$.

magnitude by a factor of approximately three compared to those in the dropped region. This causes delamination in the dropped region to be a key concern in the upper-half of the laminate. The magnitude of the interlaminar normal stresses in the dropped region is seen to increase with increasing taper angle as in the case of the in-plane load. The peak stress of $0.58\sigma_s$ in the laminate with a taper angle of 11.31° is greater by a factor of two compared to that of $0.29\sigma_s$ in the laminate with a taper angle of 3.81°. Note that in laminates under bending load, the interlaminar normal stress is anti-symmetric with respect to the mid-plane, unlike in laminates under in-plane load where it is symmetric. Therefore, in the lower-half of the laminate, the sign of the interlaminar normal stress is reversed. This implies that the interlaminar normal stress is compressive in the dropped region and tensile in the undropped region, which causes delamination to be a concern in the undropped region in the lower-half of the laminate. However, since the relative magnitude of the interlaminar tensile normal stress in the dropped region is greater than that of the interlaminar compressive normal stress in the undropped region by a factor of approximately three at the peak, delamination in the upper-half of the laminate is a greater concern.

6.2.2 Location of Terminated Plies

The effects of the location of terminated plies, with respect to the thickness direction, are investigated using four laminates with twelve continuous and four terminated plies. The layups of the laminates considered are $[0_{2D}/0_6]_s$, $[0_2/0_{2D}/0_4]_s$, $[0_4/0_{2D}/0_2]_s$ and $[0_6/0_{2D}]_s$. For the laminates with internal ply dropoffs, a taper angle of 7° is used. Diagrams of the four laminates considered are shown in Figure 6.53. The upper-half of each laminate is considered as allowed via symmetry. The interlaminar stresses along the upper and lower interfaces of the terminated ply group in the undropped region and the interface of the inner and outer continuous plies in the dropped region are considered in each laminate. The dashed lines in Figure 6.53 indicate these interfaces. Note that laminates with external ply dropoffs have only one interface where the

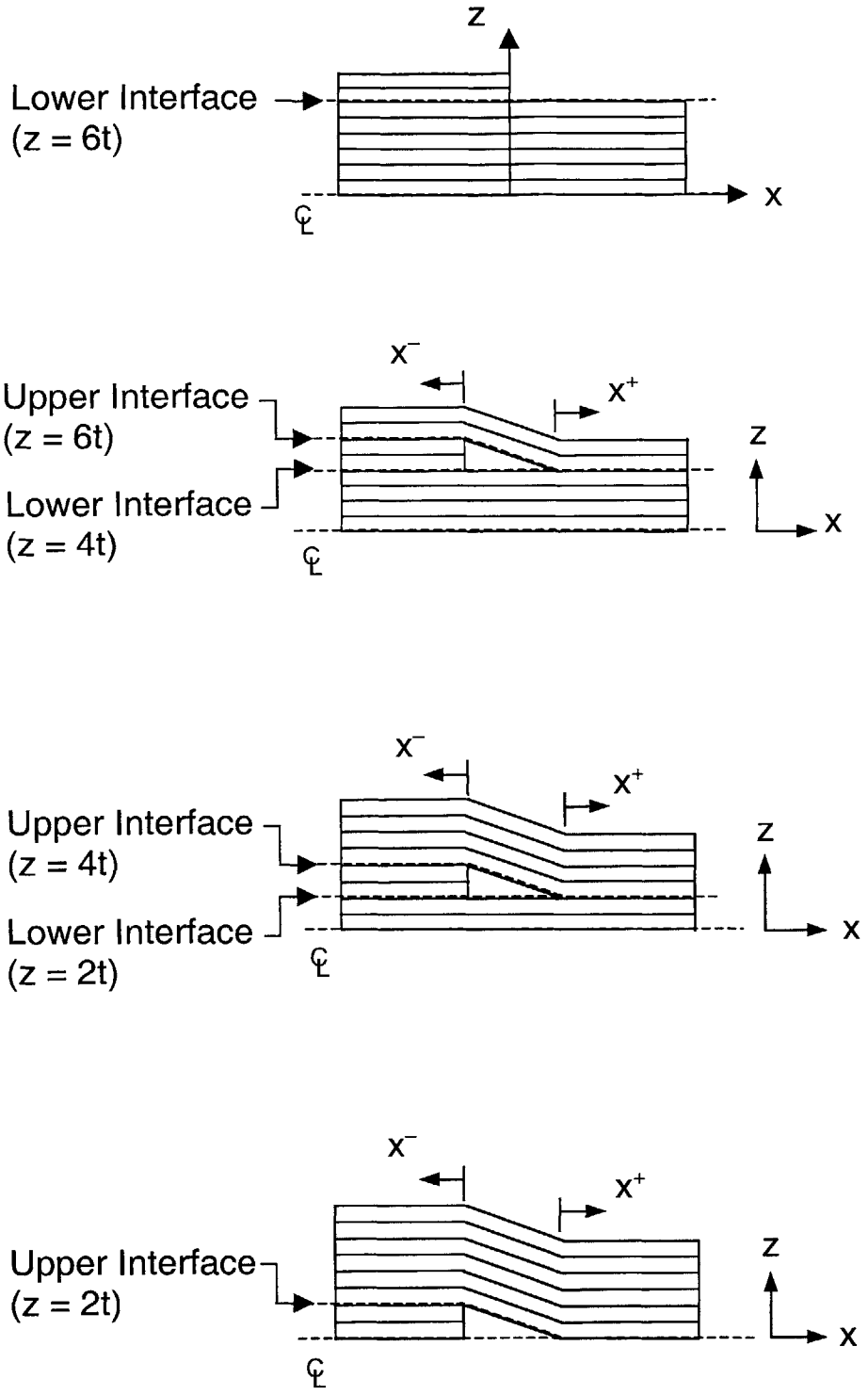

Figure 6.53 Diagrams of the upper-half of laminates with layups of $[0_{2D}/0_6]_s$, $[0_2/0_{2D}/0_4]_s$, $[0_4/0_{2D}/0_2]_s$, and $[0_6/0_{2D}]_s$ (from top to bottom) with indications of "upper" and "lower" interfaces as referenced in Figures 6.54 through 6.57.

terminated ply group and the continuous plies meet, while laminates with internal ply dropoffs have two such interfaces. An exception holds for laminates with internal ply dropoffs that are located at the mid-plane. Such laminates also have only one interface where the terminated ply groups and continuous plies meet as the lower interface, *i.e.*, the mid-plane, connects to the terminated plies in the symmetric lower-half of the laminate. All laminates are assumed to have unit width.

The interlaminar stress distributions in the laminates under in-plane load are shown in Figures 6.54 and 6.55, and those under bending load are shown in Figures 6.56 and 6.57. In order to compare the trends of the interlaminar stresses in the four types of laminates directly, the interlaminar stresses along the lower and upper interfaces in the undropped region are shown on separate plots. Thus, two plots are shown in each figure, one with the stresses along the lower interface in the undropped region and the other with the stresses along the upper interface in the undropped region. In both plots, the interlaminar stresses along the interface of the inner and outer continuous plies in the dropped region are shown as well. The interlaminar stresses are normalized by the applied in-plane stress at the undropped end, σ_0, for laminates under in-plane load and by the applied stress at the outer surface at the undropped end, σ_s, for laminates under bending load.

It can be seen in Figure 6.54 that the interlaminar shear stress distribution varies with the location of the terminated ply group. Along the lower interface in the undropped region shown in the top plot of Figure 6.54, the magnitude of the interlaminar shear stress in the laminate with external ply dropoffs is greater than those in laminates with internal ply dropoffs except in the vicinity of the cutoff (*i.e.*, in the region between the cutoff and x equal to approximately –3t). In this latter region, the interlaminar shear stress distributions in the three laminates almost overlap. Along the upper interface shown in the bottom plot of Figure 6.54, the magnitude of the interlaminar shear stress distributions in the $[0_6/0_{2D}]_s$ laminate is greater than that in the other two laminates with

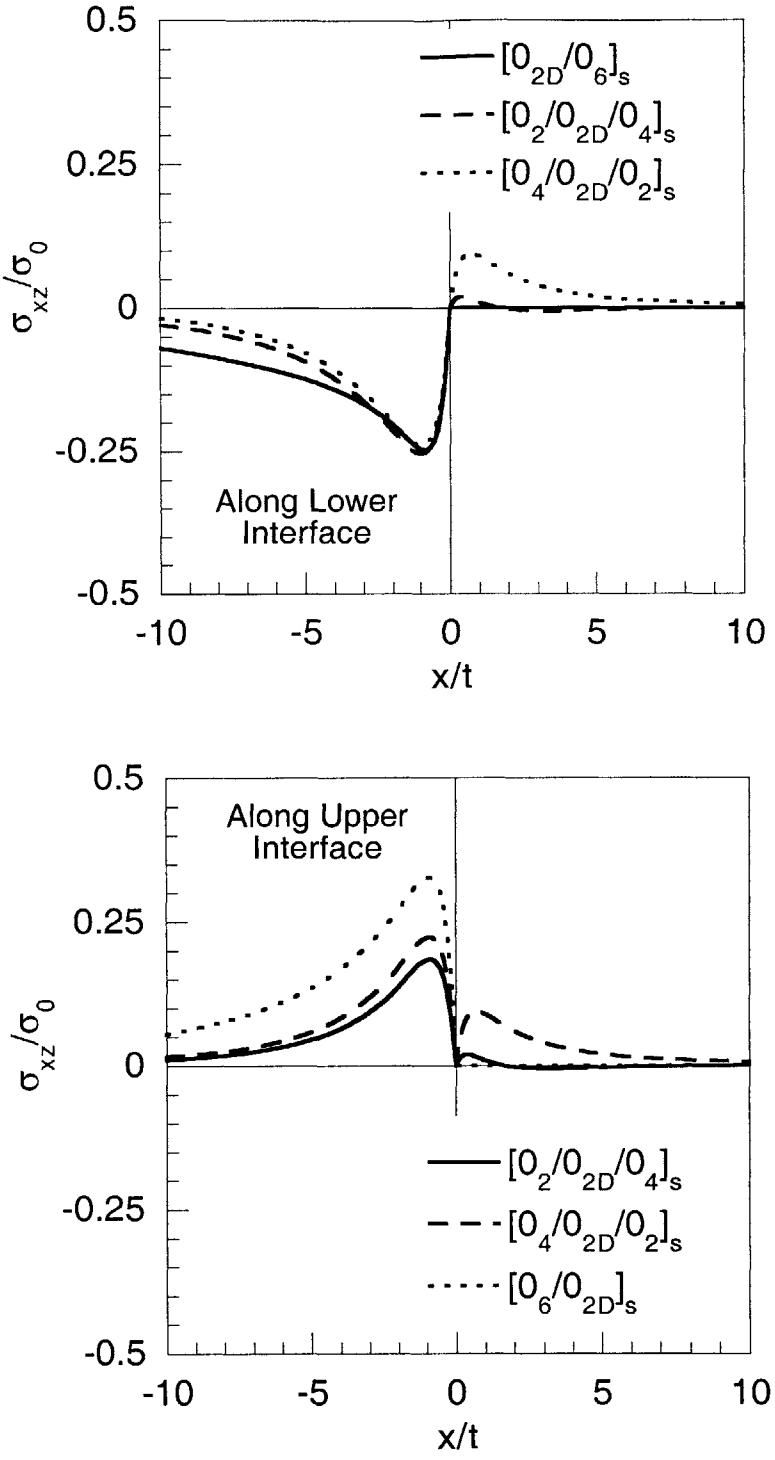

Figure 6.54 Interlaminar shear stresses along *(top)* the lower interfaces, and *(bottom)*, the upper interfaces in laminates with twelve continuous and four terminated plies under in-plane load.

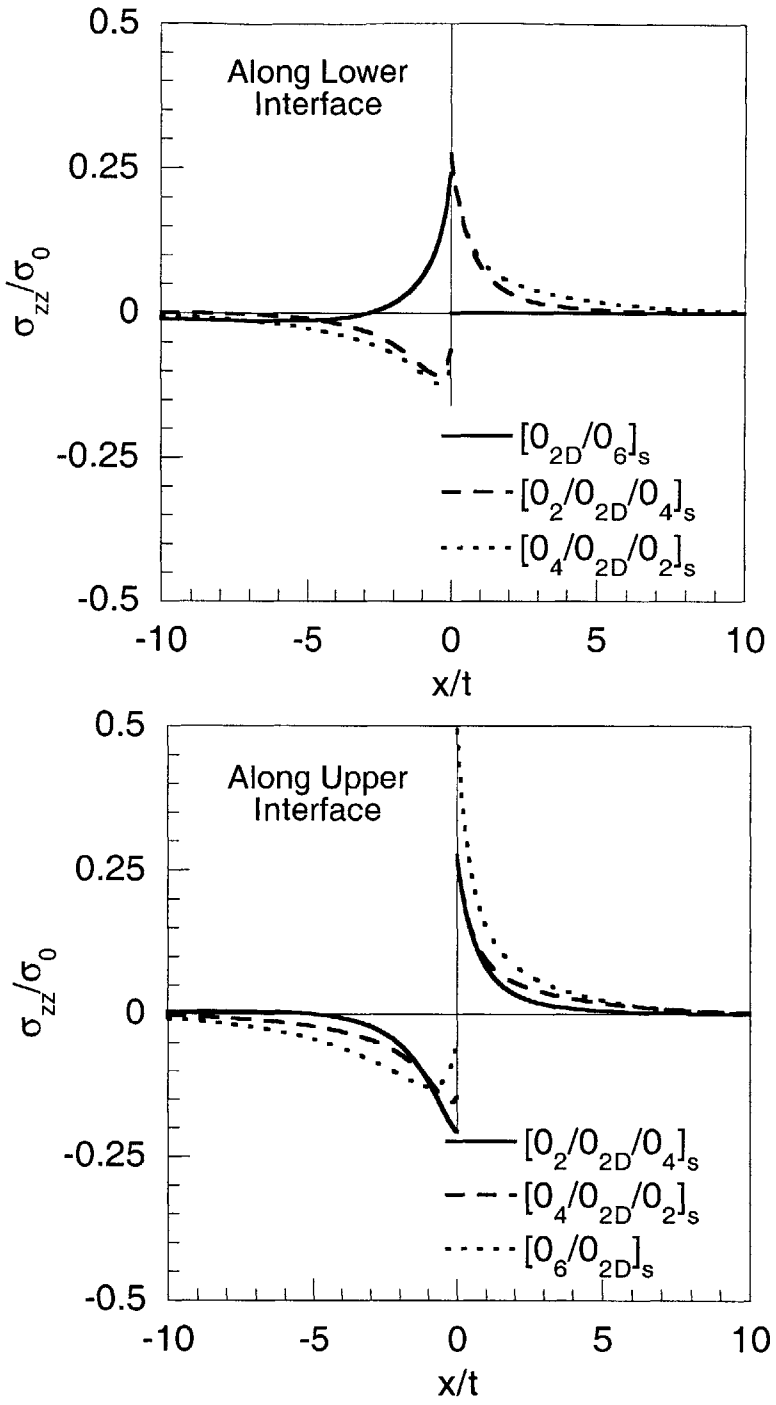

Figure 6.55 Interlaminar normal stresses along *(top)* the lower interfaces, and *(bottom)*, the upper interfaces in laminates with twelve continuous and four terminated plies under in-plane load.

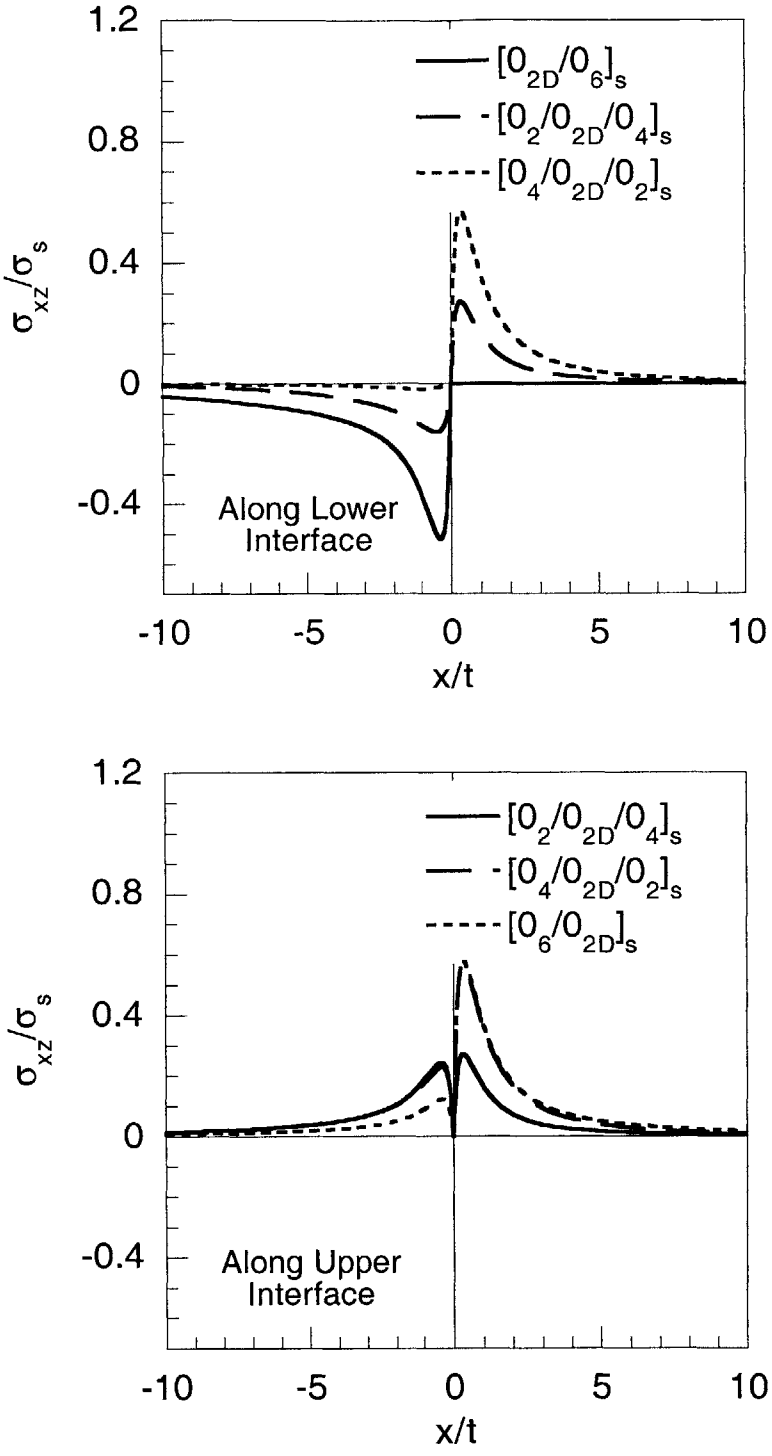

Figure 6.56 Interlaminar shear stresses along *(top)* the lower interfaces, and *(bottom)*, the upper interfaces in laminates with twelve continuous and four terminated plies under bending load.

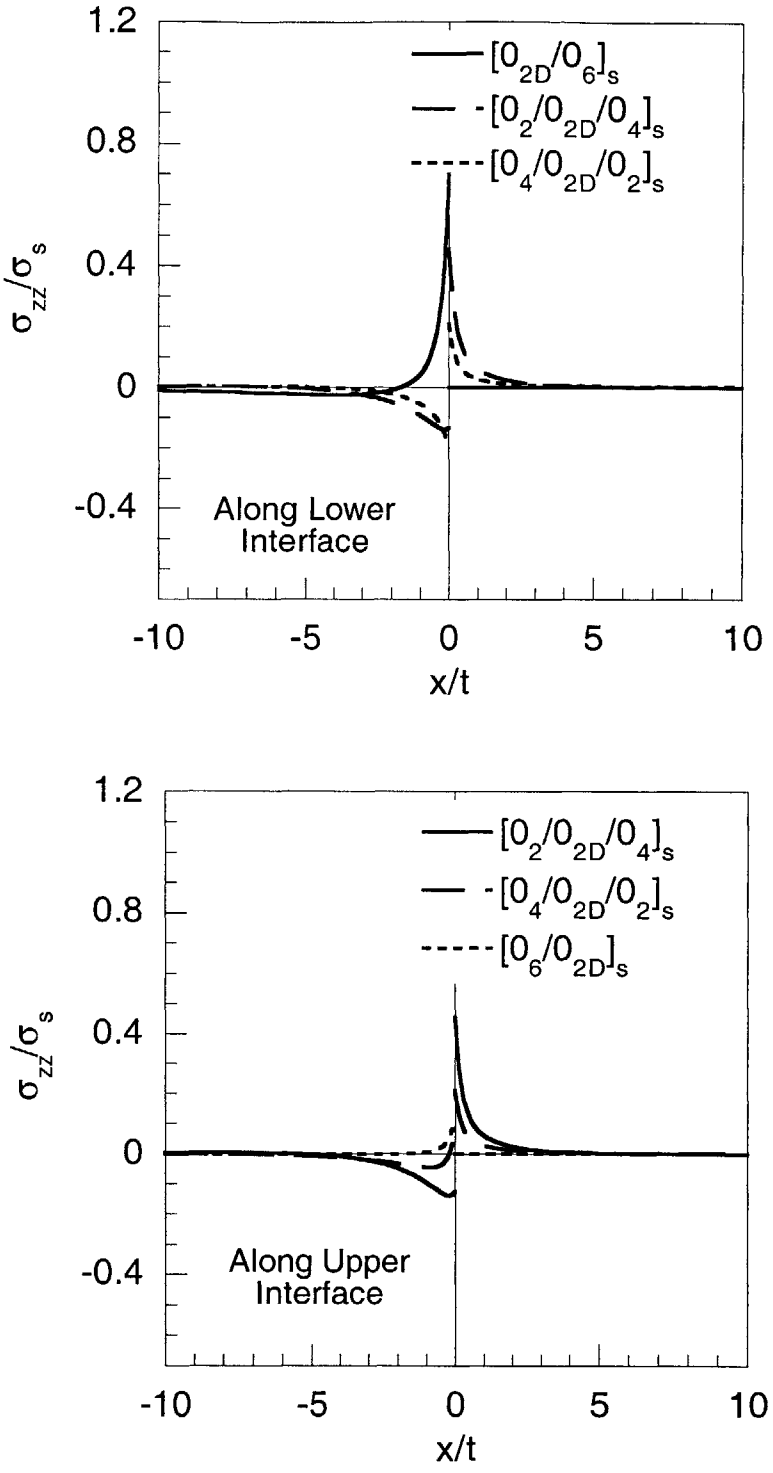

Figure 6.57 Interlaminar normal stresses along *(top)* the lower interfaces, and *(bottom)*, the upper interfaces in laminates with twelve continuous and four terminated plies under bending load.

internal ply dropoffs over the entire undropped region. In the dropped region, both the interlaminar shear and normal stresses are identically zero along the interface considered in the laminate with external ply dropoffs (z = 6t) since this interface corresponds to the outer surface. In addition, the interlaminar shear stress is also identically zero along the interface considered in the dropped region of the $[0_6/0_{2D}]_s$ laminate (z = 0) under in-plane load due to anti-symmetry about the mid-plane. The interlaminar shear stresses along the interface of the inner and outer continuous plies in the dropped region of the $[0_2/0_{2D}/0_4]_s$ and $[0_4/0_{2D}/0_2]_s$ laminates are non-zero. The magnitude of the interlaminar shear stress along this interface is greater in the $[0_4/0_{2D}/0_2]_s$ laminate compared to that in the $[0_2/0_{2D}/0_4]_s$ laminate by a factor of approximately three at the peak. However, the magnitude of the interlaminar shear stress in the dropped region is smaller than that in the undropped region by a factor of approximately three even in the $[0_4/0_{2D}/0_2]_s$ laminate. This implies that delamination due to interlaminar shear stresses in the dropped region is not a major concern in the laminates considered.

The fact that the magnitude of the interlaminar shear stress distributions in the undropped region of the $[0_{2D}/0_6]_s$ and $[0_6/0_{2D}]_s$ laminates are greater than those in the other laminates is not surprising because the far-field load carried by the terminated ply group needs to be transferred via interlaminar shear stresses along only one interface. Thus, the integral of the interlaminar shear stress, *i.e.*, the load transferred along this interface, is equal to the far-field in-plane load, $2\sigma_0 t$. The far-field loads carried by the terminated ply groups in all four laminates considered are identical because they have the same ratio of continuous to terminated plies. However, in the $[0_2/0_{2D}/0_4]_s$ and $[0_4/0_{2D}/0_2]_s$ laminates, there are two interfaces where the continuous and terminated plies in the undropped region meet. This being the case, the load transfer takes place along both interfaces, and thus, the load transferred along each interface can be lower than that when there is only one interface.

The load transferred along each interface in the undropped region is shown in

Table 6.5. It can be clearly seen that the load transferred along the two interfaces in the $[0_2/0_{2D}/0_4]_s$ and $[0_4/0_{2D}/0_2]_s$ laminates are smaller than those transferred along the single interfaces in the $[0_{2D}/0_6]_s$ and $[0_6/0_{2D}]_s$ laminates. The higher magnitude of the interlaminar shear stresses in the laminates with single interfaces between the continuous and terminated plies cause delamination along these interfaces to be a greater concern in these laminates than in those with two such interfaces.

It can also be seen in Table 6.5 that the ratio of the load transferred along the two interfaces are different in the $[0_2/0_{2D}/0_4]_s$ and $[0_4/0_{2D}/0_2]_s$ laminates. The ratio of the load transferred along the lower interface to the upper interface in the $[0_2/0_{2D}/0_4]_s$ laminate is 2.1, while the ratio in the $[0_4/0_{2D}/0_2]_s$ laminate is 1.1. In the $[0_2/0_{2D}/0_4]_s$ laminate, where there are four continuous plies below the terminated ply group and two continuous plies above it, a greater ratio of the far-field load is transferred along the lower interface. In the $[0_4/0_{2D}/0_2]_s$ laminate, approximately equal amounts of the far-field load are transferred along the upper and lower interfaces even though there are four continuous plies above the terminated ply group and two below it. This shows that the load transferred along the upper and lower interfaces of the terminated ply groups in the undropped region is related to the number of inner and outer continuous plies.

The interlaminar normal stress distributions in the four laminates with ply dropoffs at different through-thickness locations are shown in Figure 6.55. Along the lower interface shown in the top plot of Figure 6.55, the interlaminar normal stress in the undropped region of the laminate with external ply dropoffs is tensile near the cutoffs, while those in laminates with internal ply dropoffs are compressive. This suggests that there is a fundamental difference in the mechanism that causes interlaminar stresses in laminates with external and internal ply dropoffs. Along the upper interface in the undropped region shown in the bottom plot of Figure 6.55, the interlaminar normal stresses in all three laminates with internal ply dropoffs are compressive. Although the magnitude of the interlaminar normal stress in the undropped region generally increases

Table 6.5 Load (per unit width) transferred along the upper and lower interfaces in the undropped region in laminates with twelve continuous and four terminated plies under in-plane load

Interface	Laminate			
	$[0_{2D}/0_6]_s$	$[0_2/0_{2D}/0_4]_s$	$[0_4/0_{2D}/0_2]_s$	$[0_6/0_{2D}]_s$
Upper Interface (z = 6t)	–	0.65*	0.97	2.00
Lower Interface (z = 4t)	2.00	1.35	1.03	–
Total	2.00	2.00	2.00	2.00

* All values normalized by $\sigma_0 t$.

closer to the cutoffs, a sudden decrease can be observed in some laminates very close to the cutoff (within approximately two ply thicknesses). The cause of these "reversal" trends is discussed further in Section 6.4.

In the dropped region, the interlaminar normal stresses along the interface of the inner and outer continuous plies in the laminates with internal ply dropoffs are tensile and exhibit similar trends. Along this interface, the peak interlaminar normal stress occurs at the cutoff, and the interlaminar normal stress monotonically decreases and decays to zero far away from the cutoff. Since the interlaminar normal stresses in the dropped region are tensile, they are a key concern because delamination may initiate along this interface. The peak stress in the $[0_2/0_{2D}/0_4]_s$ and $[0_4/0_{2D}/0_2]_s$ laminates are almost identical and equal to $0.28\sigma_0$ while that in the $[0_6/0_{2D}]_s$ laminate is much greater and equal to $0.49\sigma_0$. The magnitude of the interlaminar normal stress in the $[0_6/0_{2D}]_s$ laminate is greater than those in the $[0_2/0_{2D}/0_4]_s$ and $[0_4/0_{2D}/0_2]_s$ laminates away from the cutoff over the entire dropped region as well.

The trends of the interlaminar stress distributions in the undropped regions of laminates under bending load are different from those in laminates under in-plane load. It can be seen in the top plot of Figure 6.56 that the magnitude of the interlaminar shear stress along the lower interface in the laminate with external ply dropoffs is greater than those with internal ply dropoffs over the entire undropped region by a factor of approximately three. In addition, the magnitude of the interlaminar shear stress along the lower interface in the $[0_2/0_{2D}/0_4]_s$ laminate is greater than that in the $[0_4/0_{2D}/0_2]_s$ laminates by approximately an order of magnitude. In contrast, the interlaminar shear stress distribution in the $[0_2/0_{2D}/0_4]_s$ and $[0_4/0_{2D}/0_2]_s$ laminates along the upper interface in the undropped region shown in the bottom plot of Figure 6.56 are almost identical and overlap, while that in the $[0_6/0_{2D}]_s$ laminate is smaller in magnitude by a factor of approximately two.

The interlaminar shear stress distribution in the undropped region of laminates

under bending load exhibits a different trend compared to those under in-plane load due to the differences in the far-field load distribution in the terminated ply group. In the in-plane load cases, the terminated ply groups in all four laminates considered carry the same amount of far-field load equal to $2\sigma_0 t$ because the in-plane stress distribution along the thickness is constant. Under bending load, the amount of far-field load carried by the terminated ply group is different in each laminate because the in-plane stress distribution under bending load varies linearly. As such, the terminated ply groups further away from the mid-plane of the laminate carry more in-plane load than those closer to the mid-plane. The far-field load carried by the terminated ply groups in each laminate is shown in Table 6.6. It can be seen that the far-field load in the $[0_{2D}/0_6]_s$ laminate is the greatest among the four laminates considered since the terminated ply group is located the furthest from the mid-plane. Therefore, the total load transferred along the lower interface in the undropped region of the $[0_{2D}/0_6]_s$ laminate is much greater than those of the $[0_2/0_{2D}/0_4]_s$ and $[0_4/0_{2D}/0_2]_s$ laminates not only because there is only one interface for the load transfer to take place, but also because more load needs to be transferred. Similarly, the far-field load in the terminated ply group in the $[0_2/0_{2D}/0_4]_s$ laminate is greater than that in the $[0_4/0_{2D}/0_2]_s$ laminate which explains the difference in magnitude of the interlaminar shear stresses along the lower interface in the two laminates.

The magnitudes of the interlaminar shear stresses in the dropped regions of laminates with internal ply dropoffs are generally greater than those in the undropped region. The peak interlaminar shear stresses along the interfaces of the inner and outer continuous plies in the dropped region of the $[0_4/0_{2D}/0_2]_s$ and $[0_6/0_{2D}]_s$ laminates are identical and equal to $0.62\sigma_s$, while those in the undropped region are less than $0.25\sigma_s$. The peak interlaminar shear stress along the same interface of the $[0_2/0_{2D}/0_4]_s$ laminate is smaller and equal to approximately $0.26\sigma_s$. These peak stresses occur approximately one half ply thickness away from the cutoff. The high magnitudes of the interlaminar shear stresses in the dropped region cause this to be a potential interface for delamination to

Table 6.6 Far-field loads (per unit width) carried in the terminated ply group in laminates with twelve continuous and four terminated plies under bending load

Laminate	Far-field Load*
$[0_{2D}/0_6]_s$	1.75
$[0_2/0_{2D}/0_4]_s$	1.26
$[0_4/0_{2D}/0_2]_s$	0.75
$[0_6/0_{2D}]_s$	0.25

* All values normalized by $\sigma_s t$.

occur. It is noted that both the interlaminar shear and normal stresses along the interface considered in the dropped region of the laminate with external ply dropoffs (z = 6t) is identically zero because this interface corresponds to the outer surface.

As in the cases of the in-plane load, it can be seen in the top plot of Figure 6.57 that the interlaminar normal stress along the lower interface in the undropped region of the laminate with external ply dropoffs is tensile while those with internal ply dropoffs are compressive. Along the upper interface in the undropped region shown in the bottom plot of Figure 6.57, the interlaminar normal stresses are also generally compressive, although in the $[0_4/0_{2D}/0_2]_s$ and $[0_6/0_{2D}]_s$ laminates, they become tensile approximately two ply thicknesses away from the cutoff. In the dropped region, the interlaminar normal stress in the $[0_6/0_{2D}]_s$ laminate is identically zero due to anti-symmetry. The interlaminar normal stresses in the $[0_2/0_{2D}/0_4]_s$ and $[0_4/0_{2D}/0_2]_s$ laminates exhibit similar trends, although the peak stress is higher in the former laminate compared to the latter with the peak stress of $0.45\sigma_s$ in the $[0_2/0_{2D}/0_4]_s$ laminate being approximately two times as high as that of $0.21\sigma_s$ in the $[0_4/0_{2D}/0_2]_s$ laminate.

6.2.3 Layup of the Terminated Ply Group

The key structural parameter affected by the layup of the terminated ply group is the stiffness. Therefore, to investigate the effects of the layup of the terminated ply group, a systematic method of varying the stiffness of the terminated ply group is useful. For this purpose, a novel method is devised in which "virtual" material properties of plies are used. In this method, plies with virtual material properties that are expressed as percentages of the in-plane longitudinal modulus, E_L, of the 0° ply are used in place of plies with actual material properties of angle plies or different materials. This method allows a more systematic investigation of the effects of elastic mismatch due to the layup of the terminated ply group and is more convenient compared to using actual material properties. The three independent moduli E_L, E_T, and G_{LT} in a transversely isotropic material are reduced by the same factor. Using this method, two specific parameters

related to the layup of the terminated ply group are considered. One is the stiffness of the terminated ply group and the other is the sequence of the layup in the terminated ply group. All laminates are assumed to have unit width.

The effect of the stiffness of the terminated ply group is considered first. In order to investigate the effect of the stiffness, a $[0_2/0_{2D}/0_4]_s$ laminate with a taper angle of 7° under in-plane and bending load is considered as the baseline. Laminates with terminated plies having 60%, 20% and 1% of the stiffness of the base plies are considered and compared to the baseline laminate. A diagram of the laminate configuration is shown in Figure 6.48. The interlaminar stresses along the upper and lower interfaces of the terminated ply group in the undropped region ($z = 6t$ and $z = 4t$) and along the interface of the inner and outer continuous plies in the dropped region ($z = 4t$) are shown in Figures 6.58 through 6.61. The interlaminar stresses in laminates under in-plane loads are normalized by the applied in-plane stress at the undropped end, σ_0, and those in laminates under bending load are normalized by the applied stress at the outer surface at the undropped end, σ_s, in the baseline laminate.

It can be seen in Figures 6.58 and 6.60 that the magnitude of interlaminar shear stresses in the undropped region is significantly affected by the decrease in stiffness of the terminated ply group. In both figures, it is seen that the magnitude of the interlaminar shear stresses in laminates under in-plane and bending loads decreases by a factor of approximately 1.5 when the stiffness of the terminated ply group is reduced by 40% (60% stiffness) and by a factor of approximately four when it is reduced by 80% (20% stiffness). The interlaminar shear stresses are negligible for the 1% stiffness case in both loading cases. The decreasing trend of interlaminar shear stresses with the stiffness of the terminated ply group is expected because the far-field load carried by the terminated ply group decreases with decreasing stiffness. The far-field loads in the terminated ply group of laminates under in-plane and bending load are shown Table 6.7. Note that these far-field loads are equal to the sum of the integrals of the interlaminar shear stresses

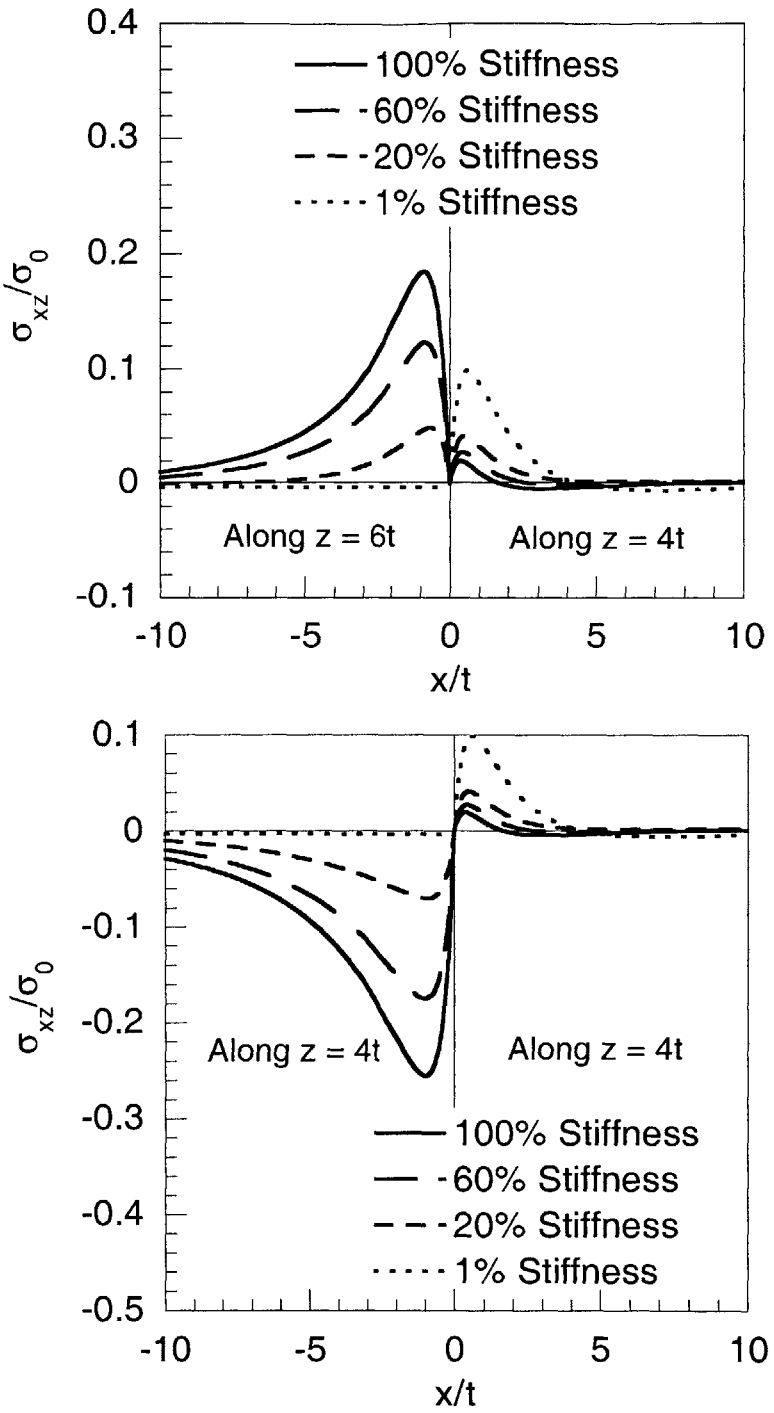

Figure 6.58 Interlaminar shear stresses along *(top)* upper interface in the undropped region (z = 6t) and the interface of the inner and outer continuous plies in the dropped region (z = 4t), and *(bottom)*, lower interface in the undropped region and the interface of the inner and outer continuous plies in the dropped region (z = 4t) in laminates with varied stiffness in the terminated ply group under in-plane load.

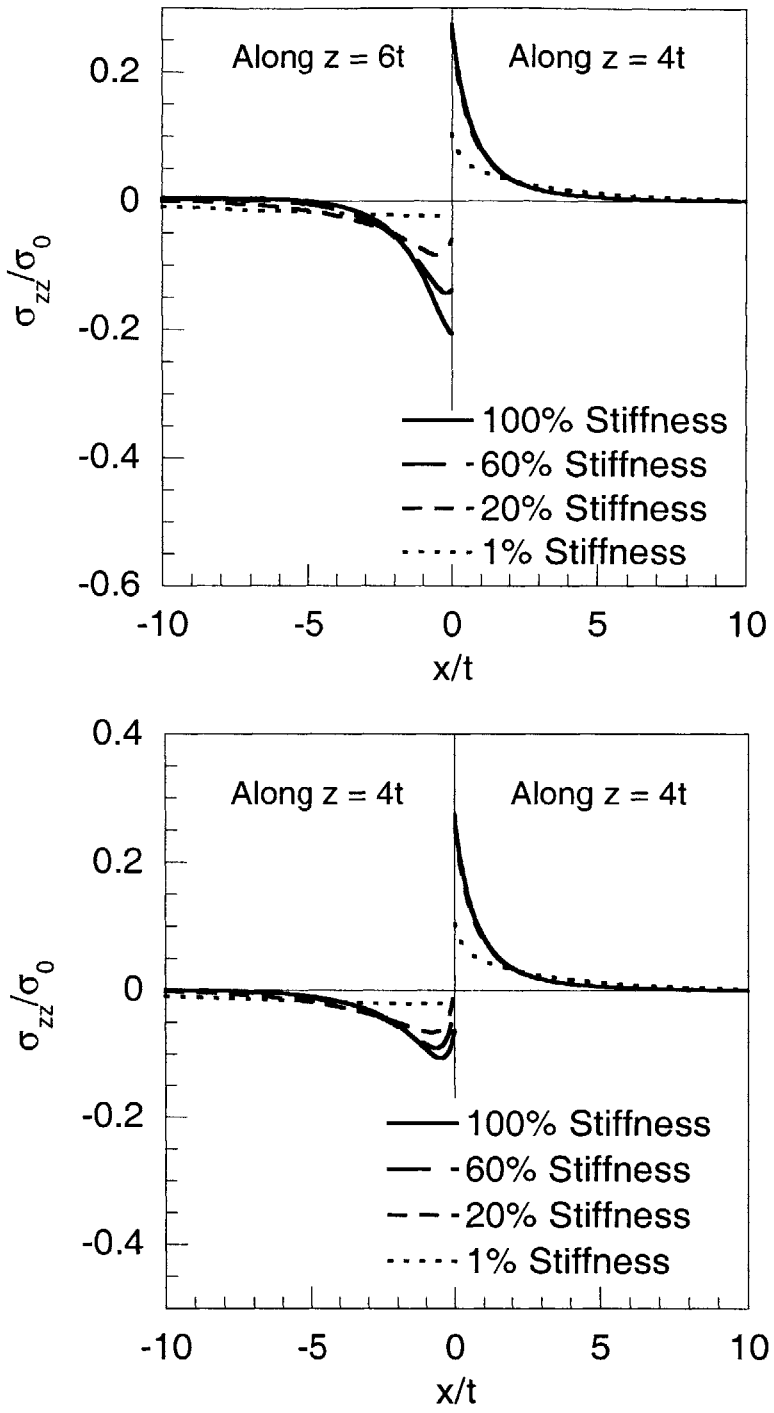

Figure 6.59 Interlaminar normal stresses along *(top)* upper interface in the undropped region (z = 6t) and the interface of the inner and outer continuous plies in the dropped region (z = 4t), and *(bottom)*, lower interface in the undropped region and the interface of the inner and outer continuous plies in the dropped region (z = 4t) in laminates with varied stiffness in the terminated ply group under in-plane load.

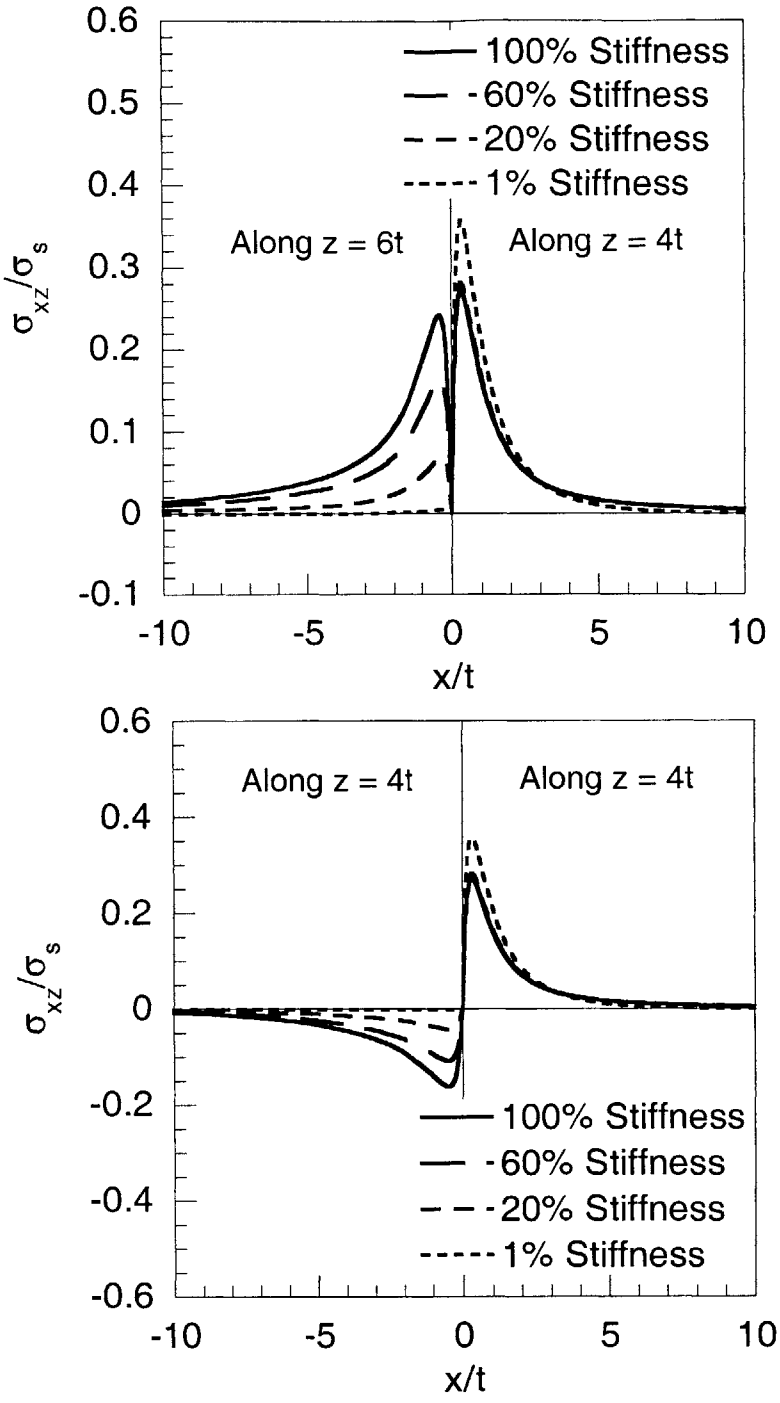

Figure 6.60 Interlaminar shear stresses along *(top)* upper interface in the undropped region (z = 6t) and the interface of the inner and outer continuous plies in the dropped region (z = 4t), and *(bottom)*, lower interface in the undropped region and the interface of the inner and outer continuous plies in the dropped region (z = 4t) in laminates with varied stiffness in the terminated ply group under bending load.

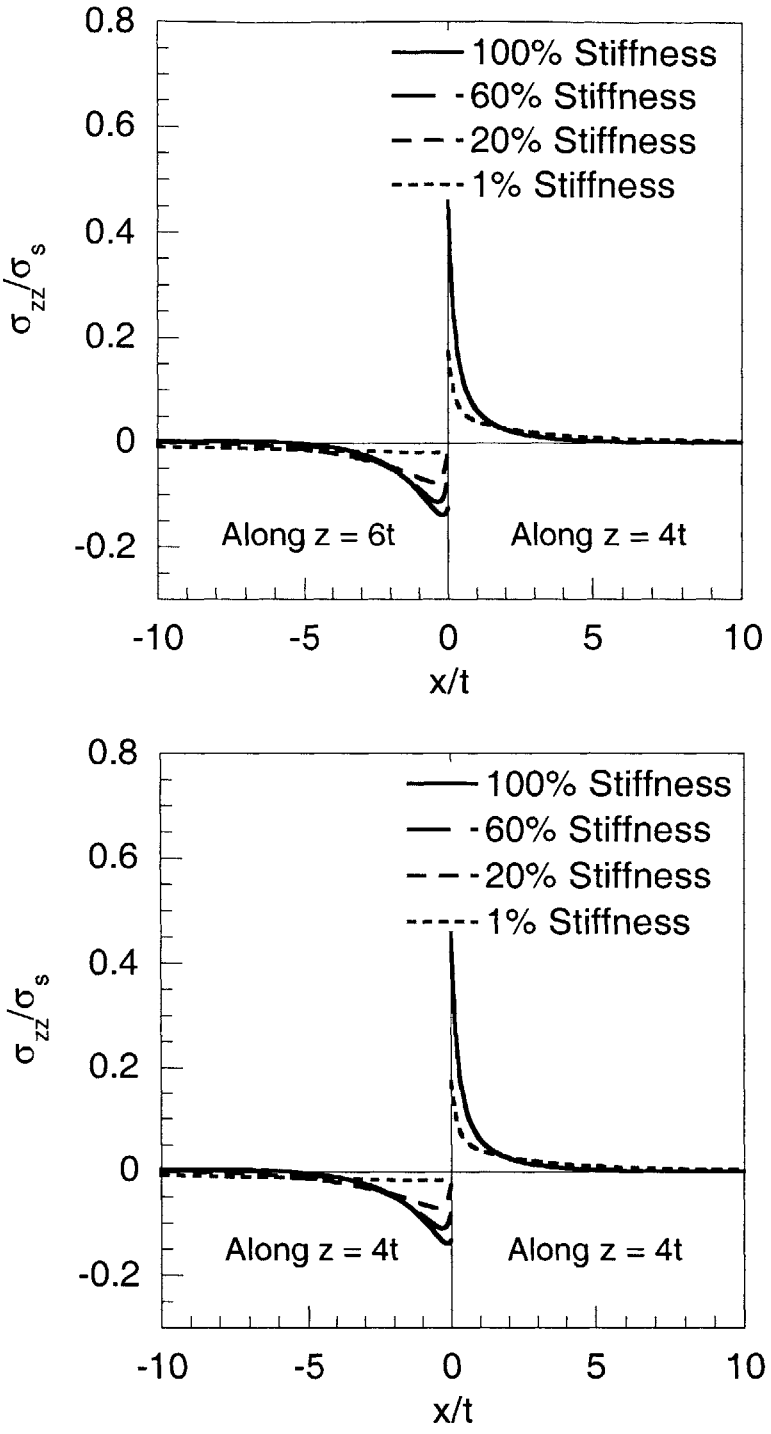

Figure 6.61 Interlaminar normal stresses along *(top)* upper interface in the undropped region (z = 6t) and the interface of the inner and outer continuous plies in the dropped region (z = 4t), and *(bottom)*, lower interface in the undropped region and the interface of the inner and outer continuous plies in the dropped region (z = 4t) in laminates with varied stiffness in the terminated ply group under bending load.

Table 6.7 Far-field loads (per unit width) carried in the terminated ply group in laminates with varied stiffness in the terminated ply group under in-plane and bending loads

Load Type	Stiffness of Terminated Ply Group			
	100%	60%	20%	1%
In-plane Load[1]	2.00	1.30	0.50	0.03
Bending Load[2]	1.26	0.85	0.33	0.02

[1] Normalized by $\sigma_s t$.

[2] Normalized by $\sigma_0 t$.

along the upper and lower interfaces of the terminated ply group in the undropped region. It can be seen that the far-field load decreases proportionally as the stiffness of the terminated ply group is decreased. The far-field load in the laminate with the 60% stiffness terminated ply group is reduced by a factor of approximately 1.5 compared to the 100% case, and by a factor of approximately four for the 20% case. The far-field load in the laminate with 1% stiffness terminated ply group is an order of magnitude smaller than those in the other laminates. It is interesting to note that this decrease in the far-field load carried in the terminated ply group varies by approximately the same factor as the magnitude of the interlaminar shear stresses.

The interlaminar shear stresses in the dropped region are also affected by the change in the stiffness as seen in Figures 6.58 and 6.60. However, the differences in magnitude of the interlaminar shear stresses in the laminates with 100%, 60% and 20% stiffnesses are small and less than approximately $0.02\sigma_0$ for the case of the in-plane load. For the case of the bending load, the differences are even smaller. In contrast to the interlaminar shear stresses in the undropped region, the magnitudes in the dropped region increase with decreasing stiffness in the terminated ply group. Under both in-plane and bending loads, the magnitudes of the interlaminar stress distribution in laminates with 1% stiffness in the terminated ply group are greater than those in other laminates (by a factor of approximately two for the case of the in-plane loads and 1.2 for the case of the bending loads).

The general trend of the interlaminar normal stresses in the undropped region is that the peak compressive values decrease with decreasing stiffness of the terminated ply group as shown in Figures 6.59 and 6.61. It is seen that the peak interlaminar normal stress decreases by a factor of approximately 1.5 when the stiffness of the terminated ply group is decreased by 40% (60% stiffness) and by a factor of approximately two when it is decreased by 80% (20% stiffness). Although the peak stress decreases with decreasing stiffness, it is seen in the two figures that the magnitude of the interlaminar normal stress

beyond approximately three ply thicknesses from the cutoff is greater in laminates with lower stiffnesses than those in laminates with higher stiffnesses. Therefore, the integral of the interlaminar normal stress, *i.e.*, the z-direction force, does not decrease significantly. The z-direction forces in the undropped region of laminates under in-plane and bending loads are shown in Table 6.8. As expected based on the characteristics of the interlaminar normal stresses, it can be seen that the z-direction force is reduced by only about 20% when the stiffness of the terminated ply group is reduced by 99% (1% stiffness). Note that based on equilibrium considerations, the z-direction forces along the upper and lower interfaces in the undropped region must be and are equal. This equality is described further in Section 6.4.

In the dropped region, it can be seen in Figures 6.59 and 6.61 that the interlaminar normal stress distributions in the laminates considered are almost identical and overlap except in the laminate with 1% stiffness where the peak interlaminar normal stress is lower than those in the laminates with higher stiffnesses by a factor of approximately three. Since the interlaminar normal stress in this region is tensile, this reduction in the peak stress may significantly increase the delamination initiation load. Despite the peak interlaminar normal stress being significantly lower, the difference in z-direction force in the dropped region of the laminate with 1% stiffness compared to the other laminates is not as significant because the magnitude of the interlaminar normal stress in the 1% stiffness case is greater than those in the other laminates beyond approximately two ply thicknesses away from the cutoff. Note that the z-direction force in the dropped region must be and is equal to that in the undropped region due to z-direction equilibrium. This is shown in Section 6.4.

The decreasing trend of the peak interlaminar normal stress in the dropped region along the interface of the inner and outer continuous plies ($z = 4t$) with respect to the stiffness of the terminated ply group is investigated further by considering three additional laminates with stiffness of the terminated ply group between 20% and 1%.

Table 6.8 Integrated force (per unit width) in the z-direction along the upper (or lower) interface of the terminated ply group in the undropped region in laminates with varied stiffness in the terminated ply group under in-plane and bending load

Load Type	Stiffness of Terminated Ply Group			
	100%	60%	20%	1%
In-plane Load[1]	0.26	0.26	0.25	0.20
Bending Load[2]	0.22	0.22	0.22	0.18

[1] Normalized by $\sigma_0 t$.

[2] Normalized by $\sigma_s t$.

The stiffnesses considered are 5.0%, 2.5% and 1.3%. The peak interlaminar normal stresses in the dropped region in each case for the laminates under in-plane and bending loads are shown in Table 6.9 along with the integrated z-direction force. It can be seen that a decrease of approximately 20% in the peak stress occurs when the stiffness of the terminated ply group is lowered from 20% to 5% in laminates under in-plane and bending loads. Note, again, that the z-direction force remains relatively unchanged with stiffness. Based on these results, it can be concluded that the stiffness of the terminated ply has to be lower than 5% of the continuous plies in order to obtain any significant decrease in the peak stress, and thereby increase the delamination load.

If the stiffness of the terminated ply group is greater than the stiffness of the continuous plies, opposite trends should occur. Three $[0_2/0_{2D}/0_4]_s$ laminates with stiffnesses of 100%, 140% and 180% in the terminated ply group under in-plane load were considered to verify this intuition. Only the interlaminar stresses along the upper interface of the terminated ply group in the undropped region ($z = 6t$) and the interface of the inner and outer continuous plies in the dropped region ($z = 4t$) are considered for this purpose. These results are shown in Figure 6.62. It can be seen in the top plot of the figure that the interlaminar shear stress in the undropped region increases in magnitude due to the increasing load carried by the terminated ply group. The magnitude of the interlaminar shear stress increases by a factor of approximately 1.3 when the stiffness is increased by 40% (140% stiffness) and by a factor of approximately 1.5 when it is increased by 80% (180% stiffness). In the dropped region, the differences among the magnitudes of the interlaminar shear stresses in the three laminates considered are very small and less than 1% of the applied in-plane stress, σ_0. The stiffness in the terminated ply group does not significantly affect the interlaminar normal stress distribution in both the undropped and dropped regions except the peak compressive stress in the undropped region which increases as the stiffness is increased. The peak stress in the undropped region increases by a factor of approximately 1.5 when the stiffness is increased by 80%

Table 6.9 Peak interlaminar normal stress and integrated z-direction force (per unit width) in laminates with varied stiffness in the terminated ply group under in-plane and bending load

Load Type	Result	Stiffness of Terminated Ply Group				
		20%	5.0%	2.5%	1.3%	1%
In-plane	Peak Stress[1]	0.26	0.21	0.18	0.12	0.10
	Z-direction Force[2]	0.25	0.24	0.22	0.21	0.20
Bending	Peak Stress[3]	0.44	0.36	0.29	0.21	0.17
	Z-direction Force[4]	0.22	0.21	0.20	0.18	0.18

[1] Normalized by σ_0.

[2] Normalized by $\sigma_0 t$.

[3] Normalized by σ_s.

[4] Normalized by $\sigma_s t$.

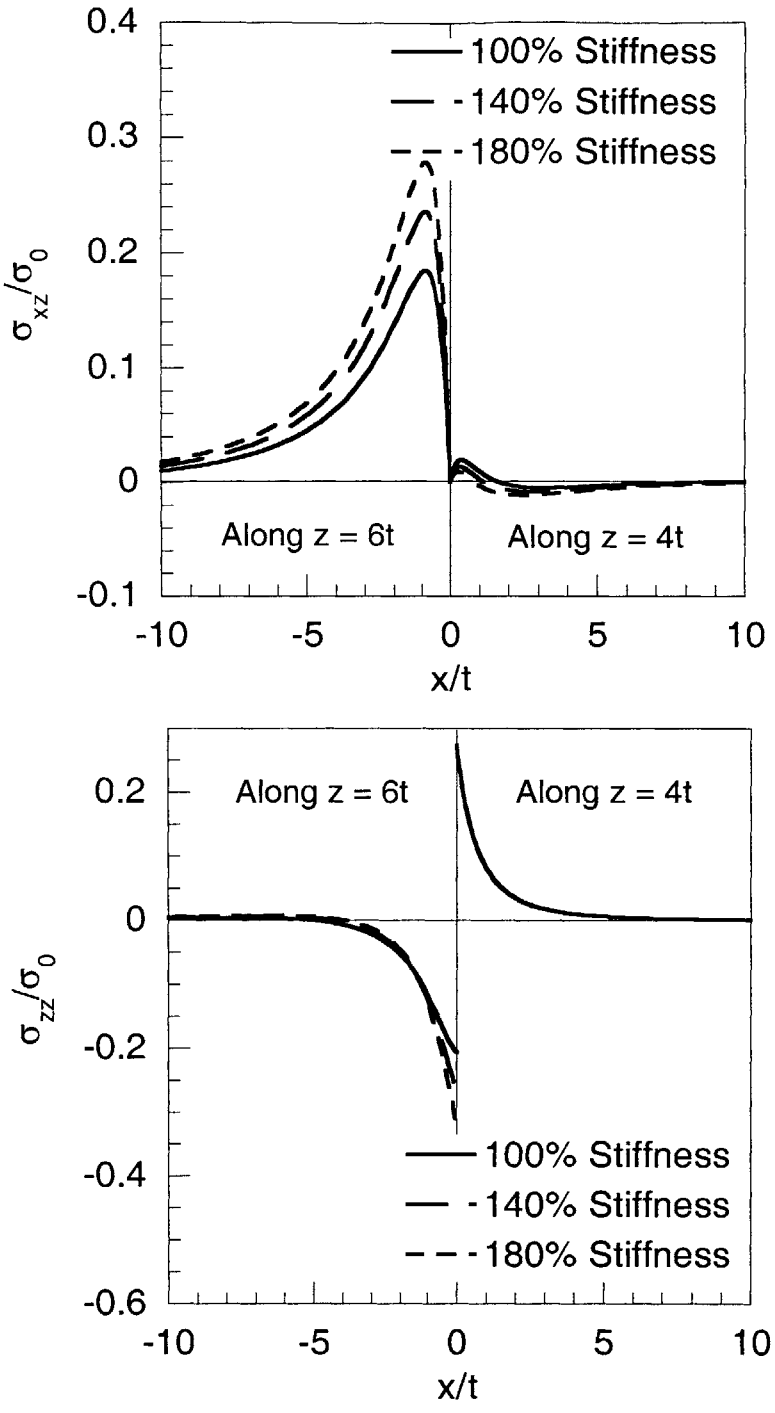

Figure 6.62 Interlaminar shear and normal stresses along the upper interface in the undropped region (z = 6t) and the interface of the inner and outer continuous plies in the dropped region (z = 4t) in laminates with varied stiffness in the terminated ply group under in-plane load.

(180% stiffness).

The effect of changing the layup sequence of the terminated ply group is considered next. For this purpose, two laminates with identical in-plane stiffness and taper angle of 7° but different layups in the terminated ply group are considered. The layup of the first laminate is $[0_2/(0/X_2/0)_D/0_3]_s$ where X denotes plies where the stiffness is reduced to 20% of the stiffness of the 0° plies and the ply group in parentheses is terminated. The layup of the second laminate is $[0_2/(X/0_2/X)_D/0_3]_s$. For convenience, the laminates are referred to as type A and B, respectively. Diagrams of the two laminates are shown in Figure 6.63. Again, these laminates are considered to be of unit width. The interlaminar stresses in the upper-half of the laminates along the upper and lower interfaces of the terminated ply group in the undropped region ($z = 7t$ and $z = 3t$) and the interface of the inner and outer continuous plies in the dropped region ($z = 3t$) are shown in Figures 6.64 through 6.69. As in previous examples, the interlaminar stresses in laminates under in-plane loads are normalized by the applied in-plane stress at the undropped end, σ_0, and those under bending load are normalized by the applied stress at the outer surface at the undropped end, σ_s, of the laminate type A.

It can be seen in Figure 6.64 that the magnitude of the interlaminar shear stress in the undropped region in the $[0_2/(0/X_2/0)_D/0_3]_s$ laminate under in-plane load is greater than that in the $[0_2/(X/0_2/X)_D/0_3]_s$ laminate along the length within approximately five ply thicknesses from the cutoff, but is smaller in the region beyond this point. This trend is seen along both the upper and lower interfaces in the undropped region. Along the upper interface shown in the top plot of Figure 6.64, the peak stress in laminate type A is $0.18\sigma_0$, while that in laminate type B is $0.09\sigma_0$, and along the lower interface shown in the bottom plot of Figure 6.64, the peak stress in laminate type A is $0.25\sigma_0$, while that in laminate type B is $0.14\sigma_0$. Thus, the peak interlaminar shear stresses in laminate type A are greater than those in laminate type B by a factor of approximately 2.

The significant reduction in the peak interlaminar shear stress in the undropped

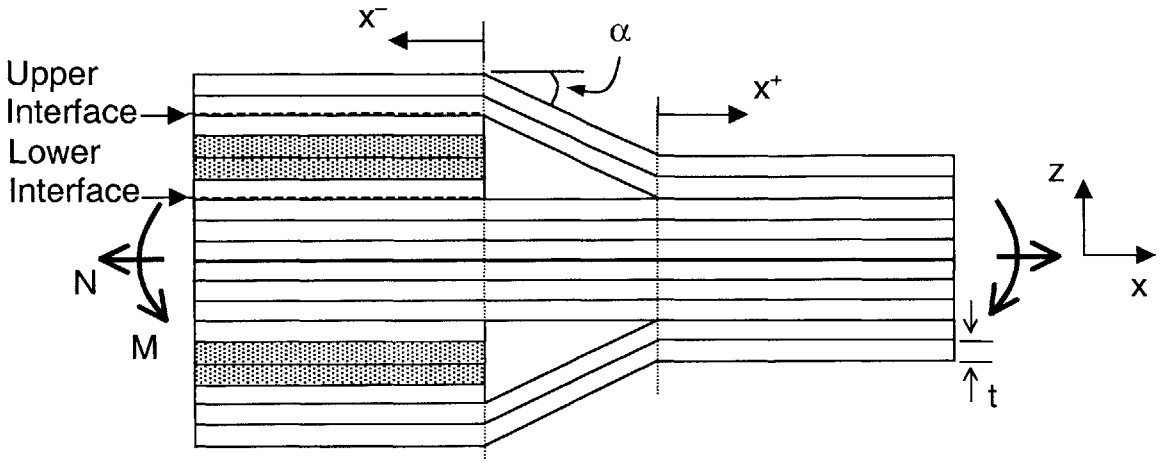

$[0_2/(0/X_2/0)_D/0_3]_s$ Laminate

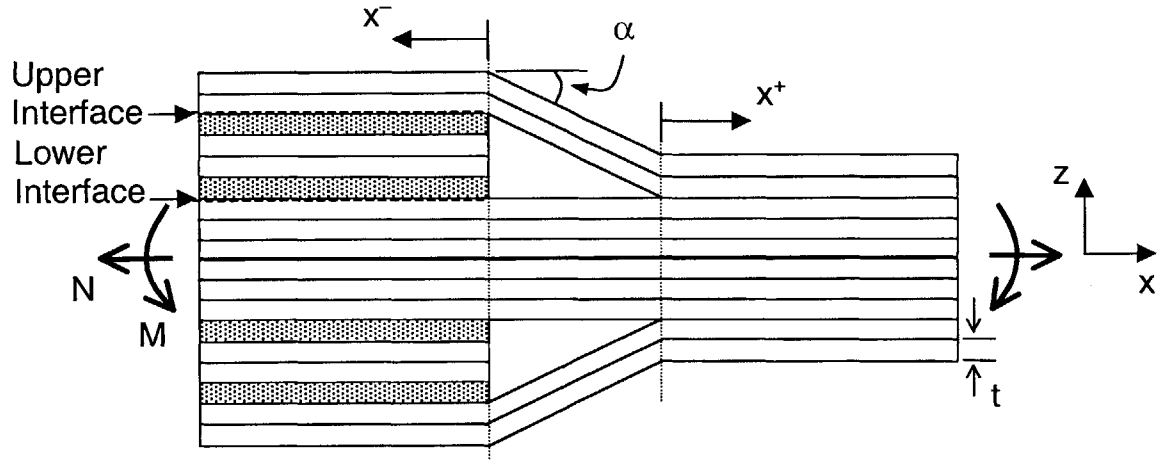

$[0_2/(X/0_2/X)_D/0_3]_s$ Laminate

Figure 6.63 Diagrams of *(top)* a laminate with a layup of $[0_2/(0/X_2/0)_D/0_3]_s$, and *(bottom)*, a laminate with a layup of $[0_2/(X/0_2/X)_D/0_3]_s$ (shaded plies denote 20% stiffness plies) with indications of "upper" and "lower" interfaces as referenced in Figures 6.64 through 6.69.

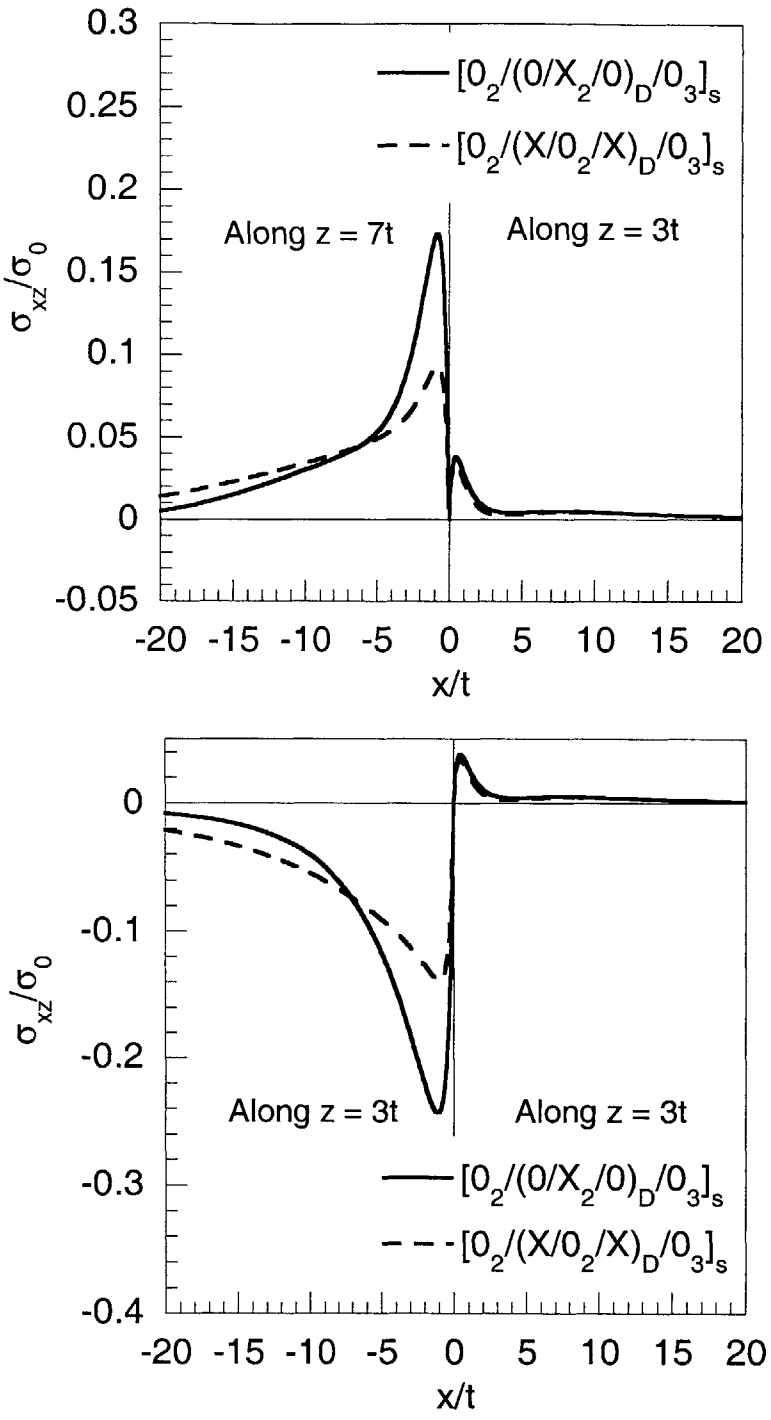

Figure 6.64 Interlaminar shear stresses along *(top)* the upper interface in the undropped region (z = 7t) and the interface of the inner and outer continuous plies in the dropped region (z = 3t), and *(bottom)*, the lower interface in the undropped region and the interface of the inner and outer continuous in the dropped region (z = 3t) in $[0_2/(0/X_2/0)_D/0_3]_s$ and $[0_2/(X/0_2/X)_D/0_3]_s$ laminates under in-plane load (note: X refers to 20% stiffness ply).

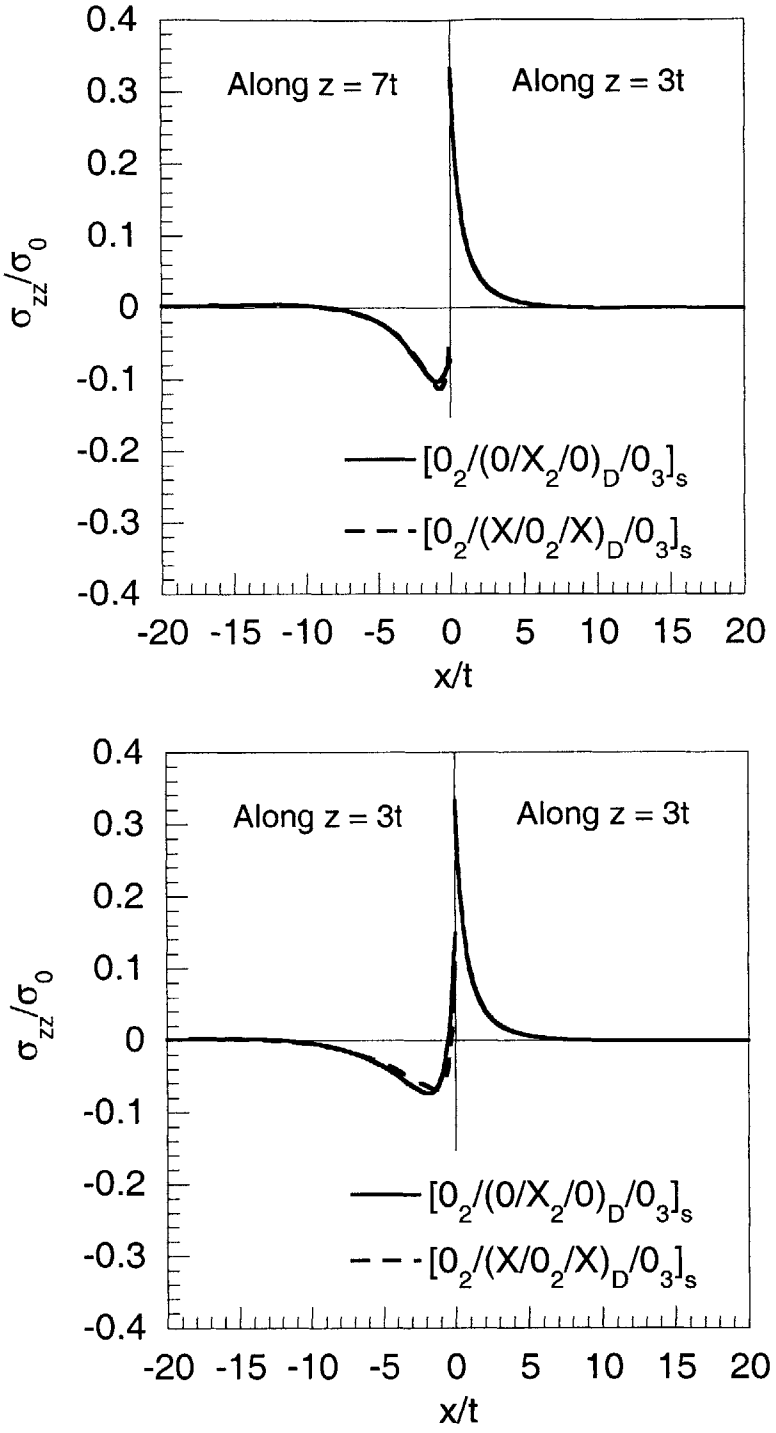

Figure 6.65 Interlaminar normal stresses along *(top)* the upper interface in the undropped region (z = 7t) and the interface of the inner and outer continuous in the dropped region (z = 3t), and *(bottom)*, the lower interface in the undropped region and the interface of the inner and outer continuous plies in the dropped region (z = 3t) in $[0_2/(0/X_2/0)_D/0_3]_s$ and $[0_2/(X/0_2/X)_D/0_3]_s$ laminates under in-plane load (note: X refers to 20% stiffness ply).

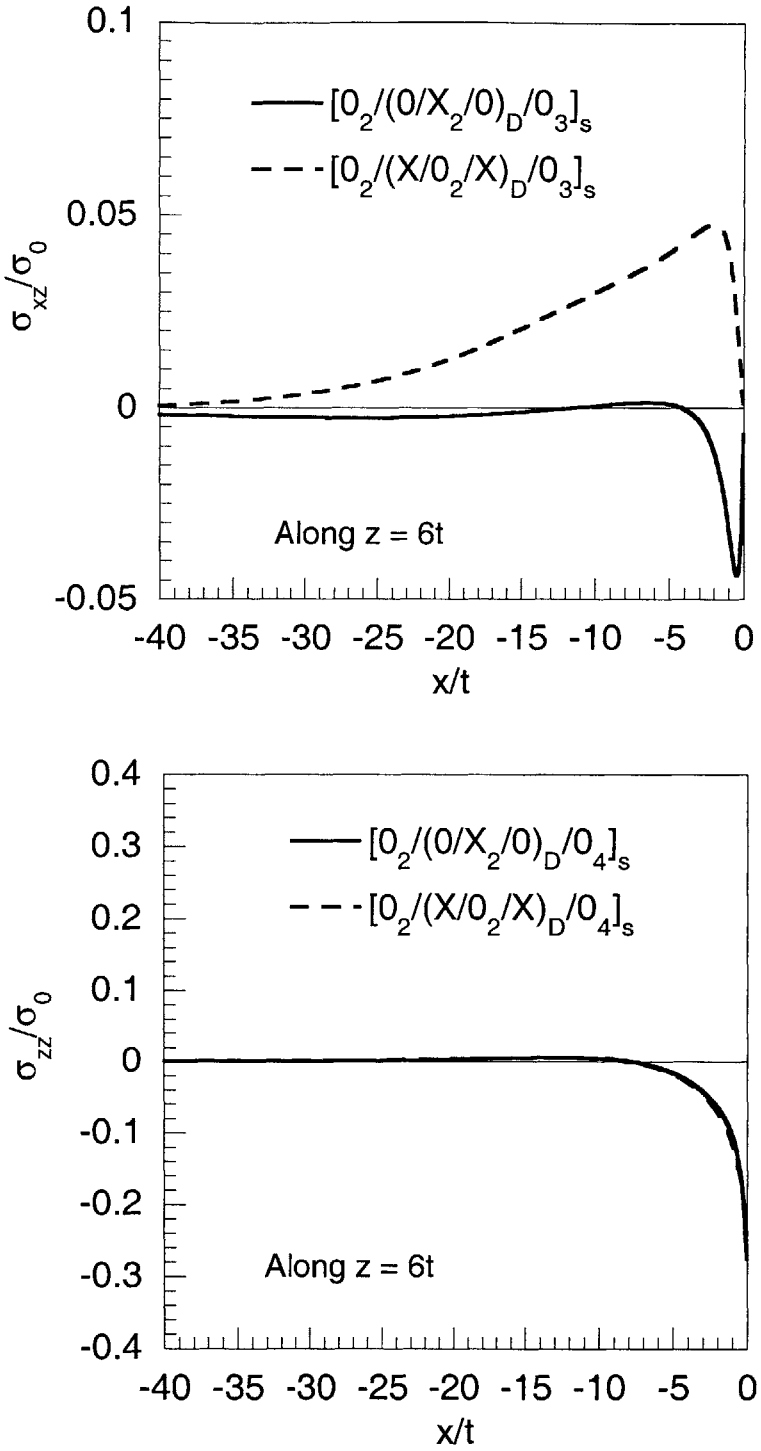

Figure 6.66 Interlaminar shear and normal stresses along the interface between 0° and 20% stiffness plies in the undropped region (z = 6t) of $[0_2/(0/X_2/0)_D/0_3]_s$ and $[0_2/(X/0_2/X)_D/0_3]_s$ laminates under in-plane load (note: X refers to 20% stiffness ply).

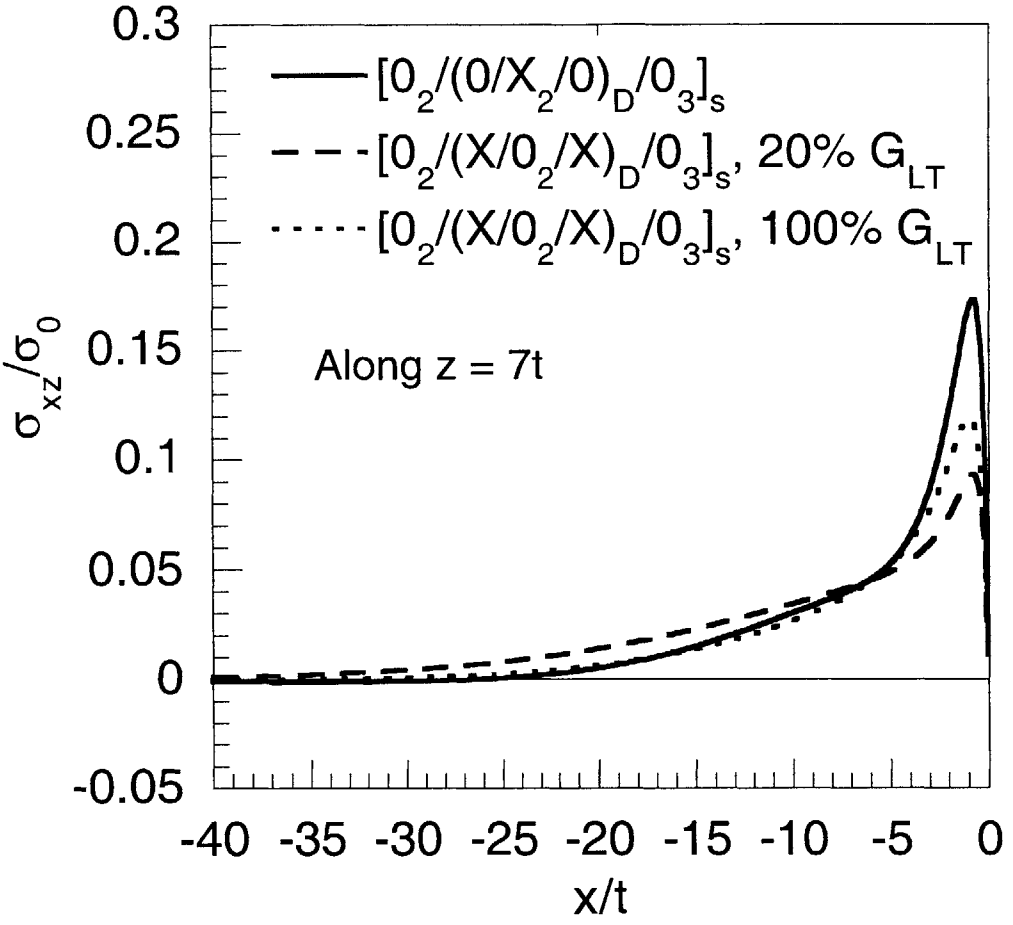

Figure 6.67 Interlaminar shear stress along the upper interface of the terminated ply group in the undropped region in $[0_2/(0/X_2/0)_D/0_3]_s$ and $[0_2/(X/0_2/X)_D/0_3]_s$ laminates with 20% G_{LT} and 100% G_{LT} under in-plane load (note: X refers to 20% stiffness ply).

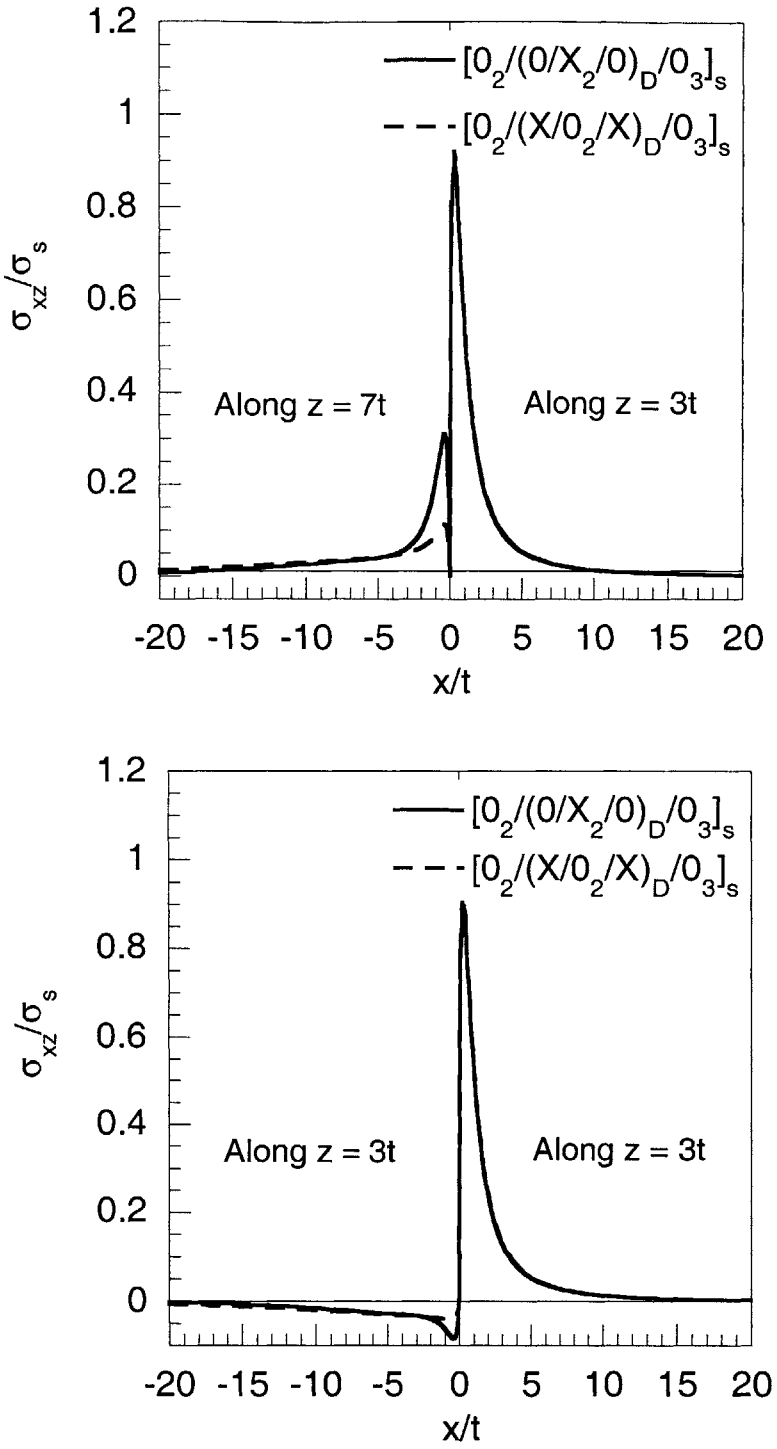

Figure 6.68 Interlaminar shear stresses along *(top)* the upper interface in the undropped region (z = 7t) and the interface of the inner and outer continuous plies in the dropped region (z = 3t), and *(bottom)*, the lower interface in the undropped region and the interface of the inner and outer continuous in the dropped region (z = 3t) in $[0_2/(0/X_2/0)_D/0_3]_s$ and $[0_2/(X/0_2/X)_D/0_3]_s$ laminates under bending load (note: X refers to 20% stiffness ply).

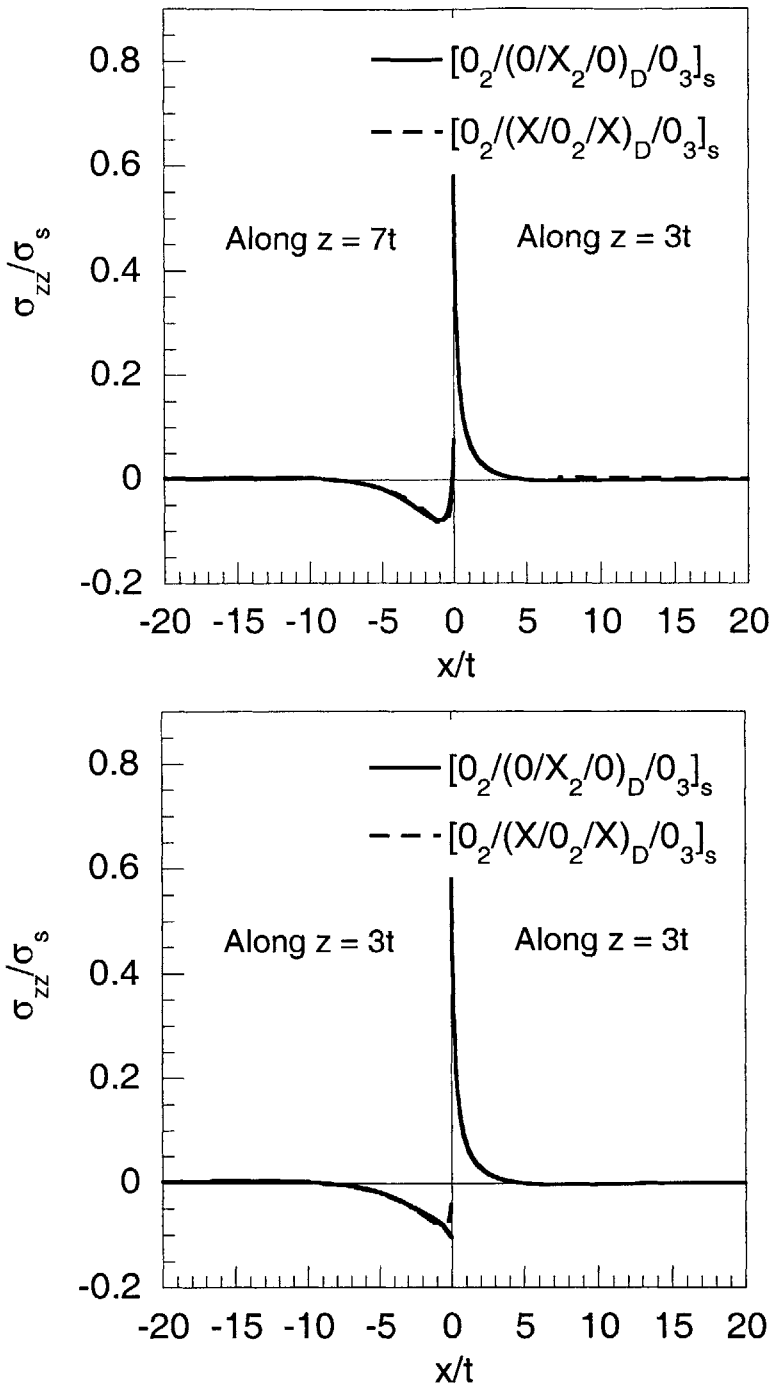

Figure 6.69 Interlaminar normal stresses along *(top)* the upper interface in the undropped region (z = 7t) and the interface of the inner and outer continuous in the dropped region (z = 3t), and *(bottom)*, the lower interface in the undropped region and the interface of the inner and outer continuous in the dropped region (z = 3t) in $[0_2/(0/X_2/0)_D/0_3]_s$ and $[0_2/(X/0_2/X)_D/0_3]_s$ laminates under bending load (note: X refers to 20% stiffness ply).

region achieved by altering the sequence of the layup in the terminated ply group should have a positive effect on the delamination characteristics. Specifically, the delamination initiation load under static loads should increase. Note, however, the integral of the interlaminar shear stress does not change significantly in the two cases. The load per unit width transferred along the upper interface is $1.02\sigma_0 t$ in laminate type A and $1.04\sigma_0$ in laminate type B, while that along the lower interface is $1.90\sigma_0 t$ in laminate type A and $1.88\sigma_0 t$ in laminate type B. The sum of the load transferred along the upper and lower interfaces is $2.92\sigma_0 t$ in both cases, which is equal to the far-field load in the terminated ply group. The magnitude of the interlaminar shear stress in the dropped region is smaller by an order of magnitude than that in the undropped region and nearly identical for the two laminates.

In contrast to the significant differences in the interlaminar shear stress distributions in the undropped region, the interlaminar normal stresses in both the undropped and dropped regions are virtually unaffected by the change in layup sequence of the terminated ply group. This can be seen in Figure 6.65. The interlaminar normal stress distributions along the interfaces in the undropped and dropped regions in the two laminates are almost identical and overlap.

There are two possible effects that contribute to reduce the peak interlaminar shear stresses in laminate type B. One is the load carried by the terminated plies immediately adjacent to the continuous plies. In both laminates, 0° terminated plies carry 83% of the load in the terminated ply group far away from the cutoff due to their higher stiffness compared to the 20% stiffness plies. However, in laminate type A, the terminated plies immediately adjacent to the continuous plies are 0° plies, whereas in laminate type B, those adjacent to the continuous plies are 20% stiffness plies. Thus, in laminate type A, the far-field load in the terminated ply group, which is mostly carried by the 0° plies, is directly transferred to the neighboring continuous plies along the two interfaces of the continuous and terminated plies ($z = 7t$ and $z = 3t$). In laminate type B,

the far-field load carried by the 0° plies is "shielded" from the continuous plies by the 20% stiffness plies. Therefore, load transfer from the 0° terminated plies needs to occur in two steps. First, the far-field load carried by the 0° plies in the terminated ply group is transferred via interlaminar shear stresses to the 20% stiffness plies. Next, the load carried by the 20% stiffness plies is transferred via interlaminar shear stresses to the continuous plies along the interfaces of the continuous and terminated plies (z = 7t and z = 3t). The interlaminar shear stresses along the interface in the undropped region of the 0° and 20% plies in the terminated ply group of laminates under in-plane load are shown in Figure 6.66. It can be seen that the interlaminar shear stress along this interface (z = 6t) in the $[0_2/(X/0_2/X)_D/0_3]_s$ laminate is positive and comparable in magnitude to that along the upper interface of the terminated ply group (z = 7t), while in the $[0_2/(0/X_2/0)_D/0_3]_s$ laminate, the interlaminar shear stress is very small and negative except near the cutoff. This illustrates the two-step load transfer process in the $[0_2/(X/0_2/X)_D/0_3]_s$ laminate. The interlaminar normal stresses in both laminates, which are also plotted in Figure 6.66, are almost identical, indicating once again that this component is not affected by the change in the layup sequence.

The other effect that may contribute to reduce the peak interlaminar shear stress is related to the in-plane shear modulus, G_{LT}, of the 20% stiffness plies in the terminated ply group. In the $[0_2/(X/0_2/X)_D/0_3]_s$ laminate, the 20% stiffness plies effectively act as a shear layer that transfers in-plane load from the 0° plies in the terminated ply group to the continuous plies. Therefore, the value of G_{LT} in these plies should affect the interlaminar shear distribution. In the current example, all moduli, including G_{LT}, were reduced by 20% in the 20% stiffness ply in accordance with the definition of the virtual material properties. From shear-lag analysis, it is known that the decay rate of the interlaminar shear stress is proportional to the shear modulus, G_{LT}. This implies that if G_{LT} remains unchanged, then the decay rate of the interlaminar shear stress will be higher, and thus, the peak interlaminar shear stress will also be greater than the case when G_{LT} is reduced

since the integral of the interlaminar shear stresses must remain constant and equal to the far-field load. A plot of the interlaminar shear stresses in the undropped region along the upper interface of the terminated ply group (z = 7t) in the three laminates are shown in Figure 6.67 to illustrate this point. The first two laminates are the same $[0_2/(0/X_2/0)_D/0_3]_s$ and $[0_2/(X/0_2/X)_D/0_3]_s$ laminates that were considered previously. The third laminate is one with a layup of $[0_2/(X/0_2/X)_D/0_3]_s$ laminates with only the longitudinal modulus, E_L, reduced by 20%. The shear modulus is left unchanged. The difference in the $[0_2/(X/0_2/X)_D/0_3]_s$ laminate with 20% G_{LT} and 100% G_{LT} is evident in Figure 6.67. It can be seen that the decay rate of the interlaminar shear stress in the laminate with 100% G_{LT} is higher than that in the laminate with 20% G_{LT}, which is expected based on the relationship between the decay rate and G_{LT}. In addition, the peak interlaminar shear stress in the laminate with 100% G_{LT} is $0.12\sigma_0$, which is 25% higher than that in the laminate with 20% G_{LT}. The peak interlaminar shear stress in the $[0_2/(X/0_2/X)_D/0_3]_s$ laminate with 100% G_{LT} is still smaller than that in the $[0_2/(0/X_2/0)_D/0_3]_s$ laminate by a factor of approximately 1.5. This difference can be attributed to the first effect described in the previous paragraph. Meanwhile, the decay rate in the $[0_2/(X/0_2/X)_D/0_3]_s$ laminate with 100% G_{LT} is comparable to that in the $[0_2/(0/X_2/0)_D/0_3]_s$ laminate, which is expected since the values of G_{LT} are the same in both cases.

Similar trends in the interlaminar stress distribution occur in the laminates under bending load. It can be seen in the top plot of Figure 6.68 that the peak interlaminar shear stress in the undropped region in laminate type A is greater than that in laminate type B by a factor of approximately three. The magnitude of the interlaminar shear stress in this region is greater in laminate type A than in laminate type B up to approximately four ply thicknesses away from the cutoff and smaller beyond this location. However, in laminates under bending load, the interlaminar shear stress along the dropped region is much higher in magnitude (by a factor of approximately three) than that in the undropped region. Therefore, the decrease in the peak stress in the undropped region may not have a

significant effect in the delamination behavior of the laminates since the dropped region is a more serious concern. Again, as can be seen in Figure 6.69, the interlaminar normal stresses are not affected by the change in layup of the terminated ply group and are almost identical in the two laminates.

6.2.4 Number of Terminated Plies

Three laminates with the same number of total plies but different numbers of terminated plies are considered to investigate the effects of the number of terminated plies on the interlaminar stress field. The layups of the laminates considered are $[0_5/0_D/0_2]_s$, $[0_4/0_{2D}/0_2]_s$ and $[0_3/0_{3D}/0_2]_s$ with a taper angle of 7°. Diagrams of these laminates are shown in Figures 6.70. For these laminates, the interlaminar stresses along only the lower interface of the terminated ply group in the undropped region ($z = 2t$) and the interface of the inner and outer continuous plies in the dropped region ($z = 2t$) are shown in Figures 6.71 and 6.72. The interlaminar stresses along the upper interface of the terminated ply group in the undropped region exhibit trends similar to those along the lower interface of the terminated ply group, and thus, add no further insights and are not considered. The interlaminar stresses in laminates under in-plane loads are normalized by the applied in-plane stress in the undropped region, σ_0, and those in laminates under bending loads by the applied bending stress at the outer surface in the undropped region, σ_s, of the $[0_3/0_{3D}/0_2]_s$ laminate.

For laminates under in-plane loads, it can be seen in the top plot of Figure 6.71 that the magnitude of the interlaminar shear stress in the undropped region increases as the number of terminated plies increases. The peak interlaminar shear stress increases by approximately $0.06\sigma_0$ as the number of terminated ply increases by one. This increasing trend is expected because the far-field load carried by the terminated ply group increases proportionally to the number of terminated plies, and thus, the load transferred via interlaminar shear stresses along the interface of the continuous and terminated plies must increase similarly. In the dropped region, the interlaminar shear stresses do not exhibit

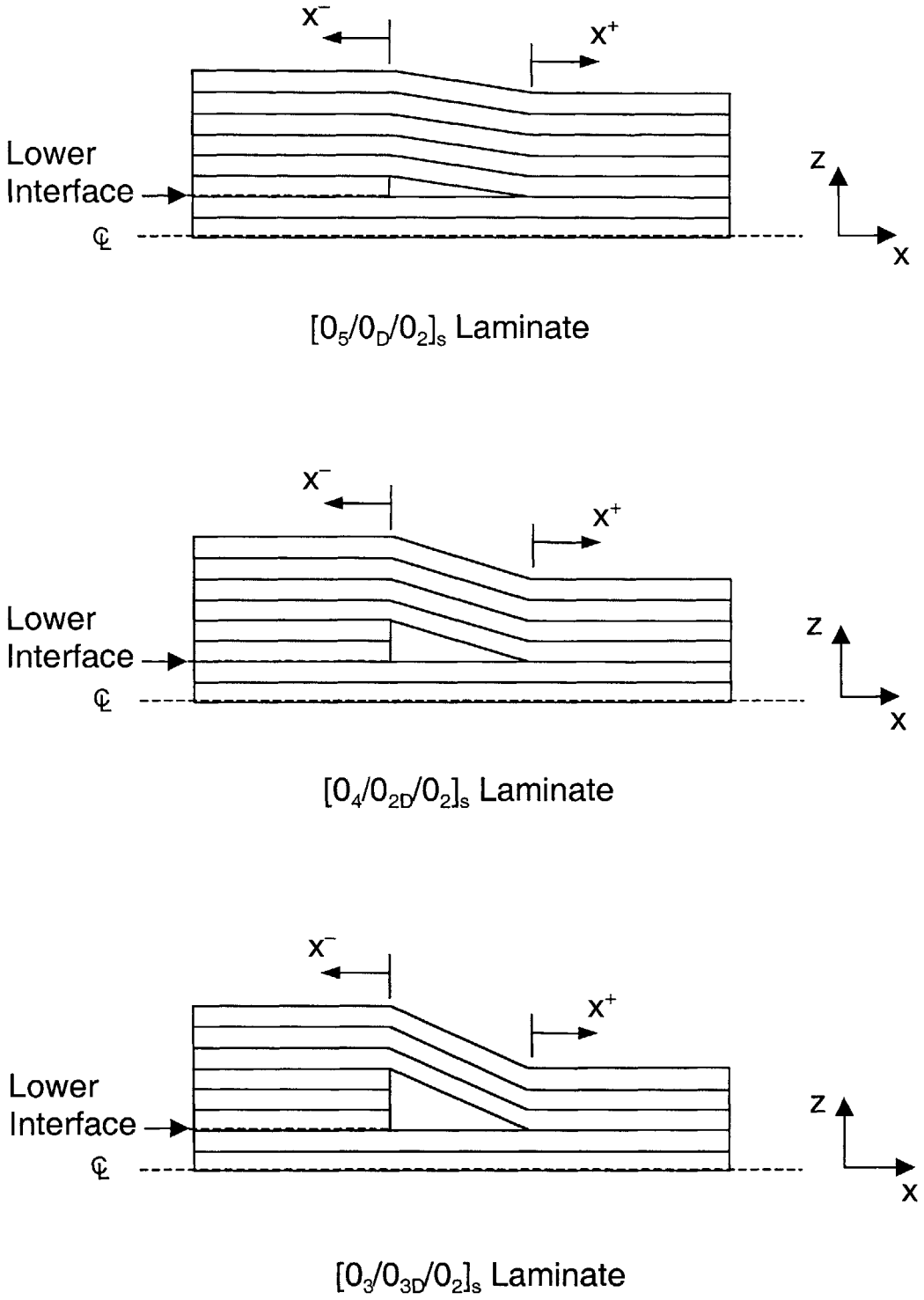

Figure 6.70 Diagrams of the upper-half of laminates with layups of $[0_5/0_D/0_2]_s$, $[0_4/0_{2D}/0_2]_s$, and $[0_3/0_{3D}/0_2]_s$ (from top to bottom) with indication of "lower" interface as reference in Figures 6.71 through 6.74.

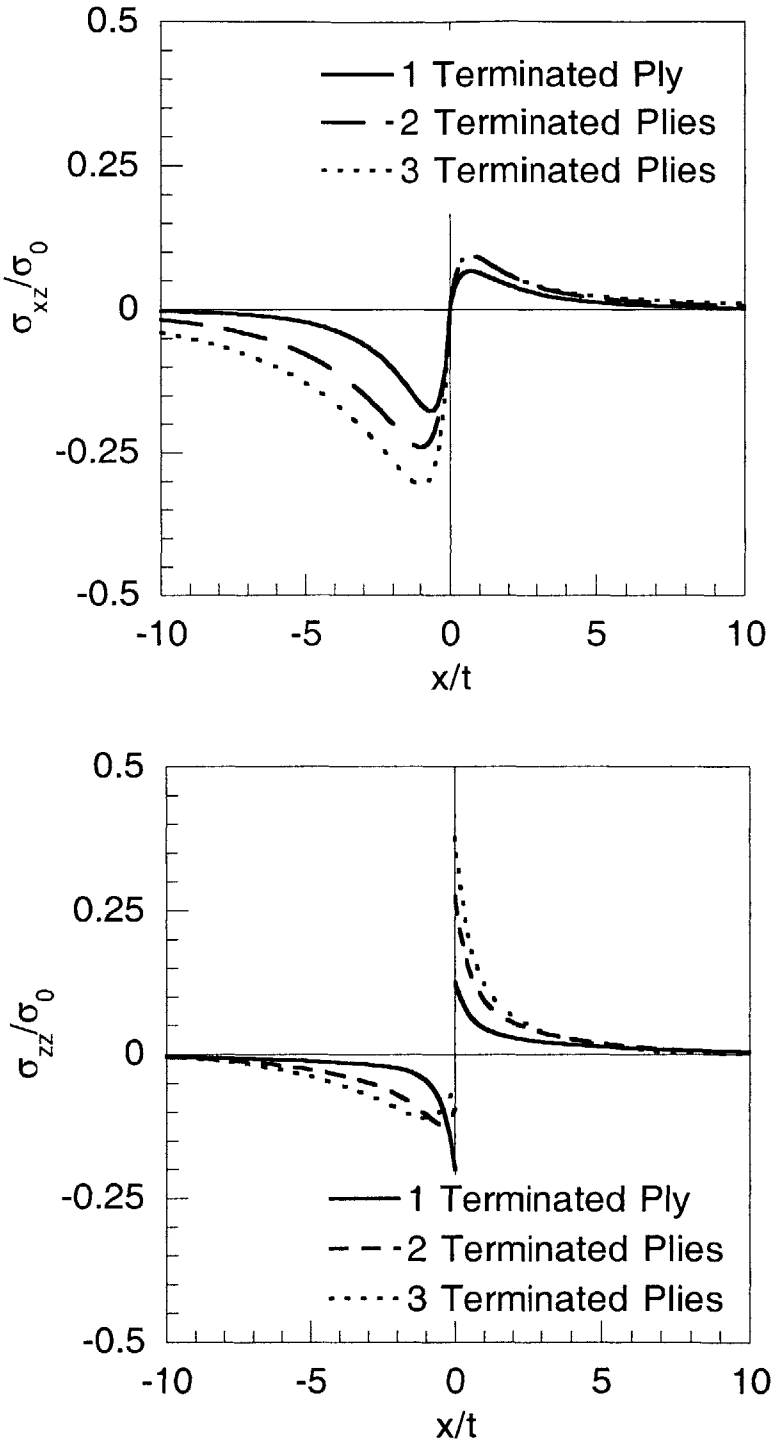

Figure 6.71 Interlaminar shear and normal stresses along lower interface in the undropped region and the interface of the inner and outer continuous plies in the dropped region (z = 2t) in 8-ply laminates with one, two and three terminated plies under in-plane load.

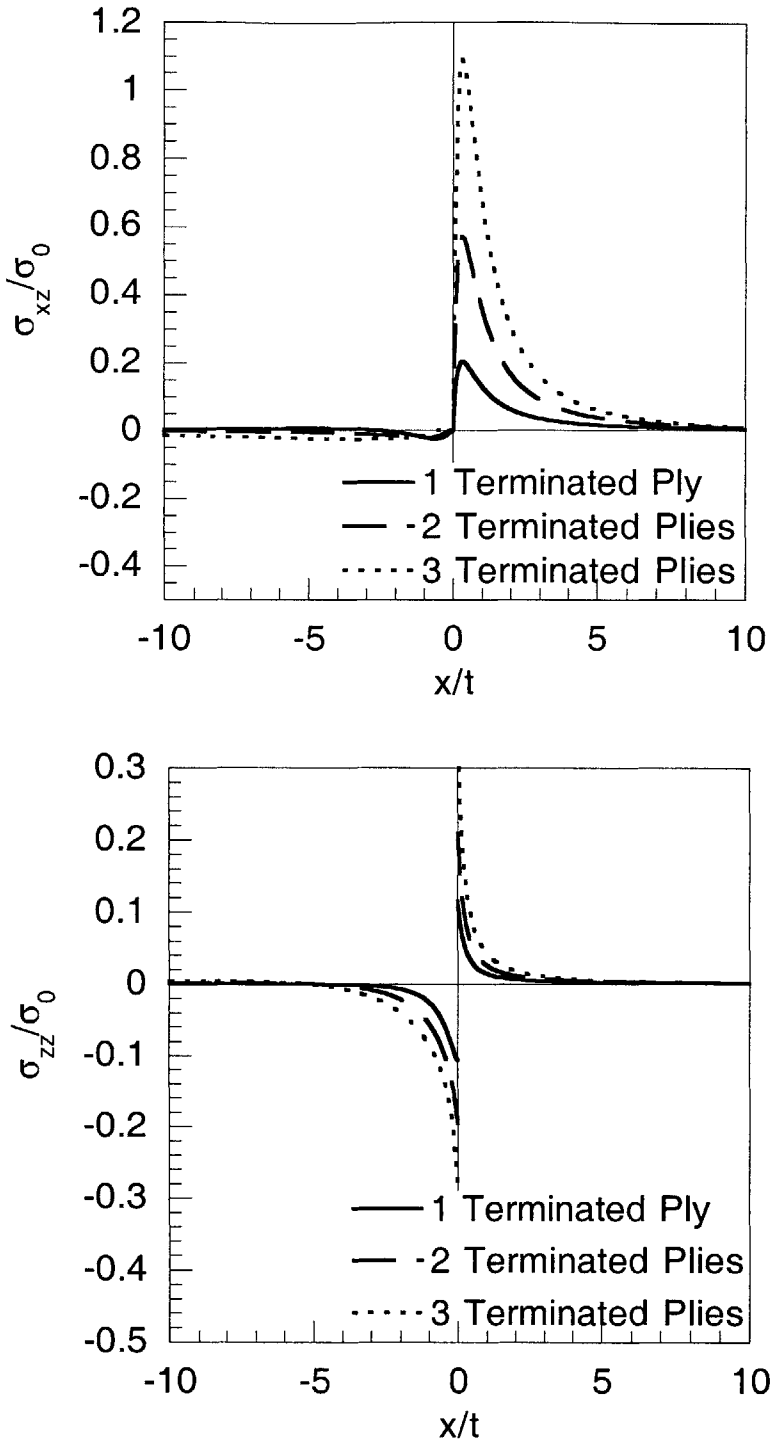

Figure 6.72 Interlaminar shear and normal stresses along lower interface in the undropped region and the interface of the inner and outer continuous plies in the dropped region (z = 2t) in 8-ply laminates with one, two and three terminated plies under bending load.

significant changes due to the change in the number of terminated plies. The interlaminar normal stresses generally increase in magnitude as the number of terminated plies is increased as seen in the bottom plot of Figure 6.71. The peak tensile interlaminar normal stress in the laminate with three terminated plies is approximately three times that in the laminate with one terminated ply and approximately 1.2 times that in the laminate with two terminated plies. Note that the peak interlaminar normal stress does not occur at the cutoff in the undropped region for the two laminates with two and three terminated plies. In these laminates, the interlaminar normal stress reaches a peak approximately one ply thickness away from the cutoff and decreases in magnitude for distances smaller than one ply thickness. This reversal trend was also observed in Section 6.2.2, and is discussed further in Section 6.4.

For the laminates under bending loads, the interlaminar shear stress in the dropped region increases significantly by a factor of approximately two as the number of terminated plies is increased by one as shown in the top plot of Figure 6.72. The magnitude of the interlaminar shear stress in the undropped region is an order of magnitude smaller than that in the dropped region. The interlaminar normal stresses in the undropped and dropped regions also increase in magnitude by a factor of approximately two as the number of terminated plies is increased by one as shown in the bottom plot of Figure 6.72.

6.3 Combined In-plane and Bending Loads

The interlaminar stress fields in laminates under combined in-plane and bending loads can be considered using the analytical models developed in this work. Since all of the analytical models are linear, the interlaminar stress field in such laminates can be obtained by appropriately superposing the stress fields for laminates under in-plane and bending loads individually. Two specific cases where laminates with ply dropoffs are subjected to combined in-plane and bending loads are considered in this section. One is

the case of symmetric laminates with ply dropoffs under applied in-plane and bending loads. This is presented in the first sub-section. The other is the case of laminates with unsymmetric ply dropoffs under in-plane load. In such laminates, the lack of symmetry about the mid-plane induces a bending load. This is presented in the second sub-section.

6.3.1 Geometrically Symmetric Laminates

Symmetric laminates under combined in-plane and bending loads can be analyzed by using superposition and summing the interlaminar stress fields due to the individual load types. Therefore, the characteristics and trends of the interlaminar stress fields in such laminates under combined loads can be deduced from those of the interlaminar stress fields obtained individually. In laminates under in-plane load, the interlaminar shear stress is anti-symmetric through the thickness about the mid-plane and the interlaminar normal stress is symmetric, while in laminates under bending load, the symmetry is reversed. Subsequently, under combined in-plane and bending loads, the magnitude of some interlaminar stress components increases due to the similar sense of the contributions from the in-plane and bending loads in one half of the laminate (about the mid-plane) while the magnitude is reduced in the other half due to opposite sense of the two contributions. The relative magnitudes of the in-plane and bending loads determine the magnitude of the interlaminar stresses under combined loads.

As an example, a $[0_2/0_{2D}/0_4]_s$ laminate with a taper angle of 7° under combined in-plane and bending loads is considered. The magnitude of the bending load is chosen such that the in-plane stress at the outer surface in the undropped region due to the bending load is equal to the applied in-plane stress, σ_0. A diagram of the laminate and the positive directions of the applied loads are shown in Figure 6.48. The interlaminar stresses in the upper-half of the same laminate under in-plane and bending loads were considered individually in Section 6.2.1. The interlaminar stresses along the interface of the continuous and terminated plies closer to the mid-plane in the undropped region and the inner and outer continuous plies in the dropped region ($z = +4t$ and $z = -4t$) are shown

in Figures 6.73 and 6.74. The interlaminar stresses along the other interface of the continuous and terminated plies in the undropped region ($z = +6t$ and $z = -6t$) exhibit a similar trend to that along the interface considered, and thus, are not shown.

As expected, the superposition of the interlaminar stress distributions in laminates under in-plane and bending loads causes the total interlaminar stress distribution to increase or decrease in magnitude. It can be seen in the top plot of Figure 6.73 that the contributions to the total interlaminar shear stress due to in-plane and bending loads are both negative along the interface considered in the upper-half of the laminate in the undropped region ($z = +4t$). Therefore, the magnitude of the total interlaminar shear stress is greater than those of the interlaminar shear stresses due to in-plane and bending loads individually. Similar, in the dropped region, the interlaminar shear stresses due to the contributions from the in-plane and bending loads are both positive, and thus, the total interlaminar shear stress is greater in magnitude. However, in this region, the contribution from the bending load is much greater than that from the in-plane load by an order of magnitude. Therefore, total interlaminar shear stress is almost identical to that due to only the bending load. In contrast, along the interface considered in the lower-half of the laminate in the undropped region ($z = -4t$) shown in the bottom plot of Figure 6.73, the interlaminar shear stress due to the in-plane load is positive, while that due to bending load is negative. Thus, the total interlaminar shear stress is smaller in magnitude compared to the cases when the two loads are applied individually. Again, in the dropped region, the interlaminar shear stress due to the in-plane load is an order of magnitude smaller than that due to the bending load.

A similar trend is seen in the total interlaminar normal stresses in Figure 6.74. Above the mid-plane ($z = +4t$), the contributions to the total interlaminar normal stresses due to both the in-plane and bending loads are tensile in the dropped region and compressive in the undropped region. Thus, the total interlaminar normal stress increases in magnitude when the two interlaminar normal stresses due to the in-plane and bending

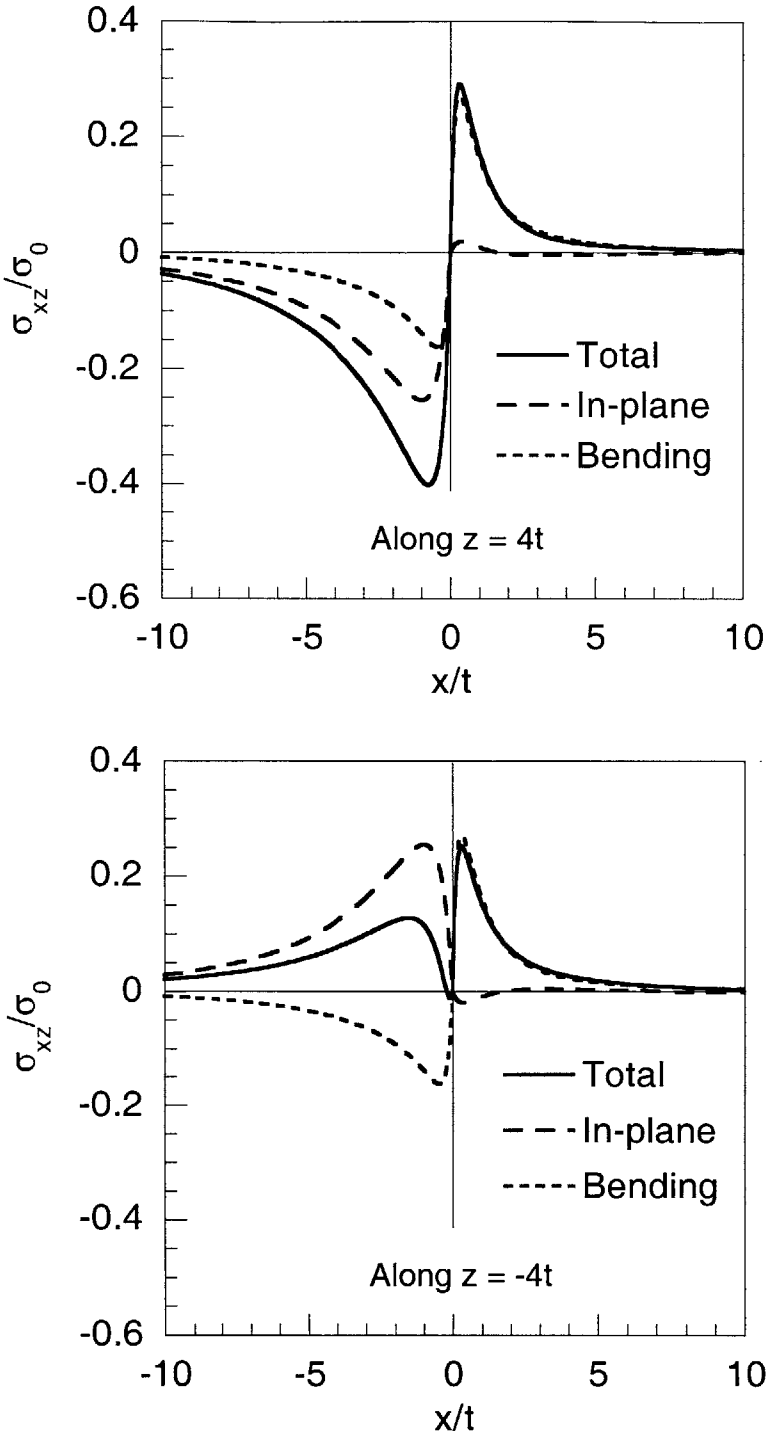

Figure 6.73 Interlaminar shear stresses along the interface of the continuous and terminated ply group closest to the mid-plane in the undropped region and the inner and outer continuous plies in the dropped region *(top)* in the upper-half (z = +4t), and *(bottom)*, in the lower-half (z = –4t) in a $[0_2/0_{2D}/0_4]_s$ laminate under combined in-plane and bending loads.

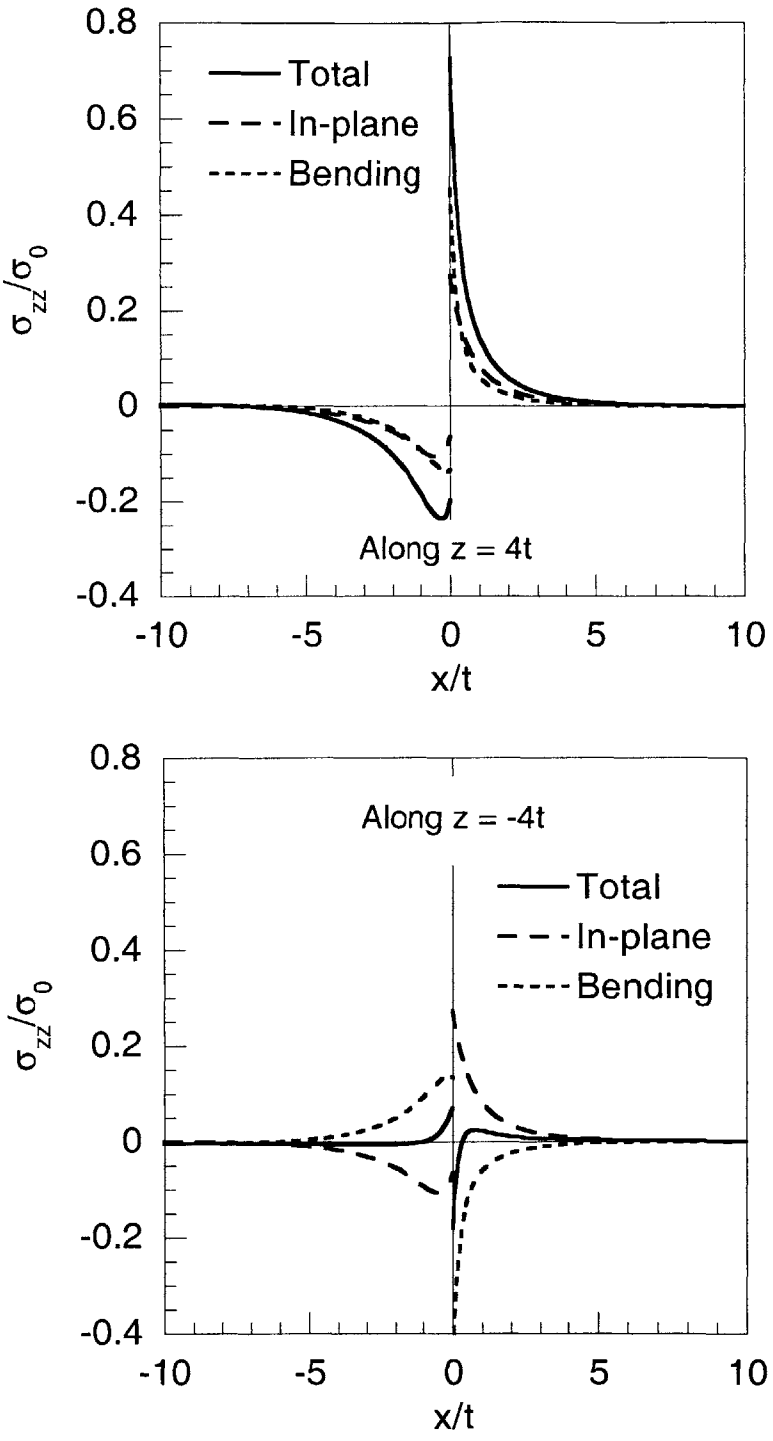

Figure 6.74 Interlaminar normal stresses along the interface of the continuous and terminated ply group closest to the mid-plane in the undropped region and the inner and outer continuous plies in the dropped region *(top)* in the upper-half (z = +4t), and *(bottom)*, in the lower-half (z = –4t) in a $[0_2/0_{2D}/0_4]_s$ laminate under combined in-plane and bending loads.

loads are superposed. On the other hand, the contributions to the interlaminar normal stress below the mid-plane ($z = -4t$) due to the in-plane and bending loads are opposite in sign. This results in the total interlaminar normal stress being smaller in magnitude compared to the cases when the two loads are applied individually. Note that for the interlaminar normal stress, the contributions from the in-plane and bending loads are comparable in the dropped region, unlike the case of the interlaminar shear stress.

Based on the two cases of combined in-plane and bending loads considered herein, it can be concluded that the characteristics of the interlaminar stresses in laminates under such loads can be derived from the characteristics of symmetric laminates under in-plane and bending loads separately. The magnitude of the interlaminar stresses in laminates under applied in-plane and bending loads are similar to those when the two loads are applied individually since they are either the summation or difference of the interlaminar stresses when the two loads are applied individually. The decay rates of the interlaminar stresses remain unchanged by such superposition. Due to the difference in symmetric and unsymmetric interlaminar stress components in symmetric laminates under in-plane and bending loads, the magnitudes of the interlaminar stresses may increase or decrease when the two effects are superposed.

6.3.2 Geometrically Unsymmetric Laminates

In laminates with ply dropoffs that are geometrically unsymmetric about the mid-plane, an in-plane load will induce an effective couple-moment due to the misalignment of the in-plane load at the undropped and dropped ends. Due to this effective couple-moment, such laminates are not under static equilibrium, and thus, require additional boundary conditions. The specific boundary conditions considered herein are that of the undropped and dropped ends being fixed in the z-direction. However, the ends are allowed to elongate in the x-direction under applied in-plane load. A diagram of an unsymmetric laminate with both ends fixed is shown in the top part of Figure 6.75. In addition, it is further assumed, for simplicity, that the layup of the laminate in the

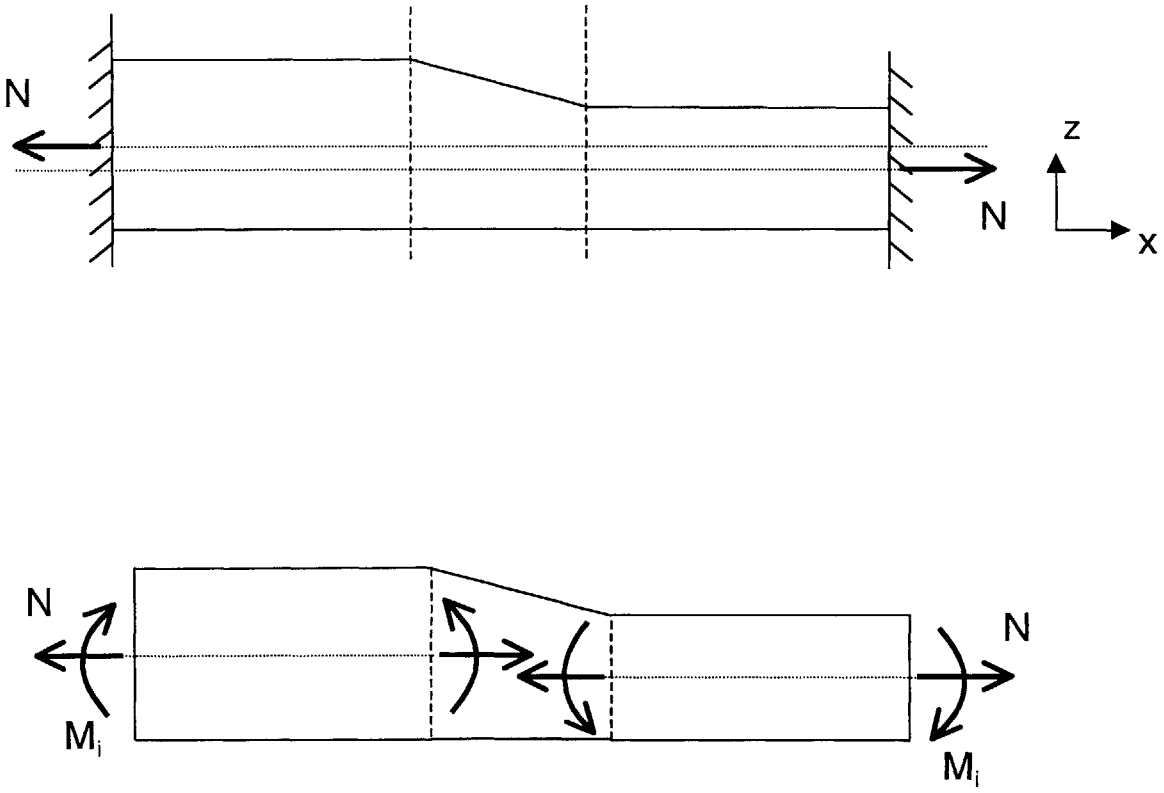

Figure 6.75 Illustrations of *(top)* an unsymmetric laminate with ply dropoffs under in-plane load, and *(bottom)*, the induced bending loads in the undropped and dropped regions.

undropped and dropped regions are symmetric and homogeneous. In such cases, the line of action of the applied in-plane load, N, in the x-direction at the undropped end is located at a distance of $nt/2$ from the lower surface (z = 0), where n is the total number of plies and t is the ply thickness, and the line of action at the dropped end is located at a distance of $n_c t/2$ from the lower surface, where n_c is the number of continuous plies. Since n is greater than n_c, the applied in-plane load gives rise to a couple-moment in the anti-clockwise direction. Therefore, in order to maintain moment equilibrium, a bending moment, M_i, in the clockwise direction is induced with a magnitude of:

$$M_i = \frac{(nt - n_c t)}{2} N \tag{6.1}$$

The clockwise direction of the net induced bending load causes the undropped and dropped region to be under local bending loads that are equal and opposite in direction. The undropped region is subjected to a bending moment that causes compression in the upper half of the laminate and tension in the bottom half, while the dropped region is subjected to a bending moment that causes tension in the upper half and compression in the bottom half. An illustration of the directions of the induced bending loads in the undropped and dropped regions is shown in the bottom part of Figure 6.75.

The interlaminar stress fields in such laminates can be approximated to first-order by superposing the solutions of one half of a symmetric laminate under appropriate combinations of in-plane and bending loads. Since the direction of the local bending loads in the undropped and dropped regions are equal and opposite, the two regions need to be considered separately. The interlaminar stress field in the undropped region is approximated by one half of a symmetric laminate under appropriate in-plane and bending loads that causes compression in the upper half of the laminate. Similarly, the dropped region is approximated by one half of a symmetric laminate under appropriate in-plane and bending loads that causes tension in the upper half. A graphical illustration

of the approximation procedure is shown in Figure 6.76. The appropriate loads to be applied to the symmetric laminate in the undropped and dropped regions to approximate the solution are found by matching the applied in-plane load and induced bending load in the unsymmetric laminate at the ends. To obtain the stress field in the undropped region, the symmetric laminate needs to be subjected to in-plane and bending loads of:

$$N_1 = 2\left(4 - 3\frac{n_c}{n}\right)N \tag{6.2}$$

$$M_1 = 4(n - n_c)Nt \tag{6.3}$$

To obtain the stress field in the dropped region, the symmetric laminate needs to subjected to in-plane and bending loads of;

$$N_2 = 2\left(4 - 3\frac{n}{n_c}\right)N \tag{6.4}$$

$$M_2 = 4(n - n_c)Nt \tag{6.5}$$

Details of the derivations for these in-plane and bending loads for the case of geometrically unsymmetric laminate with symmetric and homogeneous layup are shown in Appendix C.

An unsymmetric laminate with a taper angle of 7° and layup of $[0_2/0_{3D}/0_4]$ under in-plane load is considered as an example. For this laminate, N_1 and M_1 are equal to 4N and 12Nt, respectively, and N_2 and M_2 are equal to –N and 12Nt, respectively. The interlaminar stresses along the lower interface of the continuous and terminated plies in the undropped region (z = 4t) and along the interface of the inner and outer continuous plies in the dropped region (z = 4t) are shown in Figures 6.77 and 6.78. The interlaminar stresses along the upper interface of the continuous and terminated plies in the undropped region (z = 7t) exhibit a similar trend to that along the lower interface, and thus, are not

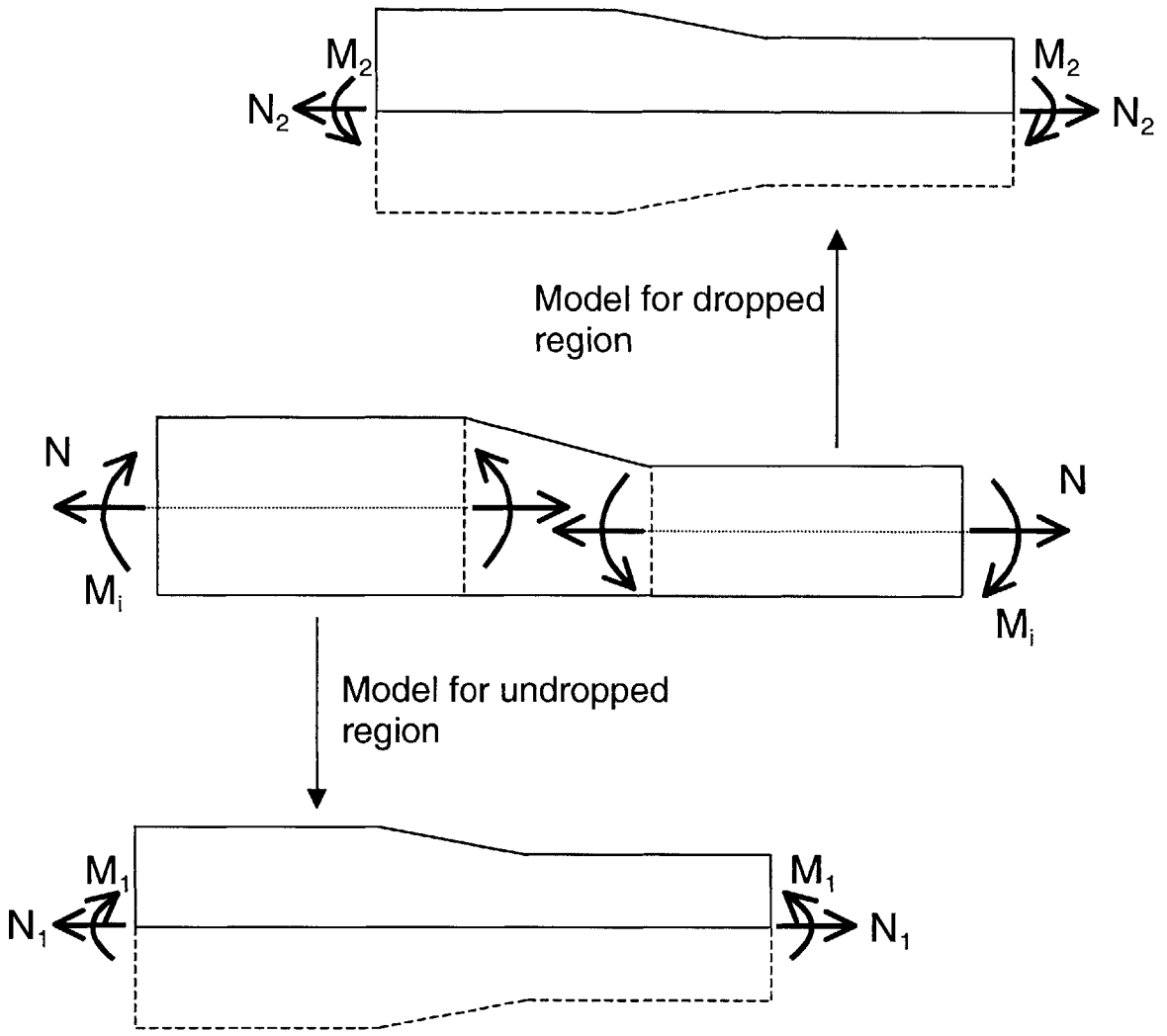

Figure 6.76 Illustrations of the models for an unsymmetric laminate using two symmetric laminates under in-plane and bending loads for the undropped and dropped regions.

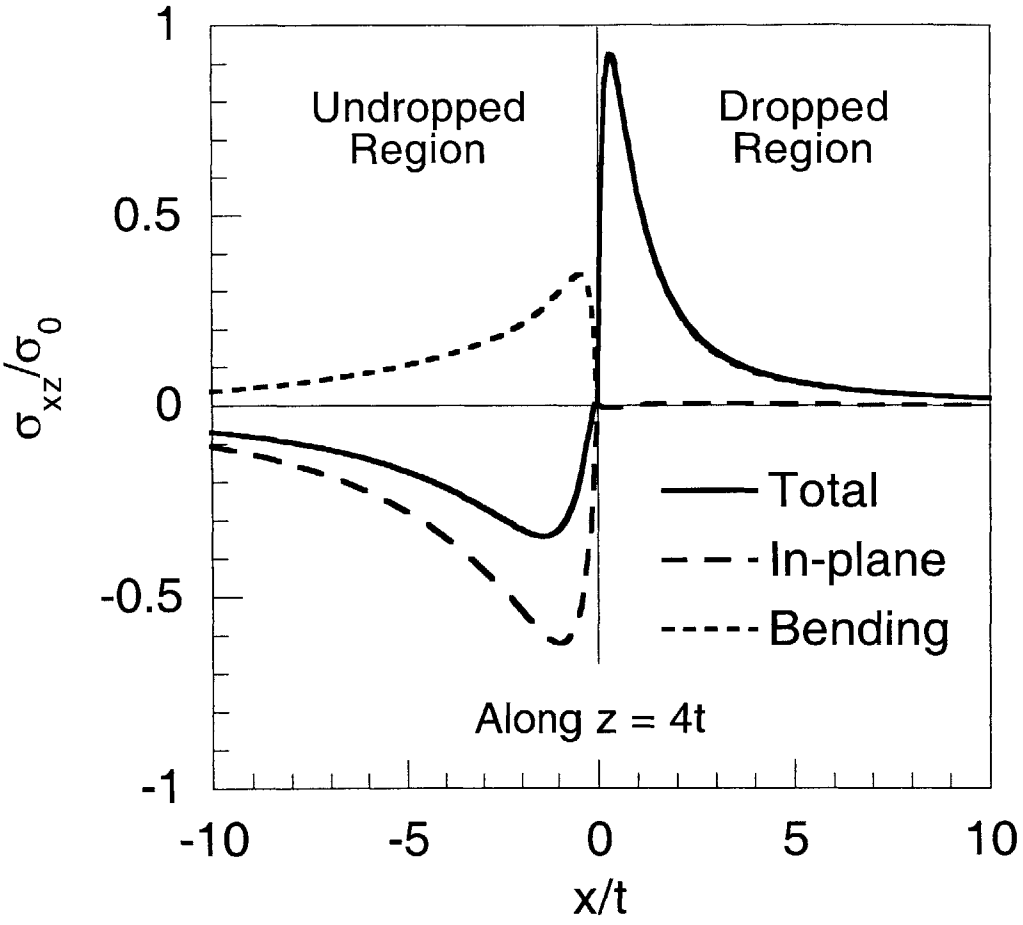

Figure 6.77 Interlaminar shear stress along lower interface of the continuous and terminated plies in the undropped region and the interface of the inner and outer continuous plies in the dropped region (z = 4t) in an unsymmetric $[0_2/0_{3D}/0_4]$ laminate under in-plane load.

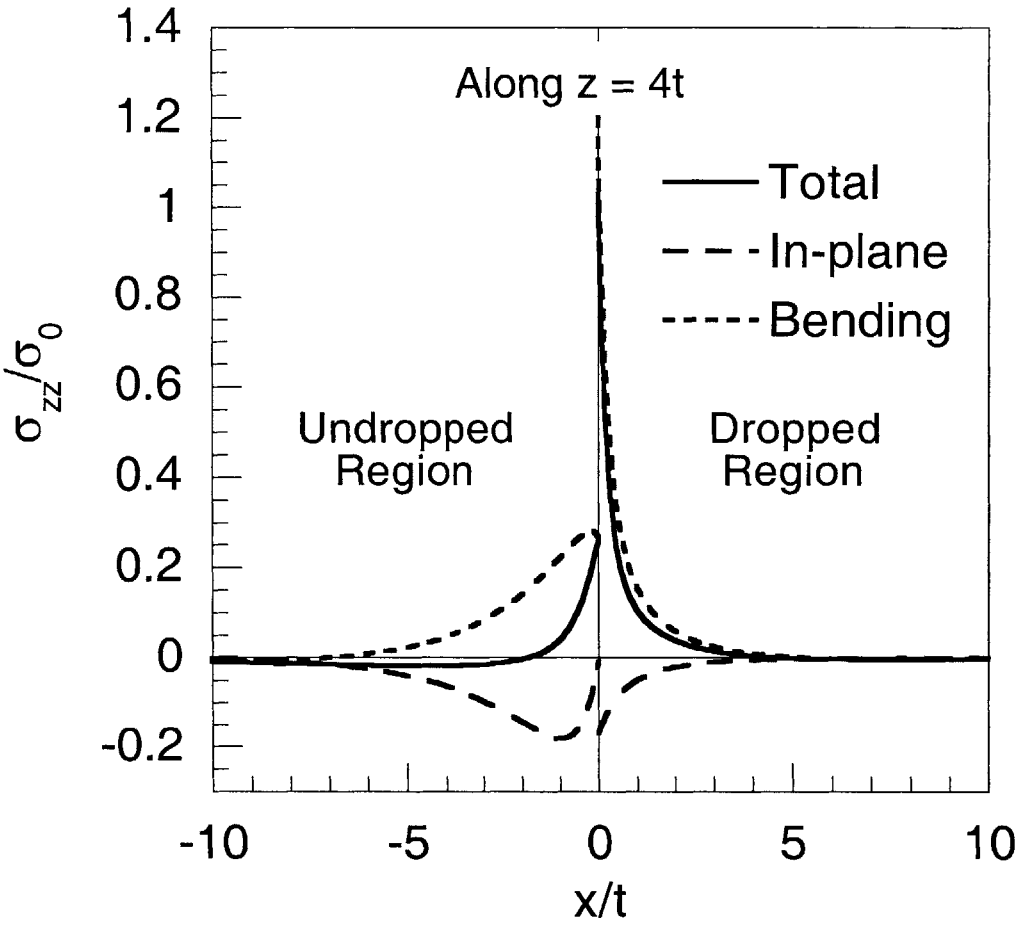

Figure 6.78 Interlaminar normal stress along lower interface of the continuous and terminated plies in the undropped region and the interface of the inner and outer continuous plies in the dropped region (z = 4t) in an unsymmetric $[0_2/0_{3D}/0_4]$ laminate under in-plane load.

shown. The interlaminar stresses are normalized by the average applied in-plane stress at the undropped end, σ_0, in the unsymmetric laminate.

It can be seen in Figures 6.77 and 6.78 that the interlaminar shear and normal stresses due to the in-plane and bending loads in the undropped region are opposite in sign, and thus, the superposition of the two contributions reduces the magnitude of the total interlaminar shear stress. In the dropped region, the interlaminar shear and normal stresses due to the in-plane and bending loads are also opposite in sign, but the magnitude of the interlaminar shear and normal stresses due to the in-plane load is much smaller than that due to the bending load (by approximately an order of magnitude). Therefore, the total interlaminar shear stress closely resembles the interlaminar shear stress due to the bending load. It is noted that N_2 would equal zero in the special case when the ratio of n to n_c is 4/3. In such cases, the interlaminar stresses in the dropped region arise solely due to the contribution from the bending load.

The preceding solution procedure for laminates with geometrically unsymmetric ply dropoffs represents a first-order approximation to the actual solution. The main drawback of this method is that the force and moment equilibrium conditions at the cutoffs are not met because two laminates under different loads are used to obtain the stress fields in the undropped and dropped regions. Therefore, the current method is not expected to yield accurate solutions especially near the cutoff, although the overall trend of the stress field can be obtained. In order to maintain equilibrium at the cutoff, the current analytical model needs to be modified to account for varying applied bending loads along the length of the laminate. In the case of the unsymmetric laminate, the induced bending loads in the undropped and dropped regions are equal and opposite as shown in Figure 6.75. However, in its current form, the current analytical model can only be used to analyze laminates under a constant bending load applied at the ends. This restriction necessitated the use of two laminates under different loads to model the undropped and dropped region. Thus, by extending the analytical model to account for

different bending loads at the undropped and dropped ends, the stress fields in laminates with unsymmetric ply dropoffs can be obtained via the use of one symmetric laminate. This would yield stress fields that satisfy the force and moment equilibrium at the cutoff, and thus, yield better approximations to the actual solution.

6.4 Discussion

The interlaminar stress distributions in various laminates with ply dropoffs obtained via the analytical models developed in the current work were presented in the previous sections. These examples show that the interlaminar stresses in the vicinity of the dropoff region in laminates with ply dropoffs can be very high and possibly singular, and that the magnitude and distribution of interlaminar stresses vary significantly with the structural parameters. A careful consideration of the characteristics and trends of the interlaminar stresses presented in the previous sections reveals two fundamental mechanisms that give rise to interlaminar stresses. The understanding of these fundamental mechanisms provides key insights that allow one to anticipate the overall characteristics and trends of the interlaminar stress distributions in laminates with ply dropoffs in general. These mechanisms are discussed in the first two sub-sections. Subsequently, in the third sub-section, the characteristics and trends of the interlaminar stresses are briefly reexamined based on the insights gained via these mechanisms to demonstrate their utility and applicability.

6.4.1 Fundamental Mechanisms

Two fundamental mechanisms cause interlaminar stresses to exist in composite laminates with ply dropoffs. The first is the transfer of load from the terminated ply group to the continuous plies. This occurs because the terminated ply group cannot carry any load at the termination location, and thus, the far-field load carried by the terminated ply group needs to be transferred to the continuous plies adjacent to the terminated ply

group via interlaminar stresses. This mechanism, which has been described in previous sections, is called the *termination effect*. The second is the redistribution of the load from the undropped region to the dropped region in the outer continuous plies through an offset in the z-direction. The offset in the z-direction occurs because the outer continuous plies are angled in the dropoff region due to the thickness discontinuity of the terminated plies, and this causes misalignment in the line of action of the far-field loads and stresses in the undropped and dropped regions. This mechanism is called the *offset effect*. Both mechanisms are generally present to give rise to interlaminar stresses in laminates with ply dropoffs. However, there are two specific laminate configurations in which each mechanism occurs individually. These configurations allow examination of each mechanism in isolation for better understanding and for identification of the factors affecting each and are subsequently considered.

The termination effect can be isolated by considering laminates with external ply dropoffs. Laminates with external ply dropoffs do not have any outer continuous plies, and thus, the offset effect does not exist. Interlaminar stresses, therefore, arise solely due to the termination effect. The interlaminar stress distribution in such a laminate was considered, for example, in Section 6.2.2 when a $[0_{2D}/0_6]_s$ laminate under in-plane and bending loads was considered. The interlaminar stresses in the $[0_{2D}/0_6]_s$ laminate are shown in the top plots of Figures 6.54 and 6.55.

A better understanding of this mechanism and the factors that affect the interlaminar stress field can be acquired by considering the equilibrium of the terminated ply group in a laminate with external ply dropoffs via a free-body diagram. A free-body diagram of the terminated ply group in the upper-half of a laminate with external ply dropoffs is shown in Figure 6.79. All faces of the terminated ply group are stress-free except the undropped end, which is under far-field load (due to applied in-plane or bending loads), and the lower interface, *i.e.*, the z^--face. Therefore, to maintain x-direction force equilibrium, interlaminar shear stress must exist along the z^--face, and the

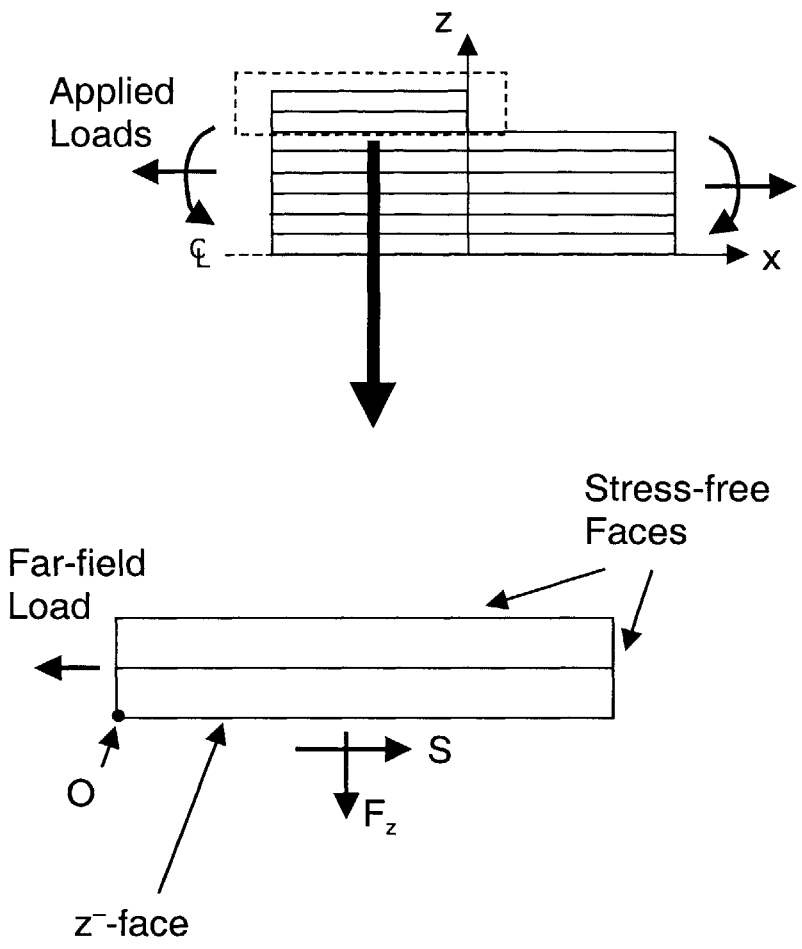

Figure 6.79 Free-body diagram of the terminated ply group in a generic laminate with external ply dropoffs.

integral of this shear stress, *i.e.*, net shear force, S, must be equal and opposite to the far-field load. This shows that interlaminar shear stress is directly related to the far-field load in the terminated ply group.

The far-field load at the undropped end and the interlaminar shear stress along the z^--face are not sufficient to keep the terminated ply group under moment equilibrium in the free-body diagram of Figure 6.79. Since the line of action of the far-field load and the interlaminar shear stress are not aligned, a counter-clockwise moment about the y-axis is induced. Taking the moment about the point O, it can be seen that the induced moment is dependent on the magnitude and the distribution of the far-field load. This induced moment must be equilibrated by interlaminar normal stress along the z^--face. Therefore, the interlaminar normal stress distribution is directly related to the far-field load in the terminated ply group and its distribution in the z-direction. In addition, to maintain z-direction force equilibrium, the interlaminar normal stress along this interface must be self-equilibrating, *i.e.*, the net normal force, F_z, is equal to zero because all other faces are stress-free. This explains why the interlaminar normal stress changes sign from tensile to compressive away from the cutoffs before decaying to zero.

The free-body analysis shows that the termination effect gives rise to interlaminar shear and normal stresses along the interface of the continuous and terminated plies in the undropped region and that these stresses are affected by the far-field stress distribution in the terminated ply group. It is clear from this analysis that the interlaminar shear and normal stresses will increase in magnitude when the magnitude of the far-field load in the terminated ply group is increased. The interlaminar shear stress increases in magnitude when the far-field load increases because the net shear force must equal the far-field load. The interlaminar normal stress increases in magnitude when the far-field load increases because the induced moment due to the far-field load increases. Under the same applied load, the magnitude of the far-field load in the terminated ply group increases if the relative stiffness of the terminated ply group with respect to that of the continuous ply

group increases. Therefore, the relative stiffness of the terminated ply group affects the interlaminar stress distribution. In addition, if the number of terminated plies is increased while the number of continuous plies and the applied load is held constant, the far-field load in the terminated ply group increases. Therefore, this is another factor that affects the interlaminar stress distribution. The distribution of the far-field load is determined by the type of load applied and the layup sequence of the terminated ply group. Thus, these factors will also affect the interlaminar stress distribution.

The offset effect can be isolated by considering laminates with internal ply dropoffs located at the mid-plane with these terminated ply groups carrying a negligible amount of far-field load. Since the terminated ply groups do not carry any significant far-field load, the load transfer that needs to occur from the terminated ply group to the continuous plies is negligible. Therefore, the interlaminar stresses in such laminates arise mainly due to the offset effect. Such laminates have not been considered previously, and thus, an example problem is considered to examine the characteristics of the interlaminar stress field due to the offset effect. For this purpose, a $[0_6/X_{2D}]_s$ laminate under in-plane load where X indicates plies with virtual material properties of 1% stiffness of the 0° plies is considered. The material properties of AS4/3501-6 composite material shown in Table 5.2 are used for the 0° plies.

The interlaminar stresses along the interface of the continuous and terminated plies in the undropped region ($z = 2t$) and along the mid-plane in the dropped region ($z = 0$) are shown in Figure 6.80 for the laminate under in-plane load. The interlaminar normal stress in the dropped region is tensile, reaches a peak at the cutoff, and decays to zero away from the cutoffs. In the undropped region, the interlaminar normal stress is compressive and decays slowly compared to that in the dropped region. The interlaminar shear stress in the undropped region is negligible, as expected, due to the low stiffness in the terminated ply group relative to the continuous plies. The interlaminar shear stress in the dropped region is identically zero due to anti-symmetry under in-plane load.

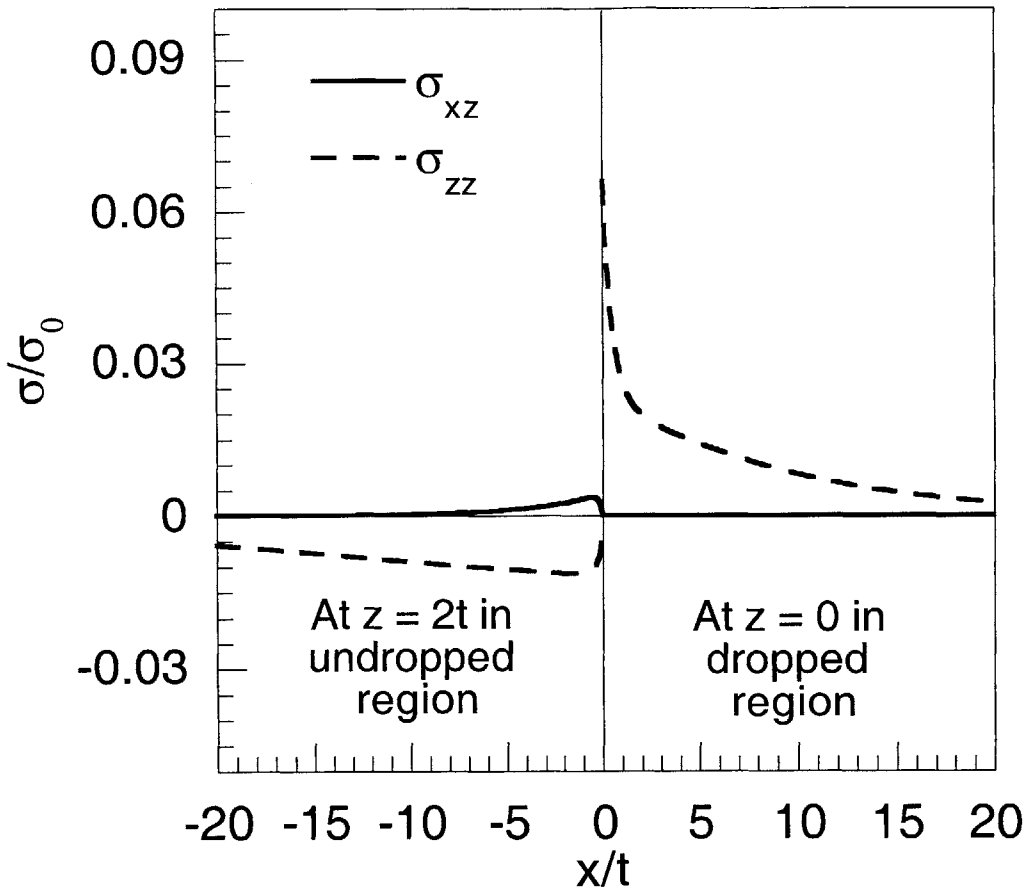

Figure 6.80 Interlaminar shear and normal stresses along the upper interface of the terminated ply group in the undropped region (z = 2t) and along the mid-plane in the dropped region (z = 0) in a $[0_6/X_{2D}]_s$ laminate where X indicates plies with 1% stiffness of 0° plies.

As in the case of the termination effect, a better understanding of the offset effect and the factors that affect it can be gained by considering the equilibrium of the outer continuous plies via a free-body diagram. A free-body diagram of the outer continuous plies in one-half of a laminate where only the offset effect exists is shown in Figure 6.81. The terminated ply group is assumed to carry no far-field load. Due to the offset in the z-direction, the far-field loads at the undropped and dropped ends of the outer continuous ply group are not aligned under in-plane or bending loads. Therefore, an induced moment about the y-axis in the counter-clockwise direction arises. The distance between the line of actions of the far-field load at the undropped and dropped ends is defined as the *offset distance*, t_d, as indicated in Figure 6.81. Thus, the magnitude of the induced moment depends on the magnitude of the far-field loads and the offset distance. This moment must be equilibrated by the interlaminar stresses on the z^--face since the outer surface and the dropoff region are assumed to be stress-free. Furthermore, the interlaminar shear stress on the z^--face in the undropped region is zero because the terminated ply group does not carry any load. In order to further describe how the interlaminar stresses on the z^--face arise to equilibrate the induced moment, the cases of the in-plane and bending loads need to be considered separately because different symmetry conditions require different components of the interlaminar stresses to be zero in the dropped region, which corresponds to the mid-plane. Under in-plane load, the interlaminar shear stress at the mid-plane is zero due to anti-symmetry, and the interlaminar normal stress is non-zero. Under bending load, the interlaminar normal stress at the mid-plane is zero due to anti-symmetry, and the interlaminar shear stress is non-zero.

The interlaminar shear stress on the z^--face being zero in the case of the in-plane load, the induced moment must be equilibrated by the interlaminar normal stresses on the z^--face in the undropped and dropped regions. One method by which this can occur is for the interlaminar normal stress on the z^--face to be identically zero in the undropped

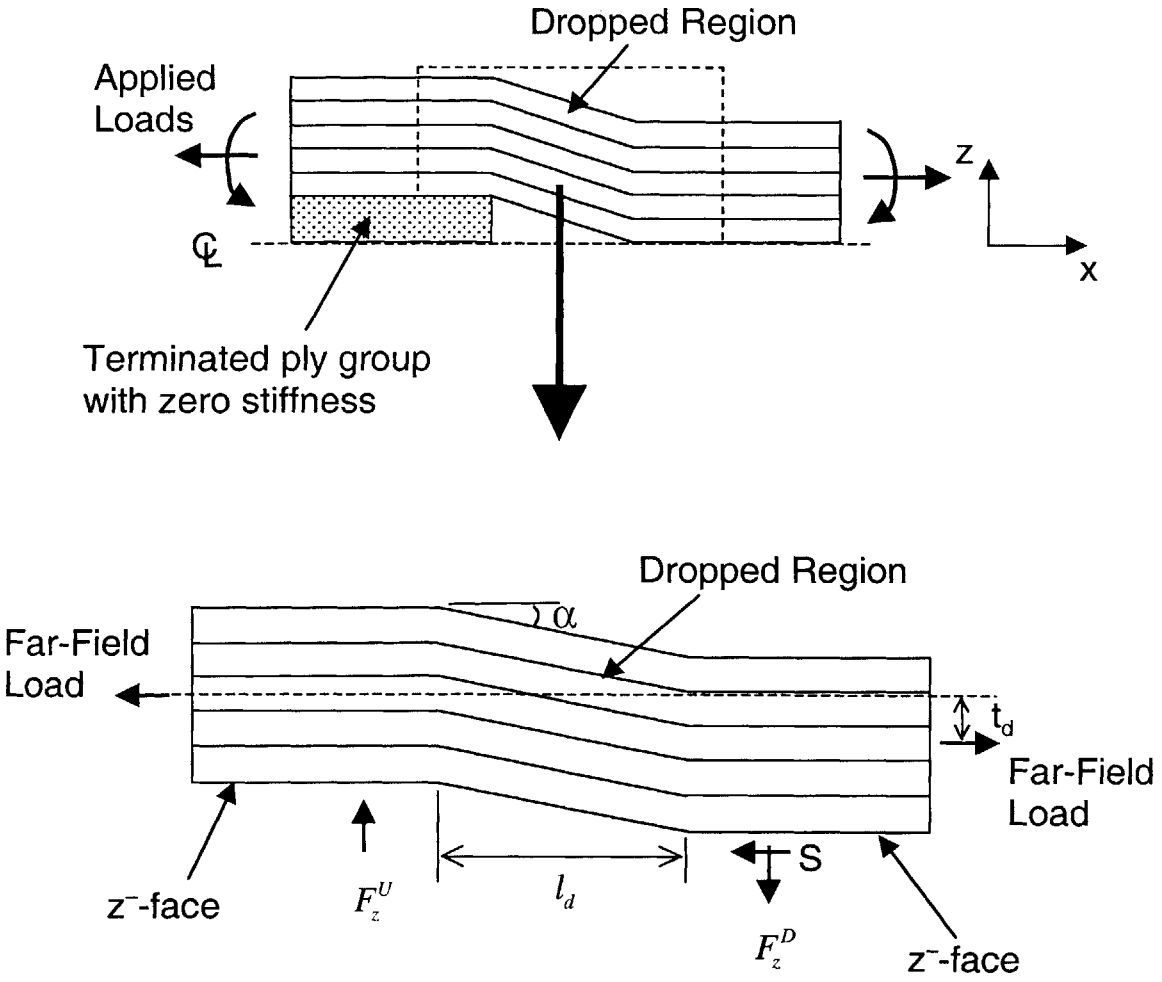

Figure 6.81 Free-body diagram of the outer continuous plies in a laminate with internal ply dropoffs with stiffness of zero and located at the mid-plane (shaded region indicates zero stiffness plies).

region and to assume a distribution in the dropped region that is self-equilibrating (no net force in the z-direction) and that generates a moment equal and opposite to the induced moment. However, since there is no physical basis for the interlaminar normal stress to be zero in the undropped region, this distribution will likely not occur. Indeed, the actual interlaminar normal stress distribution in the case considered is non-zero in the undropped region as shown in Figure 6.80. The alternative method by which the induced moment can be equilibrated is for the integral of these interlaminar normal stresses (*i.e.*, the net normal forces in the undropped region, F_z^U, and in the dropped region, F_z^D) to be such that the net moment due to the two forces is equal and opposite to the induced moment when multiplied by the distance between these two forces. The exact location where these two net normal forces act is unknown *a priori*, and thus, the distance between these forces cannot be precisely quantified. However, it is clear that this distance includes the length of the dropoff region, l_d, and thus, the moment generated by the net normal forces depends on this length. In addition, to equilibrating the induced moment, the net normal forces in the undropped and the dropped regions must be equal and opposite in magnitude to maintain z-direction force equilibrium of the outer continuous ply group. To satisfy these requirements, the net normal forces must be compressive in the undropped region and tensile in the dropped region thereby generating a moment in the clockwise direction to counter the induced moment. This is consistent with the observation from Figure 6.80. This shows that, under in-plane load, interlaminar normal stresses will generally arise in the undropped and dropped regions, and these are affected by the magnitude of the far-field load, the offset distance between the lines of action of the far-field loads in the outer continuous ply group, and the length of the dropoff region.

For the bending load case, the non-zero stress components on the z^--face are the interlaminar shear stress in the dropped region and the interlaminar normal stress in the undropped region. Thus, the summation of the moments generated by these interlaminar

stresses must be equal and opposite to the induced moment. The contribution from the interlaminar shear stress in the dropped region can be ascertained by considering the x-direction force equilibrium of the outer continuous plies. This equilibrium condition requires that the integral of the interlaminar shear stress in the dropped region, *i.e.*, the net shear force, S, must be positive on the z^--face. The reason is that the far-field loads at the undropped and dropped ends of the outer continuous plies are not equal under bending load due to the difference in the moment arm from the mid-plane at the two ends. Since the moment arm at the undropped end is greater due to the offset than that at the dropped end, the far-field load at the undropped end is smaller than that at the dropped end in order for the applied moment (*i.e.*, the far-field load multiplied by the moment arm) to be constant. The net shear force being positive on the z^--face, a clockwise moment is generated by the interlaminar shear stress in the dropped region. The other contribution is from the interlaminar normal stress in the undropped region. The direction of this moment is not known *a priori* and depends on the magnitude of the moment due to the interlaminar shear stress in the dropped region. This interlaminar normal stress distribution must be self-equilibrating because there are no other interfaces along which z-direction forces can act. Thus, the distribution of the interlaminar normal stress in the undropped region must change sign (from tensile to compressive or vice versa) away from the cutoff before decaying to zero similar to that due to the termination effect and this creates a moment dependent only on the distribution. Although the components of the interlaminar stress that arise in laminates under bending load are different from those under in-plane load, it can be seen from this analysis that the same factors affecting the interlaminar normal stress in the latter case also affect those in this case. An exception is the length of the dropoff region, which does not play a role in the case of the bending load because moments that arise to equilibrate the induced moment are not dependent on it.

The free-body analysis reveals that the interlaminar stresses due to the offset

effect is affected by the far-field load and the offset distance between the lines of action of the far-field load in the outer continuous ply group. It is clear that the magnitude of the interlaminar normal stress will increase when the far-field load and/or the offset distance or both are increased because the induced moment increases. The magnitude of the far-field load increases if the number of outer continuous plies increases and the number of inner continuous plies decreases in a laminate with a constant number of continuous and terminated plies. Therefore, the number of outer continuous plies affects the interlaminar normal stress distribution. The offset distance increases if the number of terminated plies increases when the number of outer continuous plies is held constant. Therefore, the ratio of the number of terminated plies to the number of outer continuous plies also affects the interlaminar normal stress distribution.

The free-body analysis also reveals that for laminates under in-plane loads the length of the dropoff region affects the interlaminar normal stresses on the z^--face in the undropped and dropped regions. As discussed in the free-body analysis, the length of the dropoff region affects the magnitude of the moment generated by the net normal forces, F_z^U, and F_z^D. For example, in a given laminate, if the length of the dropoff region is increased by a factor of two, the net normal forces can decrease by a factor of two because the induced moment that needs to be equilibrated is constant. The length of the dropoff region, l_d, is directly related to the taper angle, α, in the dropoff region when the number of terminated plies, n_t, is fixed. The relationship can be expressed as:

$$n_t t = l_d \tan\alpha \tag{6.6}$$

where t is the ply thickness. Therefore, it can also be stated that the interlaminar normal stresses on the z^--face in the undropped and dropped regions depend directly on the taper angle.

6.4.2 Combined Effects

Thus far, the two fundamental mechanisms that cause interlaminar stresses have

been discussed individually. In generic laminates with ply dropoffs that may be located away from the outer surface and the mid-plane, interlaminar stresses arise due to both mechanisms. Although the general characteristics and trends of the interlaminar stresses in generic laminates can be deduced from the basic understanding of the two mechanisms in the previous sub-section, there are three additional effects that arise and need to be considered when the two mechanisms are combined. These effects are discussed in the following paragraphs.

The first effect is that there can be two interfaces along which load transfer from the terminated ply group to the continuous plies can occur. Since the load transfer can occur along two interfaces, less load needs to be transferred along each interface compared to laminates with single interfaces between the continuous and terminated plies. Therefore, the magnitudes of the interlaminar shear stresses along each interface of the continuous and terminated plies are generally lower than that compared to laminates with single interfaces. This was observed in Section 6.2.2 when four laminates with twelve continuous and four terminated plies under in-plane load with the terminated ply group at different through-thickness locations were investigated (see Figure 6.54). It can be clearly seen in Table 6.5 that the loads transferred along the upper and lower interfaces in the $[0_2/0_{2D}/0_4]_s$ and $[0_4/0_{2D}/0_2]_s$ laminates are smaller than those transferred along the single interfaces in the $[0_{2D}/0_6]_s$ and $[0_6/0_{2D}]_s$ laminates. These two latter cases represent laminates with external ply dropoffs and with symmetric dropoffs at the mid-plane, respectively. It was also observed in Sections 6.2.1 and 6.2.2 that the amount of load transferred along the upper and lower interfaces of the terminated ply group is closely related to the taper angle and the number of inner and outer continuous plies. Examples in those sections show that the load transfer from the terminated ply group to the continuous plies occurs preferentially to the continuous ply group with a smaller taper angle and greater number of plies. This is not surprising because it implies that the far-field load will be transferred to the continuous ply group that offers the least resistance to

the load transfer. It is intuitively easier for the continuous ply group with a smaller taper angle and greater number of plies to carry the "extra" load from the terminated ply group than for the continuous ply group with a larger taper angle and less number of plies. Note that the number of interfaces of the continuous and terminated plies affects how the load is transferred from the terminated ply group to the continuous plies, *i.e.*, the termination effect.

The second effect is that the anti-symmetries that caused the interlaminar shear stress on the z^--face to be zero in the case of the in-plane load and the interlaminar normal stress on the z^--face to be zero in the case of the bending load, as discussed in the preceding sub-section, no longer applies since this interface generally does not correspond to the mid-plane. Therefore, both the interlaminar shear and normal stresses may exist on the z^--face of the outer continuous plies. This implies that, in generic laminates with ply dropoffs, the induced moment due to the misalignment of the far-field loads at the undropped and dropped ends of the outer continuous ply group can be equilibrated by both the interlaminar normal stresses on the z^--face in the undropped and dropped regions (as described for the case of the in-plane load when only offset effect is present) *and* by the interlaminar shear stress on the z^--face in the dropped region (as described for the case of the bending load when only the offset effect is present). The non-zero interlaminar shear stresses can be seen, for example, in Figure 6.54 for the $[0_2/0_{2D}/0_4]_s$ and $[0_4/0_{2D}/0_2]_s$ laminates under in-plane load, and the non-zero interlaminar normal stresses can be seen, for example, in Figure 6.57 for the $[0_2/0_{2D}/0_4]_s$ and $[0_4/0_{2D}/0_2]_s$ laminates under bending load. These interlaminar stresses occur due to the offset effect, and thus, the same factors that were identified to affect the interlaminar stress distributions when only the offset effect is present in the previous sub-section affect the interlaminar stress distributions in the generic case as well.

The third effect is related to the fact that one can note, based on the discussions of the interlaminar stresses due to the termination and offset effects, that the only

interlaminar stress component that arises as a direct result of both effects is the interlaminar normal stress on the z^--face of the outer continuous plies in the undropped region. For all other interlaminar stresses on the z^--face of the outer continuous plies, only one of the two fundamental mechanisms has been identified as the primary mechanism that gives rise to them. The interlaminar shear stress on the z^--face of the outer continuous plies in the undropped region arises as a primary result of the termination effect, and the interlaminar shear and normal stresses on the z^--face of the outer continuous plies in the dropped region arise as a primary result of the offset effect. In generic laminates with internal ply dropoffs, the interaction of these two fundamental mechanisms gives rise to an interesting trend of the interlaminar normal stress along the interface between the terminated ply group and the continuous plies.

Since the interlaminar normal stresses along this interface include both the termination and offset effects, the stress distributions will possess the characteristics of both the interlaminar normal stresses due to the termination effect and due to the offset effect. Therefore, the characteristics of the interlaminar normal stresses when the two effects are combined can be anticipated by simple superposition. The general trend of the interlaminar normal stress distribution due to the termination effect was discussed in the previous sub-section, and an illustration of the distribution is shown in the top-left part of Figure 6.82. It is tensile and peaks at the cutoff, decreases and turns compressive and decays to zero far away from the cutoffs. The general trend of the interlaminar normal stress distribution due to the offset effect was also discussed, and an illustration of the distribution is shown in the top-right part of Figure 6.82. It is compressive and peaks at the cutoffs and decays monotonically to zero far away from the cutoffs. Assuming that the compressive stress due to the offset effect is slightly greater in magnitude, a simple superposition of the two stress distributions results in a distribution that is compressive away from the cutoffs and the magnitude monotonically increases until the tensile contribution from the termination effect becomes significant. At this point, a reversal in

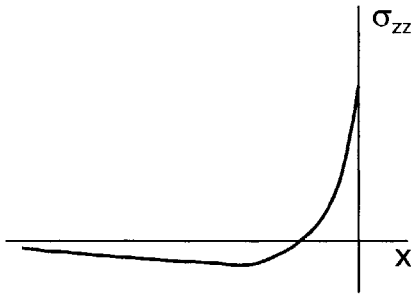

A Interlaminar normal stress distribution due to termination effect

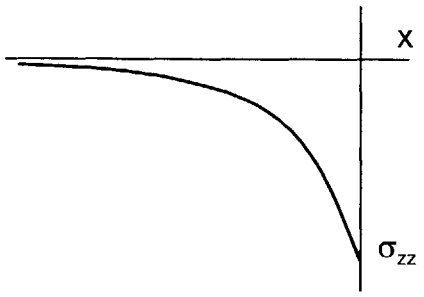

B Interlaminar normal stress distribution due to offset effect

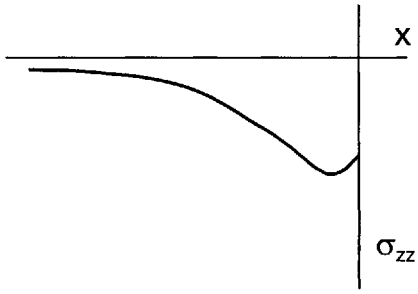

C Superposition of interlaminar normal stresses due to both effects with offset effect slightly greater

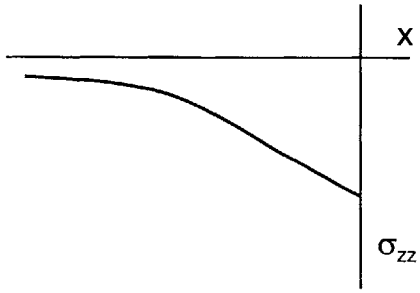

D Superposition of interlaminar normal stresses due to both effects with offset effect much greater

Figure 6.82 Illustration of interlaminar normal stresses in the undropped region in a generic laminate with internal ply dropoffs *(A)* due to the termination effect, *(B)* due to the offset effect, *(C)* due to both the termination and the offset effects when the magnitude of the offset effect is slightly greater, and *(D)* due to both the termination and the offset effects when the magnitude of the offset effect is much greater.

the trend will occur, and the magnitude of the interlaminar normal stress will decrease (see bottom-left part of Figure 6.82). Such "reversal trends" were observed, for example, in the bottom plot of Figures 6.50 where $[0_2/0_{2D}/0_4]_s$ laminates with three taper angles were considered and in the bottom plot of Figure 6.55 for the $[0_4/0_{2D}/0_2]_s$ and $[0_6/0_{2D}]_s$ laminates. If the compressive stress due to the offset effect is much greater in magnitude, the resulting distribution after superposition will simply follow the trend of the compressive stress (see bottom-right part of Figure 6.82). Such distributions were observed, for example, in the top plot of Figure 6.50 for the $[0_2/0_{2D}/0_4]_s$ laminate with a taper angle of 11.31° and in the bottom plot of Figure 6.55 for the $[0_2/0_{2D}/0_4]_s$ laminate.

6.4.3 Characteristics and Trends of Interlaminar Stresses

Based on the discussion of the mechanisms that cause interlaminar stresses in laminates with ply dropoffs in the preceding sub-sections, the key characteristics and trends of the interlaminar stress field of any laminate can be deduced through consideration of the termination and offset effects. In this sub-section, the key characteristics and trends of the interlaminar stress fields in laminates considered in the previous sections are briefly reexamined based on the insights of the two fundamental mechanisms to show the utility and applicability of such insights.

One of the factors identified as affecting the termination effect is the far-field load in the terminated ply group. If the magnitude of the far-field load in the terminated ply group increases, the magnitude of the interlaminar shear stress along the interface of the continuous and terminated plies in the undropped region increases since more load transfer needs to occur. The magnitude of the interlaminar normal stress along the same interface also increases, but this effect is generally not as discernible due to the superposition of the compressive interlaminar normal stress from the offset effect in the dropoff region as discussed in the previous sub-section. In Section 6.2.3, the magnitude of the far-field load in the terminated ply group was varied by considering laminates with terminated ply groups with virtual material properties that varied between 1% and 180%

of the stiffness of 0° plies. The in-plane load cases are shown in Figures 6.58 and 6.62, and the bending load case in Figure 6.60. As expected, the magnitude of the interlaminar shear stress along the interfaces of the continuous and terminated plies in the undropped region increases with increasing stiffness, and thus, increasing load-carrying of the terminated ply group.

The magnitude of the far-field load in the terminated ply group is also affected by the location of the terminated ply group when the laminate is under bending load. Since the far-field strain in laminates under bending load varies linearly through the thickness, the further the terminated ply group is located from the mid-plane the greater is the far-field stress, and thus load per unit width it carries. This explains the interlaminar shear stress along the interfaces of the continuous and terminated plies in the undropped region being greater in laminates with ply dropoffs located further away from the mid-plane as presented in Section 6.2.2. This trend can be seen specifically in Figure 6.56. Another example of the interlaminar shear stress along the interface of the continuous and terminated plies in the undropped region increasing with increasing magnitude of the far-field load in the terminated ply group can be found in Section 6.2.4 where laminates with the same number of continuous plies but different number of terminated plies were considered. The increasing trend of the interlaminar shear stress in the undropped region can be seen in the top plot of Figures 6.71 for the in-plane load case and the top plot of Figure 6.72 for the bending load case.

The offset effect, which gives rise to compressive interlaminar normal stresses along the interface of the continuous and terminated plies in the undropped region and tensile interlaminar normal stresses along the interface of the inner and outer continuous plies in the dropped region, is affected by the magnitude of the far-field load in the outer continuous plies. Since the magnitude of the far-field load increases with an increase in the number of outer continuous plies, the magnitude of the interlaminar normal stresses also increases. This trend can be seen in the bottom plot of Figure 6.55 where the

interlaminar normal stresses in $[0_2/0_{2D}/0_4]_s$, $[0_4/0_{2D}/0_2]_s$, and $[0_6/0_{2D}]_s$ laminates are shown. It can be seen that the magnitude of the interlaminar normal stress, and thus, the net normal force, increases with an increase in the number of outer continuous plies.

Another factor that affects the offset effect is the taper angle. As discussed in the previous sub-section, the taper angle affects the magnitude of the moment generated by the compressive and tensile interlaminar normal stresses in the undropped and dropped regions, respectively, because it is related to the distance between the undropped and dropped regions. This moment is needed to equilibrate the induced moment due to the misalignment of the far-field loads at the undropped and dropped ends. If the taper angle increases, the distance between the undropped and dropped regions decreases, and therefore, the interlaminar normal stresses must increase to maintain the magnitude of the moment needed to counter the induced moment. This trend is confirmed in the examples considered in Section 6.2.1 where $[0_2/0_{2D}/0_4]_s$ laminates with three taper angles were considered. It can be seen in Figures 6.50 and 6.52 that the interlaminar normal stresses in the undropped and dropped regions increase with increasing angles of taper.

The number of terminated plies is related to the offset distance between the lines of action of the far-field loads at the undropped and dropped ends of the outer continuous plies. Therefore, this factor also affects the interlaminar normal stresses in the undropped and dropped regions. In Section 6.4.4, three 16-ply laminates with one, two, and three symmetrically terminated plies were considered. It is seen in the bottom plots of Figures 6.71 and 6.72 that the interlaminar normal stress increases with an increase in the number of terminated plies. This is expected because an increase in the number of terminated plies increases the magnitude of the induced moment due to an increase in the offset distance of the far-field loads in the outer continuous plies in addition to an increase in the magnitude of the far-field load transferred from the terminated plies.

The preceding discussion shows that the characteristics and trends of the interlaminar stresses along key interfaces in the laminates with ply dropoffs that were

considered in this work can be anticipated based on the understanding of the two fundamental mechanisms that give rise to them. The utility of this understanding lies in the fact that they can be used to anticipate the trends of interlaminar stresses in laminates with more complex configurations than those considered in this work. Such insight would be particularly useful in preliminary design stages when many different laminate configurations and layups need to be considered. For example, the current understanding can be used to identify overall laminate configurations that alleviate the interlaminar stress concentrations.

CHAPTER 7

EXPERIMENTAL RESULTS

The results of the experimental work are presented and discussed in this chapter. The experiments were conducted on specimens with unidirectional layups and simple ply dropoff configurations in order to isolate the effect of the ply dropoffs. Specimens with six different ply dropoff configurations were tested under static and cyclic loads in order to observe damage/delamination processes and associated trends. These configurations varied in the number and through-thickness location of the terminated ply group. In the first section of the chapter, the damage/delamination initiation types and loads in specimens tested under static loads are presented. This is followed by a presentation of the damage/delamination initiation and growth characteristics observed in specimens tested under cyclic loads in section two. Finally, in section three, the results and implications of the damage/delamination characteristics and trends observed in the static and cyclic tests are discussed.

7.1 Static Tests

A typical stress-strain curve for the undropped region obtained from the static test specimens is shown in Figure 7.1. Since all specimens tested had 0° layups, the stress-strain curve of only one laminate (with a layup of $[0_{4D}/0_4]_s$) is shown. All other specimens exhibited similar behavior. Note that the stress-strain curve does not pass through zero stress and strain. This occurred because the strain gages on the specimens were not perfectly zeroed in the unstressed state. The stress is calculated by dividing the load obtained from the static test by the measured thickness and width of the undropped region of each specimen as shown in Table 5.3. The stress-strain curve is generally linear

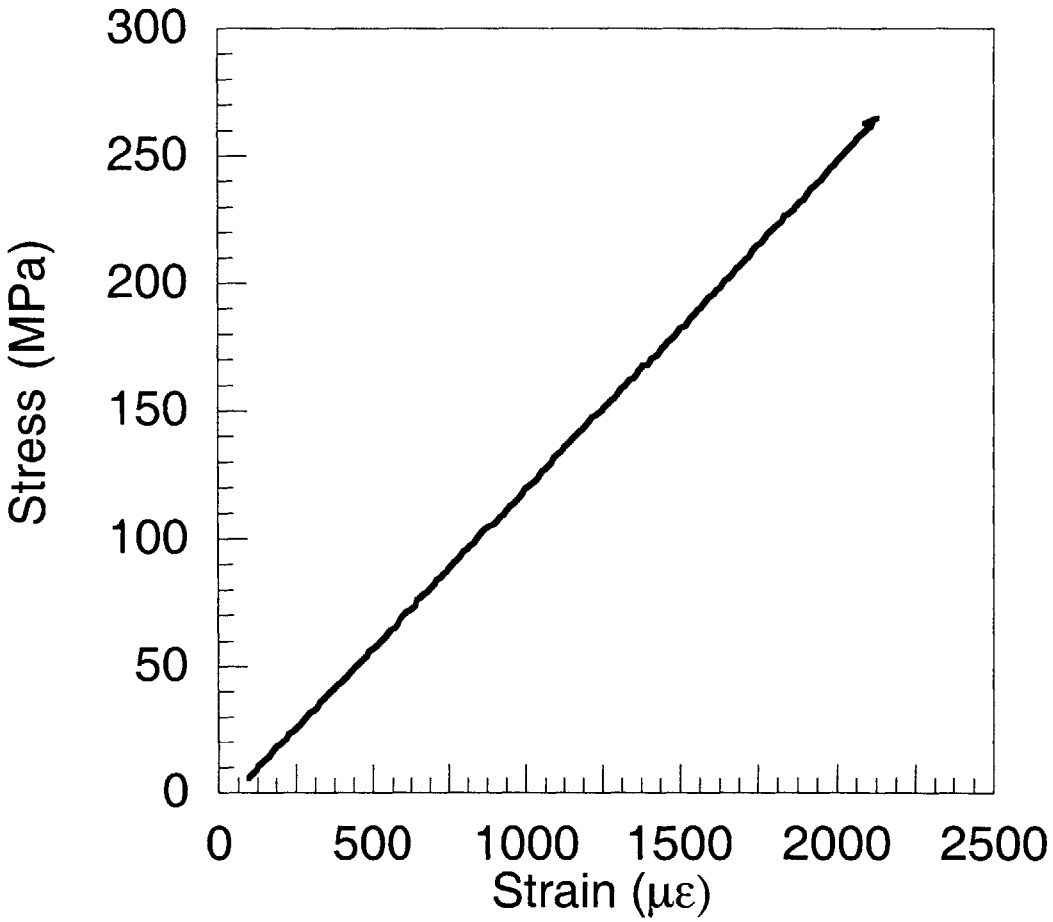

Figure 7.1 Typical stress-strain plot for the undropped region of the static test specimens.

over the entire range immediately before damage/delamination initiation. Thus, the longitudinal modulus of each specimen is calculated using a linear regression of such stress-strain curves. The average longitudinal modulus, E_{11}, of each specimen type is reported in Table 7.1. The average of the correlation coefficient squared, *i.e.*, R^2, for each specimen type is between 0.994 to 0.999. The average longitudinal modulus is 129 GPa, which is 9.1% lower than the manufacturer's reported longitudinal modulus of 142 GPa. All coefficients of variation of the longitudinal modulus for each specimen are less than 5.5%.

In all specimens, the first type of damage event to occur was matrix cracking in the resin-rich regions. These matrix cracks occurred at loads significantly lower than those at which any other damage/delamination was observed. The typical load at which these matrix cracks were observed to be first present is approximately half the static delamination load for each specimen type. The delamination loads are presented later in this sub-section. In some cases, a small drop in load and/or audible cracking noise accompanied the occurrence of these matrix cracks. The use of conservative values for the load drop margin (see Section 5.5) required the test to be stopped and inspected at frequent intervals even at low loads due to "false" stoppages. These false stoppages were useful as they allowed the detection of matrix cracks and subsequent monitoring of them.

The matrix cracks were clearly visible in the replications when viewed with a microscope. Photomicrographs of replications of the resin-rich regions in two laminates with external and internal ply dropoffs, corresponding to $[0_{2D}/0_6]_s$ and $[0_4/0_{2D}/0_2]_s$ layups, are shown in Figures 7.2 and 7.3, respectively. The matrix cracks in the two laminates shown in these figures are representative of those seen in other laminates with similar layups. In the specimen with external ply dropoffs shown in Figure 7.2, a single matrix crack can be seen at an angle to the vertical in the resin pocket with one end located at the interface of the continuous and terminated plies. In the specimen with internal ply dropoffs shown in Figure 7.3, matrix cracks can be seen at three different locations in

Table 7.1 Average longitudinal modulus for each specimen type tested under static load

Specimen Layup	Longitudinal Modulus [GPa]	Coefficient of Variation
$[0_{2D}/0_6]_s$	131	4.93 %
$[0_2/0_{2D}/0_4]_s$	131	5.43 %
$[0_4/0_{2D}/0_2]_s$	128	4.83 %
$[0_{4D}/0_4]_s$	128	3.07 %
$[0_2/0_{4D}/0_2]_s$	127	1.72 %
$[0_3/0_{4D}/0]_s$	130	1.61 %

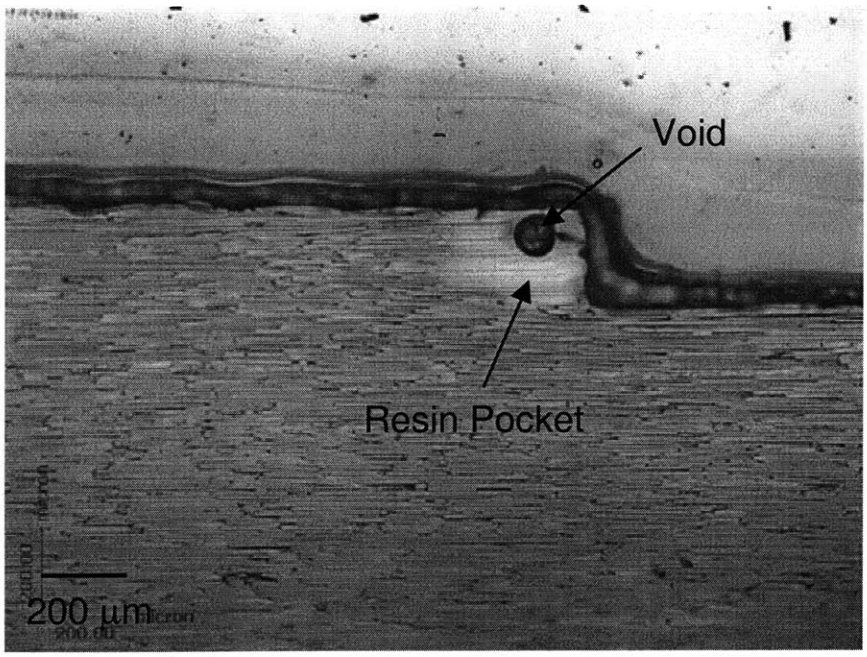

Prior to Load

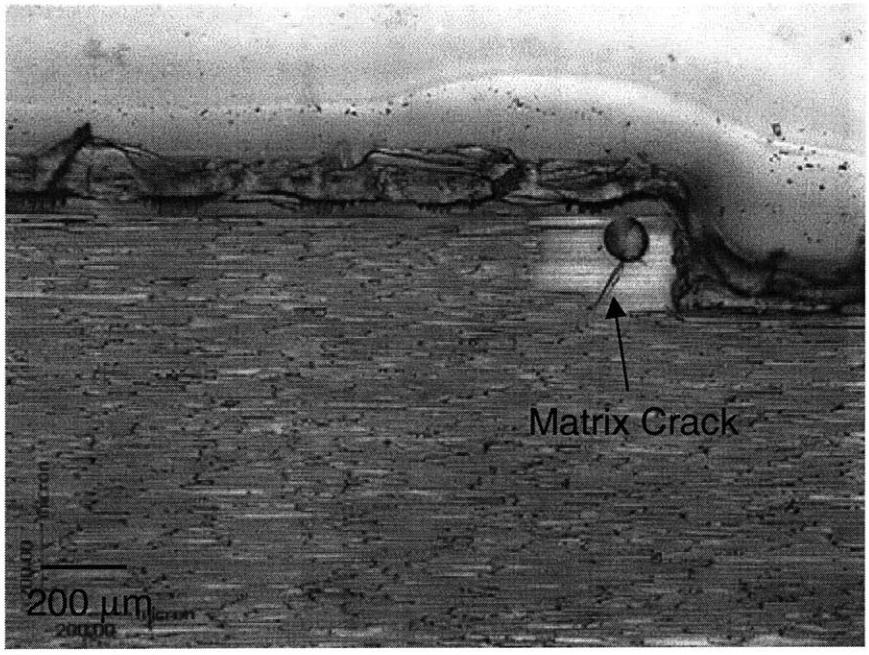

After Loading to 31.1 kN

Figure 7.2 Photomicrographs of edge replications of a $[0_{2D}/0_6]_s$ specimen *(top)* prior to load showing no matrix crack, and *(bottom)*, after loading to 31.1 kN (500 MPa) showing presence of matrix cracks.

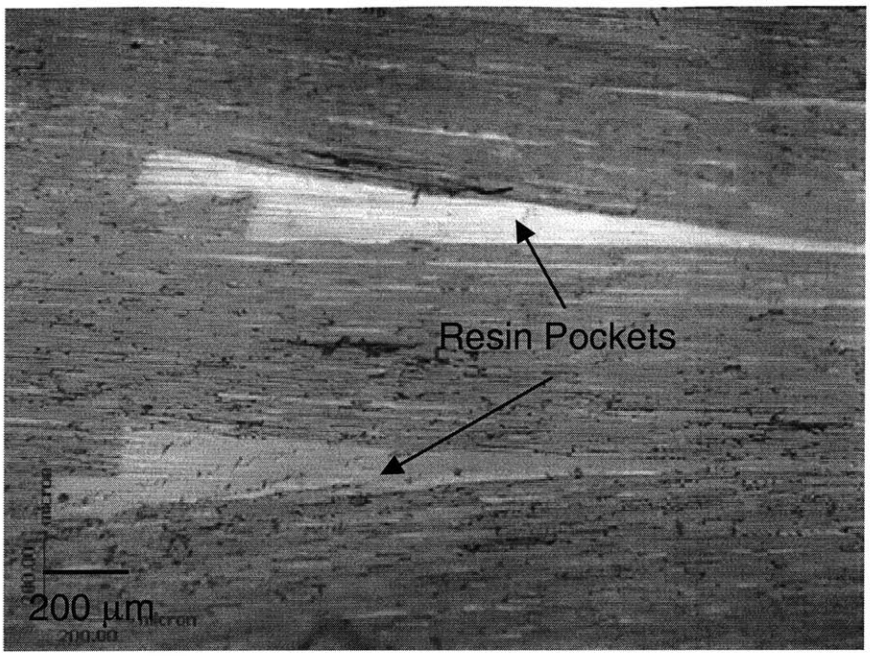

Prior to Load

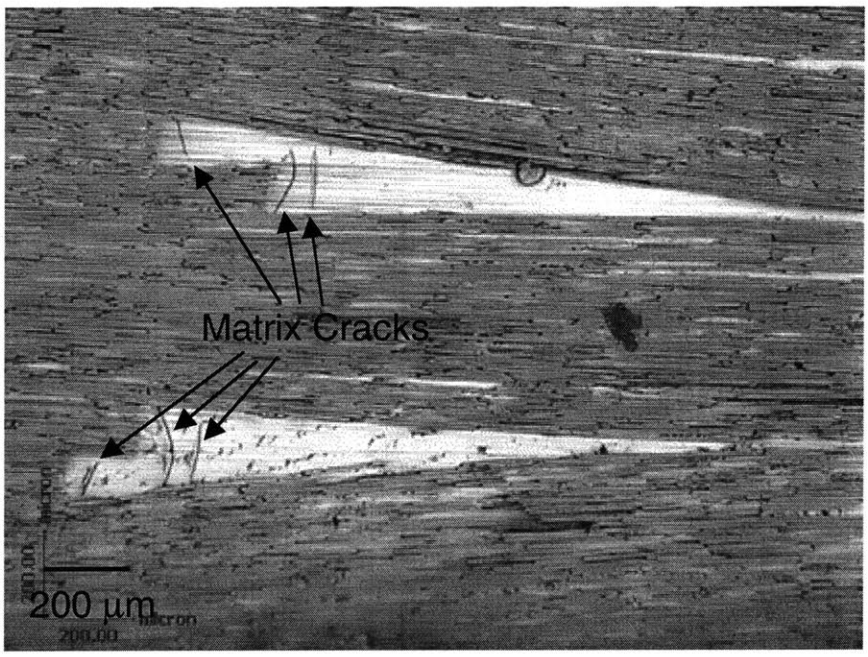

After Loading to 47.8 kN

Figure 7.3 Photomicrographs of edge replications of a $[0_4/0_{2D}/0_2]_s$ specimen *(top)* prior to load showing no matrix cracks, and *(bottom)*, after loading to 47.8 kN (758 MPa) showing presence of matrix cracks.

each resin pocket. Note that the resin pockets consist of a main, triangular region and a secondary, trapezoidal region due to a step in the ply dropoffs. The two bow-shaped cracks appeared near the base of the resin pocket perpendicular to the applied load in the triangular region, while another shorter crack appeared in the trapezoidal region. In general, the shorter cracks in the trapezoidal region occurred first followed by the two bow-shaped cracks. These matrix cracks often appeared at both edges of the laminates at corresponding locations. This suggests that the cracks extend across the width of the specimens. The location and shapes of the matrix cracks in both specimens with internal and external ply dropoffs were very uniform. These observations serve to validate to a first order the assumption in the analytical model that the terminated ply group is stress-free at the cutoffs and that the resin pockets do not carry any load prior to delamination formation.

Damage/delamination other than matrix cracking in the resin pockets generally occurred at loads approximately twice as high as the load at which matrix cracks were initially observed. Delaminations observed in many of the specimens appeared with other damage modes. Due to the difference in geometry of the specimens with external and internal ply dropoffs, there is a difference in the damage types exhibited by the two types of specimens. The damage types in specimens with external ply dropoffs are generally uniform compared to those with internal ply dropoffs, which exhibit several damage types that are more complex. The damage/delamination characteristics observed in specimens with external and internal ply dropoffs are thus described separately.

In specimens with external ply dropoffs, delaminations occurred along the interfaces of the continuous and terminated plies in the undropped region. The occurrence of delamination was usually sudden. A drop in load and audible cracking noise accompanied delamination with typical load drops ranging between 4 N and 130 N. Such load drops occurrences can be clearly seen in plots of load versus time. In most specimens, the length of the delaminations was significant enough such that they could be

detected with the naked eye when viewed from the edges. However, in other specimens, the length of the delaminations was on the order of several ply thicknesses and could not be detected with the naked eye. Such delaminations were detected via edge replication. A replication of a typical delamination is shown in Figure 7.4. The photomicrograph shows a closeup view of the delaminated edge in the vicinity of the dropoff location in a specimen with 4-ply dropoffs. The delaminations along the upper and lower interfaces of the continuous and terminated plies can be clearly seen.

The delaminations were generally unsymmetric about the mid-plane, *i.e.*, delamination occurred on only one face, front or back. In addition, some delaminations extended across the entire width of the specimen, while others extended only a short distance across the width from one edge. In some cases, these shorter delaminations ended with a ply split in the terminated ply group. A diagram of a specimen with external ply dropoffs with delaminations is shown in Figure 7.5 to illustrate the shorter delamination with a ply split. On the front face of the specimen, a delamination that extends some distance across the width and ends with a ply split is shown. Such delaminations were visible with the naked eye from the front or back of the specimen because they lifted up as depicted in the figure.

The extent of the delamination across the width of the specimen in cases where delaminations did not end with ply splits (and thus, did not lift up) can be best observed through x-ray photographs, or radiographs, using dye penetrant. The alternate method of inferring the extent of delamination from the replications of the two edges is not as reliable since information about the interior regions of the specimen cannot be obtained. Radiographs of all the specimens were taken after the static tests were completed. In Figure 7.6, two radiographs of the delaminated region that represent those that were observed in some of the specimens with external ply dropoffs are shown. The delaminated regions appear darkest in the radiographs due to the dye penetrant used. The undropped and dropped regions are represented via the lighter shades of gray regions as

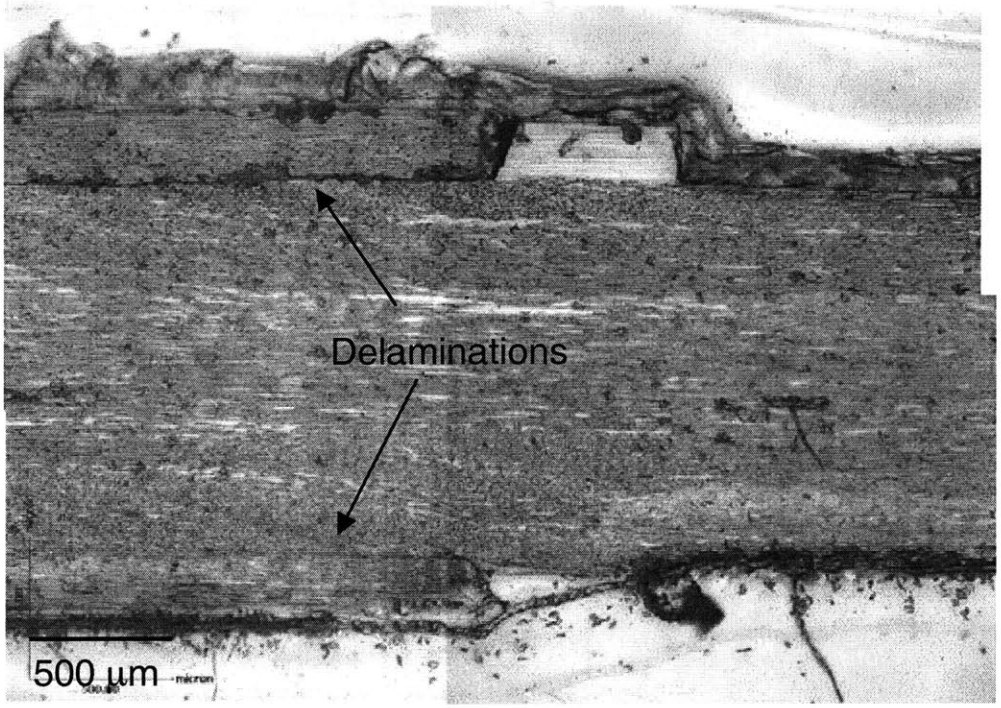

Figure 7.4 Photomicrograph of an edge replication of a $[0_{2D}/0_6]_s$ specimen with external ply dropoffs showing presence of delaminations.

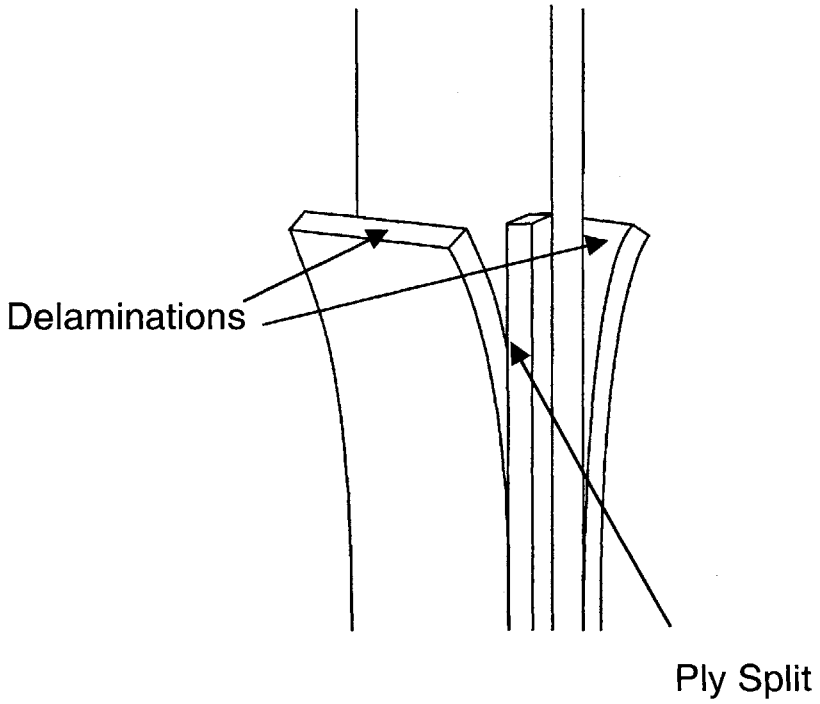

Figure 7.5 Diagram of specimen with external ply dropoffs with delamination extending from one edge across the width and ending in a ply split.

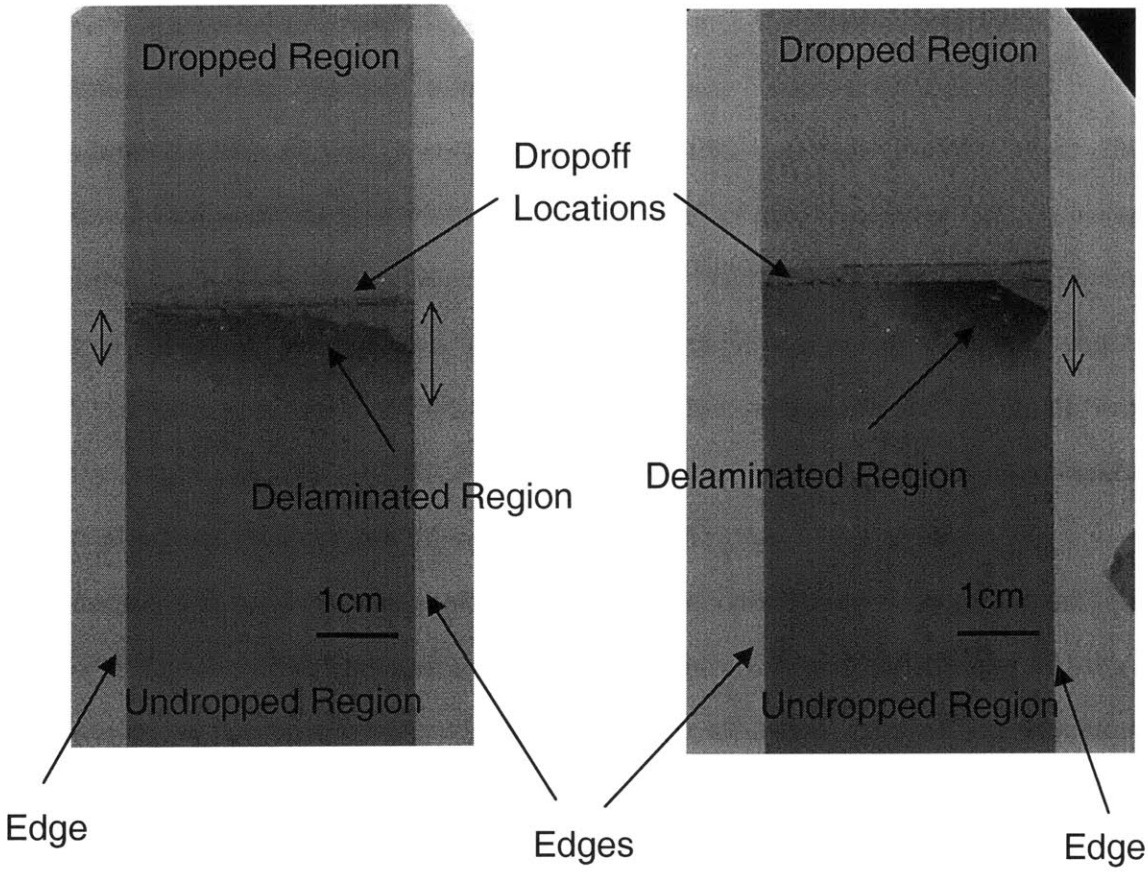

Figure 7.6 Radiographs of $[0_{4D}/0_4]_s$ specimens with *(left)* delamination that extends across the entire width, and *(right)*, delamination that spans approximately half the width.

indicated in the figure. The delamination in the specimen on the left side of the figure extends across the entire width of the specimen, while the delamination in the specimen on the right side spans approximately half the width of the specimen from one edge. In the lengthwise direction, the length of both delaminations is approximately 1 cm at the left edges as indicated by the arrows. The length of the delamination in the specimen on the left side is approximately 0.5 cm at the right edge.

In the specimens with 4-ply dropoffs, two out of four specimens delaminated on both faces. In both specimens with delaminations on either faces, the delaminations ended with ply splits as shown in Figure 7.7. None of the specimens with 8-ply dropoffs delaminated on both faces. In two of the specimens with 8-ply dropoffs, the delamination on one face extended across the entire width of the specimens, while in the other two specimens, the delamination extended a short distance from one edge. These delaminations did not end with ply splits.

The damage types observed in laminates with internal ply dropoffs were a combination of transverse matrix cracks, delaminations and/or ply splits. The damage types can be broadly divided into three distinct types as subsequently described. These damage types are not mutually exclusive, *i.e.*, two damage types were observed simultaneously in some specimens.

The first damage type, or Type I, is characterized by delaminations at the edges of the specimen. These delaminations occurred either along the interfaces of the continuous and terminated plies in the undropped region and along the interface of the inner and outer continuous plies in the dropped region or started from a transverse matrix crack at the edge of the specimen. Transverse matrix cracks generally occurred across one or two plies through the thickness where the nominally 0° fiber directions had small local angular variations at the edges due to manufacturing irregularities. These transverse matrix cracks serve as initiation points for delaminations along the length, similar to angle-ply splits. These delaminations do not extend very far across the width of the

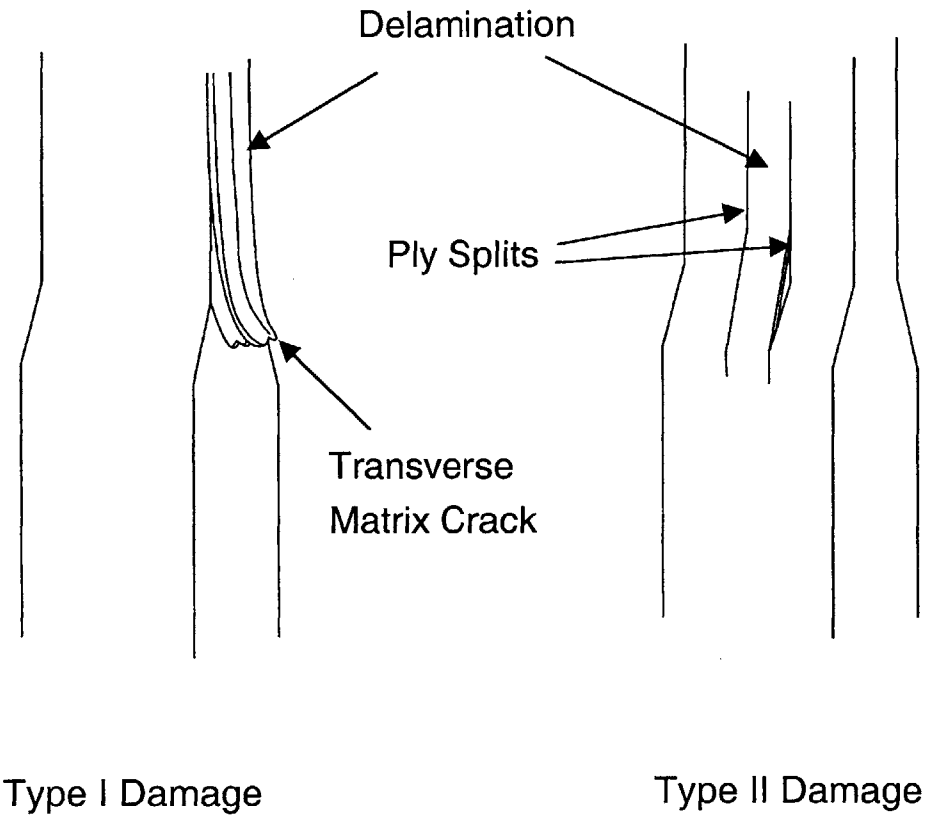

Figure 7.7 Diagrams of specimens with internal ply dropoffs showing *(left)* delamination starting from a transverse matrix crack or splinter corresponding to Type I damage, and *(right)*, delamination in the mid-section of the laminate bounded by ply splits corresponding to Type II damage.

specimens, since the local angular variations are very small. Thus, such delaminations at the edge resemble splinters, especially when the delaminated region detaches from the edge. Therefore, this form of delamination is referred to as a "splinter". A diagram of a splinter is shown on the left side of Figure 7.7. For specimens that exhibited Type I damage, the delamination load was taken to be the load at which delamination first occurred. The transverse matrix cracks that give rise to subsequent splintering occurred very shortly before delamination in some specimens.

A photomicrograph of an edge replication of a specimen that exhibited Type I damage is shown in Figure 7.8. A splinter can be seen at the edge in the dropoff region in the lower-half of the specimen in addition to a delamination along the interface of the inner and outer continuous plies in the dropped region and along the interface of the continuous and terminated plies in the undropped region. The delamination along the interface is obscured by the excess glob of replicating material, which formed due to overflow of cellulose acetate into the delaminated interface during replication.

The second damage type, or Type II, is characterized by delaminations bounded by ply splits in the mid-section of the laminate. These delaminations were clearly visible when the specimen was under load as the delaminated region "popped" out-of-plane. Such delaminations could not be detected at the edges via replication. A drop in load and an audible cracking noise usually accompanied the occurrence of such delaminations with the typical load drop ranging between 40 N and 200N. A diagram of a specimen with a delamination bounded by ply splits is shown on the right side of Figure 7.7. For specimens that exhibited Type II damage, the delamination load was taken to be the load at which the delaminated region popped out.

The extent of delamination across the width of specimens that exhibited Type II damage can be assessed using the radiographs taken after the testing was completed. Two radiographs of $[0_3/0_{4D}/0]_s$ specimens with delaminations are shown in Figure 7.9. The delaminated region appears dark in the radiographs due to the dye penetrant used. In

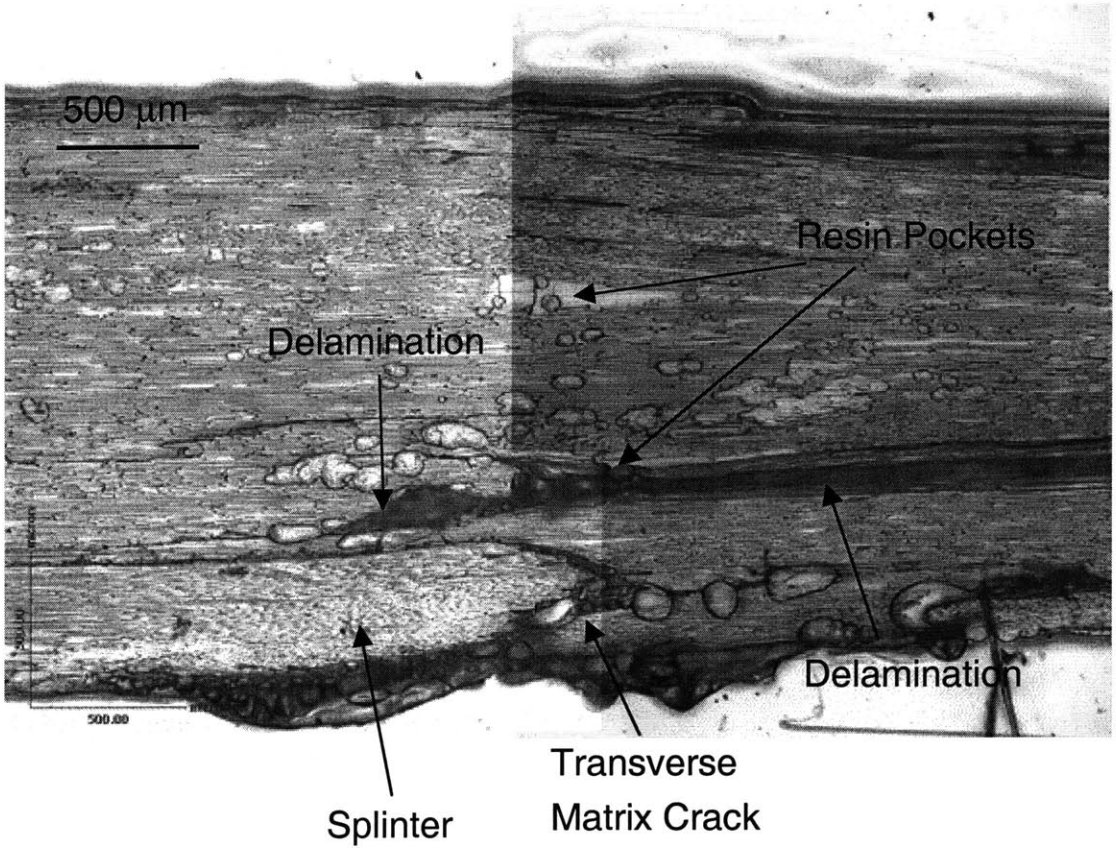

Figure 7.8 Photomicrograph of an edge replication of a $[0_4/0_{2D}/0_2]_s$ specimen with delaminations corresponding to Type I damage.

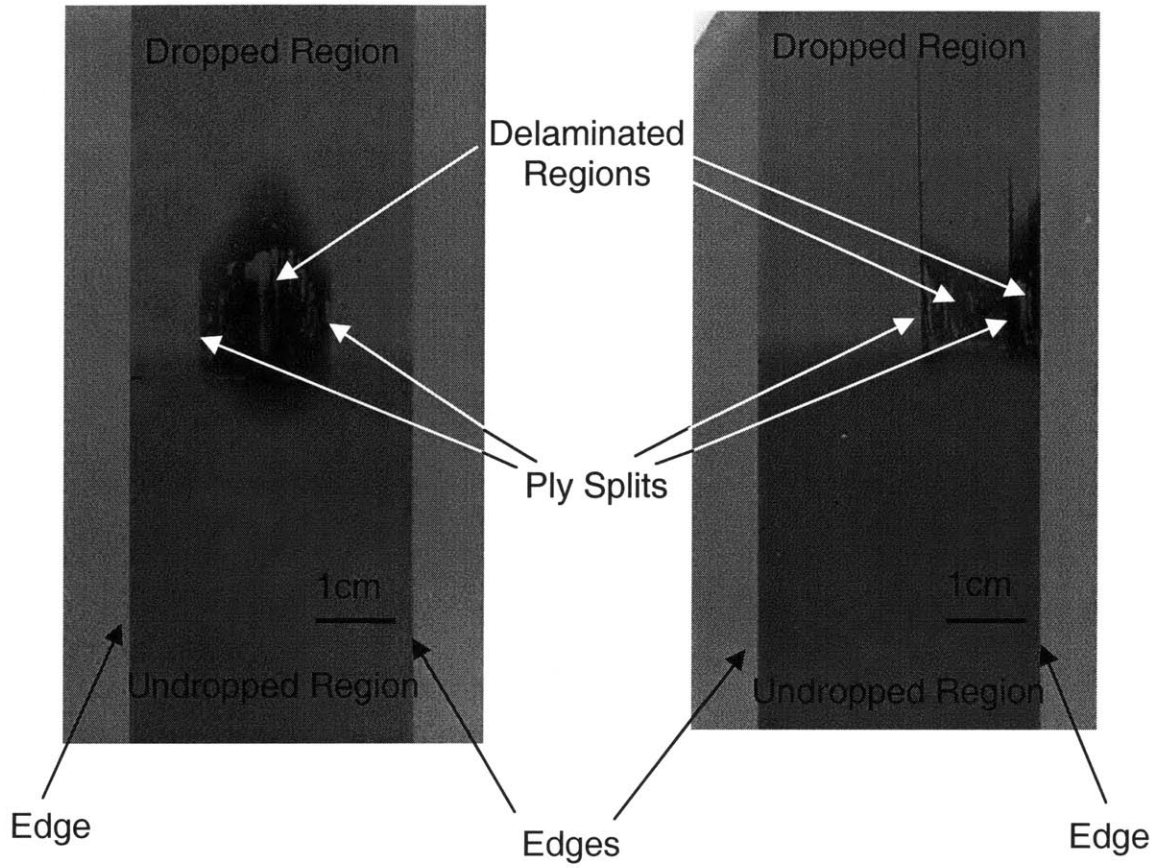

Figure 7.9 Radiographs of $[0_3/0_{4D}/0]_s$ specimens with *(left)* delamination in the mid-section bounded by ply splits corresponding to Type II damage, and *(right)*, two delaminated regions, one in the mid-section bounded by ply splits corresponding to Type II damage, and another extending from the right edge to the ply split corresponding to Type I damage.

the specimen on the left side of Figure 7.9, the delamination occurred in the mid-section of the specimen and is bounded by ply splits. This corresponds to Type II damage. In the specimen on the right side of Figure 7.9, there are two distinct delaminated regions. One delaminated region exists in the mid-section and is bounded by ply splits, while the other extends from the right edge to a ply split. As mentioned previously, each damage type was not exclusively seen in each specimen. This specimen exhibited a combination of Type I and Type II damages. Note that in both specimens shown in Figure 7.9, the delamination in the dropped region is significantly longer than that in the undropped region. Similar trends were seen in all specimens that exhibited Type II damage.

The third type of damage, or Type III, is catastrophic failure such that the specimen could not support any load. Catastrophic failure occurred in some specimens before any apparent delaminations detectable through replication of the edges, the naked eye, or load drop were observed. A photograph of a specimen that exhibited this damage type is shown in Figure 7.10.

The damage types observed in all specimens with internal ply dropoffs tested under static loads are shown in Table 7.2. More laminates with internal ply dropoffs exhibited damage type I than any other damage type, with 11 out of 16 specimens (69%) showing this type of damage. Type II damage was observed in four specimens, while Type III damage occurred in three specimens. Note that in two specimens, both Type I and Type II were observed (*e.g.*, see specimen on the right side of Figure 7.9). Based on the edge replications and radiographs of the 13 specimens that exhibited Type I or Type II damage or a combination of the two, delaminations were generally observed in the undropped, dropoff, and dropped regions. The length of the delaminations in the undropped region was on the order of 1 mm while that in the dropped region was an order of magnitude longer. In four specimens, delamination was found either in the undropped region only, or in the undropped and dropoff regions. In addition, as in the case of specimens with external ply dropoffs, the delaminations in specimens with

Figure 7.10 Photograph of a $[0_4/0_{2D}/0_2]_s$ specimen after catastrophic failure.

Table 7.2 Damage types observed in specimens with internal ply dropoffs[1]

Specimen Layup	Damage Types		
	Type I	Type II	Type III
$[0_2/0_{2D}/0_4]_s$	3	0	1
$[0_4/0_{2D}/0_2]_s$	3	0	1
$[0_2/0_{4D}/0_2]_s$	2	1	1
$[0_3/0_{4D}/0]_s$	1 +2[2]	1 +2	0
Total	9 +2	2 +2	3

[1] Damage types are classified as:

Type I: matrix cracks, delaminations and/or angle ply splitting

Type II: delamination in mid-section only (bounded by ply splits)

Type III: catastrophic failure

[2] Indicates both damage types I and II observed.

internal ply dropoffs were generally unsymmetric about the mid-plane.

The average static delamination load of each specimen type is shown in Table 7.3 along with the coefficient of variation. Specimens that failed catastrophically were not included in calculating the average delamination load. The average delamination stresses in the undropped region calculated using the delamination load and the measured thickness and width of each specimen group are also shown in Table 7.3. The coefficients of variation of the delamination loads are within 8% (and 6% for the delamination stresses) for all specimens.

These results indicate that the static delamination loads can vary significantly depending on the number and location of the terminated plies. In general, the delamination loads of specimens with 4-ply dropoffs are higher by approximately a factor of two compared to those of specimens with 8-ply dropoffs. This can be seen, for example, by taking the ratio of the delamination loads for the $[0_{2D}/0_6]_s$ specimens and the $[0_{4D}/0_4]_s$ specimens. In addition, it can be seen that the delamination loads for laminates with internal ply dropoffs are higher than those for laminates with external ply dropoffs by a factor of approximately two. The delamination load of specimens with internal ply dropoffs located further away from the mid-plane, *i.e.*, those with layups of $[0_2/0_{2D}/0_4]_s$ and $[0_2/0_{4D}/0_2]_s$, have slightly higher delaminations load than those with internal ply dropoffs located closer to the mid-plane, *i.e.*, those with layups of $[0_4/0_{2D}/0_2]_s$ and $[0_3/0_{4D}/0]_s$.

7.2 Fatigue Tests

The fatigue tests were conducted at load levels based on the static delamination loads. To ensure that the specimens did not fail statically, the maximum static delamination loads for the purposes of calculating the maximum cyclic test loads were set equal to the average static delamination loads minus one standard deviation. The average

Table 7.3 Delamination initiation loads and stresses (calculated for undropped region)

Specimen Layup	Initiation Load [kN]	Initiation Stress [MPa]
$[0_{2D}/0_6]_s$	33.4 (10.4%)[1]	544 (7.93%)
$[0_2/0_{2D}/0_4]_s$	67.2 (9.65%)	1090 (6.84%)
$[0_4/0_{2D}/0_2]_s$	59.3 (6.69%)	978 (6.04%)
$[0_{4D}/0_4]_s$	16.5 (8.64%)	268 (7.33%)
$[0_2/0_{4D}/0_2]_s$	36.3 (9.35%)	600 (7.82%)
$[0_3/0_{4D}/0]_s$	29.9 (4.23%)	491 (3.47%)

[1] Coefficient of variation in parentheses.

static delamination load minus one standard deviation is referred to as the "maximum static load" for convenience.

The three specimens in each specimen group were tested at three different maximum cyclic load levels chosen between 60% and 86% of the maximum static loads. Relatively high load levels were chosen to test the first specimen from each specimen group to increase the probability of delaminations initiating before 100,000 cycles, which was defined as run-out. For specimens with external ply dropoffs, the first specimens were tested at maximum cyclic load levels of 70% of the maximum static load, while for the specimens with internal ply dropoffs, the first specimens were tested at 80% of the maximum static load. Subsequent tests on specimens from each specimen group were performed at higher load levels if delaminations initiated close to run-out or did not initiate in the first specimen. Lower load levels were used if delaminations initiated during the fatigue test before 10,000 cycles. The maximum and minimum cyclic loads used in the fatigue test are shown in Table 7.4. As mentioned in Chapter 5, a stress ratio of 1/8 was used for all specimens. Note that two specimens in the $[0_3/0_{4D}/0]_s$ specimen group were tested at similar load levels of 80% of the maximum static load but with different inspection cycles of 10,000 cycles and 1,000 cycles. The former specimen was the first specimen to be tested under fatigue, and was used as a trial to set a suitable inspection interval. The inspection interval was chosen to be 1,000 to 5,000 cycles based on this test. The latter specimen was tested at the same load level to obtain more detailed delamination initiation data.

7.2.1 Damage Initiation

Matrix cracks in the resin pockets generally occurred prior to delamination initiation and were observed during the first several inspection intervals. These matrix cracks occurred at the same locations as those observed in specimens tested under static load. Photomicrographs of edge replications of the dropoff region in one specimen with external ply dropoffs and another with internal ply dropoffs are shown in Figure 7.11. It

Table 7.4 Maximum and minimum loads used in fatigue tests[1]

Specimen Layup	Percentage of Maximum Static Load	Maximum Cyclic Load [kN]	Minimum Cyclic Load [kN]
$[0_{2D}/0_6]_s$	60.0%	18.0	2.24
	65.0%	19.5	2.43
	70.0%	21.0	2.62
$[0_2/0_{2D}/0_4]_s$	73.0%	44.3	5.54
	75.0%	45.6	5.69
	80.0%	48.6	6.08
$[0_4/0_{2D}/0_2]_s$	75.0%	41.5	5.19
	80.0%	44.3	5.54
	82.3%	45.6	5.70
$[0_{4D}/0_4]_s$	60.0%	9.0	1.13
	65.0%	9.8	1.22
	70.0%	10.5	1.32
$[0_2/0_{4D}/0_2]_s$	69.5%	22.9	2.86
	75.0%	24.7	3.08
	80.1%	26.3	3.29
$[0_3/0_{4D}/0]_s$	79.8%	22.8	2.85
	80.0%	22.9	2.86
	86.3%	24.7	3.08

[1] R = 1/8 for all tests.

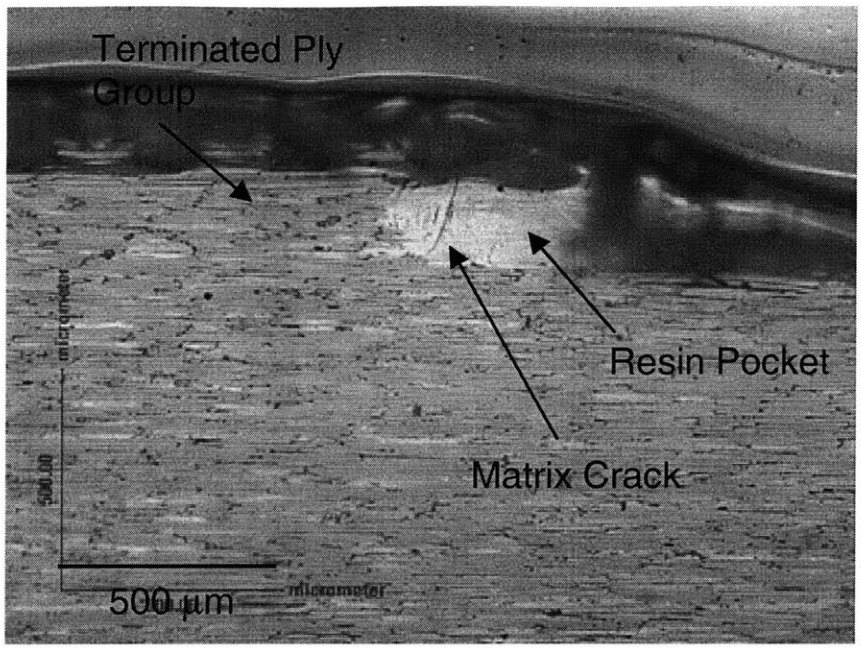

$[0_{2D}/0_6]_s$ Specimen

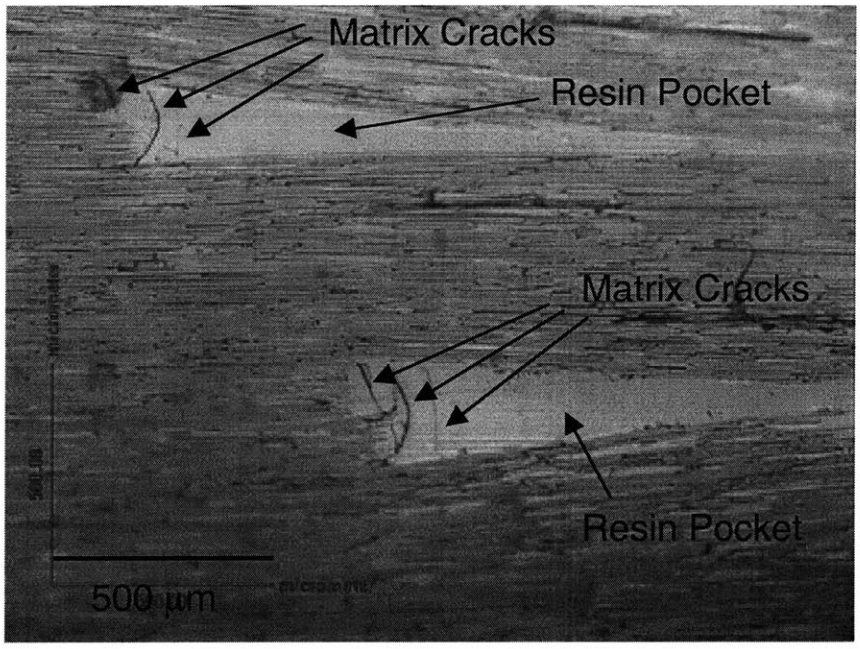

$[0_2/0_{2D}/0_4]_s$ Specimen

Figure 7.11 Photomicrographs of edge replications taken during fatigue testing of *(top)* a $[0_{2D}/0_6]_s$ specimen, and *(bottom)*, a $[0_2/0_{2D}/0_4]_s$ specimen showing presence of matrix cracks in the resin pockets.

can be seen from the replication of the specimen with external ply dropoffs that the matrix crack occurred in the resin pocket at an angle to the vertical with one end located at the interface of the continuous and terminated plies. In the specimen with internal ply dropoffs, the replication shows that three matrix cracks occurred in each resin pocket. The matrix cracks in both specimens are very similar to those shown in Figures 7.2 and 7.3 for the laminates tested under static load.

In specimens with external ply dropoffs, delaminations initiated along the interfaces of the continuous and terminated plies in the undropped region. The initial delaminations were on the order of 1 mm in length, and in general, occurred only in one-half of the specimen edge, *i.e.*, delaminations tended to initiate unsymmetrically about the mid-plane. Delaminations initiated at both left and right edges in about half of the specimens with external ply dropoffs, while delaminations initiated at one edge in the other cases. Since the initial delaminations were very short, they were generally not visible with the naked eye, and therefore, edge replications were used. A photomicrograph of a replication of a $[0_{2D}/0_6]_s$ specimen is shown in Figure 7.12. The delamination initiated after 6,000 cycles in the specimen shown. A delamination of length approximately 0.5 mm can be seen along the interface of the continuous and terminated plies.

In specimens with internal ply dropoffs, delaminations generally initiated along interfaces of two plies in the undropped, dropoff and dropped regions. In most specimens, the delaminations initiated at one edge (left or right). The length of the initial delaminations in the dropped region was generally much longer than that in the undropped region, with the length in the dropped region varying between approximately 3 mm to 8 mm and in the undropped region between 0.5 mm and 1 mm. Two specimens with four internal ply dropoffs delaminated before run-out. Initial delaminations in these specimens were detected using edge replication and observed to be unsymmetric about the mid-plane, *i.e.*, they occurred only in one-half of the specimen. In the two specimens

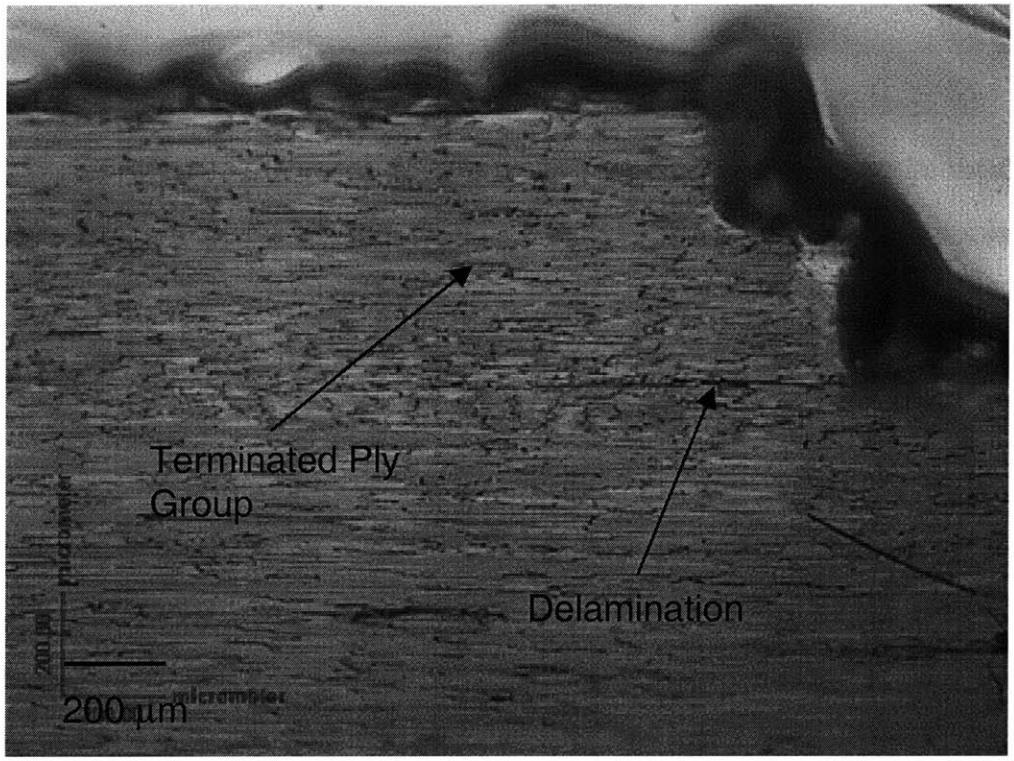

Figure 7.12 Photomicrograph of an edge replication taken during fatigue testing of a $[0_{2D}/0_6]_s$ specimen with delamination initiated along the interface of the continuous and terminated plies.

with 4-ply dropoffs that delaminated, the initial delaminations occurred along one interface between two continuous plies in the dropped region and along the interfaces of the continuous and terminated plies in the undropped region. Photomicrographs of an edge replication of a $[0_4/0_{2D}/0_2]_s$ specimen are shown in Figure 7.13. The photomicrograph in the top part of the figure shows the undropped and dropoff regions, and the photomicrograph on the bottom part of the figure shows the dropoff and dropped regions. A sketch of the specimen is shown in the middle part of the figure indicating the general regions shown in the two photomicrographs. In the photomicrograph in the top part of the figure, the initial delaminations in the undropped region have lengths of approximately 0.3 mm and can be clearly seen along the two (upper and lower) interfaces of the continuous and terminated plies. In the replication in the bottom part of the figure, the initial delamination in the dropped region can be clearly seen along the inner and outer continuous plies. The length of this delamination is approximately 8.2 mm.

Four specimens with eight internal ply dropoffs exhibited delamination initiations that were observed using edge replications during fatigue testing. The initial delaminations in these specimens generally occurred at multiple interfaces. Delaminations were not only observed along interfaces of outer and inner continuous plies in the dropped region, but they were also found along other interfaces of two continuous plies in the dropped region. Delaminations along the interfaces of the continuous and terminated plies in the undropped region were observed in two specimens, while in the other two, none were observed. A photomicrograph of an edge replication of a $[0_3/0_{4D}/0]_s$ specimen is shown in Figure 7.14. The delaminations observed in this specimen are representative of those seen in the other specimens. Four delaminations along different interfaces are seen in the dropoff and dropped regions. In the lower-half of the specimen edge, a delamination occurred along the interface of the inner and outer continuous plies in the dropped region. This delamination extends into the dropoff region as well. Another delamination that spans the dropoff and dropped

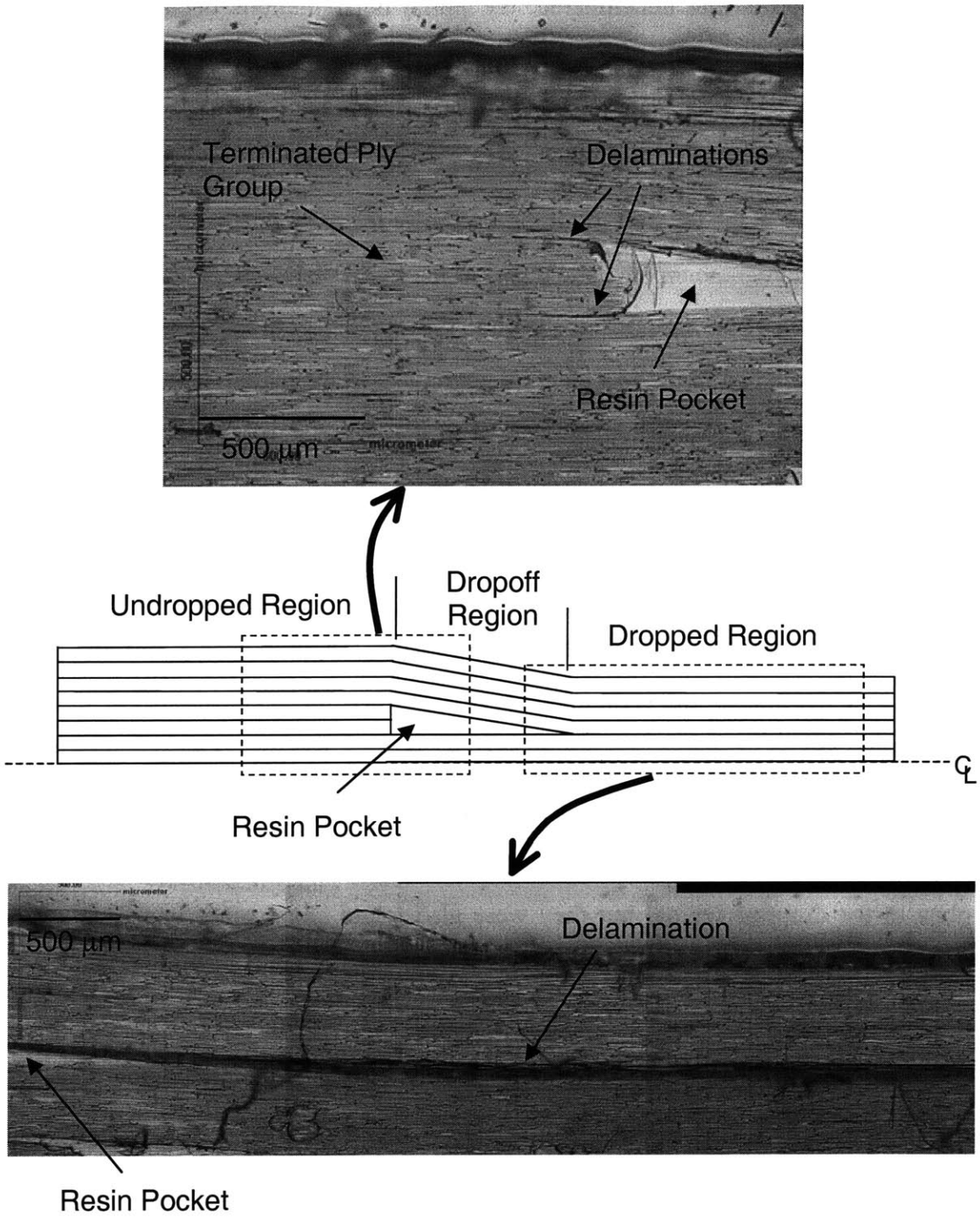

Figure 7.13 Photomicrographs of an edge replication taken during fatigue testing of a $[0_4/0_{2D}/0_2]_s$ specimen with initial delamination *(top)* along the interfaces of the continuous and terminated plies in the undropped region, and *(bottom)*, along the interface of the inner and outer continuous plies in the dropped region.

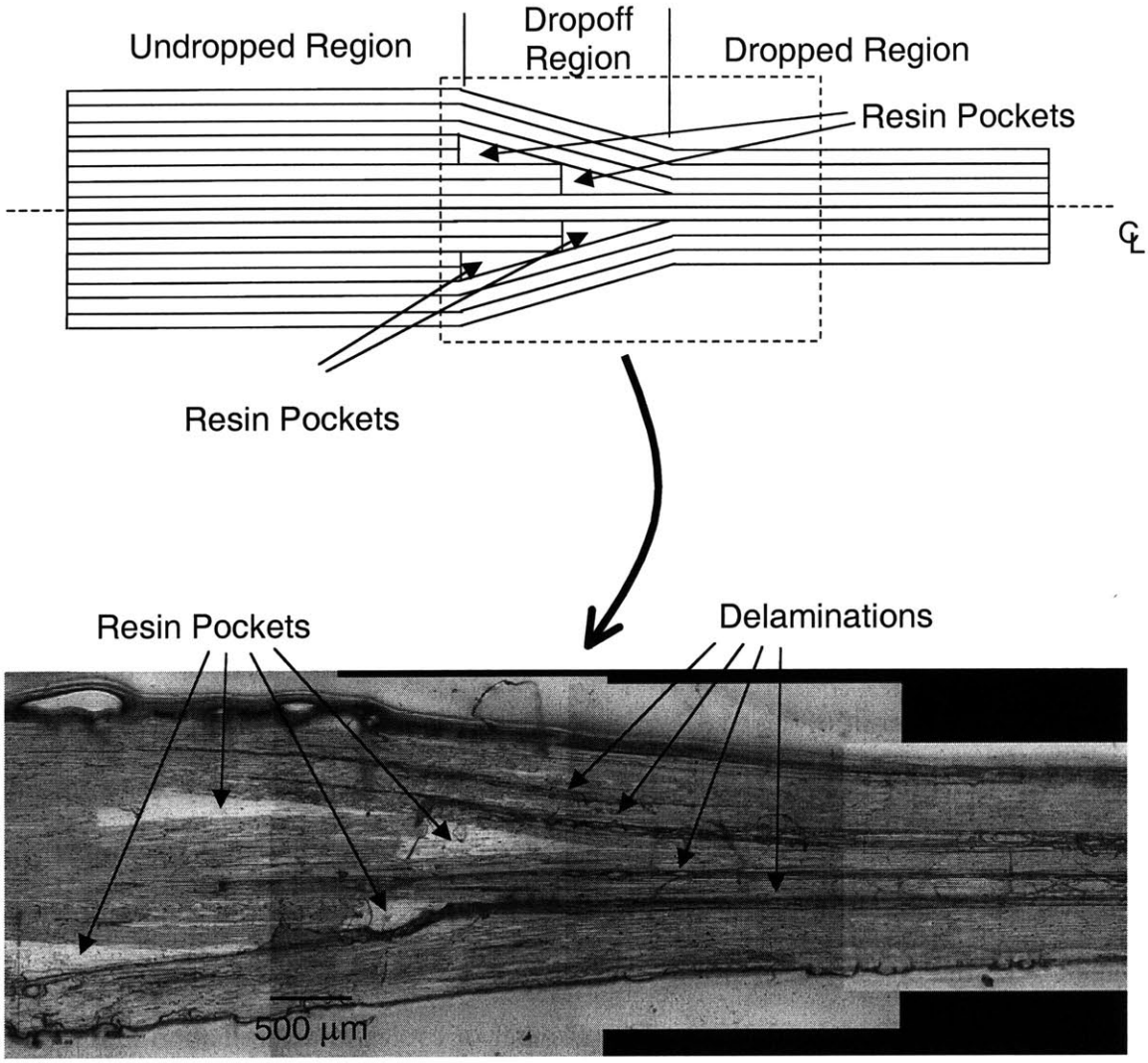

Figure 7.14 Photomicrograph of an edge replication taken during fatigue testing of a $[0_3/0_{4D}/0]_s$ specimen with initial delaminations along four interfaces in the dropoff and dropped regions.

regions is seen along the mid-plane of the specimen. In the upper-half of the specimen edge, two delaminations above the interface of the inner and outer continuous plies occurred. The delamination closer to the interface of the inner and outer continuous plies is significantly longer than the delamination above it. The initial delamination closest to the upper surface of the laminate is present only in the dropoff region, while the other three initial delaminations that extend into the dropped region were comparable in length (approximately 7 mm) with a difference of less than 1 mm among them. In this specimen, no initial delaminations were observed in the undropped region.

Three specimens with eight internal ply dropoffs exhibited ply splits along with initial delaminations. In two such specimens, the delamination initiated only in the mid-section of the specimen bounded by ply splits such that the initiation event could not be detected using edge replication. These delaminations resemble Type II damage described for the specimens tested under static loads. However, in one such specimen, the ply split was close to one edge of the specimen, and the delaminated region extended to the edge in the proximity of the ply split such that it could be observed using replicating tapes.

The number of cycles to delamination initiation is defined as the number of cycles at which delamination is first detected at the edges during inspection using edge replication. For the two specimens that exhibited delamination initiation only in the mid-section, the number of cycles at which the ply splits are first observed was recorded and taken to be the number of cycles to delamination initiation since such ply splits always occurred along with delaminations. The number of cycles to delamination initiation for each specimen tested are shown in Table 7.5. In 11 out of the 18 specimens (61%), initial delaminations that can be viewed from the edges occurred. In two specimens, initial delaminations did not extend to the edges and were observed via visual inspection of the specimen faces for ply splits. In 5 out of the 18 specimens (28%), delaminations were not observed after the full testing of 100,000 cycles. These are considered as run-outs. The results show that in four of the six specimen types, delaminations initiated earlier in

Table 7.5 Number of cycles to delamination initiation from fatigue tests

Specimen Layup	Percentage of Maximum Static Load	Maximum Cyclic Load [kN]	Number of Cycles to Initiation
$[0_{2D}/0_6]_s$	60.0%	18.0	10,000
	65.0%	19.5	6,000
	70.0%	21.0	2,000
$[0_2/0_{2D}/0_4]_s$	73.0%	44.3	run-out[1]
	75.0%	45.6	run-out
	80.0%	48.6	4,000
$[0_4/0_{2D}/0_2]_s$	75.0%	41.5	run-out
	80.0%	44.3	44,000
	82.3%	45.6	run-out
$[0_{4D}/0_4]_s$	60.0%	9.0	run-out
	65.0%	9.8	3,000
	70.0%	10.5	6,000
$[0_2/0_{4D}/0_2]_s$	69.5%	22.9	55,000
	75.0%	24.7	42,000[2]
	80.1%	26.3	1,000
$[0_3/0_{4D}/0]_s$	79.8%	22.8	20,000
	80.0%	22.9	14,000
	86.3%	24.7	2,000[2]

[1] Run-out defined as 100,000 cycles.

[2] Number of cycles to delamination initiation based on ply splits.

specimens that were tested under higher maximum cyclic loads, as expected. For example, in the $[0_2/0_{4D}/0_2]_s$ specimen group, delaminations initiated at 55,000 cycles when tested at a maximum cyclic load of 69.5% of the static delamination load, at 42,000 cycles when tested at 75.0%, and at 1,000 cycles when tested at 80.1%. In two of the six specimen types, some specimens that were tested at higher maximum cyclic loads delaminated later than those tested at lower loads. This reflects the amount of scatter in the results, which is not unexpected in fatigue testing [56].

The results shown in Table 7.5 are shown again in the form of plots in Figures 7.15 and 7.16. In these figures, the number of cycles to delamination initiation, or initiation life, is plotted against the maximum cyclic load expressed as a percentage of the maximum static load on a semi-log scale for each specimen tested. In Figure 7.15, the initiation lives of specimens with 4-ply dropoffs are shown. Note that the arrows next to data points indicate specimens that exhibited no delaminations and are considered to have run-out. A curve-fit trend line for the specimen group with four external ply dropoffs using the three data points obtained from the fatigue test is shown in Figure 7.15. The trend line is obtained using a logarithmic regression, and the R^2 value is 0.957. Trend lines for the two specimens groups with four internal ply dropoffs are not obtained due to insufficient data points. Similarly, the initiation lives of specimens with 8-ply dropoffs are shown in Figure 7.16 along with logarithmic curve-fit trend lines for the two specimen groups with internal ply dropoffs. The R^2 value is 0.775 for the $[0_2/0_{4D}/0_2]_s$ specimen group and 0.987 for the $[0_3/0_{4D}/0]_s$ specimen group. For the specimen group with eight internal ply dropoffs, a trend line is not obtained due to insufficient data points.

The plots in Figures 7.15 and 7.16 show two interesting trends. One is that the specimen groups with internal ply dropoffs tend to exhibit longer initiation lives compared to those with the same number of external ply dropoffs when loaded cyclically under a maximum cyclic load that is the same percentage of the maximum static load for

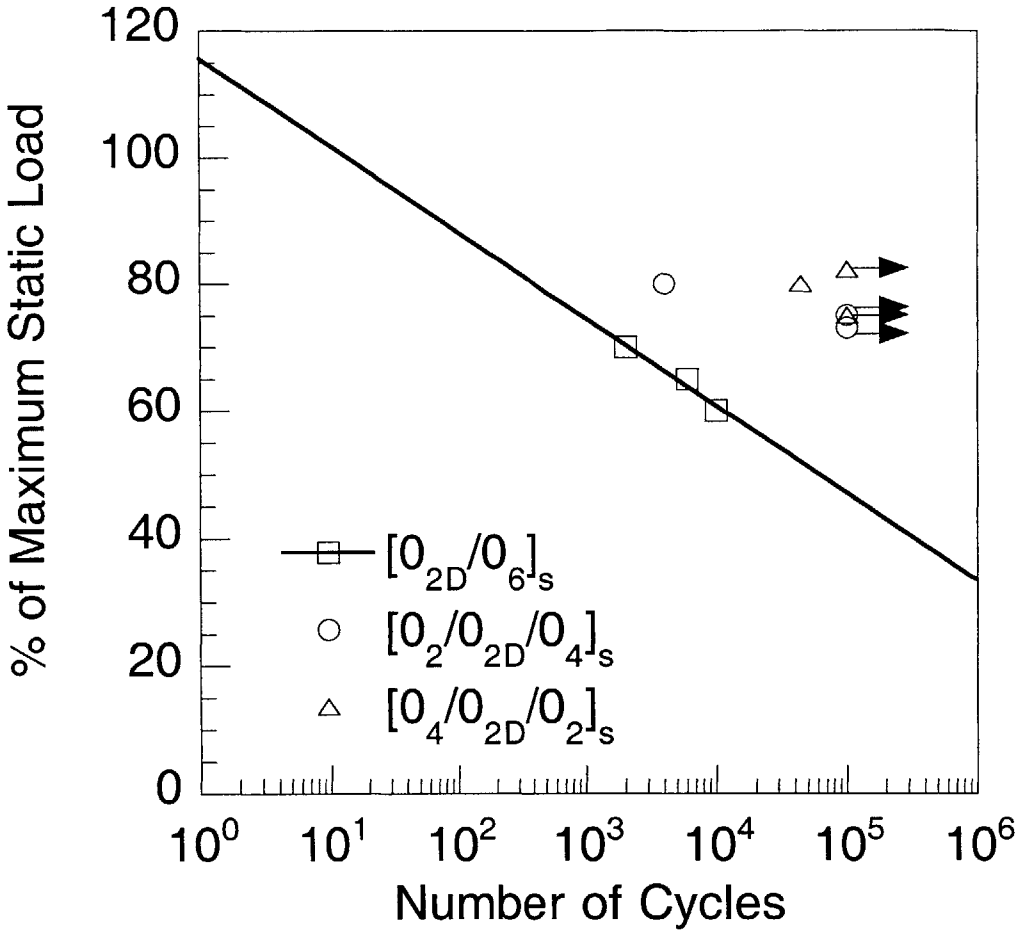

Figure 7.15 Initiation life curves (maximum cyclic load versus number of cycles to initiation) for specimens with 4-ply dropoffs.

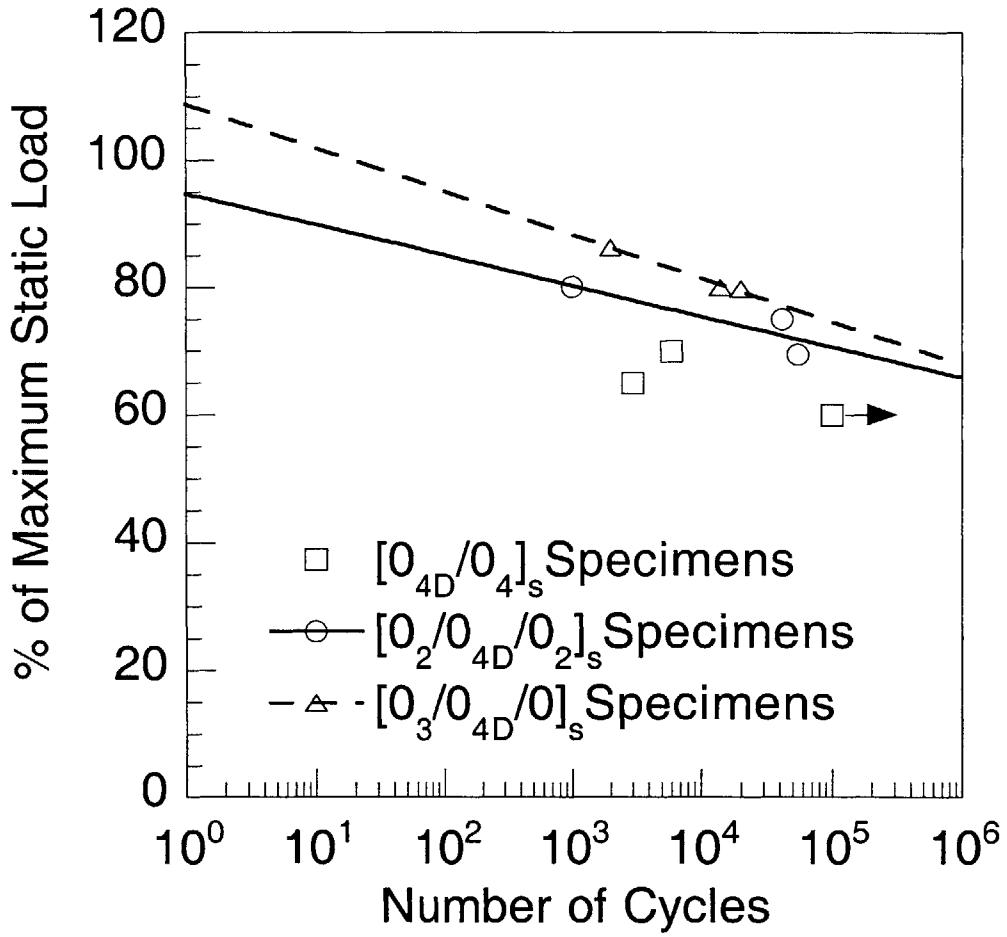

Figure 7.16 Initiation life curves (maximum cyclic load versus number of cycles to initiation) for specimens with 8-ply dropoffs.

each specimen group. This trend can be observed in both the specimen groups with four and eight ply dropoffs. In Figure 7.15, it can be seen that the two non-runout data points for the specimens with four internal ply dropoffs lie above the trend line for the specimen group with four external ply dropoffs. Similarly, in Figure 7.16, the two non-runout data points for the specimen group with eight external ply dropoffs lie below the trend lines for the specimen groups with eight internal ply dropoffs. This implies that laminates with internal ply dropoffs have greater "resistance" to delamination initiation under fatigue loads in general. Another trend is that the $[0_3/0_{4D}/0]_s$ specimen group has a longer initiation life compared to the $[0_2/0_{4D}/0_2]_s$ specimen group when loaded cyclically under a maximum cyclic load that is the same percentage of the maximum static load for each specimen group. In Figure 7.16, it can be seen that the trend line for the $[0_3/0_{4D}/0]_s$ specimen lies above the trend line for the $[0_2/0_{4D}/0_2]_s$ specimen group. This shows that laminates with internal ply dropoffs located closer to the mid-plane may have greater "resistance" to delamination initiation under fatigue loads in general. Although trend lines are not available for the specimens with four internal ply dropoffs due to insufficient non-runout data points, it can be seen that the two non-runout data points in Figure 7.15 are consistent with this trend in that the $[0_4/0_{2D}/0_2]_s$ specimen has a longer initiation life compared to the $[0_2/0_{2D}/0_4]_s$ specimen. It is emphasized, however, that both trends described herein are based on relatively few data points, and more testing would be required to obtain conclusive trends.

7.2.2 Damage Growth

The specimens in which delaminations initiated had testing continued to 100,000 cycles in order to determine growth characteristics of the delaminations and any associated damage. In specimens with external ply dropoffs, the initial delaminations at the edges along the interfaces of the continuous and terminated plies in the undropped region simply grew in length. In addition, new delaminations initiated along the interfaces of continuous and terminated plies that had not previous delaminated. These

grew in length under subsequent loading. After 100,000 cycles, specimens with external ply dropoffs generally exhibited delaminations along both interfaces of the continuous and terminated plies in the undropped region. The delaminations also extended across the entire width of the specimens. This was confirmed through radiographs taken after the fatigue tests were completed. A radiograph of a typical specimen with external ply dropoffs is shown in Figure 7.17. It can be seen from the figure that the delamination spans the entire width of the specimen, and the length of the delamination, which is indicated by the arrows, is approximately 1.3 cm at the left edge and 1 cm at the right edge.

In the specimens with internal ply dropoffs, the initial delaminations continued to grow in length with further load cycling. In addition, new delaminations along interfaces that had previously not delaminated occurred. The initial and new delaminations grew to significant lengths in the undropped region, along the entire length of the specimen in one case, while those in the dropped region did not increase significantly in length. In the widthwise direction, two trends were observed. In some specimens, the delaminations grew across the entire width of the specimen such that delaminations were seen on both edges (left and right). Such delaminations were seen in three specimens with internal ply dropoffs. Two photographs of the undropped region of the $[0_2/0_{4D}/0_2]_s$ specimen after 100,000 cycles when delamination had extended across the entire width and length of the undropped region are shown in Figure 7.18. The delaminations that occurred in this specimen are representative of the delaminations in the other two specimens. The photograph in the top part of Figure 7.18 shows a close-up view of the dropoff and undropped regions. A glob of residue from the cellulose acetate is seen in the upper-half of the dropoff region. Delaminations are seen to have occurred symmetrically in the undropped, dropped and dropoff regions. In the undropped region, it can be seen that delaminations occurred along all four interfaces of the continuous and terminated plies. The photograph in the bottom part of Figure 7.18 shows a larger view of the same

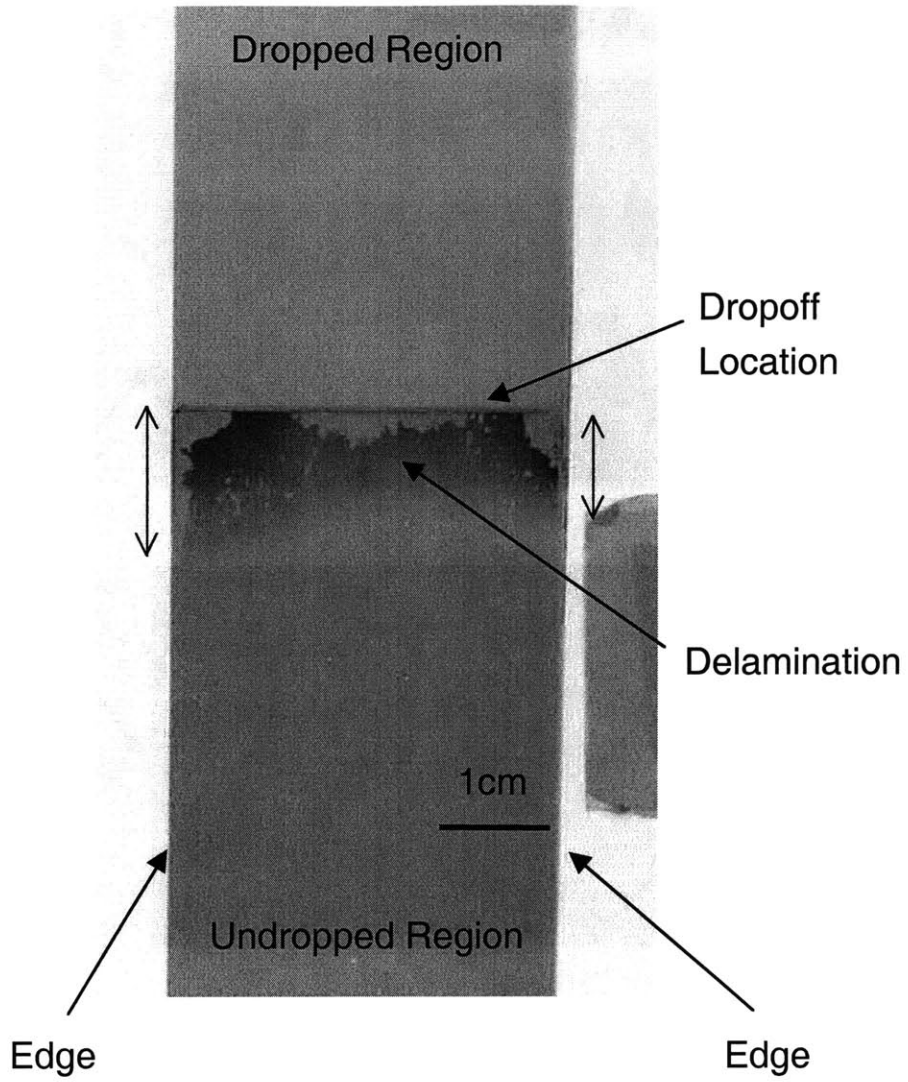

Figure 7.17 Radiograph taken after completion of fatigue testing (100,000 cycles) of a $[0_{2D}/0_6]_s$ specimen with external ply dropoffs showing delamination (arrows adjacent to edges indicate extent of delamination).

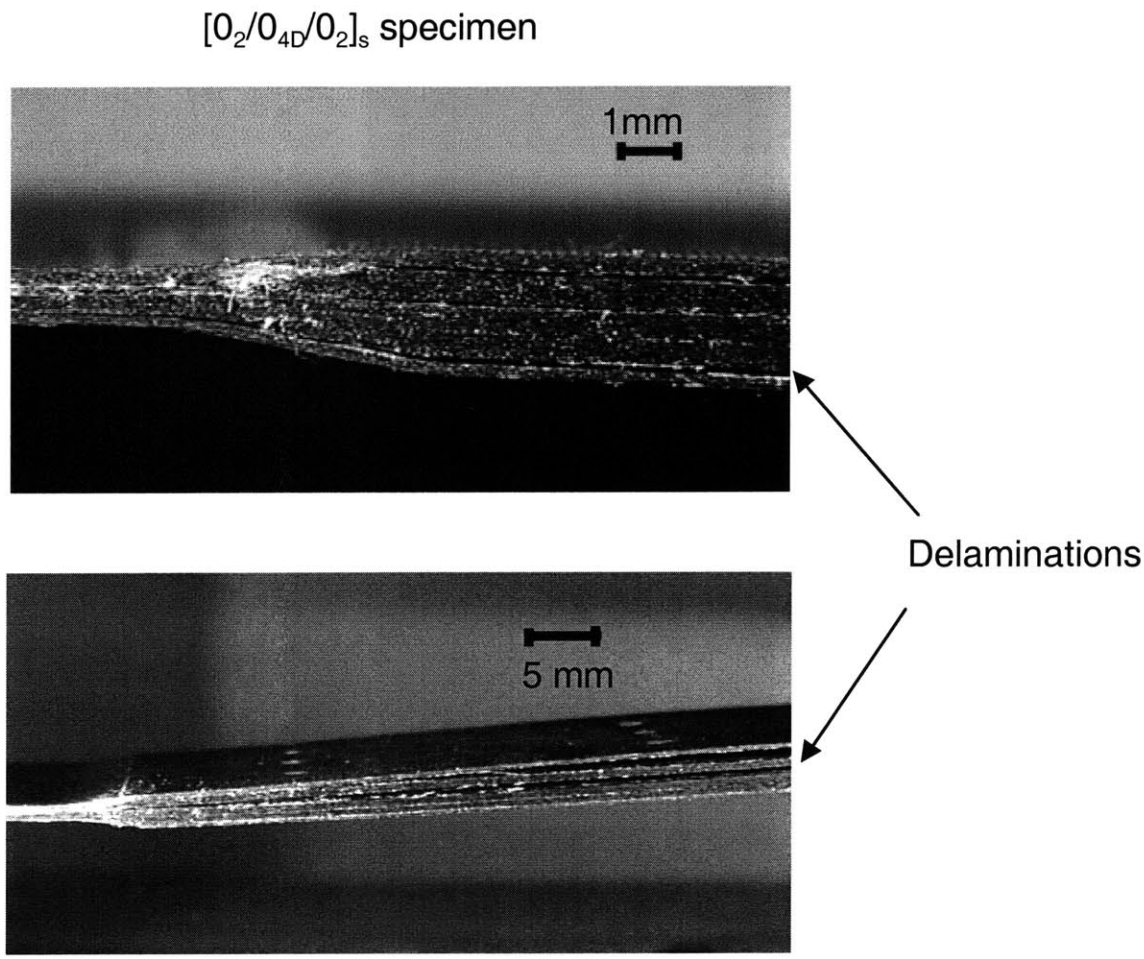

Figure 7.18 Photographs taken after completion of fatigue testing (100,000 cycles) of a $[0_2/0_{4D}/0_2]_s$ specimen where the delamination grew across the entire width and length in the undropped region.

specimen. The dropped and dropoff regions on the left are shiny from the glare produced by the flash when the photograph was taken. A lateral force was applied to the specimen to produce bending such that the delaminated regions opened and can be seen clearly. Note that these specimens can continue to carry load through their continuous plies despite the delaminations.

In the remainder of the specimens with internal ply dropoffs, the delaminated region did not grow across the entire width of the specimen. Such specimens showed two types of damage/delamination growth behavior. In some specimens, the delaminations grew in the lengthwise direction mainly in the undropped region without extension in the widthwise direction. A radiograph taken after 100,000 cycles of a $[0_3/0_{4D}/0]_s$ specimen that exhibited this behavior is shown in Figure 7.19. It can be seen that the delaminated region is bounded by the right edge of the specimen and a ply split to the left. Note the length of the delaminated region in the undropped region is greater than that in the dropped region. Since the initial delamination in the dropped region was much greater in length compared to that in the undropped region. This implies that the delamination grew faster in the undropped region than in the dropped region. In other specimens, additional delaminations that were either bounded by two new ply splits or a ply split and one edge of the specimen occurred. In such specimens, the length of the delamination in the undropped region tended to grow faster than the length of the delamination in the dropped region. Radiographs taken after 100,000 cycles of two specimens that exhibited this type of behavior are shown in Figure 7.20. In the left side of the figure, a $[0_3/0_{4D}/0]_s$ specimen with two distinct delaminated regions each bounded by a ply split and one edge is shown. In this specimen, the delamination in the left edge occurred first and the delamination in the right edge occurred under continued testing. The radiograph of a $[0_2/0_{4D}/0_2]_s$ specimen in the right side of Figure 7.20 shows multiple delaminated regions bounded by ply splits that occurred under continued cyclic loading. For this specimen, the sequence of occurrence of the delaminated regions is not very clear because the

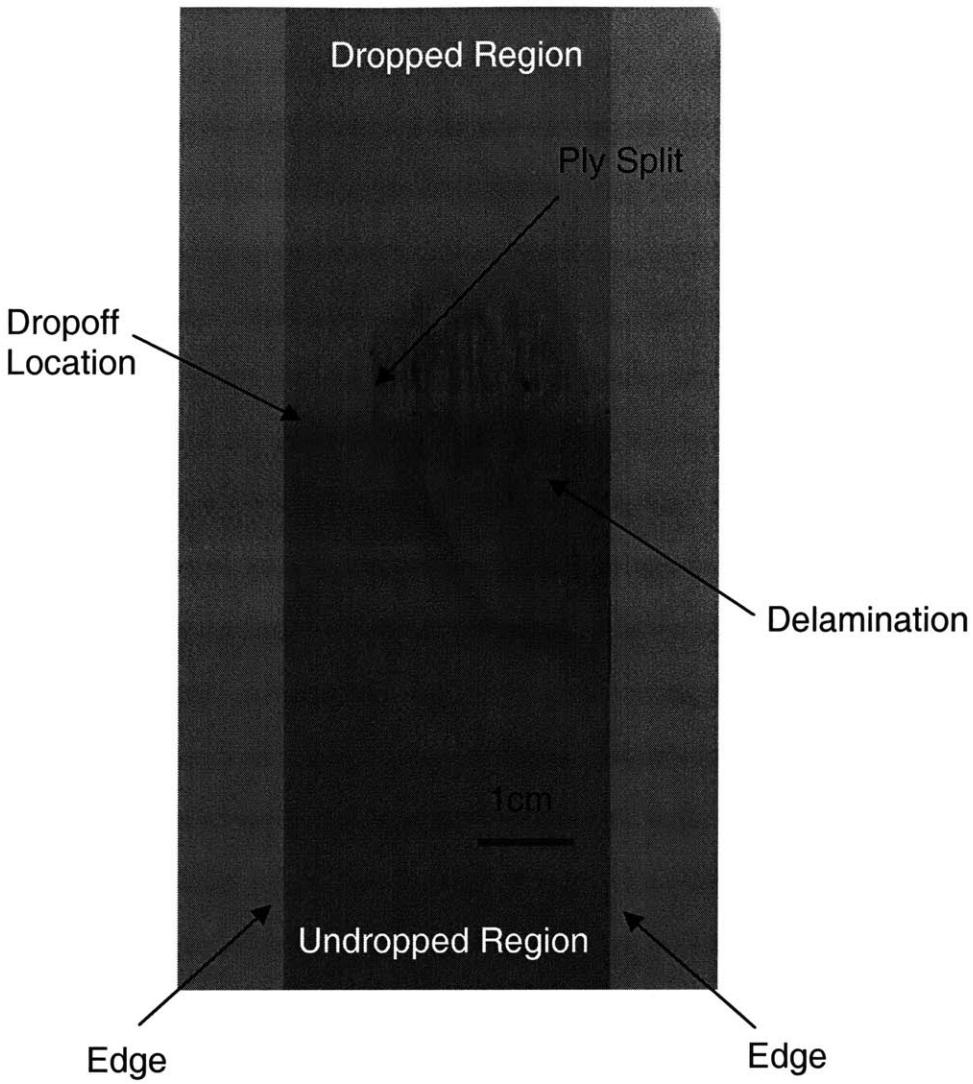

Figure 7.19 Radiograph taken after completion of fatigue testing (100,000 cycles) of a $[0_3/0_{4D}/0]_s$ specimen showing delamination bounded by a ply split and the right edge.

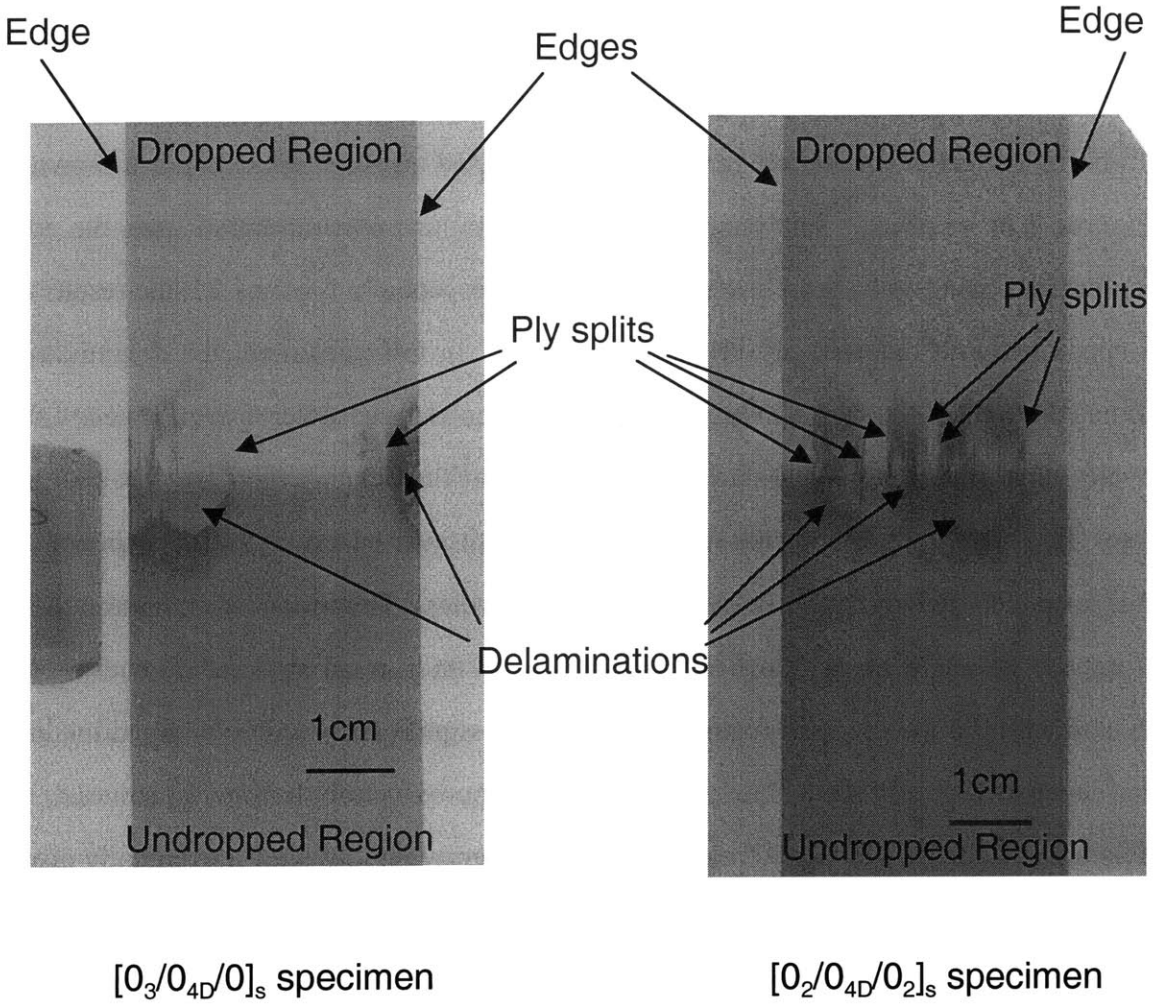

Figure 7.20 Radiographs taken after completion of fatigue testing (100,000 cycles) of two specimens with eight internal ply dropoffs showing *(left)* two delaminated regions bounded by a ply split and one edge in a $[0_3/0_{4D}/0]_s$ specimen, and *(right)*, three delaminated regions bounded by ply splits in a $[0_2/0_{4D}/0_2]_s$ specimen.

delaminations did not extend to the edges.

The delamination growth data based on edge replications in specimens with internal ply dropoffs cannot adequately quantify the growth behavior of such specimens under cyclic load as the growth is not independent of width. As such, extracting specific growth trends for each specimen group from such data would be inappropriate. However, in order to obtain a general sense for the behavior in laminates with ply dropoffs, typical delamination growth data plots based on edge replication are shown in Figures 7.21 and 7.22. The length of the delaminations was measured from the edge replications using an X-Y table attached to the microscope. In Figure 7.21, the results for a specimen with external ply dropoffs is shown. In this specimen, the delamination initiated after 2,000 cycles and grew at a relatively quick rate. After approximately 4,000 cycles, the growth rate decreased, and the length of the delamination grew at a slower rate. In Figure 7.22, the results for a specimen with internal ply dropoffs is shown. In this specimen, delamination initiated after 1,000 cycles. The initial delamination in the dropped region is much longer than that in the undropped region. However, the delamination in the dropped region does not grow significantly with continued loading, but levels off almost immediately at a length of approximately 8 mm. In contrast, the delamination in the undropped region continues to grow rapidly until it eventually grows longer than that in the dropped region. This plot suggests that there may be a "saturation" delamination length in the dropped region after which delamination will not grow under the same applied cyclic load but that this does not exist in the undropped region.

7.3 Discussion

The results from the experimental work reveal details of the damage/delamination characteristics and show trends that help to better understand the effects of ply dropoffs in composite laminates. The key damage/delamination characteristics from the static and cyclic tests are recapitulated and their implications are discussed in the first sub-section.

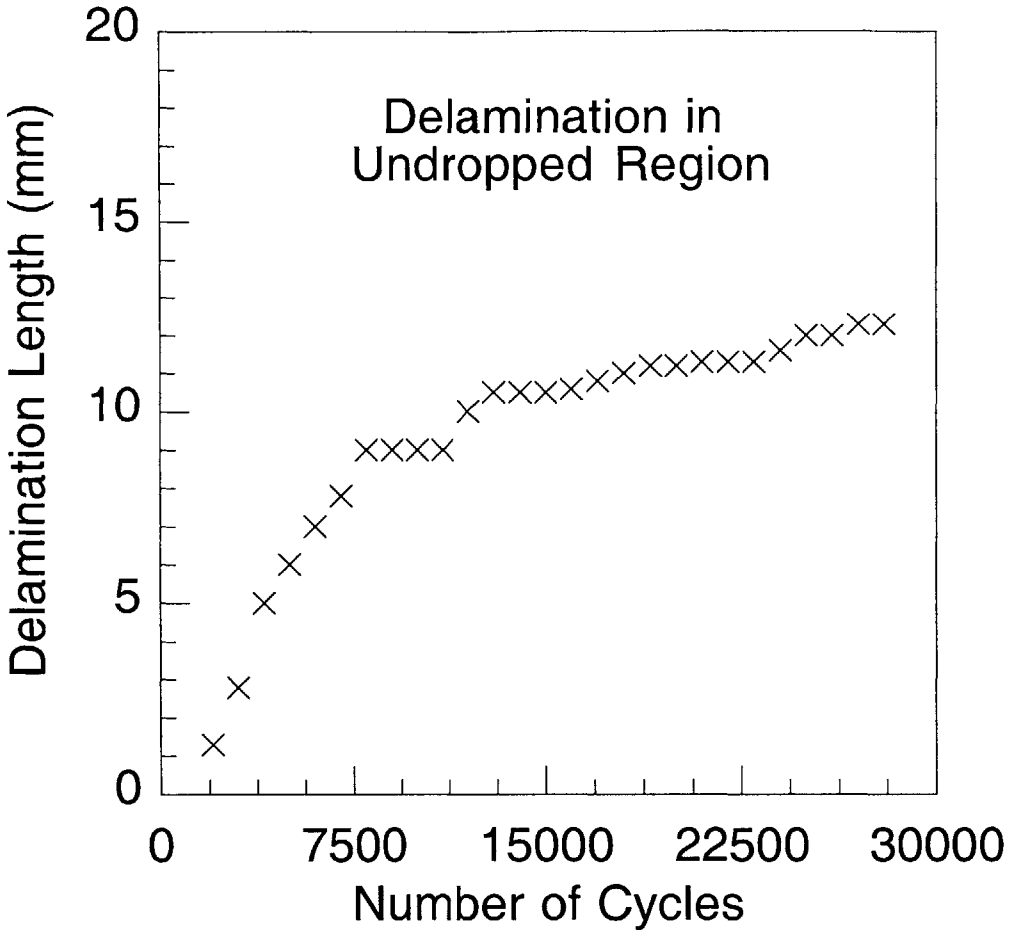

Figure 7.21 Plot of delamination length in undropped region versus the number of cycles in a $[0_{2D}/0_6]_s$ specimen tested under maximum cyclic load of 70% of maximum static load.

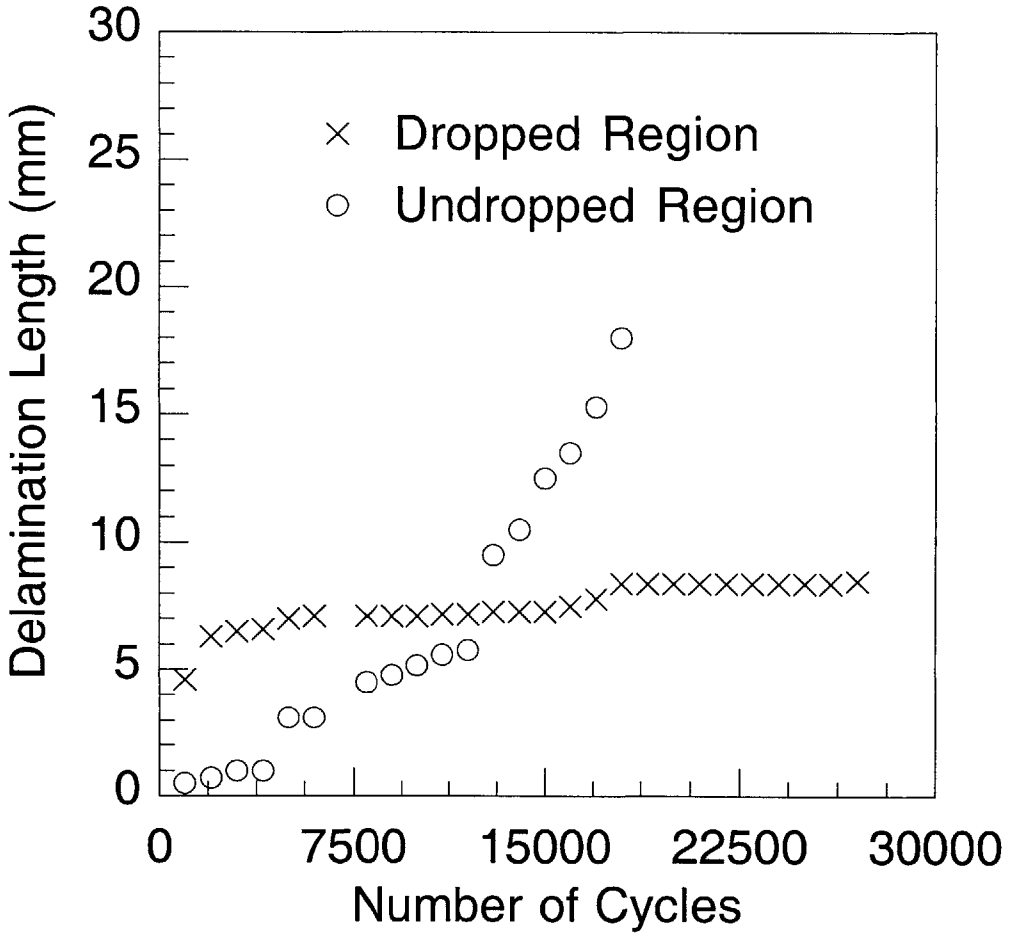

Figure 7.22 Plot of delamination length in undropped and dropped regions versus the number of cycles in a $[0_2/0_{4D}/0_2]_s$ specimen tested under maximum cyclic load of 80% of maximum static load.

The damage/delamination initiation and growth trends are discussed in the second sub-section.

7.3.1 Damage/Delamination Characteristics

Most of the specimens tested under static loads exhibited delamination as a damage mode, as expected based on the stress characterization in Chapter 6 and from previous investigations. The exceptions were specimens that failed catastrophically where it is unknown if delamination preceded final failure. Delamination being the key concern, it is important to know the critical location(s) for delamination occurrence in order to predict delamination initiation loads. As mentioned in Chapter 2, the critical location in laminates with internal ply dropoffs has been a subject of debate among previous investigators.

The current results provide the critical location only for laminates with external ply dropoffs. Based on the location of the delaminations observed in specimens with external ply dropoffs, it is clear that the ply dropoff location, *i.e.*, the cutoff, is the critical location in such laminates. Delaminations were observed to start from the cutoff along the interfaces of continuous and terminated plies in the undropped region in all cases.

Two characteristics of the delaminations observed in specimens with internal ply dropoffs make it impossible to identify the critical location from the current work. One is that delaminations were observed in the vicinity of the dropoff region over finite regions that were often several times the length of the dropoff region itself and extended into the undropped and dropped regions. Since the interlaminar stresses may be very high at various locations along several interfaces, as observed in Chapter 6, the precise location of delamination initiation cannot be identified based on the observation of these finite length delaminations that extend across the various locations where the interlaminar stresses are high. This is a limitation of the experimental procedure used in the current work. In order to obtain the critical location for delamination initiation in laminates with internal ply dropoffs, it is not sufficient to examine specimens visually or otherwise after

the delamination event since delaminations always occur over finite regions. As such, various *in situ* methods may be required to identify the critical location. Recommendations for static test methods to obtain the critical location are made in Chapter 9. Another characteristic is that delaminations were observed at various interfaces, even in different specimens from the same specimen group. This suggests that critical locations in specimens with internal ply dropoffs may depend on local manufacturing variations from specimen to specimen.

The type of delamination not visible from the edges and bounded by ply splits in the mid-section of the specimen, *i.e.*, the Type II damage, is an interesting damage mode that has not been previously reported in the literature. It is hypothesized that the ply splits are induced by the mismatch in the Poisson contraction due to the difference in the thickness of the undropped and dropped regions. In these specimens where the Poisson's ratio is the same for the undropped and dropped regions and the widths of the two regions are identical, the dropped region undergoes a greater amount of Poisson contraction than the undropped region under the same load since the dropped region is under a greater stress. Therefore, in the vicinity of the dropoff region where the undropped and dropped regions meet, the undropped region is under overall transverse compression while the dropped region is under overall transverse tension. A simple quasi-one-dimensional analysis can be used to obtain the order of magnitude of the transverse tensile stresses.

Using the quasi-one-dimensional analysis, a first-order estimate of the transverse tensile stress in the dropped region, σ_d, can be expressed as;

$$\sigma_d = \frac{\nu P}{w t_d}\left(\frac{t_u - t_d}{t_u + t_d}\right) \tag{7.1}$$

where P is the applied load in the longitudinal direction, ν is the Poisson's ratio, w is the specimen width, and the t_u and t_d are the thicknesses in the undropped and dropped regions, respectively. Details of the analysis are presented in the Appendix D. The

transverse tensile stress in the dropped region of the specimens at the static delamination load can be obtained by substituting the appropriate numbers into equation (7.1). For the specimens with eight internal ply dropoffs, the average applied longitudinal load at delamination initiation is 33 kN (from Table 7.3) and the nominal thicknesses, t_u and t_d, are 0.0021 m and 0.0011 m, respectively. The Poisson's ratio, ν, is 0.3, and the nominal width, w, 0.031 m, yielding a transverse tensile stress in the dropped region of 88 MPa for the specimens with 8-ply dropoffs. Similarly, for the specimens with four internal ply dropoffs the transverse tensile stress in the dropped region is 52 MPa at the average applied longitudinal load at delamination of 63 kN (from Table 7.3) and the nominal thicknesses, t_u and t_d, of 0.0021 m and 0.0016 m, respectively, are used. According to the manufacturer, the transverse strength is 53.4 MPa for the AS4/3501-6 composite material system. Since the calculated transverse tensile stress in the dropped region of specimens with 8-ply dropoffs are greater than the reported transverse strength value, ply splits are likely to occur in these specimens. For the specimens with 4-ply dropoffs, the transverse tensile stress in the dropped region is smaller than the transverse strength, and thus, ply splits should not occur. Therefore, the fact that ply splits were observed only in the specimens with 8-ply dropoffs strengthens the hypothesis that the ply splits are induced by the mismatch in the Poisson contraction.

The damage initiation modes in specimens tested under cyclic load are similar to those tested under static load. In specimens with external ply dropoffs, delaminations that were approximately 1 cm in length started from the dropoff location and along the interfaces of the continuous and terminated plies in the undropped region. It is therefore clear that the critical location for delamination initiation in specimens with external ply dropoffs under cyclic load is identical to the critical location in those under static load, *i.e.*, the cutoff. In specimens with internal ply dropoffs, delaminations were observed over finite regions along various interfaces in the undropped, dropoff, and dropped regions. Therefore, the critical location for delamination initiation cannot be identified as

in the static case.

7.3.2 Delamination Initiation and Growth Trends

The static and fatigue tests show that specimens with different configurations exhibit different delamination initiation and growth trends. These trends are discussed in the following paragraphs.

The static delamination initiation loads in Table 7.3 clearly show dependence on the through-thickness location of the terminated ply group and the number of terminated plies. It is seen that specimens with external ply dropoffs delaminate at significantly lower loads than those with internal ply dropoffs when the same number of plies is terminated. This implies that external dropoffs create a state of higher interlaminar stresses to induce delamination at lower loads than internal dropoffs. In addition, it can be seen that delamination loads in specimens with more terminated plies are generally lower than those with less terminated plies. Although both trends are expected based on intuition, it is surprising that the delamination load in specimens with external ply dropoffs is lower by more than a factor of two compared to those with internal ply dropoffs with the same number of terminated plies depending on the internal location. Thus, it is desirable to avoid placing terminated plies at the outer surfaces of composite laminates and terminate fewer plies to achieve higher static delamination load. It can also be seen in Table 7.3 that specimens with internal ply dropoffs located further away from the mid-plane delaminate at a higher load than those with internal ply dropoffs located closer to the mid-plane when the same number of plies are terminated. The difference in the delamination loads is 12% in the case of specimens with 4-ply dropoffs and 18% in the case of specimens with 8-ply dropoffs. Again, this implies that the overall magnitude of the interlaminar stresses in the specimens with internal ply dropoffs located closer to the mid-plane is larger than those located further away from the mid-plane. The correlation between the static delamination loads and the interlaminar stresses in the specimens tested are further discussed in Chapter 8.

The delamination initiation lives in Figures 7.15 and 7.16 also show dependence on the through-thickness location of the terminated ply group. As noted in Section 7.2, specimens with internal ply dropoffs generally have greater resistance to delamination initiation than those with external ply dropoffs, and specimens with internal ply dropoffs located closer to the mid-plane generally have greater resistance to delamination initiation than those located further away from the mid-plane. However, the dependence of delamination initiation lives on the number of terminated plies is inconclusive due to insufficient data. Although it can be seen in Figures 7.15 and 7.16 that the slope of the logarithmic regression curve of approximately –14 for the specimens with four external ply dropoffs differs significantly from those of approximately –6 for the specimens with eight internal ply dropoffs, there is not enough data to be conclude that the number of cycles to initiation depends on the number of terminated plies.

Delaminations in the undropped region were observed to grow in length along the interface of the continuous and terminated plies under continued cyclic load after delamination initiation in specimens with internal or external ply dropoffs. Qualitatively, this implies that the magnitude of the interlaminar stresses along these interfaces remains large enough for delaminations to grow as the length of the delamination increases. In contrast, delaminations in the dropped region were observed to no longer grow after reaching a certain length (or after a certain number of cycles). This implies that the magnitude of the interlaminar stresses ahead of the delamination must decrease as the length of the delamination increases. Although quantitative characterizations of the delamination growth behavior are available from the current experiments, *e.g.*, in Figures 7.21 and 7.22, such characterizations may not accurately represent delamination growth. As mentioned in Section 7.2, the delaminations did not occur over the entire width of the laminate in most cases, causing delaminations to grow a non-self-similar manner along the length. In order to obtain more accurate growth data in laminates with ply dropoffs, pre-cracks across the width using inserts may be useful in future experiments. Such

possibilities are further noted in Chapter 9.

The results from both the static and fatigue tests show that external ply dropoff configurations are undesirable due to relatively low static delamination initiation loads and short initiation lives compared to internal ply dropoff configurations. In this sense, the static and fatigue delamination initiation trends are consistent. The results also show that specimens with internal ply dropoffs located further away from the mid-plane delaminated at higher loads compared to those with internal ply dropoffs located closer to the mid-plane under static load. However, specimens with internal ply dropoffs located closer to the mid-plane exhibited greater resistance to fatigue than those with internal ply dropoffs located further away from the mid-plane. Therefore, the static and fatigue delamination initiation trends for the specimens with internal ply dropoffs show different trends. This indicates that the critical location(s) for delamination initiation and/or mechanism that cause delamination in specimens under static and cyclic loads may be different.

CHAPTER 8

DELAMINATION PREDICTION

According to the strength of materials approach, laminates (or interfaces within each laminate) under a higher state of stress are more likely to delaminate than those under a lower state of stress, and delamination is postulated to occur when the stress state exceeds a certain limit. In this chapter, qualitative and quantitative examinations of the stress field in the laminates that were tested, as obtained via the analytical methods, and the delamination characteristics, as observed via the experiments, are performed to correlate the two based on the strength of materials approach. In the first section, the characteristics and trends of the interlaminar stresses in each laminate are compared qualitatively with the delamination characteristics observed from the experiments. In the second section, a quantitative assessment via a strength of materials based criterion, the Quadratic Delamination Criterion with the average stress method, is presented using the interlaminar stresses obtained in the first section and the static delamination stresses from the experiments. The qualitative comparison and the quantitative assessments are then discussed in the third section.

8.1 Qualitative Comparison

In this section, the interlaminar stress fields along various interfaces in the laminate configurations considered in the experiments are obtained and examined to see if their characteristics and trends are consistent with experimental observations concerning delamination. To this end, the interlaminar stress distributions in each type of laminate along various interfaces obtained using the global and mixed models are presented first. Subsequently, three experimental observations from Chapter 7 are

considered in separate sub-sections. In addition, a qualitative prediction is made on the type of delamination surface expected along certain interfaces based on the characteristics of the interlaminar stresses. This is compared with fractographs from the experiments and presented in the fourth sub-section.

The interlaminar stresses in laminates with external ply dropoffs are shown in Figures 8.1 and 8.2. For these laminates, the interlaminar stresses along the interface of the continuous and terminated plies in the undropped region and the two interfaces immediately below this interface are considered. Thus, for the $[0_{2D}/0_6]_s$ laminate, the interlaminar stresses along the interface of the continuous and terminated plies in the undropped region and the outer surface in the dropped region ($z = 6t$), and the two interfaces between two continuous plies immediately below ($z = 5t$ and $z = 4t$) are plotted in Figure 8.1. Similarly, for the $[0_{4D}/0_4]_s$ laminate, the interlaminar stresses along the interface of the continuous and terminated plies in the undropped region and the outer surface in the dropped region ($z = 4t$), and the two interfaces immediately below ($z = 3t$ and $z = 2t$) are plotted in Figure 8.2. For convenience, these interfaces are referred to as the first, second and third interface, with the interface furthest from the mid-plane being the first interface and the one closest to the mid-plane being the third. The magnitude of the interlaminar stresses along other interfaces through the thickness direction are smaller by approximately an order of magnitude compared to those considered, and thus, are not shown or considered further. All stresses are normalized by the applied in-plane stress in the undropped region, σ_0.

The interlaminar stresses in laminates with internal ply dropoffs are shown in Figures 8.3 through 8.6. For these laminates, a taper angle of 7° in the dropoff region was used in order to be consistent with the nominal angle in the experimental work. The interfaces considered are indicated in the top part of each figure. In the undropped region, the interlaminar stresses along the upper and lower interfaces of the terminated ply group and the two interfaces immediately above and below these interfaces are

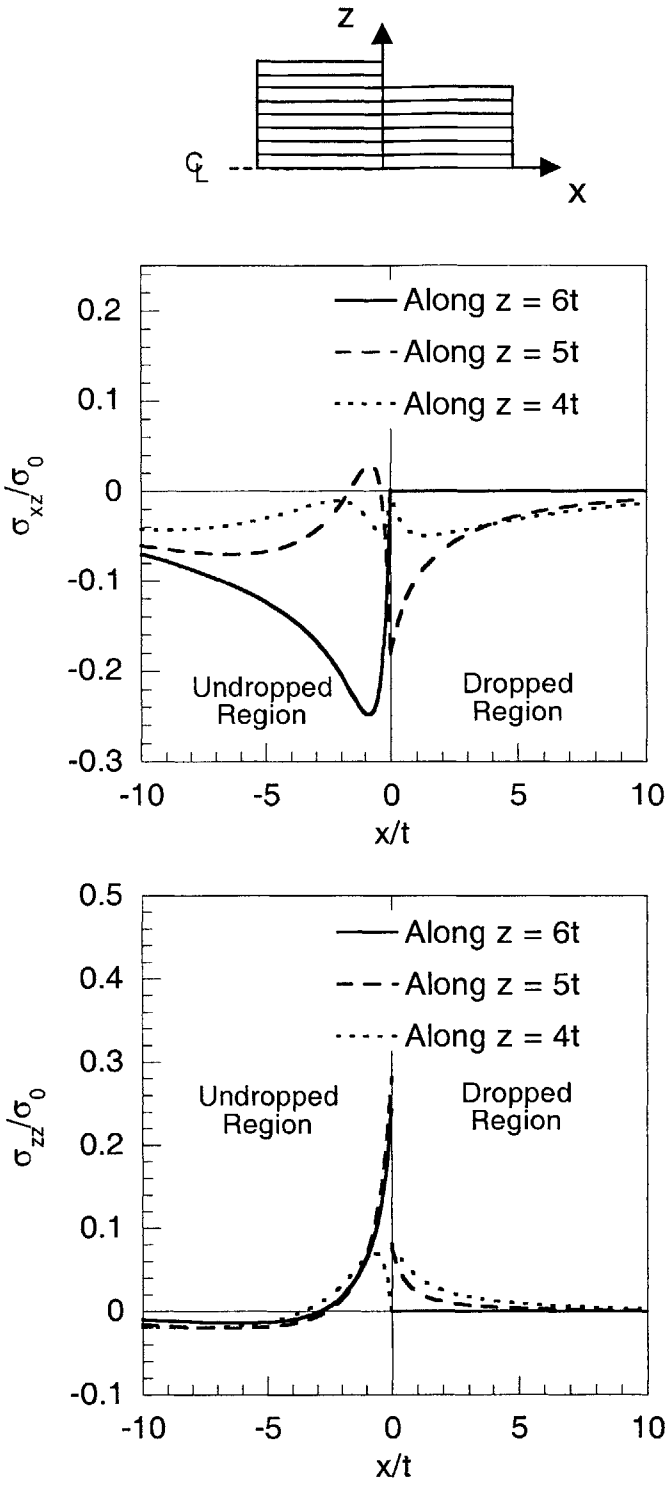

Figure 8.1 Normalized interlaminar shear and normal stresses in a $[0_{2D}/0_6]_s$ laminate along three interfaces (z = 6t, 5t and 4t).

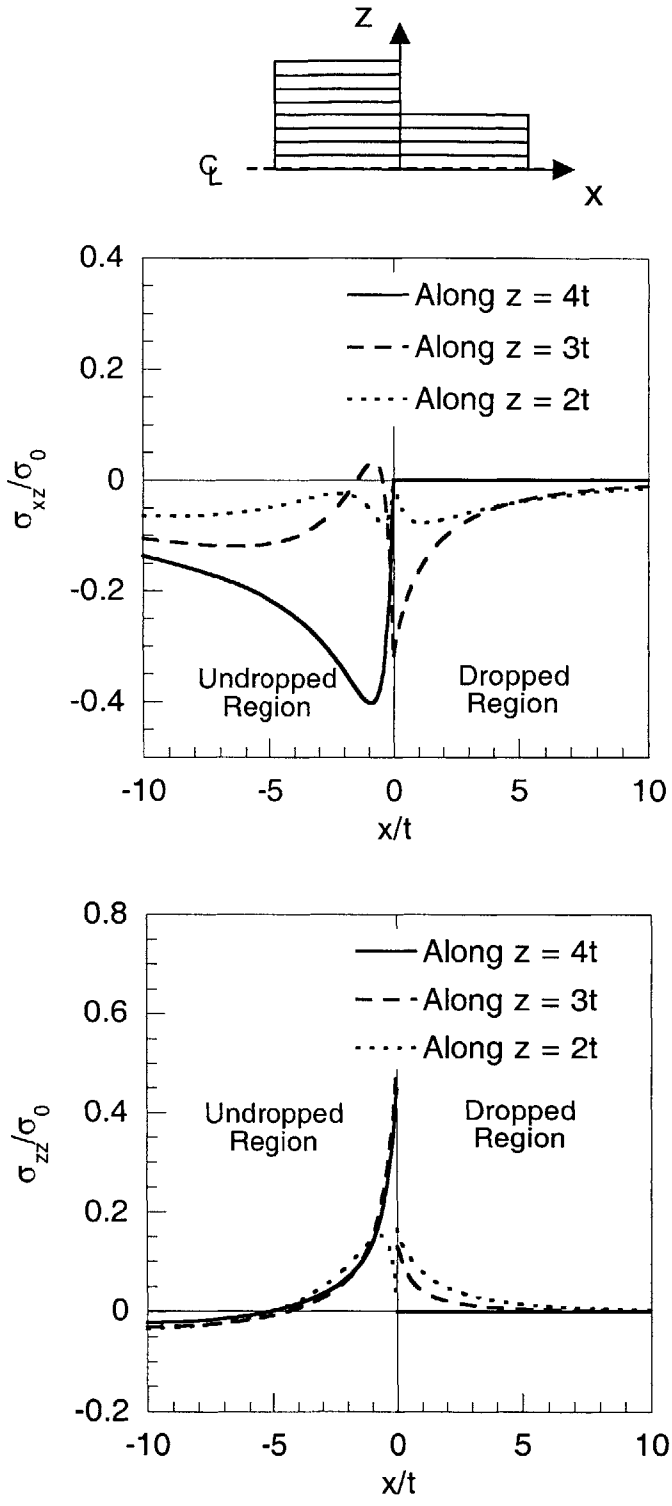

Figure 8.2 Normalized interlaminar shear and normal stresses in a $[0_{4D}/0_4]_s$ laminate along three interfaces (z = 4t, 3t and 2t).

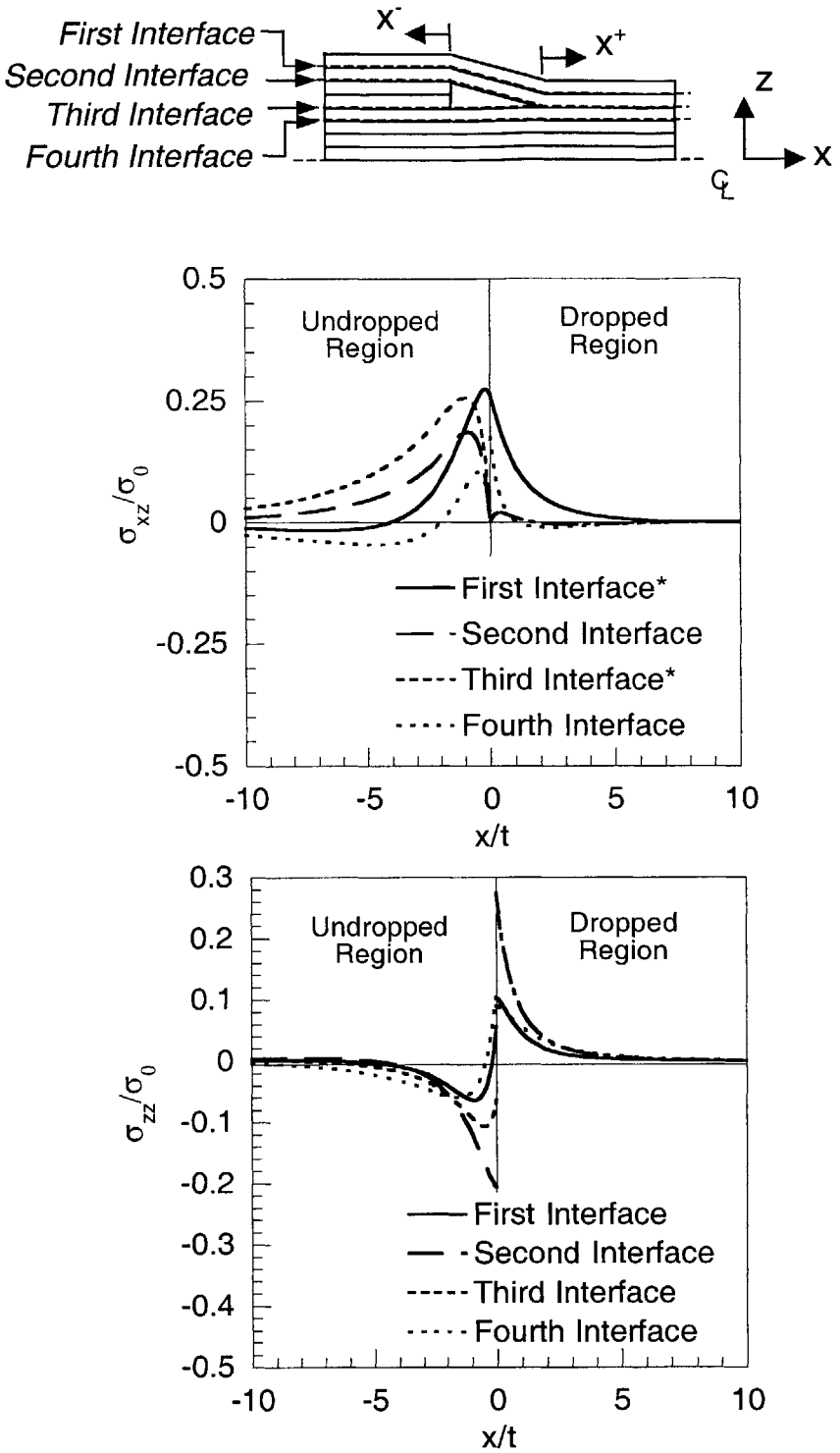

Figure 8.3 Normalized interlaminar shear and normal stresses in a $[0_2/0_{2D}/0_4]_s$ laminate along the four interfaces indicated in the top diagram (* indicates multiplied by –1).

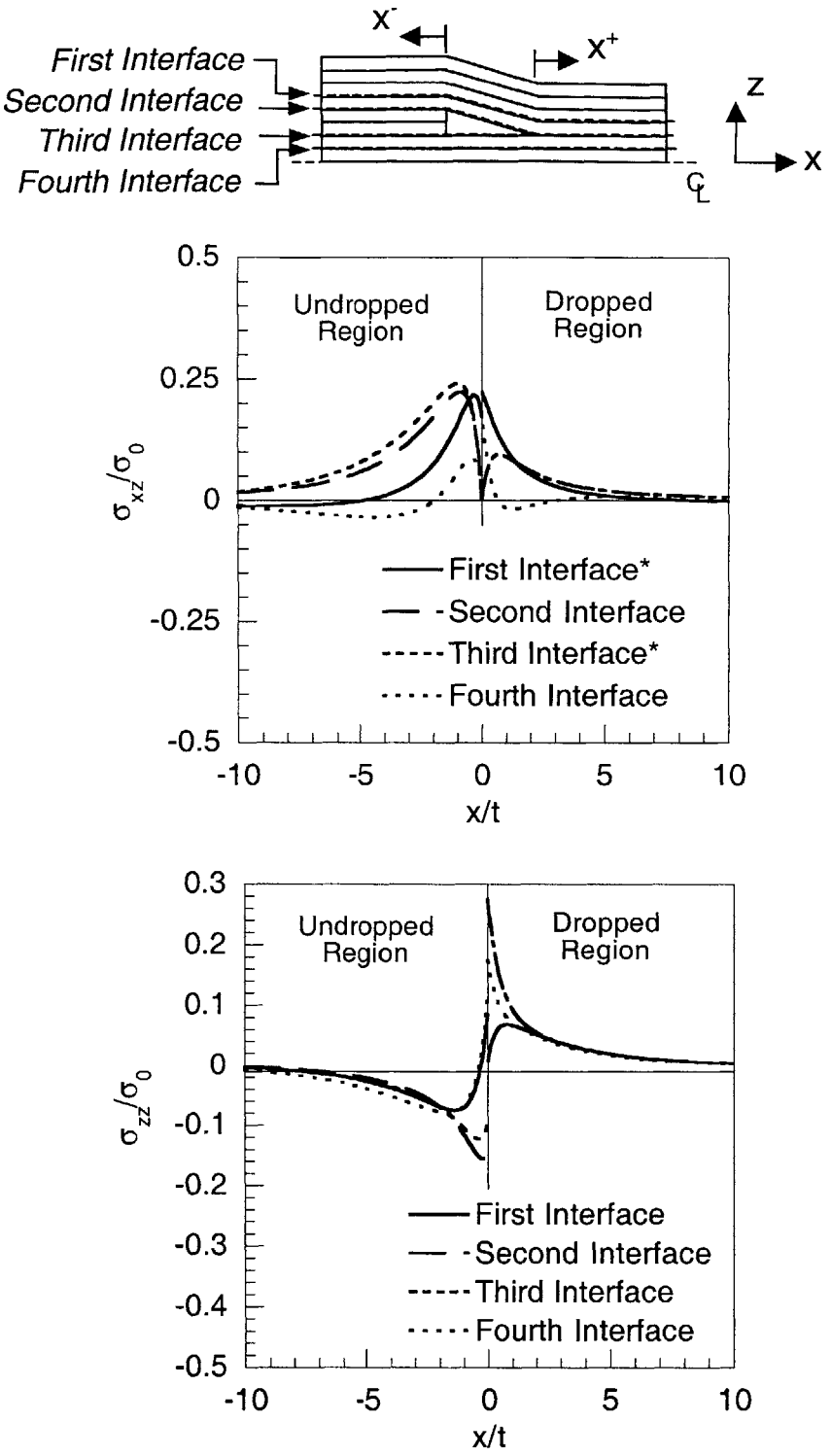

Figure 8.4 Normalized interlaminar shear and normal stresses in a $[0_4/0_{2D}/0_2]_s$ laminate along the four interfaces indicated in the top diagram (* indicates multiplied by –1).

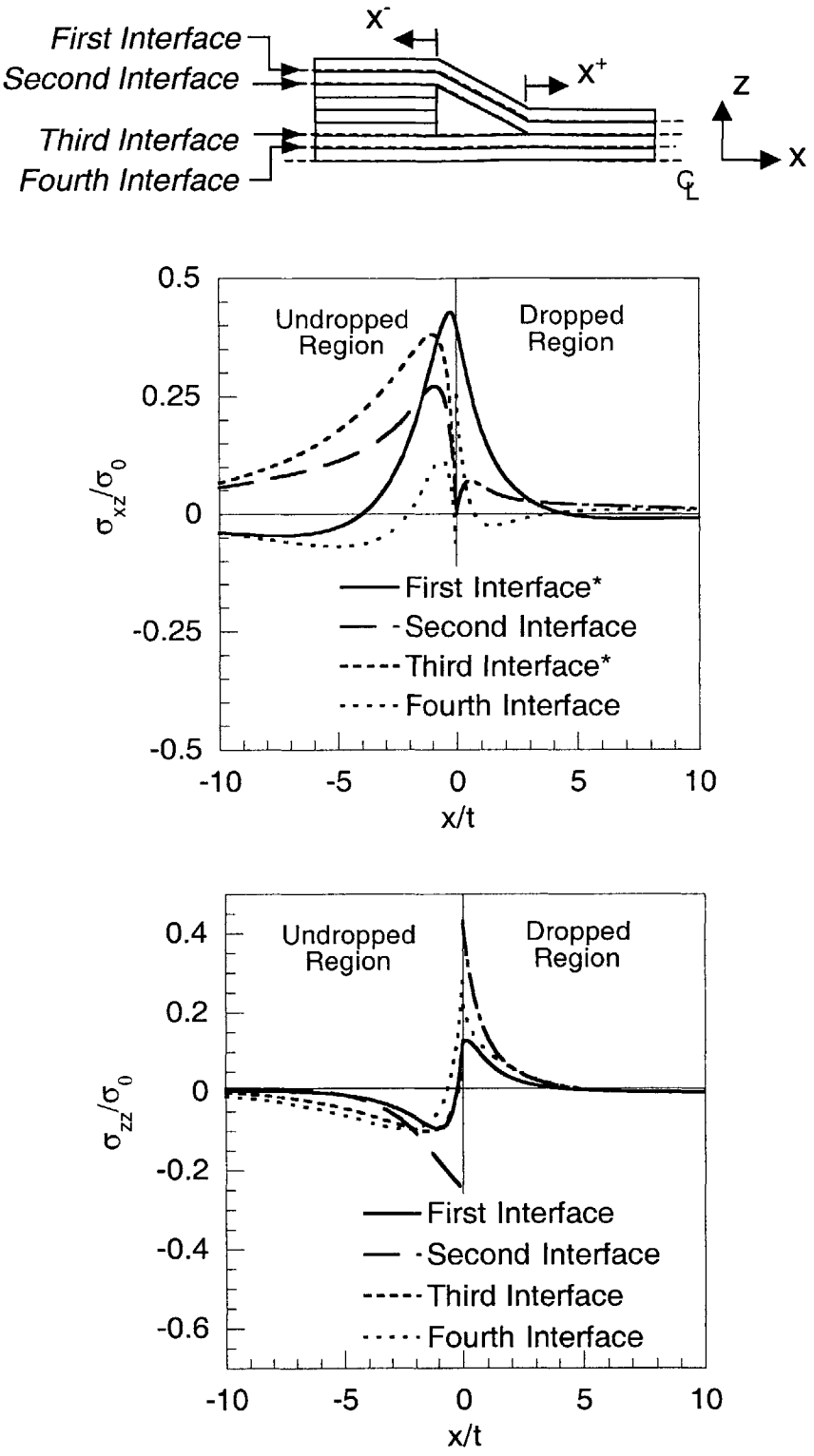

Figure 8.5 Normalized interlaminar shear and normal stresses in a $[0_2/0_{4D}/0_2]_s$ laminate along the four interfaces indicated in the top diagram (* indicates multiplied by –1).

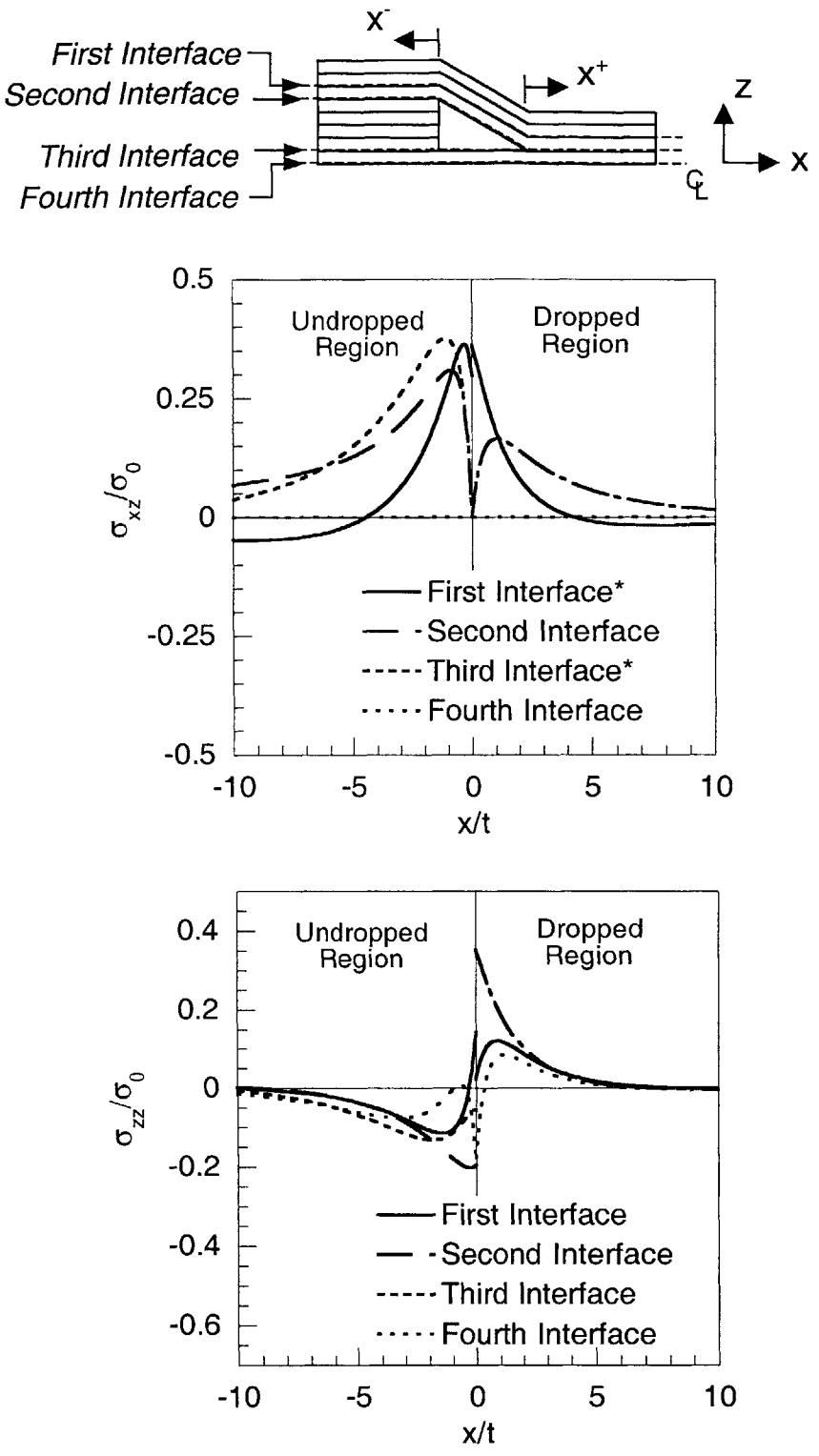

Figure 8.6 Normalized interlaminar shear and normal stresses in a $[0_3/0_{4D}/0]_s$ laminate along the four interfaces indicated in the top diagram (* indicates multiplied by –1).

considered. In the dropped region, the interlaminar stresses along the inner and outer continuous plies and the interfaces immediately above and below these interfaces are considered. Interlaminar stresses along other interfaces are approximately an order of magnitude smaller compared to those along these interfaces and are not shown or considered further. For convenience, the four interfaces considered are referred to as the first, second, third and fourth interfaces starting with the uppermost interface in the undropped region. Thus, the second and third interfaces correspond to the upper and lower interfaces, respectively, of the terminated ply group in the undropped region, and the first and fourth interfaces correspond to the interfaces immediately above and below these interfaces, respectively. The second and third interfaces in the dropped region coincide and correspond to the interface of the inner and outer continuous plies, and thus, the interlaminar stresses along these two interfaces in the dropped region are identical.

In order to allow direct comparison of the relative magnitudes of the interlaminar shear stresses along the four interfaces considered, interlaminar shear stresses along some interfaces in Figures 8.3 through 8.6 are multiplied by -1 such that the peak values near the cutoff are positive. These interfaces are the first interface in the undropped and dropped regions and the third interface in the undropped region only. Interlaminar shear stress distributions multiplied by -1 are indicated by an asterisk (*) in the figures. Such direct comparison allows one to see along which interface the interlaminar shear stress is highest, and thus, a sense of where delamination may be more likely to occur. The sign of the interlaminar shear stress is unimportant when considering whether it will cause delamination, only its magnitude. On the other hand, the sign of the interlaminar normal stress is important because only tensile stresses will cause delamination. Compressive interlaminar stresses are generally not considered to cause delamination although there have been suggestions that these may work to suppress delamination [73].

8.1.1 Critical Interfaces

It can be seen in the top plots of Figures 8.1 and 8.2 that the magnitudes of the

interlaminar shear stresses in both laminates with external ply dropoffs are the greatest along the first interface in the undropped region over the entire undropped region. In the bottom plots of Figures 8.1 and 8.2, it can be seen that the magnitudes of the interlaminar normal stresses are the greatest along the first and second interfaces in the undropped region, and these interlaminar stresses almost overlap. Based on these observations, it can be concluded that the first interface, *i.e.*, the interface of the continuous and terminated plies in the undropped region, is the critical interface in both laminates. Along this interface, both the interlaminar shear and normal stresses are the greatest among those along all interfaces, and as such, delamination is most likely to initiate at this location. This is consistent with the observations from static and fatigue tests where delaminations occurred along the interfaces of continuous and terminated plies in the undropped region in specimens with external ply dropoffs. Photomicrographs of edge replications of $[0_{2D}/0_6]_s$ specimens tested under static and fatigue loads that exhibited delamination along these interfaces are shown in Figures 7.4 and 7.12, respectively.

The critical interface where delamination is most likely to occur in laminates with internal ply dropoffs is more difficult to identify based on the interlaminar stress distributions because the magnitudes of the interlaminar stresses are comparable along several interfaces. For example, it can be seen in the top plot of Figure 8.3 that the peak interlaminar shear stress along the first and third interfaces are comparable in the $[0_2/0_{2D}/0_4]_s$ laminate. Similar observations can be made for the cases shown in Figures 8.4 through 8.6. It is therefore not possible to identify one critical interface where delamination is likely to occur based on qualitative comparison for these laminates. Thus, for laminates with internal ply dropoffs, multiple interfaces along which interlaminar stresses are relatively high compared to other interfaces are chosen as potential critical interfaces.

Based on the interlaminar stress distributions in the laminates with internal ply dropoffs shown in Figures 8.3 through 8.6, there are two interfaces each in the undropped

and dropped regions where the interlaminar stresses are relatively high compared to other interfaces. In the dropped region, the magnitudes of the interlaminar normal stresses along the coinciding second and third interface in all four laminates are the highest among those along the entire length of these interfaces. Therefore, this interface, which corresponds to the interface of the inner and outer continuous plies in the dropped region, may be a critical interface. Another interface where the interlaminar stresses are relatively high is the first interface in the dropped region. The peak interlaminar shear stresses along this interface are the greatest among those along all interfaces in the dropped region, and the interlaminar normal stresses are also relatively high, with the peak stress being approximately half of that along the second and third interface. The combination of the high interlaminar shear and normal stresses may cause this first interface to be critical.

In the undropped region, the magnitudes of the interlaminar shear stresses along the third interface in all laminates are the highest among those along all interfaces over the entire undropped region shown except in the $[0_3/0_{4D}/0]_s$ laminate. In the $[0_3/0_{4D}/0]_s$ laminate, the magnitude of the interlaminar shear stress along the third interface is the highest over approximately 60% of the undropped region. Therefore, this third interface may be a critical interface. In addition, the peak interlaminar shear stresses along the first interface are also among the highest in the undropped region. Therefore, delaminations may also initiate along this first interface in the undropped region, and thus, it is chosen as a potential critical interface. It is noted that the interlaminar shear stress along the second interface in the undropped region is also relatively high, causing delamination initiation along this interface to be a concern as well. However, since the magnitude of the interlaminar shear stress along this second interface is always smaller than that along the third interface over the entire undropped region except in the $[0_3/0_{4D}/0]_s$ laminate (where the magnitude is higher in the region further than approximately 6t from the cutoff) by a factor of approximately 0.8, this interface is not chosen as a potentially

critical interface. The interlaminar normal stresses along the two potential critical interfaces, *i.e.*, along the first and third interfaces in the undropped region are generally compressive except for a small region near the cutoff, and thus, are not expected to contribute significantly to delamination.

The fact that multiple interfaces can be identified as critical interfaces indicates that there is no clearly single dominant interface in laminates with internal ply dropoffs unlike the case of laminates with external ply dropoffs. This implies that the location of delamination initiation may vary from specimen to specimen depending on local material and manufacturing variability or defects. It also implies that multiple delaminations may occur along several or all of the potential critical interfaces. The delaminations observed in the static and fatigue test specimens with internal ply dropoffs generally reflect these characteristics as discussed in Section 7.3, and thus, are consistent with the qualitative examination of the interlaminar stress field. Delaminations were observed along the first, second, and third interfaces as well as along other interfaces as shown in the photomicrographs of edge replications of specimens tested under static and fatigue loads in Figures 7.8, 7.13 and 7.14.

8.1.2 Effect of Number of Terminated Plies

In the top plots of Figures 8.1 and 8.2, it can be seen that the interlaminar shear stress along the critical interface in the laminate with eight external ply dropoffs is approximately twice as high as that in the laminate with four external ply dropoffs. This trend is expected based on the previous stress analyses of laminates with different numbers of ply dropoffs as considered in Section 6.2.4. It was seen that, in general, the magnitude of the interlaminar shear stress increases with an increase in the number of terminated plies because the far-field load carried by the terminated ply group increases. In addition, the magnitude of the interlaminar normal stress increases as well because the moment resulting from the far-field load in the terminated ply group increases. In the bottom plots of Figures 8.1 and 8.2, it can be seen that the interlaminar normal stress

along the same interface in the former laminate is approximately 1.5 times as high as that in the latter laminate. Since higher interlaminar stresses generally imply lower delamination loads, the trend of the interlaminar stress distribution is in good agreement with the experimental results where the static delamination load in the specimens with 8-ply dropoffs is smaller than that in the specimens with 4-ply dropoffs by a factor of approximately two (see Table 7.3). Note that this factor is nearly the same as the ratio of the interlaminar shear and normal stresses in the two laminates.

It can similarly be seen in Figures 8.3 through 8.6 that the magnitudes of the interlaminar stresses in laminates with eight internal ply dropoffs are generally greater than those in laminates with four internal ply dropoffs. For example, the peak interlaminar shear stresses along the first and second interfaces in the undropped region of the $[0_2/0_{4D}/0_4]_s$ laminate is greater than those along the first and second interfaces in the $[0_2/0_{2D}/0_4]_s$ laminate by a factor of approximately 1.5, and the magnitude of the interlaminar shear stresses along the same interfaces are also greater over the entire undropped region. Again, this trend is expected based on the previous stress analyses in Section 6.2.4. The peak interlaminar normal stress in the former laminate is also greater than that in the latter laminate by a factor of approximately 1.5. Similar differences can be seen between the $[0_3/0_{4D}/0]_s$ and $[0_4/0_{2D}/0_2]_s$ laminates. Since the magnitudes of the interlaminar stresses are greater in laminates with 8-ply dropoffs than for those with 4-ply dropoffs, the delamination initiation load should be smaller in those laminates. The trends of the magnitudes of the interlaminar stresses in laminates with four and eight internal ply dropoffs are in good agreement with the experimental result. As shown in Table 7.3, it was observed from the experiments that static delamination loads in laminates with four internal ply dropoffs are higher than those with four internal ply dropoffs by a factor of approximately 2.

8.1.3 Effect of Location of Terminated Plies

The magnitudes of the interlaminar shear and normal stresses along the potential

critical interfaces in the three laminates with 4-ply dropoffs are comparable as shown in Figure 8.1, 8.3, and 8.4. In all three laminates, the peak interlaminar shear stresses along the potential critical interfaces are equal to approximately $0.25\sigma_0$, and the peak interlaminar normal stresses are equal to approximately $0.3\sigma_0$, except along the first interface in the two laminates with four internal ply dropoffs. Along these latter interfaces in the internal cases, the peak interlaminar normal stresses are equal to approximately $0.1\sigma_0$. Given the similarities in the magnitudes, the interlaminar stresses along the critical interface in the $[0_{2D}/0_6]_s$ laminate are expected to be most "severe" because both the interlaminar shear and normal stresses are relatively high. Along the two potential critical interfaces in the undropped regions, *i.e.*, the first and third interfaces of the $[0_2/0_{2D}/0_4]_s$ laminate and the $[0_4/0_{2D}/0_2]_s$ laminate, only the interlaminar shear stresses are relatively high. Along the coinciding second and third interfaces in the dropped regions of the two internal cases, which was also identified as a potential critical interface, only the interlaminar normal stresses are relatively high. The first interfaces in the dropped regions of the two internal cases were also identified as potential critical interfaces due to the interlaminar shear and normal stresses, but the magnitude of the interlaminar normal stress is lower than that in the laminate with external ply dropoffs. Therefore, it can be concluded that laminates with four external ply dropoffs should delaminate at lower loads compared to those with four internal ply dropoffs. The same observations can be made for laminates with eight ply dropoffs. Therefore, the same conclusion that laminates with eight external ply dropoffs should delamination at lower loads compared to those with eight internal ply dropoffs can be made. These conclusions are consistent with the experimental results shown in Table 7.3 where the laminates with external ply dropoffs delaminate at loads smaller by a factor of approximately two compared to those with internal ply dropoffs for the same number of terminated plies.

8.1.4 Delamination Surfaces

Based on the interlaminar stress distributions in the laminates with internal ply

dropoffs as shown in Figures 8.3 through 8.6, it is most likely that delamination in the undropped region along the second and third interfaces will be caused mainly by interlaminar shear stresses because the interlaminar normal stresses are generally compressive in this region. This implies that the delamination surfaces along these interfaces would exhibit mode II (*i.e.*, shearing) characteristics. In the dropped region, the interlaminar normal stresses are tensile and greater in magnitude than the interlaminar shear stresses. Considering the fact that the interlaminar normal strength is generally lower than the interlaminar shear strength in composite laminates [42], the contribution of the interlaminar normal stresses to delamination in the dropped region should be greater than that of the interlaminar shear stresses. This implies that the delamination surface along this interface would exhibit mode I (*i.e.*, opening) characteristics.

To validate whether interlaminar shear or normal stresses contributed more to delamination along these interfaces, the delamination surfaces of a $[0_3/0_{4D}/0]_s$ specimen tested under static load were inspected using an environmental scanning electron microscope (SEM). The radiograph of this specimen was shown in the left side of Figure 7.9. Fractographs along the interface of the continuous and terminated plies in the undropped region (the second interface: $z = 5t$) and of the inner and outer continuous plies in the dropped region (the second/third interface: $z = t$) are shown in Figure 8.7. The fractographs were taken approximately five ply thicknesses away from the cutoff. The fractograph of the undropped region in the top part of Figure 8.7 clearly shows visible hackle markings that are indicative of delamination dominated by interlaminar shear stress (mode II) [74]. This is in good agreement with the prediction based on the interlaminar stress field characteristics. The fractograph of the dropped region in the bottom part of Figure 8.7 reveals a relatively smooth delamination surface with small markings that suggest delamination dominated by interlaminar normal stress (mode I) [74]. Again, this is consistent with the prediction based on the interlaminar stress field characteristics.

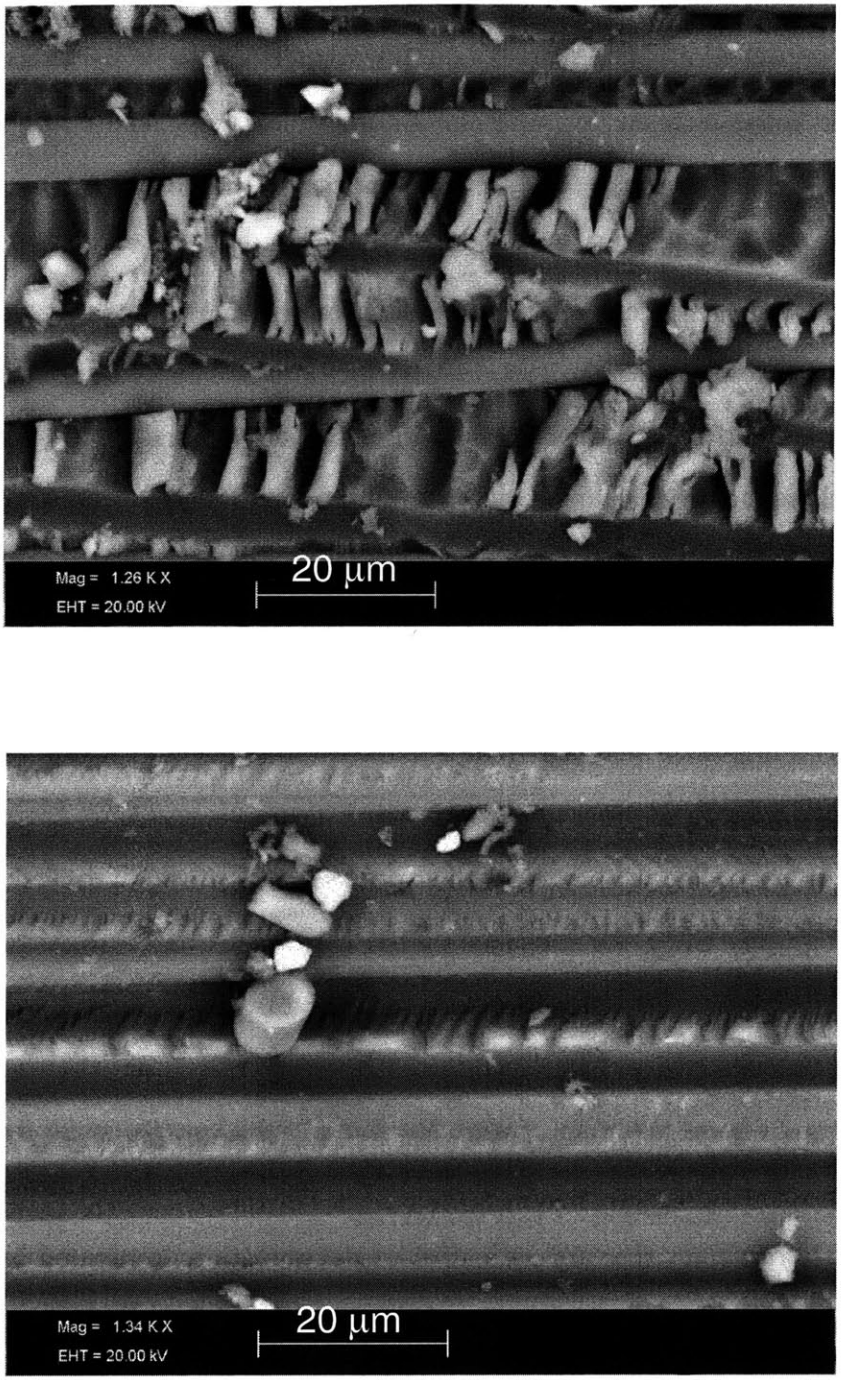

Figure 8.7 Fractographs of a $[0_3/0_{4D}/0]_s$ specimen with internal ply dropoffs taken approximately five ply thicknesses away from the cutoff *(top)* along the interface of the continuous and terminated plies in the undropped region (z = 5t), and *(bottom)*, along the interface of the inner and outer continuous plies in the dropped region (z = t).

8.2 Quantitative Assessment of the Quadratic Delamination Criterion with the Average Stress Method

Having qualitatively examined the characteristics and trends of the interlaminar stresses in the laminates that were tested and identified the potential critical interfaces, the next step is to assess the static delamination loads or stresses quantitatively using a delamination criterion. In this work, the Quadratic Delamination Criterion (QDC) with the average stress method [42], which is based on strength of materials, is used for this purpose. According to the QDC with the average stress method, delamination is assumed to occur when the combination of average interlaminar stresses over a characteristic distance, commonly referred to as the averaging length, exceeds the interlaminar strengths. The interlaminar strengths are material system constants that are available from the manufacturer and/or from previous investigations. The averaging length is not as readily available although it has been suggested that this may also be a material system constant [42]. In any case, for this criterion to be useful in predicting delamination stresses, the averaging length should be single-valued for all laminates with ply dropoffs. Thus, in this section, the averaging lengths for the tested laminates are obtained using the experimental delamination stresses. Based on the results, the utility of the QDC with the average stress method is discussed.

The form of the QDC used for correlation of the experimental data in the current work can be expressed as,

$$\left(\frac{\bar{\sigma}_{1z}}{Z^{s1}}\right)^2+\left(\frac{\bar{\sigma}_{zz}}{Z^{t}}\right)^2=1 \tag{8.1}$$

where the bar denotes average stress, and Z^{s1} and Z^{t} are the interlaminar shear and normal strengths. The interlaminar shear stress, σ_{2z}, is not considered since unidirectional laminates were tested and these stress components are identically zero. The average

stresses are defined as,

$$\overline{\sigma}_{iz} = \frac{1}{l_{ave}} \int_0^{l_{ave}} \sigma_{iz} dx \tag{8.2}$$

where l_{ave} is the averaging length and σ_{iz} are the interlaminar stresses along the appropriate interface. As is normally the case when QDC is applied, only the tensile part of the interlaminar normal stress is considered in the equation (8.1). The compressive part of the interlaminar normal stress is not considered to contribute to delamination. The interlaminar shear strength from short beam shear tests is 128 MPa according to the manufacturer, Hexcel® Composites [75]. The interlaminar normal strength of 43.0 MPa is used as reported previously [76].

Given the interlaminar shear and normal strengths, the averaging length along a specific interface in a laminate can be calculated using the interlaminar stresses obtained in the previous section and the static delamination stress using equations (8.1) and (8.2). The static delamination stresses from the experiments, shown in Table 7.3, are used. In all cases, these calculated lengths are expressed as multiples of the ply thickness, t, for convenience. For the laminates with external ply dropoffs, the averaging length along the critical interface as identified in the previous section, *i.e.*, the interface of the continuous and terminated plies in the undropped region, is calculated. The averaging lengths for these laminates are shown in Table 8.1. For the laminates with internal ply dropoffs, the averaging length along each of the four potential critical interfaces as identified in the previous section is obtained. The averaging lengths for these laminates are shown in Table 8.2.

Two observations can be made from the averaging lengths shown Tables 8.1 and 8.2. One is that the averaging lengths along the four potential interfaces in each laminate with internal ply dropoffs are different. For example, in the $[0_2/0_{2D}/0_4]_s$ laminate, the averaging length of 3.80t, where t is the ply thickness, along the first interface in the

Table 8.1 Averaging lengths (normalized by ply thickness) along the critical interface for laminates with external ply dropoffs

Layup	Averaging Length
$[0_{2D}/0_6]_s$	3.67
$[0_{4D}/0_4]_s$	3.42

Table 8.2 Averaging lengths (normalized by ply thickness) along the four potential critical interfaces for laminates with internal ply dropoffs

Layup	Undropped Region		Dropped Region	
	First Interface[1]	Third Interface	First Interface	Third Interface[2]
$[0_2/0_{2D}/0_4]_s$	3.80	9.55	4.21	6.60
$[0_4/0_{2D}/0_2]_s$	2.62	6.92	5.72	8.77
$[0_2/0_{4D}/0_2]_s$	3.10	8.50	3.48	5.91
$[0_3/0_{4D}/0]_s$	2.15	5.17	3.96	6.80

[1] Interfaces are as described in Figures 8.3 through 8.6.

[2] Second and third interfaces are identical in the dropped region.

undropped region is smaller than that of 9.55t along the third interface in the undropped region by a factor of approximately 2.5. This variation is expected because the interlaminar stress distributions along the different interfaces in each laminate are different. It indicates the predicted delamination stresses along each interface will be different if a single value of the averaging length is used.

The other observation is that the averaging lengths along the potential critical interfaces in the laminates with external and internal ply dropoffs exhibit significant differences depending on the interface. For example, the averaging lengths obtained along the third interfaces in the undropped region for laminates with internal ply dropoffs is greater than that for laminates with external ply dropoffs by a factor of approximately 2.5. This implies that if the critical interface in laminates with internal ply dropoffs turns out to be the third interface in the undropped region, the averaging lengths in laminate with internal and external ply dropoffs will differ by a factor of approximately 2.5.

The two observations suggest that the averaging length may not be single-valued in laminates with ply dropoffs. The large variation of the averaging lengths makes it difficult to choose a single value of the averaging length. Therefore, the QDC with the average stress method is not immediately useful in predicting accurate static delamination stresses all of the laminates with ply dropoffs that were considered in the current work. The possible causes and implications of the large variation in the averaging lengths are discussed in the next section.

8.3 Discussion

In the preceding sections, it was shown that the characteristics and trends of the interlaminar stress fields in the tested laminates are consistent with the experimental observations concerning delamination from a qualitative viewpoint. However, in a quantitative approach using the QDC, a single value for the averaging length could not be found. This would limit the utility of the QDC with the average stress method since the

delamination stresses in other types of laminates with ply dropoffs could not be predicted using an averaging length obtained for a specific type of laminate with ply dropoffs. In this section, the possible causes of the inability to find a single averaging length and the implications thereof to the applicability of the QDC with the average stress method are discussed. Following this discussion, the QDC with the average stress method is utilized in a limited capacity to further obtain useful information such as the predicted delamination initiation location and the sensitivity of delamination to various structural parameters.

As discussed in Section 8.2, the averaging length in laminates with ply dropoffs does not appear to be single-valued, much less a material system constant. This result is somewhat unexpected based on previous investigations of the QDC with the average stress method. The majority of previous work on the QDC with the average stress method has been performed using experimental data for flat laminates with straight free edges, *e.g.*, [42,44], and these have shown that the averaging length in several types of laminates of the same material were relatively constant. The typical averaging lengths obtained from such laminates were 1.33t for the AS1/3501-6 composite material and 2.73t for the T300/5208 composite material. One of the concerns in using this criterion that has been mentioned in the previous investigations is the reliability of the interlaminar strength data. The problem lies in the fact that these through-thickness quantities are inherently difficult to measure *in situ*, and thus, reliable values are often not available. Indeed, several values of the interlaminar strengths for a given composite material have been used with the QDC in the literature, *e.g.*, different values of the interlaminar normal strengths for the T300/5208 were used in two previous investigations referenced [42,44]. Since the averaging length is sensitive to the interlaminar strengths, the inaccuracy of the interlaminar strength values may be one of the reasons that a single value of the averaging length cannot be found.

Another possible explanation for the apparent non-uniqueness of the averaging

lengths is that the averaging length may be dependent on the nature of the interlaminar stress field. Different laminate or interface configurations give rise to different interlaminar stress distributions with varying orders of singularities that may necessitate the use of different averaging lengths. It can be seen that the averaging lengths in laminates with external ply dropoffs in Tables 8.1 are comparable to the typical values obtained from flat laminates with straight free edges but that the averaging lengths in laminates with internal ply dropoffs in Tables 8.1 are much larger (by a factor of approximately 2.5 to 3) along some potential critical interfaces. These interfaces are the third interfaces in the undropped region and the third (or second) interfaces in the dropped region. Based on this observation, it can suggested that there may exist one value of the averaging length for laminates with external ply dropoffs and another value for laminates with internal ply dropoffs due to the differences in the geometry of the interfaces considered. In the external cases, both the interlaminar shear and normal stresses are high along the critical interface with the interlaminar normal stress possibly being singular. In the internal cases, only the interlaminar shear stress is high along the third interface in the undropped region and is non-singular, while only the interlaminar normal stress is high along the third (or second) interface in the dropped region and is possibly singular. In order to validate this and other similar possibilities, a more precise stress analysis for the order of singularity at various interfaces and additional experimental data for other types of laminates with external and internal ply dropoffs would be required.

Although the results suggest that the QDC with the average stress method cannot be used to predict accurate delamination stresses in laminates with ply dropoffs using a single averaging length, the approach can be used to obtain general trends of the static delamination stresses. Since the qualitative comparisons have already shown good correlation between the interlaminar stress fields and the experimental observations concerning delamination, application of the QDC with the average stress method for this

capacity is also expected to show good agreement. In addition, this will also reveal which interfaces are the critical ones in laminates with internal ply dropoffs as shown in the following discussion.

To obtain the general trends of the static delamination stresses using the QDC with the average stress method, a suitable value of the averaging length is needed. Since a single value of the averaging length could not be found as discussed in the preceding section, it needs to be shown that general relative trends of the static delamination stresses are relatively insensitive to the choice of the averaging length in order for this delamination criterion to be useful. If this is the case, then it can be implied that one can judiciously choose a suitable averaging length to predict general delamination trends in other types of laminates with ply dropoffs as well. Thus, several averaging lengths within the range of the averaging lengths obtained in Tables 8.1 and 8.2 are used as a basis to predict the static delamination stresses. Specifically, four averaging lengths of 3.55t, 4.80t, 6.19t, and 7.54t are used. The first of the four averaging lengths of 3.55t is the mean averaging length of laminates with external ply dropoffs in Table 8.1, and the fourth averaging length of 7.54t is the mean averaging length of laminates with internal ply dropoffs along the third interface in the undropped region. The second and third averaging lengths of 4.80t and 6.19t were chosen to represent lengths between the first and fourth averaging lengths. The predicted delamination stresses obtained using these averaging lengths are shown in Tables 8.3 and 8.4 along with the experimental delamination stresses. The average experimental delamination stresses from Table 7.3 and the range of these loads is shown to indicate their variability. All delamination stresses are calculated using the thickness of the undropped region.

It can be seen in Tables 8.3 and 8.4 that the predicted static delamination stress increases with an increase in the averaging length for all laminates along each potential critical interface. For example, the predicted static delamination stress is 534 MPa in the $[0_{2D}/0_6]_s$ laminate when an averaging length of 3.55t is used, 628 MPa when 4.80t is

Table 8.3 Predicted and experimental delamination stresses for laminates with external ply dropoffs using four averaging lengths (units of [MPa])

Layup	Averaging Length				Experimental Average (range)
	3.55t	4.80t	6.19t	7.54t	
$[0_{2D}/0_6]_s$	534	628	718	796	544 (480 - 573)
$[0_{4D}/0_4]_s$	270	317	368	415	268 (240 - 283)

Table 8.4 Predicted[1] and experimental delamination stresses for laminates with internal ply dropoffs with a taper angle of 7° based on nominal angle used in experiments using four averaging lengths (units of [MPa])

Layup	Interface/ Region	Averaging Length				Experimental Average (range)
		3.55t	4.80t	6.19t	7.54t	
$[0_2/0_{2D}/0_4]_s$	First/ Undropped	1023	1386	1868	2400	1090 (1011-1160)
	Third/ Undropped	647	**724**	**822**	**926**	
	First/ Dropped	948	1222	1539	1858	
	Third[2]/ Dropped	**631**	815	1024	1233	
$[0_4/0_{2D}/0_2]_s$	First/ Undropped	1229	1622	2129	2688	978 (911-1023)
	Third/ Undropped	698	790	909	1036	
	First/ Dropped	750	878	1035	1199	
	Third[1]/ Dropped	**501**	**610**	**734**	**860**	
$[0_2/0_{4D}/0_2]_s$	First/ Undropped	605	825	1139	1521	600 (549-662)
	Third/ Undropped	416	**453**	**503**	**555**	
	First/ Dropped	612	801	1031	1268	
	Third[1]/ Dropped	**380**	493	626	761	
$[0_3/0_{4D}/0]_s$	First/ Undropped	682	906	1224	1625	491 (465-500)
	Third/ Undropped	429	474	536	604	
	First/ Dropped	457	563	699	845	
	Third[1]/ Dropped	**285**	**359**	**447**	**539**	

[1] Critical stress indicated in bold.

[2] Second and third interfaces are identical in the dropped region.

used, 718 MPa when 6.19t is used, and 796 MPa when 7.54t is used. Similar trends are seen in laminates with internal ply dropoffs as well. This increasing trend is expected because the average interlaminar stresses decrease with an increase in the averaging length based on the general distributions of interlaminar stresses, which peak in the vicinity of the cutoff and decay away from it.

Three general trends of the predicted delamination stresses in Tables 8.3 and 8.4 can be observed and compared with the trends of the experimental delamination stresses. One, it can be seen that predicted delamination stresses along the four potential critical interfaces in each laminate are different for a given averaging length. Thus, the lowest stress among the four stresses is the critical delamination stress and the interface along which this occurs is the critical interface. These critical delamination stresses for a given averaging length in each laminate are indicated in bold. It can be seen in Table 8.4 that the critical delamination stresses occur along the third interfaces in the undropped region in the $[0_2/0_{2D}/0_4]_s$ and $[0_2/0_{4D}/0_2]_s$ laminates and the third (or second) interfaces in the dropped region in the $[0_4/0_{2D}/0_2]_s$ and $[0_3/0_{4D}/0]_s$ laminates for all averaging lengths except when the averaging length of 3.55t is used. In such cases, the lowest predicted delamination stresses occur along the third (or second) interfaces in the dropped region in all laminates with internal ply dropoffs. Regardless of the location of the lowest predicted delamination stresses, it can be seen that the trend of the lowest predicted delamination stresses in the four laminates with internal ply dropoffs is consistent with the trend observed in the experimental data in that laminates with internal ply dropoffs closer to the mid-plane have lower delamination stresses than those with internal ply dropoffs further away from the mid-plane for all averaging lengths considered. It is noted that this trend may change when the averaging length exceeds 7.54t based on the rate of increase of the critical delamination stresses with averaging length.

The second observation is that the predicted delamination stresses in the two laminates with external ply dropoffs are lower than the critical delamination stresses in

laminates with internal ply dropoffs when the same number of plies are terminated for all averaging lengths with the exception of two averaging lengths in the $[0_4/0_{2D}/0_2]_s$ laminate. In the cases when the averaging length of 3.55t and 4.80t are used, the predicted critical delamination stresses in the $[0_4/0_{2D}/0_2]_s$ laminate are slightly smaller by approximately 5% than those in the $[0_{2D}/0_6]_s$ laminate. This shows that the trend of the predicted delamination stresses generally agree with the trend of the experimental delamination stresses, as expected from the qualitative comparison. The third observation is that the predicted delamination stresses in the laminates with 8-ply dropoffs are lower than those in laminates with 4-ply dropoffs for all averaging lengths. This trend is also consistent with the trend of the experimental delamination stresses.

These observations show that the QDC with the average stress method is capable of predicting the general trends of the static delamination stresses in laminates with ply dropoffs. Since the averaging length does not significantly affect the general trends of the delamination stresses within the range of the averaging lengths as shown herein, it is expected that general delamination trends in other types of laminates with ply dropoffs can be obtained in a similar manner using a judiciously chosen averaging length (or a range of averaging lengths).

Two further observations can be made in Tables 8.3 and 8.4. One, it can be seen that when a single averaging length is used, the critical delamination stresses do not exhibit good agreement with the experimental stresses for all the tested laminates, as expected. For example, when the averaging length of 7.54t is used, the predicted delamination stress of 796 MPa in the $[0_{2D}/0_6]_s$ laminate is greater than the experimental stress of 544 MPa by a factor of approximately 1.5, while the critical delamination stress of 555 MPa in the $[0_2/0_{4D}/0_2]_s$ laminate is comparable to the experimental stress of 600 MPa. In general, when the averaging length of 7.54t is used, it can be seen that the critical delamination stresses in laminates with internal ply dropoffs are comparable to those obtained experimentally, while the predicted delamination stresses in laminates

with external ply dropoffs are overestimated by a factor of approximately 1.5. On the other hand, when the averaging length of 3.55t is used, the predicted delamination stresses in laminates with external ply dropoffs are comparable to those obtained experimentally, while those in laminates with internal ply dropoffs are underestimated by a factor of approximately 1.5. This observation is another manifestation of the observation made previously based on which it was suggested that different averaging lengths may exist for laminates with internal and external ply dropoffs.

The other interesting observations is that although different averaging lengths yield different critical delamination stresses, the ratios of the predicted delamination stresses between the two laminates with external ply dropoffs remain relatively constant and comparable to the ratios of the experimental delamination stresses. The ratio of the predicted delamination stresses in the $[0_{2D}/0_6]_s$ laminate to the $[0_{4D}/0_4]_s$ laminate is approximately 2 (and range between 1.92 and 1.98) for all averaging lengths This is the same as the ratio between the experimental delamination stresses in the two laminates. The ratios of the predicted critical delamination stresses among the four laminates with internal ply dropoffs are also comparable to the ratios of the experimental delamination stresses although they exhibit slightly greater variations than those with external ply dropoffs. For example, the ratios of the predicted critical delamination stresses in the $[0_2/0_{2D}/0_4]_s$ laminates to the $[0_2/0_{4D}/0_2]_s$ laminates range between 1.60 and 1.67 for all averaging lengths while the ratio of the experimental delamination stresses between the two laminates is 1.82. For the $[0_4/0_{2D}/0_2]_s$ and the $[0_3/0_{4D}/0]_s$ laminates, the ratios range between 1.60 and 1.78 while the ratio of the experimental delamination stresses is 2.00. Similarly, the ratios between predicted critical delamination stresses of the $[0_2/0_{4D}/0_2]_s$ and $[0_3/0_{4D}/0]_s$ laminates range between 1.03 and 1.33, and those of the $[0_2/0_{2D}/0_4]_s$ and $[0_4/0_{2D}/0_2]_s$ laminates range between 1.08 and 1.26. The ratios from the experiments for the two pairs of laminates fall within these ranges and are equal to 1.22 and 1.11, respectively, for the former and latter pair of laminates.

In addition to the number and location of the terminated ply group, the predicted delamination stresses and critical locations may change in laminates with internal ply dropoffs when the taper angle changes. In order to investigate the sensitivity of the delamination stresses and critical locations with respect to the taper angle, the laminates with internal ply dropoffs were also analyzed using different angles of 3° and 10° as compared to the experimental angle of 7°. The averaging length of 7.54t used in the preceding discussion is used again for convenience. The predicted delamination stresses along all four potential critical interfaces in the laminates with internal ply dropoffs with taper angles of 3° are shown in Table 8.5 and those in laminates with taper angles of 10° are shown in Table 8.6. Again, the lowest predicted delamination stresses are shown in bold.

It can be seen in Table 8.5 that the predicted delamination stresses along the third interfaces in the dropped region are the lowest, and thus, the delamination initiation should occur along this interface in all four laminates with taper angles of 3°. The trend of the delamination stresses in these laminates shows that laminates with 8-ply dropoffs are smaller than those in laminates with 4-ply dropoffs as observed for the laminates with taper angles of 7°. However, unlike the laminates with taper angles of 7°, it can be seen that the laminates with ply dropoffs closer to the mid-plane have higher delamination stresses than those with ply dropoffs further away from the mid-plane. In Table 8.6, it can be seen that the lowest predicted delaminations stresses occur along the third interfaces in the undropped region in the $[0_2/0_{2D}/0_4]_s$ and $[0_2/0_{4D}/0_2]_s$ laminates and the third (or second) interfaces in the dropped region in the $[0_4/0_{2D}/0_2]_s$ and $[0_3/0_{4D}/0]_s$ laminates for the case of taper angles of 10°. This trend is similar to that observed for laminates with taper angles of 7°. For the case of taper angles of 10°, the delamination stresses in laminates with 8-ply dropoffs are smaller than those in laminates with 4-ply dropoffs and laminates with ply dropoffs closer to the mid-plane have lower delamination stresses than those with ply dropoffs further away from the mid-plane. These results

Table 8.5 Predicted delamination stresses[1] in laminates with taper angles of 3° using averaging length of 7.54t

Layup	Undropped Region		Dropped Region	
	First Interface [MPa]	Third Interface [MPa]	First Interface [MPa]	Third Interface[2] [MPa]
$[0_2/0_{2D}/0_4]_s$	5375	**992**	4051	2502
$[0_4/0_{2D}/0_2]_s$	6178	**1116**	2189	1488
$[0_2/0_{4D}/0_2]_s$	3049	**592**	2793	1622
$[0_3/0_{4D}/0]_s$	3607	**655**	1729	982

[1] Critical stress indicated in bold.

[2] Second and third interfaces are identical in the dropped region.

Table 8.6 Predicted delamination stresses[1] in laminates with taper angles of 10° using averaging length of 7.54t

Layup	Undropped Region		Dropped Region	
	First Interface [MPa]	Third Interface [MPa]	First Interface [MPa]	Third Interface[2] [MPa]
$[0_2/0_{2D}/0_4]_s$	1760	**883**	1400	965
$[0_4/0_{2D}/0_2]_s$	2061	992	1006	**740**
$[0_2/0_{4D}/0_2]_s$	1137	**527**	937	573
$[0_3/0_{4D}/0]_s$	1187	566	643	**422**

[1] Critical stress indicated in bold.

[2] Second and third interfaces are identical in the dropped region.

show that the trend of the delamination stresses in laminates with internal ply dropoffs may vary with the variation of the taper angle.

In addition to the varying trend of the delamination stresses, the magnitude of the delamination stress is seen to be relatively sensitive to the taper angle. To better observe this sensitivity, the lowest predicted delamination stresses in each laminate are shown again in Table 8.7. It can be seen that the lowest predicted delamination stress decreases with increasing taper angle for the three angles considered. For example, in the $[0_2/0_{2D}/0_4]_s$ laminate, the predicted critical stress decreases by approximately 10% when the taper angle is increased from 3° to 10°, and in the $[0_4/0_{2D}/0_2]_s$ laminate, the predicted critical stress increases by approximately 35% when the taper angle is increased by the same amount. This trend is reasonable based on the intuition that less stress concentration will occur in laminates with small taper angles than those with larger taper angles. The sensitivity of the predicted delamination stresses implies that irregularities in the taper angle due to manufacturing defects may significantly affect the static delamination stresses.

It is noted that in addition to the possible causes and implications of the lack of a single averaging length that were discussed herein, other possibilities need to be explored. One possibility is the suppression effect of the compressive interlaminar normal stresses that occur along the two potential critical interfaces in the undropped region [73]. Another possibility is that the interlaminar stresses obtained via the analytical method differ from those in the actual specimens due to simplifying assumptions such as the assumption that the resin pockets carry no load and that the taper angle in the dropoff region is constant. In actual specimens, the resin pockets are filled with matrix that do carry a small amount of load, and the taper angle is not constant over the entire dropped region because smooth transitions must occur between the dropoff region and undropped and dropped regions. Therefore, these assumptions may cause the interlaminar stresses obtained via the analytical method to be greater than those in actual

Table 8.7 Lowest predicted delamination stresses in laminates with internal ply dropoffs from Tables 8.4 through 8.6 using an averaging length of 7.54t (units of [MPa])

Layup	Taper Angle		
	3°	7°	10°
$[0_2/0_{2D}/0_4]_s$	992	926	883
$[0_4/0_{2D}/0_2]_s$	1116	860	740
$[0_2/0_{4D}/0_2]_s$	592	555	527
$[0_3/0_{4D}/0]_s$	655	539	422

specimens.

Based on the preceding discussion, it can be concluded that although the QDC with the average stress method could not be used to predict accurate delamination stresses in laminates with ply dropoffs using a single averaging length, the general trends of the delamination stresses can be obtained using this criterion.

CHAPTER 9

CONCLUSIONS AND RECOMMENDATIONS

In this work, the characteristics and trends of the interlaminar stress fields and delamination/damage in laminates with ply dropoffs under static and cyclic loads were investigated with the objective of obtaining a fundamental understanding of the mechanisms and structural parameters affecting such. To this end, analytical models that provide valuable insights in addition to accurate stress fields were developed; systematic experiments on laminates with simplified ply dropoff configurations were performed; and the static delamination characteristics from the experiments were correlated qualitatively and quantitatively with the obtained stress fields. In this section, the conclusions, as drawn from the preceding results and discussions, are presented, and recommendations for further investigations are proposed based on the understanding of laminates with ply dropoffs acquired from this work.

The following conclusions can be drawn from the current investigation of composite laminates with ply dropoffs:

1. The use of the building-block approach in the development of the analytical models provides a systematic framework in which the key features of generic laminates with ply dropoffs can be isolated and models developed in a hierarchical manner of increasing complexity. This approach provides the opportunity to gain overall insights to a complex problem via the process of isolating the key features and developing models based on those features as well as through the use of analytical models themselves.
2. The analytical models developed based on the building-block approach yield valid stress fields for laminates with ply dropoffs under in-plane and bending loads as

shown via comparison with numerical methods from the literature and from the current investigation. The stress fields in laminates with external ply dropoffs can be obtained most accurately using the global model and those in laminates with internal ply dropoffs using the mixed model.

3. The main advantages of the analytical models are that they are efficient and yield analytical expressions for the stress field. This allows many different configurations of laminates with ply dropoffs to be examined to identify the characteristics and trends of the interlaminar stress fields and for easy integration and incorporation into a delamination criterion.
4. It is important to consider and understand how various "global" structural parameters (*e.g.*, the layup of the undropped and dropped regions and the location of the ply dropoffs) affect the stress field in laminates with ply dropoffs in contrast to the "local" parameters (*e.g.*, effects of different termination sequences and the shape of the dropoff region and resin pocket) that have been considered in previous investigations on laminates with ply dropoffs because these global parameters can cause significant variations in the stress field.
5. A clear understanding of the variation of the stress field can be obtained by isolating the two fundamental mechanisms that give rise to interlaminar stresses in laminates with ply dropoffs: the *termination effect*, that is caused by the transfer of load from the terminated ply group to the continuous plies, and the *offset effect*, that is caused by the redistribution of the load from the undropped region to the dropped region in the outer continuous plies through an offset in the z-direction.
6. Interlaminar stresses due to the termination effect are affected by the magnitude of the far-field load in the terminated ply group and any associated factors that affect this. These factors include the magnitude and type of the applied load, the relative stiffness of the terminated ply group and the number of terminated plies.
7. Interlaminar stresses due to the offset effect are affected by the offset distance

between the lines of action of the far-field loads and the magnitudes of the far-field loads in the outer continuous ply group, the taper angle and any associated factors that affect these three items. These factors include the number of outer continuous plies and the ratio of the number of terminated plies to the number of outer continuous plies.

8. The utility of isolating and separately considering the two fundamental mechanisms in generic laminates with ply dropoffs separately is that the overall interlaminar stress distribution due to each mechanism can be predicted based on the understanding of the factors that affect them. This allows the overall characteristics and trends of the interlaminar stresses to be anticipated, and thereby helps to identify laminate configurations that alleviate the interlaminar stress fields.
9. The method of "virtual material properties" provides a convenient and systematic procedure to simulate the effects of varying the layup in composite laminates.
10. The characteristics of the interlaminar stresses in symmetric laminates under combined in-plane and bending loads and in geometrically unsymmetric laminates under in-plane load can be derived from the characteristics of symmetric laminates under in-plane and bending loads separately (to a first-order for the latter type of laminates).
11. Delamination is a key concern in the damage of unidirectional laminates with ply dropoffs under both static and fatigue cases as this mode was observed in most specimens tested along with other modes such as matrix cracks and ply splits.
12. The mismatch in the Poisson contraction in the undropped and dropped regions of the laminates with ply dropoffs can cause ply splits. This is a damage mode not previously reported for laminates with ply dropoffs in the literature.
13. The critical location for delamination initiation in specimens with external ply dropoffs under both static and fatigue loads is the ply dropoff location along the interface of the continuous and terminated plies.

14. There may be several critical locations for delamination initiation in specimens with internal ply dropoffs. The potential interfaces include the upper and lower interfaces of the continuous and terminated plies in the undropped region and the interface of the inner and outer continuous plies in the dropped region. The precise location(s) for delamination initiation in specimens with internal ply dropoffs under both static and cyclic loads could not be identified because finite length delaminations that extend across the various locations where the interlaminar stresses are high were observed along various interfaces.
15. The through-thickness location of the terminated ply group when the same number of plies are terminated significantly affects the delamination behavior. Ply dropoffs placed in the interior region of composite laminates as opposed to at the outer surfaces result in higher static delamination loads (by a factor of approximately two in unidirectional laminates) and longer initiation lives under cyclic loads. The location of the terminated ply group in laminates with internal ply dropoffs also affects the static delamination load and number of cycles to delamination initiation.
16. The number of terminated plies significantly affects the delamination behavior when the location of the terminated ply group is fixed. Laminates with fewer terminated plies result in higher static delamination loads (by a factor of approximately two in unidirectional laminates when the number of terminated plies are reduced by a factor of two).
17. The growth of delaminations in laminates with internal ply dropoffs under cyclic load is a greater concern in the undropped region because the length of these delaminations continue to increase indefinitely as compared to delaminations in the dropped region that are retarded after reaching a certain length (approximately 8 mm).
18. The critical location for delamination initiation and/or the mechanisms that cause delamination in laminates with internal ply dropoffs under static and cyclic loads

may be different as the static and fatigue delamination initiation trends exhibit differences.

19. The characteristics and trends of the interlaminar stress field in the tested laminates are consistent with the experimental observations concerning delamination.
20. Unlike the case of flat laminates with straight free edges from previous investigations, it was not possible to use the Quadratic Delamination Criterion with the average stress method and a single value of the averaging length to predict accurate delamination loads.
21. The Quadratic Delamination Criterion with the average stress method can be used to predict delamination trends in laminates with ply dropoffs using a carefully chosen averaging length due to the relative insensitivity of this parameter within a certain range (3.55 to 7.54 times the ply thickness, herein).

The following recommendations are proposed as future work based on the understanding established in the current work:

1. To build on and extend the current understanding of laminates with simplified dropoff configurations, further analysis should be performed on laminates with higher levels of complexity using the systematic framework based on the building-block approach proposed in the current work (see Figure 3.3). Since models at the next level of complexity require local details of the dropoff region, this will allow one to obtain a better understanding of the local effects of the ply dropoffs in addition to the overall effects from the current work. In addition, to obtain accurate stress fields in multidirectional laminates with ply dropoffs, the interlaminar stresses due to the free edges should be considered.
2. The analytical model for laminates with existing delaminations is a simple and efficient alternative compared to time-consuming finite element analysis, and thus, deserves further investigation for extension to include the realistic effect of contact.

Such would allow more accurate stress fields to be obtained for laminates with existing delaminations.

3. To obtain better approximations to the interlaminar stresses in geometrically unsymmetric laminates, the analytical model should be extended to account for varying applied moments along the length of the laminate. Analysis using such a model will yield more accurate interlaminar stresses in the vicinity of the dropoffs, which is of primary interest.
4. Further experiments should be conducted on specimens with layups other than those considered in the current set of experiments to validate the results from the current analytical work. One, specimens with different taper angles should be tested to compare delamination characteristics with the analytical result that interlaminar normal stresses in the dropped region are directly related to the taper angle. Two, specimens with various layup sequences should be tested to determine whether the interlaminar stress field can be alleviated as proposed based on the analytical results. Specifically, stress analysis shows that lower interlaminar stresses occur in the cases where laminates have terminated ply groups with stiffnesses lower than those of the continuous ply groups and in laminates that have terminated plies with lower stiffness immediately adjacent to continuous plies (see Section 6.2.3).
5. In order to determine the precise location of delamination initiation in laminates with internal ply dropoffs, careful *in situ* experiments with high-speed camera(s) and/or placement of small sensors such as strain-gages in the vicinity of the dropoff region need to be performed. The identification of the precise location will help obtain a more reliable value for the averaging length by eliminating the need to calculate the mean averaging lengths of several potential critical interfaces as was done in the current work.
6. The phenomenon of delamination retardation in the dropped region and its interaction with the delamination growth in the undropped region of laminates with

internal ply dropoffs under cyclic load deserves further investigation. The characteristics of the retardation phenomenon such as the length of the delamination at and the rate of retardation should be quantified and compared with analysis of interlaminar stresses and/or stress intensity factor at the delamination tip to identify the conditions under with such conditions arise. In addition, the effect of this phenomenon on subsequent structural response such as residual strength should be explored to understand its implications on damage tolerance.

7. In order to better quantify delamination growth in laminates with ply dropoffs, experiments should be conducted on laminates with pre-cracks inserted at the interfaces of interest via teflon inserts in the undropped and dropped regions so as to avoid delamination initiations that do not extend across the width of the laminate and thereby induce non-self-similar growth.
8. Further investigation should be performed to determine whether or not the averaging length in laminates with ply dropoffs is multi-valued as suggested by the current work. To do so, further tests are recommended on specimens with the same layups as those considered in this work to obtain a statistically significant set of data as well as on specimens with other layups. In addition, reliable *in situ* interlaminar strengths need to be obtained in order to better apply the delamination criterion. If the averaging length is found to be non-unique, methods should be devised to identify its generic dependence on the laminate/interface configurations in order to predict accurate delamination loads using strength-based delamination criteria that use the average stress method, including the Quadratic Delamination Criterion used in the current work.

REFERENCES

[1] Jones, R. M., "Mechanics of Composite Materials, 2nd Ed.", Philadelphia, Taylor & Francis, 1998.

[2] Hoskin, B. C. and Baker, A. A. Eds., "Composite Materials for Aircraft Structures", in *AIAA Education Series*, J. S. Przemieniecki, Ed., New York, AIAA, 1986.

[3] Middleton, D. H., Ed., "Composite Materials in Aircraft Structures", New York, John Wiley & Sons, Inc., 1990.

[4] Sen, J. K., "Application of Composites in Commercial Helicopters", in *Vertiflite*, vol. 43 (2), 1996, pp. 58-65.

[5] Vizzini, A. J. and Lee, S. W., "Damage Analysis of Composite Tapered Beams", *Journal of the American Helicopter Society*, 40(2), 1995, pp. 43-49.

[6] Lagace, P. A., "On Delamination Failures in Composite Laminates", *Composite Structures: Testing, Analysis and Design*, J. N. Reddy and A. V. K. Murty, Eds., Berlin, Springer-Verlag, 1992, pp. 111-132.

[7] Fish, J. C. and Lee, S. W., "Delamination of Tapered Composite Structures", *Engineering Fracture Mechanics*, 4(1), 1989, pp. 43-54.

[8] Lee, S. and Knauss, W. G., "Failure of Laminated Composites at Thickness Discontinuities Under Complex Loading and Elevated Temperatures", *International Journal of Solids and Structures*, 37, 2000, pp. 3479-3501.

[9] Cannon, R. K., "The Effects of Ply Dropoffs on the Tensile behavior of Graphite/Epoxy Laminates", Massachusetts Institute of Technology, Department of Aeronautics and Astronautics, TELAC Report #87-12, S.M. Thesis, Cambridge, MA, 1987.

[10] Curry, J. M., Johnson, E. R., and Starnes, J. H., "Effect of Dropped Plies on the Strength of Graphite-Epoxy Laminates", *AIAA Journal*, 30, 1992, pp. 449-456.

[11] Grimes, G. C. and Dusablon, E. G., "Study of Compression Properties of Graphite/Epoxy Composites with Discontinuities", *Composite Materials: Design and Testing (Sixth Conference)*, I. M. Daniels, Ed., Philadelphia, PA, ASTM STP 787, 1982, pp. 513-538.

[12] Botting, A. D., Vizzini, A. J., and Lee, S. W., "Effect of Ply-drop Configuration on Delamination Strength of Tapered Composite Structures", *AIAA Journal*, 34(8), 1996, pp. 1650-1656.

[13] Wisnom, M. R., Jones, M. I., and Cui, W., "Delamination in Composites with Terminating Internal Plies Under Tension Fatigue Loading", *Composite Materials: Fatigue and Fracture (Fifth Volume)*, R. H. Martin, Ed., Philadelpia, PA, ASTM STP 1230, 1995, pp. 486-508.

[14] DiNardo, M. T. and Lagace, P. A., "Buckling and Post Buckling of Laminated Composite Plates with Ply Drop-offs", *AIAA Journal*, 27, 1989, pp. 1392-1398.

[15] Herakovich, C. T., "Mechanics of Fibrous Composites", New York, John Wiley & Sons Inc., 1998.

[16] Cui, W., Wisnom, M. R., and Jones, M. I., "Effect of Through Thickness Tensile and Compressive Stresses on Delamination Propagation Fracture Energy", *Journal of Composites Technology & Research*, 16(4), 1994, pp. 329-335.

[17] Wisnom, M. R., Jones, M. I., and Cui, W., "Failure of Tapered Composites Under Static and Fatigue Tension Loading", *AIAA Journal*, 33(5), 1995, pp. 911-918.

[18] Miravete, A., "Strain and Stress Analysis in Tapered Laminated Composite Structures", *Composite Structures*, 16, 1990, pp. 65-84.

[19] Gopal, P., Yen, S. C., and Dharani, L. R., "Flexural Behavior of Stepped Graphite/Epoxy Laminates", *Polymer Composites*, 15(1), 1994, pp. 18-24.

[20] Kassapoglou, C. and Lagace, P. A., "An Efficient Method for the Calculation of Interlaminar Stresses in Composite Materials", *Journal of Applied Mechanics*, 53, 1986, pp. 744-749.

[21] Wisnom, M. R., "Delamination in Tapered Unidirectional Glass Fibre-Epoxy Under Static Tension Loading", AIAA Paper No. 91-1142-CP, *Proceedings of the 30th AIAA/ASME/ASCE/AHS/ASC Structures, Structural Dynamics and Materials Conference*, Baltimore, MD, 1991, pp. 1162-1172.

[22] Wisnom, M. R., "Prediction of Delamination in Tapered Unidirectional Glass Fibre Epoxy with Dropped Plies Under Static Tension and Compression", *AGARD, Debonding/Delamination of Composites*, 1992, pp. 25-1~25-7.

[23] Murri, G. B., Salpekar, S. A., and O'Brien, T. K., "Fatigue Delamination Onset Prediction in Unidirectional Tapered Laminates", *Composite Materials: Fatigue and Fracture (Third Volume)*, T. K. O'Brien, Ed., Philadelphia, PA, ASTM STP 1110, 1991, pp. 312-339.

[24] Murri, G. B., O'Brien, T. K., and Salekar, S. A., "Tension Fatigue of Glass/Epoxy and Graphite/Epoxy Tapered Laminates", *Journal of the American Helicopter Society*, Jan., 1993, pp. 29-37.

[25] Hoa, S. V., Daoust, J., Du, B. L., and Vu-Khanh, T., "Interlaminar Stresses in Tapered Laminates", *Polymer Composites*, 9(5), 1988, pp. 337-344.

[26] Kemp, B. L. and Johnson, E. R., "Response and Failure Analysis of a Graphite-Epoxy Laminate Containing Terminating Internal Plies", AIAA Paper No. 85-0608, *Proceedings of the 26th AIAA/ASME/ASCE/AHS Structures, Structural Dynamics and Materials Conference*, Monterey, CA, 1985, pp. 13-24.

[27] Wu, C. M. L. and Webber, J. P. H., "Analysis of Tapered (in Steps) Laminated Plates Under Uniform In-plane Load", *Composite Structures*, 5, 1986, pp. 87-100.

[28] Daoust, J. and Hoa, S. V., "Parameters Affecting Interlaminar Stresses in Tapered Laminates Under Static Loading Conditions", *Polymer Composites*, 10(5), 1989, pp. 374-383.

[29] Poon, C. Y., Ruiz, C., and Allen, C. B., "Finite Element Analysis of a Tapered Composite", *Composites Science and Technology*, 51, 1994, pp. 429-440.

[30] Wu, C. M. L., "Non-linear Analysis of Tapered (in Steps) Laminated Plates Under Uniform In-plane Load", *Composite Structures*, 7, 1987, pp. 205-223.

[31] Wang, S. S., "Delamination Crack Growth in Unidirectional Fiber-Reinforced Composites under Static and Cyclic Loading", *Composite Materials: Testing and Design (Fifth Conference)*, S. W. Tsai, Ed., ASTM STP 674, 1979, pp. 642-663.

[32] Fish, J. C., "Tensile Strength of Composite Structures with Internal Ply Drops and Free-Edge Effects", University of Maryland, Department of Aerospace Engineering, Tensile Strength of Composite Structures with Internal Ply Drops and Free-Edge Effects, Ph.D. Thesis, College Park, MD, 1988.

[33] Llanos, A. S. and Vizzini, A. J., "The Effect of Film Adhesive on the Delamination Strength of Tapered Composites", *Journal of Composite Materials*, 26(13), 1992, pp. 1968-1983.

[34] Vizzini, A. J., "Influence of Realistic Ply-drop Geometries on Interlaminar Stresses in Tapered Laminates", *Composite Materials: Fatigue and Fracture (Fifth Volume)*, R. H. Martin, Ed., Philadelphia, PA, ASTM STP 1230, 1995, pp. 467-485.

[35] Varughese, B. and Mukherjee, A., "A Ply Drop-off Element for Analysis of Tapered Laminated Composites", *Composite Structures*, 39, 1997, pp. 123-144.

[36] Armanios, E. A. and Parnas, L., "Delamination Analysis of Tapered Laminated Composites Under Tensile Loading", *Composite Materials: Fatigue and Fracture (Third Volume)*, T. K. O'Brien, Ed., Philadelphia, PA, ASTM STP 1110, 1991, pp. 340-358.

[37] Vizzini, A. J., "Shear-lag Analysis About an Internally-Dropped Ply", *Journal of Reinforced Plastics and Composites*, 16(1), 1997, pp. 73-85.

[38] Kassapoglou, C., "Stress Determination at Skin-Stiffener Interfaces of Composite

Stiffened Panels under Generalized Loading", *Journal of Reinforced Plastics and Composites*, 13, 1994, pp. 555-572.

[39] Harrison, P. N. and Johnson, E. R., "A Mixed Variational Formulation for Interlaminar Stresses in Thickness Tapered Composite Laminates", *International Journal of Solids and Structures*, 33(16), 1996, pp. 2377-2399.

[40] Thomsen, O. T., Rits, W., Eaton, D. C. G., and Brown, S., "Ply Drop-off Effects in CFRP/Honeycomb Sandwich Panels - Theory", *Composites Science and Technology*, 56, 1996, pp. 407-422.

[41] Rose, C. A. and Starnes, J. H., "Approximate Analysis for Interlaminar Stresses in Composite Structures with Thickness Discontinuities", AIAA Paper No. 96-1497-CP, *Proceedings of the 39th AIAA/ASME/ASCE/AHS/ASC Structures, Structural Dynamics, and Materials Conference and Exhibit*, Salt Lake City, UT, 1996, pp. 1623-1638.

[42] Brewer, J. C. and Lagace, P. A., "Quadratic Stress Criterion for Initiation of Delamination", *Journal of Composite Materials*, 22, 1988, pp. 1141-1155.

[43] Whitney, J. M. and Nuismer, R. J., "Stress Fracture Criteria for Laminated Composites Containing Stress Concentrations", *Journal of Composite Materials*, 8, 1974, pp. 253-265.

[44] Kim, R. Y. and Soni, S. R., "Experimental and Analytical Studies on the Onset of Delamination in Laminated Composites", *Journal of Composite Materials*, 18, 1984, pp. 70-80.

[45] Wu, E. M., "Fracture Mechanics of Anisotropic Plates", *Composite Materials Workshop*, J. C. H. S.W. Tsai, and N.J. Pagano, Ed., Technomic Publishing Co., 1968, pp. 20-43.

[46] Rybicki, E. F., Schmueser, D. W., and Fox, J., "An Energy Release Rate Approach for Stable Crack Growth in the Free-edge Delamination Problem", *Journal of Composite Materials*, 11, 1977, pp. 470-487.

[47] O'Brien, T. K., "Mixed-mode Strain-Energy-Release Rate Effects on Edge Delamination of Composites", *Effects of Defects in Composite Materials*, ASTM STP 836, 1984, pp. 125-142.

[48] Davidson, B. D., Gharibian, S.J., and Yu, Lije, "Evaluation of Energy Release Rate-Based Approaches for Predicting Growth in Laminated Composites", *International Journal of Fracture*, 105, 2000, pp. 343-365.

[49] "Standard Test Method for Plane Strain Fracture Toughness of Metallic Materials", E399-90, ASTM, 1997.

[50] Tada, H., Paris, P.C., and Irwin, G.R., "The Stress Analysis of Cracks Handbook",

Hellertown, PA, Del Research Corp., 1973.

[51] "Standard Test Method for Mode I Interlaminar Fracture Toughness of Unidirectional Fiber-Reinforced Polymer Matrix Composites", D 5528-94a, ASTM, 2001.

[52] O'Brien, T. K., "Characterization of Delamination Onset and Growth in a Composite Laminate", *Damage in Composite Materials*, K. L. Reifsnider, Ed., ASTM STP 775, 1982, pp. 140-167.

[53] Petrossian, Z. and Wisnom, M. R., "Parametric Study of Delamination in Composites with Discontinuous Plies Using an Analytical Solution Based on Fracture Mechanics", *Composites Part A*, 29A, 1998, pp. 403-414.

[54] Cui, W., Wisnom, M. R., and Jones, M. I., "New Model to Predict Static Strength of Tapered Laminates", *Composites*, 26, 1995, pp. 141-146.

[55] Paris, P. C. and Erdogan, F., "A Critical Analysis of Crack Propagation Laws", *Journal of Basic Engineering*, 85, 1963, pp. 528-534.

[56] Suresh, S., "Fatigue of Materials", Cambridge, Cambridge University Press, 1998.

[57] O'Brien, T. K., "Towards a Damage Tolerance Philosophy for Composite Materials and Structures", *Composite Materials: Testing and Design (Ninth Volume)*, S. P. Garbo, Ed., Philadelphia, PA, ASTM STP 1059, 1990, pp. 7-33.

[58] Murri, G. B., O'Brien, T. K., and Rousseau, C. Q., "Fatigue Life Methodology for Tapered Composite Flexbeam Laminates", *Journal of the American Helicopter Society*, April, 1998, pp. 146-155.

[59] "The Composite Materials Handbook MIL-17 Vol. 1: Guidelines for Characterization of Structural Materials", MIL-HDBK-17-1E, Department of Defense, 1999.

[60] Saeger, K. J., "An Efficient Semi-Analytical Method for the Calculation of Interlaminar Stresses Around Holes", Massachusetts Institute of Technology, Department of Aeronautics and Astronautics, TELAC Report #89-11, Ph.D. Thesis, Cambridge, MA, 1989.

[61] Bhat, N. V. and Lagace, P. A., "An Analytical Method for the Evaluation of Interlaminar Stresses Due to Material Discontinuities", *Journal of Composite Materials*, 28(3), 1994, pp. 190-210.

[62] "ABAQUS/Standard User's Manual v6.2", Hibbitt, Karlsson & Sorensen, Inc., 2001.

[63] Whitcomb, J. D. and Raju, I. S., "Superposition Method for Analysis of Free-Edge Stresses", *Journal of Composite Materials*, 17, 1983, pp. 492-507.

[64] Bhat, N. V., "Delamination Suppression in Graphite/Epoxy Composites via Efficient Use of Film Adhesive", Massachusetts Institute of Technology, Department of Aeronautics and Astronautics, TELAC Report #89-14, S.M. Thesis, Cambridge, MA, 1990.

[65] Lekhnitskii, S. G., "Theory of Elasticity of an Anisotropic Elastic Body", P. Fern trans., San Francisco, Holden-Day, 1963.

[66] Bathe, K. J., "Finite Element Procedures", Englewood Cliffs, NJ, Prentice-Hall, Inc., 1996.

[67] "Standard Test Method for Tensile Properties of Polymer Matrix Composite Materials", D 3039M-00a, ASTM, 2000.

[68] Lagace, P. A., Beaumont, M., Brewer, J.C., and Varnerin, C.F., "TELAC Manufacturing Course Class Notes", TELAC Report 88-4b, TELAC, MIT, 1991.

[69] Wang, A. S. D. and Crossman, F. W., "Some New Results on Edge Effect in Symmetric Composite Laminates", *Journal of Composite Materials*, 11, 1977, pp. 92-106.

[70] Salamon, N. J., "Interlaminar Stresses in a Layered Composite Laminate in Bending", *Fibre Science and Technology*, 11, 1978, pp. 305-317.

[71] Zwiers, R. I., Ting, T. C. T., and Spilker, R. L., "On the Logarithmic Singularity of Free-Edge Stress in Laminated Composites Under Uniform Extension", *Journal of Applied Mechanics*, 49(3), 1982, pp. 561-569.

[72] Di Sciuva, M., "A General Quadrilateral Multilayered Plate Element with Continuous Interlaminar Stresses", *Computers and Structures*, 47, 1993, pp. 91-105.

[73] Kim, R. Y. and Soni, S. R., "Failure of Composite Laminates due to Combined Interlaminar Normal and Shear Stresses", *Composites '86: Recent Advances in Japan and the United States, Proceedings of the Japan-US CCM-III*, Tokyo, 1986.

[74] Yamashita, M. M., Hua, C.T., Stumpff, P., "Expansion of Fractographic Database for Carbon Fiber Reinforced Plastics (CFRP)", *Proceedings of the International Symposium on Testing and Failure Analysis*, Los Angeles, CA, 1988, pp. 289-297.

[75] "3501-6 Epoxy Matrix Product Data", Hexcel Composites, Pleasanton, CA, 1998.

[76] Lagace, P. A. and Weems, D. B., "A Through-the-thickness Strength Specimen for Composites", *Test Methods and Design Allowables for Fibrous Composites*, Philadelphia, PA, 1989, pp. 197-207.

APPENDIX A

SOURCE CODE LISTING FOR ANALYSIS OF LAMINATES WITH PLY DROPOFFS UNDER IN-PLANE LOAD

The source codes of the programs for analysis of laminates with ply dropoffs under in-plane load are listed in this appendix. One main program, named 'inplane.m', was written for this loading condition where the user is prompted to input the laminate configuration and material properties, and the eigenvalues and eigenvectors for equations (4.28) and (4.29) are calculated. Separate subroutines were written to obtain the unknown constants, a_j and b_j, for the global model (from equation (4.54)), mixed model (from equation (4.60)) and model for laminates with existing delaminations (from equation (4.69)). The program named 'global_i.m' is the subroutine for the global model, 'mixed_i.m' for the mixed model, and 'delam_i.m' for the model with existing delamination. Other subroutines called by these programs are also listed. A plotting program, 'plot_i.m' is also listed. This program is used to visualize the stress field in the laminates analyzed. All programs are written for Matlab® Release 12.

```
% ------------------------------------------------------------
%                          inplane.m
%   Stress Analysis Program for Laminates Under In-plane Loads
%                             by
%                          DJ Shim
%
%      Copyright 2002, Massachusetts Institute of Technology
%
% Permission to use, copy, modify, and distribute this software
% for any purpose and without fee is hereby granted, provided that
% the above copyright notice appear in all copies and that both
% that copyright notice and this permission notice appear in
% supporting documentation, and that the name of MIT not be used
% in advertising or publicity pertaining to distribution of the
% software without specific, written prior permission. MIT makes no
% representations about the suitability or merchantability of the
% documentation (or its associated software) for any purpose.
% It is provided "as is" without express or implied warranty.
% This software is a research program, and MIT does not represent
% that it is free of errors or bugs or suitable for any particular
% task.
% ------------------------------------------------------------

clear all

% ------------------------------------------------------------
% User input query
% ------------------------------------------------------------

model = input('>> Select Analytical Model (default = 2) \n>> [1] Global Model
[2] Mixed Model [3] Existing Delamination \n?? ');
if isempty(model) model = 2; end;
Fx = input('>> Applied Force (default = 8000 N)? \n?? ');
if isempty(Fx) Fx = 8000; end;
% Symmetric layups (100 refers to terminated plies, 2xx refers to variable
stiffness plies)
LayUp = input('\n>> Layup of Half Laminate (default = [0t2/0t4D/0t2]s)? \n??
');
if isempty(LayUp) LayUp = [0 0 0 0 0 0 0 0;
                           0 0 100 100 100 100 0 0];
end;
LayUp = LayUp*pi/180;
alpha = 0;
if LayUp(2,1) ~= 100*pi/180
    alpha = input('\n>> Taper Angle (default = 7deg)? ');
    if isempty(alpha) alpha = 7; end % Taper angle (in degrees)
end
t = input('\n>> Normalized Ply Thickness (default = 1)? ');
if isempty(t) t = 1; % Each layer thickness is 1
end
[EL ET GLT GTT NuLT NuTT] = as4_3501d6; % Material constants
F = [Fx;0;0]; % Applied force
b = 80*t; % Length of laminate in undropped and dropped regions

% ------------------------------------------------------------
% Initialize variables
% ------------------------------------------------------------

NuTL = (ET/EL) * NuLT;
MaterialConstants = [EL ET NuLT NuTL NuTT GLT GTT];
RegionALayUp = LayUp(1,:);
RegionBLayUp = LayUp(2,:);
for region = 1:2
```

```
   tempLayUp = LayUp(region,:);
   tempNumHalfPly = size(tempLayUp);
   tempNumHalfPly = tempNumHalfPly(2);
   CurrentLayUp = [];
   for i = 1:tempNumHalfPly
      if LayUp(region,i) ~= 100*pi/180
         CurrentLayUp = [CurrentLayUp LayUp(region,i)];
      end
   end
   CurrentNumHalfPly = size(CurrentLayUp);
   CurrentNumHalfPly = CurrentNumHalfPly(2);
   n(region) = CurrentNumHalfPly;
end

for i = 1:n(1)
   if RegionBLayUp(i) == 100*pi/180
      TestDropPly(i) = 1;
      DropPly = i;
   else
      TestDropPly(i) = 0;
   end
end

% ------------------------------------------------------------------
% Solve CLPT problem
% ------------------------------------------------------------------

for region = 1:2
   CurrentLayUp = [];
   for i = 1:n(1)
      if LayUp(region,i) ~= 100*pi/180
         CurrentLayUp = [CurrentLayUp LayUp(region,i)];
      end
   end
   [tempstrain,tempcltstress,tempcltnstress] =
clt2(F,MaterialConstants,CurrentLayUp,t);
   if region == 1
      strain(:,:,region) = tempstrain;
      cltstress(:,:,region) = tempcltstress;
      cltnstress(:,:,region) = tempcltnstress;
   else
      strain(:,:,region) = tempstrain;
      j = 1;
      for i = 1:n(1)
         if TestDropPly(i) == 1
            cltstress(:,i,region) = zeros(3,1);
            cltnstress(:,i,region) = zeros(3,1);
         else
            cltstress(:,i,region) = tempcltstress(:,j);
            cltnstress(:,i,region) = tempcltnstress(:,j);
            j = j+1;
         end
      end
   end
end
ncltstress = cltstress; % CLT stresses normalized to one

% ------------------------------------------------------------------
% Solve companion problem
% ------------------------------------------------------------------

% Calculate eigenvalues and eigenvectors
eigval = zeros(1,2*(2*(n(1)-1))-(n(1)-1),2);
```

```
eigvec = zeros(2*(2*(n(1)-1))-2*(n(1)-1),2*(2*(n(1)-1))-(n(1)-1),2);
Oa_A = zeros(2*(2*(n(1)-1))-(n(1)-1),2*(2*(n(1)-1))-(n(1)-1));
Oa_B = zeros(2*(2*(n(2)-1))-(n(2)-1),2*(2*(n(2)-1))-(n(2)-1));
for region = 1:2
   M = zeros(2*(2*(n(region)-1))-(n(region)-1),2*(2*(n(region)-1))-(n(region)-
1),n(region),9);
   CurrentLayUp = [];
   for i = 1:tempNumHalfPly
      if LayUp(region,i) ~= 100*pi/180
         CurrentLayUp = [CurrentLayUp LayUp(region,i)];
      end
   end
   [AA,BB,CC,S,BS,Ss_L] = companion2(MaterialConstants,CurrentLayUp,t);
   ALPHA = [BB AA;AA zeros(2*(n(region)-1),2*(n(region)-1))];
   BETA = [-CC zeros(2*(n(region)-1),2*(n(region)-1));zeros(2*(n(region)-
1),2*(n(region)-1)) AA];
   [v,d] = eig(BETA,ALPHA);
   v = v(1:2*(2*(n(region)-1))-2*(n(region)-1),1:2*(2*(n(region)-1))-
(n(region)-1));
   d = diag(d);

   % Choose decaying eigenvalues and corresponding eigenvector pair
   if region == 1
      sqrtd = sqrt(d(1:2*(2*(n(region)-1))-(n(region)-1)));
      for i = 1:2*(2*(n(region)-1))-(n(region)-1)
         eigval(1,i,region) = sqrtd(i);
         eigvec(:,i,region) = v(:,i);
      end
   else
      sqrtd = -sqrt(d(1:2*(2*(n(region)-1))-(n(region)-1)));
      for i = 1:2*(2*(n(region)-1))-(n(region)-1)
         eigval(1,i,region) = sqrtd(i);
         for j = 1:2*(n(region)-1)
            eigvec(j,i,region) = v(j,i);
         end
      end
   end
   eval = eigval(:,:,region);
   evec_F = eigvec(1:n(region)-1,:,region);
   evec_G = eigvec(n(region):2*(n(region)-1),:,region);
   for p = 1:2*(2*(n(region)-1))-(n(region)-1)
      for q = 1:2*(2*(n(region)-1))-(n(region)-1)
         for i = 1:n(region)
            if i == 1
               M(p,q,i,1) = 1/(eval(p)+eval(q))*evec_F(i,p)*evec_F(i,q);
               M(p,q,i,2) =
3*(eval(p)*eval(q))^2/(eval(p)+eval(q))*evec_F(i,p)*evec_F(i,q);
               M(p,q,i,3) = 1/(eval(p)+eval(q))*evec_G(i,p)*evec_G(i,q);
               M(p,q,i,4) =
eval(p)*eval(q)/(eval(p)+eval(q))*evec_G(i,p)*evec_G(i,q);
               M(p,q,i,5) =
eval(p)*eval(q)/(eval(p)+eval(q))*evec_F(i,p)*evec_F(i,q);
               M(p,q,i,6) =
eval(q)^2/(eval(p)+eval(q))*evec_F(i,p)*evec_F(i,q);
               M(p,q,i,7) = 1/(eval(p)+eval(q))*evec_F(i,p)*evec_G(i,q);
               M(p,q,i,8) = eval(p)^2/(eval(p)+eval(q))*evec_G(p)*evec_F(q);
               M(p,q,i,9) =
eval(p)*eval(q)/(eval(p)+eval(q))*evec_F(i,p)*evec_G(i,q);
            elseif i == n(region)
               M(p,q,i,1) = 1/(eval(p)+eval(q))*evec_F(i-1,p)*evec_F(i-1,q);
               for m = 1:i-1
                  for l = 1:i-1
```

```
                    M(p,q,i,2) = M(p,q,i,2) +
60*(eval(p)*eval(q))^2/(eval(p)+eval(q))*evec_F(m,p)*evec_F(l,q);
                end
                M(p,q,i,2) = M(p,q,i,2) -
20*(eval(p)*eval(q))^2/(eval(p)+eval(q))*evec_F(i-1,p)*evec_F(m,q);
                M(p,q,i,6) = M(p,q,i,6) -
6*(eval(q))^2/(eval(p)+eval(q))*evec_F(i-1,p)*evec_F(m,q);
                M(p,q,i,8) = M(p,q,i,8) -
6*(eval(q))^2/(eval(p)+eval(q))*evec_G(i-1,p)*evec_F(m,q);
             end
             M(p,q,i,2) = M(p,q,i,2) +
3*(eval(p)*eval(q))^2/(eval(p)+eval(q))*evec_F(i-1,p)*evec_F(i-1,q);
             M(p,q,i,3) = 1/(eval(p)+eval(q))*evec_G(i-1,p)*evec_G(i-1,q);
             M(p,q,i,4) = eval(p)*eval(q)/(eval(p)+eval(q))*evec_G(i-
1,p)*evec_G(i-1,q);
             M(p,q,i,5) = eval(p)*eval(q)/(eval(p)+eval(q))*evec_F(i-
1,p)*evec_F(i-1,q);
             M(p,q,i,6) = M(p,q,i,6) + eval(q)^2/(eval(p)+eval(q))*evec_F(i-
1,p)*evec_F(i-1,q);
             M(p,q,i,7) = 1/(eval(p)+eval(q))*evec_F(i-1,p)*evec_G(i-1,q);
             M(p,q,i,8) = M(p,q,i,8) + eval(q)^2/(eval(p)+eval(q))*evec_G(i-
1,p)*evec_F(i-1,q);
             M(p,q,i,9) = eval(p)*eval(q)/(eval(p)+eval(q))*evec_F(i-
1,p)*evec_G(i-1,q);
          else
             M(p,q,i,1) = 1/(eval(p)+eval(q))*evec_F(i-1,p)*evec_F(i-1,q) ...
                - 2*1/(eval(p)+eval(q))*(evec_F(i-1,p)*evec_F(i,q)) ...
                + 1/(eval(p)+eval(q))*evec_F(i,p)*evec_F(i,q) ;
             for m = 1:i-1
                for l = 1:i-1
                   M(p,q,i,2) = M(p,q,i,2) +
60*(eval(p)*eval(q))^2/(eval(p)+eval(q))*evec_F(m,p)*evec_F(l,q);
             end
             M(p,q,i,2) = M(p,q,i,2) -
20*(eval(p)*eval(q))^2/(eval(p)+eval(q))*evec_F(m,p)*evec_F(i-1,q) ...
              +
20*(eval(p)*eval(q))^2/(eval(p)+eval(q))*evec_F(m,p)*evec_F(i,q);
             M(p,q,i,6) = M(p,q,i,6) -
6*(eval(q))^2/(eval(p)+eval(q))*evec_F(i-1,p)*evec_F(m,q) ...
                + 6*(eval(q))^2/(eval(p)+eval(q))*evec_F(i,p)*evec_F(m,q);
             M(p,q,i,8) = M(p,q,i,8) -
6*(eval(q))^2/(eval(p)+eval(q))*evec_G(i-1,p)*evec_F(m,q) ...
                + 6*(eval(q))^2/(eval(p)+eval(q))*evec_G(i,p)*evec_F(m,q);
          end
             M(p,q,i,2) = M(p,q,i,2) +
3*(eval(p)*eval(q))^2/(eval(p)+eval(q))*evec_F(i-1,p)*evec_F(i-1,q) ...
                - (eval(p)*eval(q))^2/(eval(p)+eval(q))*evec_F(i-
1,p)*evec_F(i,q) ...
                +
3*(eval(p)*eval(q))^2/(eval(p)+eval(q))*evec_F(i,p)*evec_F(i,q);
             M(p,q,i,3) = 1/(eval(p)+eval(q))*evec_G(i-1,p)*evec_G(i-1,q) ...
                - 2/(eval(p)+eval(q))*(evec_G(i-1,p)*evec_G(i,q)) ...
                + 1/(eval(p)+eval(q))*evec_G(i,p)*evec_G(i,q);
             M(p,q,i,4) = eval(p)*eval(q)/(eval(p)+eval(q))*evec_G(i-
1,p)*evec_G(i-1,q) ...
                + eval(p)*eval(q)/(eval(p)+eval(q))*(evec_G(i-
1,p)*evec_G(i,q)) ...
                + eval(p)*eval(q)/(eval(p)+eval(q))*evec_G(i,p)*evec_G(i,q);
             M(p,q,i,5) = eval(p)*eval(q)/(eval(p)+eval(q))*evec_F(i-
1,p)*evec_F(i-1,q) ...
                + eval(p)*eval(q)/(eval(p)+eval(q))*(evec_F(i-
1,p)*evec_F(i,q)) ...
                + eval(p)*eval(q)/(eval(p)+eval(q))*evec_F(i,p)*evec_F(i,q);
```

```
                M(p,q,i,6) = M(p,q,i,6) + eval(q)^2/(eval(p)+eval(q))*evec_F(i-
1,p)*evec_F(i-1,q) ...
                    - eval(q)^2/(eval(p)+eval(q))*evec_F(i-1,p)*evec_F(i,q) ...
                    - eval(q)^2/(eval(p)+eval(q))*evec_F(i,p)*evec_F(i-1,q) ...
                    + eval(q)^2/(eval(p)+eval(q))*evec_F(i,p)*evec_F(i,q);
                M(p,q,i,7) = 1/(eval(p)+eval(q))*evec_F(i-1,p)*evec_G(i-1,q) ...
                    - 1/(eval(p)+eval(q))*evec_F(i-1,p)*evec_G(i,q) ...
                    - 1/(eval(p)+eval(q))*evec_F(i,p)*evec_G(i-1,q) ...
                    + 1/(eval(p)+eval(q))*evec_F(i,p)*evec_G(i,q);
                M(p,q,i,8) = M(p,q,i,8) + eval(q)^2/(eval(p)+eval(q))*evec_G(i-
1,p)*evec_F(i-1,q) ...
                    - eval(q)^2/(eval(p)+eval(q))*evec_G(i-1,p)*evec_F(i,q) ...
                    - eval(q)^2/(eval(p)+eval(q))*evec_G(i,p)*evec_F(i-1,q) ...
                    + eval(q)^2/(eval(p)+eval(q))*evec_G(i,p)*evec_F(i,q);
                M(p,q,i,9) = eval(p)*eval(q)/(eval(p)+eval(q))*evec_F(i-
1,p)*evec_G(i-1,q) ...
                    + 1/2*eval(p)*eval(q)/(eval(p)+eval(q))*evec_F(i-
1,p)*evec_G(i,q) ...
                    + 1/2*eval(p)*eval(q)/(eval(p)+eval(q))*evec_F(i,p)*evec_G(i-
1,q) ...
                    + eval(p)*eval(q)/(eval(p)+eval(q))*evec_F(i,p)*evec_G(i,q);
            end
         end
      end
   end

   if region == 1
      for p = 1:2*(2*(n(region)-1))-(n(region)-1)
         for q = 1:2*(2*(n(region)-1))-(n(region)-1)
            for i = 1:n(region)
               Oa_A(p,q) = Oa_A(p,q) + BS(1,1,i)/2*(M(p,q,i,1)+M(q,p,i,1)) +
BS(2,2,i)/2*(M(p,q,i,2)+M(q,p,i,2)) ...
                    + BS(5,5,i)/2*(M(p,q,i,3)+M(q,p,i,3)) +
BS(4,4,i)/2*(M(p,q,i,4)+M(q,p,i,4)) + BS(3,3,i)/2*(M(p,q,i,5)+M(q,p,i,5)) ...
                    + BS(1,2,i)/2*(M(p,q,i,6)+M(q,p,i,6)) +
BS(1,5,i)/2*(M(p,q,i,7)+M(q,p,i,7)) + BS(2,5,i)/2*(M(p,q,i,8)+M(q,p,i,8)) ...
                    + BS(3,4,i)/2*(M(p,q,i,9) + M(q,p,i,9));
            end
         end
      end
   else
      for p = 1:2*(2*(n(region)-1))-(n(region)-1)
         for q = 1:2*(2*(n(region)-1))-(n(region)-1)
            for i = 1:n(region)
               Oa_B(p,q) = Oa_B(p,q) + BS(1,1,i)/2*(M(p,q,i,1)+M(q,p,i,1)) +
BS(2,2,i)/2*(M(p,q,i,2)+M(q,p,i,2)) ...
                    + BS(5,5,i)/2*(M(p,q,i,3)+M(q,p,i,3)) +
BS(4,4,i)/2*(M(p,q,i,4)+M(q,p,i,4)) + BS(3,3,i)/2*(M(p,q,i,5)+M(q,p,i,5)) ...
                    + BS(1,2,i)/2*(M(p,q,i,6)+M(q,p,i,6)) +
BS(1,5,i)/2*(M(p,q,i,7)+M(q,p,i,7)) + BS(2,5,i)/2*(M(p,q,i,8)+M(q,p,i,8)) ...
                    + BS(3,4,i)/2*(M(p,q,i,9) + M(q,p,i,9));
            end
         end
      end
   end
end
Oa_A = Oa_A*2;
Oa_B = Oa_B*2;

% Calculate unknown coefficients, aj and bj, using boundary conditions
% a_A = aj, a_B = bj

if model == 1 % global model
```

```
   [a_A,a_B] = global_i(eigval,eigvec,Oa_A,Oa_B,n,ncltstress,TestDropPly,t);
elseif model == 2 % mixed model
   [a_A,a_B] =
mixed_i(eigval,eigvec,Oa_A,Oa_B,n,ncltstress,TestDropPly,DropPly,t,alpha);
else % model with existing delamination
   [a_A,a_B] =
delam_i(eigval,eigvec,Oa_A,Oa_B,n,ncltstress,TestDropPly,DropPly,t,alpha);
end

plot_i



% ------------------------------------------------------------------
%                          global_i.m
%       Calculates unknown coefficients using global model
%
%                          Function for
%   Stress Analysis Program for Laminates Under In-plane Loads
% ------------------------------------------------------------------

function [a_A,a_B] =
global_i(eigval,eigvec,Oa_A,Oa_B,n,ncltstress,TestDropPly,t);

B = zeros(2*(2*(n(1)-1))-(n(1)-1) + 2*(2*(n(2)-1))-(n(2)-1),1);
for i = 1:n(1)-1
   if TestDropPly(i) == 1
      B = [B; -t*ncltstress(1,i,1)];
   else
      B = [B; t*(ncltstress(1,i,2)-ncltstress(1,i,1))];
   end
end
for i = 1:n(1)-1
   if TestDropPly(i) == 1
      B = [B; -t*ncltstress(3,i,1)];
   else
      B = [B; t*(ncltstress(3,i,2)-ncltstress(3,i,1))];
   end
end
for i = 1:n(1)-1
   B = [B; 0]
end
GaF_A = [];
GaF_B = [];
GaG_A = [];
GaG_B = [];
Te_A = [];
Te_B = [];
k = 0;
for i = 1:(n(1)-1)
   tGaF_A = [];
   tGaF_B = [];
   tGaG_A = [];
   tGaG_B = [];
   tTe_A = [];
   tTe_B = [];
   for j = 1:2*(2*(n(1)-1))-(n(1)-1)
      if i == 1
         tGaF_A = [tGaF_A -eigvec(i,j,1)];
         tGaG_A = [tGaG_A -eigvec((n(1)-1)+i,j,1)];
         tTe_A = [tTe_A eigval(1,j,1)*eigvec(i,j,1)];
      else
```

```
            tGaF_A = [tGaF_A (eigvec(i-1,j,1)-eigvec(i,j,1))];
            tGaG_A = [tGaG_A (eigvec((n(1)-1)+i-1,j,1)-eigvec((n(1)-1)+i,j,1))];
            tTe_A = [tTe_A eigval(1,j,1)*eigvec(i,j,1)];
         end
      end
      if TestDropPly(i) ~= 1
         k = k+1;
      end
      for j = 1:2*(2*(n(2)-1))-(n(2)-1)
         if TestDropPly(i) == 1
            tGaF_B = [tGaF_B 0];
            tGaG_B = [tGaG_B 0];
            tTe_B = [tTe_B 0];
         elseif k == 1
            tGaF_B = [tGaF_B eigvec(k,j,2)];
            tGaG_B = [tGaG_B eigvec((n(2)-1)+k,j,2)];
            tTe_B = [tTe_B -eigval(1,j,2)*eigvec(k,j,2)];
         elseif k == n(2)
            tGaF_B = [tGaF_B -eigvec(k-1,j,2)];
            tGaG_B = [tGaG_B -eigvec((n(2)-1)+k-1,j,2)];
            tTe_B = [tTe_B -eigval(1,j,2)*eigvec(k,j,2)];
         else
            tGaF_B = [tGaF_B -(eigvec(k-1,j,2)-eigvec(k,j,2))];
            tGaG_B = [tGaG_B -(eigvec((n(2)-1)+k-1,j,2)-eigvec((n(2)-1)+k,j,2))];
            tTe_B = [tTe_B -eigval(1,j,2)*eigvec(k,j,2)];
         end
      end
      GaF_A = [GaF_A; tGaF_A];
      GaF_B = [GaF_B; tGaF_B];
      GaG_A = [GaG_A; tGaG_A];
      GaG_B = [GaG_B; tGaG_B];
      Te_A = [Te_A; tTe_A];
      Te_B = [Te_B; tTe_B];
   end

   fill = zeros(2*(2*(n(1)-1))-(n(1)-1),2*(2*(n(2)-1))-(n(2)-1));
   A = [Oa_A fill GaF_A.' GaG_A.' Te_A.';
        fill' -Oa_B GaF_B.' GaG_B.' Te_B.';
        GaF_A GaF_B zeros((n(1)-1),2*(2*(n(1)-1))-(n(1)-1));
        GaG_A GaG_B zeros((n(1)-1),2*(2*(n(1)-1))-(n(1)-1));
        Te_A Te_B zeros((n(1)-1),2*(2*(n(1)-1))-(n(1)-1))];

   xx = inv(A)*B;
   a_A = xx(1:2*(2*(n(1)-1))-(n(1)-1));
   a_B = xx(2*(2*(n(1)-1))-(n(1)-1)+1:2*(2*(n(1)-1))-(n(1)-1)+2*(2*(n(2)-1))-
   (n(2)-1));



   % ------------------------------------------------------------------
   %                            mixed_i.m
   %        Calculates unknown coefficients using mixed model
   %
   %                          Function for
   %   Stress Analysis Program for Laminates Under In-plane Loads
   % ------------------------------------------------------------------

   function [a_A,a_B] =
   mixed_i(eigval,eigvec,Oa_A,Oa_B,n,ncltstress,TestDropPly,DropPly,t,alpha);

   nt = n(1)-n(2);
   i1 = 0;
```

```
i2 = 0;
i3 = 0;
PlyNumsUKU = [];
for i = 1:n(1)
   if TestDropPly(i) == 1
      i2 = i2 + 1;
      PlyNumsDrop(i2) = i;
   end
   if TestDropPly(i) ~= 1
      if i2 ~= 0
         i3 = i3 + 1;
         % PlyNumsUKU = ply numbers of plies in unkinked region in the
undropped region
         PlyNumsUKU(i3) = i;
      elseif i3 == 0
         i1 = i1 + 1;
         % PlyNumKU = ply numbers of plies in kinked region in the undropped
region
         PlyNumsKU(i1) = i;
      end
   end
end
% tf = ply number of first terminated ply
tf = PlyNumsDrop(1);
% tl = ply number of last terminated ply
tl = PlyNumsDrop(n(1)-n(2));
% PlyNumsKD = ply numbers of plies in kinked region in the dropped region
PlyNumsKD = PlyNumsKU;
for i = 1:size(PlyNumsUKU,2)
   % PlyNumsUKD = ply numbers of plies in unkinked region in the dropped region
   PlyNumsUKD(i) = i + (tf-1);
end
B = zeros(3*(n(1)-1) + 3*(n(2)-1),1);

% Boundary conditions for terminated plies
S11T = [];S11T_CLPT = [];S12T = [];S12T_CLPT = [];S1ZT = [];S1ZT_CLPT = [];
Drop = zeros(1,3*(n(1)-1));
for i = 1:size(PlyNumsDrop,2)
   if i == size(PlyNumsDrop,2) & isempty(PlyNumsUKU)
      S11T = [S11T; eigvec(PlyNumsDrop(i)-1,:,1)];
      S11T_CLPT = [S11T_CLPT; -t*ncltstress(1,PlyNumsDrop(i),1)];
      S12T = [S12T; eigvec((n(1)-1)+(PlyNumsDrop(i)-1),:,1)];
      S12T_CLPT = [S12T_CLPT; -t*ncltstress(3,PlyNumsDrop(i),1)];
   else
      S11T = [S11T; eigvec(PlyNumsDrop(i)-1,:,1)-eigvec(PlyNumsDrop(i),:,1)];
      S11T_CLPT = [S11T_CLPT; -t*ncltstress(1,PlyNumsDrop(i),1)];
      S12T = [S12T; eigvec((n(1)-1)+(PlyNumsDrop(i)-1),:,1)-eigvec((n(1)-
1)+PlyNumsDrop(i),:,1)];
      S12T_CLPT = [S12T_CLPT; -t*ncltstress(3,PlyNumsDrop(i),1)];
      S1ZT = [S1ZT; eigval(1,:,1).*eigvec(PlyNumsDrop(i),:,1)];
      S1ZT_CLPT = [S1ZT_CLPT; 0];
   end
end
Drop = eigval(1,:,1).*eigvec(PlyNumsDrop(1)-1,:,1);

% Boundary conditions for undropped region
FXKU = zeros(1,3*(n(1)-1));FYKU = FXKU;FZKU = FXKU;MKU = FXKU;FZUKU = FXKU;MUKU
= FXKU;FZU = FXKU;MU = FZKU;
FXKU_CLPT = 0;FYKU_CLPT = 0;MKU_CLPT = 0;MUKU_CLPT = 0;
for i = 1:n(1)
   if i <= tf-1
      r = (i-1)*t;
      if i == 1
```

```
         FXKU = FXKU + 1/t*( -eigvec(i,:,1) );
         FYKU = FYKU + 1/t*( -eigvec((n(1)-1)+i,:,1) );
         FZKU = FZKU + t/2*( eigval(1,:,1).*eigvec(i,:,1) );
         MKU = MKU + 1/2*( -eigvec(i,:,1) )*(t+2*r);
      else
         FXKU = FXKU + 1/t*( eigvec(i-1,:,1)-eigvec(i,:,1) );
         FYKU = FYKU + 1/t*( eigvec((n(1)-1)+i-1,:,1)-eigvec((n(1)-1)+i,:,1) );
         if i == tf-1
            FZKU = FZKU + t/2*( eigval(1,:,1).*eigvec(i,:,1)*2 +
eigval(1,:,1).*eigvec(i-1,:,1) );
         else
            FZKU = FZKU + t/2*( eigval(1,:,1).*eigvec(i,:,1) +
eigval(1,:,1).*eigvec(i-1,:,1) );
         end
         MKU = MKU + 1/2*( eigvec(i-1,:,1)-eigvec(i,:,1) )*(t+2*r);
      end
      FXKU_CLPT = FXKU_CLPT + ncltstress(1,i,1);
      FYKU_CLPT = FYKU_CLPT + ncltstress(3,i,1);
      MKU_CLPT = MKU_CLPT + ncltstress(1,i,1)*1/2*t*(t+2*r);
   elseif i >= tl+1
      r = (i-1-tl)*t;
      if i < n(1)
         if i == tl+1
            FZUKU = FZUKU + t/2*( eigval(1,:,1).*eigvec(i,:,1) +
2*eigval(1,:,1).*eigvec(i-1,:,1));
         else
            FZUKU = FZUKU + t/2*( eigval(1,:,1).*eigvec(i,:,1) +
eigval(1,:,1).*eigvec(i-1,:,1) );
         end
         MUKU = MUKU + 1/2*( eigvec(i-1,:,1)-eigvec(i,:,1) )*(t+2*r);
      else
         FZUKU = FZUKU + t/2*( eigval(1,:,1).*eigvec(i-1,:,1) );
         MUKU = MUKU + 1/2*( eigvec(i-1,:,1) )*(t+2*r);
      end
      MUKU_CLPT = MUKU_CLPT + ncltstress(1,i,1)*1/2*t*(t+2*r);
   end
   if i <= n(1)-1
      FZU = FZU - t*eigval(1,:,1).*eigvec(i,:,1);
      MU = MU + t*eigvec(i,:,1);
   end
end

% Boundary condition for dropped region
FXKD = zeros(1,3*(n(2)-1));FYKD = FXKD;FZKD = FXKD;MKD = FXKD;FZUKD = FXKD;MUKD
= FXKD;FZD = FXKD;MD = FZKD;
FXKD_CLPT = 0;FYKD_CLPT = 0;MKD_CLPT = 0;MUKD_CLPT = 0;
clpt = [ncltstress(:,PlyNumsKU,2) ncltstress(:,PlyNumsUKU,2)];
THETA = eigvec(1:n(2)-1,1:3*(n(2)-1),2);
GAMMA = eigvec(n(2):2*(n(2)-1),1:3*(n(2)-1),2);
lambda = eigval(1,1:3*(n(2)-1),2);
for i = 1:n(2)
   if i <= tf-1
      r = (i-1)*t;
      if i == 1
         FXKD = FXKD + 1/t*( -THETA(i,:) );
         FYKD = FYKD + 1/t*( -GAMMA(i,:) );
         FZKD = FZKD + t/2*( lambda(1,:).*THETA(i,:) );
         MKD = MKD + 1/2*( -THETA(i,:) )*(t+2*r);
      else
         if (i == tf-1) & isempty(PlyNumsUKU)
            FXKD = FXKD + 1/t*( THETA(i-1,:) );
            FYKD = FYKD + 1/t*( GAMMA(i-1,:) );
            FZKD = FZKD + t/2*( lambda(1,:).*THETA(i-1,:) );
```

```
            MKD = MKD + 1/2*( THETA(i-1,:) )*(t+2*r);
         else
            FXKD = FXKD + 1/t*( THETA(i-1,:)-THETA(i,:) );
            FYKD = FYKD + 1/t*( GAMMA(i-1,:)-GAMMA(i,:) );
            if i == tf-1
               FZKD = FZKD + t/2*( lambda(1,:).*THETA(i,:)*2 +
lambda(1,:).*THETA(i-1,:) );
            else
               FZKD = FZKD + t/2*( lambda(1,:).*THETA(i,:) +
lambda(1,:).*THETA(i-1,:) );
            end
            MKD = MKD + 1/2*( THETA(i-1,:)-THETA(i,:) )*(t+2*r);
         end
      end
      FXKD_CLPT = FXKD_CLPT + clpt(1,i);
      FYKD_CLPT = FYKD_CLPT + clpt(3,i);
      MKD_CLPT = MKD_CLPT + clpt(1,i)*1/2*t*(t+2*r);
   elseif i >= PlyNumsUKD(1)
      r = (i-PlyNumsDrop(1))*t;
      if i < n(2)
         if i == PlyNumsUKD(1)
            FZUKD = FZUKD + t/2*( lambda(1,:).*THETA(i,:) +
2*lambda(1,:).*THETA(i-1,:) );
         else
            FZUKD = FZUKD + t/2*( lambda(1,:).*THETA(i,:) +
lambda(1,:).*THETA(i-1,:) );
         end
         MUKD = MUKD + 1/2*( THETA(i-1,:)-THETA(i,:) )*(t+2*r);
      else
         FZUKD = FZUKD + t/2*( lambda(1,:).*THETA(i-1,:) );
         MUKD = MUKD + 1/2*( THETA(i-1,:) )*(t+2*r);
      end
      MUKD_CLPT = MUKD_CLPT + clpt(1,i)*1/2*t*(t+2*r);
   end
   if i <= n(2)-1
      FZD = FZD + t*lambda(1,:).*THETA(i,:);
      MD = MD - t*THETA(i,:);
   end
end
sina = sin(alpha*pi/180);
cosa = cos(alpha*pi/180);
l = nt*t/sina;

if DropPly == 1 | DropPly == n(1)
   fill = zeros(2*(2*(n(1)-1))-(n(1)-1),2*(2*(n(2)-1))-(n(2)-1));
   fill2 = zeros(2*(2*(n(2)-1))-(n(2)-1),3*nt);
   fill3 = zeros(nt,2*(2*(n(2)-1))-(n(2)-1));
   if nt == 1
      B = [B; S11T_CLPT; S12T_CLPT; 0];
      B = [B; 0;MKD_CLPT-MKU_CLPT+FXKD_CLPT*l*sina];
      A = [Oa_A  fill    S11T.'              S12T.' Drop.' FZKU.' MKU.';
           fill' -Oa_B   fill2              -FZKD.' FZKD.'*l*cosa-MKD.'-
FXKD.'*l*sina*t ;
           S11T          fill3
zeros(nt,2+3*nt);
           S12T          fill3
zeros(nt,2+3*nt);
           Drop          zeros(1,3*(n(2)-1))
zeros(1,2+3*nt);
           FZKU          -FZKD
zeros(1,2+3*nt);
           MKU           FZKD*l*cosa-MKD-FXKD*l*sina*t
zeros(1,2+3*nt)];
```

```
   else
      B = [B; S11T_CLPT; S12T_CLPT; S1ZT_CLPT; 0];
      B = [B; 0;MKD_CLPT-MKU_CLPT+FXKD_CLPT*l*sina];
      A = [Oa_A  fill    S11T.'                      S12T.' S1ZT.' Drop.'
FZKU.' MKU.' ;
           fill' -Oa_B   fill2                      -FZKD.' FZKD.'*l*cosa-
MKD.'-FXKD.'*l*sina*t ;
           S11T          fill3
zeros(nt,2+3*nt);
           S12T          fill3
zeros(nt,2+3*nt);
           S1ZT          zeros(nt-1,2*(2*(n(2)-1))-(n(2)-1))          zeros(nt-
1,2+3*nt);
           Drop          zeros(1,3*(n(2)-1))
zeros(1,2+3*nt);
           FZKU          -FZKD
zeros(1,2+3*nt);
           MKU           FZKD*l*cosa-MKD-FXKD*l*sina*t
zeros(1,2+3*nt)];
   end
else
   B = [B; S11T_CLPT; S12T_CLPT; S1ZT_CLPT; 0];
   B = [B; FXKD_CLPT-FXKU_CLPT; FYKD_CLPT-FYKU_CLPT; 0;MKD_CLPT-
MKU_CLPT+FXKD_CLPT*l*sina*t];
   B = [B; 0];
   fill = zeros(2*(2*(n(1)-1))-(n(1)-1),2*(2*(n(2)-1))-(n(2)-1));
   fill2 = zeros(2*(2*(n(2)-1))-(n(2)-1),1+3*nt);
   fill3 = zeros(nt,2*(2*(n(2)-1))-(n(2)-1));
   A = [Oa_A  fill    S11T.'                    S12T.'  S1ZT.'  Drop.' FXKU.'
FYKU.'  FZKU.' MKU.'         FZUKU.'+FZU.' ;
        fill' -Oa_B   fill2                    -FXKD.' -FYKD.' -FZKD.'
FZKD.'*l*cosa-MKD.'-FXKD.'*l*sina*t -FZUKD.'+FZD.' ;
        S11T          fill3
zeros(nt,6+3*nt);
        S12T          fill3
zeros(nt,6+3*nt);
        S1ZT          fill3
zeros(nt,6+3*nt);
        Drop          zeros(1,3*(n(2)-1))
zeros(1,6+3*nt);
        FXKU          -FXKD
zeros(1,6+3*nt);
        FYKU          -FYKD
zeros(1,6+3*nt);
        FZKU          -FZKD
zeros(1,6+3*nt);
        MKU           FZKD*l*cosa-MKD-FXKD*l*sina*t
zeros(1,6+3*nt);
        FZUKU+FZU     -FZUKD+FZD
zeros(1,6+3*nt)];
end

xx = inv(A)*B;
a_A = xx(1:2*(2*(n(1)-1))-(n(1)-1));
a_B = xx(2*(2*(n(1)-1))-(n(1)-1)+1:2*(2*(n(1)-1))-(n(1)-1)+2*(2*(n(2)-1))-
(n(2)-1));



% ------------------------------------------------------------
%                          delam_i.m
%         Calculates unknown coefficients using model for
```

```
%              laminate with existing delamination
%
%                          Function for
%   Stress Analysis Program for Laminates Under In-plane Loads
% ------------------------------------------------------------

function [a_A,a_B] =
delam_i(eigval,eigvec,Oa_A,Oa_B,n,ncltstress,TestDropPly,DropPly,t,alpha);

if TestDropPly(1) == 1 % if external dropoff

   % Use boundary conditions at drop-off to find coefficients
   nt = n(1)-n(2);
   i1 = 0;
   i2 = 0;
   i3 = 0;
   PlyNumsUKU = [];
   PlyNumsKU = [];
   for i = 1:n(1)
      if TestDropPly(i) == 1
         i1 = i1 + 1;
         PlyNumsDrop(i1) = i;
      end
      if TestDropPly(i) ~= 1
         if i1 ~= 0
            i2 = i2 + 1;
            % PlyNumsUKU = ply numbers of plies in unkinked region in the
undropped region
            PlyNumsUKU = [PlyNumsUKU i];
         elseif i2 == 0
            i3 = i3 + 1;
            % PlyNumKU = ply numbers of plies in kinked region in the undropped
region
            PlyNumsKU = [PlyNumsKU i];
         end
      end
   end
   % tf = ply number of first terminated ply
   tf = PlyNumsDrop(1);
   % tl = ply number of last terminated ply
   tl = PlyNumsDrop(n(1)-n(2));
   % PlyNumsKD = ply numbers of plies in kinked region in the dropped region
   PlyNumsKD = PlyNumsKU;
   % nDrop = number of plies in dropped plies
   nDrop = size(PlyNumsDrop,2);
   % nUKU = number of plies in unkinked region in the undropped region
   nUKU = size(PlyNumsUKU,2);
   % nKU = number of plies in kinked region in the undropped region
   nKU = size(PlyNumsKU,2);
   for i = 1:size(PlyNumsUKU,2)
      % PlyNumsUKD = ply numbers of plies in unkinked region in the dropped
region
      PlyNumsUKD(i) = i + (tf-1);
   end

   FXT = zeros(1,3*(n(1)-1));FYT = FXT;FZT = FXT;MT = FXT;MT_CLPT = 0;
   B = zeros(2*(2*(n(1)-1))-(n(1)-1) + 2*(2*(n(2)-1))-(n(2)-1),1);
   for i = tl+1:n(1)
      if TestDropPly(i) == 1
         B = [B; -t*ncltstress(1,i,1)];
      else
         B = [B; t*(ncltstress(1,i,2)-ncltstress(1,i,1))];
      end
```

```
   end
   for i = tl+1:n(1)
      if TestDropPly(i) == 1
         B = [B; -t*ncltstress(3,i,1)];
      else
         B = [B; t*(ncltstress(3,i,2)-ncltstress(3,i,1))];
      end
   end
   for i = tl+1:n(1)
      B = [B; 0];
   end
   GaF_A = [];
   GaF_B = [];
   GaG_A = [];
   GaG_B = [];
   Te_A = [];
   Te_B = [];
   k = 0;
   for i = 1:n(1)
      tGaF_A = [];
      tGaF_B = [];
      tGaG_A = [];
      tGaG_B = [];
      tTe_A = [];
      tTe_B = [];
      if i <= tl
         r = (i-1)*t;
         if i == 1
            FXT = FXT - eigvec(i,:,1);
            FYT = FYT - eigvec((n(1)-1)+i,:,1);
            FZT = FZT + t/2*( eigval(1,:,1).*eigvec(i,:,1) );
            MT = MT + 1/2*( -eigvec(i,:,1) )*(t+2*r);
         else
            FXT = FXT + (eigvec(i-1,:,1)-eigvec(i,:,1));
            FYT = FYT + (eigvec((n(1)-1)+i-1,:,1)-eigvec((n(1)-1)+i,:,1));
            FZT = FZT + t/2*( eigval(1,:,1).*eigvec(i,:,1) +
eigval(1,:,1).*eigvec(i-1,:,1) );
            MT = MT + 1/2*(eigvec(i-1,:,1)-eigvec(i,:,1))*(t+2*r);
         end
         MT_CLPT = MT_CLPT + ncltstress(1,i,1)*1/2*t*(t+2*r);
      else
         for j = 1:2*(2*(n(1)-1))-(n(1)-1)
             if i == n(1)
                tGaF_A = [tGaF_A (eigvec(i-1,j,1))];
                tGaG_A = [tGaG_A (eigvec((n(1)-1)+i-1,j,1))];
                tTe_A = [tTe_A eigval(1,j,1)*eigvec(i,j,1)];
             else
                tGaF_A = [tGaF_A (eigvec(i-1,j,1)-eigvec(i,j,1))];
                tGaG_A = [tGaG_A (eigvec((n(1)-1)+i-1,j,1)-eigvec((n(1)-
1)+i,j,1))];
                tTe_A = [tTe_A eigval(1,j,1)*eigvec(i,j,1)];
             end
         end
         if TestDropPly(i) ~= 1
            k = k+1;
         end
         for j = 1:2*(2*(n(2)-1))-(n(2)-1)
            if k == 1
               tGaF_B = [tGaF_B eigvec(k,j,2)];
               tGaG_B = [tGaG_B eigvec((n(2)-1)+k,j,2)];
               tTe_B = [tTe_B -eigval(1,j,2)*eigvec(k,j,2)];
            elseif k == n(2)
               tGaF_B = [tGaF_B -eigvec(k-1,j,2)];
```

```
            tGaG_B = [tGaG_B -eigvec((n(2)-1)+k-1,j,2)];
            tTe_B = [tTe_B -eigval(1,j,2)*eigvec(k,j,2)];
         else
            tGaF_B = [tGaF_B -(eigvec(k-1,j,2)-eigvec(k,j,2))];
            tGaG_B = [tGaG_B -(eigvec((n(2)-1)+k-1,j,2)-eigvec((n(2)-
1)+k,j,2))];
            tTe_B = [tTe_B -eigval(1,j,2)*eigvec(k,j,2)];
         end
      end
   end
   GaF_A = [GaF_A; tGaF_A];
   GaF_B = [GaF_B; tGaF_B];
   GaG_A = [GaG_A; tGaG_A];
   GaG_B = [GaG_B; tGaG_B];
   Te_A = [Te_A; tTe_A];
   Te_B = [Te_B; tTe_B];
end
fill = zeros(2*(2*(n(1)-1))-(n(1)-1),2*(2*(n(2)-1))-(n(2)-1));
B = [B;-MT_CLPT;0];
A = [Oa_A   fill  GaF_A.' GaG_A.' Te_A.' MT.' FZT.';
     fill' -Oa_B  GaF_B.' GaG_B.' Te_B.' zeros(size(Te_B,2),2);
     GaF_A  GaF_B zeros((n(1)-nDrop),3*(n(1)-nDrop)+2);
     GaG_A  GaG_B zeros((n(1)-nDrop),3*(n(1)-nDrop)+2);
     Te_A   Te_B  zeros((n(1)-nDrop),3*(n(1)-nDrop)+2);
     MT     zeros(1,size(Te_B,2))      zeros(1,3*(n(1)-nDrop)+2);
     FZT    zeros(1,size(Te_B,2))      zeros(1,3*(n(1)-nDrop)+2)];
xx = inv(A)*B;
a_A = xx(1:2*(2*(n(1)-1))-(n(1)-1));
a_B = xx(2*(2*(n(1)-1))-(n(1)-1)+1:2*(2*(n(1)-1))-(n(1)-1)+2*(2*(n(2)-1))-
(n(2)-1));

else % if internal dropoff

   da = input('>> Delamination length? \n?? ');
   if isempty(da) da = 10; end;
   da = da*t;

   nt = n(1)-n(2);
   i1 = 0;
   i2 = 0;
   i3 = 0;
   PlyNumsUKU = 0;
   for i = 1:n(1)
      if TestDropPly(i) == 1
         i2 = i2 + 1;
         PlyNumsDrop(i2) = i;
      end
      if TestDropPly(i) ~= 1
         if i2 ~= 0
            i3 = i3 + 1;
            % PlyNumsUKU = ply numbers of plies in unkinked region in the
undropped region
            PlyNumsUKU(i3) = i;
         elseif i3 == 0
            i1 = i1 + 1;
            % PlyNumKU = ply numbers of plies in kinked region in the undropped
region
            PlyNumsKU(i1) = i;
         end
      end
   end
   % tf = ply number of first terminated ply
   tf = PlyNumsDrop(1);
```

```
   % tl = ply number of last terminated ply
   tl = PlyNumsDrop(n(1)-n(2));
   % PlyNumsKD = ply numbers of plies in kinked region in the dropped region
   PlyNumsKD = PlyNumsKU;
   for i = 1:size(PlyNumsUKU,2)
      % PlyNumsUKD = ply numbers of plies in unkinked region in the dropped
region
      PlyNumsUKD(i) = i + (tf-1);
   end

   B = zeros(3*(n(1)-1) + 3*(n(2)-1),1);
   % Boundary conditions for terminated plies
   FXT = zeros(1,3*(n(1)-1));FYT = FXT;FZT = FXT;MT = FXT;
   FXT_CLPT = 0; FYT_CLPT = 0; FZT_CLPT = 0; MT_CLPT = 0;
   Drop = zeros(1,3*(n(1)-1));
   for i = 1:size(PlyNumsDrop,2)
      r = (i-1)*t;
      FXT = FXT + 1/t*( eigvec(PlyNumsDrop(i)-1,:,1)-eigvec(PlyNumsDrop(i),:,1)
);
      FXT_CLPT = FXT_CLPT + ncltstress(1,PlyNumsDrop(i),1);
      FYT = FYT + 1/t*( eigvec((n(1)-1)+(PlyNumsDrop(i)-1),:,1)-eigvec((n(1)-
1)+PlyNumsDrop(i),:,1) );
      FYT_CLPT = FYT_CLPT + ncltstress(3,PlyNumsDrop(i),1);
      FZT = FZT + t/2*( eigval(1,:,1).*eigvec(PlyNumsDrop(i),:,1) +
eigval(1,:,1).*eigvec(PlyNumsDrop(i)-1,:,1) );
      MT = MT + 1/2*(eigvec(PlyNumsDrop(i)-1,:,1)-
eigvec(PlyNumsDrop(i),:,1))*(t+2*r);
      MT_CLPT = MT_CLPT + ncltstress(1,PlyNumsDrop(i),1)*1/2*t*(t+2*r);
   end

   Drop = eigval(1,:,1).*eigvec(PlyNumsDrop(1)-1,:,1);

   % Boundary conditions for undropped region
   FXKU = zeros(1,3*(n(1)-1));FYKU = FXKU;FZKU = FXKU;MKU = FXKU;FZUKU =
FXKU;MUKU = FXKU;FZU = FXKU;MU = FZKU;
   FXKU_CLPT = 0;FYKU_CLPT = 0;MKU_CLPT = 0;MUKU_CLPT = 0;
   for i = 1:n(1)
      if i <= tf-1
         r = (i-1)*t;
         if i == 1
            FXKU = FXKU + 1/t*( -eigvec(i,:,1) );
            FYKU = FYKU + 1/t*( -eigvec((n(1)-1)+i,:,1) );
            FZKU = FZKU + t/2*( eigval(1,:,1).*eigvec(i,:,1) );
            MKU = MKU + 1/2*( -eigvec(i,:,1) )*(t+2*r);
         else
            FXKU = FXKU + 1/t*( eigvec(i-1,:,1)-eigvec(i,:,1) );
            FYKU = FYKU + 1/t*( eigvec((n(1)-1)+i-1,:,1)-eigvec((n(1)-1)+i,:,1)
);
            if i == tf-1
               FZKU = FZKU + t/2*( eigval(1,:,1).*eigvec(i,:,1)*2 +
eigval(1,:,1).*eigvec(i-1,:,1) );
            else
               FZKU = FZKU + t/2*( eigval(1,:,1).*eigvec(i,:,1) +
eigval(1,:,1).*eigvec(i-1,:,1) );
            end
            MKU = MKU + 1/2*( eigvec(i-1,:,1)-eigvec(i,:,1) )*(t+2*r);
         end
         FXKU_CLPT = FXKU_CLPT + ncltstress(1,i,1);

         FYKU_CLPT = FYKU_CLPT + ncltstress(3,i,1);
         MKU_CLPT = MKU_CLPT + ncltstress(1,i,1)*1/2*t*(t+2*r);
      elseif i >= tl+1
         r = (i-1-tl)*t;
```

```
         if i < n(1)
            if i == t1+1
               FZUKU = FZUKU + t/2*( eigval(1,:,1).*eigvec(i,:,1) +
2*eigval(1,:,1).*eigvec(i-1,:,1));
            else
               FZUKU = FZUKU + t/2*( eigval(1,:,1).*eigvec(i,:,1) +
eigval(1,:,1).*eigvec(i-1,:,1) );
            end
            MUKU = MUKU + 1/2*( eigvec(i-1,:,1)-eigvec(i,:,1) )*(t+2*r);
         else
            FZUKU = FZUKU + t/2*( eigval(1,:,1).*eigvec(i-1,:,1) );
            MUKU = MUKU + 1/2*( eigvec(i-1,:,1) )*(t+2*r);
         end
         MUKU_CLPT = MUKU_CLPT + ncltstress(1,i,1)*1/2*t*(t+2*r);
      end
      if i <= n(1)-1
         FZU = FZU - t*eigval(1,:,1).*eigvec(i,:,1);
         MU = MU + t*eigvec(i,:,1);
      end
   end
   % Boundary condition for dropped region
   FXKD = zeros(1,3*(n(2)-1));FYKD = FXKD;FZKD = FXKD;MKD = FXKD;FZUKD =
FXKD;MUKD = FXKD;FZD = FXKD;MD = FZKD;
   FXKD_CLPT = 0;FYKD_CLPT = 0;MKD_CLPT = 0;MUKD_CLPT = 0;
   clpt = [ncltstress(:,PlyNumsKU,2) ncltstress(:,PlyNumsUKU,2)];
   THETA = eigvec(1:n(2)-1,1:3*(n(2)-1),2);
   GAMMA = eigvec(n(2):2*(n(2)-1),1:3*(n(2)-1),2);
   lambda = eigval(1,1:3*(n(2)-1),2);
   for i = 1:n(2)
      if i <= tf-1
         r = (i-1)*t;
         if i == 1
            FXKD = FXKD + 1/t*( -THETA(i,:) );
            FYKD = FYKD + 1/t*( -GAMMA(i,:) );
               FZKD = FZKD + t/2*( lambda(1,:).*THETA(i,:) );
            MKD = MKD + 1/2*( -THETA(i,:) )*(t+2*r);
         elseif i == n(2)
            FXKD = FXKD + 1/t*( THETA(i-1,:) );
            FYKD = FYKD + 1/t*( GAMMA(i-1,:) );
            if i == tf-1
               FZKD = FZKD + t/2*( lambda(1,:).*THETA(i-1,:) );
            else
               FZKD = FZKD + t/2*( lambda(1,:).*THETA(i-1,:) );
            end
            MKD = MKD + 1/2*( THETA(i-1,:) )*(t+2*r);
         else
            FXKD = FXKD + 1/t*( THETA(i-1,:)-THETA(i,:) );
            FYKD = FYKD + 1/t*( GAMMA(i-1,:)-GAMMA(i,:) );
            if i == tf-1
               FZKD = FZKD + t/2*( lambda(1,:).*THETA(i,:)*2 +
lambda(1,:).*THETA(i-1,:) );
            else
               FZKD = FZKD + t/2*( lambda(1,:).*THETA(i,:) +
lambda(1,:).*THETA(i-1,:) );
            end
            MKD = MKD + 1/2*( THETA(i-1,:)-THETA(i,:) )*(t+2*r);
         end
         FXKD_CLPT = FXKD_CLPT + clpt(1,i);
         FYKD_CLPT = FYKD_CLPT + clpt(3,i);
         MKD_CLPT = MKD_CLPT + clpt(1,i)*1/2*t*(t+2*r);
      elseif i >= PlyNumsUKD(1)
         r = (i-PlyNumsDrop(1))*t;
         if i < n(2)
```

```
            if i == PlyNumsUKD(1)
               FZUKD = FZUKD + t/2*( lambda(1,:).*THETA(i,:) +
2*lambda(1,:).*THETA(i-1,:) );
            else
               FZUKD = FZUKD + t/2*( lambda(1,:).*THETA(i,:) +
lambda(1,:).*THETA(i-1,:) );
            end
            MUKD = MUKD + 1/2*( THETA(i-1,:)-THETA(i,:) )*(t+2*r);
         else
            FZUKD = FZUKD + t/2*( lambda(1,:).*THETA(i-1,:) );
            MUKD = MUKD + 1/2*( THETA(i-1,:) )*(t+2*r);
         end
         MUKD_CLPT = MUKD_CLPT + clpt(1,i)*1/2*t*(t+2*r);
      end
      if i <= n(2)-1
         FZD = FZD + t*lambda(1,:).*THETA(i,:);
         MD = MD - t*THETA(i,:);
      end
   end
   sina = sin(alpha*pi/180);
   cosa = cos(alpha*pi/180);
   l = nt*t/sina;
   B = [B; -FXT_CLPT; -FYT_CLPT; -FZT_CLPT; -MT_CLPT;FXKD_CLPT-FXKU_CLPT;
FYKD_CLPT-FYKU_CLPT; 0;MKD_CLPT-MKU_CLPT+FXKD_CLPT*l*sina];

   fill = zeros(2*(2*(n(1)-1))-(n(1)-1),2*(2*(n(2)-1))-(n(2)-1));
   fill2 = zeros(2*(2*(n(2)-1))-(n(2)-1),1+3*nt);
   fill3 = zeros(nt,2*(2*(n(2)-1))-(n(2)-1));
   A = [Oa_A  fill    FXT.' FYT.' FZT.' MT.'  FXKU.'  FYKU.'  FZKU.'
MKU.'+FZKU.'*da;
        fill' -Oa_B   zeros(size(FXKD,2),4)  -FXKD.' -FYKD.' -FZKD.'
FZKD.'*l*cosa-MKD.'-FXKD.'*l*sina;
        FXT           zeros(1,size(FXKD,2))                          zeros(1,8);
        FYT           zeros(1,size(FXKD,2))                          zeros(1,8);
        FZT           zeros(1,size(FXKD,2))                          zeros(1,8);
        MT            zeros(1,size(FXKD,2))                          zeros(1,8);
        FXKU          -FXKD                                          zeros(1,8);
        FYKU          -FYKD                                          zeros(1,8);
        FZKU          -FZKD                                          zeros(1,8);
        MKU+FZKU*da    FZKD*l*cosa-MKD-FXKD*l*sina                   zeros(1,8)];


   xx = inv(A)*B;
   a_A = xx(1:2*(2*(n(1)-1))-(n(1)-1));
   a_B = xx(2*(2*(n(1)-1))-(n(1)-1)+1:2*(2*(n(1)-1))-(n(1)-1)+2*(2*(n(2)-1))-
(n(2)-1));

end



% ------------------------------------------------------
%                       clt2.m
%        Calculate CLPT stresses and strains
%
%                     Function for
%       Mixed Model for Laminates Under In-plane Loads
% ------------------------------------------------------

function [strain,stress,nstress] = clt2(F,MaterialConstants,LayUp,t)

NumHalfPly = size(LayUp);
```

```
NumHalfPly = NumHalfPly(2);

[A,D] = stiffv2(MaterialConstants,LayUp,t);
for i = 1:NumHalfPly
   if LayUp(i) >= 200*pi/180
      [Q(:,:,i)] = VariableStiff(MaterialConstants,LayUp(i)*180/pi-200);
   else
      [Q(:,:,i)] = SLStiff2v2(MaterialConstants,LayUp(i));
   end
end
strain = inv(A)*F;
for i = 1:NumHalfPly
   stress(:,i) = Q(:,:,i)*strain;
end

nstress = stress/strain(1); % Stresses normalized to applied strain



% ------------------------------------------------------
%                      companion2.m
%     Calculate matrices A,B and C from equation (4.19)
%
%                      Function for
%       Mixed Model for Laminates Under In-plane Loads
% ------------------------------------------------------

% AA == A, BB == B, CC == C
function [AA,BB,CC,S,B,Ss_L] = companion2(MaterialConstants,LayUp,t)

NumHalfPly = size(LayUp);
NumHalfPly = NumHalfPly(2);

for i = 1:NumHalfPly
   if LayUp(i) >= 200*pi/180
      S_L = VariableComp(MaterialConstants,LayUp(i)*180/pi-200);
   else
      S_L = SLComp3(MaterialConstants,LayUp(i));
   end
   Ss_L(:,:,i) = [S_L(1,1)-S_L(1,2)*S_L(1,2)/S_L(2,2) S_L(1,3)-
S_L(1,2)*S_L(2,3)/S_L(2,2)    0      0   S_L(1,6)-S_L(1,2)*S_L(2,6)/S_L(2,2);
                  S_L(1,3)-S_L(1,2)*S_L(2,3)/S_L(2,2) S_L(3,3)-
S_L(2,3)*S_L(2,3)/S_L(2,2)    0      0   S_L(3,6)-S_L(2,3)*S_L(2,6)/S_L(2,2);
                                     0                          0
S_L(4,4) S_L(4,5)             0;
                                     0                          0
S_L(4,5) S_L(5,5)             0;
                  S_L(6,1)-S_L(1,2)*S_L(2,6)/S_L(2,2) S_L(6,3)-
S_L(2,3)*S_L(2,6)/S_L(2,2)    0      0   S_L(6,6)-S_L(2,6)*S_L(2,6)/S_L(2,2)];
   S(:,:,i) = S_L;
end

AA = zeros(2*(NumHalfPly-1),2*(NumHalfPly-1));
BB = zeros(2*(NumHalfPly-1),2*(NumHalfPly-1));
CC = zeros(2*(NumHalfPly-1),2*(NumHalfPly-1));

for i = 1:NumHalfPly
   for l = 1:2*(NumHalfPly-1)
      for m = 1:2*(NumHalfPly-1)

         if i == 1
            if l == 1 & m == 1
```

```
      AA(l,m) = AA(l,m) + 1/10*t^3*Ss_L(2,2,i);
      BB(l,m) = BB(l,m) + 2/3*t*Ss_L(1,2,i) - 2/3*t*Ss_L(3,3,i);
      CC(l,m) = CC(l,m) + 2*Ss_L(1,1,i)/t;
   elseif l == 1 & m == NumHalfPly
      BB(l,m) = BB(l,m) - 2/3*t*Ss_L(3,4,i) + 1/3*t*Ss_L(2,5,i);
      CC(l,m) = CC(l,m) + 2*Ss_L(1,5,i)/t;
   elseif l == NumHalfPly & m == NumHalfPly
      BB(l,m) = BB(l,m) - 2/3*t*Ss_L(4,4,i);
      CC(l,m) = CC(l,m) + 2*Ss_L(5,5,i)/t;
   else
      AA(l,m) = AA(l,m) + 0;
   end
elseif i == NumHalfPly
   if l+2 <= i & m+2 <= i
      AA(l,m) = AA(l,m) + 2*t^3*Ss_L(2,2,i);
      BB(l,m) = BB(l,m) + 0;
   elseif l+2 <= i & m+1 == i
      AA(l,m) = AA(l,m) + 5/3*t^3*Ss_L(2,2,i);
      BB(l,m) = BB(l,m) - 2*t*Ss_L(1,2,i);
   elseif l+2 <= i & m == i+(NumHalfPly-3)+1
      BB(l,m) = BB(l,m) - 2*t*Ss_L(2,5,i);
   elseif l+1 == i & m+1 == i
      AA(l,m) = AA(l,m) + 43/30*t^3*Ss_L(2,2,i);
      BB(l,m) = BB(l,m) - 10/3*t*Ss_L(1,2,i) - 2/3*t*Ss_L(3,3,i);
      CC(l,m) = CC(l,m) + 2*Ss_L(1,1,i)/t;
   elseif l+1 == i & m == i+(NumHalfPly-3)+1
      BB(l,m) = BB(l,m) - 2/3*t*Ss_L(3,4,i) - 5/3*t*Ss_L(2,5,i);
      CC(l,m) = CC(l,m) + 2*Ss_L(1,5,i)/t;
   elseif l == 2*(NumHalfPly-1) & m == 2*(NumHalfPly-1)
      BB(l,m) = BB(l,m) - 2/3*t*Ss_L(4,4,i) ;
      CC(l,m) = CC(l,m) + 2*Ss_L(5,5,i)/t;
   end
else
   if l+2 <= i & m+2 <= i
      AA(l,m) = AA(l,m) + 2*t^3*Ss_L(2,2,i);
      BB(l,m) = BB(l,m) + 0;
   elseif l+2 <= i & m+1 == i
      AA(l,m) = AA(l,m) + 5/3*t^3*Ss_L(2,2,i);
      BB(l,m) = BB(l,m) - 2*t*Ss_L(1,2,i);
   elseif l+2 <=i & m == i
      AA(l,m) = AA(l,m) + 1/3*t^3*Ss_L(2,2,i);
      BB(l,m) = BB(l,m) + 2*t*Ss_L(1,2,i);
   elseif l+2 <= i & m == i+(NumHalfPly-3)+1
      BB(l,m) = BB(l,m) - 2*t*Ss_L(2,5,i);
   elseif l+2 <= i & m == i+(NumHalfPly-3)+2
      BB(l,m) = BB(l,m) + 2*t*Ss_L(2,5,i);
   elseif l+1 == i & m+1 == i
      AA(l,m) = AA(l,m) + 43/30*t^3*Ss_L(2,2,i);
      BB(l,m) = BB(l,m) - 10/3*t*Ss_L(1,2,i) - 2/3*t*Ss_L(3,3,i);
      CC(l,m) = CC(l,m) + 2*Ss_L(1,1,i)/t;
   elseif l+1 == i & m == i
      AA(l,m) = AA(l,m) + 19/60*t^3*Ss_L(2,2,i);
      BB(l,m) = BB(l,m) + 4/3*t*Ss_L(1,2,i) - 1/3*t*Ss_L(3,3,i);
      CC(l,m) = CC(l,m) - 2*Ss_L(1,1,i)/t;
   elseif l+1 == i & m == i+(NumHalfPly-3)+1
      BB(l,m) = BB(l,m) - 2/3*t*Ss_L(3,4,i) - 5/3*t*Ss_L(2,5,i);
      CC(l,m) = CC(l,m) + 2*Ss_L(1,5,i)/t;
   elseif l+1 == i & m == i+(NumHalfPly-3)+2
      BB(l,m) = BB(l,m) - 1/3*t*Ss_L(3,4,i) + 5/3*t*Ss_L(2,5,i);
      CC(l,m) = CC(l,m) - 2*Ss_L(1,5,i)/t;
   elseif l == i & m == i
      AA(l,m) = AA(l,m) + 1/10*t^3*Ss_L(2,2,i);
      BB(l,m) = BB(l,m) + 2/3*t*Ss_L(1,2,i) - 2/3*t*Ss_L(3,3,i);
```

```
            CC(l,m) = CC(l,m) + 2*Ss_L(1,1,i)/t;
         elseif l == i & m == i+(NumHalfPly-3)+1
            BB(l,m) = BB(l,m) - 1/3*t*Ss_L(3,4,i) - 1/3*t*Ss_L(2,5,i);
            CC(l,m) = CC(l,m) - 2*Ss_L(1,5,i)/t;
         elseif l == i & m == i+(NumHalfPly-3)+2
            BB(l,m) = BB(l,m) - 2/3*t*Ss_L(3,4,i) + 1/3*t*Ss_L(2,5,i);
            CC(l,m) = CC(l,m) + 2*Ss_L(1,5,i)/t;
         elseif l == i+(NumHalfPly-3)+1 & m == i+(NumHalfPly-3)+1
            BB(l,m) = BB(l,m) - 2/3*t*Ss_L(4,4,i);
            CC(l,m) = CC(l,m) + 2*Ss_L(5,5,i)/t;
         elseif l == i+(NumHalfPly-3)+1 & m == i+(NumHalfPly-3)+2
            BB(l,m) = BB(l,m) - 1/3*t*Ss_L(4,4,i);
            CC(l,m) = CC(l,m) -2*Ss_L(5,5,i)/t;
         elseif l == i+(NumHalfPly-3)+2 & m == i+(NumHalfPly-3)+2
            BB(l,m) = BB(l,m) - 2/3*t*Ss_L(4,4,i);
            CC(l,m) = CC(l,m) + 2*Ss_L(5,5,i)/t;
         end
      end

   end
end

for l = 1:2*(NumHalfPly-1)
   for m = l:2*(NumHalfPly-1)
      if l ~= m
         AA(m,l) = AA(l,m);
         BB(m,l) = BB(l,m);
         CC(m,l) = CC(l,m);
      end
   end
end

for i = 1:NumHalfPly
   B(:,:,i) = [Ss_L(1,1,i)/t Ss_L(1,2,i)*t/3          0            0
Ss_L(1,5,i)*2/t;
                     0       Ss_L(2,2,i)*t^3/60      0            0
Ss_L(2,5,i)*t/3;
                     0               0         Ss_L(3,3,i)*t/3
2*Ss_L(3,4,i)*t/3       0;
                     0               0                 0       Ss_L(4,4,i)*t/3
0;
                     0               0                 0            0
Ss_L(5,5,i)/t];
end



% ---------------------------------------------------------
%                      slcomp3.m
%       Calculate compliance in new axis when axis is
%          rotated from principal material axis
%                by an angle 'theta'(3D)
%
%                     Function for
% Mixed Model for Laminates Under In-plane & Bending Loads
% ---------------------------------------------------------

function[Sm] = SLComp3(MaterialConstants,theta);

EL = MaterialConstants(1);
ET = MaterialConstants(2);
```

```
NuLT = MaterialConstants(3);
NuTL = MaterialConstants(4);
NuTT = MaterialConstants(5);
GLT = MaterialConstants(6);
GTT = MaterialConstants(7);
c = cos(theta);
s = sin(theta);

R = [c^2  s^2  0 0 0   2*c*s;
     s^2  c^2  0 0 0  -2*c*s;
      0    0   1 0 0     0;
      0    0   0 c -s    0;
      0    0   0 s c     0;
     -c*s c*s  0 0 0  c^2-s^2];

Sp = [  1/EL   -NuTL/ET -NuTL/ET   0      0      0;
      -NuLT/EL   1/ET   -NuTT/ET   0      0      0;
     -NuLT/EL -NuTT/ET   1/ET     0      0      0;
        0         0       0     1/GTT   0      0;
         0         0       0       0   1/GLT   0;
        0         0       0       0     0   1/GLT];

Sm = R'*Sp*R;



% ------------------------------------------------------------------
%                          slstiff2v2.m
%           Calculate stiffness in new axis when axis is
%              rotated from principal material axis
%                    by an angle 'theta'(2D)
%
%                          Function for
%   Mixed Model for Laminates Under In-plane and Bending Loads
% ------------------------------------------------------------------

function[Qm] = SLStiff2v2(MaterialConstants,theta);

EL = MaterialConstants(1);
ET = MaterialConstants(2);
NuLT = MaterialConstants(3);
NuTL = MaterialConstants(4);
NuTT = MaterialConstants(5);
GLT = MaterialConstants(6);
GTT = MaterialConstants(7);

m = cos(theta);
n = sin(theta);

T1 = [m^2 n^2 2*m*n;
      n^2 m^2 -2*m*n;
      -m*n m*n m^2-n^2];

T2 = [m^2 n^2 m*n;
      n^2 m^2 -m*n;
      -2*m*n 2*m*n m^2-n^2];

Qp = [EL/(1 - NuLT*NuTL) NuLT*ET/(1-NuLT*NuTL) 0;
      NuLT*ET/(1-NuLT*NuTL) ET/(1 - NuLT*NuTL) 0;
     0                      0         GLT];

Qm = inv(T1)*Qp*T2;
```

```
% ------------------------------------------------------------
%                       stiffv2.m
%        Calculate laminate stiffnesses A, B, and D
%                      (from CLPT)
%
%                      Function for
%   Mixed Model for Laminates Under In-plane and Bending Loads
% ------------------------------------------------------------

function [A,D] = stiffv2(MaterialConstants,LayUp,t) % t = ply thickness

EL = MaterialConstants(1);
ET = MaterialConstants(2);
NLT = MaterialConstants(3);
NTL = MaterialConstants(4);
NTT= MaterialConstants(5);
GLT = MaterialConstants(6);
GTT = MaterialConstants(7);
NumPly = size(LayUp,2);

A = zeros(3,3);
D = zeros(3,3);
z = linspace(0,NumPly*t,NumPly+1);
for i = 1:NumPly
   PlyAngle = LayUp(NumPly+1-i);
   if PlyAngle >= 200*pi/180
      [Q] = VariableStiff(MaterialConstants,PlyAngle*180/pi-200);
   else
      [Q] = SLStiff2v2(MaterialConstants,PlyAngle);
   end
   A = A + 2*Q*(z(i+1)-z(i));
   D = D + 2*1/3*Q*(z(i+1)^3-z(i)^3);
end
```

```
% ------------------------------------------------------------
%                       variablecomp.m
%        Calculate reduced principal material direction
%              compliance by 'ReductionRatio' (3D)
%
%                       Function for
%    Mixed Model for Laminates Under In-plane and Bending Loads
% ------------------------------------------------------------

function [S] = VariableComp(MaterialConstants,ReductionRatio);

if ReductionRatio == 0
   EL = 1e-10;
   ET = 1e-10;
   NuLT = MaterialConstants(3);
   NuTL = MaterialConstants(4);
   NuTT = MaterialConstants(5);
   GLT = 1e-10;
   GTT = 1e-10;
else
   EL = MaterialConstants(1)/ReductionRatio;
   ET = MaterialConstants(2)/ReductionRatio;
   NuLT = MaterialConstants(3);
   NuTL = MaterialConstants(4);
   NuTT = MaterialConstants(5);
   GLT = MaterialConstants(6)/ReductionRatio;
```

```
   GTT = MaterialConstants(7)/ReductionRatio;
end

S = [  1/EL   -NuTL/ET -NuTL/ET   0      0      0;
      -NuLT/EL   1/ET   -NuTT/ET   0      0      0;
     -NuLT/EL -NuTT/ET   1/ET      0      0      0;
        0          0        0     1/GTT   0      0;
         0          0        0       0   1/GLT   0;
        0          0        0       0     0   1/GLT];



% ------------------------------------------------------
%                    variablestiff.m
%      Calculate reduced principal material direction
%            stiffness by 'ReductionRatio' (2D)
%
%                      Function for
%       Mixed Model for Laminates Under In-plane Loads
% ------------------------------------------------------

function[Q] = variablestiff(MaterialConstants,ReductionRatio);

if ReductionRatio == 0
   EL = 0;
   ET = 0;
   NuLT = MaterialConstants(3);
   NuTL = MaterialConstants(4);
   NuTT = MaterialConstants(5);
   GLT = 0;
   GTT = 0;
else
   EL = MaterialConstants(1)/ReductionRatio;
   ET = MaterialConstants(2)/ReductionRatio;
   NuLT = MaterialConstants(3);
   NuTL = MaterialConstants(4);
   NuTT = MaterialConstants(5);
   GLT = MaterialConstants(6)/ReductionRatio;
   GTT = MaterialConstants(7)/ReductionRatio;
end

Q = [EL/(1 - NuLT*NuTL) NuLT*ET/(1-NuLT*NuTL) 0;
      NuLT*ET/(1-NuLT*NuTL) ET/(1 - NuLT*NuTL) 0;
      0                     0         GLT];



% ------------------------------------------------------------
%                          plot_i.m
%                        Plot stresses
%
%                          Script for
%   Stress Analysis Program for Laminates Under In-plane Loads
% ------------------------------------------------------------

flag = 0;
while flag == 0
   Orientation = input('>> Choose Orientation of Plot \n>> [1] Along the Length
[2] Along the Thickness \n?? ');
   if Orientation == 1
      % Stress field along length of laminate (x-direction)
```

```
      StressComp = input('\n>> Choose Stress Component(s) to Plot \n>> [1] in-
plane components (sig_xx, sig_xy)  [2] out-of-plane components (sig_zz, sig_xz,
sig_yz) \n?? ');
      PlotLayer = input('\n>> Choose Layer to Plot (bottom layer is layer 1)
\n?? ');
      Plotz = input('\n>> Choose z-location to Plot (local z, -0.5 to 0.5) \n??
')*t;
      interval = 1000;
      sigma_yz = zeros(interval*2,1);
      sigma_xz = zeros(interval*2,1);
      sigma_xy = zeros(interval*2,1);
      sigma_xx = zeros(interval*2,1);
      sigma_zz = zeros(interval*2,1);
      bplot = 60*t;
      x = [linspace(-bplot,0,interval) linspace(0,bplot,interval)];
      x = x.';
      for i = 1:interval*2
         y = x(i);
         if i <= interval
            region = 1;
            coe = a_A;
            F = zeros((n(region)-1),1);
            G = zeros((n(region)-1),1);
            dF = zeros((n(region)-1),1);
            dG = zeros((n(region)-1),1);
            ddF = zeros((n(region)-1),1);
            for j = 1:2*(2*(n(region)-1))-(n(region)-1)
               F = F + coe(j)*eigvec(1:(n(region)-
1),j,region)*exp(eigval(1,j,region)*y);
               G = G + coe(j)*eigvec((n(region)-1)+1:2*(n(region)-
1),j,region)*exp(eigval(1,j,region)*y);
               dF = dF + coe(j)*eigvec(1:(n(region)-
1),j,region)*exp(eigval(1,j,region)*y)*eigval(1,j,region);
               dG = dG + coe(j)*eigvec((n(region)-1)+1:2*(n(region)-
1),j,region)*exp(eigval(1,j,region)*y)*eigval(1,j,region);
               ddF = ddF + coe(j)*eigvec(1:(n(region)-
1),j,region)*exp(eigval(1,j,region)*y)*eigval(1,j,region)^2;
            end

            % ---------------
            if i == interval
               BVF_A = F;
               BVdF_A = dF;
               BVddF_A = ddF;
               BVG_A = G;
               BVdG_A = dG;
            end
            % ---------------

            if PlotLayer == 1
               sigma_xz(i) = real(dF(PlotLayer)*(Plotz/t + 1/2));
               sigma_yz(i) = real(dG(PlotLayer)*(Plotz/t + 1/2));
               sigma_xy(i) = real(-G(PlotLayer)/t) +
ncltstress(3,PlotLayer,region);
               sigma_xx(i) = real(-F(PlotLayer)/t) +
ncltstress(1,PlotLayer,region);
               sa_yy(i) = real(-F(PlotLayer)/t);
               sigma_zz(i) = real(-t/2*ddF(PlotLayer)*(Plotz/t + 1/2)^2);
            elseif PlotLayer == n(region)
               sigma_xz(i) = real(-dF(PlotLayer-1)*(Plotz/t - 1/2));
               sigma_yz(i) = real(-dG(PlotLayer-1)*(Plotz/t - 1/2));
               sigma_xy(i) = real(G(PlotLayer-1)/t) +
ncltstress(3,PlotLayer,region);
```

```
                sigma_xx(i) = real(F(PlotLayer-1)/t) +
ncltstress(1,PlotLayer,region);
                sa_yy(i) = real(F(PlotLayer-1)/t);
                sum = 0;
                for k = 1:PlotLayer-1
                   sum = sum + t*ddF(k);
                end
                sigma_zz(i) = real(t/2*ddF(PlotLayer-1)*(Plotz/t - 1/2)^2 -
sum);
             else
                sigma_xz(i) = real(dF(PlotLayer)*(Plotz/t + 1/2) - dF(PlotLayer-
1)*(Plotz/t - 1/2));
                sigma_yz(i) = real(dG(PlotLayer)*(Plotz/t + 1/2) - dG(PlotLayer-
1)*(Plotz/t - 1/2));
                sigma_xy(i) = real((G(PlotLayer-1)-G(PlotLayer))/t) +
ncltstress(3,PlotLayer,region);
                sigma_xx(i) = real((F(PlotLayer-1)-F(PlotLayer))/t) +
ncltstress(1,PlotLayer,region);
                sa_yy(i) = real((F(PlotLayer-1)-F(PlotLayer))/t);
                sum = 0;
                for k = 1:PlotLayer-1
                   sum = sum + t*ddF(k);
                end
                sigma_zz(i) = real(t/2*ddF(PlotLayer-1)*(Plotz/t - 1/2)^2 -
t/2*ddF(PlotLayer)*(Plotz/t + 1/2)^2 - sum);
             end
          else  % if i <= interval
             region = 2;
             coe = a_B;
             F = zeros((n(region)-1),1);
             G = zeros((n(region)-1),1);
             dF = zeros((n(region)-1),1);
             dG = zeros((n(region)-1),1);
             ddF = zeros((n(region)-1),1);
             RealPlotLayer = 0;
             for j = 1:PlotLayer
                if TestDropPly(j) ~= 1
                   RealPlotLayer = RealPlotLayer + 1;
                end
             end
             if (n(region)-1) == 0
                F = 0;
                G = 0;
                dF = 0;
                dG = 0;
                ddF = 0;
             end
             if TestDropPly(PlotLayer) ~= 1
                for j = 1:2*(2*(n(region)-1))-(n(region)-1)
                   F = F + coe(j)*eigvec(1:(n(region)-
1),j,region)*exp(eigval(1,j,region)*y);
                   G = G + coe(j)*eigvec((n(region)-1)+1:2*(n(region)-
1),j,region)*exp(eigval(1,j,region)*y);
                   dF = dF + coe(j)*eigvec(1:(n(region)-
1),j,region)*exp(eigval(1,j,region)*y)*eigval(1,j,region);
                   dG = dG + coe(j)*eigvec((n(region)-1)+1:2*(n(region)-
1),j,region)*exp(eigval(1,j,region)*y)*eigval(1,j,region);
                   ddF = ddF + coe(j)*eigvec(1:(n(region)-
1),j,region)*exp(eigval(1,j,region)*y)*eigval(1,j,region)^2;
                end
             % ---------------
             if i == interval+1
                BVF_B = F;
```

```
            BVdF_B = dF;
            BVddF_B = ddF;
            BVG_B = G;
            BVdG_B = dG;
         end
         % ---------------
            if RealPlotLayer == 1
               sigma_xz(i) = real(dF(RealPlotLayer)*(Plotz/t + 1/2));
               sigma_yz(i) = real(dG(RealPlotLayer)*(Plotz/t + 1/2));
               sigma_xy(i) = real(-G(RealPlotLayer)/t) +
ncltstress(3,PlotLayer,region);
               sigma_xx(i) = real(-F(RealPlotLayer)/t) +
ncltstress(1,PlotLayer,region);
               sigma_zz(i) = real(-t/2*ddF(RealPlotLayer)*(Plotz/t +
1/2)^2);
            elseif RealPlotLayer == n(region)
               sigma_xz(i) = real(-dF(RealPlotLayer-1)*(Plotz/t - 1/2));
               sigma_yz(i) = real(-dG(RealPlotLayer-1)*(Plotz/t - 1/2));
               sigma_xy(i) = real(G(RealPlotLayer-1)/t) +
ncltstress(3,PlotLayer,region);
               sigma_xx(i) = real(F(RealPlotLayer-1)/t) +
ncltstress(1,PlotLayer,region);
               sum = 0;
               for k = 1:RealPlotLayer-1
                  sum = sum + t*ddF(k);
               end
               sigma_zz(i) = real(t/2*ddF(RealPlotLayer-1)*(Plotz/t - 1/2)^2
- sum);
            else
               sigma_xz(i) = real(dF(RealPlotLayer)*(Plotz/t + 1/2) -
dF(RealPlotLayer-1)*(Plotz/t - 1/2));
               sigma_yz(i) = real(dG(RealPlotLayer)*(Plotz/t + 1/2) -
dG(RealPlotLayer-1)*(Plotz/t - 1/2));
               sigma_xy(i) = real((G(RealPlotLayer-1)-G(RealPlotLayer))/t) +
ncltstress(3,PlotLayer,region);
               sigma_xx(i) = real((F(RealPlotLayer-1)-F(RealPlotLayer))/t) +
ncltstress(1,PlotLayer,region);
               sum = 0;
               for k = 1:RealPlotLayer-1
                  sum = sum + t*ddF(k);
               end
               sigma_zz(i) = real(t/2*ddF(RealPlotLayer-1)*(Plotz/t - 1/2)^2
- t/2*ddF(RealPlotLayer)*(Plotz/t + 1/2)^2 - sum);
            end
         end
      end   % if i <= interval
   end  % for i = 1:interval*2
   if StressComp == 1
      figure(1)

plot(x(1:interval),sigma_xx(1:interval),x(1:interval),sigma_xy(1:interval),':')
; hold on

plot(x(interval+1:interval*2),sigma_xx(interval+1:interval*2),x(interval+1:inte
rval*2),sigma_xy(interval+1:interval*2),':');
      xlabel('Length');
      ylabel('Stress');
      title1 = ['In-plane Stress, Layer: ' num2str(PlotLayer) ', Local z: '
num2str(Plotz)];
      title(title1);
      grid on
      hold off
   else
```

```
         figure(1)

plot(x(1:interval),sigma_xz(1:interval),x(1:interval),sigma_yz(1:interval),':',
x(1:interval),sigma_zz(1:interval),'--');hold on

plot(x(interval+1:interval*2),sigma_xz(interval+1:interval*2),x(interval+1:inte
rval*2),sigma_yz(interval+1:interval*2),':',x(interval+1:interval*2),sigma_zz(i
nterval+1:interval*2),'--');
         xlabel('Length');
         ylabel('Stress');
         title2 = ['Interlaminar Stress, Layer: ' num2str(PlotLayer) ', Local
z: ' num2str(Plotz)];
         title(title2);
         grid on
         hold off
      end

   elseif Orientation == 2
      % Stress field along length of laminate (x-direction)
      StressComp = input('\n>> Choose Stress Component to Plot \n>> [1] sig_xx
[2] sig_yy   [3] sig_zz   [4] sig_xz   [5] sig_yz   [6] sig_xy \n?? ');
      Plotz = [];
      PointsPerPly = 10;
      for i = 1:n(1)
         Plotz = [linspace(-i*t,(-i+1)*t,10) Plotz];
      end
      sigma_xx_zA = zeros(1,size(Plotz,2));
      sigma_xz_zA = zeros(1,size(Plotz,2));
      sigma_zz_zA = zeros(1,size(Plotz,2));
      currentlayer = 1;
      for i = 1:size(Plotz,2)
         if i > PointsPerPly*currentlayer
            currentlayer = currentlayer + 1;
         end
         z = Plotz(i) + (n(1)-(2*currentlayer-1)/2)*t;
         if currentlayer == 1
            sigma_xx_zA(i) = real(-
BVF_A(currentlayer)/t)+ncltstress(1,currentlayer,1);
            sigma_xz_zA(i) = real(BVdF_A(currentlayer))*(z/t + 1/2);
            sigma_zz_zA(i) = real(-t/2*BVddF_A(currentlayer)*(z/t + 1/2)^2);
            sigma_xy_zA(i) = real(-
BVG_A(currentlayer)/t)+ncltstress(3,currentlayer,1);
            sigma_yz_zA(i) = real(BVdG_A(currentlayer))*(z/t + 1/2);
         elseif currentlayer == n(1)
            sigma_xx_zA(i) = real(BVF_A(currentlayer-
1)/t)+ncltstress(1,currentlayer,1);
            sigma_xz_zA(i) = real(-BVdF_A(currentlayer-1)*(z/t - 1/2));
            sum = 0;
            for k = 1:currentlayer-1
                sum = sum + t*BVddF_A(k);
            end
            sigma_zz_zA(i) = real(t/2*BVddF_A(currentlayer-1)*(z/t - 1/2)^2 -
sum);
            sigma_xy_zA(i) = real(BVG_A(currentlayer-
1)/t)+ncltstress(3,currentlayer,1);
            sigma_yz_zA(i) = real(-BVdG_A(currentlayer-1)*(z/t - 1/2));
         else
            sigma_xx_zA(i) = real(BVF_A(currentlayer-1)/t-
BVF_A(currentlayer)/t)+ncltstress(1,currentlayer,1);
            sigma_xz_zA(i) = real(BVdF_A(currentlayer)*(z/t + 1/2) -
BVdF_A(currentlayer-1)*(z/t - 1/2));
            sum = 0;
            for k = 1:currentlayer-1
```

```
                sum = sum + t*BVddF_A(k);
            end
            sigma_zz_zA(i) = real(t/2*BVddF_A(currentlayer-1)*(z/t - 1/2)^2 -
t/2*BVddF_A(currentlayer)*(z/t + 1/2)^2 - sum);
            sigma_xy_zA(i) = real(BVG_A(currentlayer-1)/t-
BVG_A(currentlayer)/t)+ncltstress(3,currentlayer,1);
            sigma_yz_zA(i) = real(BVdG_A(currentlayer)*(z/t + 1/2) -
BVdG_A(currentlayer-1)*(z/t - 1/2));
        end
    end

    if StressComp == 1
        figure(2)
        subplot(1,2,1); plot(sigma_xx_zA,Plotz);
        xlabel('\sigma_x_x');
        ylabel('z');
        title1 = ['In-plane Stress at x = 0 in Undropped Region'];
        title(title1);
        grid on
    elseif StressComp == 4
        figure(2)
        subplot(1,2,1); plot(sigma_xz_zA,Plotz);
        xlabel('\sigma_x_z');
        ylabel('z');
        title1 = ['Shear Stress at x = 0 in Undropped Region'];
        title(title1);
        grid on

    elseif StressComp == 3
        figure(2)
        subplot(1,2,1); plot(sigma_zz_zA,Plotz);
        xlabel('\sigma_z_z');
        ylabel('z');
        title1 = ['Normal Stress at x = 0 in Undropped Region'];
        title(title1);
        grid on
    elseif StressComp == 6
        figure(2)
        subplot(1,2,1); plot(sigma_xy_zA,Plotz);
        xlabel('\sigma_x_y');
        ylabel('z');
        title1 = ['In-plane Stress at x = 0 in Undropped Region'];
        title(title1);
        grid on
    elseif StressComp == 5
        figure(2)
        subplot(1,2,1); plot(sigma_yz_zA,Plotz);
        xlabel('\sigma_y_z');
        ylabel('z');
        title1 = ['Shear Stress at x = 0 in Undropped Region'];
        title(title1);
        grid on
    end

    Plotz = [];
    PointsPerPly = 10;
    for i = 1:n(2)
        Plotz = [linspace(-i*t,(-i+1)*t,10) Plotz];
    end
    sigma_xx_zB = zeros(1,size(Plotz,2));
    sigma_xz_zB = zeros(1,size(Plotz,2));
    currentlayer = 1;
    RealPlotLayer = 1;
```

```
      for i = 1:size(Plotz,2)
         if i > PointsPerPly*currentlayer
            currentlayer = currentlayer + 1;
            RealPlotLayer = currentlayer;
            if currentlayer > PlyNumsDrop(1)-1
               RealPlotLayer = RealPlotLayer + nt;
            end
         end
         z = Plotz(i) + (n(2)-(2*currentlayer-1)/2)*t;
         if currentlayer == 1
            sigma_xx_zB(i) = real(-
BVF_B(currentlayer)/t)+ncltstress(1,RealPlotLayer,2);
            sigma_xz_zB(i) = real(BVdF_B(currentlayer))*(z/t + 1/2);
            sigma_zz_zB(i) = real(-t/2*BVddF_B(currentlayer)*(z/t + 1/2)^2);
            sigma_xy_zB(i) = real(-
BVG_B(currentlayer)/t)+ncltstress(3,RealPlotLayer,2);
            sigma_yz_zB(i) = real(BVdG_B(currentlayer))*(z/t + 1/2);
         elseif currentlayer == n(2)
            sigma_xx_zB(i) = real(BVF_B(currentlayer-
1)/t)+ncltstress(1,RealPlotLayer,2);
            sigma_xz_zB(i) = real(-BVdF_B(currentlayer-1)*(z/t - 1/2));
            sum = 0;
            for k = 1:currentlayer-1
                sum = sum + t*BVddF_B(k);
            end
            sigma_zz_zB(i) = real(t/2*BVddF_B(currentlayer-1)*(z/t - 1/2)^2 -
sum);
            sigma_xy_zB(i) = real(BVG_B(currentlayer-
1)/t)+ncltstress(3,RealPlotLayer,2);
            sigma_yz_zB(i) = real(-BVdG_B(currentlayer-1)*(z/t - 1/2));
         else
            sigma_xx_zB(i) = real(BVF_B(currentlayer-1)/t-
BVF_B(currentlayer)/t)+ncltstress(1,RealPlotLayer,2);
            sigma_xz_zB(i) = real(BVdF_B(currentlayer)*(z/t + 1/2) -
BVdF_B(currentlayer-1)*(z/t - 1/2));
            sum = 0;
            for k = 1:currentlayer-1
                sum = sum + t*BVddF_B(k);
            end
            sigma_zz_zB(i) = real(t/2*BVddF_B(currentlayer-1)*(z/t - 1/2)^2 -
t/2*BVddF_B(currentlayer)*(z/t + 1/2)^2 - sum);
            sigma_xy_zB(i) = real(BVG_B(currentlayer-1)/t-
BVG_B(currentlayer)/t)+ncltstress(3,RealPlotLayer,2);
            sigma_yz_zB(i) = real(BVdG_B(currentlayer)*(z/t + 1/2) -
BVdG_B(currentlayer-1)*(z/t - 1/2));
         end
      end

      if StressComp == 1
         subplot(1,2,2); plot(sigma_xx_zB,Plotz);
         xlabel('\sigma_x_x');
         ylabel('z');
         title1 = ['and Dropped Region'];
         title(title1);
         grid on;
      elseif StressComp == 4
         subplot(1,2,2); plot(sigma_xz_zB,Plotz);
         xlabel('\sigma_x_z');
         ylabel('z');
         title1 = ['and Dropped Region'];
         title(title1);
         grid on;
      elseif StressComp == 3
```

```
         subplot(1,2,2); plot(sigma_zz_zB,Plotz);
         xlabel('\sigma_z_z');
         ylabel('z');
         title1 = ['and Dropped Region'];
         title(title1);
         grid on;
      elseif StressComp == 6
         subplot(1,2,2); plot(sigma_xy_zB,Plotz);
         xlabel('\sigma_x_y');
         ylabel('z');
         title1 = ['and Dropped Region'];
         title(title1);
         grid on;
      elseif StressComp == 5
         subplot(1,2,2); plot(sigma_yz_zB,Plotz);
         xlabel('\sigma_y_z');
         ylabel('z');
         title1 = ['and Dropped Region'];
         title(title1);
         grid on
      end

   end % if Orientation == 1

   ContPlot = input('\n>> Continue (Yes or No, default Yes) \n?? ','s');
   switch ContPlot,
      case 'No',
         flag = 1;
      end

end % while flag == 0



% AS4/3501-6 in Metric units
function[EL,ET,GLT,GTT,NuLT,NuTT] = as4_3501d6

EL = 142e9; %Pa
ET = 9.81e9; %Pa
GLT = 6e9; %Pa
GTT = 6e9;
NuLT = 0.3;
NuTT = 0.34;
```

APPENDIX B

SOURCE CODE LISTING FOR ANALYSIS OF LAMINATES WITH PLY DROPOFFS UNDER BENDING LOAD

The source codes of the programs for analysis of laminates with ply dropoffs under bending load are listed in this appendix. One main program, named 'bending.m', was written for this loading condition where the user is prompted to input the laminate configuration and material properties, and the eigenvalues and eigenvectors for equations (4.51) and (4.52) are calculated. Separate subroutines were written to obtain the unknown constants, a_j and b_j, for the global model (from equation (4.54)), and mixed model (from equation (4.60)). The program named 'global_b.m' is the subroutine for the global model and 'mixed_b.m' for the mixed model. Other sub-routines called by these programs are also listed. A plotting program, 'plot_b.m' is also listed. This program is used to visualize the stress field in the laminates analyzed. All programs are written for Matlab® Release 12.

```
% ------------------------------------------------------------
%                          bending.m
%   Stress Analysis Program for Laminates Under Bending Loads
%                             by
%                          DJ Shim
%
%      Copyright 2002, Massachusetts Institute of Technology
%
% Permission to use, copy, modify, and distribute this software
% for any purpose and without fee is hereby granted, provided that
% the above copyright notice appear in all copies and that both
% that copyright notice and this permission notice appear in
% supporting documentation, and that the name of MIT not be used
% in advertising or publicity pertaining to distribution of the
% software without specific, written prior permission. MIT makes no
% representations about the suitability or merchantability of the
% documentation (or its associated software) for any purpose.
% It is provided "as is" without express or implied warranty.
% This software is a research program, and MIT does not represent
% that it is free of errors or bugs or suitable for any particular
% task.
% ------------------------------------------------------------

clear all

% ------------------------------------------------------------------
% User input query
% ------------------------------------------------------------------

model = input('>> Select Analytical Model (default = 2) \n>> [1] Global Model
[2] Mixed Model \n?? ');
if isempty(model) model = 2; end;
Mx = input('>> Applied Moment (default = 10000)? \n?? ');
if isempty(Mx) Mx = 10000; end;
% Symmetric layups (100 refers to terminated plies, 2xx refers to variable
stiffness plies)
LayUp = input('\n>> Layup of Laminate (default = [0t2/02tD/0t4]s)? \n?? ');
if isempty(LayUp)
   fprintf('... default layup used ...');
      LayUp = [0 0 0 0 0 0 0 0;
            0 0 100 100 0 0 0 0]
else
   LayUp
end;
LayUp = LayUp*pi/180;
alpha = 0;
if LayUp(2,1) ~= 100*pi/180
    alpha = input('\n>> Taper Angle (default = 7deg)? ');
    if isempty(alpha) alpha = 7; end % Taper angle (in degrees)
end
t = input('\n>> Ply Thickness (default = 1)? ');
if isempty(t) t = 1; % Each layer thickness is 1
end
[EL ET GLT GTT NuLT NuTT] = as4_3501d6; % Material constants
M = [Mx;0;0]; % Applied force
b = 100*t; % Length of laminate

% ------------------------------------------------------------------
% Initialize variables
% ------------------------------------------------------------------

% A and B are integration intervals
A = -0.5*t;
```

```
B = 0.5*t;
alp = alpha*pi/180;
NuTL = (ET/EL) * NuLT;
% MC = material constants
MC = [EL ET NuLT NuTL NuTT GLT GTT];
RegionALayUp = LayUp(1,:);
RegionBLayUp = LayUp(2,:);
for region = 1:2
   tempLayUp = LayUp(region,:);
   tempNumHalfPly = size(tempLayUp);
   tempNumHalfPly = tempNumHalfPly(2);
   % ContractedLayUp = real layup, without '100' -- important for dropped
region layup
   ContractedLayUp = [];
   for i = 1:tempNumHalfPly
      if LayUp(region,i) ~= 100*pi/180
         ContractedLayUp = [ContractedLayUp LayUp(region,i)];
      end
   end
   CurrentNumHalfPly = size(ContractedLayUp);
   CurrentNumHalfPly = CurrentNumHalfPly(2);
   n(region) = CurrentNumHalfPly;
end

% LUU = LayUp of undropped region
LUU = LayUp(1,:);
% LUD = LayUp of dropped region (without terminated plies)
LUD = [];
for i = 1:n(1)
   if LayUp(2,i) ~= 100*pi/180
      LUD = [LUD LayUp(region,i)];
   end
end

% NTP = Number of Terminated Plies
NTP = 0;
% DropPlies = Ply Number of Dropped Plies
DropPlies = [];
for i = 1:n(1)
   if RegionBLayUp(i) == 100*pi/180
      NTP = NTP + 1;
      TestDropPly(i) = 1;
      DropPlies = [DropPlies i];
   else
      TestDropPly(i) = 0;
   end
end

% Gauss Integration Points and Weights
r = [-.861136311594053 -.339981043584856 .339981043584856 .861136311594053];
al = [.347854845137454 .652145154862546 .652145154862546 .347854845137454];

r = (A+B)/2+(B-A)/2*r;
al = (B-A)/2*al;

% ---------------------------------------------------------------
% Solve companion problem
% ---------------------------------------------------------------

for region = 1:2

% Calculate Matrix Components
```

```
   E0 = zeros(n(region)*4-2,n(region)*4-2); E1 = E0; E2 = E0; E3 = E0; E4 = E0;
E5 = E0; E5 = E0; E6 = E0; E7 = E0; E8 = E0;
   for i = 1:n(region)
      if region == 1
            CurrentLayUp = LUU;
      else
                  CurrentLayUp = LUD;
          end
      if CurrentLayUp(i) >= 200*pi/180
         S_L = VariableComp(MC,CurrentLayUp(i)*180/pi-200);
      else
         S_L = SLComp3(MC,CurrentLayUp(i));
      end
      Ss_L(:,:,i,region) = [S_L(1,1)-S_L(1,2)*S_L(1,2)/S_L(2,2) S_L(1,3)-
S_L(1,2)*S_L(2,3)/S_L(2,2)    0      0   S_L(1,6)-S_L(1,2)*S_L(2,6)/S_L(2,2);
                             S_L(1,3)-S_L(1,2)*S_L(2,3)/S_L(2,2) S_L(3,3)-
S_L(2,3)*S_L(2,3)/S_L(2,2)    0      0   S_L(3,6)-S_L(2,3)*S_L(2,6)/S_L(2,2);
                                                  0                          0
S_L(4,4) S_L(4,5)             0;
                                                  0                          0
S_L(4,5) S_L(5,5)             0;
                             S_L(6,1)-S_L(1,2)*S_L(2,6)/S_L(2,2) S_L(6,3)-
S_L(2,3)*S_L(2,6)/S_L(2,2)    0      0   S_L(6,6)-S_L(2,6)*S_L(2,6)/S_L(2,2)];
      fill = i*2-3;
      for j = 1:4
          s33 = [s33function(n(region),i,i,r(j),t), zeros(1,(n(region)-i)*2)];
          s33 = [s33(1:n(region)*2-1), zeros(1,n(region)*2-1)];
          s13 = [s13function(n(region),i,i,r(j),t), zeros(1,(n(region)-i)*2)];
          s13 = [s13(1:n(region)*2-1), zeros(1,n(region)*2-1)];
          s11 = [zeros(1,fill), s11function(n(region),i,i,r(j),t),
zeros(1,(n(region)-i)*2)];
          s11 = [s11(1:n(region)*2-1), zeros(1,n(region)*2-1)];
          s23 = [s23function(n(region),i,i,r(j),t), zeros(1,(n(region)-i)*2)];
          s23 = [zeros(1,n(region)*2-1), s23(1:n(region)*2-1)];
          s12 = [zeros(1,fill), s12function(n(region),i,i,r(j),t),
zeros(1,(n(region)-i)*2)];
          s12 = [zeros(1,n(region)*2-1), s12(1:n(region)*2-1)];
          E0 = E0 + 2*al(j)*(s33.'*s33)*Ss_L(2,2,i,region);
          E1 = E1 - 2*al(j)*(s13.'*s13)*Ss_L(3,3,i,region);
          E2 = E2 - 2*al(j)*(s23.'*s23)*Ss_L(4,4,i,region);
          E3 = E3 + 2*al(j)*(s33.'*s11+s11.'*s33)*Ss_L(1,2,i,region);
          E4 = E4 - 2*al(j)*(s13.'*s23+s23.'*s13)*Ss_L(3,4,i,region);
          E5 = E5 + 2*al(j)*(s12.'*s33+s33.'*s12)*Ss_L(2,5,i,region);
          E6 = E6 + 2*al(j)*(s11.'*s11)*Ss_L(1,1,i,region);
          E7 = E7 + 2*al(j)*(s12.'*s12)*Ss_L(5,5,i,region);
          E8 = E8 + 2*al(j)*(s11.'*s12+s12.'*s11)*Ss_L(1,5,i,region);
      end
   end
   AA = E0;
   BB = E1+E2+E3+E4+E5;
   CC = E6+E7+E8;

   ALPHA = [BB AA;AA zeros((n(region)*2-1)*2)];
   BETA = [-CC zeros((n(region)*2-1)*2);zeros((n(region)*2-1)*2) AA];
   [v,d] = eig(BETA,ALPHA);
   temp1 = zeros((n(region)*2-1)*2,(n(1)*2)*3-(n(region)*2)*3);
   temp2 = zeros((n(1)*4)-n(region)*4,(n(region)*2-1)*3);
   evec_R(:,:,region) = [v(1:(n(region)*2-1)*2,1:(n(region)*2-1)*3) temp1;
                         temp2 zeros(n(1)*4-n(region)*4,(n(1)*2-
n(region)*2)*3)];
   evec_F(:,:,region) = [evec_R(1:n(region)*2-1,1:(n(region)*2-1)*3,region)
zeros(n(region)*2-1,(n(1)*2-n(region)*2)*3);
```

```
                                                        zeros(n(1)*2-
n(region)*2,(n(region)*2-1)*3) zeros(n(1)*2-n(region)*2,(n(1)*2-
n(region)*2)*3)];
   evec_G(:,:,region) = [evec_R(n(region)*2:(n(region)*2-1)*2,1:(n(region)*2-
1)*3,region) zeros(n(region)*2-1,(n(1)*2-n(region)*2)*3);
                                                        zeros(n(1)*2-
n(region)*2,(n(region)*2-1)*3) zeros(n(1)*2-n(region)*2,(n(1)*2-
n(region)*2)*3)];
   diagd = diag(d);
   eval_R(1,:,region) = [sqrt(diagd(1:(n(region)*2-1)*3)).' zeros(1,(n(1)*2-
n(region)*2)*3)];
   if region == 2
      eval_R(1,:,region) = -eval_R(1,:,region);
   end
end

Oa_A = zeros((n(1)*2-1)*3,(n(1)*2-1)*3);
Oa_B = zeros((n(2)*2-1)*3,(n(2)*2-1)*3);

for region = 1:2

% Calculate Matrix Components
   E0 = zeros((n(region)*2-1)*3,(n(region)*2-1)*3); E1 = E0; E2 = E0; E3 = E0;
E4 = E0; E5 = E0; E6 = E0; E7 = E0; E8 = E0;
   for i = 1:n(region)
      fill = i*2-3;
      for j = 1:4
          tevec_R = evec_R(1:(n(region)*2-1)*2,1:(n(region)*2-1)*3,region);
          teval_R = eval_R(1,1:(n(region)*2-1)*3,region);
          s33 = [s33function(n(region),i,i,r(j),t), zeros(1,(n(region)-i)*2)];
          s33 = [s33(1:n(region)*2-1), zeros(1,n(region)*2-1)];
          s13 = [s13function(n(region),i,i,r(j),t), zeros(1,(n(region)-i)*2)];
          s13 = [s13(1:n(region)*2-1), zeros(1,n(region)*2-1)];
          s11 = [zeros(1,fill), s11function(n(region),i,i,r(j),t),
zeros(1,(n(region)-i)*2)];
          s11 = [s11(1:n(region)*2-1), zeros(1,n(region)*2-1)];
          s23 = [s23function(n(region),i,i,r(j),t), zeros(1,(n(region)-i)*2)];
          s23 = [zeros(1,n(region)*2-1), s23(1:n(region)*2-1)];
          s12 = [zeros(1,fill), s12function(n(region),i,i,r(j),t),
zeros(1,(n(region)-i)*2)];
          s12 = [zeros(1,n(region)*2-1), s12(1:n(region)*2-1)];
          E0 = E0 +
2*al(j)*((s33*de(teval_R,de(teval_R,tevec_R))).'*(s33*de(teval_R,de(teval_R,tev
ec_R))))*Ss_L(2,2,i,region);
          E1 = E1 +
2*al(j)*((s13*de(teval_R,tevec_R)).'*(s13*de(teval_R,tevec_R)))*Ss_L(3,3,i,regi
on);
          E2 = E2 +
2*al(j)*((s23*de(teval_R,tevec_R)).'*(s23*de(teval_R,tevec_R)))*Ss_L(4,4,i,regi
on);
          E3 = E3 +
2*al(j)*((s33*de(teval_R,de(teval_R,tevec_R))).'*(s11*tevec_R)+(s11*tevec_R).'*
(s33*de(teval_R,de(teval_R,tevec_R))))*Ss_L(1,2,i,region);
          E4 = E4 +
2*al(j)*((s13*de(teval_R,tevec_R)).'*(s23*de(teval_R,tevec_R))+(s23*de(teval_R,
tevec_R)).'*(s13*de(teval_R,tevec_R)))*Ss_L(3,4,i,region);
          E5 = E5 +
2*al(j)*((s33*de(teval_R,de(teval_R,tevec_R))).'*(s12*tevec_R)+(s12*tevec_R).'*
(s33*de(teval_R,de(teval_R,tevec_R))))*Ss_L(2,5,i,region);
          E6 = E6 + 2*al(j)*((s11*tevec_R).'*(s11*tevec_R))*Ss_L(1,1,i,region);
          E7 = E7 + 2*al(j)*((s12*tevec_R).'*(s12*tevec_R))*Ss_L(5,5,i,region);
```

```
            E8 = E8 +
2*al(j)*((s11*tevec_R).'*(s12*tevec_R)+(s12*tevec_R).'*(s11*tevec_R))*Ss_L(1,5,
i,region);
        end
    end
    if region == 1
        Oa_A = Oa_A+E0+E1+E2+E3+E4+E5+E6+E7+E8;
        for j = 1:size(Oa_A,1)
            for k = 1:size(Oa_A,2)
                Oa_A(j,k) = Oa_A(j,k)/(teval_R(j)+teval_R(k));
            end
        end
    else
        Oa_B = Oa_B+E0+E1+E2+E3+E4+E5+E6+E7+E8;
        for j = 1:size(Oa_B,1)
            for k = 1:size(Oa_B,2)
                Oa_B(j,k) = Oa_B(j,k)/(teval_R(j)+teval_R(k));
            end
        end
    end
end

% Calculate unknown coefficients, aj and bj, using boundary conditions
% a_A = aj, a_B = bj

if model == 1 % global model
    [a_A,a_B] =
global_b(eval_R,evec_R,evec_F,evec_G,Oa_A,Oa_B,M,MC,n,LUU,LUD,NTP,TestDropPly,D
ropPlies,t);
else % mixed model
    [a_A,a_B] =
mixed_b(eval_R,evec_R,evec_F,evec_G,Oa_A,Oa_B,M,MC,n,LUU,LUD,NTP,TestDropPly,t,
alp);
end

eigvec = evec_R;
eigval = eval_R;

plot_b



% ------------------------------------------------------------------
%                            global_b.m
%        Calculates unknown coefficients using global model
%
%                          Function for
%   Stress Analysis Program for Laminates Under Bending Loads
% ------------------------------------------------------------------

function [a_A,a_B] =
global_b(eval_R,evec_R,evec_F,evec_G,Oa_A,Oa_B,M,MC,n,LUU,LUD,NTP,TestDropPly,D
ropPlies,t);

B = zeros((n(1)*2-1)*3+(n(2)*2-1)*3,1);
s11BCs = [];
s12BCs = [];
s1zBCs = [];
rhs_s11BCs = [];
rhs_s12BCs = [];
rhs_s1zBCs = [];
for region = 1:2
```

```
   temps11BCs = [];
   temps12BCs = [];
   temps1zBCs = [];
   rhs_temps11BCs = [];
   rhs_temps12BCs = [];
   rhs_temps1zBCs = [];
   ri = 0;
   sizeof = (n(region)*2-1)*3;
   for i = 1:n(1)
      if region == 1
         ri = ri + 1; % ri = real i
         flag = 1;
         CLU = LUU; % CLU = Current Layup
      else
         if TestDropPly(i) == 1
             temps11BCs = [temps11BCs; zeros(2,sizeof)];
             temps12BCs = [temps12BCs; zeros(2,sizeof)];
             temps1zBCs = [temps1zBCs; zeros(2,sizeof)];
             rhs_temps11BCs = [rhs_temps11BCs; zeros(2,1)];
             rhs_temps12BCs = [rhs_temps12BCs; zeros(2,1)];
             rhs_temps1zBCs = [rhs_temps1zBCs; zeros(2,1)];
             CLU = LUD;
             flag = 0;
         else
             CLU = LUD;
             ri = ri + 1;
             flag = 1;
         end
      end
      if flag == 1
         temps11BCs = [temps11BCs;
sigma11(evec_F(:,:,region),eval_R(:,:,region),-1/2*t,ri,n(region),t)]; % s11 at
z = -1/2t
         temps11BCs = [temps11BCs;
sigma11(evec_F(:,:,region),eval_R(:,:,region),1/2*t,ri,n(region),t)]; % s11 at
z = 1/2t
         temps12BCs = [temps12BCs;
sigma12(evec_G(:,:,region),eval_R(:,:,region),-1/2*t,ri,n(region),t)]; % s12 at
z = -1/2t
         temps12BCs = [temps12BCs;
sigma12(evec_G(:,:,region),eval_R(:,:,region),1/2*t,ri,n(region),t)]; % s12 at
z = 1/2t
         temps1zBCs = [temps1zBCs;
sigma1z(evec_F(:,:,region),eval_R(:,:,region),0,ri,n(region),t)]; % s1z at z =
0
         temps1zBCs = [temps1zBCs;
sigma1z(evec_F(:,:,region),eval_R(:,:,region),1/2*t,ri,n(region),t)]; % s1z at
z = 1/2t
         rhs_temps11BCs = [rhs_temps11BCs; bcltc2(M,n(region),-
1/2*t,ri,MC,CLU,t,'s11')];
         rhs_temps11BCs = [rhs_temps11BCs;
bcltc2(M,n(region),1/2*t,ri,MC,CLU,t,'s11')];
         rhs_temps12BCs = [rhs_temps12BCs; bcltc2(M,n(region),-
1/2*t,ri,MC,CLU,t,'s12')];
         rhs_temps12BCs = [rhs_temps12BCs;
bcltc2(M,n(region),1/2*t,ri,MC,CLU,t,'s12')];
         rhs_temps1zBCs = [rhs_temps1zBCs; zeros(2,1)];
      end
   end
   if region == 1
      s11BCs = [s11BCs temps11BCs];
      s12BCs = [s12BCs temps12BCs];
      s1zBCs = [s1zBCs temps1zBCs];
```

```
      rhs_s11BCs = -rhs_temps11BCs;
      rhs_s12BCs = -rhs_temps12BCs;
      rhs_s1zBCs = -rhs_temps1zBCs;
   else
      s11BCs = [s11BCs -temps11BCs];
      s12BCs = [s12BCs -temps12BCs];
      s1zBCs = [s1zBCs -temps1zBCs];
      rhs_s11BCs = rhs_s11BCs + rhs_temps11BCs;
      rhs_s12BCs = rhs_s12BCs + rhs_temps12BCs;
   end
end
s11BCs = s11BCs(1:n(1)*2-1,:);
s12BCs = s12BCs(1:n(1)*2-1,:);
s1zBCs = s1zBCs(1:n(1)*2-1,:);
rhs_s11BCs = rhs_s11BCs(1:(n(1)*2-1),1);
rhs_s12BCs = rhs_s12BCs(1:(n(1)*2-1),1);
rhs_s1zBCs = rhs_s1zBCs(1:(n(1)*2-1),1);

% Extra conditions for internal cases
if TestDropPly(1) ~= 1
   if max(DropPlies) == n(1)
      s11BCs = [s11BCs; sigma11(evec_F(:,:,1),eval_R(:,:,1),1/2*t,n(1),n(1),t)
zeros(1,(n(2)*2-1)*3)];
      s12BCs = [s12BCs; sigma12(evec_G(:,:,1),eval_R(:,:,1),1/2*t,n(1),n(1),t)
zeros(1,(n(2)*2-1)*3)];
      s1zBCs = [s1zBCs; sigma1z(evec_F(:,:,1),eval_R(:,:,1),1/2*t,DropPlies(1)-
1,n(1),t) zeros(1,sizeof)];
      rhs_s11BCs = [rhs_s11BCs; 0];
      rhs_s12BCs = [rhs_s12BCs; 0];
      rhs_s1zBCs = [rhs_s1zBCs; 0];
   else
      s11BCs = [s11BCs; sigma11(evec_F(:,:,1),eval_R(:,:,1),1/2*t,n(1),n(1),t)
...
                          -
sigma11(evec_F(:,:,2),eval_R(:,:,2),1/2*t,n(2),n(2),t)]; % s11 at z = 1/2t of
ply n
      s12BCs = [s12BCs; sigma12(evec_G(:,:,1),eval_R(:,:,1),1/2*t,n(1),n(1),t)
...
                          -
sigma12(evec_G(:,:,2),eval_R(:,:,2),1/2*t,n(2),n(2),t)]; % s12 at z = 1/2t of
ply n
      s1zBCs = [s1zBCs; sigma1z(evec_F(:,:,1),eval_R(:,:,1),1/2*t,DropPlies(1)-
1,n(1),t) zeros(1,sizeof)];
      rhs_s11BCs = [rhs_s11BCs; bcltc2(M,n(2),1/2*t,n(2),MC,LUD,t,'s11')-
bcltc2(M,n(1),1/2*t,n(1),MC,LUU,t,'s11')];
      rhs_s12BCs = [rhs_s12BCs; bcltc2(M,n(2),1/2*t,n(2),MC,LUD,t,'s12')-
bcltc2(M,n(1),1/2*t,n(1),MC,LUU,t,'s12')];
      rhs_s1zBCs = [rhs_s1zBCs; 0];
   end
end

fill = [zeros((n(1)*2-1)*3,(n(2)*2-1)*3)];

A = [Oa_A fill;
     fill' -Oa_B];

B = [B; rhs_s11BCs; rhs_s12BCs; rhs_s1zBCs];

A = [A s11BCs.' s12BCs.' s1zBCs.';
       s11BCs [zeros(size(s11BCs,1),size(s11BCs,1))
zeros(size(s11BCs,1),size(s12BCs,1)) zeros(size(s11BCs,1),size(s1zBCs,1))];
       s12BCs [zeros(size(s12BCs,1),size(s11BCs,1))
zeros(size(s12BCs,1),size(s12BCs,1)) zeros(size(s12BCs,1),size(s1zBCs,1))];
```

```
       s1zBCs [zeros(size(s1zBCs,1),size(s11BCs,1))
zeros(size(s1zBCs,1),size(s12BCs,1)) zeros(size(s1zBCs,1),size(s1zBCs,1))]];

xx = A\B;
a_A = xx(1:(n(1)*2-1)*3);
a_B = xx((n(1)*2-1)*3+1:(n(1)*2-1)*3+(n(2)*2-1)*3);



% ------------------------------------------------------------
%                          mixed_b.m
%        Calculates unknown coefficients using mixed model
%
%                         Function for
%   Stress Analysis Program for Laminates Under Bending Loads
% ------------------------------------------------------------

function [a_A,a_B] =
mixed_b(eval_R,evec_R,evec_F,evec_G,Oa_A,Oa_B,M,MC,n,LUU,LUD,NTP,TestDropPly,t,
alp);

nt = n(1)-n(2);
i1 = 0;
i2 = 0;
i3 = 0;
PlyNumsKU = [];
PlyNumsUKU = 0;
for i = 1:n(1)
   if TestDropPly(i) == 1
      i2 = i2 + 1;
      PlyNumsDrop(i2) = i;
   end
   if TestDropPly(i) ~= 1
      if i2 ~= 0
         i3 = i3 + 1;
         % PlyNumsUKU = ply numbers of plies in unkinked region in the
undropped region
         PlyNumsUKU(i3) = i;
      elseif i3 == 0
         i1 = i1 + 1;
         % PlyNumKU = ply numbers of plies in kinked region in the undropped
region
         PlyNumsKU(i1) = i;
      end
   end
end
% tf = ply number of first terminated ply
tf = PlyNumsDrop(1);
% tl = ply number of last terminated ply
tl = PlyNumsDrop(n(1)-n(2));
% PlyNumsKD = ply numbers of plies in kinked region in the dropped region
PlyNumsKD = PlyNumsKU;
for i = 1:size(PlyNumsUKU,2)
   % PlyNumsUKD = ply numbers of plies in unkinked region in the dropped region
   PlyNumsUKD(i) = i + (tf-1);
end

B = zeros((n(1)*2-1)*3+(n(2)*2-1)*3,1);
sizeof = (n(2)*2-1)*3;

% Separate Internal Dropoff Cases From External Dropoff Cases
s11BCs_Dropoff = [];
```

```
s12BCs_Dropoff = [];
s1zBCs_Dropoff = [];
mBCs1_Dropoff = [];
mBCs2_Dropoff = [];
mBCs3_Dropoff = [];
mBCs4_Dropoff = [];
rhs_s11BC_Dropoff = [];
rhs_s12BC_Dropoff = [];
rhs_s1zBC_Dropoff = [];
BCsm_Dropoff = [];

s11BCs_Continuous = [];
s12BCs_Continuous = [];
s1zBCs_Continuous = [];
rhs_s11BC_Continuous = [];
rhs_s12BC_Continuous = [];
rhs_s1zBC_Continuous = [];

if tf ~= 1 % Internal Dropoff Case

% Force Balance in Dropoff Region, Kinked Plies
s11BCs_Dropoff = 0;
s12BCs_Dropoff = 0;
s1zBCs_Dropoff = 0;
mBCs1_Dropoff = 0;
mBCs2_Dropoff = 0;
mBCs3_Dropoff = 0;
mBCs4_Dropoff = 0;
rhs_s11BC_Dropoff = 0;
rhs_s12BC_Dropoff = 0;
rhs_s1zBC_Dropoff = 0;
BCsm_Dropoff = 0;
       midpoint = (0.5 - (n(1)-(2*(size(PlyNumsKU,2)/2)-1)/2));
       for i = 1:size(PlyNumsKU,2)
         s11BCs_Dropoff = s11BCs_Dropoff + [int_sigma11(evec_F(:,:,1),i,n(1),t)
-int_sigma11(evec_F(:,:,2),i,n(2),t)]; % x direction force equilibrium in
dropoff region
         s12BCs_Dropoff = s12BCs_Dropoff + [int_sigma12(evec_G(:,:,1),i,n(1),t)
-int_sigma12(evec_G(:,:,2),i,n(2),t)]; % y direction force equilibrium in
dropoff region
         s1zBCs_Dropoff = s1zBCs_Dropoff +
[int_sigma1z(evec_F(:,:,1),eval_R(:,:,1),i,n(1),t) -
int_sigma1z(evec_F(:,:,2),eval_R(:,:,2),i,n(2),t)]; % z direction force
equilibrium in dropoff region
         rhs_s11BC_Dropoff = rhs_s11BC_Dropoff - t*(bcltc2(M,n(1),-
1/2*t,i,MC,LUU,t,'s11')+bcltc2(M,n(1),1/2*t,i,MC,LUU,t,'s11'))/2 ...
                                                + t*(bcltc2(M,n(2),-
1/2*t,i,MC,LUD,t,'s11')+bcltc2(M,n(2),1/2*t,i,MC,LUD,t,'s11'))/2;
         rhs_s12BC_Dropoff = rhs_s12BC_Dropoff - t*(bcltc2(M,n(1),-
1/2*t,i,MC,LUU,t,'s12')+bcltc2(M,n(1),1/2*t,i,MC,LUU,t,'s12'))/2 ...
                                                + t*(bcltc2(M,n(2),-
1/2*t,i,MC,LUD,t,'s12')+bcltc2(M,n(2),1/2*t,i,MC,LUD,t,'s12'))/2;
         r = -( midpoint + (n(1)-(2*i-1)/2));
       mBCs1_Dropoff = mBCs1_Dropoff +
int_z_sigma11(evec_F(:,:,1),eval_R(:,:,1),i,n(1),r*2,t);
         mBCs2_Dropoff = mBCs2_Dropoff +
int_sigma1z(evec_F(:,:,2),eval_R(:,:,2),i,n(2),t);
         mBCs3_Dropoff = mBCs3_Dropoff +
int_z_sigma11(evec_F(:,:,2),eval_R(:,:,2),i,n(2),r*2,t);
         mBCs4_Dropoff = mBCs4_Dropoff + int_sigma11(evec_F(:,:,2),i,n(2),t);
         BCsm_Dropoff = BCsm_Dropoff + int_z_clts11(M,n(2),i,r*2,MC,LUD,t)-
int_z_clts11(M,n(1),i,r*2,MC,LUU,t)+ ...
```

```
                                + t*(bcltc2(M,n(2),-
1/2*t,i,MC,LUD,t,'s11')+bcltc2(M,n(2),1/2*t,i,MC,LUD,t,'s11'))/2*NTP*t;
      end
      mBCs = [mBCs1_Dropoff mBCs2_Dropoff/tan(alp)*NTP*t-(mBCs3_Dropoff +
mBCs4_Dropoff*NTP*t)];

else % External Dropoff Case

      for i = 1:size(PlyNumsUKU,2)
            if i ~= size(PlyNumsUKU,2)
               s11BCs_Continuous = [s11BCs_Continuous;...

      sigma11(evec_F(:,:,1),eval_R(:,:,1),-1/2*t,PlyNumsUKU(i),n(1),t) -
sigma11(evec_F(:,:,2),eval_R(:,:,2),-1/2*t,PlyNumsUKU(i)-nt,n(2),t);...

      sigma11(evec_F(:,:,1),eval_R(:,:,1),1/2*t,PlyNumsUKU(i),n(1),t) -
sigma11(evec_F(:,:,2),eval_R(:,:,2),1/2*t,PlyNumsUKU(i)-nt,n(2),t)]; % x
direction force equilibrium in dropoff region
               s12BCs_Continuous = [s12BCs_Continuous;...

      sigma12(evec_G(:,:,1),eval_R(:,:,1),-1/2*t,PlyNumsUKU(i),n(1),t) -
sigma12(evec_G(:,:,2),eval_R(:,:,2),-1/2*t,PlyNumsUKU(i)-nt,n(2),t);...

      sigma12(evec_G(:,:,1),eval_R(:,:,1),1/2*t,PlyNumsUKU(i),n(1),t) -
sigma12(evec_G(:,:,2),eval_R(:,:,2),1/2*t,PlyNumsUKU(i)-nt,n(2),t)];% y
direction force equilibrium in dropoff region
               s1zBCs_Continuous = [s1zBCs_Continuous;...

      sigma1z(evec_F(:,:,1),eval_R(:,:,1),0,PlyNumsUKU(i),n(1),t) -
sigma1z(evec_F(:,:,2),eval_R(:,:,2),0,PlyNumsUKU(i)-nt,n(2),t);...

      sigma1z(evec_F(:,:,1),eval_R(:,:,1),1/2*t,PlyNumsUKU(i),n(1),t) -
sigma1z(evec_F(:,:,2),eval_R(:,:,2),1/2*t,PlyNumsUKU(i)-nt,n(2),t)]; % z
direction force equilibrium in dropoff region
               rhs_s11BC_Continuous = [rhs_s11BC_Continuous;...

      bcltc2(M,n(2),-1/2*t,PlyNumsUKU(i)-nt,MC,LUD,t,'s11')-bcltc2(M,n(1),-
1/2*t,PlyNumsUKU(i),MC,LUU,t,'s11');...

      bcltc2(M,n(2),1/2*t,PlyNumsUKU(i)-nt,MC,LUD,t,'s11')-
bcltc2(M,n(1),1/2*t,PlyNumsUKU(i),MC,LUU,t,'s11')];
               rhs_s12BC_Continuous = [rhs_s12BC_Continuous;...

      bcltc2(M,n(2),-1/2*t,PlyNumsUKU(i)-nt,MC,LUD,t,'s12')-bcltc2(M,n(1),-
1/2*t,PlyNumsUKU(i),MC,LUU,t,'s12');...

      bcltc2(M,n(2),1/2*t,PlyNumsUKU(i)-nt,MC,LUD,t,'s12')-
bcltc2(M,n(1),1/2*t,PlyNumsUKU(i),MC,LUU,t,'s12')];
               rhs_s1zBC_Continuous = [rhs_s1zBC_Continuous; 0; 0];
            else
               s11BCs_Continuous = [s11BCs_Continuous;...

      sigma11(evec_F(:,:,1),eval_R(:,:,1),-1/2*t,PlyNumsUKU(i),n(1),t) -
sigma11(evec_F(:,:,2),eval_R(:,:,2),-1/2*t,PlyNumsUKU(i)-nt,n(2),t)];% x
direction force equilibrium in dropoff region
               s12BCs_Continuous = [s12BCs_Continuous;...

      sigma12(evec_G(:,:,1),eval_R(:,:,1),-1/2*t,PlyNumsUKU(i),n(1),t) -
sigma12(evec_G(:,:,2),eval_R(:,:,2),-1/2*t,PlyNumsUKU(i)-nt,n(2),t)];% y
direction force equilibrium in dropoff region
               s1zBCs_Continuous = [s1zBCs_Continuous;...

      sigma1z(evec_F(:,:,1),eval_R(:,:,1),0,PlyNumsUKU(i),n(1),t) -
```

```
sigma1z(evec_F(:,:,2),eval_R(:,:,2),0,PlyNumsUKU(i)-nt,n(2),t)]; % z direction
force equilibrium in dropoff region
                rhs_s11BC_Continuous = [rhs_s11BC_Continuous;...

       bcltc2(M,n(2),-1/2*t,PlyNumsUKU(i)-nt,MC,LUD,t,'s11')-bcltc2(M,n(1),-
1/2*t,PlyNumsUKU(i),MC,LUU,t,'s11')];
                rhs_s12BC_Continuous = [rhs_s12BC_Continuous;...

       bcltc2(M,n(2),-1/2*t,PlyNumsUKU(i)-nt,MC,LUD,t,'s12')-bcltc2(M,n(1),-
1/2*t,PlyNumsUKU(i),MC,LUU,t,'s12')];
                rhs_s1zBC_Continuous = [rhs_s1zBC_Continuous; 0];
             end
       end

end

% Stress-Free Conditions in Terminated Plies at Cutoffs
s11BCs_Terminated = [];
s12BCs_Terminated = [];
s1zBCs_Terminated = [];
rhs_s11BC_Terminated = [];
rhs_s12BC_Terminated = [];
rhs_s1zBC_Terminated = [];
for i = 1:size(PlyNumsDrop,2)
   s11BCs_Terminated = [s11BCs_Terminated;...

       sigma11(evec_F(:,:,1),eval_R(:,:,1),-1/2*t,PlyNumsDrop(i),n(1),t)
zeros(1,sizeof);...

       sigma11(evec_F(:,:,1),eval_R(:,:,1),1/2*t,PlyNumsDrop(i),n(1),t)
zeros(1,sizeof)];
   s12BCs_Terminated = [s12BCs_Terminated;...

       sigma12(evec_G(:,:,1),eval_R(:,:,1),-1/2*t,PlyNumsDrop(i),n(1),t)
zeros(1,sizeof);...

       sigma12(evec_G(:,:,1),eval_R(:,:,1),1/2*t,PlyNumsDrop(i),n(1),t)
zeros(1,sizeof)];
   s1zBCs_Terminated = [s1zBCs_Terminated;...

       sigma1z(evec_F(:,:,1),eval_R(:,:,1),0,PlyNumsDrop(i),n(1),t)
zeros(1,sizeof);...

       sigma1z(evec_F(:,:,1),eval_R(:,:,1),1/2*t,PlyNumsDrop(i),n(1),t)
zeros(1,sizeof)];
   rhs_s11BC_Terminated = [rhs_s11BC_Terminated;...
                                                    -bcltc2(M,n(1),-
1/2*t,PlyNumsDrop(i),MC,LUU,t,'s11');...
                                                    -
bcltc2(M,n(1),1/2*t,PlyNumsDrop(i),MC,LUU,t,'s11')];
   rhs_s12BC_Terminated = [rhs_s12BC_Terminated;...
                                                     -bcltc2(M,n(1),-
1/2*t,PlyNumsDrop(i),MC,LUU,t,'s12');...
                                                     -
bcltc2(M,n(1),1/2*t,PlyNumsDrop(i),MC,LUU,t,'s12')];
   rhs_s1zBC_Terminated = [rhs_s1zBC_Terminated; 0; 0];
end

s11BCs = [s11BCs_Dropoff; s11BCs_Continuous; s11BCs_Terminated];
s12BCs = [s12BCs_Dropoff; s12BCs_Continuous; s12BCs_Terminated];
s1zBCs = [s1zBCs_Dropoff; s1zBCs_Continuous; s1zBCs_Terminated];
rhs_s11BCs = [rhs_s11BC_Dropoff; rhs_s11BC_Continuous; rhs_s11BC_Terminated];
rhs_s12BCs = [rhs_s12BC_Dropoff; rhs_s12BC_Continuous; rhs_s12BC_Terminated];
```

```
rhs_s1zBCs = [rhs_s1zBC_Dropoff; rhs_s1zBC_Continuous; rhs_s1zBC_Terminated];

% Extra condition for Internal Dropoff Case Only
if PlyNumsDrop(1) ~= 1
   s1zBCs = [s1zBCs; sigma1z(evec_F(:,:,1),eval_R(:,:,1),-
1/2*t,PlyNumsDrop(1),n(1),t) zeros(1,sizeof)]; % s1z at z = -1/2t of first ply
drop
   rhs_s1zBCs = [rhs_s1zBCs; 0];
   s1zBCs = [s1zBCs;zeros(1,(n(1)*2-1)*3) sigma1z(evec_F(:,:,2),eval_R(:,:,2),-
1/2*t,PlyNumsDrop(1),n(2),t)]; % s1z at z = -1/2t of first ply drop
   rhs_s1zBCs = [rhs_s1zBCs; 0];
end

fill = [zeros((n(1)*2-1)*3,(n(2)*2-1)*3)];
A = [Oa_A fill;
     fill' -Oa_B];

if PlyNumsDrop(1) == 1 % External Dropoff
   fill1 = zeros(n(1)*2,(n(1)*2-1)*2+2);
   fill2 = zeros(n(1)*2,(n(1)*2-1)*2+2);
   B = [B; rhs_s11BCs; rhs_s12BCs; rhs_s1zBCs];
else % Internal Dropoff
   fill1 = zeros(n(1)*2,(n(1)*2-1)*2+2);
   fill2 = zeros(n(1)*2,(n(1)*2-1)*2+2);
   B = [B; rhs_s11BCs; rhs_s12BCs; rhs_s1zBCs];
      B = [B;BCsm_Dropoff];
end

if PlyNumsDrop(1) == 1 % External Dropoff
   A = [A s11BCs.' s12BCs.' s1zBCs.';
        s11BCs
zeros(size(s11BCs,1),size(s11BCs,1)+size(s12BCs,1)+size(s1zBCs,1));
        s12BCs
zeros(size(s11BCs,1),size(s11BCs,1)+size(s12BCs,1)+size(s1zBCs,1));
        s1zBCs
zeros(size(s1zBCs,1),size(s11BCs,1)+size(s12BCs,1)+size(s1zBCs,1))];
else  % Internal Dropoff
   A = [A s11BCs.' s12BCs.' s1zBCs.' mBCs.';
        s11BCs
zeros(size(s11BCs,1),size(s11BCs,1)+size(s12BCs,1)+size(s1zBCs,1)+size(mBCs,1))
;
        s12BCs
zeros(size(s11BCs,1),size(s11BCs,1)+size(s12BCs,1)+size(s1zBCs,1)+size(mBCs,1))
;
        s1zBCs
zeros(size(s1zBCs,1),size(s11BCs,1)+size(s12BCs,1)+size(s1zBCs,1)+size(mBCs,1))
;
        mBCs
zeros(size(mBCs,1),size(s11BCs,1)+size(s12BCs,1)+size(s1zBCs,1)+size(mBCs,1))];
end

xx = A\B;
a_A = xx(1:(n(1)*2-1)*3);
a_B = xx((n(1)*2-1)*3+1:(n(1)*2-1)*3+(n(2)*2-1)*3);



% ------------------------------------------------------------------
%                          bcltc2.m
%   Calculates CLPT stresses and returns appropriate component
%
%                          Function for
```

```
%   Stress Analysis Program for Laminates Under Bending Loads
% ------------------------------------------------------------

function [stresscomponent,stress,rz] =
bcltc2(M,n,z,i,MaterialConstants,LayUp,t,returncomponent)
% returncomponent = component of stress that needs to be returned by this
function

[A,D] = stiffv2(MaterialConstants,LayUp,t);
if LayUp(i) >= 200*pi/180
   [Q] = VariableStiff(MaterialConstants,LayUp(i)*180/pi-200);
else
   [Q] = SLStiff2v2(MaterialConstants,LayUp(i));
end
rz = z - (n-(2*i-1)/2)*t;
curvature = inv(D)*M;
stress = rz*Q*curvature;
if returncomponent == 's11'
   stresscomponent = stress(1);
elseif returncomponent == 's22'
   stresscomponent = stress(2);
else
   stresscomponent = stress(3);
end
```

```
% ------------------------------------------------------------
%                          s11function.m
%      Calculates matrix function g11 from equation (4.39a)
%
%                          Function for
%    Stress Analysis Program for Laminates Under Bending Loads
% ------------------------------------------------------------

% n=number of half-plies, i=current ply in recursion, r=Gauss integration point

function [s11]=s11function(n,CurrentPly,i,r,t)

ThirdLastTerm = [1/(2*(2+3*(-CurrentPly+n)))-r/t/(2+3*(-CurrentPly+n))];

LastTwoTerms = [1/(2*(1+3*(-CurrentPly+n)))-1/(2*(2+3*(-CurrentPly+n)))+ ...
                r/t/(1+3*(-CurrentPly+n))+r/t/(2+3*(-CurrentPly+n)), ...
                -1/(2*(1+3*(-CurrentPly+n)))-r/t/(1+3*(-CurrentPly+n))];

if i == 1
   s11 = LastTwoTerms;
else
   s11 = [ThirdLastTerm, LastTwoTerms];
end
```

```
% ------------------------------------------------------------
%                          s12function.m
%      Calculates matrix function g12 from equation (4.39b)
%
%                          Function for
%    Stress Analysis Program for Laminates Under Bending Loads
% ------------------------------------------------------------
```

```
% n=number of half-plies, i=current ply in recursion, r=Gauss integration point

function [s12]=s12function(n,CurrentPly,i,r,t)

ThirdLastTerm = [1/(2*(2+3*(-CurrentPly+n)))-r/t/(2+3*(-CurrentPly+n))];

LastTwoTerms = [1/(2*(1+3*(-CurrentPly+n)))-1/(2*(2+3*(-CurrentPly+n)))+ ...
                r/t/(1+3*(-CurrentPly+n))+r/t/(2+3*(-CurrentPly+n)), ...
                -1/(2*(1+3*(-CurrentPly+n)))-r/t/(1+3*(-CurrentPly+n))];

if i == 1
   s12 = LastTwoTerms;
else
   s12 = [ThirdLastTerm, LastTwoTerms];
end



% ---------------------------------------------------------------
%                          s13function.m
%      Calculates matrix function g13 from equation (4.39c)
%
%                          Function for
%    Stress Analysis Program for Laminates Under Bending Loads
% ---------------------------------------------------------------

% n=number of half-plies, i=current ply in recursion, r=Gauss integration point

function [s13]=s13function(n,CurrentPly,i,r,t)

FirstTerm = [-t/(2*(1+3*(-(CurrentPly-i+1)+n)))+t/(2*(2+3*(-(CurrentPly-
i+1)+n)))];

SecondTerm = [-t/(2*(2+3*(-(CurrentPly-i+2)+n)))+t/(2*(1+3*(-(CurrentPly-
i+1)+n)))];

ThirdLastTerm = [-3*t/(8*(2+3*(-CurrentPly+n)))+t/(2*(1+3*(-(CurrentPly-
1)+n)))-r/(2*(2+3*(-CurrentPly+n)))+r^2/t/(2*(2+3*(-CurrentPly+n)))];

LastTwoTerms = [-t/(8*(1+3*(-CurrentPly+n)))+3*t/(8*(2+3*(-CurrentPly+n)))-
r/(2*(1+3*(-CurrentPly+n)))+r/(2*(2+3*(-CurrentPly+n)))- ...
                r^2/t/(2*(1+3*(-CurrentPly+n)))-r^2/t/(2*(2+3*(-
CurrentPly+n))), ...
                t/(8*(1+3*(-CurrentPly+n)))+r/(2*(1+3*(-
CurrentPly+n)))+r^2/t/(2*(1+3*(-CurrentPly+n)))];

if i == 1
   s13 = LastTwoTerms;
elseif i == 2
   s13 = [FirstTerm, ThirdLastTerm, s13function(n,CurrentPly,i-1,r,t)];
else
   s13 = [FirstTerm, SecondTerm, s13function(n,CurrentPly,i-1,r,t)];
end



% ---------------------------------------------------------------
%                          s23function.m
%      Calculates matrix function g23 from equation (4.39d)
%
%                          Function for
```

```
%    Stress Analysis Program for Laminates Under Bending Loads
% ------------------------------------------------------------

% n=number of half-plies, i=current ply in recursion, r=Gauss integration point

function [s23]=s23function(n,CurrentPly,i,r,t)

FirstTerm = [-t/(2*(1+3*(-(CurrentPly-i+1)+n)))+t/(2*(2+3*(-(CurrentPly-
i+1)+n)))];

SecondTerm = [-t/(2*(2+3*(-(CurrentPly-i+2)+n)))+t/(2*(1+3*(-(CurrentPly-
i+1)+n)))];

ThirdLastTerm = [-3*t/(8*(2+3*(-CurrentPly+n)))+t/(2*(1+3*(-(CurrentPly-
1)+n)))-r/(2*(2+3*(-CurrentPly+n)))+r^2/t/(2*(2+3*(-CurrentPly+n)))];

LastTwoTerms = [-t/(8*(1+3*(-CurrentPly+n)))+3*t/(8*(2+3*(-CurrentPly+n)))-
r/(2*(1+3*(-CurrentPly+n)))+r/(2*(2+3*(-CurrentPly+n)))- ...
                r^2/t/(2*(1+3*(-CurrentPly+n)))-r^2/t/(2*(2+3*(-
CurrentPly+n))), ...
                t/(8*(1+3*(-CurrentPly+n)))+r/(2*(1+3*(-
CurrentPly+n)))+r^2/t/(2*(1+3*(-CurrentPly+n)))];

if i == 1
   s23 = LastTwoTerms;
elseif i == 2
   s23 = [FirstTerm, ThirdLastTerm, s23function(n,CurrentPly,i-1,r,t)];
else
   s23 = [FirstTerm, SecondTerm, s23function(n,CurrentPly,i-1,r,t)];
end



% ------------------------------------------------------------
%                          s33function.m
%      Calculates matrix function g33 from equation (4.39e)
%
%                          Function for
%    Stress Analysis Program for Laminates Under Bending Loads
% ------------------------------------------------------------

% n=number of half-plies, i=current ply in recursion, r=Gauss integration point

function [s33]=s33function(n,CurrentPly,i,r,t)

FirstTerm = [(6*i-7)*t^2/(12*(1+3*(-(CurrentPly-i+1)+n)))-(6*i-
5)*t^2/(12*(2+3*(-(CurrentPly-i+1)+n)))+r*t/(2*(1+3*(-(CurrentPly-i+1)+n)))-
r*t/(2*(2+3*(-(CurrentPly-i+1)+n)))];

SecondTerm = [(6*i-11)*t^2/(12*(2+3*(-(CurrentPly-i+2)+n)))-(6*i-
7)*t^2/(12*(1+3*(-(CurrentPly-i+1)+n)))+r*t/(2*(2+3*(-(CurrentPly-i+2)+n)))-
r*t/(2*(1+3*(-(CurrentPly-i+1)+n)))];

ThirdLastTerm = [5*t^2/(48*(2+3*(-CurrentPly+n)))-5*t^2/(12*(1+3*(-(CurrentPly-
1)+n)))+3*r*t/(8*(2+3*(-CurrentPly+n)))-r*t/(2*(1+3*(-(CurrentPly-1)+n)))+ ...
                r^2/(4*(2+3*(-CurrentPly+n)))-r^3/t/(6*(2+3*(-CurrentPly+n)))];

LastTwoTerms = [t^2/(48*(1+3*(-CurrentPly+n)))-5*t^2/(48*(2+3*(-
CurrentPly+n)))+r*t/(8*(1+3*(-CurrentPly+n)))-3*r*t/(8*(2+3*(-CurrentPly+n)))+
...
```

```
                r^2/(4*(1+3*(-CurrentPly+n)))-r^2/(4*(2+3*(-
CurrentPly+n)))+r^3/t/(6*(1+3*(-CurrentPly+n)))+r^3/t/(6*(2+3*(-
CurrentPly+n))), ...
                -t^2/(48*(1+3*(-CurrentPly+n)))-r*t/(8*(1+3*(-CurrentPly+n)))-
r^2/(4*(1+3*(-CurrentPly+n)))-r^3/t/(6*(1+3*(-CurrentPly+n)))];

if i == 1
   s33 = LastTwoTerms;
elseif i == 2
   s33 = [FirstTerm, ThirdLastTerm, s33function(n,CurrentPly,i-1,r,t)];
else
   s33 = [FirstTerm, SecondTerm, s33function(n,CurrentPly,i-1,r,t)];
end
```

```
% ------------------------------------------------------------------
%                          sigma11.m
%       Calculates sigma_11 stress from companion problem
%
%                         Function for
%    Stress Analysis Program for Laminates Under Bending Loads
% ------------------------------------------------------------------

function [vector] = sigma11(F,l,z,i,n,t)

s = (n*2-1)*3;
if i == 1
   vector = -1/(3*(n-i)+2)*(-F(2*i-1,1:s))*(z/t-1/2)+1/(3*(n-i)+1)*(F(2*i-
1,1:s)-F(2*i,1:s))*(z/t+1/2);
elseif i == n
   vector = -1/(3*(n-i)+2)*(F(2*i-2,1:s)-F(2*i-1,1:s))*(z/t-1/2)+1/(3*(n-
i)+1)*(F(2*i-1,1:s))*(z/t+1/2);
else
   vector = -1/(3*(n-i)+2)*(F(2*i-2,1:s)-F(2*i-1,1:s))*(z/t-1/2)+1/(3*(n-
i)+1)*(F(2*i-1,1:s)-F(2*i,1:s))*(z/t+1/2);
end
```

```
% ------------------------------------------------------------------
%                          sigma12.m
%       Calculates sigma_12 stress from companion problem
%
%                         Function for
%    Stress Analysis Program for Laminates Under Bending Loads
% ------------------------------------------------------------------

function [vector] = sigma12(G,l,z,i,n,t)

s = (n*2-1)*3;
if i == 1
   vector = -1/(3*(n-i)+2)*(-G(2*i-1,1:s))*(z/t-1/2)+1/(3*(n-i)+1)*(G(2*i-
1,1:s)-G(2*i,1:s))*(z/t+1/2);
elseif i == n
   vector = -1/(3*(n-i)+2)*(G(2*i-2,1:s)-G(2*i-1,1:s))*(z/t-1/2)+1/(3*(n-
i)+1)*(G(2*i-1,1:s))*(z/t+1/2);
else
   vector = -1/(3*(n-i)+2)*(G(2*i-2,1:s)-G(2*i-1,1:s))*(z/t-1/2)+1/(3*(n-
i)+1)*(G(2*i-1,1:s)-G(2*i,1:s))*(z/t+1/2);
end
```

```
% ------------------------------------------------------------
%                          sigma1z.m
%       Calculates sigma_1z stress from companion problem
%
%                         Function for
%    Stress Analysis Program for Laminates Under Bending Loads
% ------------------------------------------------------------

function [vector] = sigma1z(F,l,z,i,n,t)

s = (n*2-1)*3;
if i == 1
   j = 1;
   sum = t/2*(1/(3*(n-j)+2)*(-F(2*j-1,1:s).*l(1,1:s)));
   vector = t/2/(3*(n-i)+2)*(-F(2*i-1,1:s).*l(1,1:s))*(z/t-1/2)^2 ...
            - t/2/(3*(n-i)+1)*(F(2*i-1,1:s).*l(1,1:s)-
F(2*i,1:s).*l(1,1:s))*(z/t+1/2)^2 - sum;
elseif i >= n
   sum = [];
   for j = 1:i
       if j == 1
          sum = t/2*(1/(3*(n-j)+2)*(-F(2*j-1,1:s).*l(1,1:s)));
       else
          sum = sum + t/2*(1/(3*(n-j)+2)*(F(2*j-2,1:s).*l(1,1:s)-F(2*j-
1,1:s).*l(1,1:s)) ...
                          + 1/(3*(n-(j-1))+1)*(F(2*j-3,1:s).*l(1,1:s)-F(2*j-
2,1:s).*l(1,1:s)));
       end
   end
   vector = t/2/(3*(n-i)+2)*(F(2*i-2,1:s).*l(1,1:s)-F(2*i-
1,1:s).*l(1,1:s))*(z/t-1/2)^2 ...
            - t/2/(3*(n-i)+1)*(F(2*i-1,1:s).*l(1,1:s))*(z/t+1/2)^2 - sum;
else
   sum = [];
   for j = 1:i
       if j == 1
          sum = t/2*(1/(3*(n-j)+2)*(-F(2*j-1,1:s).*l(1,1:s)));
       else
          sum = sum + t/2*(1/(3*(n-j)+2)*(F(2*j-2,1:s).*l(1,1:s)-F(2*j-
1,1:s).*l(1,1:s)) ...
                          + 1/(3*(n-(j-1))+1)*(F(2*j-3,1:s).*l(1,1:s)-F(2*j-
2,1:s).*l(1,1:s)));
       end
   end
   vector = t/2/(3*(n-i)+2)*(F(2*i-2,1:s).*l(1,1:s)-F(2*i-
1,1:s).*l(1,1:s))*(z/t-1/2)^2 ...
            - t/2/(3*(n-i)+1)*(F(2*i-1,1:s).*l(1,1:s)-
F(2*i,1:s).*l(1,1:s))*(z/t+1/2)^2 - sum;
end
```

```
% ------------------------------------------------------------
%                       int_sigma11.m
%         Calculates the integral of sigma_11 stress
%                   from companion problem
%
%                         Function for
%    Stress Analysis Program for Laminates Under Bending Loads
% ------------------------------------------------------------

function [vector] = int_sigma11(F,i,n,t)
```

```
s = (n*2-1)*3;
if i == 1
   vector = -1/(3*(n-i)+2)*(-F(2*i-1,1:s))*(-1/2)*t+1/(3*(n-i)+1)*(F(2*i-
1,1:s)-F(2*i,1:s))*(1/2)*t;
elseif i == n
   vector = -1/(3*(n-i)+2)*(F(2*i-2,1:s)-F(2*i-1,1:s))*(-1/2)*t+1/(3*(n-
i)+1)*(F(2*i-1,1:s))*(1/2)*t;
else
   vector = -1/(3*(n-i)+2)*(F(2*i-2,1:s)-F(2*i-1,1:s))*(-1/2)*t+1/(3*(n-
i)+1)*(F(2*i-1,1:s)-F(2*i,1:s))*(1/2)*t;
end
```

```
% ------------------------------------------------------------
%                        int_sigma12.m
%          Calculates the integral of sigma_12 stress
%                    from companion problem
%
%                         Function for
%    Stress Analysis Program for Laminates Under Bending Loads
% ------------------------------------------------------------

function [vector] = int_sigma12(G,i,n,t)

s = (n*2-1)*3;
if i == 1
   vector = -1/(3*(n-i)+2)*(-G(2*i-1,1:s))*(-1/2)*t+1/(3*(n-i)+1)*(G(2*i-
1,1:s)-G(2*i,1:s))*(1/2)*t;
elseif i == n
   vector = -1/(3*(n-i)+2)*(G(2*i-2,1:s)-G(2*i-1,1:s))*(-1/2)*t+1/(3*(n-
i)+1)*(G(2*i-1,1:s))*(1/2)*t;
else
   vector = -1/(3*(n-i)+2)*(G(2*i-2,1:s)-G(2*i-1,1:s))*(-1/2)*t+1/(3*(n-
i)+1)*(G(2*i-1,1:s)-G(2*i,1:s))*(1/2)*t;
end
```

```
% ------------------------------------------------------------
%                        int_sigma1z.m
%          Calculates the integral of sigma_1z stress
%                    from companion problem
%
%                         Function for
%    Stress Analysis Program for Laminates Under Bending Loads
% ------------------------------------------------------------

function [vector] = int_sigma1z(F,l,i,n,t)

s = (n*2-1)*3;
if i == 1
   j = 1;
   sum = t/2*(1/(3*(n-j)+2)*(-F(2*j-1,1:s).*l(1,1:s)));
   vector = t/2/(3*(n-i)+2)*(-F(2*i-1,1:s).*l(1,1:s))*(1/3)*t ...
            - t/2/(3*(n-i)+1)*(F(2*i-1,1:s).*l(1,1:s)-
F(2*i,1:s).*l(1,1:s))*(1/3)*t - sum*t;
elseif i == n
   sum = [];
   for j = 1:i
```

```
       if j == 1
          sum = t/2*(1/(3*(n-j)+2)*(-F(2*j-1,1:s).*l(1,1:s)));
       else
          sum = sum + t/2*(1/(3*(n-j)+2)*(F(2*j-2,1:s).*l(1,1:s)-F(2*j-
1,1:s).*l(1,1:s)) ...
                          + 1/(3*(n-(j-1))+1)*(F(2*j-3,1:s).*l(1,1:s)-F(2*j-
2,1:s).*l(1,1:s)));
       end
   end
   vector = t/2/(3*(n-i)+2)*(F(2*i-2,1:s).*l(1,1:s)-F(2*i-
1,1:s).*l(1,1:s))*(1/3)*t ...
            - t/2/(3*(n-i)+1)*(F(2*i-1,1:s).*l(1,1:s))*(1/3)*t - sum*t;
else
   sum = [];
   for j = 1:i
       if j == 1
          sum = t/2*(1/(3*(n-j)+2)*(-F(2*j-1,1:s).*l(1,1:s)));
       else
          sum = sum + t/2*(1/(3*(n-j)+2)*(F(2*j-2,1:s).*l(1,1:s)-F(2*j-
1,1:s).*l(1,1:s)) ...
                          + 1/(3*(n-(j-1))+1)*(F(2*j-3,1:s).*l(1,1:s)-F(2*j-
2,1:s).*l(1,1:s)));
       end
   end
   vector = t/2/(3*(n-i)+2)*(F(2*i-2,1:s).*l(1,1:s)-F(2*i-
1,1:s).*l(1,1:s))*(1/3)*t ...
            - t/2/(3*(n-i)+1)*(F(2*i-1,1:s).*l(1,1:s)-
F(2*i,1:s).*l(1,1:s))*(1/3)*t - sum*t;
end
```

```
% ---------------------------------------------------------------
%                          int_z_cltsl1.m
%          Calculates integral of sigma_11*z from CLPT
%
%                          Function for
%   Stress Analysis Program for Laminates Under Bending Loads
% ---------------------------------------------------------------

function [value,rz] = int_z_cltsl1(M,n,i,m,MaterialConstants,LayUp,t)

% M = moment, n = number of half plies, i = ply number,
% m = integer distance from mid-point, t = thickness

[s,vecstress,rz] = bcltc2(M,n,-0.5*t,i,MaterialConstants,LayUp,t,'s11');
s = s/rz;
rz = -(n-(2*i-1)/2);
rz = -rz*2;
value = s*(t^3/12-1/4*rz*m*t^3);
```

```
% ---------------------------------------------------------------
%                        int_z_sigma11.m
%    Calculates integral of sigma_11*z from companion problem
%
%                          Function for
%    Stress Analysis Program for Laminates Under Bending Loads
% ---------------------------------------------------------------
```

```
function [vector] = int_z_sigma11(F,l,i,n,m,t)

s = (n*2-1)*3;
if i == 1
   vector = ( -1/(3*(n-i)+2)*(-F(2*i-1,1:s)) + 1/(3*(n-i)+1)*(F(2*i-1,1:s)-
F(2*i,1:s)) )/12*t^2 ...

             + ( 1/(3*(n-i)+2)*(-F(2*i-1,1:s)) + 1/(3*(n-i)+1)*(F(2*i-1,1:s)-
F(2*i,1:s)) )/4*m*t^2;
elseif i == n
   vector = ( -1/(3*(n-i)+2)*(F(2*i-2,1:s)-F(2*i-1,1:s))+1/(3*(n-i)+1)*(F(2*i-
1,1:s)) )/12*t^2 ...
             + ( 1/(3*(n-i)+2)*(F(2*i-2,1:s)-F(2*i-1,1:s))+1/(3*(n-
i)+1)*(F(2*i-1,1:s)) )/4*m*t^2;
else
   vector = ( -1/(3*(n-i)+2)*(F(2*i-2,1:s)-F(2*i-1,1:s))+1/(3*(n-i)+1)*(F(2*i-
1,1:s)-F(2*i,1:s)) )/12*t^2 ...
             + ( 1/(3*(n-i)+2)*(F(2*i-2,1:s)-F(2*i-1,1:s))+1/(3*(n-
i)+1)*(F(2*i-1,1:s)-F(2*i,1:s)) )/4*m*t^2;
end
```

```
% ------------------------------------------------------------------
%                          de.m
%         Calculates the derivative of F(x) = exp(lam*x)
%
%                       Function for
%    Stress Analysis Program for Laminates Under Bending Loads
% ------------------------------------------------------------------

function [vector] = de(eval,evec)

sevec = size(evec,1);
vector = [];

for i = 1:sevec
   vector = [vector; eval.*evec(i,:)];
end
```

```
% ------------------------------------------------------------------
%                           plot_b.m
%                         Plot stresses
%
%                           Script for
%   Stress Analysis Program for Laminates Under Bending Loads
% ------------------------------------------------------------------

flag = 0;
while flag == 0
   % Ouput request
   Orientation = input('>> Choose Orientation of Plot \n>> [1] Along the Length
[2] Along the Thickness \n?? ');
   StressComp = input('\n>> Choose Stress Component to Plot \n>> [1] sig_xx
[2] sig_yy   [3] sig_zz   [4] sig_xz   [5] sig_yz   [6] sig_xy \n?? ');
   if Orientation == 1
      % Output request
      PL = input('\n>> Choose Layer to Plot (bottom layer is layer 1) \n?? ');
```

```
      z = input('\n>> Choose z-location to Plot (local z, -0.5 to 0.5) \n??
')*t*t;
      interval = 500;
      sigma_yz = zeros(interval*2,1);
      sigma_xz = zeros(interval*2,1);
      sigma_xy = zeros(interval*2,1);
      sigma_xx = zeros(interval*2,1);
      sigma_zz = zeros(interval*2,1);
      % Plot stress field across the width(y)
      bplot = 40*t;
      x = [linspace(-bplot,0,interval) linspace(0,bplot,interval)];
      x = x.';
      for i = 1:interval*2
         y = x(i);
         if i <= interval
            region = 1;
                        N = n(region);
            coe = a_A;
            F = zeros(2*n(region)-1,1);
            G = zeros(2*n(region)-1,1);
            dF = zeros(2*n(region)-1,1);
            dG = zeros(2*n(region)-1,1);
            ddF = zeros(2*n(region)-1,1);
            for j = 1:3*(2*n(region)-1)
               F = F + coe(j)*eigvec(1:2*n(region)-
1,j,region)*exp(eigval(1,j,region)*y);
               G = G + coe(j)*eigvec(2*n(region):2*(2*n(region)-
1),j,region)*exp(eigval(1,j,region)*y);
               dF = dF + coe(j)*eigvec(1:2*n(region)-
1,j,region)*exp(eigval(1,j,region)*y)*eigval(1,j,region);
               dG = dG + coe(j)*eigvec(2*n(region):2*(2*n(region)-
1),j,region)*exp(eigval(1,j,region)*y)*eigval(1,j,region);
               ddF = ddF + coe(j)*eigvec(1:2*n(region)-
1,j,region)*exp(eigval(1,j,region)*y)*eigval(1,j,region)^2;
            end
            if PL == 1
               sigma_xx(i) = real( 1/(3*(N-PL)+1)*(F(2*PL-1)-F(2*PL))*(z/t+1/2)
- 1/(3*(N-PL)+2)*(-F(2*PL-1))*(z/t-1/2) ) + bcltc2(M,N,z/t,PL,MC,LUU,t,'s11');
               sigma_xy(i) = real( 1/(3*(N-PL)+1)*(G(2*PL-1)-G(2*PL))*(z/t+1/2)
- 1/(3*(N-PL)+2)*(-G(2*PL-1))*(z/t-1/2) ) + bcltc2(M,N,z/t,PL,MC,LUU,t,'s12');
               sum = 0;
               sumG = 0;
               for j = 1:PL
                  if j == 1
                        sum = sum + 1/(3*(N-j)+2)*(-dF(2*j-1));
                        sumG = sumG + 1/(3*(N-j)+2)*(-dG(2*j-1));
                  else
                        sum = sum + 1/(3*(N-j)+2)*(dF(2*j-2)-dF(2*j-1)) +
1/(3*(N-(j-1))+1)*(dF(2*j-3)-dF(2*j-2));
                        sumG = sumG + 1/(3*(N-j)+2)*(dG(2*j-2)-dG(2*j-1)) +
1/(3*(N-(j-1))+1)*(dG(2*j-3)-dG(2*j-2));
                  end
               end
               sigma_xz(i) = real( -t/(2*(3*(N-PL)+1))*(dF(2*PL-1)-
dF(2*PL))*(z/t+1/2)^2 + t/(2*(3*(N-PL)+2))*(-dF(2*PL-1))*(z/t-1/2)^2 ...
                                    - 1/2*t*sum );
               sigma_yz(i) = real( -t/(2*(3*(N-PL)+1))*(dG(2*PL-1)-
dG(2*PL))*(z/t+1/2)^2 + t/(2*(3*(N-PL)+2))*(-dG(2*PL-1))*(z/t-1/2)^2 ...
                                    - 1/2*t*sumG );
               sum1 = 0;
               sum2 = 0;
               for j = 1:PL
                  if j == 1
```

```
                        sum1 = sum1 + 1/(3*(N-j)+2)*(-ddF(2*j-1));
                    sum2 = sum2 + (1/3 + (PL-j)/2)/(3*(N-j)+2)*(-ddF(2*j-1));
                else
                        sum1 = sum1 + 1/(3*(N-j)+2)*(ddF(2*j-2)-ddF(2*j-1)) +
1/(3*(N-(j-1))+1)*(ddF(2*j-3)-ddF(2*j-2));
                    sum2 = sum2 + (1/3 + (PL-j)/2)/(3*(N-j)+2)*(ddF(2*j-2)-
ddF(2*j-1)) + (2/3 + (PL-j)/2)/(3*(N-(j-1))+1)*(ddF(2*j-3)-ddF(2*j-2));
                end
            end
            sigma_zz(i) = real( t^2/(6*(3*(N-PL)+1))*(ddF(2*PL-1)-
ddF(2*PL))*(z/t+1/2)^3 - t^2/(6*(3*(N-PL)+2))*(-ddF(2*PL-1))*(z/t-1/2)^3 ...
                                + 1/2*t^2*sum1*(z/t-1/2)+t^2*sum2);
        elseif PL == n(region)
            sigma_xx(i) = real( 1/(3*(N-PL)+1)*F(2*PL-1)*(z/t+1/2) -
1/(3*(N-PL)+2)*(F(2*PL-2)-F(2*PL-1))*(z/t-1/2) ) +
bcltc2(M,N,z/t,PL,MC,LUU,t,'s11');
            sigma_xy(i) = real( 1/(3*(N-PL)+1)*G(2*PL-1)*(z/t+1/2) -
1/(3*(N-PL)+2)*(G(2*PL-2)-G(2*PL-1))*(z/t-1/2) ) +
bcltc2(M,N,z/t,PL,MC,LUU,t,'s12');
            sum = 0;
            sumG = 0;
            for j = 1:PL
                if j == 1
                        sum = sum + 1/(3*(N-j)+2)*(-dF(2*j-1));
                        sumG = sumG + 1/(3*(N-j)+2)*(-dG(2*j-1));
                else
                        sum = sum + 1/(3*(N-j)+2)*(dF(2*j-2)-dF(2*j-1)) +
1/(3*(N-(j-1))+1)*(dF(2*j-3)-dF(2*j-2));
                        sumG = sumG + 1/(3*(N-j)+2)*(dG(2*j-2)-dG(2*j-1)) +
1/(3*(N-(j-1))+1)*(dG(2*j-3)-dG(2*j-2));
                end
            end
            sigma_xz(i) = real( -t/(2*(3*(N-PL)+1))*(dF(2*PL-1))*(z/t+1/2)^2
+ t/(2*(3*(N-PL)+2))*(dF(2*PL-2)-dF(2*PL-1))*(z/t-1/2)^2 ...
                                - 1/2*t*sum );
            sigma_yz(i) = real( -t/(2*(3*(N-PL)+1))*(dG(2*PL-1))*(z/t+1/2)^2
+ t/(2*(3*(N-PL)+2))*(dG(2*PL-2)-dG(2*PL-1))*(z/t-1/2)^2 ...
                                - 1/2*t*sumG );
            sum1 = 0;
            sum2 = 0;
            for j = 1:PL
                if j == 1
                        sum1 = sum1 + 1/(3*(N-j)+2)*(-ddF(2*j-1));
                    sum2 = sum2 + (1/3 + (PL-j)/2)/(3*(N-j)+2)*(-ddF(2*j-1));
                else
                        sum1 = sum1 + 1/(3*(N-j)+2)*(ddF(2*j-2)-ddF(2*j-1)) +
1/(3*(N-(j-1))+1)*(ddF(2*j-3)-ddF(2*j-2));
                    sum2 = sum2 + (1/3 + (PL-j)/2)/(3*(N-j)+2)*(ddF(2*j-2)-
ddF(2*j-1)) + (2/3 + (PL-j)/2)/(3*(N-(j-1))+1)*(ddF(2*j-3)-ddF(2*j-2));
                end
            end
            sigma_zz(i) = real( t^2/(6*(3*(N-PL)+1))*(ddF(2*PL-
1))*(z/t+1/2)^3 - t^2/(6*(3*(N-PL)+2))*(ddF(2*PL-2)-ddF(2*PL-1))*(z/t-1/2)^3
...
                                + 1/2*t^2*sum1*(z/t-1/2)+t^2*sum2);
        else
            sigma_xx(i) = real( 1/(3*(N-PL)+1)*(F(2*PL-1)-F(2*PL))*(z/t+1/2)
- 1/(3*(N-PL)+2)*(F(2*PL-2)-F(2*PL-1))*(z/t-1/2) ) +
bcltc2(M,N,z/t,PL,MC,LUU,t,'s11');
            sigma_xy(i) = real( 1/(3*(N-PL)+1)*(G(2*PL-1)-G(2*PL))*(z/t+1/2)
- 1/(3*(N-PL)+2)*(G(2*PL-2)-G(2*PL-1))*(z/t-1/2) ) +
bcltc2(M,N,z/t,PL,MC,LUU,t,'s12');
            sum = 0;
```

```
                sumG = 0;
                for j = 1:PL
                   if j == 1
                          sum = sum + 1/(3*(N-j)+2)*(-dF(2*j-1));
                          sumG = sumG + 1/(3*(N-j)+2)*(-dG(2*j-1));
                   else
                          sum = sum + 1/(3*(N-j)+2)*(dF(2*j-2)-dF(2*j-1)) +
1/(3*(N-(j-1))+1)*(dF(2*j-3)-dF(2*j-2));
                          sumG = sumG + 1/(3*(N-j)+2)*(dG(2*j-2)-dG(2*j-1)) +
1/(3*(N-(j-1))+1)*(dG(2*j-3)-dG(2*j-2));
                   end
                end
                sigma_xz(i) = real( -t/(2*(3*(N-PL)+1))*(dF(2*PL-1)-
dF(2*PL))*(z/t+1/2)^2 + t/(2*(3*(N-PL)+2))*(dF(2*PL-2)-dF(2*PL-1))*(z/t-1/2)^2
...
                                      - 1/2*t*sum );
                sigma_yz(i) = real( -t/(2*(3*(N-PL)+1))*(dG(2*PL-1)-
dG(2*PL))*(z/t+1/2)^2 + t/(2*(3*(N-PL)+2))*(dG(2*PL-2)-dG(2*PL-1))*(z/t-1/2)^2
...
                                      - 1/2*t*sumG );
                sum1 = 0;
                sum2 = 0;
                for j = 1:PL
                   if j == 1
                          sum1 = sum1 + 1/(3*(N-j)+2)*(-ddF(2*j-1));
                      sum2 = sum2 + (1/3 + (PL-j)/2)/(3*(N-j)+2)*(-ddF(2*j-1));
                   else
                          sum1 = sum1 + 1/(3*(N-j)+2)*(ddF(2*j-2)-ddF(2*j-1)) +
1/(3*(N-(j-1))+1)*(ddF(2*j-3)-ddF(2*j-2));
                      sum2 = sum2 + (1/3 + (PL-j)/2)/(3*(N-j)+2)*(ddF(2*j-2)-
ddF(2*j-1)) + (2/3 + (PL-j)/2)/(3*(N-(j-1))+1)*(ddF(2*j-3)-ddF(2*j-2));
                   end
                end
                sigma_zz(i) = real( t^2/(6*(3*(N-PL)+1))*(ddF(2*PL-1)-
ddF(2*PL))*(z/t+1/2)^3 - t^2/(6*(3*(N-PL)+2))*(ddF(2*PL-2)-ddF(2*PL-1))*(z/t-
1/2)^3 ...
                                      + 1/2*t^2*sum1*(z/t-1/2)+t^2*sum2);
             end
          else
             region = 2;
             N = n(region);
             coe = a_B;
             F = zeros(2*n(region)-1,1);
             G = zeros(2*n(region)-1,1);
             dF = zeros(2*n(region)-1,1);
             dG = zeros(2*n(region)-1,1);
             ddF = zeros(2*n(region)-1,1);
             RealPL = 0;
             for j = 1:PL
                if TestDropPly(j) ~= 1
                   RealPL = RealPL + 1;
                end
             end
             if (n(region)-1) == 0
                F = 0;
                G = 0;
                dF = 0;
                dG = 0;
                ddF = 0;
             end
             if TestDropPly(PL) ~= 1
                for j = 1:3*(2*n(region)-1)
```

```
                F = F + coe(j)*eigvec(1:2*n(region)-
1,j,region)*exp(eigval(1,j,region)*y);
                G = G + coe(j)*eigvec(2*n(region):2*(2*n(region)-
1),j,region)*exp(eigval(1,j,region)*y);
                dF = dF + coe(j)*eigvec(1:2*n(region)-
1,j,region)*exp(eigval(1,j,region)*y)*eigval(1,j,region);
                dG = dG + coe(j)*eigvec(2*n(region):2*(2*n(region)-
1),j,region)*exp(eigval(1,j,region)*y)*eigval(1,j,region);
                ddF = ddF + coe(j)*eigvec(1:2*n(region)-
1,j,region)*exp(eigval(1,j,region)*y)*eigval(1,j,region)^2;
             end
             if RealPL == 1
                sigma_xx(i) = real( 1/(3*(N-RealPL)+1)*(F(2*RealPL-1)-
F(2*RealPL))*(z/t+1/2) - 1/(3*(N-RealPL)+2)*(-F(2*RealPL-1))*(z/t-1/2) ) +
bcltc2(M,N,z/t,RealPL,MC,LUD,t,'s11');
                sigma_xy(i) = real( 1/(3*(N-RealPL)+1)*(G(2*RealPL-1)-
G(2*RealPL))*(z/t+1/2) - 1/(3*(N-RealPL)+2)*(-G(2*RealPL-1))*(z/t-1/2) ) +
bcltc2(M,N,z/t,RealPL,MC,LUD,t,'s12');
                sa_yy(i) = real(-F(RealPL)/t);
                sum = 0;
                sumG = 0;
                for j = 1:RealPL
                   if j == 1
                          sum = sum + 1/(3*(N-j)+2)*(-dF(2*j-1));
                          sumG = sumG + 1/(3*(N-j)+2)*(-dG(2*j-1));
                   else
                          sum = sum + 1/(3*(N-j)+2)*(dF(2*j-2)-dF(2*j-1)) +
1/(3*(N-(j-1))+1)*(dF(2*j-3)-dF(2*j-2));
                          sumG = sumG + 1/(3*(N-j)+2)*(dG(2*j-2)-dG(2*j-1)) +
1/(3*(N-(j-1))+1)*(dG(2*j-3)-dG(2*j-2));
                   end
                end
                sigma_xz(i) = real( -t/(2*(3*(N-RealPL)+1))*(dF(2*RealPL-1)-
dF(2*RealPL))*(z/t+1/2)^2 + t/(2*(3*(N-RealPL)+2))*(-dF(2*RealPL-1))*(z/t-
1/2)^2 ...
                                          - 1/2*t*sum );
                sigma_yz(i) = real( -t/(2*(3*(N-RealPL)+1))*(dG(2*RealPL-1)-
dG(2*RealPL))*(z/t+1/2)^2 + t/(2*(3*(N-RealPL)+2))*(-dG(2*RealPL-1))*(z/t-
1/2)^2 ...
                                          - 1/2*t*sumG );
                sum1 = 0;
                sum2 = 0;
                for j = 1:RealPL
                   if j == 1
                          sum1 = sum1 + 1/(3*(N-j)+2)*(-ddF(2*j-1));
                      sum2 = sum2 + (1/3 + (RealPL-j)/2)/(3*(N-j)+2)*(-
ddF(2*j-1));
                   else
                          sum1 = sum1 + 1/(3*(N-j)+2)*(ddF(2*j-2)-ddF(2*j-1))
+ 1/(3*(N-(j-1))+1)*(ddF(2*j-3)-ddF(2*j-2));
                       sum2 = sum2 + (1/3 + (RealPL-j)/2)/(3*(N-
j)+2)*(ddF(2*j-2)-ddF(2*j-1)) + (2/3 + (RealPL-j)/2)/(3*(N-(j-1))+1)*(ddF(2*j-
3)-ddF(2*j-2));
                   end
                end
                sigma_zz(i) = real( t^2/(6*(3*(N-RealPL)+1))*(ddF(2*RealPL-
1)-ddF(2*RealPL))*(z/t+1/2)^3 - t^2/(6*(3*(N-RealPL)+2))*(-ddF(2*RealPL-
1))*(z/t-1/2)^3 ...
                                          + 1/2*t^2*sum1*(z/t-1/2)+t^2*sum2);
             elseif RealPL == n(region)
                sigma_xx(i) = real( 1/(3*(N-RealPL)+1)*F(2*RealPL-
1)*(z/t+1/2) - 1/(3*(N-RealPL)+2)*(F(2*RealPL-2)-F(2*RealPL-1))*(z/t-1/2) ) +
bcltc2(M,N,z/t,RealPL,MC,LUD,t,'s11');
```

```
                sigma_xy(i) = real( 1/(3*(N-RealPL)+1)*G(2*RealPL-
1)*(z/t+1/2) - 1/(3*(N-RealPL)+2)*(G(2*RealPL-2)-G(2*RealPL-1))*(z/t-1/2) ) +
bcltc2(M,N,z/t,RealPL,MC,LUD,t,'s12');
                sa_yy(i) = real(F(RealPL-1)/t);
                sum = 0;
                sumG = 0;
                for j = 1:RealPL
                   if j == 1
                          sum = sum + 1/(3*(N-j)+2)*(-dF(2*j-1));
                          sumG = sumG + 1/(3*(N-j)+2)*(-dG(2*j-1));
                   else
                          sum = sum + 1/(3*(N-j)+2)*(dF(2*j-2)-dF(2*j-1)) +
1/(3*(N-(j-1))+1)*(dF(2*j-3)-dF(2*j-2));
                          sumG = sumG + 1/(3*(N-j)+2)*(dG(2*j-2)-dG(2*j-1)) +
1/(3*(N-(j-1))+1)*(dG(2*j-3)-dG(2*j-2));
                   end
                end
                sigma_xz(i) = real( -t/(2*(3*(N-RealPL)+1))*(dF(2*RealPL-
1))*(z/t+1/2)^2 + t/(2*(3*(N-RealPL)+2))*(dF(2*RealPL-2)-dF(2*RealPL-1))*(z/t-
1/2)^2 ...
                                        - 1/2*t*sum );
                sigma_yz(i) = real( -t/(2*(3*(N-RealPL)+1))*(dG(2*RealPL-
1))*(z/t+1/2)^2 + t/(2*(3*(N-RealPL)+2))*(dG(2*RealPL-2)-dG(2*RealPL-1))*(z/t-
1/2)^2 ...
                                        - 1/2*t*sumG );
                sum1 = 0;
                sum2 = 0;
                for j = 1:RealPL
                   if j == 1
                          sum1 = sum1 + 1/(3*(N-j)+2)*(-ddF(2*j-1));
                      sum2 = sum2 + (1/3 + (RealPL-j)/2)/(3*(N-j)+2)*(-
ddF(2*j-1));
                   else
                       sum1 = sum1 + 1/(3*(N-j)+2)*(ddF(2*j-2)-ddF(2*j-1)) +
1/(3*(N-(j-1))+1)*(ddF(2*j-3)-ddF(2*j-2));
                      sum2 = sum2 + (1/3 + (RealPL-j)/2)/(3*(N-
j)+2)*(ddF(2*j-2)-ddF(2*j-1)) + (2/3 + (RealPL-j)/2)/(3*(N-(j-1))+1)*(ddF(2*j-
3)-ddF(2*j-2));
                   end
                end
                sigma_zz(i) = real( t^2/(6*(3*(N-RealPL)+1))*(ddF(2*RealPL-
1))*(z/t+1/2)^3 - t^2/(6*(3*(N-RealPL)+2))*(ddF(2*RealPL-2)-ddF(2*RealPL-
1))*(z/t-1/2)^3 ...
                                        + 1/2*t^2*sum1*(z/t-1/2)+t^2*sum2);
             else
                sigma_xx(i) = real( 1/(3*(N-RealPL)+1)*(F(2*RealPL-1)-
F(2*RealPL))*(z/t+1/2) - 1/(3*(N-RealPL)+2)*(F(2*RealPL-2)-F(2*RealPL-1))*(z/t-
1/2) ) + bcltc2(M,N,z/t,RealPL,MC,LUD,t,'s11');
                sigma_xy(i) = real( 1/(3*(N-RealPL)+1)*(G(2*RealPL-1)-
G(2*RealPL))*(z/t+1/2) - 1/(3*(N-RealPL)+2)*(G(2*RealPL-2)-G(2*RealPL-1))*(z/t-
1/2) ) + bcltc2(M,N,z/t,RealPL,MC,LUD,t,'s12');
                sa_yy(i) = real((F(RealPL-1)-F(RealPL))/t);
                sum = 0;
                sumG = 0;
                for j = 1:RealPL
                   if j == 1
                          sum = sum + 1/(3*(N-j)+2)*(-dF(2*j-1));
                          sumG = sumG + 1/(3*(N-j)+2)*(-dG(2*j-1));
                   else
                          sum = sum + 1/(3*(N-j)+2)*(dF(2*j-2)-dF(2*j-1)) +
1/(3*(N-(j-1))+1)*(dF(2*j-3)-dF(2*j-2));
                          sumG = sumG + 1/(3*(N-j)+2)*(dG(2*j-2)-dG(2*j-1)) +
1/(3*(N-(j-1))+1)*(dG(2*j-3)-dG(2*j-2));
```

```
                    end
                end
                sigma_xz(i) = real( -t/(2*(3*(N-RealPL)+1))*(dF(2*RealPL-1)-
dF(2*RealPL))*(z/t+1/2)^2 + t/(2*(3*(N-RealPL)+2))*(dF(2*RealPL-2)-dF(2*RealPL-
1))*(z/t-1/2)^2 ...
                                        - 1/2*t*sum );
                sigma_yz(i) = real( -t/(2*(3*(N-RealPL)+1))*(dG(2*RealPL-1)-
dG(2*RealPL))*(z/t+1/2)^2 + t/(2*(3*(N-RealPL)+2))*(dG(2*RealPL-2)-dG(2*RealPL-
1))*(z/t-1/2)^2 ...
                                        - 1/2*t*sumG );
                sum1 = 0;
                sum2 = 0;
                for j = 1:RealPL
                    if j == 1
                            sum1 = sum1 + 1/(3*(N-j)+2)*(-ddF(2*j-1));
                        sum2 = sum2 + (1/3 + (RealPL-j)/2)/(3*(N-j)+2)*(-
ddF(2*j-1));
                    else
                            sum1 = sum1 + 1/(3*(N-j)+2)*(ddF(2*j-2)-ddF(2*j-1))
+ 1/(3*(N-(j-1))+1)*(ddF(2*j-3)-ddF(2*j-2));
                        sum2 = sum2 + (1/3 + (RealPL-j)/2)/(3*(N-
j)+2)*(ddF(2*j-2)-ddF(2*j-1)) + (2/3 + (RealPL-j)/2)/(3*(N-(j-1))+1)*(ddF(2*j-
3)-ddF(2*j-2));
                    end
                end
                sigma_zz(i) = real( t^2/(6*(3*(N-RealPL)+1))*(ddF(2*RealPL-
1)-ddF(2*RealPL))*(z/t+1/2)^3 - t^2/(6*(3*(N-RealPL)+2))*(ddF(2*RealPL-2)-
ddF(2*RealPL-1))*(z/t-1/2)^3 ...
                                        + 1/2*t^2*sum1*(z/t-1/2)+t^2*sum2);
            end
        end
    end
end
figure(1)
if StressComp == 1 | StressComp == 2 | StressComp == 6
    figure(1)

plot(x(1:interval),sigma_xx(1:interval),x(1:interval),sigma_xy(1:interval),':')
; hold on

plot(x(interval+1:interval*2),sigma_xx(interval+1:interval*2),x(interval+1:inte
rval*2),sigma_xy(interval+1:interval*2),':');
    %legend('\sigma_x_x','\sigma_x_y');
    xlabel('Length');
    ylabel('Stress');
    title1 = ['In-plane Stress, Layer: ' num2str(PL) ', Local z: '
num2str(z)];
    title(title1);
    grid on
    hold off
else
    figure(1)

plot(x(1:interval),sigma_xz(1:interval),x(1:interval),sigma_yz(1:interval),':',
x(1:interval),sigma_zz(1:interval),'--');hold on

plot(x(interval+1:interval*2),sigma_xz(interval+1:interval*2),x(interval+1:inte
rval*2),sigma_yz(interval+1:interval*2),':',x(interval+1:interval*2),sigma_zz(i
nterval+1:interval*2),'--');
    %legend('\sigma_x_z','\sigma_y_z','\sigma_z_z');
    xlabel('Length');
    ylabel('Stress');
```

```
         title2 = ['Interlaminar Stress, Layer: ' num2str(PL) ', Local z: '
num2str(z)];
         title(title2);
         grid on
         hold off
      end
   elseif Orientation == 2
      region = 1;
      N = n(region);
            sigma_yz_zA = zeros(1,20*N);
            sigma_xz_zA = sigma_yz_zA;
            sigma_xy_zA = sigma_yz_zA;
            sigma_xx_zA = sigma_yz_zA;
            sigma_zz_zA = sigma_yz_zA;
         y = input('\n>> Choose a Positive Lengthwise Location to Plot (default
y=0) \n?? ')*(-1);
         if isempty(y) y = 0; end
         coe = a_A;
         F = zeros(2*n(region)-1,1);
         G = zeros(2*n(region)-1,1);
         dF = zeros(2*n(region)-1,1);
         dG = zeros(2*n(region)-1,1);
         ddF = zeros(2*n(region)-1,1);
         for j = 1:3*(2*n(region)-1)
            F = F + coe(j)*eigvec(1:2*n(region)-
1,j,region)*exp(eigval(1,j,region)*y);
            G = G + coe(j)*eigvec(2*n(region):2*(2*n(region)-
1),j,region)*exp(eigval(1,j,region)*y);
            dF = dF + coe(j)*eigvec(1:2*n(region)-
1,j,region)*exp(eigval(1,j,region)*y)*eigval(1,j,region);
            dG = dG + coe(j)*eigvec(2*n(region):2*(2*n(region)-
1),j,region)*exp(eigval(1,j,region)*y)*eigval(1,j,region);
            ddF = ddF + coe(j)*eigvec(1:2*n(region)-
1,j,region)*exp(eigval(1,j,region)*y)*eigval(1,j,region)^2;
         end
         Plotz = [];
         PLall = [];
         for j = 1:N
             Plotz = [Plotz linspace(-(N-j+1),-(N-j),20)];
             PLall = [PLall j*ones(1,20)];
         end

         for i = 1:20*N
            PL = PLall(i);
            z = Plotz(i) + (N-(2*PL-1)/2)*t;
            if PL == 1
               sigma_xx_zA(i) = real( 1/(3*(N-PL)+1)*(F(2*PL-1)-
F(2*PL))*(z/t+1/2) - 1/(3*(N-PL)+2)*(-F(2*PL-1))*(z/t-1/2) ) +
bcltc2(M,N,z/t,PL,MC,LUU,t,'s11');
               sigma_xy_zA(i) = real( 1/(3*(N-PL)+1)*(G(2*PL-1)-
G(2*PL))*(z/t+1/2) - 1/(3*(N-PL)+2)*(-G(2*PL-1))*(z/t-1/2) ) +
bcltc2(M,N,z/t,PL,MC,LUU,t,'s12');
               sum = 0;
               sumG = 0;
               for j = 1:PL
                  if j == 1
                        sum = sum + 1/(3*(N-j)+2)*(-dF(2*j-1));
                        sumG = sumG + 1/(3*(N-j)+2)*(-dG(2*j-1));
                  else
                        sum = sum + 1/(3*(N-j)+2)*(dF(2*j-2)-dF(2*j-1)) +
1/(3*(N-(j-1))+1)*(dF(2*j-3)-dF(2*j-2));
                        sumG = sumG + 1/(3*(N-j)+2)*(dG(2*j-2)-dG(2*j-1)) +
1/(3*(N-(j-1))+1)*(dG(2*j-3)-dG(2*j-2));
```

```
                end
            end
            sigma_xz_zA(i) = real( -t/(2*(3*(N-PL)+1))*(dF(2*PL-1)-
dF(2*PL))*(z/t+1/2)^2 + t/(2*(3*(N-PL)+2))*(-dF(2*PL-1))*(z/t-1/2)^2 ...
                                    - 1/2*t*sum );
            sigma_yz_zA(i) = real( -t/(2*(3*(N-PL)+1))*(dG(2*PL-1)-
dG(2*PL))*(z/t+1/2)^2 + t/(2*(3*(N-PL)+2))*(-dG(2*PL-1))*(z/t-1/2)^2 ...
                                    - 1/2*t*sumG );
            sum1 = 0;
            sum2 = 0;
            for j = 1:PL
               if j == 1
                     sum1 = sum1 + 1/(3*(N-j)+2)*(-ddF(2*j-1));
                  sum2 = sum2 + (1/3 + (PL-j)/2)/(3*(N-j)+2)*(-ddF(2*j-1));
               else
                     sum1 = sum1 + 1/(3*(N-j)+2)*(ddF(2*j-2)-ddF(2*j-1)) +
1/(3*(N-(j-1))+1)*(ddF(2*j-3)-ddF(2*j-2));
                  sum2 = sum2 + (1/3 + (PL-j)/2)/(3*(N-j)+2)*(ddF(2*j-2)-
ddF(2*j-1)) + (2/3 + (PL-j)/2)/(3*(N-(j-1))+1)*(ddF(2*j-3)-ddF(2*j-2));
               end
            end
            sigma_zz_zA(i) = real( t^2/(6*(3*(N-PL)+1))*(ddF(2*PL-1)-
ddF(2*PL))*(z/t+1/2)^3 - t^2/(6*(3*(N-PL)+2))*(-ddF(2*PL-1))*(z/t-1/2)^3 ...
                                    + 1/2*t^2*sum1*(z/t-1/2)+t^2*sum2);
         elseif PL == n(region)
            sigma_xx_zA(i) = real( 1/(3*(N-PL)+1)*F(2*PL-1)*(z/t+1/2) -
1/(3*(N-PL)+2)*(F(2*PL-2)-F(2*PL-1))*(z/t-1/2) ) +
bcltc2(M,N,z/t,PL,MC,LUU,t,'s11');
            sigma_xy_zA(i) = real( 1/(3*(N-PL)+1)*G(2*PL-1)*(z/t+1/2) -
1/(3*(N-PL)+2)*(G(2*PL-2)-G(2*PL-1))*(z/t-1/2) ) +
bcltc2(M,N,z/t,PL,MC,LUU,t,'s12');
            sum = 0;
            sumG = 0;
            for j = 1:PL
               if j == 1
                     sum = sum + 1/(3*(N-j)+2)*(-dF(2*j-1));
                     sumG = sumG + 1/(3*(N-j)+2)*(-dG(2*j-1));
               else
                     sum = sum + 1/(3*(N-j)+2)*(dF(2*j-2)-dF(2*j-1)) +
1/(3*(N-(j-1))+1)*(dF(2*j-3)-dF(2*j-2));
                     sumG = sumG + 1/(3*(N-j)+2)*(dG(2*j-2)-dG(2*j-1)) +
1/(3*(N-(j-1))+1)*(dG(2*j-3)-dG(2*j-2));
               end
            end
            sigma_xz_zA(i) = real( -t/(2*(3*(N-PL)+1))*(dF(2*PL-
1))*(z/t+1/2)^2 + t/(2*(3*(N-PL)+2))*(dF(2*PL-2)-dF(2*PL-1))*(z/t-1/2)^2 ...
                                    - 1/2*t*sum );
            sigma_yz_zA(i) = real( -t/(2*(3*(N-PL)+1))*(dG(2*PL-
1))*(z/t+1/2)^2 + t/(2*(3*(N-PL)+2))*(dG(2*PL-2)-dG(2*PL-1))*(z/t-1/2)^2 ...
                                    - 1/2*t*sumG );
            sum1 = 0;
            sum2 = 0;
            for j = 1:PL
               if j == 1
                     sum1 = sum1 + 1/(3*(N-j)+2)*(-ddF(2*j-1));
                  sum2 = sum2 + (1/3 + (PL-j)/2)/(3*(N-j)+2)*(-ddF(2*j-1));
               else
                     sum1 = sum1 + 1/(3*(N-j)+2)*(ddF(2*j-2)-ddF(2*j-1)) +
1/(3*(N-(j-1))+1)*(ddF(2*j-3)-ddF(2*j-2));
                  sum2 = sum2 + (1/3 + (PL-j)/2)/(3*(N-j)+2)*(ddF(2*j-2)-
ddF(2*j-1)) + (2/3 + (PL-j)/2)/(3*(N-(j-1))+1)*(ddF(2*j-3)-ddF(2*j-2));
               end
            end
```

```
                sigma_zz_zA(i) = real( t^2/(6*(3*(N-PL)+1))*(ddF(2*PL-
1))*(z/t+1/2)^3 - t^2/(6*(3*(N-PL)+2))*(ddF(2*PL-2)-ddF(2*PL-1))*(z/t-1/2)^3
...
                                        + 1/2*t^2*sum1*(z/t-1/2)+t^2*sum2);
            else
                sigma_xx_zA(i) = real( 1/(3*(N-PL)+1)*(F(2*PL-1)-
F(2*PL))*(z/t+1/2) - 1/(3*(N-PL)+2)*(F(2*PL-2)-F(2*PL-1))*(z/t-1/2) ) +
bcltc2(M,N,z/t,PL,MC,LUU,t,'s11');
                sigma_xy_zA(i) = real( 1/(3*(N-PL)+1)*(G(2*PL-1)-
G(2*PL))*(z/t+1/2) - 1/(3*(N-PL)+2)*(G(2*PL-2)-G(2*PL-1))*(z/t-1/2) ) +
bcltc2(M,N,z/t,PL,MC,LUU,t,'s12');
                sum = 0;
                sumG = 0;
                for j = 1:PL
                   if j == 1
                          sum = sum + 1/(3*(N-j)+2)*(-dF(2*j-1));
                          sumG = sumG + 1/(3*(N-j)+2)*(-dG(2*j-1));
                   else
                          sum = sum + 1/(3*(N-j)+2)*(dF(2*j-2)-dF(2*j-1)) +
1/(3*(N-(j-1))+1)*(dF(2*j-3)-dF(2*j-2));
                          sumG = sumG + 1/(3*(N-j)+2)*(dG(2*j-2)-dG(2*j-1)) +
1/(3*(N-(j-1))+1)*(dG(2*j-3)-dG(2*j-2));
                   end
                end
                sigma_xz_zA(i) = real( -t/(2*(3*(N-PL)+1))*(dF(2*PL-1)-
dF(2*PL))*(z/t+1/2)^2 + t/(2*(3*(N-PL)+2))*(dF(2*PL-2)-dF(2*PL-1))*(z/t-1/2)^2
...
                                        - 1/2*t*sum );
                sigma_yz_zA(i) = real( -t/(2*(3*(N-PL)+1))*(dG(2*PL-1)-
dG(2*PL))*(z/t+1/2)^2 + t/(2*(3*(N-PL)+2))*(dG(2*PL-2)-dG(2*PL-1))*(z/t-1/2)^2
...
                                        - 1/2*t*sumG );
                sum1 = 0;
                sum2 = 0;
                for j = 1:PL
                   if j == 1
                          sum1 = sum1 + 1/(3*(N-j)+2)*(-ddF(2*j-1));
                      sum2 = sum2 + (1/3 + (PL-j)/2)/(3*(N-j)+2)*(-ddF(2*j-1));
                   else
                          sum1 = sum1 + 1/(3*(N-j)+2)*(ddF(2*j-2)-ddF(2*j-1)) +
1/(3*(N-(j-1))+1)*(ddF(2*j-3)-ddF(2*j-2));
                      sum2 = sum2 + (1/3 + (PL-j)/2)/(3*(N-j)+2)*(ddF(2*j-2)-
ddF(2*j-1)) + (2/3 + (PL-j)/2)/(3*(N-(j-1))+1)*(ddF(2*j-3)-ddF(2*j-2));
                   end
                end
                sigma_zz_zA(i) = real( t^2/(6*(3*(N-PL)+1))*(ddF(2*PL-1)-
ddF(2*PL))*(z/t+1/2)^3 - t^2/(6*(3*(N-PL)+2))*(ddF(2*PL-2)-ddF(2*PL-1))*(z/t-
1/2)^3 ...
                                        + 1/2*t^2*sum1*(z/t-1/2)+t^2*sum2);
            end
         end
   if StressComp == 1
      figure(2)
      subplot(1,2,1); plot(sigma_xx_zA,Plotz);
      xlabel('\sigma_x_x');
      ylabel('z');
      title1 = ['In-plane Stress at x = 0 in Undropped Region'];
      title(title1);
      %axis([0 2500 -n(1)*t 0])
      grid on
   elseif StressComp == 4
      figure(2)
      subplot(1,2,1); plot(sigma_xz_zA,Plotz);
```

```
      xlabel('\sigma_x_z');
      ylabel('z');
      title1 = ['Shear Stress at x = 0 in Undropped Region'];
      title(title1);
      %axis tight
      grid on
   elseif StressComp == 3
      figure(2)
      subplot(1,2,1); plot(sigma_zz_zA,Plotz);
      xlabel('\sigma_z_z');
      ylabel('z');
      title1 = ['Normal Stress at x = 0 in Undropped Region'];
      title(title1);
      %axis tight
      grid on
   elseif StressComp == 6
      figure(2)
      subplot(1,2,1); plot(sigma_xy_zA,Plotz);
      xlabel('\sigma_x_y');
      ylabel('z');
      title1 = ['In-plane Stress at x = 0 in Undropped Region'];
      title(title1);
      %axis tight
      grid on
   elseif StressComp == 5
      figure(2)
      subplot(1,2,1); plot(sigma_yz_zA,Plotz);
      xlabel('\sigma_y_z');
      ylabel('z');
      title1 = ['Shear Stress at x = 0 in Undropped Region'];
      title(title1);
      %axis tight
      grid on
   end % if StressComp == 1

         region = 2;
         y = -y;
                N = n(region);
         sigma_yz_zB = zeros(1,20*N);
         sigma_xz_zB = sigma_yz_zB;
         sigma_xy_zB = sigma_yz_zB;
         sigma_xx_zB = sigma_yz_zB;
         sigma_zz_zB = sigma_yz_zB;
         coe = a_B;
         F = zeros(2*n(region)-1,1);
         G = zeros(2*n(region)-1,1);
         dF = zeros(2*n(region)-1,1);
         dG = zeros(2*n(region)-1,1);
         ddF = zeros(2*n(region)-1,1);
         for j = 1:3*(2*n(region)-1)
            F = F + coe(j)*eigvec(1:2*n(region)-
1,j,region)*exp(eigval(1,j,region)*y);
            G = G + coe(j)*eigvec(2*n(region):2*(2*n(region)-
1),j,region)*exp(eigval(1,j,region)*y);
            dF = dF + coe(j)*eigvec(1:2*n(region)-
1,j,region)*exp(eigval(1,j,region)*y)*eigval(1,j,region);
            dG = dG + coe(j)*eigvec(2*n(region):2*(2*n(region)-
1),j,region)*exp(eigval(1,j,region)*y)*eigval(1,j,region);
            ddF = ddF + coe(j)*eigvec(1:2*n(region)-
1,j,region)*exp(eigval(1,j,region)*y)*eigval(1,j,region)^2;
         end
         Plotz = [];
         PLall = [];
```

```
        for j = 1:N
            Plotz = [Plotz linspace(-(N-j+1),-(N-j),20)];
            PLall = [PLall j*ones(1,20)];
        end
        for i = 1:20*N
           PL = PLall(i);
           z = Plotz(i) + (N-(2*PL-1)/2)*t;
           if PL == 1
              sigma_xx_zB(i) = real( 1/(3*(N-PL)+1)*(F(2*PL-1)-
F(2*PL))*(z/t+1/2) - 1/(3*(N-PL)+2)*(-F(2*PL-1))*(z/t-1/2) ) +
bcltc2(M,N,z/t,PL,MC,LUD,t,'s11');
              sigma_xy_zB(i) = real( 1/(3*(N-PL)+1)*(G(2*PL-1)-
G(2*PL))*(z/t+1/2) - 1/(3*(N-PL)+2)*(-G(2*PL-1))*(z/t-1/2) ) +
bcltc2(M,N,z/t,PL,MC,LUD,t,'s12');
              sum = 0;
              sumG = 0;
              for j = 1:PL
                 if j == 1
                        sum = sum + 1/(3*(N-j)+2)*(-dF(2*j-1));
                        sumG = sumG + 1/(3*(N-j)+2)*(-dG(2*j-1));
                 else
                        sum = sum + 1/(3*(N-j)+2)*(dF(2*j-2)-dF(2*j-1)) +
1/(3*(N-(j-1))+1)*(dF(2*j-3)-dF(2*j-2));
                        sumG = sumG + 1/(3*(N-j)+2)*(dG(2*j-2)-dG(2*j-1)) +
1/(3*(N-(j-1))+1)*(dG(2*j-3)-dG(2*j-2));
                 end
              end
              sigma_xz_zB(i) = real( -t/(2*(3*(N-PL)+1))*(dF(2*PL-1)-
dF(2*PL))*(z/t+1/2)^2 + t/(2*(3*(N-PL)+2))*(-dF(2*PL-1))*(z/t-1/2)^2 ...
                                    - 1/2*t*sum );
              sigma_yz_zB(i) = real( -t/(2*(3*(N-PL)+1))*(dG(2*PL-1)-
dG(2*PL))*(z/t+1/2)^2 + t/(2*(3*(N-PL)+2))*(-dG(2*PL-1))*(z/t-1/2)^2 ...
                                    - 1/2*t*sumG );
              sum1 = 0;
              sum2 = 0;
              for j = 1:PL
                 if j == 1
                        sum1 = sum1 + 1/(3*(N-j)+2)*(-ddF(2*j-1));
                     sum2 = sum2 + (1/3 + (PL-j)/2)/(3*(N-j)+2)*(-ddF(2*j-1));
                 else
                        sum1 = sum1 + 1/(3*(N-j)+2)*(ddF(2*j-2)-ddF(2*j-1)) +
1/(3*(N-(j-1))+1)*(ddF(2*j-3)-ddF(2*j-2));
                     sum2 = sum2 + (1/3 + (PL-j)/2)/(3*(N-j)+2)*(ddF(2*j-2)-
ddF(2*j-1)) + (2/3 + (PL-j)/2)/(3*(N-(j-1))+1)*(ddF(2*j-3)-ddF(2*j-2));
                 end
              end
              sigma_zz_zB(i) = real( t^2/(6*(3*(N-PL)+1))*(ddF(2*PL-1)-
ddF(2*PL))*(z/t+1/2)^3 - t^2/(6*(3*(N-PL)+2))*(-ddF(2*PL-1))*(z/t-1/2)^3 ...
                                    + 1/2*t^2*sum1*(z/t-1/2)+t^2*sum2);
           elseif PL == n(region)
              sigma_xx_zB(i) = real( 1/(3*(N-PL)+1)*F(2*PL-1)*(z/t+1/2) -
1/(3*(N-PL)+2)*(F(2*PL-2)-F(2*PL-1))*(z/t-1/2) ) +
bcltc2(M,N,z/t,PL,MC,LUD,t,'s11');
              sigma_xy_zB(i) = real( 1/(3*(N-PL)+1)*G(2*PL-1)*(z/t+1/2) -
1/(3*(N-PL)+2)*(G(2*PL-2)-G(2*PL-1))*(z/t-1/2) ) +
bcltc2(M,N,z/t,PL,MC,LUD,t,'s12');
              sum = 0;
              sumG = 0;
              for j = 1:PL
                 if j == 1
                        sum = sum + 1/(3*(N-j)+2)*(-dF(2*j-1));
                        sumG = sumG + 1/(3*(N-j)+2)*(-dG(2*j-1));
                 else
```

```
                        sum = sum + 1/(3*(N-j)+2)*(dF(2*j-2)-dF(2*j-1)) +
1/(3*(N-(j-1))+1)*(dF(2*j-3)-dF(2*j-2));
                        sumG = sumG + 1/(3*(N-j)+2)*(dG(2*j-2)-dG(2*j-1)) +
1/(3*(N-(j-1))+1)*(dG(2*j-3)-dG(2*j-2));
                    end
                end
                sigma_xz_zB(i) = real( -t/(2*(3*(N-PL)+1))*(dF(2*PL-
1))*(z/t+1/2)^2 + t/(2*(3*(N-PL)+2))*(dF(2*PL-2)-dF(2*PL-1))*(z/t-1/2)^2 ...
                                    - 1/2*t*sum );
                sigma_yz_zB(i) = real( -t/(2*(3*(N-PL)+1))*(dG(2*PL-
1))*(z/t+1/2)^2 + t/(2*(3*(N-PL)+2))*(dG(2*PL-2)-dG(2*PL-1))*(z/t-1/2)^2 ...
                                    - 1/2*t*sumG );
                sum1 = 0;
                sum2 = 0;
                for j = 1:PL
                   if j == 1
                           sum1 = sum1 + 1/(3*(N-j)+2)*(-ddF(2*j-1));
                      sum2 = sum2 + (1/3 + (PL-j)/2)/(3*(N-j)+2)*(-ddF(2*j-1));
                   else
                           sum1 = sum1 + 1/(3*(N-j)+2)*(ddF(2*j-2)-ddF(2*j-1)) +
1/(3*(N-(j-1))+1)*(ddF(2*j-3)-ddF(2*j-2));
                      sum2 = sum2 + (1/3 + (PL-j)/2)/(3*(N-j)+2)*(ddF(2*j-2)-
ddF(2*j-1)) + (2/3 + (PL-j)/2)/(3*(N-(j-1))+1)*(ddF(2*j-3)-ddF(2*j-2));
                   end
                end
                sigma_zz_zB(i) = real( t^2/(6*(3*(N-PL)+1))*(ddF(2*PL-
1))*(z/t+1/2)^3 - t^2/(6*(3*(N-PL)+2))*(ddF(2*PL-2)-ddF(2*PL-1))*(z/t-1/2)^3
...
                                    + 1/2*t^2*sum1*(z/t-1/2)+t^2*sum2);
             else
                sigma_xx_zB(i) = real( 1/(3*(N-PL)+1)*(F(2*PL-1)-
F(2*PL))*(z/t+1/2) - 1/(3*(N-PL)+2)*(F(2*PL-2)-F(2*PL-1))*(z/t-1/2) ) +
bcltc2(M,N,z/t,PL,MC,LUD,t,'s11');
                sigma_xy_zB(i) = real( 1/(3*(N-PL)+1)*(G(2*PL-1)-
G(2*PL))*(z/t+1/2) - 1/(3*(N-PL)+2)*(G(2*PL-2)-G(2*PL-1))*(z/t-1/2) ) +
bcltc2(M,N,z/t,PL,MC,LUD,t,'s12');
                sum = 0;
                sumG = 0;
                for j = 1:PL
                   if j == 1
                           sum = sum + 1/(3*(N-j)+2)*(-dF(2*j-1));
                           sumG = sumG + 1/(3*(N-j)+2)*(-dG(2*j-1));
                   else
                           sum = sum + 1/(3*(N-j)+2)*(dF(2*j-2)-dF(2*j-1)) +
1/(3*(N-(j-1))+1)*(dF(2*j-3)-dF(2*j-2));
                           sumG = sumG + 1/(3*(N-j)+2)*(dG(2*j-2)-dG(2*j-1)) +
1/(3*(N-(j-1))+1)*(dG(2*j-3)-dG(2*j-2));
                   end
                end
                sigma_xz_zB(i) = real( -t/(2*(3*(N-PL)+1))*(dF(2*PL-1)-
dF(2*PL))*(z/t+1/2)^2 + t/(2*(3*(N-PL)+2))*(dF(2*PL-2)-dF(2*PL-1))*(z/t-1/2)^2
...
                                    - 1/2*t*sum );
                sigma_yz_zB(i) = real( -t/(2*(3*(N-PL)+1))*(dG(2*PL-1)-
dG(2*PL))*(z/t+1/2)^2 + t/(2*(3*(N-PL)+2))*(dG(2*PL-2)-dG(2*PL-1))*(z/t-1/2)^2
...
                                    - 1/2*t*sumG );
                sum1 = 0;
                sum2 = 0;
                for j = 1:PL
                   if j == 1
                           sum1 = sum1 + 1/(3*(N-j)+2)*(-ddF(2*j-1));
                      sum2 = sum2 + (1/3 + (PL-j)/2)/(3*(N-j)+2)*(-ddF(2*j-1));
```

```
                else
                        sum1 = sum1 + 1/(3*(N-j)+2)*(ddF(2*j-2)-ddF(2*j-1)) +
1/(3*(N-(j-1))+1)*(ddF(2*j-3)-ddF(2*j-2));
                    sum2 = sum2 + (1/3 + (PL-j)/2)/(3*(N-j)+2)*(ddF(2*j-2)-
ddF(2*j-1)) + (2/3 + (PL-j)/2)/(3*(N-(j-1))+1)*(ddF(2*j-3)-ddF(2*j-2));
                end
            end
            sigma_zz_zB(i) = real( t^2/(6*(3*(N-PL)+1))*(ddF(2*PL-1)-
ddF(2*PL))*(z/t+1/2)^3 - t^2/(6*(3*(N-PL)+2))*(ddF(2*PL-2)-ddF(2*PL-1))*(z/t-
1/2)^3 ...
                                + 1/2*t^2*sum1*(z/t-1/2)+t^2*sum2);
        end
    end
if StressComp == 1
   subplot(1,2,2); plot(sigma_xx_zB,Plotz);
   xlabel('\sigma_x_x');
   ylabel('z');
   title1 = ['and Dropped Region'];
   title(title1);
   %axis([0 2500 -n(1)*t 0])
   grid on;
elseif StressComp == 4
   subplot(1,2,2); plot(sigma_xz_zB,Plotz);
   xlabel('\sigma_x_z');
   ylabel('z');
   title1 = ['and Dropped Region'];
   title(title1);
   %axis tight
   grid on;
elseif StressComp == 3
   subplot(1,2,2); plot(sigma_zz_zB,Plotz);
   xlabel('\sigma_z_z');
   ylabel('z');
   title1 = ['and Dropped Region'];
   title(title1);
   %axis tight
   grid on;
elseif StressComp == 6
   subplot(1,2,2); plot(sigma_xy_zB,Plotz);
   xlabel('\sigma_x_y');
   ylabel('z');
   title1 = ['and Dropped Region'];
   title(title1);
   %axis tight
   grid on;
elseif StressComp == 5
   subplot(1,2,2); plot(sigma_yz_zB,Plotz);
   xlabel('\sigma_y_z');
   ylabel('z');
   title1 = ['and Dropped Region'];
   title(title1);
   %axis tight
   grid on
end

end % if Orientation == 1

ContPlot = input('\n>> Continue (Yes or No, default Yes) \n?? ','s');
switch ContPlot,
   case 'No',
      flag = 1;
   end
end % while flag == 0
```

APPENDIX C

CALCULATION OF EFFECTIVE IN-PLANE AND BENDING LOADS FOR GEOMETRICALLY UNSYMMETRIC LAMINATES

A bending load is induced in geometrically unsymmetric laminates under applied in-plane load due to the misalignment of the in-plane load at the undropped and dropped ends. Thus, the in-plane stress distribution through the thickness due to the applied in-plane load in such laminates can be obtained by superposing the constant in-plane stress due to the applied in-plane load and a linearly varying in-plane stress due to the induced bending load. In order to model such a laminate using one half of a symmetric laminate, the appropriate combination of the in-plane and bending loads must be applied such that one half of the symmetric laminate is under the identical in-plane stress state as the unsymmetric laminate at the undropped and dropped ends. In this appendix, these appropriate in-plane and bending loads are derived. For simplicity, the laminate is assumed to be homogeneous, *i.e.*, all plies are unidirectional, furthermore resulting in symmetric sections within each region. Using a similar procedure shown herein, extensions to general laminated cases can be obtained. In addition, all laminates are assumed to be of unit width in the following derivation.

Consider the unsymmetric laminate shown in Figure 6.75. The magnitude of the induced bending load was found to be,

$$M_i = \frac{(nt - n_c t)}{2} N, \tag{C.1}$$

where n is the total number of plies in the unsymmetric laminate, n_c is the number of continuous plies, and t is the ply thickness. Expressing the applied in-plane load in terms of the applied stress, σ_0, at the undropped end, equation (C.1) becomes:

$$M_i = \frac{(nt - n_c t)}{2}\sigma_0 nt \tag{C.2}$$

At the undropped end of the unsymmetric laminate, the in-plane stress due to the applied in-plane load is equal to σ_0, and that due to the induced bending load is equal to,

$$\sigma_{bending} = -\frac{M_i}{I}z' = -\left[\frac{12}{(nt)^3}\frac{(nt - n_c t)}{2}\sigma_0 nt\right]z' \tag{C.3}$$

where the induced bending load from equation (C.2) was substituted for M_i and the second moment of inertia of a rectangular cross-section was substituted for I. Note that the coordinate z' in the unsymmetric laminate is defined such that the origin is located at nt/2 above the bottom surface (see top diagram in Figure C.1).

Summing the in-plane stresses due to the two loads results in a linearly varying in-plane stress in the undropped region as illustrated in Figure C.1. The in-plane stresses at the top and bottom surfaces are equal to:

$$\sigma_{top} = \sigma_0 - \sigma_s = \sigma_0 - \left[\frac{12}{(nt)^3}\frac{(nt - n_c t)}{2}\sigma_0 nt\right]\frac{nt}{2} \tag{C.3a}$$

and

$$\sigma_{bottom} = \sigma_0 + \sigma_s = \sigma_0 + \left[\frac{12}{(nt)^3}\frac{(nt - n_c t)}{2}\sigma_0 nt\right]\frac{nt}{2} \tag{C.3b}$$

The in-plane and bending loads that need to be applied to a symmetric laminate such that the in-plane stress distribution in one half of the symmetric laminate is identical to that in the unsymmetric laminate can obtained from equations (C.3a) and (C.3b). They are obtained such that the bottom surface of the unsymmetric laminate corresponds to the mid-plane in the symmetric laminate, and the upper surface in the unsymmetric laminate corresponds to the upper surface in the symmetric laminate. In order to satisfy this condition, the in-plane load in the symmetric laminate needs to produce a stress equal to the in-plane stress at the bottom surface in the unsymmetric laminate in equation (C.3b).

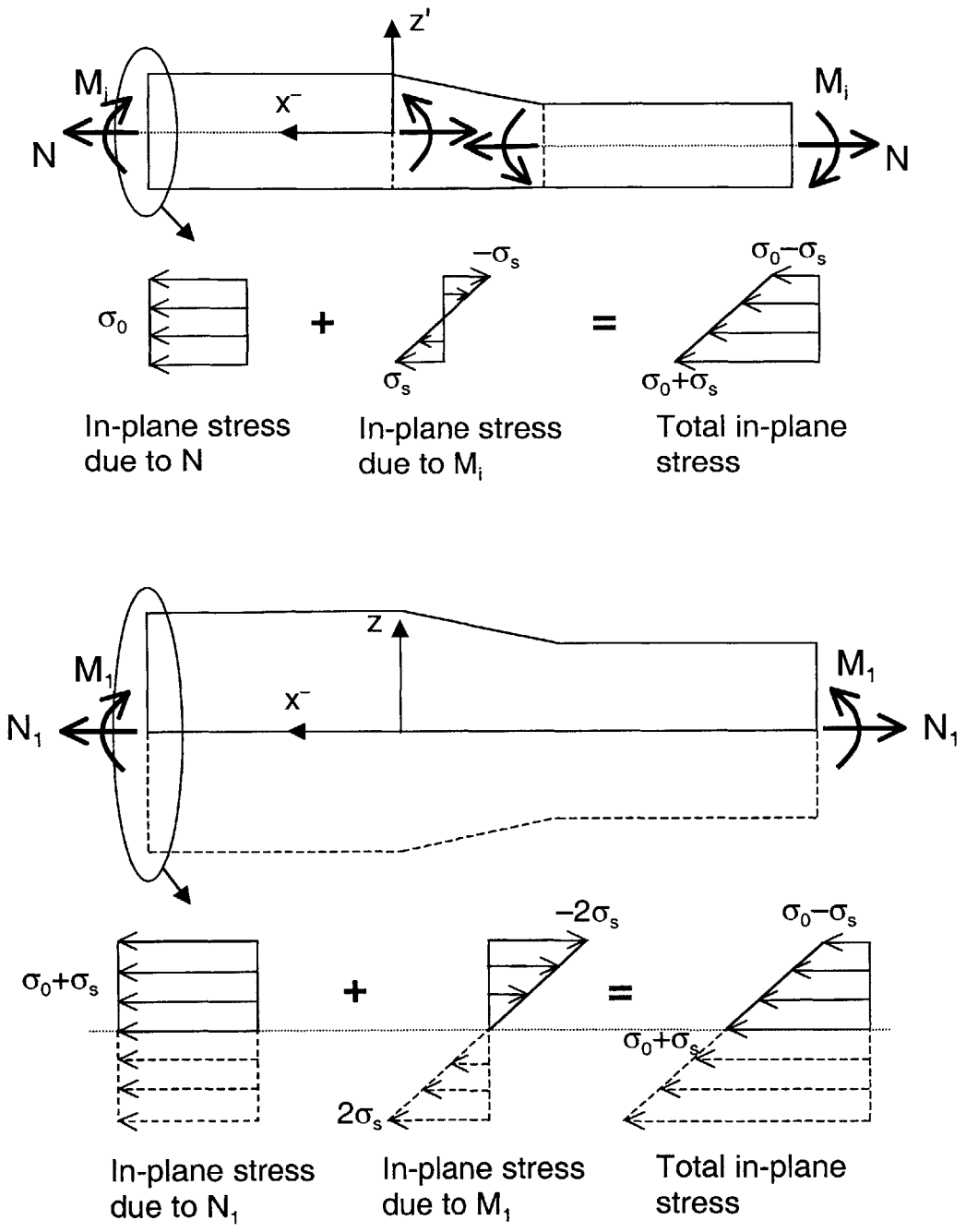

Figure C.1 Illustrations of the total in-plane stress at the undropped end *(top)* in the unsymmetric laminate due to the applied in-plane and the induced bending load, and *(bottom)*, in a symmetric laminate due to applied in-plane and bending loads.

Since there are twice as many plies in the symmetric laminate, the in-plane load per unit width is equal to twice the in-plane stress at the bottom surface multiplied by the total number of plies in the undropped region of the unsymmetric laminate, *i.e.*;

$$N_1 = 2\sigma_{bottom} nt = 2\left\{\sigma_0 nt + \left[\frac{12}{(nt)^3}\frac{(nt - n_c t)}{2}\sigma_0 nt\right]\frac{(nt)^2}{2}\right\} \tag{C.4}$$

The bending moment in the symmetric laminate must be such that the sum of the in-plane stress due to N_1 and that due to the bending moment at the top surface of the laminate is equal to the in-plane stress at the top surface in the unsymmetric laminate in equation (C.3) (see bottom part of Figure (C.1)). Since the in-plane stress in the symmetric laminate due to a bending load can be expressed as,

$$\sigma_{bending} = -\frac{M_1}{I}z = -\frac{12}{(2nt)^3}M_1 z \tag{C.5}$$

the magnitude of the bending load, M_1, in the symmetric laminate needs to be equal to

$$M_1 = \left(\sigma_{bottom} - \sigma_{top}\right)\frac{(2nt)^3}{12}\frac{1}{nt} = \left\{\left[\frac{12}{(nt)^3}\frac{(nt - n_c t)}{2}\sigma_0 nt\right]nt\right\}\frac{(2nt)^3}{12}\frac{1}{nt} \tag{C.6}$$

Note that the coordinate z in the symmetric laminate is defined such that the origin coincides with the mid-plane (see lower diagram in Figure C.1). Equations (C.4) and (C.5) can be simplified to:

$$N_1 = 2(4nt - 3n_c t)\sigma_0 = 2\left(4 - 3\frac{n_c}{n}\right)N \tag{C.6}$$

and

$$M_1 = 4(nt - n_c t)\sigma_0 nt = 4(n - n_c)Nt \tag{C.7}$$

Similarly, at the dropped end, the in-plane stresses at the top and bottom surfaces are equal to:

$$\sigma_{top} = \sigma_0 \frac{n}{n_c} + \left[\frac{12}{(n_c t)^3} \frac{(nt - n_c t)}{2} \sigma_0 nt \right] \frac{n_c t}{2} \tag{C.8a}$$

and

$$\sigma_{bottom} = \sigma_0 \frac{n}{n_c} - \left[\frac{12}{(n_c t)^3} \frac{(nt - n_c t)}{2} \sigma_0 nt \right] \frac{n_c t}{2} \tag{C.8b}$$

In equation (C.8), the in-plane stress due to the induced bending load is added to the in-plane stress due to the in-plane load at the top surface and subtracted at the bottom surface to account for the opposite direction of the bending load. Thus, the in-plane load in the symmetric laminate must be equal to,

$$N_2 = 2\sigma_{bottom} n_c t = 2\left(nt - 3(nt - n_c t)\frac{n}{n_c} \right)\sigma_0 \tag{C.9}$$

and the bending load to:

$$M_2 = \left(\sigma_{top} - \sigma_{bottom}\right)\frac{(2n_c t)^3}{12}\frac{1}{n_c t} \tag{C.10}$$

Again, these can be simplified to:

$$N_2 = 2\left(4 - 3\frac{n}{n_c} \right)N \tag{C.11}$$

and

$$M_2 = 4(n - n_c)Nt \tag{C.12}$$

APPENDIX D

CALCULATION OF TRANSVERSE STRESSES DUE TO MISMATCH IN POISSON CONTRACTION

Laminates with ply dropoffs under in-plane load generally undergo different amounts of Poisson contraction in the transverse direction. This is true even in cases where the Poisson's ratio is the same in the undropped and dropped regions due to the difference in the thickness between the two regions. A quasi-one-dimensional analysis is presented herein to obtain a first-order estimate of the transverse tensile and compressive stresses in the undropped and dropped regions. For simplicity, the material is assumed to be isotropic.

Consider the undropped and dropped regions of a laminate with ply dropoffs as shown in Figure D.1. The laminate is under applied longitudinal load, P. If the width of the laminate is w, the thicknesses in the undropped and dropped regions are t_u and t_d, respectively, the longitudinal modulus is E and the Poisson's ratio is ν, the transverse strains due to P can be expressed as:

$$\varepsilon_u = -\nu \frac{P}{Ewt_u} \tag{D.1a}$$

and

$$\varepsilon_d = -\nu \frac{P}{Ewt_d} \tag{D.1b}$$

where ε_u and ε_d are the far-field transverse (y-direction) strains in the undropped and dropped regions, respectively. Since the transverse strains in the two regions are different, tensile and compressive stresses must develop at the cutoff location where the two regions meet in order to satisfy compatibility. Specifically, transverse compressive

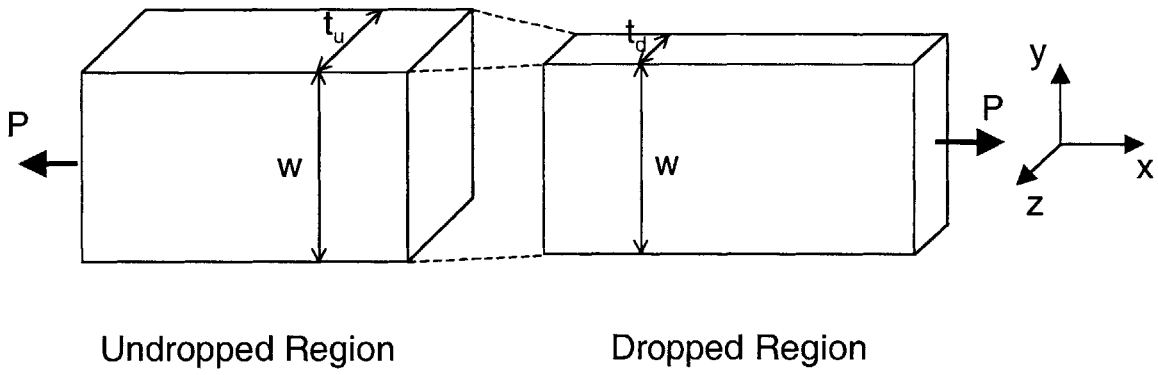

Figure D.1 Diagram of laminate with ply dropoffs under in-plane load.

stress must occur in the undropped region because the transverse strain is smaller in this region compared to the dropped region. Likewise, transverse tensile stress must occur in the dropped region since the transverse strain is greater in this region.

The transverse compressive stress in the undropped region, σ_u, and the transverse tensile stress in the dropped regions σ_d can be obtained by considering the transverse direction compatibility condition and force equilibrium. In order for the undropped and dropped regions to match at the cutoff, the transverse strains in the undropped and dropped region at the cutoff must be equal. The transverse strains in the undropped and dropped regions at the cutoffs are the sum of the strains due to the longitudinal (x-direction) load, P, in equation (D.1) and the strains due to the transverse stress at the cutoff. Thus, the strains in the undropped and dropped regions are:

$$\varepsilon_u = -\nu\frac{P}{Ewt_u} + \frac{\sigma_u}{E} \tag{D.2a}$$

and

$$\varepsilon_d = -\nu\frac{P}{Ewt_d} + \frac{\sigma_d}{E} \tag{D.2b}$$

The compatibility condition mandates that the transverse strains in the two regions be equal:

$$-\nu\frac{P}{Ewt_u} + \frac{\sigma_u}{E} = -\nu\frac{P}{Ewt_d} + \frac{\sigma_d}{E} \tag{D.3}$$

In addition, the force equilibrium in the transverse direction must be satisfied. This requires that:

$$\sigma_u wt_u + \sigma_d wt_d = 0 \tag{D.4}$$

The tensile and compressive stresses, σ_u and σ_d, can be obtained by simultaneously

solving equations (D.3) and (D.4). This yields the following expressions for the transverse stresses:

$$\sigma_d = \frac{\nu P}{w t_d}\left(\frac{t_u - t_d}{t_u + t_d}\right) \tag{D.5a}$$

and

$$\sigma_u = -\frac{\nu P}{w t_u}\left(\frac{t_u - t_d}{t_u + t_d}\right) \tag{D.5b}$$

The analysis presented herein provides a first-order estimate of the transverse tensile and compressive stresses in the dropped and undropped regions that arise due to a mismatch in the Poisson contraction in isotropic materials. To obtain more accurate transverse stresses, the geometry of the dropoff region, such as the length of the dropoff region, would need to be taken into account. Intuitively, a long dropoff region would allow the mismatch in Poisson contraction in the undropped and dropped regions to be "resolved" gradually thereby decreasing the magnitude of the transverse stresses while a short dropoff region would have the opposite effect. Based on this intuition, the current analysis yields a conservative estimate of the transverse stresses since the dropoff region is assumed to be zero. In addition, to extend this first-order analysis to more general cases of laminates with arbitrary ply angles and orthotropic material properties, the mismatch in the laminate longitudinal moduli and the Possion's ratios in the undropped and dropped regions need to be taken into account.